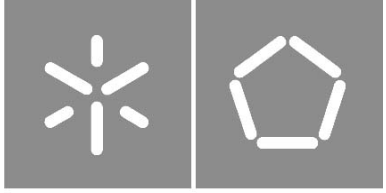

Universidade do Minho
Escola de Engenharia

Vladimir Guilherme Haach

Development of a design method for reinforced masonry subjected to in-plane loading based on experimental and numerical analysis

Tese de Doutoramento
Engenharia Civil / Estruturas

Trabalho efectuado sob a orientação do(a)
Professor Doutor Paulo B. Lourenço
Professora Doutora Graça Vasconcelos

Junho de 2009

…to my parents and my wife.

ACKNOWLEDGEMENTS

Firstly, I would like to thank God that was a major source of strength during the work on my thesis research. This thesis would not be completed without the encouragement of my family. I would like specially to express my gratitude to Lourdes, my wife, who was present in every good and bad time of this stage of my life.

I acknowledge Professor Paulo Lourenço and Professor Graça Vaconcelos, my supervisors for their supports, discussions, patience, careful reading and valuable suggestions.

I would like to thanks the Programme Alβan, the European Union Programme of High Level Scholarships for Latin America which supported this PhD research providing the scholarship nº E06D100148BR.

This work would not be possible without the support, hard work and endless efforts of technicians of the Laboratory of Civil Engineering of University of Minho: Matos, Marco, Pokee, Gonçalves and Palha who always provided great technical suggestions and friendship. I would like specially to thank technician José Manuel who help me very much in all experimental programs, working several times out of his time schedule.

I am really grateful to SIKA® and SECIL® for given away materials to development of experiments.

Finally, I wish to acknowledge all friends made in this phase of my life and my sincere thanks to all the people who have contributed to development of this research.

“There are men who fight one day and are good.
There are men who fight one year and are better.
There are some who fight many years and they are better still.
But there are some that fight their whole lives,
these are the ones that are indispensable.”

Bertolt Brecht

ABSTRACT

Masonry walls consist of the main elements responsible for the global stability of masonry buildings when subjected to lateral loads such as wind and seismic forces. These elements are subjected to gravity forces, bending moments and shear forces due to the horizontal loading. The masonry beams above the openings are important structural elements promoting the coupling behaviour of the masonry piers enabling the transfer of forces between them. Besides, the consideration of these elements leads to higher stiffness of the building. The anisotropic behaviour added to bi-axial stress state generated by the combination of those efforts becomes the behaviour of masonry walls and beams very complex. Therefore, this research aims at better understanding the behaviour of masonry walls and beams subjected to in-plane loading and propose analytical methodology for their design. Based on the literature review, an extensive experimental program is planned, being composed by experimental tests for the characterization of mechanical behaviour of masonry and masonry materials, in-plane cyclic tests on masonry walls and tests on masonry beams under flexure and shear. Based on experimental results, calibration of numerical micro-model using software DIANA® is presented. Moreover, a parametric analysis of masonry walls and beams is performed in order to assess the influence of different boundary conditions, aspect ratios, loading and reinforcement arrangements that could not by studied in experimental program. Results indicates that masonry walls and beams are described by similar flexural and shear resisting mechanisms. Unreinforced walls and beams present a very brittle behaviour. On the other hand, the application of reinforcement increases the deformation capacity, controls the crack opening and allows a better distribution of stresses. Longitudinal reinforcements (vertical in case of walls and horizontal in case of beams) increase the flexural strength, even if they seem not to influence the shear behaviour. Transversal reinforcements (horizontal in case of walls and vertical in case of beams) increase the shear strength, even if they do not influence the flexural behaviour. Effectiveness of reinforcements on the increase of the resistance of masonry walls and beams is highly related to the failure mode of the element. Based on numerical and experimental results, a new analytical method is proposed for the design of masonry walls and beams subjected to in-plane loading. Comparison between the results provided by the proposed method with other design methods presented in literature and experimental results of several authors is presented.

x

RESUMO

As paredes consistem no elemento estrutural responsável pela estabilidade global dos edifícios em alvenaria estrutural quando sujeitos a acções laterais como vento e sismos. Estes elementos estão sujeitos a forças verticais e adicionalmente a momentos flectores e esforços de corte devido as forças laterais. Um elemento estrutural secundário mas muito importante na interacção de paredes são as vigas sobre as aberturas. Este elemento permite a transferência de esforços entre os troços de parede e confere uma maior rigidez à estrutura. O comportamento anisotrópico da alvenaria aliado ao estado bi-axial de tensão provocado pela combinação dos esforços referidos torna o comportamento das paredes e vigas bastante complexo. Desta forma, este trabalho tem como principal objectivo a melhor compreensão do comportamento de paredes e vigas de alvenaria quando sujeitos a acções no plano e a proposição de um método de dimensionamento para estes elementos. Assim, com base na revisão bibliográfica relativa ao comportamento de paredes e vigas de alvenaria, tanto em termos numéricos quanto experimentais, é proposto um plano extenso de ensaios para a caracterização mecânica dos materiais, para o estudo do comportamento de paredes sob a acção combinada de forças verticais e horizontais cíclicas aplicadas no plano das paredes e, finalmente, para o estudo do comportamento de vigas de alvenaria sujeitos à flexão e ao corte. Com base nos resultados experimentais é feita a calibração de um micro-modelo numérico com o aplicativo DIANA®, utilizando como ferramenta básica o método dos elementos finitos (MEF). Além disso, uma análise paramétrica é realizada nas paredes e nas vigas para avaliar o efeito das condições de fronteira, da geometria, da relação altura/largura dos elementos e das percentagens de armadura transversal e longitudinal. Os resultados indicam que o comportamento das paredes e vigas é descrito pelos mesmos mecanismos de resistência. Ambos os elementos apresentam um comportamento bastante frágil quando não são armados. Por outro lado, a utilização de armaduras aumenta a capacidade de deformação, controla a abertura de fissuras e permite uma melhor distribuição de tensões. As armaduras longitudinais (verticais no caso das paredes e horizontais no caso das vigas) aumentam a resistência à flexão dos elementos mas parecem não ter grande influência no comportamento ao corte. As armaduras transversais (horizontais no caso das paredes e verticais no caso das vigas) aumentam a resistência ao corte dos elementos não tendo grande influência no comportamento à flexão. A eficiência das armaduras no aumento de resistência das paredes e vigas está bastante relacionada com o modo de ruptura. Com base nos resultados numéricos e experimentais é proposto um método de dimensionamento de paredes e vigas sujeitos a acções no plano. A comparação dos resultados fornecidos pelo método proposto e por outros métodos de dimensionamento com resultados experimentais de diversos autores é apresentada.

SUMMARY

LIST OF FIGURES

LIST OF TABLES

1 INTRODUCTION

1.1 Overview of masonry

Masonry is one of the most antique structural systems in the world and began to be developed when the men made a simple pile of stone. There are several evidences of the masonry used by ancient civilizations (Taly, 2001) such as zigurats built by Sumerians and Babylonics with sun dried lumps of mud or clay, the pyramids of Egypt, Romans' aqueducts, etc., see Figure 1.1. The availability of natural materials, solidity, durability and the simple and easy method of construction, by laying brick over brick joined with mortar, probably explain why the technique has been used since ancient cultures.

(a) (b)

Figure 1.1 – Ancient masonry: (a) ziggurat[1] Dur-Untash built in 13th century B.C. and (b) Roman aqueduct[2] in Carthage, Tunísia.

[1] *http://en.wikipedia.org/wiki/Image:Choghazanbil2.jpg* acessed on May of 2008.

[2] *http://en.wikipedia.org/wiki/Image:Aqueduc.jpg* acessed on May of 2008.

The masonry structures were understood only empirically by experienced masons who were responsible to transmit the empirical knowledge to other generations. The application of structural mechanics to the design and assessment of the strength and stability of masonry structures dates back to 17th century when the principles of static were applied to an investigation of the stability of arches and domes (Hendry, 2002). In spite some tests carried out in the beginning of 20th century masonry structures were designed using mainly empirical rules and with limited engineering principles. The sixteen storeys Monadnock Building in Chicago, in which the wall thickness at ground level is 1.80 m, is an example. It is believed that if this building was designed by the current standards and with the same materials, the wall thickness should be lower than 30 cm (Ramalho and Corrêa, 2003).

Figure 1.2 – Monadnock Building in Chicago[3].

The result of scarce or even absence of rules, recommendations and design methods available for masonry and with the advance of other structural systems such as reinforced concrete and steel, masonry structures lost prestige and practically they are no longer used. The interest in masonry structures became evident again after 1950's, when Paul Haller in Switzerland built apartment buildings of up to eighteen-storeys with wall thickness of only 150 mm following his research work at the Swiss Federal Institute of Technology in Zurich (Haller, 1969 and Ramalho and Corrêa, 2003).

The results of several investigations that have been carried out through recent decades led to the preparation of codes (BS 5628, 1992; Eurocode 6, 2005) pushing the design of masonry structures to a more competitive approach (Carvalho *et al.*, 2001).

Differently of other industries, civil construction does not allow serial production which hinders the organization and quality control of work. In general, limited qualifications of workers added to the acceptance of unfeasible periods of construction leads to a very flexible system with low level of quality. Therefore, the rationalization of construction system through

[3] *http://www.chicagoarchitecture.info* acessed on May of 2008.

simplification of tasks, optimization of the execution processes and consequently improvement on quality control provide a better performance of the built environment (Rauber, 2005). The masonry technology encompasses this rationalization in several aspects such as reduction of moulds, reduction of specialities of labour, reduction in thickness of coatings due to the better quality of units. Besides it contributes to minimize the waste of materials due to the breakage of walls to install the hydraulics and other installations.

One of the most important characteristic of the masonry structures is the simple method of construction. It can be considered as a precast structure since the building is assembled by separated pieces (concrete blocks, bricks, stone). Mortar can be the unique material that have to be produced or prepared (pre-mixed mortars) in the local of construction if precast slabs are used, promoting a clean work place. Besides, in masonry structures the phase of constructive process of infill frames is excluded. Thus, masonry walls act as structural element, they make the division of space, promote thermal and acoustic insulation, as well as fire and weather protection. The material is relatively cheap and durable, can provide infinite flexibility in plan form and can offer and attractive external appearance (Hendry, 1998).

On the other hand, the interaction of architectural conception, structural design, electrical and hydraulic projects is essential (Carvalho *et al.*, 2001). In masonry structures, attention should be given to the phase of design project regarding to the compatibility of all specialities generating a final draw rich of details. The main disadvantage of masonry structures is that unexpected changes in layout of walls during or after the construction such as holes to air-conditioning system are impossible.

It is important that all professionals involved in project have a general knowledge about the masonry system, about its possibilities and restrictions. In terms of architectural aspects, the modulation is the basis of the dimensional co-ordination system used for the design of buildings in structural masonry. The architect, since the early stages of the design, should work on a mesh to modulate the building according to the dimensions of the structural components (Carvalho *et al.*, 2001), see Figure 1.3.

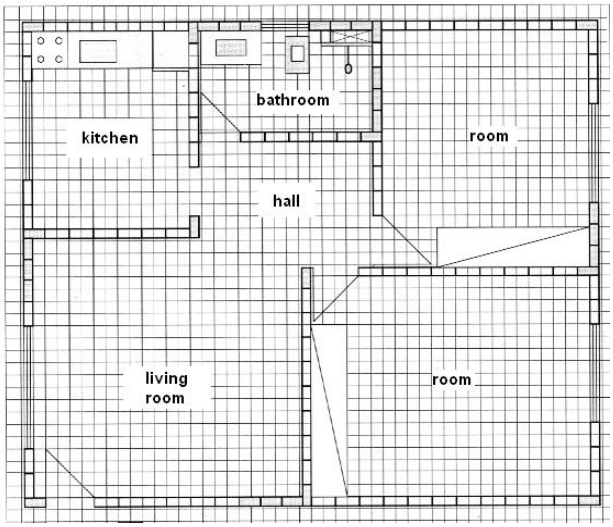

Figure 1.3 - Mesh used in a modular planning of masonry (Carvalho *et al.*, 2001).

Other important point during the design is the definition of the walls layout, including the scheme to be used by positioning various load-bearing walls over the floor/roof slab which will be supported, see Figure 1.4 (Hendry, 1998). According to Taly (2001), proper layout is crucial to a successful masonry project. The author still affirms that the layout should be such that floor slabs can be economically installed avoiding too much distance between the walls.

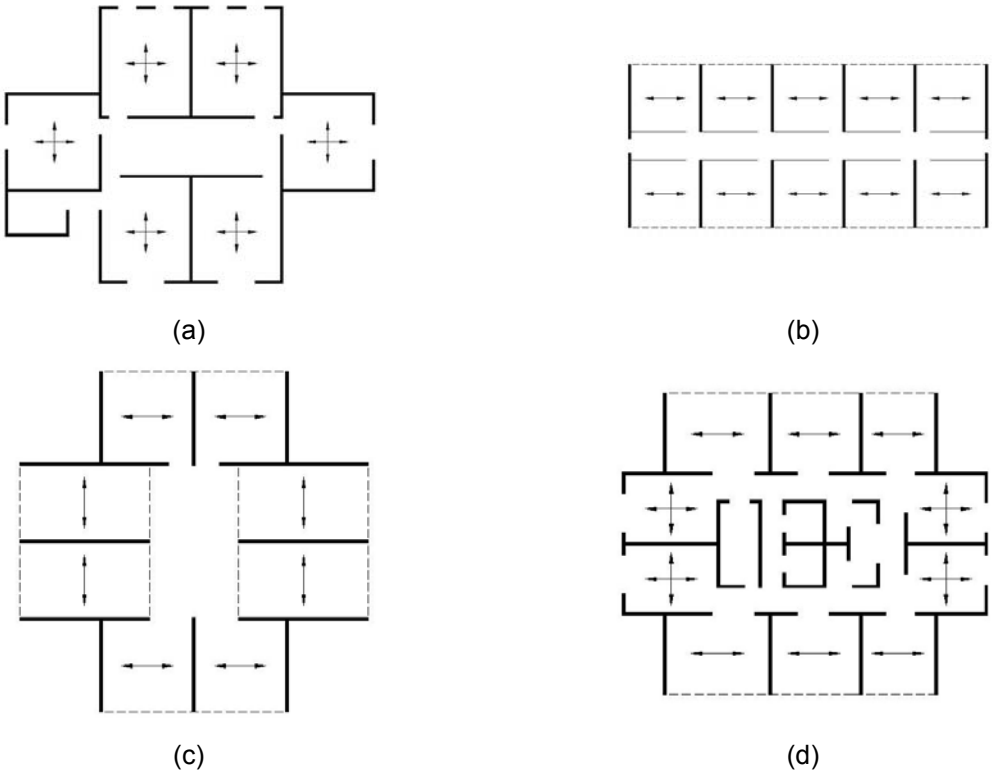

Figure 1.4 – Possible layouts of resistant walls: (a) cellular, (b) simple cross-wall structure, (c) double cross-wall system and (d) core-wall structure.

Finally, the work of all professionals involved in the project should be compatible and the project manager must control this process to avoid resolution of interferences during the construction. Thus, the final project should present the detail of the first and second courses of masonry walls, detail of the intersection of walls, detail of the lintels above and below openings, detail of the connection between walls and slabs, detail of the vertical and horizontal reinforcements, detail of movement joints and a detail of the correct position of the electrical, hydraulical and gas installations. The final result should be a structure that is capable of resisting design loads, functional for the intend occupancy and free of maintenance problems.

In Portugal, masonry is being used almost exclusively as traditional infill material for reinforced concrete frames. Nevertheless, recently, modern engineered masonry is becoming increasingly popular as long as horizontally reinforced non-load bearing walls in large non-residential buildings (Lourenço, 2006). For example, three new stadiums in Portugal were built for the European Championship 2004 using masonry with bed joint reinforcement (Lourenço, 2004). Lack of knowledge about modern masonry technology and simple technology required by reinforced concrete are the main factors contributing to the reduced use of structural masonry in Portugal. Therefore, a major challenge that has to be faced by the Portuguese brick and block producers is the finding of an effective and attractive load bearing masonry system that is able to convince contractors and designers to use it in low and medium-rise buildings. The adoption of such a renewed building technology by contractors seems obvious due to the economical and technological advantages (Lourenço *et al.*, 2006). In this context, some research projects have been carried out by University of Minho in conjunct with the industry to develop and disseminate the structural masonry into the Portuguese civil construction market.

1.2 Objectives

Masonry is an excellent material to resist compression stresses generated by gravity loads. However, masonry buildings should be also capable to resist lateral loads, which produce tensile and shear stresses. Wind and seismic actions are the main lateral loadings supported by masonry buildings. The main structural elements which resist these actions are the walls subjected to in-plane loadings connected by beams located over the openings. The use of steel reinforcement is one of the more reliable solutions for making masonry buildings adequately safe when subjected to seismic actions. In this way, prefabricated reinforcements are being highly applied aiming at improving on-site productivity.

Thus, the main objective of this research is the evaluation of the behaviour of masonry structural elements (walls and beams) reinforced with longitudinal and transversal prefabricated truss type bars under in-plane loading. The evaluation of the in-plane behaviour of masonry walls and beams aims at performing: (a) an experimental assessment of the influence of variables like longitudinal and transversal reinforcement ratios, level of pre-compression and distinct masonry bond patterns in order to propose a solution technologically more efficient; (b) validation of a numerical model and perform a parametric study in order to assess the influence of geometry and boundary conditions and additionally the presence of transversal and longitudinal reinforcements and variation of their ratio and filling of vertical joints (c) proposal of an analytical model for the design of masonry walls and beams.

1.3 Research Significance

Due to the poor performance of masonry under tensile stresses, the lateral actions are critical during the design of masonry buildings. On the other hand, shear walls are the main structural elements on masonry buildings responsible for resisting the lateral loads. Even if several researches has been performed on the unreinforced and reinforced masonry up to date, there are many doubts and lack of knowledge on several issues such the influence of the longitudinal and transversal reinforcement ratio on the lateral resistance of masonry walls. Besides, standards present design methods much simplified or empirical and in most cases underestimate the capacity of shear walls. Masonry beams connect the shear walls and provide a better distribution of the lateral forces through the wall panels reducing the efforts at the base of building. There are few works evaluating these elements and in general they are designed using the same methods applied in reinforced concrete beams. In addition, the use of prefabricated truss type bars for transversal and longitudinal directions is considered to be a challenge. The use of these bars can increase the productivity in construction of reinforced masonry buildings due to the facility of application.

Thus, the major significance of the present thesis relies on the clarification of the in-plane behaviour of reinforced masonry structures by achieving a better insight on the main parameters influencing their in-plane behaviour. The major outputs of the thesis is the experimental research, advance numerical simulation of reinforced masonry structures, relatively to which scarce information exists in literature, and in the proposal of an analytical model to assist the design of masonry walls and beams.

1.4 Methodology

Firstly, an extensive literature review was carried out aiming to better understand the behaviour of shear walls and masonry beams and to gather the information related to past and recent experimental, numerical and design procedures on reinforced masonry walls and beams.

The second phase encompasses the planning of the work of the thesis, including experimental, numerical and analytical analysis of masonry walls and beams. It was decided to analyse reinforced masonry walls that are suitable to be used on seismic areas. Besides, concrete blocks, cement mortar and prefabricated truss type reinforcements were adopted as the main materials of masonry. The experimental work is divided in three parts: (1) the experimental program I aims at performing the mechanical characterization and evaluation of mechanical behaviour of masonry and masonry materials. It includes the mechanical characterization of the concrete units, mortar, reinforcements and the masonry as composite material; (2) the experimental program II intends to evaluate the experimental behaviour of reinforced masonry walls under cyclic lateral loads, namely the failure modes, force-displacement diagrams, lateral resistance, stiffness degradation and energy dissipation capacity. Ten shear walls were built with distinct reinforcement ratios, geometry of units, pre-compression levels and masonry bond patterns; (3) in the experimental program III, twenty four masonry beams were tested under monotonic loading. Four and three load point configuration tests were considered to evaluate the flexure and shear in masonry beams.

Furthermore, a numerical model was calibrated using the experimental results and a parametrical analysis was carried out to evaluate the influence of other variables in behaviour of shear walls and masonry beams not observed in experimental tests. A design model was proposed for the design of reinforced masonry walls and beams. An evaluation of its performance was carried out by comparing the experimental and analytical lateral resistance of reinforced masonry walls with design models available in literature. A database containing about 100 walls was built in order to validate the design model for masonry walls. Unfortunately, this procedure could not be applied in design methods of masonry beams due to the absence of results of experiments in literature. Finally, in order to exemplify the proposed design model, an example of elastic design of a masonry building is presented. Figure 1.5 presents a scheme of the methodology used in this research.

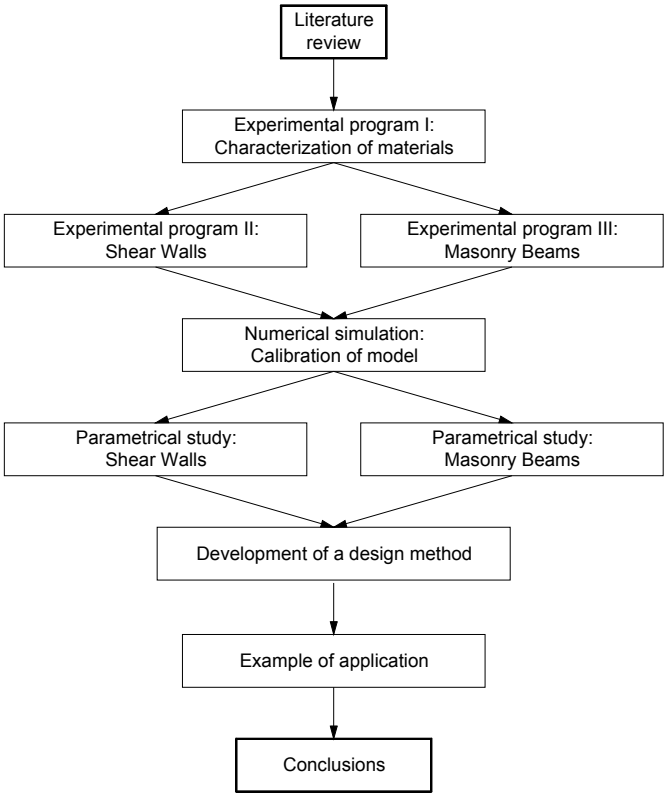

Figure 1.5 – Flow chart of the methodology of the research.

1.5 Outline of the thesis

Thesis was divided in eight chapters: (1) introduction, (2) literature review, (3) experimental program I: characterization of materials, (4) experimental program II: shear walls, (5) experimental program III: masonry beams, (6) numerical simulation, (7) new analytical method for design of masonry walls and beams subjected to in-plane loading and (8) conclusions and final remarks.

Chapter 2 presents a literature review about shear walls and masonry beams. Resistant mechanisms and the variables that influence the behaviour of these elements are discussed. Some experimental works are reported mainly for shear walls. Besides, an overview of the numerical modelling of masonry is presented pointing out the main characteristics of micro- and macro-modelling approaches.

Chapter 3 details the characterization of materials that are used in the construction of masonry walls and beams. In case of concrete units, some tests are carried out to evaluate the compressive strength normal and parallel to hollow cores, tensile strength, water absorption, dimensions and voids' percentages. In case of mortar, some tests are carried out to evaluate the workability through the flow table, compressive and flexural strength. In case of reinforcements, direct tensile tests are carried out to obtain the yield strength and the

elastic modulus. Besides, some tests are carried out to evaluate the behaviour of masonry as a composite such as compressive strength parallel and perpendicular to bed joints, diagonal strength, flexural strength and initial shear strength.

Chapter 4 describes the experimental program of shear walls. Details of the construction of specimens, layout of test, test procedures and instrumentation are explained. Results of test are presented in terms of failure modes and force *vs.* displacements diagrams. Seismic performance of the specimens is discussed based on the stiffness degradation, energy dissipation capacity, ductility and the bi-linear idealization of the experimental monotonic envelops.

Chapter 5 describes the experimental program of masonry beams. Details of the specimens, layout of test, test procedures and instrumentation are explained. Results of test are presented in terms of failure modes and force *vs.* displacements diagrams and resistant mechanisms are discussed.

Chapter 6 presents the numerical modelling of shear walls and masonry beams. Firstly, the calibration of the micro-model is presented based on experimental results of the tests in shear walls and masonry beams. Furthermore, a parametric study is carried out for shear walls and masonry beams in order to evaluate in detail the main factors influencing their in-plane behaviour.

Chapter 7 presents a new analytical method based on experimental and numerical results for the design of masonry walls and beams. In case of shear walls a database with 100 masonry walls collected from the literature review is used to validate the proposed method and compare its performance with analytical models available in literature. Besides, a Windows application is developed to design shear walls and masonry beams through the proposed model and also through the models selected from the literature. Besides, a masonry building is designed using the model proposed in this thesis to design the shear walls and masonry beams in order to exemplify its use.

Chapter 8 presents a summary of the research with the main conclusions and some suggestions for further works.

2 LITERATURE REVIEW

2.1 Introduction

Structures are often subjected to lateral loads from wind or, in zones of moderate or high seismicity, from seismic actions, meaning that structural systems have to be designed to resist these types of loading. In masonry buildings walls are the main structural elements that assure the structural stability for in-plane loads and out-of-plane loads. Due to the cyclic random nature of the seismic and wind actions, any wall of a building can be subjected to in-plane and out-of-plane loads, as shown in Figure 2.1. Masonry walls are the main elements that resist the in-plane loads and act in conjunction with beams over doors or windows connecting the masonry piers. The masonry walls are particularly vulnerable to out-of-plane loads and its adequate in-plane behaviour is only ensured if the walls resist the out-of-plane loading. Besides lateral loads, the walls are submitted to vertical loads since they constitute the main supports of slabs, vaults and domes, meaning that a complex stress state develops in masonry walls.

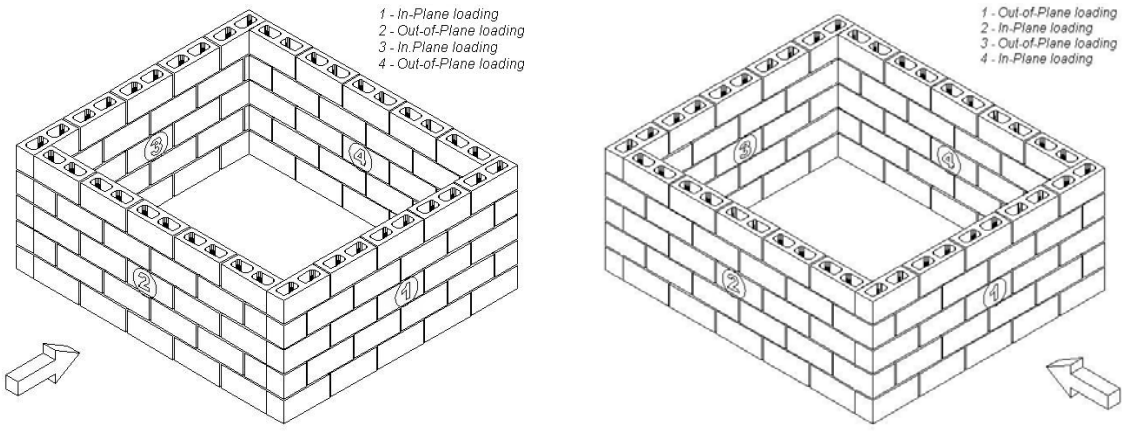

Figure 2.1 – Behaviour of the walls due to cyclic random nature seismic action.

Unreinforced masonry is an excellent structural material when compressive stresses are preponderant. However, it is well known that the low tensile strength of masonry becomes it inadequate to be use when lateral forces reach high values. Therefore, the use of steel reinforcement appears to be a good solution to increase the tensile strength and, thus, to improve the mechanical behaviour of masonry under lateral loading.

Although several investigations have been performed in the scope of unreinforced masonry, mainly due to the need of preserving historical constructions, its behaviour under lateral forces is not still completely clear. Masonry exhibits a complex structural behaviour since it is a composite material with anisotropic behaviour subjected to a tri-axial stress state (Drysdale *et al.*, 1999). The complexity of the in-plane behaviour of masonry walls increases when the presence of steel reinforcement is considered. Besides the material properties of the components (units and mortar) and of the unit-mortar interface (tensile bond and shear behaviour), the interaction between masonry material and reinforcement has to be analyzed.

The correct understanding of the in-plane behaviour and of the factors that influence the response of reinforced masonry walls based on experimental and numerical approaches remains an important research topic. The main focus of this thesis is the in-plane behaviour of reinforced masonry walls and masonry beams. Thus, a brief overview on the structural behaviour of resisting masonry structural elements to the in-plane lateral loading is presented in the next sections.

2.2 Shear walls

The walls subjected to in-plane loading are known as “shear walls” due to the predominance of the shear efforts. A shear wall acts as vertical cantilever or fixed end structural element and its stiffness depends basically on its aspect ratio defined as the relation between the height and length of the wall. As observed by several authors (Anthoine and Magonette, 1995; Schultz *et al.*, 1998; Kikuchi *et al.*, 2003), the aspect ratio has a great influence on the failure mode of the walls. For low aspect ratios shear failure predominates, whereas flexural behaviour governs the in-plane behaviour of slender walls. The failure mode of a particular shear wall also depends on the combination of applied loads, properties of the materials and as recently pointed out by Vasconcelos (2005) on the bond pattern. Besides, in reinforced masonry walls the details of the vertical and horizontal reinforcement also influence their in-plane behaviour. Figure 2.2 shows the distinct crack patterns associated to different stress states exhibited by shear walls.

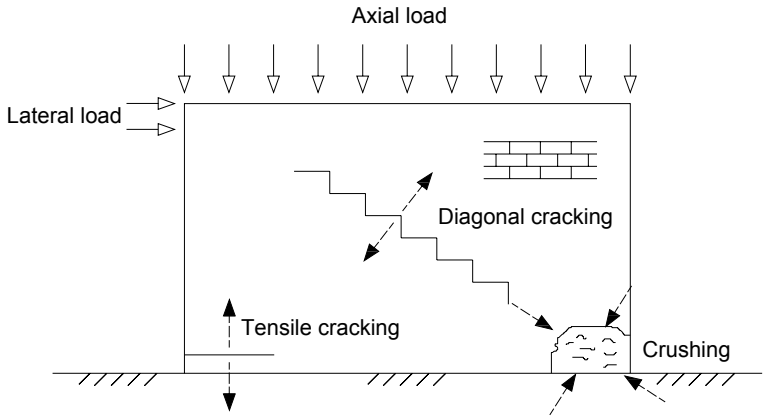

Figure 2.2 – Typical cracking patterns of shear walls.

Shear walls are subjected to flexure and shear efforts in conjunction with compressive stresses associated to the gravity loads. Its behaviour under flexure is well-defined and follows the same rules applied to concrete structures. However, in terms of shear, masonry walls exhibit a complex behaviour due to the presence of weakness planes along head and bed joints. Thus, there has been considerable research works focused on the analysis of shear behaviour of masonry walls (Abrams, 1986; Shing *et al.*, 1989; Anthoine and Magonette, 1995; Tomaževič, 1999; Dhanasekar and Haider, 2004; Vasconcelos, 2005; Voon and Ingham, 2006). According to Tomaževič (1999), the axial load has a significant influence on the shear strength of masonry walls. If the axial load is within moderate values and depending on the aspect ratio the wall may fail by shear or flexure. In shear mode diagonal cracks develop at the unit-mortar interface or both at the unit-mortar interface and through units as result of a biaxial tension-compression stress state, which in unreinforced masonry generally mean the collapse. In flexural mode, horizontal cracks opens at the unit-mortar interfaces as a result of the reduced tensile bond strength of masonry. This crack pattern represents only an intermediate and local failure mechanism since global failure of wall does not develop if it occurs. However, these cracks reduce the resisting cross section, leading to a concentration of compressive stresses and to the failure of the wall by toe crushing.

In case of unreinforced masonry, it is widely accepted that axial compression increases the shear strength according to a Coulomb failure criterion until a limit value, see Figure 2.3, being the failure mode mainly characterized by diagonal stair stepped cracks along unit-mortar interfaces. After this point, the increase on the axial compression leads only to a slight increase on the shear strength. Diagonal shear cracks can be followed by the reduction of the shear strength with the increase on the axial compressive stress (Drysdale *et al.*, 1999).

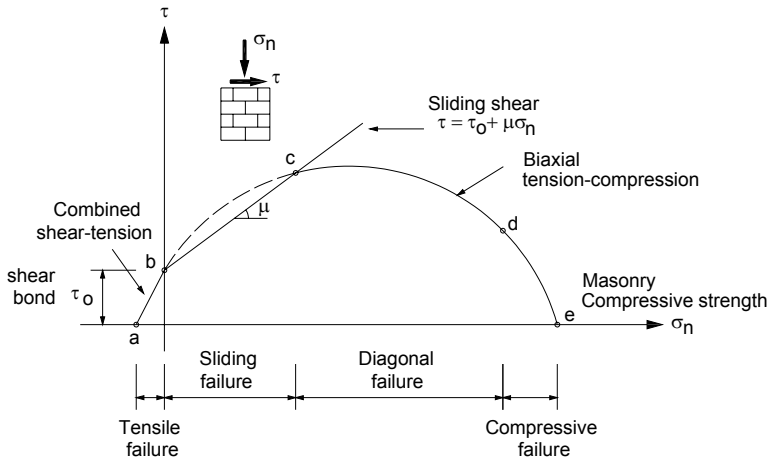

Figure 2.3 – Behavior of unreinforced masonry under combined shear and normal stresses (Drysdale *et al.*, 1999).

Andreaus (1996) identified ten mechanisms of failure to masonry subjected to in-plane loading defined by three failure criterions: Mohr-Coulomb (slipping), Saint-Venant (splitting) and Navier (spalling) as follow:

1. *Slipping of mortar joints*

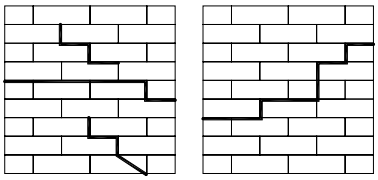

This failure is predominantly observed in the mortar joints and corresponds to the practical range of compression found in shear walls up to about 2MPa. This mechanism may not constitute the ultimate failure.

2. *Slipping of bed joints.*

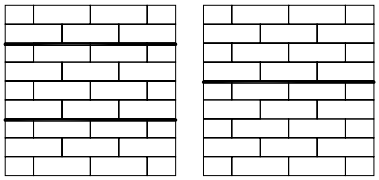

In case of low axial load the lateral loading may lead to shear failure by the horizontal sliding of the joints. This failure usually happens in upper storeys of buildings, where high seismic accelerations are associated to low axial loads.

3. *Splitting and slipping of bed joints.*

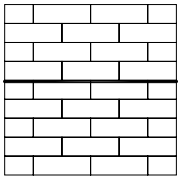

Failure was observed to take place along the bed joints and constitute the ultimate failure of the wall.

4. *Splitting of bricks and slipping of mortar joints.*

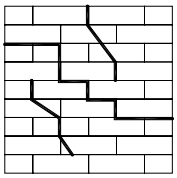

Depending on the relative magnitudes of shear and compressive stresses, failure of the panels occurs by cracking and sliding along bed and/or head joints, or in a combined mechanism involving cracking in brick and joints.

5. *Splitting of bricks and head joints.*

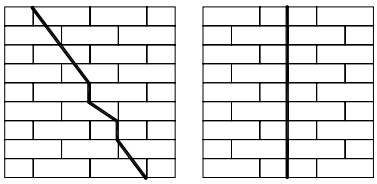

This failure mode is a tension failure by tensile debonding between the mortar and the brick along the head joints and/or tensile failure of brick in some courses.

6. *Slipping of bed joints and splitting of head joints.*

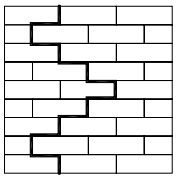

This failure is very similar to the previous mechanism however the failure only happens along head joints because weaker mortar.

7. *Splitting of bed joints.*

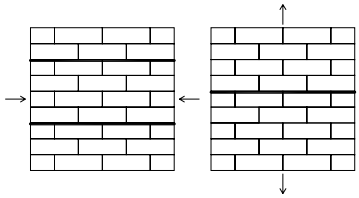

Failure occurs or by compression parallel to bed joints or by tension perpendicular to bed joints.

8. *Slipping and splitting of mortar joints.*

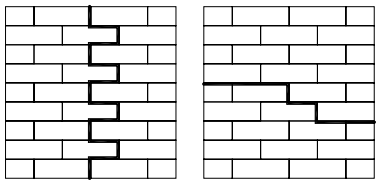

A zig-zag pattern through the head and bed joints occurs because a combined slipping and splitting failure mechanism.

9. *Biaxial deformation.*

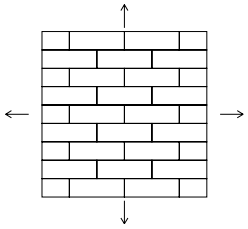

All failures in this range will propagate along the joint planes and the final failure will occur when a sufficient number of joints have failed to allow a collapse mechanism to form.

10. *Middle plane spalling.*

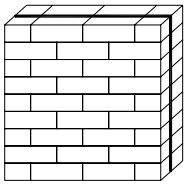

This is a brittle failure that occurs in case of biaxial compression with very high compressive stresses with respect to shear stress.

Another factor that have a strong influence on the structural behaviour of the masonry walls are the boundary conditions. In real buildings the walls are generally restrained in three or four sides: at upper and bottom edges by slabs/wood diaphragms and at lateral edges by perpendicular walls. Abrams (1986) and Modena *et al.* (2004) tested two-story reinforced masonry building systems in a real scale, which enabled to simulate the real connection between the structural elements. Nevertheless, these types of specimens are expensive and need special apparatus to be tested. Therefore, single walls, commonly cantilever or fixed end walls are the most common system for in-plane and out-of-plane testing. Lateral restraints can be simulated by flanged panels (Zhang *et al.*, 2001; Yoshimura *et al.*, 2003; Modena *et al.*, 2004) as shown in Figure 2.4. However, the interaction between walls is still a subject not well understood. This type of specimen is particularly used when the main aim is the assessment of the influence of the level of connection between walls on the in-plane or on the out-of-plane behaviour.

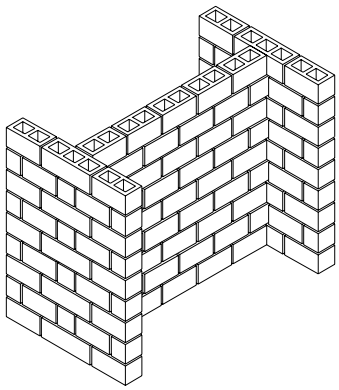

Figure 2.4 – Lateral restraints simulated by flanged walls.

In the recent decades, several works have been carried out for the evaluation of the behaviour of unreinforced masonry walls since it is a constructive system existing in the most impressive monumental buildings and presently it is a constructive alternative of easy application, practical, fast to be built and economically competitive (Jingqian *et al.*, 1986; Mahmoud *et al.*, 1995; Zhuge *et al.*, 1996; Bosiljkov *et al.*, 2003; Steelman and Abrams, 2007). However, serious damages in unreinforced masonry walls have been observed in some past earthquakes such as in the 1931 Hawke's Bay in New Zealand, 1976 Friuli in

Italy, 1949 Olympia and 1965 Seattle-Tacoma earthquakes, see Figure 2.5. This led to the idea that unreinforced masonry walls behave in an inappropriate manner under seismic loading, being not allowed in zones with moderate to high seismic hazard.

(a) (b)

Figure 2.5 – Examples of damages caused by an earthquake in unreinforced masonry walls: (a) 1965 Seattle-Tacoma (Noson *et al.*, 1988) and (b) 1976 Friuli in Italy[4].

The brittle failure of unreinforced masonry shear walls, which is more remarkable with high axial loads, may be reduced by the use of steel reinforcement. According to several authors, the introduction of reinforcement in the masonry ensures the increase on the ductility due to redistribution of lateral loads, and provides better energy dissipation under seismic loading (Schultz *et al.*, 1998; Yoshimura *et al.*, 2003; Dhanasekar and Haider, 2004; Voon and Ingham, 2006). This is very important in areas with high seismicity. According to Tomaževič (1999), when diagonal cracking develops in an unreinforced masonry shear wall subjected to lateral loading a severe deterioration of the wall strength occurs and a brittle collapse takes place. The presence of the horizontal reinforcement prevents the separation of the wall's cracked parts at shear failure and provides the load transfer between the edges of the cracks Schultz *et al.* (1998), see Figure 2.6a.

After diagonal cracking and separation of the wall in two parts, the horizontal reinforcement is subjected to increasing tensile stresses and to tendency for pull-out from the joint. According to Voon and Ingham (2006), this resisting mechanism enables the redistribution of lateral loads improving the resistance and energy dissipation capacity of the wall when subjected to repeated reversal lateral loads. Therefore, the walls with bed joint reinforcement present smeared cracking in opposition to the localized shear crack of unreinforced masonry walls.

[4]http://www.gfz-potsdam.de/pb5/pb53/projekt/ems/guide/illustrations/illustrations.htm acessed in April of 2007.

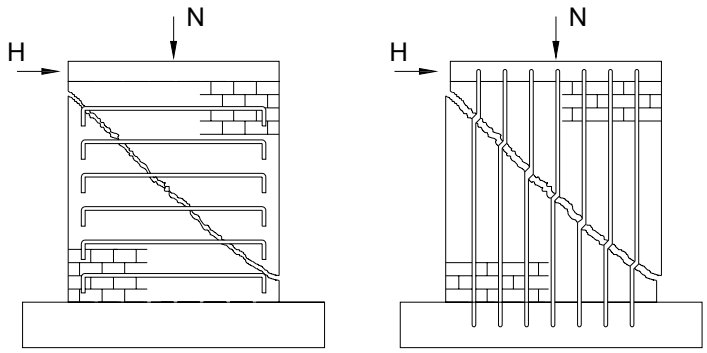

Figure 2.6 – Resisting mechanisms of reinforced masonry walls: (a) horizontal reinforcement and (b) vertical reinforcement (Tomaževič, 1999).

Yoshimura *et al.* (2003) observed that specimens with horizontal reinforcement present higher ductility and ultimate load in relation to unreinforced masonry. However, concerning the contribution of horizontal reinforcement for the improvement of the lateral strength there is no clear agreement. According to Shing *et al.* (1990b), the use of horizontal reinforcement exhibits a small influence both in ultimate and diagonal cracking load and only a high horizontal reinforcement ratio improves ductility and energy dissipation capacity of masonry walls. Similar results are pointed by Schultz *et al.* (1998) that stated that horizontal reinforcements have only a modest influence on ultimate shear stress and deformation capacity.

The resisting mechanism developed in vertical reinforcements is quite different. The vertical reinforcement is particularly effective in case of flexural behavior governs the lateral response, increasing the flexural strength of masonry walls. Additionally it contributes to the shear resistance of masonry walls through the dowel action mechanism, see Figure 2.6b and Figure 2.7. Experimental tests performed by Tomaževič (1999) confirmed that the shear resistance of reinforced masonry walls can be more easily assessed as a sum of contributions of the masonry wall panel and vertical reinforcement.

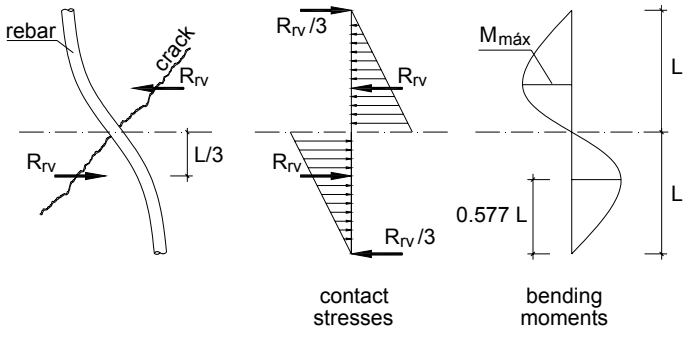

Figure 2.7 – Dowel mechanism of vertical reinforcement at shear failure of a reinforced masonry wall (Tomaževič, 1999).

Dhanasekar and Haider (2004) studied the influence of the spacing ratio of vertical reinforcement. Authors concluded that shear walls with vertical reinforcement spaced uniformly exhibited good level of lateral strength and ductility. These specimens degraded gradually when compared with the walls with non-uniform distribution of vertical reinforcement and exhibited gradual reduction on the lateral strength with increasing spacing ratio of vertical reinforcement.

On the other hand, as assessed in post-earthquake damage observations and through experimental results, only vertical steel reinforcement is not able of contributing to the shear resistance of masonry. Walls reinforced with vertical reinforcement fail in shear, despite their predicted flexural behaviour (Tomaževič, 1999).

2.3 Masonry beams

In masonry buildings the masonry beams are the structural elements responsible for the distribution of vertical loads over openings, see Figure 4.2. Combined with shear walls, masonry beams play a major role on the distribution of lateral actions in masonry buildings providing the coupling of masonry piers. They may be built by using other materials such as steel profiles and precast reinforced concrete elements. However, in these cases, special care should be taken to consider the composite behaviour of masonry and the other material.

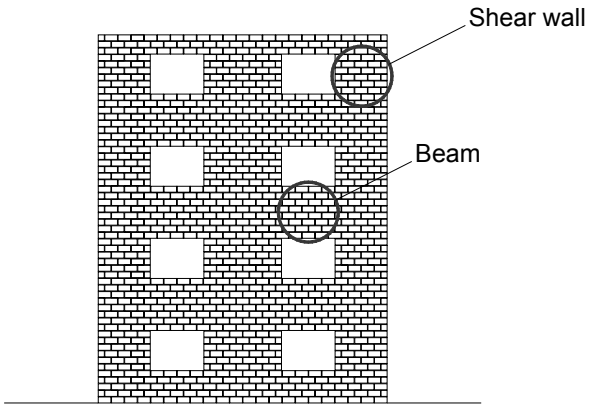

Figure 2.8 – Localization of masonry beams.

In masonry walls and beams an interesting phenomenon can develop denominated “arch action”, corresponding to the direct transfer of the applied in-plane vertical load to the supports. When arching mechanism develops, a triangular part of the beam immediately above the opening could be removed without affecting the load capacity of the element. According to Taly (2001), the development of arching action depends on the mass of

masonry in each side of the opening providing adequate restraint to resist the horizontal thrust. If the adjacent masonry is found to be unable to resist these forces, tension ties are required to provide resistance to tensile stresses developed at the bottom edge. Taly (2001) considers that there is a great degree of uncertainty about which span to depth ratios leads to the development of arching action, however pointed out a maximum value of about 2.0. According to Haseltine and Moore (1981), the equivalent arch has a thickness of about 60% of the span length and an internal radius of about 0.25L, see Figure 2.9. This subject has been analyzed by some researchers in the analysis of composite masonry beams above openings in which a reinforced concrete beam is embedded at the lower edge (Wood, 1952; Stafford Smith and Riddington, 1977; Tomazela, 1995; Paes, 2008).

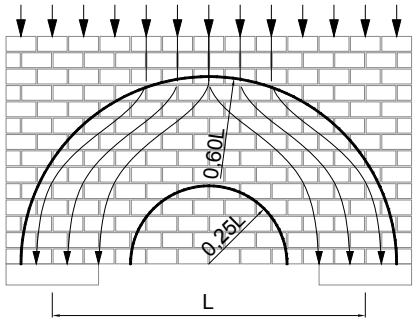

Figure 2.9 – Development of the arching effect.

The span to depth ratio has also influence on the behaviour of masonry beams and in the corresponding design approach. According to several authors, the design of masonry beams can be performed using the ultimate strength design method used in reinforced concrete structures (Khalaf *et al.*, 1983; Hendry, 1998; Drysdale *et al.*, 1999; Taly, 2001). However, this method is not valid to deep beams. Deep beams are structural elements in which a significant amount of the load is transferred to the supports by compression struts connecting the load and the supports. The strain distribution is no longer considered linear and the shear deformations become significant when compared to pure flexure, being the strut-and-tie model recommended for the design, see Figure 2.10. European standard Eurocode 6 (2005) considers deep beams in case of span to depth ratio is lower than 2.0.

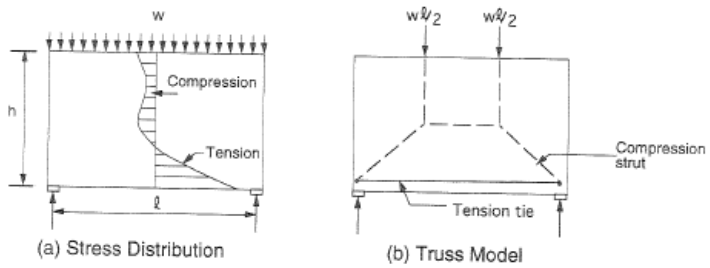

Figure 2.10 – Deep beam behaviour (Drysdale, 1999).

According to Drysdale *et al.* (1999) for shallow masonry beams (span to depth ratio higher than 5 for simply supported beams) the fundamental assumptions considered in the analysis of reinforced concrete elements under flexure can be adopted:

- Internal forces at any section of a member are in equilibrium with the effects of external loads;
- Plane sections before bending remain plane after the bending;
- After the cracking, the contribution of tension in the masonry is ignored;
- Complete bond between steel and masonry is considered.

Khalaf *et al.* (1983) tested a total of eight fully grouted concrete block masonry beams divided in two series: a series with span to depth ratio of about 9 and another series with span to depth ratio of about 6. In both series varying levels of tensile reinforcement were considered aiming at assessing the load-deflection behaviour and at obtaining the strength in flexure. Authors confirmed the assumption that plane sections remain plane during bending and obtained an ultimate compressive strain for masonry of about 0.003.

Limón *et al.* (2000) tested ten brick masonry beams (span to depth ratio equal to 4.5) reinforced with truss type prefabricated bars through four point load configuration aiming at analysing the flexural behaviour of the masonry. Variables like the depth of the neutral axis, the quantity of reinforcement, the overlap of wires and the shear behaviour of masonry were considered in the analysis. Specimens exhibited an ultimate load up to 100% higher than the predicted values from flexural strength method. Authors assumed that the high value of the resistance was attributed to the lower reinforcement area considered in the calculations as the diagonal bars were not taken into account. Taking into account the area of diagonal bars Limón *et al.* (2000) obtained experimental resistances in some specimens close to theoretical values.

In the calculation of flexural strength of masonry beams the compressive strength of masonry in the parallel direction to bed joints is needed, contrarily to masonry walls, whose calculation of the in-plane flexural strength needs the knowledge of the compressive strength of masonry in perpendicular direction to bed joints, see Figure 2.11.

According to Eurocode 6 (2005) the compressive strength of masonry in the parallel direction to bed joints should be calculated by using the same equation adopted for the calculation of the compressive strength of masonry perpendicular to bed joints. For this, the normalized compressive strength of the masonry units obtained from experimental tests in the parallel direction to bed joints must be considered. Besides, for units of group 2 and 3 the value of the coefficient K used in the formula presented by Eurocode 6 (2005), related to the type of mortar and grouping of units, should be multiplied by 0.5.

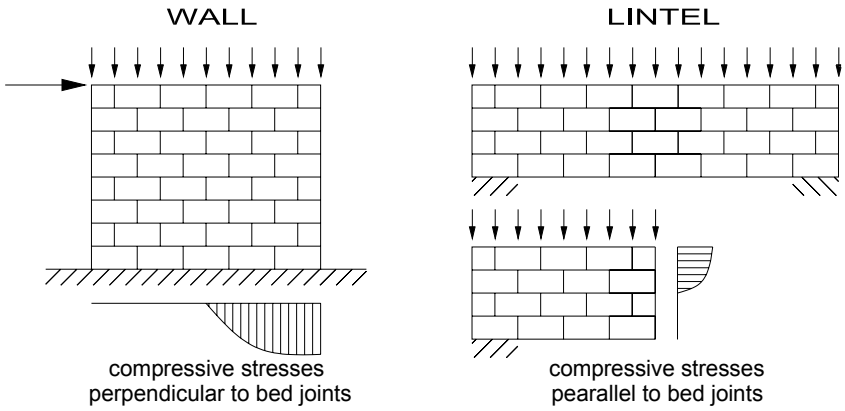

Figure 2.11 – Stress diagram along the length of shear walls and along the height of masonry beams.

Chen *et al.* (2008) performed a parametric study of reinforced masonry sections under flexure and observed that compressive strength of masonry has a large influence on the resisting moment, whereas the tensile strength has only a marginal effect. Another aspect analyzed by some authors is the distribution of longitudinal reinforcements in masonry beams (Jang and Hart, 1995; Adell *et al.*, 2008). Results showed that uniform distribution of reinforcement has advantages over concentrated reinforcements both at top and bottom layers, providing better shear resistance by dowel action, even if displacement ductility decreases.

As in case of walls, shear resisting mechanisms in masonry beams appear to be very complex. Also in this case, the shear efforts are mostly due to lateral loads such as wind and earthquakes. Maximum shear stresses generally develop near the supports leading to diagonal cracking oriented approximately to 45º. From experimental tests several researchers concluded that lower shear strength was observed in masonry beams with the same geometry of reinforced concrete beams (Fereig, 1994; Li and Neis; 1986). Fereig (1994) observed this behaviour in masonry specimens with a/d < 2.0 (ratio of shear span and effective depth) and assigned to the “arch action”. Besides, Fereig (1994) did not observe significant increase in the shear strength by providing an increase of the longitudinal reinforcement ratio. According to Drysdale *et al.* (1999) stronger arches correspond to lower span to height ratios. The shear strength increases when the beams have rigid ties provided by the addition of high amount of tension reinforcements. The formation of a tied arch represents an ultimate resisting mechanism, which is considered to be particularly a dangerous mode of failure due to its brittleness.

Based on a significant number of tests, Suter *et al.* (1984) proposed a shear strength design equation for masonry beams fully grouted without vertical reinforcement (stirrups). According to the design model, the shear strength is a function of the span to length ratio and of the longitudinal reinforcement ratio, ρ, see Figure 2.12.

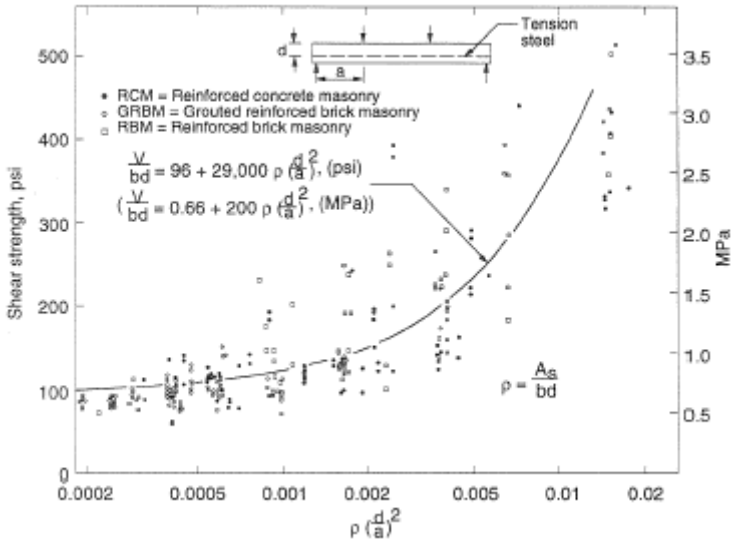

Figure 2.12 – Shear strength of beams without shear reinforcement (Suter *et al.,* 1984).

As in reinforced concrete beams, vertical reinforcements in masonry beams, crossing diagonal cracks, control crack opening and crack propagation can be considered in masonry beams. Through experimental tests Fereig (1994) observed that vertical reinforcement prevents diagonal tension failure and allows the development of full flexural strength.

Comparing to the experimental and numerical information available in literature related to masonry shear walls, there is much more reduced information on the behaviour of masonry beams. In general, design codes for masonry use the same assumptions available for reinforced concrete beams. However, considering that the common height of masonry beams is approximately 1600 mm (800 mm above the openings plus 800 mm under the opening of the other floor), the span of the beam should be at least 8000 mm in order to the span to depth ratio to comply with the requirement pointed out by Drysdale *et al.* (1999) in relation to the span to depth ratio of the beams (5.0) to be considered regular beams. Thus, more research is needed to better understanding the flexural and shear behaviour of masonry beams and the influence of the vertical and horizontal reinforcements on their shear and flexural strength.

2.4 Design models

Design of masonry structures subjected to in-plane loading encompasses two major resisting mechanisms: flexure and shear. According to Shing *et al.* (1990b) flexural strength and deformation can be accurately evaluated by means of the simple flexure theory used for reinforced concrete structural elements. However, shear resisting mechanisms are

considerably more complex. Design models consider that shear strength is the result of the contribution of resisting masonry and reinforcements. The calculation of the contribution of masonry to shear strength is complex to define since it depends on the biaxial behaviour of masonry, which is an anisotropic material. In relation to the contribution of reinforcements, the main difficulty is the definition of the percentage of transversal reinforcement that is really active since the shear stresses are not homogeneous through the section of masonry elements. Besides, longitudinal reinforcements are subjected to transversal efforts resulting on its bending, which is known as the dowel action mechanism. Thus, part of the shear capacity of the masonry elements can also be attributed to this mechanism. Still related with shear mechanism, the sliding between the joints is an interesting effect which is related to the interface unit-mortar. However, in case of shear walls, sliding normally can be neglect since its evaluation is important only when there is none pre-compression, according to Tomaževič (1999) and Shing *et al.* (1990a).

This section aims at presenting some well known approaches for the calculation of shear and flexural strength of reinforced masonry walls and masonry beams.

2.4.1 Shear walls

2.4.1.1 Eurocode 6 (2005)

According to Eurocode 6 (2005) the design of shear walls should be performed by considering different failure modes, namely failure in shear and in flexure. The evaluation of flexural strength of reinforced masonry walls shall be based on the following assumptions:

- the reinforcement is subjected to the same variations in strain as the adjacent masonry;
- the tensile strength of the masonry is taken to be zero;
- the tensile strain of the reinforcement should be limited to 10%;
- the maximum compressive strain of the masonry is chosen according to the material;
- the maximum tensile strength in the reinforcement is chosen according to the material;
- the stress-strain relationship of masonry is taken to be linear, parabolic, parabolic rectangular or rectangular ($\lambda = 0{,}8x$);
- the stress-strain relationship of the reinforcement is defined according to Eurocode 2 (2004);

- for cross-sections not fully in compression, the compressive strain should be taken not greater than ε_{mu} = -0,0035 for Group 1 units and ε_{mu} = -0,002 for Group 2, 3 and 4 units.

The flexural strength is obtained by defining the equilibrium of the section in terms of forces and bending moments (Eq. 2.1 and Eq. 2.2), taking into account the constitutive laws for masonry and reinforcements(Eq. 2.3 and Eq. 2.4) and the compatibility of strains (Eq. 2.5), see Figure 2.13:

$$N = F_m - \sum_i F_{si} \quad \text{Eq. 2.1}$$

$$M_R = F_m\left(\frac{b_w}{2} - 0.4x\right) + \sum_i F_{si}\left(d_i - \frac{b_w}{2}\right) \quad \text{Eq. 2.2}$$

$$F_m = 0.8 f_a t_w x \quad \text{Eq. 2.3}$$

$$F_{si} = E_s \varepsilon_{si} A_{svi} \quad \text{Eq. 2.4}$$

$$\frac{-\varepsilon_m}{x} = \frac{\varepsilon_{si}}{d_i - x} \quad \text{Eq. 2.5}$$

Where, N and M_R are the axial force and moment applied to the section, F_m is the force resisted by masonry, ε_m is the strain of compressed masonry, f_a is the compressive strength of masonry, E_s is the elastic modulus of reinforcements, A_{svi} is the area of i- reinforcement, F_{si} is the force resisted by the i- reinforcement, d_i is the depth of the i-reinforcement, ε_{si} is the strian of the i- reinforcement, x is the position of neutral axis and b_w and t_w are the length and thickness of walls, respectively.

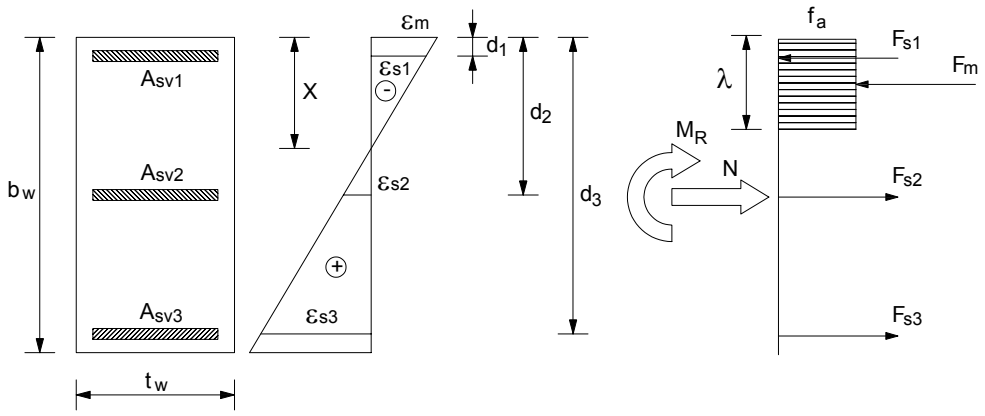

Figure 2.13 – Stress and strain distribution in the wall section assuming a rectangular stress-strain approach (Eurocode 6, 2005).

When shear failure mode is considered, Eurocode 6 (2005) proposes the calculation of the shear strength by taking into account the contribution of masonry and reinforcements through Eq. 2.6.

$$V = V_{R1} + V_{R2}$$
$$V = f_v b_w t_w + 0.9 A_{sh} f_{yh} \leq (2MPa) t_w b_w \quad \text{Eq. 2.6}$$

Where, V_{R1} and V_{R2} are the contribution of masonry and horizontal reinforcement respectively, A_{sh} is the area of horizontal reinforcement, f_{yh} is the yield strength of horizontal reinforcement.

The contribution of masonry for shear strength follows the law of Mohr-Coulomb with the initial shear strength considered as the cohesion of masonry and the friction coefficient equal to 0.4, see Eq. 2.7. The upper limit of the characteristic shear strength is given by Eq. 2.8. This limitation accounts for a possible failure by shear of the units instead of the mortar joints.

$$f_v = f_{v0} + 0.4\sigma \quad \text{Eq. 2.7}$$
$$f_v \leq 0.065 f_b \quad \text{Eq. 2.8}$$

Where, f_v is the shear strength of the masonry, f_{v0} is the initial shear strength of masonry, σ is the normal stress and f_b is the normalized compressive strength of the masonry unit.

The contribution of reinforcements is considered to be the yield force of all horizontal reinforcements distributed along the height of the wall. This approach leads to high values of shear strength as, in fact, only part of the reinforcement contributes to the shear strength. However, Eurocode 6 (2005) defines a limit to the shear stress equal to 2.0 MPa, ensure low values of shear strength in case of high steel ratio.

In case of unreinforced walls, Eurocode 6 (2005) considers that only the compressed length of the wall should be considered to contribute to the shear strength being the tension part neglected, see Eq. 4.17.

$$V = f_v l_c t_w \quad \text{Eq. 2.9}$$

Where, f_v is the shear strength of interface unit-mortar and l_c is the compressed length of the wall in flexure. The compressed part of the wall is calculated assuming a linear elastic distribution of the normal compressive stresses.

When the main reinforcement is placed in pockets, cores or cavities filled with concrete infill Eurocode 6 (2005) in informative Annex J suggest that the vertical reinforcement in conjunct to the infill material contributes to the shear strength and recommend that the value of f_v shall be obtained by Eq. 2.10.

$$f_v = 0.35 + 17.5\rho_v \qquad \text{Eq. 2.10}$$

Where, ρ_v is the vertical reinforcement ratio.

2.4.1.2 MSJC (2002)

According to the Masonry Standard Joint Committee (MSJC, 2002) unreinforced masonry walls should be designed under flexure as an elastic material ensuring that the tensile stresses are lower than the tensile bond strength. In Table 2.1 a summary of the tensile bond strength to different masonry types and for distinct masonry mortars (Portland Cement-lime mortar (PCL), cement mortar and air-entrained Portland Cement-Lime mortar) is shown.

For partially grouted masonry, allowable stresses shall be determined from linear interpolation between fully grouted hollow units and ungrouted units based on the amount of grouting.

Table 2.1 – Flexural strength for clay and concrete masonry (MSJC, 2002).

Masonry Type	Mortar types			
	PCL or cement mortar		Masonry cement or air-entrained PCL	
	M or S	N	M or S	N
Normal to bed joints				
Solid units	0.689	0.517	0.413	0.262
Hollow units[1]				
Ungrouted	0.431	0.331	0.262	0.158
Fully grouted	1.124	1.089	1.055	1.000
Parallel to bed joints in running bond				
Solid units	1.379	1.033	0.827	0.517
Hollow units				
Ungrouted	0.862	0.655	0.517	0.331
Fully grouted	1.379	1.033	0.827	0.517
Parallel to bed joints in stack bond	0	0	0	0

For the shear strength of unreinforced masonry walls, MSJC (2002) recommends the values provided in Eq. 2.11 to Eq. 2.15.

$$V = 0{,}083\left(3{,}8A_n\sqrt{f_a}\right) \quad \text{Eq. 2.11}$$

$$V = 0{,}083\left(300A_n\right) \quad \text{Eq. 2.12}$$

$V = 0{,}083\left(56A_n\right) + 0{,}45N$ → running bond masonry not solidly grouted and for stack bond masonry with open end units and grouted solid. Eq. 2.13

$V = 0{,}083\left(90A_n\right) + 0{,}45N$ → running bond masonry grouted solid. Eq. 2.14

$V = 0{,}083\left(23A_n\right)$ → stack bond other than open end units and grouted solid. Eq. 2.15

Where, A_n is the net area of the wall, f_a is the compressive strength of masonry and N is the axial force of wall.

Design of reinforced shear walls under flexure should be performed considering similar assumptions to those used in reinforced concrete structures according to MSJC (2002). The shear strength of masonry walls is considered to be the sum of the contribution of masonry and of the contribution of reinforcements similarly to Eurocode 6 (2005), see Eq. 2.16.

$$V = V_{R1} + V_{R2}$$

$$V = 0.083\left[4.0 - 1.75\left(\frac{M_u}{V_u d_v}\right)\right]A_n\sqrt{f_a} + 0.25N + 0.5\left(\frac{A_{sh}}{s}\right)f_{yh}d_v \quad \text{Eq. 2.16}$$

Where, M_u and V_u are the maximum bending moment and shear force of the section, d_v is the actual depth of the section of masonry wall and s is the spacing of reinforcement.

The maximum values for the shear strength need not to be greater than the values of Eq. 2.17 and Eq. 2.18. The maximum value of nominal shear strength is permitted to be calculated by linear interpolation between the presented limits for values of $M_u/V_u d_v$ between 0.25 and 1.00.

$$\frac{M_u}{V_u d_v} \le 0.25 \;\rightarrow\; V \le 0.083\left(6A_n\sqrt{f_a}\right) \qquad \text{Eq. 2.17}$$

$$\frac{M_u}{V_u d_v} \ge 1.00 \;\rightarrow\; V \le 0.083\left(4A_n\sqrt{f_a}\right) \qquad \text{Eq. 2.18}$$

2.4.1.3 Tomaževič (1999)

Tomaževič (1999) evaluates the flexural strength shear walls using the classical formulation presented in Eurocode 6 (2005) but with some simplifications: (a) the vertical reinforcements with the same area are assumed to be concentrated near the lateral edges of the wall leading to a symmetrical reinforcement distribution, see Figure 2.14; (b) the reinforcements, both in compression and tension are assumed to be yielded, meaning that both reinforcements carry the same forces.

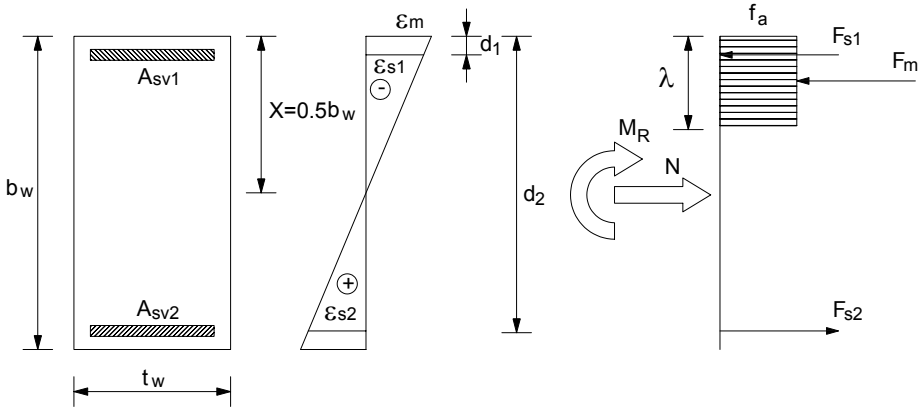

Figure 2.14 – Stress and strain distribution in wall section (Tomaževič, 1999).

Thus, the procedure to obtain the flexural resisting moment consists of considering in a first phase the equilibrium of forces (Eq. 2.19) from which it is possible to obtain the value of λ (Eq. 2.20) and in the second phase by the equilibrium of bending moments acting in the wall's section through Eq. 2.21.

$$N = F_m + F_{s1} - F_{s2} \qquad \text{Eq. 2.19}$$

$$F_{s1} = F_{s2} \;\rightarrow\; b_w t_w \sigma = f_a \lambda t_w \;\rightarrow\; \lambda = \frac{\sigma b_w}{f_a} \qquad \text{Eq. 2.20}$$

$$M_R = \frac{t_w b_w^2 \sigma}{2}\left(1 - \frac{\sigma}{f_a}\right) + A_{svi} f_{yv}\left(b_w - 2d_1\right) \qquad \text{Eq. 2.21}$$

For practical calculations, Tomaževič (1999) considers the shear strength of reinforced masonry walls as the sum of the contributions of masonry, vertical and horizontal reinforcement see Eq. 2.22:

$$V_{sh} = V_{R1} + V_{R2} + V_{R3}$$

$$V_{sh} = b_w t_w \left(\frac{f_t}{b}\right)\sqrt{\frac{\sigma}{f_t} + 1} + \Phi A_{sh} f_{yh} + 1.026 A_{sv}\sqrt{f_m f_{yv}} \qquad \text{Eq. 2.22}$$

Where, f_t is the tensile strength of the masonry, f_m is the compressive strength of the mortar, b is the shear stress distribution factor and Φ is the horizontal reinforcement capacity reduction factor, A_{sv} and A_{sh} are the area of vertical and horizontal reinforcements respectively, f_{yv} and f_{yh} are the yield strength of vertical and horizontal reinforcements respectively.

For the contribution of the masonry to shear resistance Tomaževič (1999) used the equation proposed by Turnšek and Čačovič (1971) assuming that the diagonal shear cracking develops when the maximum principal, corresponding to the combination of the vertical and horizontal loads, attains the tensile strength of masonry, see Figure 2.15. Therefore, the shear strength of unreinforced masonry is calculated considering it as an elastic, homogeneous and isotropic material, to which the elementary theory of elasticity, is valid, see Eq. 2.23.

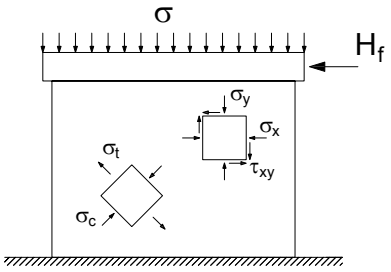

Figure 2.15 – Principal stresses in wall when subjected to a combination of vertical and lateral load.

$$\sigma_t = \frac{\sigma_x + \sigma_y}{2} + \sqrt{\left(\frac{\sigma_x - \sigma_y}{2}\right)^2 + \tau_{xy}^2} \rightarrow f_t = \frac{\sigma}{2} + \sqrt{\left(\frac{\sigma}{2}\right)^2 + (b\tau)^2} \qquad \text{Eq. 2.23}$$

$$\tau = \frac{f_t}{b}\sqrt{\frac{\sigma}{f_t} + 1}$$

According to Turnšek and Čačovič (1971) Eq. 2.22 is valid when the aspect ratio of the wall is larger than 1.5. This expression is also valid when aspect ratio is higher than 0.67, however in this case maximum eccentricity should be lower than *d/6*. In case of aspect ratios smaller than 0.67 the calculated value is larger than the actual one. Factor *b* is used to take into account the real parabolic stress distribution on rectangular sections in which the maximum shear stress is 50% higher than the average shear stress (*b* = 1.5), simply obtained by dividing the shear force by the area of cross section.

Similarly to Eurocode 6 (2005) the contribution of the horizontal is calculated based on its yielding force even if experimental results indicated that in the case of masonry walls with bed joint reinforcement the tensile capacity of horizontal steel cannot be fully used due to the bond failure between mortar and steel. Thus, a reduction factor *Φ* is considered to the shear strength resisted by horizontal reinforcements. According to Tomaževič (1999) this value depends on the characteristics of masonry units and mortar, as well as on the conditions of anchoring the reinforcement. Due to the lack of experimental data, it is suggested that horizontal reinforcement capacity reduction factor *Φ* is considered to be equal to 0.3. Besides, the contribution of the vertical reinforcements due to the dowel action is also taken into account in the shear strength.

Tomaževič (1999) still considers the possibility of masonry walls fail by sliding. According to the author, this type of failure occurs in walls with low compression forces, through horizontal cracking developing in wide extension of the wall. This failure mode can occur in the upper storeys of buildings, where vertical loading acting on the wall is low but horizontal loads from the seismic action are considerably high. In this case, Tomaževič (1999) also considers the influence of vertical reinforcement acting in bending, see Eq. 2.24. It is interesting to notice that the author does not consider the contribution of cohesion of masonry in sliding strength.

$$V_{sl} = \mu\sigma A_w + 1.026 A_{sv}\sqrt{f_m f_{yv}} \qquad \text{Eq. 2.24}$$

Where, μ is the friction coefficient of the unit-mortar interface and A_w is the area of wall.

2.4.1.4 Brunner and Shing (1996)

Based on the finite element method using a combined smeared and discrete crack model approach, Shing *et al.* (1993) investigated the shear resisting mechanisms of reinforced fully grouted masonry shear walls and through a parametric study, calibrated with

experimental results, proposed a novel equation for the calculation of the shear resistance. According to the authors, the shear behaviour of masonry walls is characterized by diagonal tensile cracking, followed by toe crushing and the shear resistance of the shear walls is the combination of three major resisting mechanisms, see Figure 2.16.

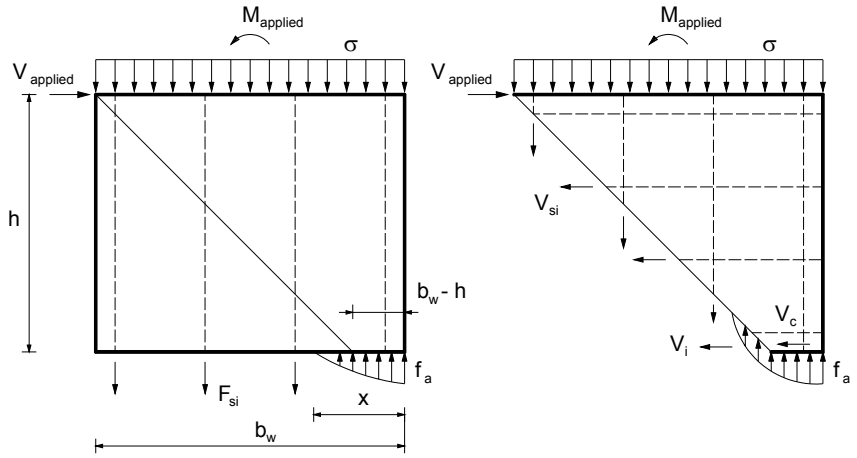

Figure 2.16 – Resistance mechanisms of Brunner and Shing´s model.

The first mechanism is the resistance developed at the compression toe of wall (V_c). This force is limited either by crushing of masonry due to the combination of compressive and shear stresses, or by sliding of the wall relatively to the foundation. As in case of Tomaževič's approach, this model considers the masonry wall as an elastic, homogeneous and isotropic structural material. The basic equation describing the resistance developed at the compression toe of the wall (V_c) can be derived by taking into account the assumptions of principal stresses of the elementary theory of elasticity, see Eq. 2.25.

$$\sigma_c = \frac{\sigma_x + \sigma_y}{2} - \sqrt{\left(\frac{\sigma_x - \sigma_y}{2}\right)^2 + \tau_{xy}^2} \rightarrow f_a = \frac{\sigma}{2} - \sqrt{\left(\frac{\sigma}{2}\right)^2 + \tau^2}$$

$$\tau = f_a \sqrt{1 - \frac{\sigma}{f_a}} \rightarrow V_c = C_1 f_a b_w t_w \sqrt{1 - \frac{C_2 \sigma}{f_a}} \qquad \text{Eq. 2.25}$$

Where, C_1 is a factor to accounts for the percentage of the total wall area effective in resisting shear at the compression toe and C_2 is a multiplier used to estimate the level of compressive stress at the compression toe.

The second shear resisting mechanism is related to the aggregate interlocking developed along the diagonal crack, to which forces V_i are associated, see Figure 2.16. From experimental results Shing *et al.* (1990a) observed that the shear resistance increased with

axial compression and vertical reinforcement ratio as these variables tend to avoid the opening of the diagonal cracking increasing the interlocking between both lips of the diagonal crack. The contribution of the aggregate interlocking resisting mechanism to shear resistance is defined through Eq. 2.26:

$$V_i = C_3\left(C_4 \rho_v f_{yv} + \sigma\right) b_w t_w \qquad \text{Eq. 2.26}$$

Where, C_3 is the coefficient of friction along the crack and C_4 accounts for the fact that not all of the vertical steel will have reached its tensile yield stress when the shear capacity is reached due to the different distance of the reinforcement to the neutral axis.

The third shear resisting mechanism is attributed to the horizontal reinforcement acting in tension across the diagonal crack contributing to the shear lateral strength with the force H_s. Shing *et al.* (1990a) considers that the diagonal crack occurs at 45º, as is shown in Figure 2.17, meaning that the contribution of the reinforcement to the shear lateral strength depends on the height to length ratio. In fact, in case of walls with the height much higher than the length there will be some bars that will not contribute to the shear strength. The contribution of the horizontal reinforcement to the lateral strength is given by Eq. 2.27.

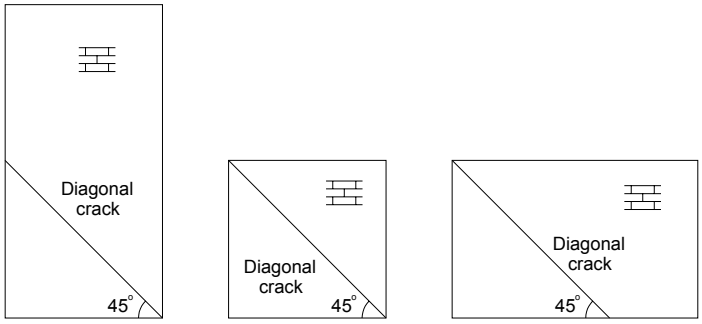

Figure 2.17 – Diagonal crack to distinct aspect ratios.

$$V_s = C_5 C_6 A_{sh} f_{yh}$$
$$C_6 = \left(\frac{b_w - 2 * d_1}{s} - 1\right) \qquad \text{Eq. 2.27}$$

Where, C_5 is a factor to account for that not all of the horizontal steel have reached its tensile yield stress when the shear capacity is reached, C_6 represents the number of effective horizontal reinforcements, s is the vertical spacing of the horizontal steel, A_{sh} is the area of the horizontal reinforcements and f_{yh} is the yielding strength of the steel. The coefficient C_6 enables to consider that only horizontal bars located in a height equal to the distance

between the vertical reinforcements near the edges of the wall are effective for the resisting mechanism.

Taking into account the contribution of the three main shear resisting mechanisms, the shear resistance of the reinforced masonry walls is obtained from Eq. 2.28.

$$V = V_c + V_i + V_s \qquad \text{Eq. 2.28}$$

The coefficients appearing in Eq. 2.25 to Eq. 2.27 were obtained through a parametric study based on a finite element model validated from experimental results (Shing *et al.*1993), see Table 2.2.

Table 2.2 – Values of the coefficients defining the contribution of each resisting shear mechanism Shing *et al.* (1993).

C1	C2	C3	C4	C5
0.040	4.500	0.250	0.667	0.750

Brunner and Shing (1996) presented a generalization of the methodology for the calculation of the shear strength of reinforced masonry walls for any aspect ratio and considering the interaction with the flexural design. Thus, the contribution regarding the shear resistance of the compressed toe, V_c, is calculated based on the stress-strain diagram obtained for masonry from experimental results carried out on specimens under uniaxial compression load, see Figure 2.18. It is assumed that a linear strain distribution along the section of the walls is valid and that the relation between strains and stresses in masonry is parabolic.

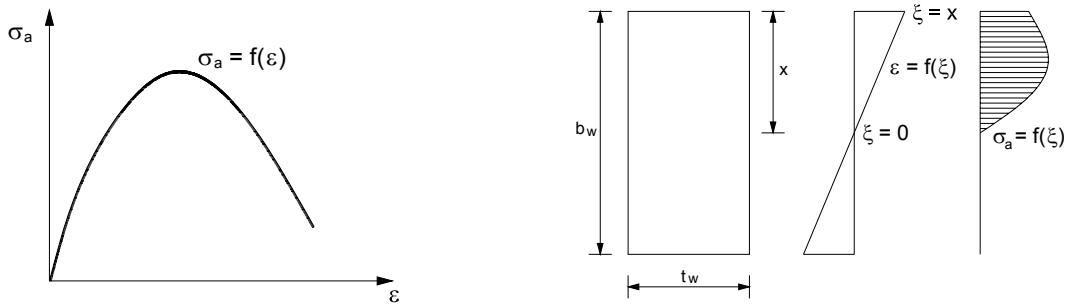

Figure 2.18 – Design details; (a) Compressive stress *vs.* strain diagram of masonry under compression load; (b) distribution of normal strains and stresses along the length of the wall under a bending moment.

The shear resistance at the compressed toe, V_c, is obtained by integrating the shear stresses along the effective area of the bottom toe, defined as the area under compression between the tip of the diagonal crack and the point corresponding to the maximum compressive stress and is given by Eq. 2.29.

$$V_c = t_w \int_{\xi 1}^{\xi 2} \tau(\xi) d\xi \rightarrow V_c = t_w \int_{\xi 1}^{\xi 2} f_a \sqrt{1 - \frac{\sigma_a(\xi)}{f_a}} d\xi \quad \text{Eq. 2.29}$$

$$\sigma_a = f(\varepsilon) \rightarrow \varepsilon = f(\xi) \quad \text{Eq. 2.30}$$

Where, f_a is the compressive strength of masonry, ξ is the local coordinate of the section with its origin at the neutral axis.

The integration bounds ξ_1 and ξ_2 are governed by the diagonal crack and the maximum masonry compressive strength see Figure 2.19. The bound ξ_1 corresponds to the point defined by the intersection of the diagonal crack and the compressed part of the wall and ξ_2 is the coordinate of the point corresponding to the compressive strength.

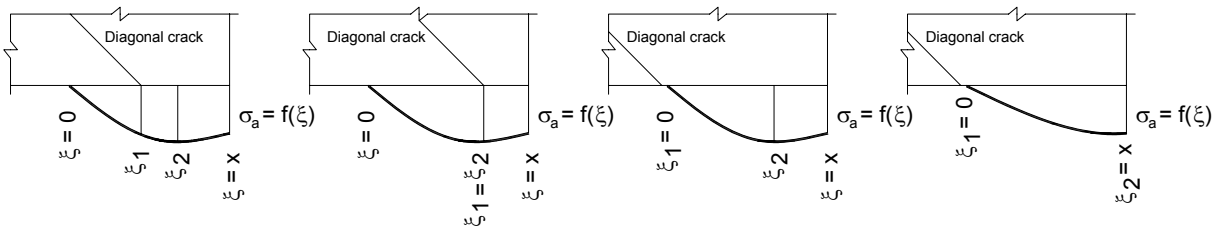

Figure 2.19 – Integration bounds of the compressive stress diagram of masonry at the toe of wall.

As aggregate interlock resistance (V_i) is derived from forces developed along the diagonal crack, the authors assume that it is derived from two sources: friction and cohesion. The friction force is equal to the vertical force acting on the crack, F_i, multiplied by the coefficient C_3. The cohesive force acts at the relatively intact area at the tip of the diagonal crack, c_0, multiplied by the area on which it acts, defined by the compressed area between the neutral axis and the tip of the diagonal crack, ξ_1. As the compression force (F_i) depends on the compressive stress in masonry, the influence of vertical reinforcement in shear strength is implicit in the calculus of this compressive stress.

Therefore, the contribution of the aggregate interlocking to the shear resistance is given by Eq. 2.31.

$$V_i = C_3 F_i + c_o t_w \xi_1 \quad \text{Eq. 2.31}$$

$$F_i = t_w * \int_0^{\xi 1} \sigma_a(\xi) d\xi \qquad \text{Eq. 2.32}$$

Where, c_o is the cohesion of masonry and the vertical compressive force.

In case of the contribution of the horizontal reinforcement to the shear strength no modifications are necessary to generalize the method.

Using the simple flexure theory and the equations proposed by Brunner and Shing (1996), the shear strength can be determined through an interactive procedure, see Figure 2.20. If the flexural strength governs the behaviour of the wall, the horizontal equilibrium never is satisfied since V is higher than $V_{applied}$. With this approach, the strength of a wall panel can be predicted in case of shear or flexure mode predominates.

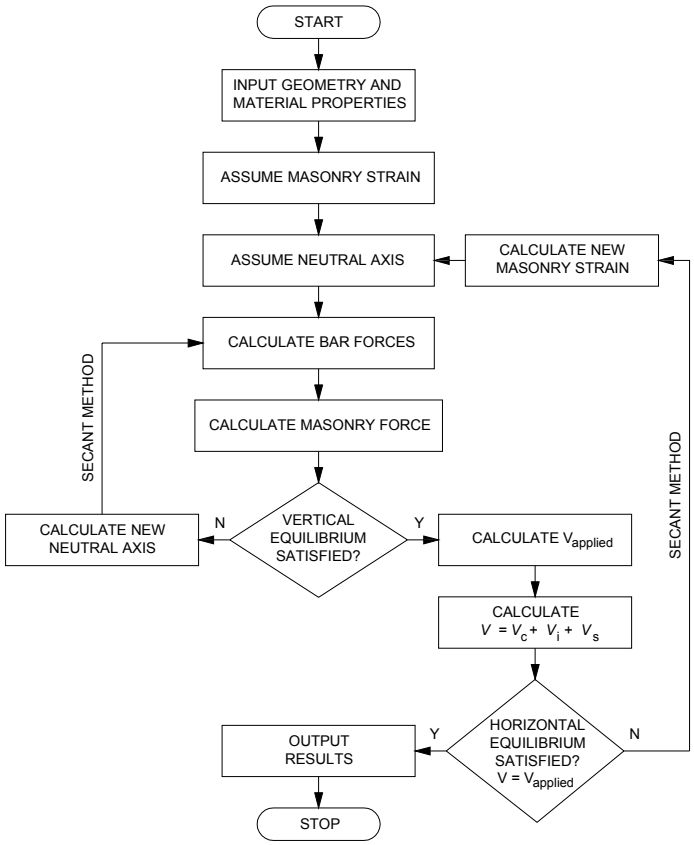

Figure 2.20 – Flow chart for determining shear strength (Brunner and Shing, 1996).

2.4.2 Masonry beams

2.4.2.1 Eurocode 6 (2005)

The flexural strength of masonry beams can be calculated following the approach pointed out in section 2.4.1.1 for shear walls. The unique adaptation concerns the

compressive behaviour of masonry as the compressive strength in the parallel direction to bed joints should be used. In case of shear design, Eurocode 6 (2005) determines that the shear strength of masonry beams is given by the resistance of masonry added by the yield strength of transversal reinforcements, see Eq. 2.33.

$$V_{R1} = f_v bd \quad \text{and} \quad V_{R2} = 0{,}9 A_{sh} f_{yh} \qquad \text{Eq. 2.33}$$

Where, f_v is the shear strength of interface unit-mortar and b is the width of the beam, d is the depth of the beam, A_{sh} is the area of horizontal reinforcement, f_{yh} is the yield strength of horizontal reinforcement.

The shear strength (V_{R1}) near the support should be increased by a factor (Eq. 2.34), due to the arch effect.

$$\frac{2d}{\alpha_x} \leq 4 \qquad \text{Eq. 2.34}$$

Where, α_x is the distance from the face of the support to the cross-section being considered.

The maximum shear resistance is still limited by the compressive strength of masonry according to Eq. 2.35:

$$V_{R1} + V_{R2} \leq 0{,}25 f_{a//} bd \qquad \text{Eq. 2.35}$$

Where, $f_{a//}$ is the compressive strength of masonry in parallel direction to bed joints.

2.4.2.2 MSJC (2002)

For MSJC (2002), the shear and flexural design of masonry beams follows the same rules of the design of shear walls. However, compressive strength of masonry parallel to bed joints should be considered.

2.4.2.3 Sorić (1994)

Sorić (1994) proposed an analytical model describing the shear stress distribution in the first mortar bed joint of the masonry beam, Figure 2.21. The model is able to determine

the ultimate load at shear failure. It considers a linear distribution for the compressive stresses along the height of the beams and neglects the tensile strength of masonry.

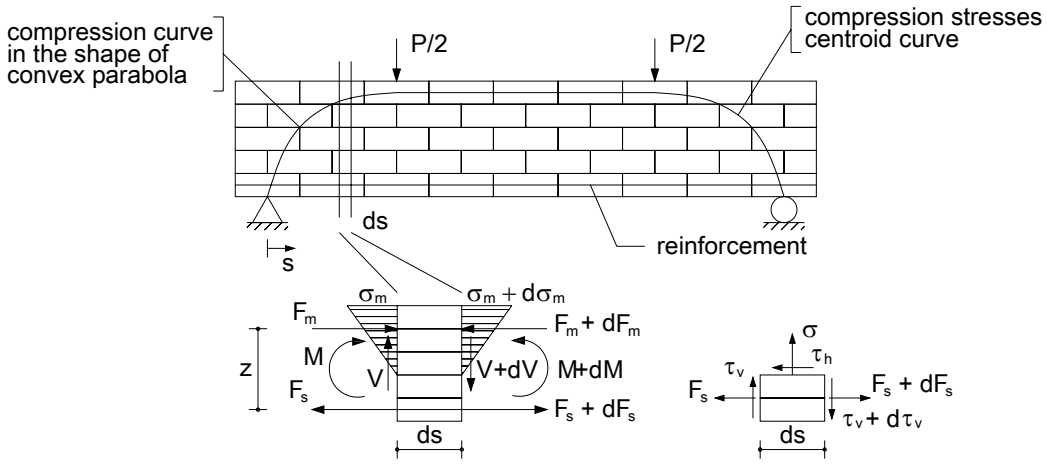

Figure 2.21 – Masonry beam and stresses caused by external load at free body diagram (Sorić, 1994).

Horizontal shear stresses at bed joints can be calculated through the equilibrium of horizontal forces on the cracked section of an infinitesimal length *ds* "cut out" from masonry beam, see Eq. 2.36. Based on the bending moment equilibrium equation, the tensile strength on the longitudinal reinforcement can be calculated by Eq. 2.37.

$$dF_s - \tau_h ds b = 0 \qquad \text{Eq. 2.36}$$

$$F_s = \frac{M}{z} \qquad \text{Eq. 2.37}$$

Where, *b* is the thickness of the cross section of the masonry beam and *z* is the lever arm of the longitudinal reinforcement.

By combining Eq. 2.36 and Eq. 2.37, the shear stresses along bed joints are calculated from Eq. 2.38.

$$\tau_h = \frac{1}{b}\frac{d\left(\frac{M}{z}\right)}{ds} \qquad \text{Eq. 2.38}$$

Bending moment *M* is easy to calculate for any type of loading, but the distance *z* between internal forces F_s and F_m, as a function of *s* is not quite simple to determine. Author

presents 5 curves *z* = f(*s*): concave parabola (Eq. 2.39), straight line (Eq. 2.40), convex parabola (Eq. 2.41), curve in form of square root function (Eq. 2.42) and ellipse (Eq. 2.43).

$$z = \frac{z_m}{a^2} s^2 \quad \text{Eq. 2.39}$$

$$z = \frac{z_m}{a} s\left(2 - \frac{s}{a}\right) \quad \text{Eq. 2.40}$$

$$z = \frac{z_m}{a} s \quad \text{Eq. 2.41}$$

$$z = z_m \sqrt{\frac{s}{a}} \quad \text{Eq. 2.42}$$

$$z = z_m \sqrt{1 - \left(1 - \frac{s}{a}\right)^2} \quad \text{Eq. 2.43}$$

Where, z_m is the distance between internal forces in middle span of beam and *a* is the distance between support and first external load P/2.

In case of a simply supported beam, in beam's portion between support and external force, bending moment follows Eq. 2.44. Inserting Eq. 2.43 and Eq. 2.44 in Eq. 2.38 a function which describes the shear stresses distribution along mortar bed joint is obtained, see Eq. 2.45.

$$M = \frac{P}{2} s \quad \text{Eq. 2.44}$$

$$\tau_h = \frac{a^2 P}{2 b z_m (2a - s)\sqrt{s(2a - s)}} \quad \text{Eq. 2.45}$$

Coulmob's function is a failure criterion which relates shear and normal stresses by Eq. 2.46.

$$\tau_u = c - \sigma\mu \quad \text{Eq. 2.46}$$

Where, τ_u is the failure shear strength, c is the cohesion and μ is friction coefficient

Normal stress in a bed joint can be calculated from equilibrium of vertical forces, see Figure 2.21 and Eq. 2.47. From equilibrium of bending moments about mid point and neglecting product of small values as $ds d\tau_v$ can obtain Eq. 2.48.

$$b\sigma ds + \left[\tau_v - \left(\tau_v + d\tau_v\right)\right]d_1 b = 0$$

$$\sigma = \frac{d\tau_v}{ds} d1 \qquad \text{Eq. 2.47}$$

$$\tau_h b d_s \frac{d_1}{2} - \tau_v b d_1 \frac{ds}{2} - \left(\tau_v + d\tau_v\right) b d_1 \frac{ds}{2} = 0$$

$$\tau_v = \frac{\tau_h}{2} \qquad \text{Eq. 2.48}$$

Where, τ_v is the vertical shear stress and d1 is the distance from the bottom of beam to the respective bed joint.

Inserting Eq. 2.48 in Eq. 2.47 and differentiating τ_h related to s obtain the value of normal stress, see Eq. 2.49. According to failure criteria τ_h defined by Eq. 2.45 should be smaller than τ_u value in order to prevent shear failure.

$$\sigma = \frac{Pd1}{4bz_m}\left[\frac{a^2(2s-a)}{s(2a-s)^2\sqrt{s(2a-s)}} - \frac{1}{a}\right] - \frac{a^2 P}{2bz_m(2a-s)\sqrt{s(2a-s)}} \qquad \text{Eq. 2.49}$$

2.5 Finite element method

Numerical modelling based on Finite Element Method (FEM) provides a powerful tool to perform complex analysis of masonry structures and it can assist in practical design situations. FEM is very useful to study the static or dynamic behaviour of masonry structures in case of complex geometry. The major concern of numerical modelling is related to the material model to be adopted that represents the behaviour of masonry material with reasonable approach.

Masonry is a composite material composed of units, mortar and unit-mortar interfaces. The complexity of the masonry material is essentially due to the behaviour of the unit-mortar interface and it is commonly the weakest link in which the major nonlinear phenomena are concentrated, namely the propagation of cracking. This is the main reason by which masonry behaves as an anisotropic material with distinct directional properties, making the numerical simulation of masonry assemblages rather complex.

In recent decades, several studies have been carried out in the scope of structural mechanics aiming at providing theoretical and numerical tools for better understanding the complex behaviour of masonry structures. Two main approaches have been formulated for

the appropriate constitutive description of masonry material: macro-modelling and micro-modelling, see Figure 2.22.

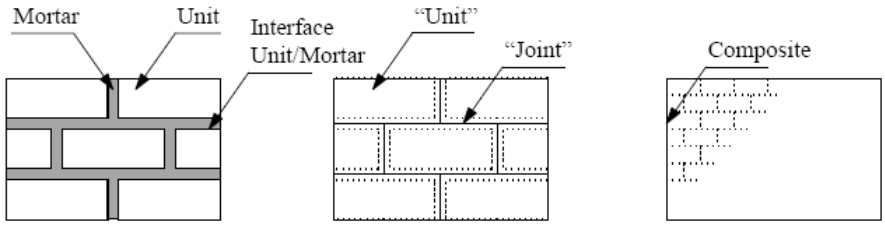

Figure 2.22 - Modelling strategies for masonry structures: (a) detailed micro-modelling; (b) simplified micro-modelling; (c) macro-modelling (Lourenço, 1996).

It is well known that both approaches provide satisfactory results. Macro-models are applicable when the dimensions of the analysed structure are sufficiently large so that the stresses across or along a macro length will be essentially uniform. Besides, the low computational cost supports its use on the analysis of large structures. On the other hand, micro-models are applicable in very specific problems where local failures should be analysed.

In the macro-modelling approach the masonry is considered as a continuum material, where the two-phase masonry is represented by the constitutive equations of an equivalent homogeneous medium whose characteristics have to be obtained through homogenisation techniques (Gambarota and Lagomarsino, 1997; Lourenço and Rots, 2000; Asteris and Tzamtzis, 2003; El-Dakhakhni *et al.*, 2006). One of the advantages of the macro-modelling approach is the possibility of building a continuous finite element mesh, which has considerable computational advantages when large wall panels are to be analyzed. Researches on macro-modelling of masonry seeking for improved techniques for material homogenization and for enhanced constitutive models that provides a satisfactory representation of the masonry behaviour.

The major difficulty of modelling masonry is the uncertainty or absence of reliable mechanical material data. This is particularly important, when it is intended to represent the orthotropic behaviour of masonry through a homogenised solution. Very reduced experimental information is available in literature on the orthotropic masonry mechanical properties due to the complexity of conducting some tests.

In case of micro-modelling approach, the masonry material is considered as a discontinuous assembly of units connected by dry or mortar joints and taking into account appropriate constitutive laws. There are two types of micro-modelling: detailed and simplified. In detailed micro-modelling, continuum elements are adopted to represent units and mortar

and the unit-mortar interfaces are described by interface elements. In case of simplified micro-modelling, units are represented by continuum elements while mortar joints and unit/mortar interface are lumped in discontinuous elements.

The great advantage of micro-modelling is the ability for the detection of all possible failure modes of masonry. As observed by Lourenço (1996), an accurate micro-model for masonry has to include the basic failure mechanisms that characterize the material: (a) tensile cracking at the joints; (b) sliding along the bed and head joints for low values of normal stress; (c) cracking of the masonry units in direct tension; (d) diagonal tensile cracking of masonry for combined normal and shear stresses; and (e) splitting of units in tension as a result of mortar dilatancy at high values of normal compressive stress.

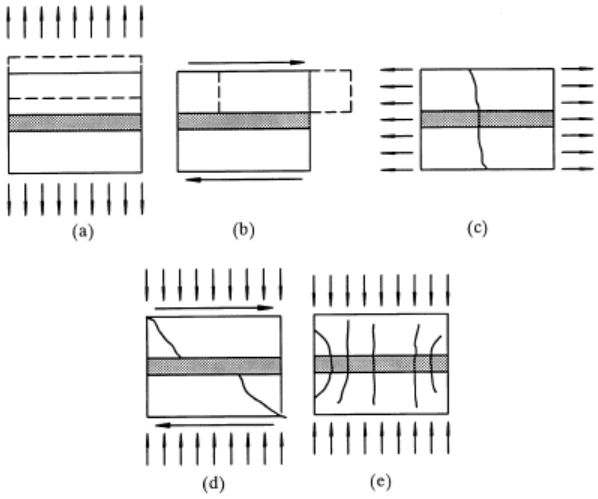

Figure 2.23 – Failure mechanisms of masonry: (a) tensile cracking at joints, (b) joint slipping, (c) tensile cracking of units (d) diagonal tensile cracking of masonry and (e) masonry crushing. (Lourenço, 1996).

Lourenço (1996) proposed an interface cap model with modern plasticity concepts, able to capture all masonry failure mechanisms. The model includes a tension cut-off model to capture Mode I failure, a Coulomb friction envelope to describe Mode II failure and a cap model for compressive failure, see Figure 2.24. This model concentrates all the damage in the relatively weak joints and, if necessary, in potential pure tensile cracks in the units placed vertically at the middle of each unit. According to the authors, the model is able to reproduce the complete failure patterns until total degradation without numerical difficulties.

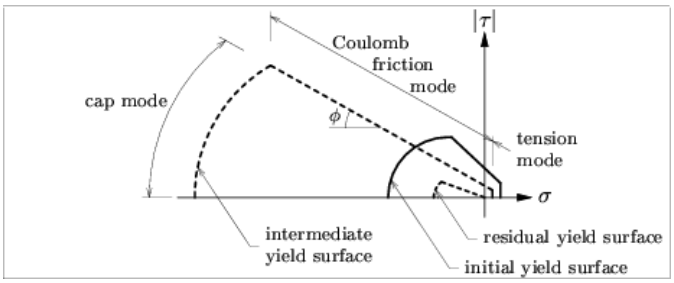

Figure 2.24 – Proposed interface cap model (Lourenço and Rots, 1997).

Another micro-modelling approach has been proposed by Sutcliffe *et al.* (2001), which considers that from a macroscopic point of view, masonry exhibits similar behaviour of rock joints or reinforced earth. Therefore, the authors proposed a model based on the lower bound theorem of classical plasticity. Authors consider a simplified micro-model where the units are assumed to be isotropic, homogeneous and obey to the Mohr-Coulomb failure condition, whereas joints are represented by a simplified interface cap model proposed by Lourenço (1996), as shown in Figure 2.25. In the context of linear programming and lower bound limit analysis, a linear approximation to the spherical cap model proposed by Lourenço (1996) is considered. A linear tension cut-off is considered as according to the authors it seems to be more realistic, given that the tensile failure the joint should be associated to zero shear strength. Authors presented numerical examples that suggest the proposed numerical procedure can be used successfully for limit analysis of unreinforced masonry structures for in-plane behaviour.

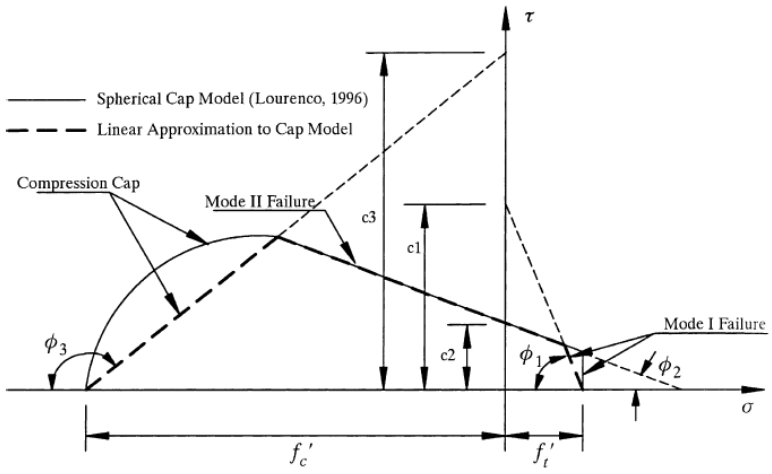

Figure 2.25 – Simplified interface cap model (Sutcliffe *et al.*, 2001).

A linear compression cap model, similar to Sutcliffe *et al.* (2001), was proposed by Chaimoon and Attard (2007), which defined a criterion to obtain the intersection point between the Mohr-Coulomb yield surface and the compression cap. The angle γ

(supplementary angle of ϕ_3 in Sutcliffe's model) between the normal stress axis and the compression cap is given by Eq. 2.50.

$$\gamma = \frac{\pi}{4} - \frac{\phi}{2} \qquad \text{Eq. 2.50}$$

Where, ϕ is the mortar friction angle.

The consideration of a linear compression cap model adopted by Sutcliffe *et al.* (2001) and Chaimoon and Attard (2007) seems to be an interesting simplification that can be applied in complex analysis of masonry structures.

In spite of the complexity of the models presented previously any detailed analysis on the possible shear phenomenon of dilatancy has been pointed out. Pluijm (1999) observed an increasing of volume on specimens submitted to shear tests, following the inelastic shearing deformations. The increasing of volume is prevented by confining structural elements which leads to pressure build up. In the case of pressure-dependent strength, which is a well known characteristic of the dilatational materials, a significant strength increase may result from such confined boundary conditions. Thus, Van Zijl (2004) proposed an enhancement for the micro-model proposed by Lourenço (1996) by incorporating a variable dilatancy coefficient to reproduce experimental measurements of brick normal uplift during shearing along a brick-mortar interface, see Figure 2.26. The author defined the dilatancy angle according to Eq. 2.51.

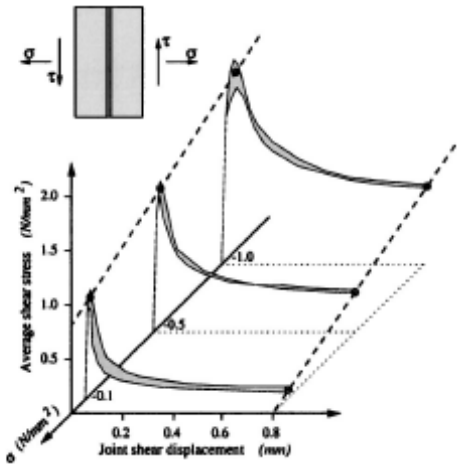

Figure 2.26 – Shear test for characterizing masonry joint behaviour. (Van Zijl., 2004).

$$\psi = \psi_o \left(1 - \frac{\sigma}{\sigma_u}\right) e^{-\delta v_p} \qquad \text{Eq. 2.51}$$

Where, ψ_o is the dilatancy at zero normal confining stress and shear-slip, σ_u is confining compressive stress at which the dilatancy becomes zero, δ is the dilatancy shear-slip degradation coefficient and v_p is the shear-slip.

According to the author, inappropriate modelling of shear dilatancy with the discrete approach can lead to large errors, see Figure 2.27. A dilatancy coefficient of zero reproduces the unconfined shear response, which represents the lower limit of the confined shear resistance, being in general conservative.

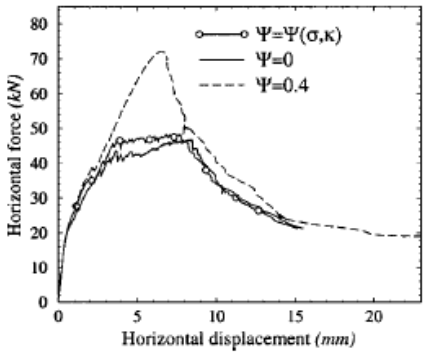

Figure 2.27 – Sensitivity analysis of the influence of dilatancy on the shear force-drift response (Van Zijl, 2004).

Observing the researches about micro-modelling, it is easy to conclude that it enables the best insight into the behaviour of masonry structures if a detailed analysis is required. It enables that distinct failure modes can be captured, giving a better understanding of the several interactions that can occur at a local level (Chaimoon and Attard, 2007). However, according to Gambarotta and Lagomarsino (1997), it is extremely burdensome from a computational point of view and the calibration of the model parameters from experimental data is not straightforward.

2.6 Summary and conclusions

In this chapter a brief literature review was presented about the behaviour of masonry structures under lateral loading. The main resistant elements of a masonry building subjected to horizontal forces, shear walls and beams, are presented and their behaviours are described according to studies carried out by other researchers.

The behaviour of shear walls under flexure is well defined and can be accurately evaluated through the simple flexure theory based on the plane-section assumption. On the other hand, the behaviour of these elements under shear is very complex and it is influenced by several variables such as axial force, reinforcement ratios, aspect ratio and masonry bond pattern. Failure modes of shear walls can be preponderantly by flexure characterized by horizontal cracks on the base of wall generated by tensile stresses due to the uplift, or preponderantly by shear characterized by diagonal cracking. The use of reinforcements in shear walls improve their behaviour as flexure as shear providing a better ductility and energy dissipation. There are several works related to shear walls, however the complex behaviour of these elements added to the influence of a large amount of variables generate divergent conclusions of the researchers which become this subject extremely open to new works.

In case of beams, there is little information in literature about their mechanical behaviour. It is admitted that masonry beams simply supported with span to depth ratio higher than 5 can be accurately evaluated through the simple flexure theory based on the plane-section assumption. And, masonry beams simply supported with span to depth ratio lower than 2 should be analysed through strut and tie models for deep beams. However, there is lack of information about the behaviour of beams with span to depth ratio in the range between 2 and 5.

The different approaches used to simulate masonry structures through numerical modelling based on finite element method were presented. Macro- and micro modelling can be used to analyse masonry elements. In first case, the analysed element is represented by continuum elements with material properties that try to represent the material composite. On the other hand, micro-modelling considers units connecting by the vertical and horizontal joints which allow observing localized failures in masonry. However, the use of numerical modelling in practical design situations can be too costly.

Finally, this chapter provided information about masonry structures subjected to lateral loading in order to introduce this thesis and insert it in the context of previous researches.

3 EXPERIMENTAL PROGRAM I: CHARACTERIZATION OF MATERIALS

3.1 Introduction

Even as timber structures, masonry is the most antique construction material. It is present not only in most impressive historical constructions but also in custom architecture. Masonry is a composite material composed of units connected by mortar layers. Masonry behaves reasonably well under compressive loads however; its tensile strength is much reduced, leading to early cracking due to shear and tensile stresses. This is the main reason by which unreinforced masonry is not allowed in high seismic zones when new construction is needed. However, if reinforced masonry is used, a very good mechanical performance can be achieved (Manos *et al.*, 2001; Schultz *et al.*, 1998) and it can effectively be used as a reliable construction material. Even in low seismicity zones, unreinforced masonry appears to be a possible structural solution. This means that it is important to enhance the knowledge on the behaviour of unreinforced and reinforced masonry in order to contribute for achievement of reliable design methods that assist engineers on the professional design and stimulate its use by contractors.

As aforementioned, this thesis aims at obtaining a better insight on the in-plane behaviour of key structural masonry elements of masonry buildings, namely masonry walls and beams. Masonry walls play a central role on the stability of masonry buildings subjected to vertical and horizontal loadings and masonry beams above or below openings connect the masonry piers resulting in much more stiffness to the global structure.

The understanding of experimental results carried out on the masonry structural elements, the numerical simulation and the analytical modelling are key tasks for the improvement on the knowledge about the in-plane masonry behaviour. An accurate

experimental, numerical and analytical analysis is only possible if detailed information on the mechanical properties of masonry materials and masonry as a composite is known.

This chapter represents the first phase of an enlarged experimental program on the characterization of masonry. It refers the characterization of masonry materials under tension and compression such as units and mortar, the shear behaviour of unit-mortar assemblages to shear loading and mechanical characterization of masonry as a composite under tensile, flexural and compressive loading. Besides, mechanical characterization of reinforcements applied in reinforced masonry elements is presented.

3.2 Units

Given the traditional use of concrete blocks for non-loadbearing walls such enclosure and partition walls in Portugal, it was decided to develop two new structural concrete masonry blocks in order to make the use of distinct masonry bond patterns possible and also to enable the introduction of horizontal and vertical reinforcements. Two (2C-units) and three cell (3C-units) concrete blocks were designed according to the shape and geometry indicated in Figure 3.1. The concrete units were produced in reduced scale (1:2) in order to comply with technical limitations at the structural laboratory of University of Minho to perform real scale tests on masonry walls. The idea of using frogged ends in 3C-units is the placement of vertical reinforcements in a continuous vertical joint in order to simplify the construction technology. The 2C-units has a geometry very similar to non structural concrete blocks existing in the Portuguese market and are a real possibility for the traditional masonry bond.

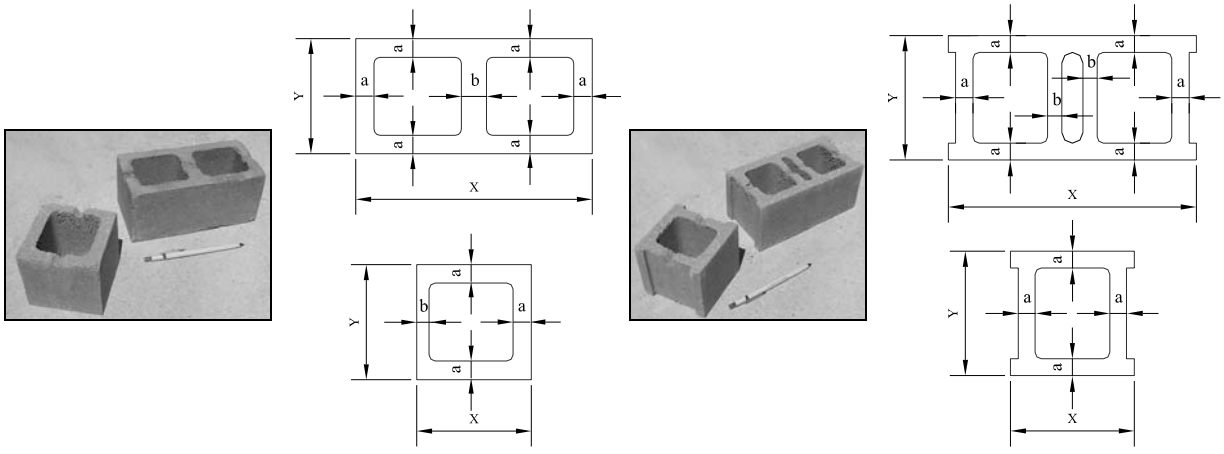

(a) (b)

Figure 3.1 – Concrete masonry units: (a) two cells and (b) three cells.

Physical properties such as dimensions and dimensional variability, percentage of vertical perforation and water absorption due to capillarity action were obtained to the concrete units according to EN 772-16 (2000), EN 772-2 (1998) and EN 772-11 (2000) respectively, see Table 2.1. In all tests 6 concrete units were used.

In Eurocode 6 (2005), units are classified in four groups according to geometrical requirements such as percentage of voids and thickness of webs and shells. According to the classification proposed in Eurocode 6 (2005) both units belong to group 2.

Table 3.1 – Physical properties of units.

	X (mm)	Y (mm)	Z (mm)	a (mm)	b (mm)	Net area of blocks (cm^2)	Area of voids (cm^2)	Percentage of voids (%)	Coefficient of water absorption ($g/(mm^2s^{0,5})$)
Block (2C-units)	196	94	94	16	21	97.96	87.45	47	171.83
Half block (2C-units)	96	94	94	17	12	47.81	41.81	47	246.72
Block (3C-units)	201	100	93	16	14	110.14	93.92	46	228.29
Half Block (3C-units)	101	100	93	16	-	57.20	46.10	45	226.67

EN 772-11 (2000) specified the coefficient of water absorption due to capillarity after the immersion time of 10 minutes. In the tests the measurements were carried out in intermediate steps to evaluate the behaviour of absorption with time, see Figure 3.2 and Figure 3.3. Results indicated that the absorption is very high at the beginning of test and exhibited a progressive reduction with time reaching a stable value close to 10 minutes.

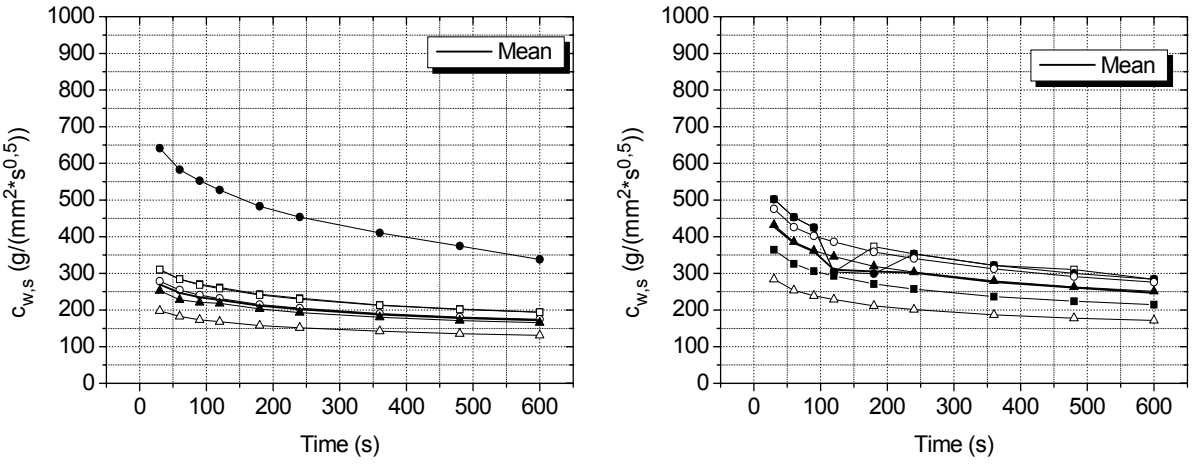

Figure 3.2 – Water absorption of the units: (a) blocks and (b) half blocks (2C-units)

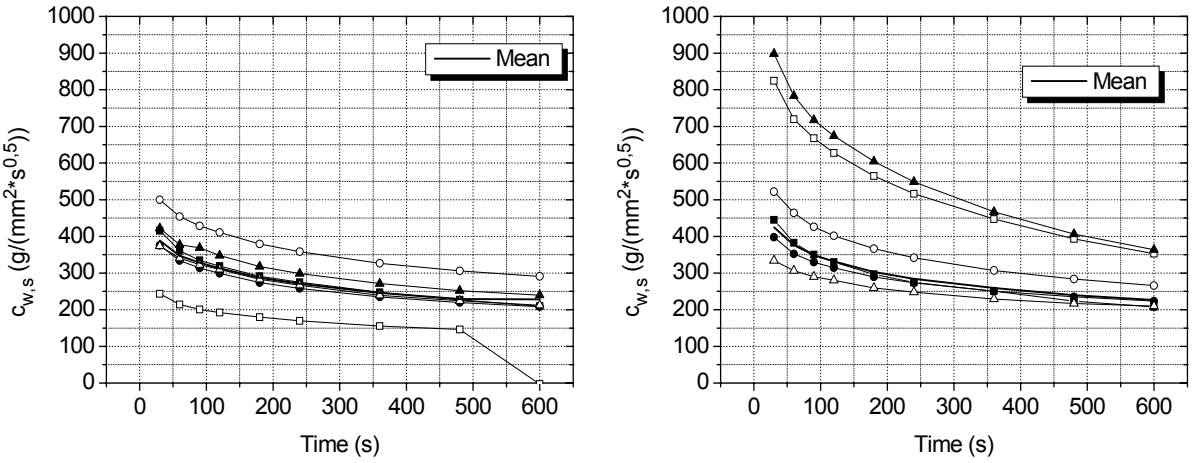

Figure 3.3 – Water absorption of units: (a) blocks and (b) ½ blocks (3C-units).

The 3C-units exhibited a coefficient of water absorption very similar comparing blocks and half bocks. In case of 2C-units half blocks presented a coefficient of water absorption higher than blocks. This higher value may be the result of a thinner shell in the half blocks. Because the small width, the half block is more sensitive to damages during the production process, mainly at the stage of removing the mould, see Figure 3.4. These regions of small damages have a higher amount of voids and consequently increase the coefficient of water absorption. 2C-units had low coefficient of water absorption when compared to 3C-units possibly to the thicker central web influencing the effect of capillarity.

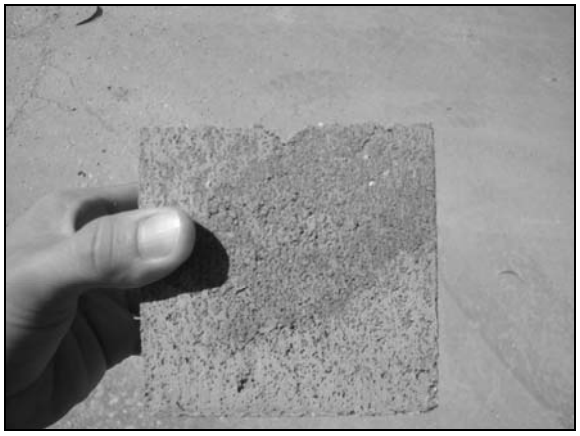

Figure 3.4 – Damages in half blocks of 2C-units.

Mechanical properties of units are fundamental to the design of masonry walls and beams as well as to carry out numerical analysis. The mechanical properties of concrete units include the tensile strength, f_{bt}, and compressive strength in the direction perpendicular, $f_{b\perp}$, and parallel, $f_{b//}$, to the bed joints. The tensile strength of units was measured following the test setup used by Vasconcelos (2005) and Mohamad (2007). The tests were performed

in specimens cut from the shells of units, see Figure 3.5. According to Vasconcelos (2005), the adoption of a constant cross section for the specimens leads to uncertainty about the localization of the microcraks, which represents the usual supplementary difficulty for the control method of this type of tests. Thus, it was decided to introduce two lateral notches with a depth of 6mm at mid height of the specimen in order to localize the fracture surface. Twelve specimens of each type of unit were prepared.

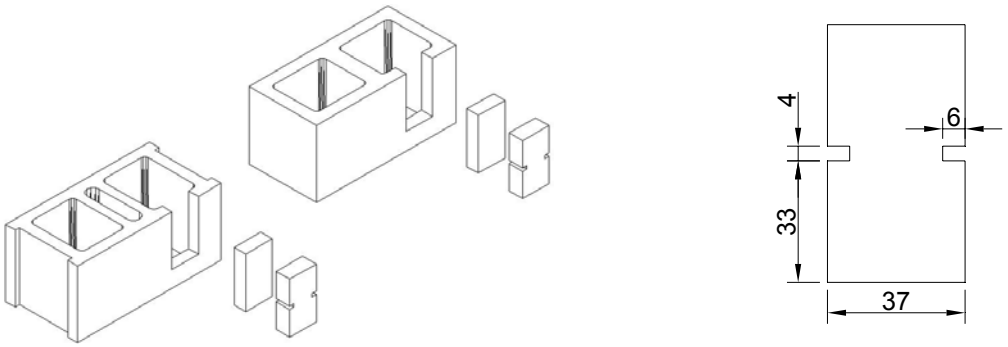

Figure 3.5 – Specimens used in direct tensile tests of units.

The direct tensile were performed by using a CS7400S servo-controlled universal testing machine with fixed end plates. This equipment has a load cell connected to the vertical actuator with a maximum capacity of 22 kN, being particularly suitable to small specimens. Specimens were glued to the steel plates of the equipment and two LVDTs were used to measure the crack opening.

There were practically no differences in the results of the 2C-units and 3C-units, which was expected since the both blocks were produced at same time, with the same concrete and were cured at the same environmental conditions. In most specimens the crack appeared in notched section, see Figure 3.6a. However, in few specimens the crack appeared in region with higher cross section close to the fixed end, see Figure 3.6b. This behaviour can be explained by the fact that the localization of the smaller cross section zone may be not compatible with the weakest zone of the material (Wittman. *et al.*, 1994).

It was very difficult to avoid the rotation of the specimens because their small size. This fact generated distinct behaviour between the LVDTs. Besides, in spite of the low velocity used in load application (0.08 μm/s) it was not possible to obtain the post-peak behaviour of the specimen. Only in three of the twenty four tested specimens it was possible to obtain the post-peak behaviour, see Figure 3.7.

(a) (b)

Figure 3.6 – Fracture of the specimens in direct tensile test: (a) common fracture and (b) fracture in zone with higher cross section.

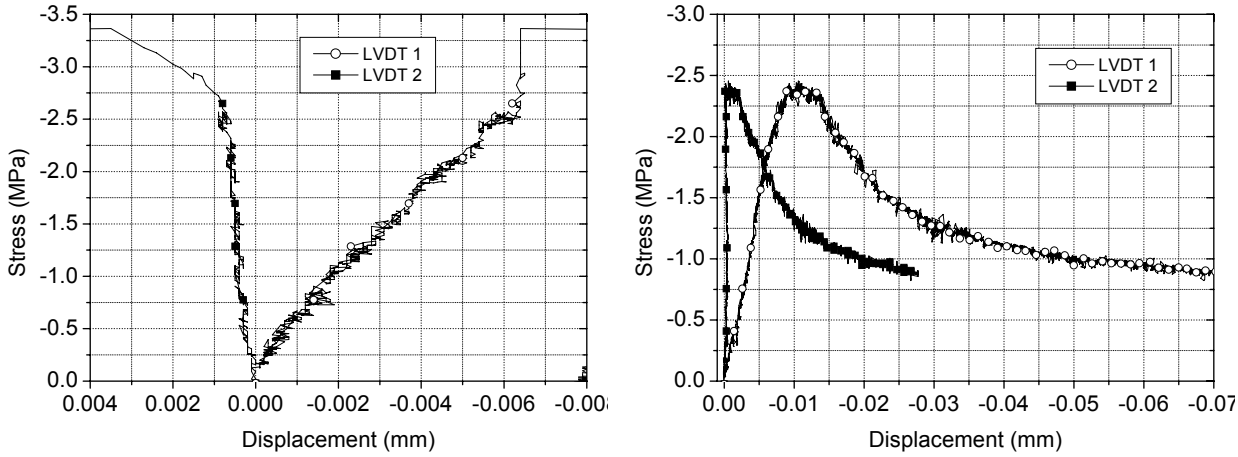

(a) (b)

Figure 3.7 – Stress-displacement diagrams (σ *vs.* δ) of the specimens in tensile tests: (a) common behaviour and (b) specimen with post-peak.

According to Eurocode 8 (2003), units used to build masonry structures in seismic areas should have a normalized compressive strength normal to bed joints not lower than 5 MPa and a normalized compressive strength parallel to bed joints not lower than 2 MPa. Uniaxial compressive tests in the direction perpendicular to bed joint direction were carried out according to EN 772-1 (2000). Twelve concrete blocks and half blocks of 3C-units and 2C-units were considered. Specimens were tested between two plates of steel with 50 mm of thickness to ensure a homogeneous distribution of vertical stresses and avoid flexural effects of the steel plate. Horizontal and vertical deformations of the specimens were measured using 4 and 2 LVDTs respectively, to evaluate elastic modulus and Poisson's ratio of the units, see Figure 3.8. Tests were carried out under displacement control by means of a vertical LVDT connected to the actuator at a rate of 5 μm/s.

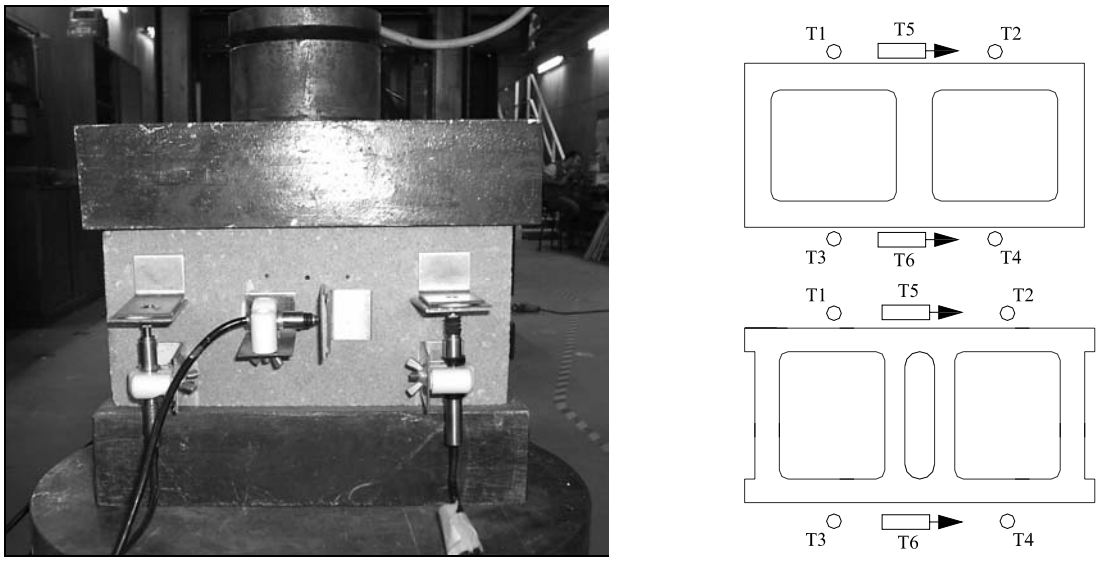

(a)

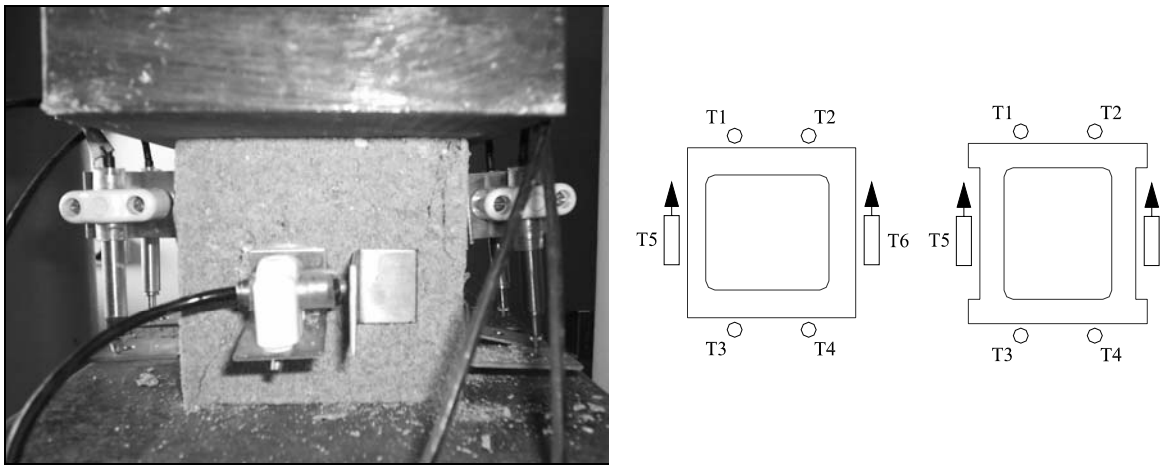

(b)

Figure 3.8 – Test setup of the compressive tests normal to bed joints: (a) blocks and (b) half blocks.

Failure mode of all tested units, both in 3C-units and 2C-units was pyramidal-trunk, see Figure 3.9. In blocks and half blocks, the first cracks appeared vertically in corners of the units, see Figure 3.10. In case of 3C-units, some specimens were completely burst. As observed by Page and Kleeman (1991), this behaviour can be explained by the lateral restrictions caused by the steel plates at top and bottom of the specimen leading to friction forces. With the increase of the loading, in most cases the vertical cracks were connected by a horizontal crack in superior region of the unit as shown in Figure 3.11. This horizontal crack occurs because the superior part of the units slides over the pyramidal-trunk surface of rupture. In some specimens near to the collapse a vertical crack also appeared in central region of the unit. This failure mode is very similar to that pointed out by Mohamad (2007).

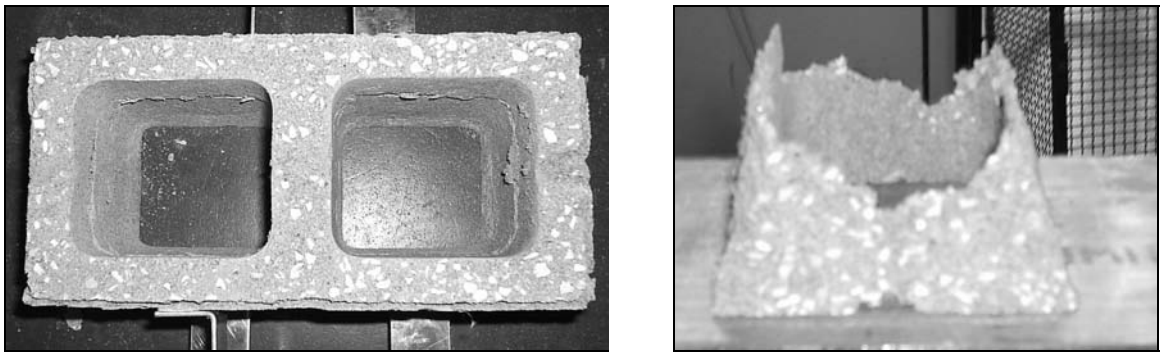

Figure 3.9 – Pyramidal-trunk failure mode of the units.

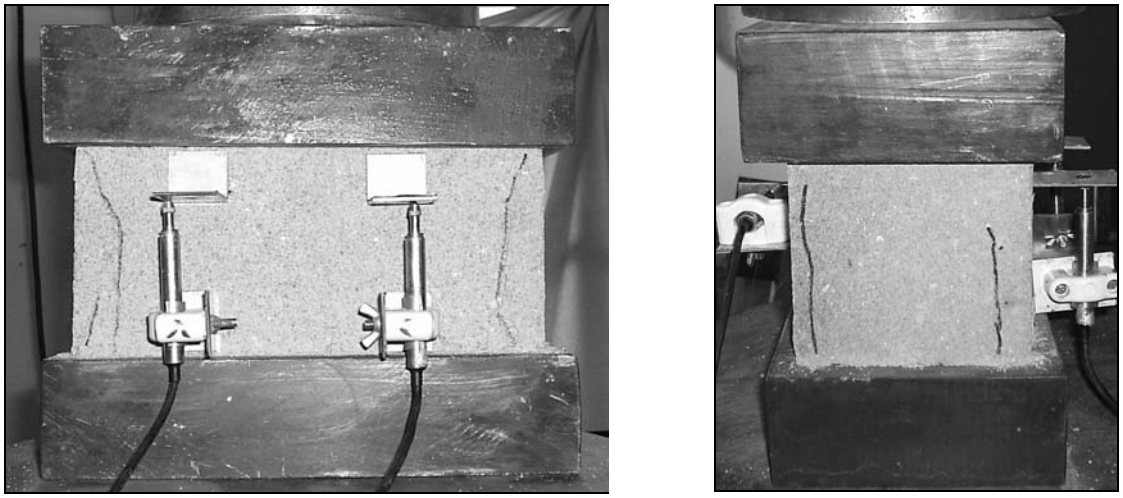

Figure 3.10 – Vertical cracks in corners of units.

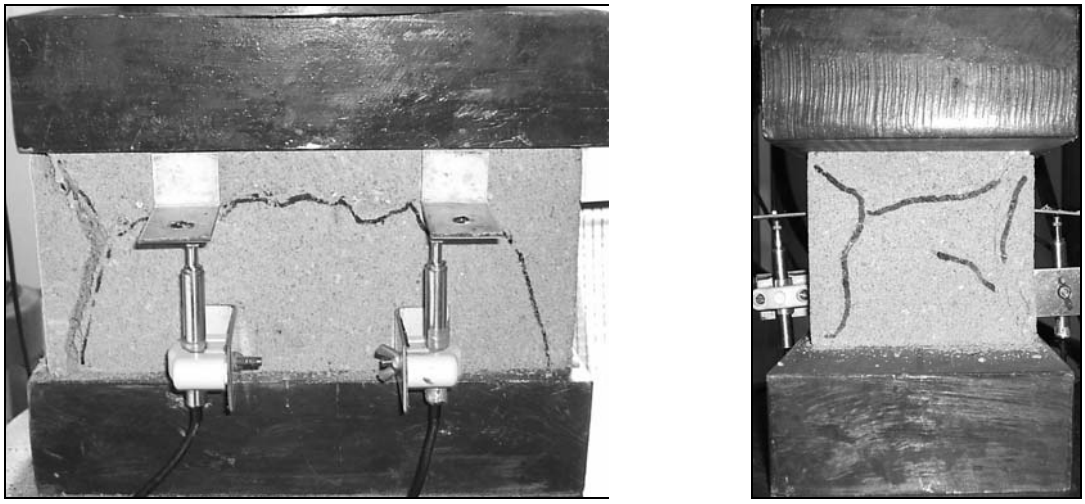

Figure 3.11 – Horizontal cracks connecting vertical cracks.

It was not possible to obtain the entire stress-strain diagram due to some complications. The small size of the specimen difficult the evaluation of the deformations. Even using LVDTs with a precision of 0.50 mm, it was not possible to record accurate horizontal deformations to obtain accurate Poisson's ratios. In addition, the fragile behaviour

of the units avoided the attainment of the post-peak behaviour of the units. The elastic modulus was calculated through a linear regression of the data up to 50% of the maximum load.

Units were also tested under compression in the direction parallel to bed joint. This test was carried out given that in case of the masonry beams, the compressive stresses in masonry develop in the parallel direction to the bed joints. Compressive tests in the parallel direction to bed joints were carried out in 6 specimens of blocks and half blocks of 3C-units and 2C-units. Specimens were tested in same conditions of those tested under compression normal to bed joints. Vertical deformations of the specimens were measured using 2 LVDTs to evaluate elastic modulus, see Figure 3.12. Tests were carried out under displacement control by means of a vertical LVDT connected to the actuator at a rate of 5 μm/s. Two steel plates supported by transversal cables were used to insure the safety in test because the fragile behaviour of the units.

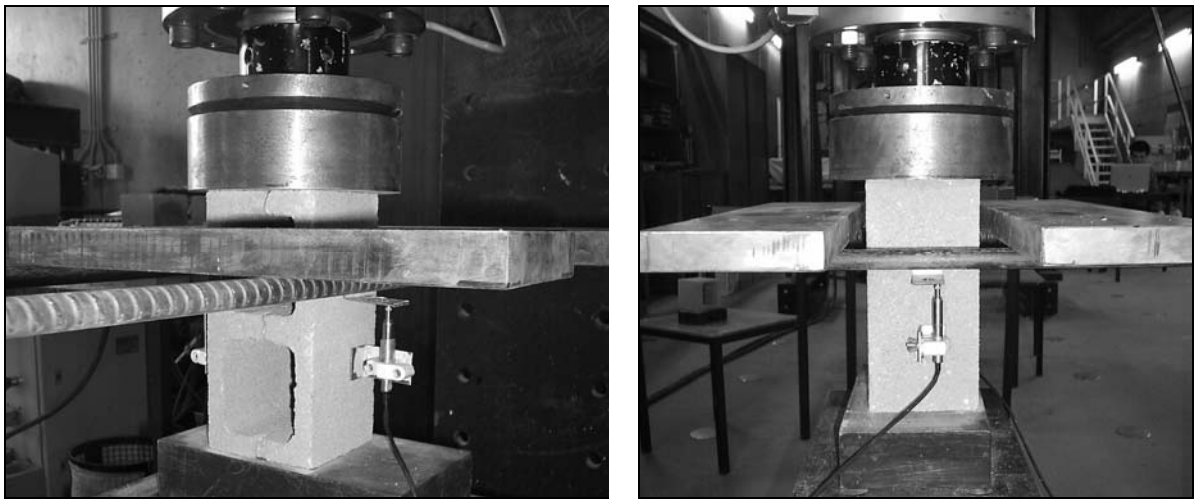

Figure 3.12 – Test setup of the compressive tests in direction parallel to bed joints.

2C-units and 3C-units presented distinct behaviours as the geometry of unit had significant influence. The behaviour of blocks of 2C-units can be divided in two phases. Firstly, unit exhibited compressive deformations due to the increasing of vertical loading. However, the distributed vertical load at the top and at the base of the unit created flexural efforts. The flexure in shells of unit was prevented by the presence of web, leading to tensile stresses in webs, see Figure 3.13. When tensile stresses in webs reached the tensile strength of the concrete, a crack appeared in this element. After this point, LVDTs began to register tensile strains in shells since there was no resistance of the web and flexure was predominant, see Figure 3.14.

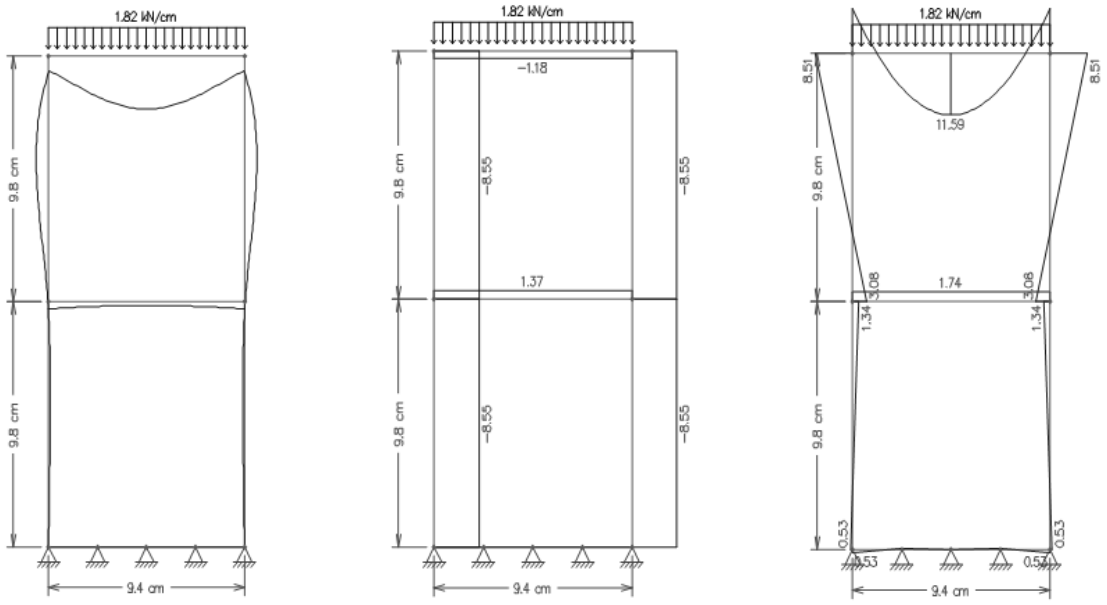

(a) (b) (c)

Figure 3.13 – Behaviour of blocks of 2C-units tested under compression parallel to bed joint before cracking of the web: (a) deformed state, (b) diagram of normal forces and (c) diagram of bending moments.

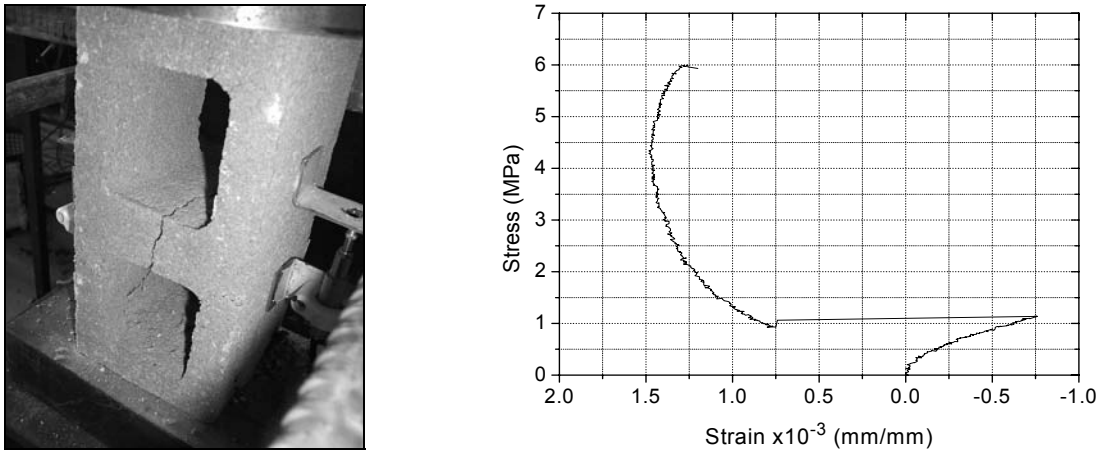

Figure 3.14 – Behaviour of 2C blocks under compression parallel to bed joints.

It is perfectly clear the onset of the cracking of the web, which is identified by the discontinuity on the stress *vs.* strain diagram. This test can be seen as an indirect tensile test of the units if the tensile strength of the units is the tensile strength of the web of the units. With the assumption, the tensile strength of the units can be calculated by using Eq. 3.1:

$$f_{bt//} = \frac{Nt_{web} + 6M}{h_b t_{web}^2} \qquad \text{Eq. 3.1}$$

Where, $f_{bt//}$ is the tensile strength of unit through the compressive test in the direction parallel to bed joints, h_b is the height of the unit, t_{web} is the thickness of the web and *N* and *M* are the normal force and bending moment acting in web respectively.

The value of $f_{bt//}$ measured in tested specimens was 3.21 MPa with a coefficient of variation equal to 35%. Tensile strength evaluated through the compressive test in the direction parallel to bed joints was only 2% higher than the value found in direct tensile test. Thus, the compressive test seems to be an alternative method of measuring the tensile strength of unit. It is easier to carry out and avoid problems like rotation of the specimen and debonding of the specimens to the plates.

Half blocks of 2C-units were also tested under compression in the direction parallel to bed joints. The failure of these units developed by flexure-compression of the shells, see Figure 3.15. As in case of the blocks, a concentration of stress occurs at the corners. The failure occurred from the increasing damage in the shells in which tensile stresses developed.

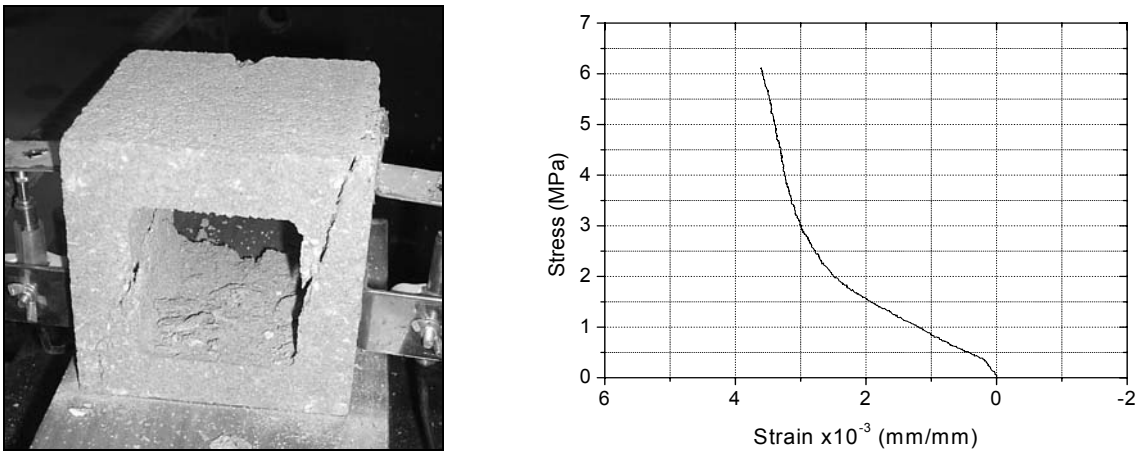

Figure 3.15 – Behaviour of half blocks of 2C-units tested under compression in direction parallel to bed joints.

In case of 3C-units, two samples were prepared to the test: units with capping and without capping. Firstly, the use of capping had the objective to avoid the rupture of the frogged ends of blocks due to the concentration of stresses. However, it was decided to test units without capping since the concentration of stresses in bands of units really happen in a masonry structure built with this unit. Both specimens had a similar failure mode, although specimens with capping reached lower forces probably because the flexure.

Blocks of 3C-units also showed cracks in the webs as in case of 2C-units, see Figure 3.16. However, these cracks appeared only at the end of test probably caused by the instability of the shells of the unit. Half blocks of 3C-units also developed compressive strains during whole test and reached a higher strength than 2C-units, see Figure 3.17. Specimens

of 3C-units without capping had no flexure in webs or shells since the vertical loading was applied directly on the transversal shells. Possible flexure caused by the slenderness of the shells was resisted by the webs, which improved the behaviour of the 3C blocks.

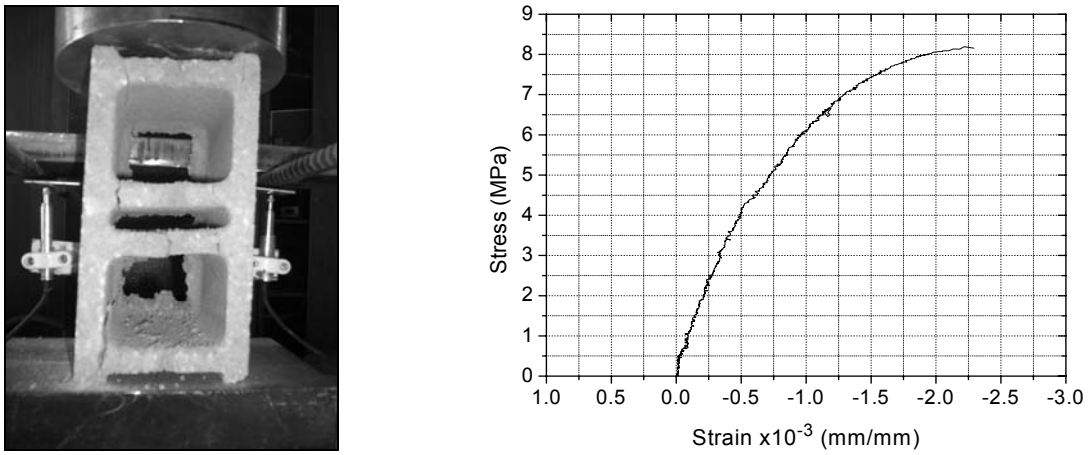

Figure 3.16 – Behaviour of 3C-units tested under compression in direction parallel to bed joint.

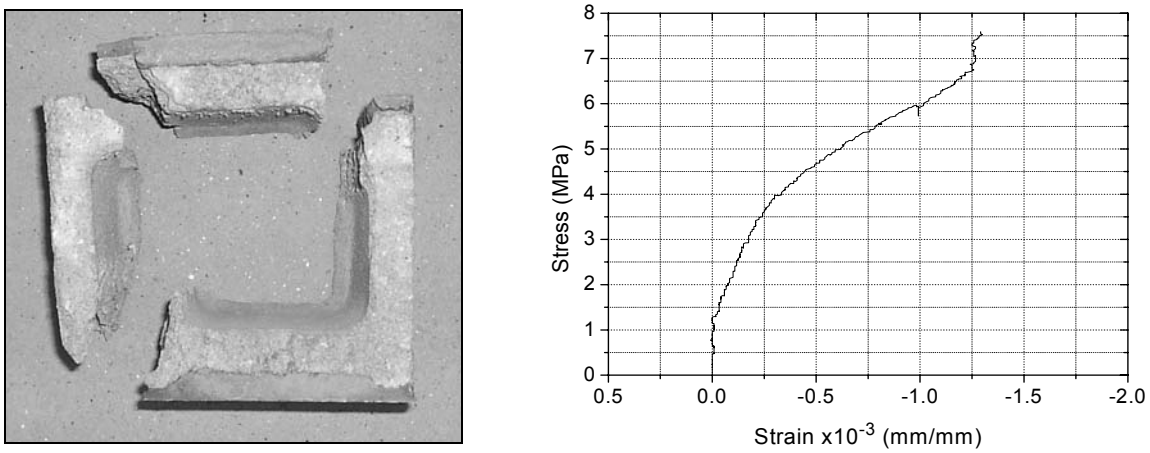

Figure 3.17 – Behaviour of ½ blocks of 3C-units tested under compression parallel in direction parallel to bed joint.

A summary of the results on the mechanical properties of concrete blocks under tension and compression is indicated in Table 2.2. All mechanical properties were calculated in relation to gross area of the specimens. In Table 2.2, f_{bt} is the tensile strength of the units, η is the coefficient of normalization of the compressive strength, $f_{bm\perp}$ is the mean compressive strength normal to bed joints, $f_{b\perp}$ is the normalized strength of the units normal to bed joints, $E_{bm\perp}$ is the average of elastic modulus of the units normal to bed joints, $f_{bm//}$ is the mean compressive strength of the units parallel to bed face and $f_{b//}$ is the normalized strength of the units parallel to bed face. According to EN 772-1 (2000) compressive strength

should be normalized by factor η to design application. This normalization considers the air-dry conditioning regime and the shape of the unit.

Table 3.2 – Mechanical properties of units.

	f_{bt} *(MPa)*	η	$f_{bm\perp}$ *(MPa)*	$f_{b\perp}$ *(MPa)*	$E_{bm\perp}$ **(GPa)**	$f_{bm//}$ *(MPa)*	$f_{b//}$ *(MPa)*
Block (2C-units)	3.13 (24%)	0.99	9.38 (19%)	9.29	8.80 (66%)	6.59 (10%)	6.52
Half block (2C-units)		0.99	9.27 (21%)	9.18	8.21 (40%)	6.39 (14%)	6.33
Block (3C-units)	3.19 (21%)	0.97	12.13 (22%)	11.77	9.57 (40%)	7.88 (5%)	7.64
Half Block (3C-units)		0.97	10.33 (19%)	10.02	9.44 (47%)	7.20 (14%)	6.98

3.3 Mortar

Mortar is one of the components of the anisotropic masonry material. It is responsible for the stress uniform distribution, correction in irregularities of blocks and accommodation of deformations associated to thermal expansions and shrinkage. In spite of mortar has been often neglected in terms of structural analysis of masonry structures, it is well known that it influences the final behavior of the masonry such as compressive and bond strengths, and deformability (Edgell and Haseltine, 2005). In this research, mortar was used simultaneously used to lay the concrete masonry blocks and also as infill material of the hollow cells of the concrete blocks, where vertical reinforcement is added, in substitution of the traditional grout. According to Biggs (2005), in some regions of the United States contractors commonly substitute grout by mortar in reinforced masonry construction. This preference is justified as the use of mortar reduces installation costs in low-lift applications when the masonry is to be total or partially grouted and reduce the number of materials. This means that the mortar has to present a consistence that enables the laying of the concrete units and fills appropriately the reinforced hollow cells.

Previous studies were carried out (Haach *et al.*; 2007) aiming at obtaining a mortar mix with an adequate consistence to use as embedding and infill material with a minimum compressive strength of 10 MPa. This value of compressive strength of mortar was chosen because it is recommended by Eurocode 8 (2003) in case of reinforced masonry structures in seismic areas. Thus, a general purpose mortar was adopted, being composed of cement and sand in the proportion of 1:3 (cement/sand) with water/cement ratio equal to 0.9. The cement used was CEM II/B-L 32.5N, according to EN 197-1 (2000). The sand had a fineness

modulus of 1.8 and a maximum diameter of 2.35mm, see Figure 3.18. Some physical properties of materials are indicated in Table 3.3.

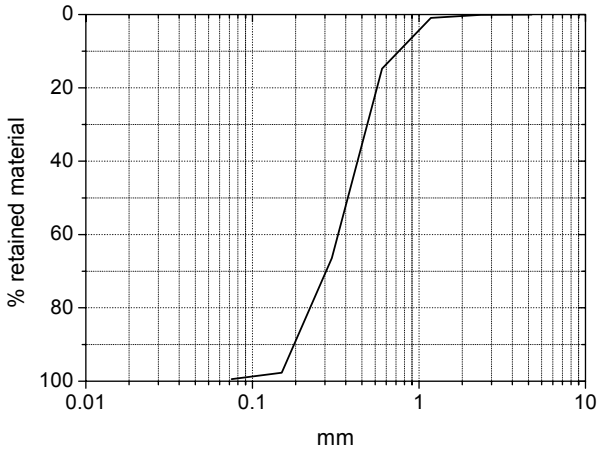

Figure 3.18 – Grading curve of sand.

Table 3.3 – Properties of materials used in mortar.

Property	*Cement*	*Sand*
Density (kg/m^3)	3210	2640
Unit mass (kg/m^3)	1080	1450

Workability of mortars plays an important role on the construction process of masonry structures. According to Sabbatini (1984), the workability may be considered one of the most important properties because it influences directly the bricklayer's work as it can facilitate or complicate the construction quality. It is important to stress that the quality of the workmanship can influence considerably the mechanical properties of masonry. The definition of workability is somewhat subjective as it depends on the person who evaluates the mortar. Panarese (1991) considers the workability as an assembly of several properties such as, consistence, plasticity and cohesion. Provided that plasticity and cohesion are properties of difficult determination, consistence is frequently used as the measure of the workability. Thus, fresh behaviour of applied mortar was evaluated by means of the value of consistence obtained through the flow table test according to EN 1015-3 (2002), see Figure 3.19.

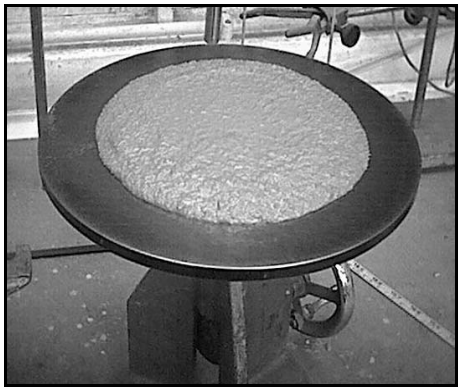

Figure 3.19 – Flow table test.

Mechanical behaviour of mortar was defined through compressive and flexural strength and elastic properties (elastic modulus and Poisson's ratio). Compressive and flexural tests were carried out on prismatic specimens 40mmx40mmx160mm according to EN 1015-11(1999), see Figure 3.20a. The elastic properties were obtained from compressive tests carried out on cylinders with 50mm of diameter and 100mm of height (height to diameter ratio of 2) according to NBR 13279 (1995). The elastic modulus and Poisson's ratio were calculated by averaging the measurements of strain-gauges attached to the specimen placed in the vertical and horizontal directions, see Figure 3.20b.

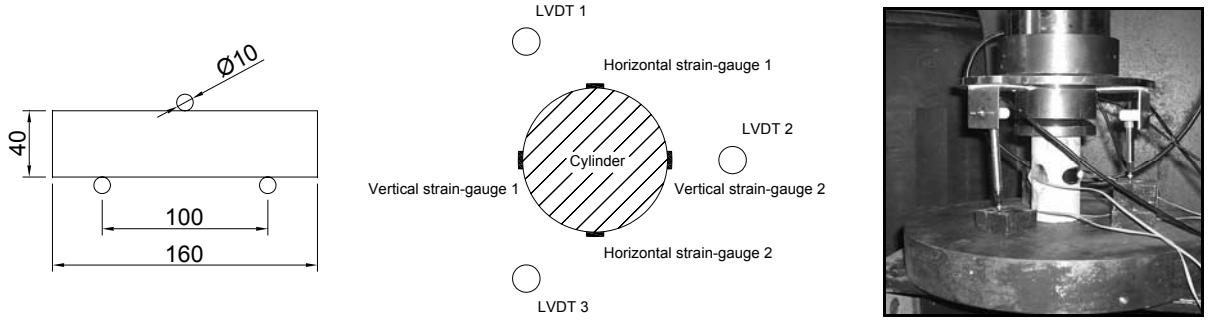

Figure 3.20 – Details of the experimental tests in mortar: (a) compressive and flexural test in prismatic specimens and (b) compressive tests in cylinder specimens.

In addition, three LVDTs were also used in the tests of the cylinders to evaluate the complete stress-strain diagrams. In spite of LVDTs and strain-gauges had been used to measure vertical deformations, only results given by the strain gauges were considered for the calculation of the elastic modulus. As the LVDTs were placed between steel plates, the measurements included the accommodation of the interfaces between the specimen and the steel plates, leading to considerable higher deformations, see Figure 3.21.

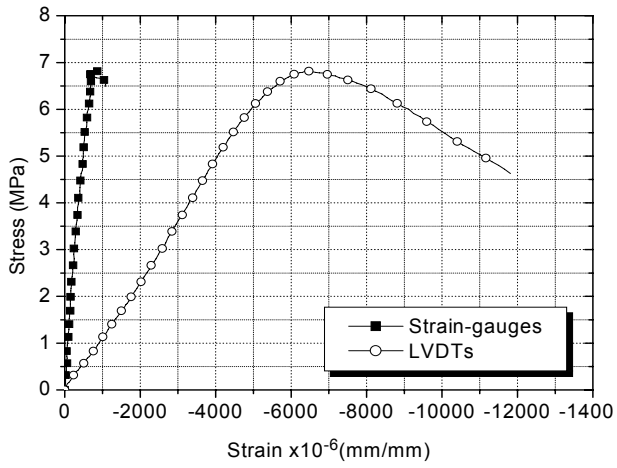

Figure 3.21 – Comparison between the elastic modulus measured by LVDTs and strain-gauges.

Differences ranging between 12 and 30% were also pointed out by Vasconcelos (2005). An alternative scheme to measure the vertical displacements consists of the positioning of the LVDTs in the specimen by using special steel rings. A summary of the fresh and mechanical properties of mortar are indicated Table 3.4. The coefficient of variation obtained for the elastic modulus was in average of 14%.

Table 3.4 – Mechanical and fresh properties of the mortar.

Compressive cylinder strength (MPa)	*Compressive cubic strength (MPa)*	*Flexural Strength (MPa)*	*Elastic Modulus (GPa)*	*Poisson's ratio*	*Flow Table (mm)*
7.53 (1%)	11.81 (1%)	2.91 (13%)	9.02 (14%)	0.18 (17%)	180

3.4 Interface unit-mortar

Masonry is a composite material made by units embedded in mortar. Collapse of masonry structures may be occurs because the failure of units, mortar or interface of unit-mortar. Interface behaviour can be basically defined by the properties normal and parallel to bed joint direction. In this study only the behaviour parallel to bed joints was characterized through initial shear test.

3.4.1 Initial shear test

Initial shear tests were carried out according to EN1052-3 (2002). Three distinct pre-compression levels (σ) were applied in specimens (4 kN, 12 kN and 20 kN equivalent to 0.22 MPa, 0.66 MPa and 1.10 MPa in case of 2C-units and 0.2 MPa, 0.6 MPa and 1.0 MPa in case of 3C-units). Six specimens were built for each pre-compression level, totalizing 18 samples for each type of unit used in this study. Specimens were built with one unit of length and three courses with a 8mm joint, see Figure 3.22a. The pre-compression was applied through four steel cables forming a self equilibrated system, see Figure 3.22b. The mortar the specimens presented a flexural strength equal to 2.11 MPa and a compressive strength equal to 8.35 MPa.

Rubber pieces were used at the extremities of the samples to avoid concentration of stresses. A set of LVDTs was used in both sides of specimens to analyse the behaviour of unit-mortar interface under shear stresses. Three LVDTs were used to evaluate horizontal

displacements of the joints: two LVDTs measuring horizontal displacements of each individual joint and one LVDT, indicating measuring the global horizontal displacement. Besides, two LVDTs were attached to the specimen to record the shear displacement of the joints.

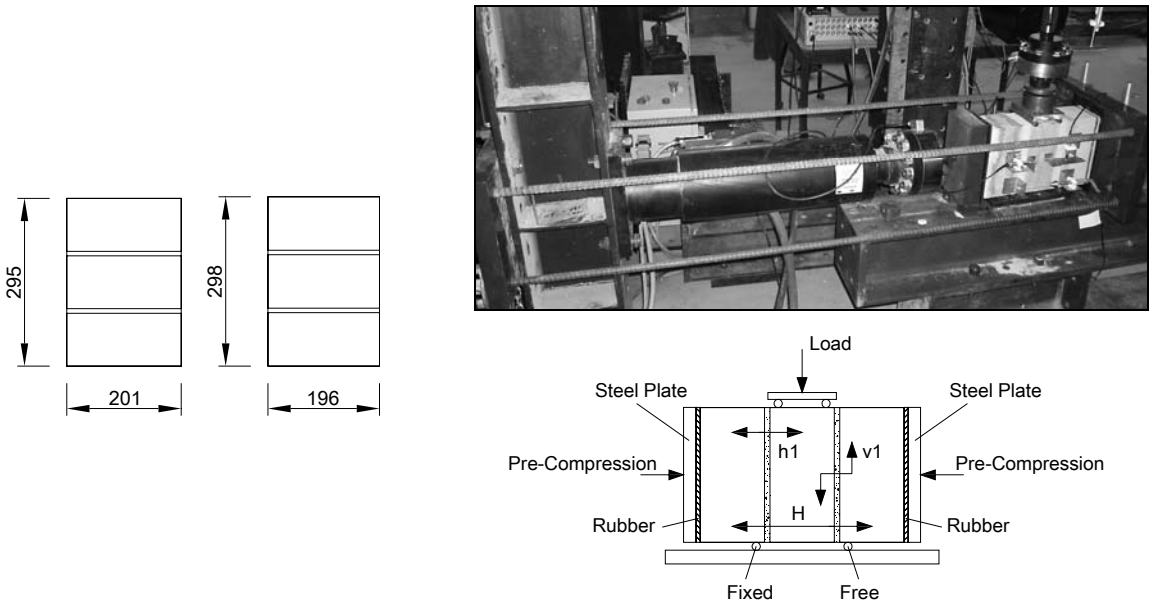

Figure 3.22 – Initial shear tests: (a) Geometry of specimens and (b) Test setup.

According to EN 1052-3 (2002), test specimens should have one of four different types of failure.

a) Shear failure in the unit/mortar bond area either on one or divided between two units face;
b) Shear failure of the mortar;
c) Shear failure of the unit;
d) Crushing and/or splitting failure of the units.

All tested specimens presented the failure at the unit-mortar bond area either on only one or divided between two units face. In some specimens, horizontal cracks on the units appeared at the end of test, after the slide of the central unit, see Figure 3.23. This behaviour can be caused by some expansion of the interface as observed by horizontal LVDTs.

A summary of the shear strength properties obtained in shear tests, namely the initial cohesion, f_{vo} (f_{vok} is the characteristic value), and the coefficient of friction, μ (μ_k is the characteristic value), is shown in see Table 3.5. All properties were calculated in relation to gross area of the specimen. The cohesion is practically the double in case of 3C-units. ON the other hand, it is seen that the coefficient of friction is similar in both geometries of the concrete blocks, see Table 3.5 and Figure 3.24. The friction coefficient depends only on the

concrete-mortar surface contact. As the concrete and mortar was the same for both geometries of the blocks the friction coefficient was expected to be similar. The higher cohesion recorded in 3C-units can probably be attributed to the proximity of the internal webs leading to the union of the excess of mortar during the laying providing a better adherence between the courses.

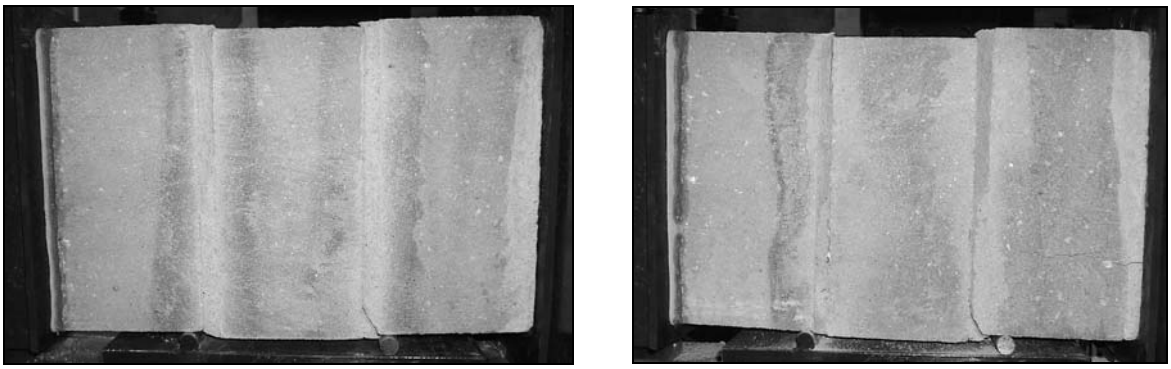

(a) (b)

Figure 3.23 – Failure mode of shear tests: (a) sliding and (b) sliding with horizontal crack.

Table 3.5 – Results of peak shear strength properties.

Type of unit	f_{vo} *(MPa)*	f_{vok} *(MPa)*	μ	μ_k
2C-units	0.21	0.17	0.49	0.39
3C-units	0.42	0.34	0.49	0.40

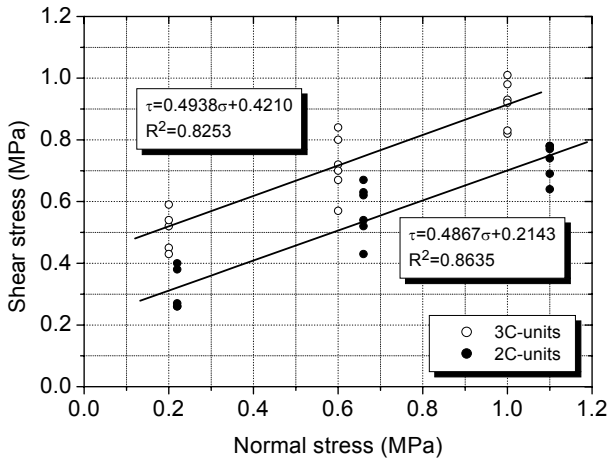

Figure 3.24 – Shear stress *vs.* normal stress diagram.

As observed by other authors (Vasconcelos, 2005; Abdou *et al.*, 2006), after the peak the shear stress had a gradual decrease and stabilizes in a residual value, see Figure 3.25. The residual shear strength properties are presented in Table 3.6. In the Table $f_{vo,res}$ is the residual cohesion, $f_{vok,res}$ is the characteristic value of residual cohesion, α_{res} is the residual coefficient of friction and $\alpha_{k,res}$ is the characteristic value of the residual coefficient of friction. The relation between normal and shear stresses fit also reasonably well a linear function, see Figure 3.26.

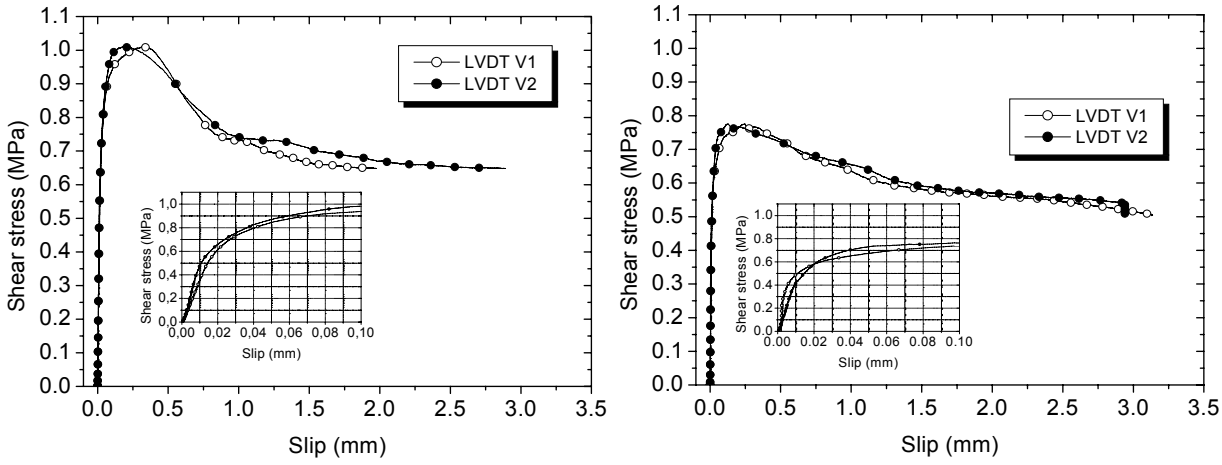

Figure 3.25 – Shear-slipping diagrams: (a) 3C-units – σ = 1.00 MPa and (b) 2C-units – σ = 1.10 MPa.

Table 3.6 – Results of residual values of initial-shear tests.

Type of unit	$f_{vo,res}$ *(MPa)*	$f_{vok,res}$ *(MPa)*	α_{res}	$\alpha_{k,res}$
2C-units	0.14	0.12	0.32	0.25
3C-units	0.16	0.13	0.43	0.34

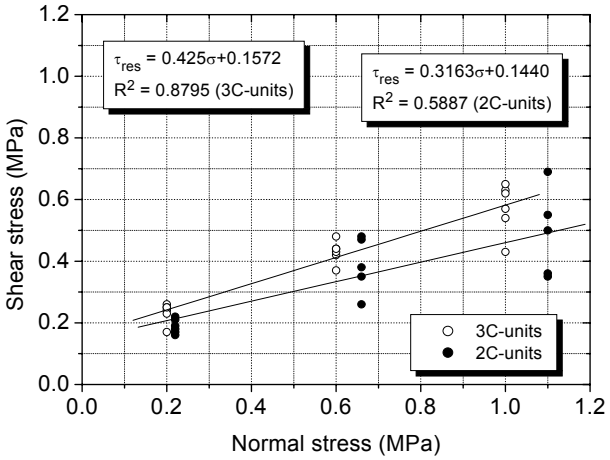

Figure 3.26 – Residual shear stress *vs.* normal stress diagram.

The cohesion reduced approximately 62% and 33% for specimens built with 3C-units and 2C-units respectively, meaning that if cohesion is neglected in design of masonry walls underestimated shear strength can be achieved. According to Abdou *et al.* (2006), the existence of this residual cohesion can be explained by the penetration of mortar into the holes, which avoids the separation of the blocks. Thus, this value can be used for evaluation of the shear sliding resistance of walls or piers submitted to seismic action failing along horizontal sliding joints (Calvi *et al.*, 1996). The residual friction coefficient is 12% and 35% lower than peak friction coefficient in specimens built with 3C-units and 2C-units respectively. In this case the higher reduction occurs for 2C-Units.

Mode II fracture energy was calculated according to Pluijm (1999), see Figure 3.27. A high variation was observed in results. However, it was clear that G_f^{II} depends of the normal stress applied on the mortar joints, see Table 3.7 and Figure 3.28. All properties were

calculated in relation to gross area of the specimen. From the linear fitting to the experimental results it is possible to conclude that the mode II fracture energy can be calculated from Eq. 3.3:

$$G_f^{II} = A + B\sigma \qquad \text{Eq. 3.2}$$

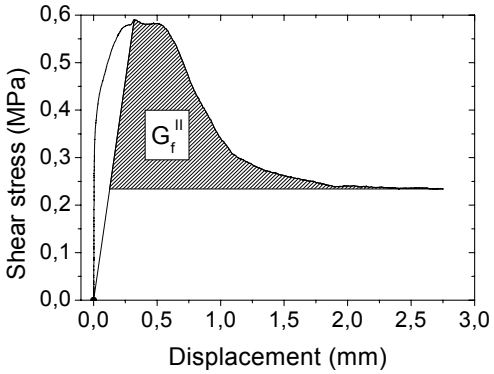

Figure 3.27 – Mode II fracture energy.

Specimens built with 3C-units exhibited higher values of mode II fracture energy than specimens built with 2C-units. This behavior is probably due to the higher penetration of mortar into the holes blocks in 3C-units.

Table 3.7 – Results of mode II fracture energy obtained from initial-shear tests.

Type of unit	*A*	*B*
2C-units	0.02	0.30
3C-units	0.19	0.13

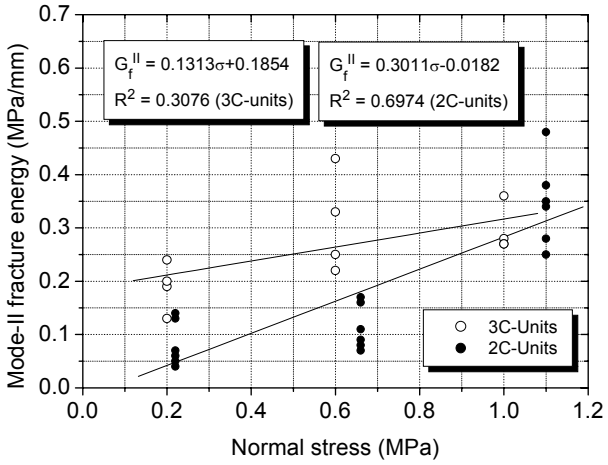

Figure 3.28 – Variation of mode II fracture energy with normal stresses.

The shear stiffness of the unit-mortar interface was also calculated from the shear stress *vs.* shear slipping. It seems not to be influenced by the normal stresses, see Figure 3.29. However, the scatter of the results was very high, which means that more tests should be carried out to evaluate this mechanical property.

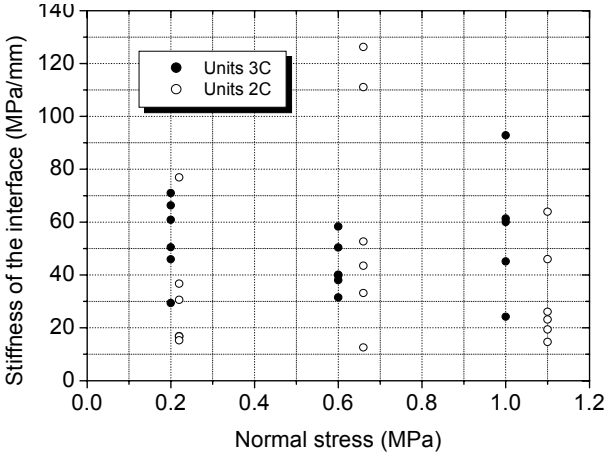

Figure 3.29 – Relation between shear stiffness and normal stress.

Horizontal deformation of the specimens was also observed during the test. All horizontal LVDTs exhibited similar behaviour at the beginning of the test and presented small values. With no symmetrical damages of the interface some rotations appeared in specimen and the horizontal displacements became quite different, see Figure 3.30.

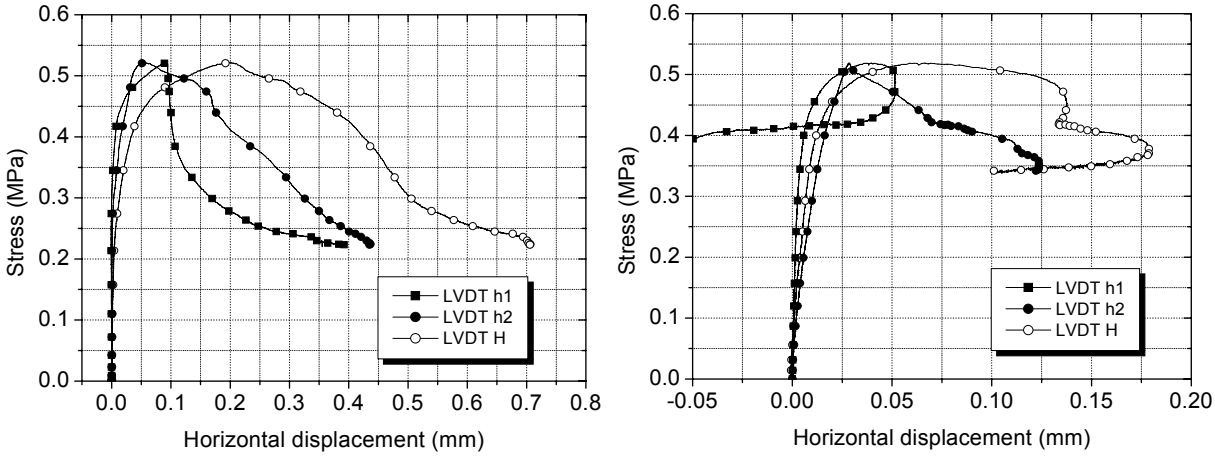

(a) (b)

Figure 3.30 – Horizontal behaviour of the specimens in initial shear tests: (a) 3C-units – σ = 0.20 MPa and (b) 2C-units – σ = 0.66 MPa.

The relation between the horizontal displacement and vertical displacement define the tangent of the dilatancy angle (*tan* ψ). As after the beginning of damage there were some rotations, LVDT H was used to define the dilatancy. Half of the values recorded in LVDT H were considered since there were two joints in the measured distance. Thus, dilatancy was calculated as the tangent of the horizontal displacements *vs.* vertical displacements diagrams, see Figure 3.31. As observed by Pluijm (1999) and Vasconcelos (2005), dilatancy

decreases with the increasing of pre-compression, see Figure 3.32. Dilatancy seems to have a linear variation in relation to normal stress and can be given by Eq. 3.3.

$$\tan\psi = A + B\sigma \qquad \text{Eq. 3.3}$$

The values of the variables *A* and *B* in the equation are defined in Table 3.8.

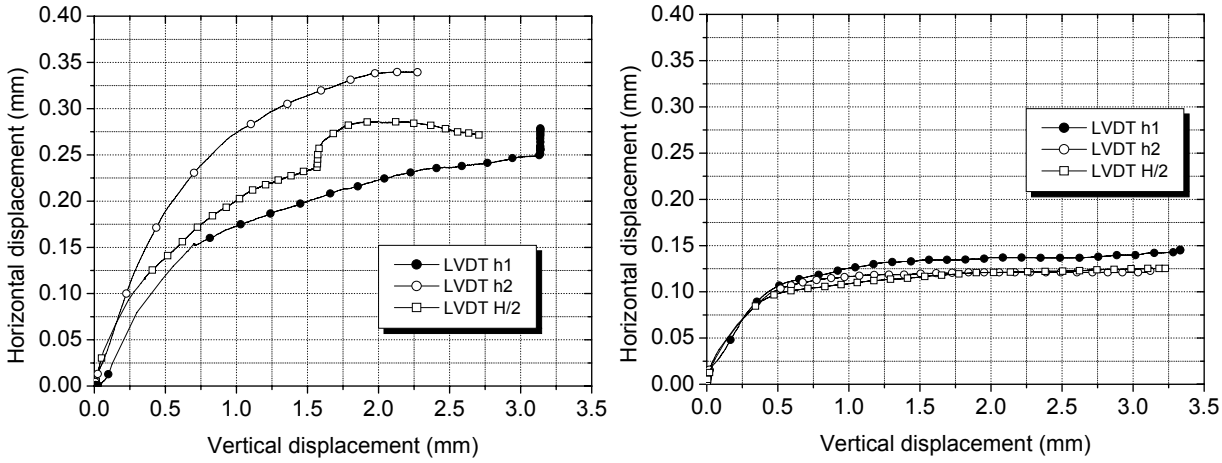

Figure 3.31 – Horizontal displacements *vs.* vertical displacements of the specimens in initial-shear tests: (a) 3C-units – σ = 0.20 MPa and (b) 2C-units – σ = 0.66 MPa.

Specimens built with 3C-units had a high coefficient of correlation equal to 0.91. On the other hand, specimens built with 2C-units had a high scatter on the results.

Table 3.8 – Results of dilatancy of initial shear tests.

Type of unit	*A*	*B*
2C-units	0.41	-0.19
3C-units	0.52	-0.38

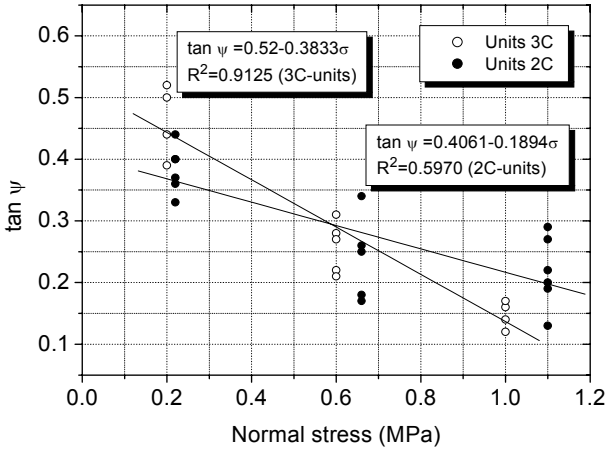

Figure 3.32 – Relation between dilatancy and normal stress.

3.5 Reinforcements

Aiming at analysing the behaviour of reinforced masonry walls and beams, it was decided to use pre-fabricated truss type reinforcements both for bed joints and as vertical reinforcement, see Figure 3.33. This is a prefabricated reinforcement consisting of two parallel wires welded to a continuous zig-zag wire.

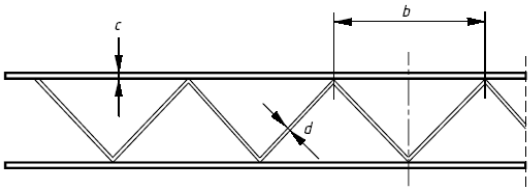

Figure 3.33 – Pre-fabricated trussed type reinforcement.

Reinforcements with 4mm and 5mm diameter and spacing between longitudinal bars of 80 mm and 50mm were used for the bed joints and vertical hollow cells of the units respectively. Reinforcements of two classes of strength were applied due to the usage of different productions. Three specimens were submitted to direct tensile tests, see Figure 3.34. The average value of the yield stress was of 580 MPa and 700 MPa (ε_y = 2.96 ‰ and ε_y = 3.57 ‰) and the elastic modulus was about 196 GPa, see Figure 3.34.

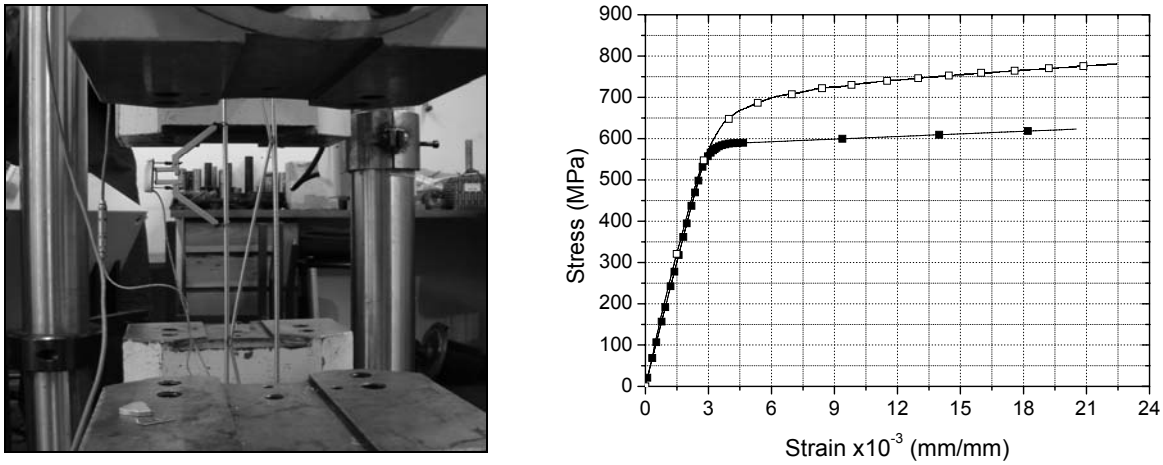

Figure 3.34 – Stress *vs.* strain diagram of the trussed reinforcements.

Straight bars were also used in the construction of masonry beams at the bed joints, when the flexural failure was to be prevented. Straight bars with 6 mm of diameter were used. As in case of trussed type reinforcement, three specimens were submitted to direct

tensile tests, being the average value of the yield stress of 448 MPa (ε_y = 2.50 ‰) and the elastic modulus of about 179.3 GPa, see Figure 3.35.

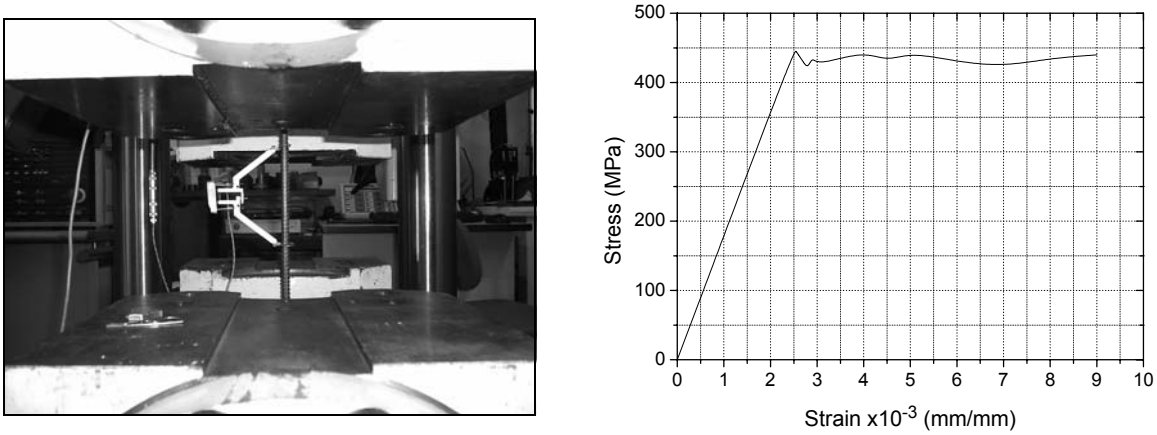

Figure 3.35 – Stress *vs.* strain diagram of the straight reinforcement.

3.6 Masonry

Besides the characterization of the masonry materials and unit-mortar interfaces, experimental characterization was carried out to evaluate the composite behaviour of masonry. Uniaxial compressive tests were carried out in order to characterize the compressive behaviour of masonry in normal and parallel direction to the bed joints. Diagonal tests were also carried out to evaluate the shear and indirect tensile behaviour of masonry. Finally, flexural tests were performed in order to obtain the flexural strength of masonry with plane of failure parallel to bed joints.

3.6.1 Compressive tests in direction normal to bed joints

Six masonry wallets were built considering each geometry of the units in order to evaluate the compressive behaviour normal to bed joints according to EN 1052-1 (1999). The geometry of the specimens was defined according to the recommendations of the European standard, being composed of two units length and five courses height with an 8mm horizontal joints, see Figure 3.36a. Six LVDTs were used to measure the deformations of the samples. Four LVDTs were attached to the specimen in order to measure the vertical strain and calculate the elastic modulus of the masonry assembles. Two additional LVDTs were used to measure the horizontal strains, see Figure 3.36b. The horizontal strains were measured in the middle of unit and in the vertical joint. The mortar used in the construction of

the specimen presented a flexural strength equal to 2.74 MPa and a compressive strength equal to 11.52 MPa.

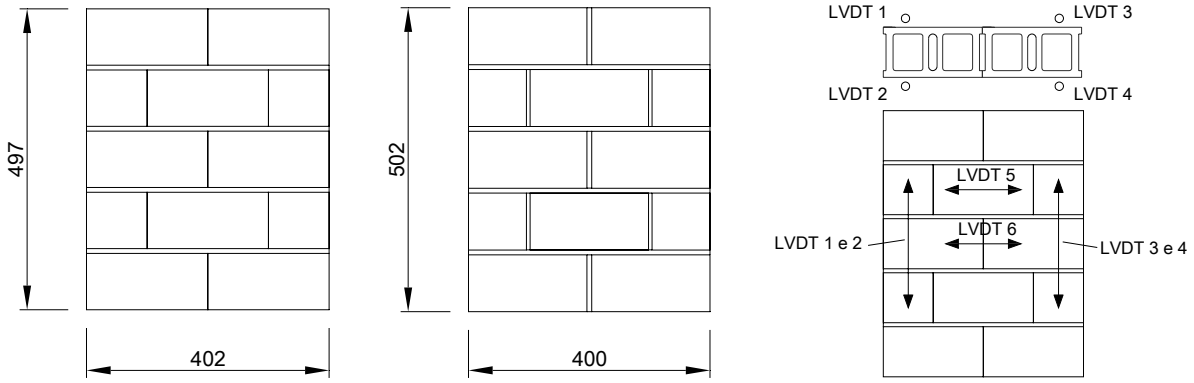

Figure 3.36 – Specimens used in compressive tests normal to bed joints: (a) geometry and (b) instrumentation.

The masonry built with the distinct geometry of the concrete blocks presented similar behaviour under compression, see

Table 3.9. In the Table 3.9, $f_{am\perp}$ is the mean of compressive strength normal to bed joints, $f_{ak\perp}$ is the characteristic value of compressive strength normal to bed joints, $E_{am\perp}$ is the mean of elastic modulus normal to bed joints, $\nu_{am\perp}$ is the mean of Poisson's ratio normal to bed face, $\varepsilon_{aym\perp}$ is the mean of yield strain normal to bed joints and $f_{ak,Eurocode\ 6\ (2005)\perp}$ is the characteristic compressive strength normal to bed face of masonry measured according to Eurocode 6 (2005). All properties were calculated in relation to gross area of the specimen. The compressive strength calculated according to Eurocode 6 (2005) is given by Eq. 3.4.

$$f_{ak} = 0.45 f_b^{0.7} f_m^{0.3} \qquad \text{Eq. 3.4}$$

Where, f_{ak} is the characteristic value of compressive strength of masonry, f_b is the normalized compressive strength of the units and f_m is the compressive strength of the mortar.

It is observed that the values calculated according to Eurocode 6 (2005) were 8.6% lower and 8.2% higher than the characteristic compressive strength obtained in 2C-units and 3C-units respectively, meaning that good agreement was find between experimental values and those suggested by the European code. In spite of the compressive strength normal to bed joints of 3C-units was higher than the compressive strength of 2C-units, the compressive strength of the masonry normal to bed joints was very similar for both types of units.

Table 3.9 – Compressive strength of masonry normal to bed joints.

Type of unit	$f_{am}^{\perp}$ *(MPa)*	$f_{ak}^{\perp}$ *(MPa)*	$E_{am}^{\perp}$ *(GPa)*	$\nu_{am}^{\perp}$	$\varepsilon_{aym}^{\perp}$ (‰)	$f_{ak,Eurocode\ 6\ (2005)}^{\perp}$ *(MPa)*
2C-units	5.44 (6%)	4.88	10.48 (23%)	0.47 (53%)	0.93 (13%)	4.46
3C-units	5.95 (11%)	4.86	10.51 (23%)	0.55 (37%)	1.00 (25%)	5.26

Masonry panels presented a fragile behaviour with an explosive collapse in most of specimens, see Figure 3.37 and Figure 3.38. Cracking began in vertical joint at the middle of specimen due to tensile stresses in direction parallel to bed joints. The crack propagates and passes through the upper and lower units when tensile stresses reached the tensile strength of the concrete block. Mortar in horizontal joint of the top of specimen crushed and vertical cracks appeared in the upper and middle course units in following the vertical joints. The basic difference on the failure mode of specimens built with 3C-units and 2C-units seemed to be the gradual and higher cracking of the masonry built with filled vertical joints.

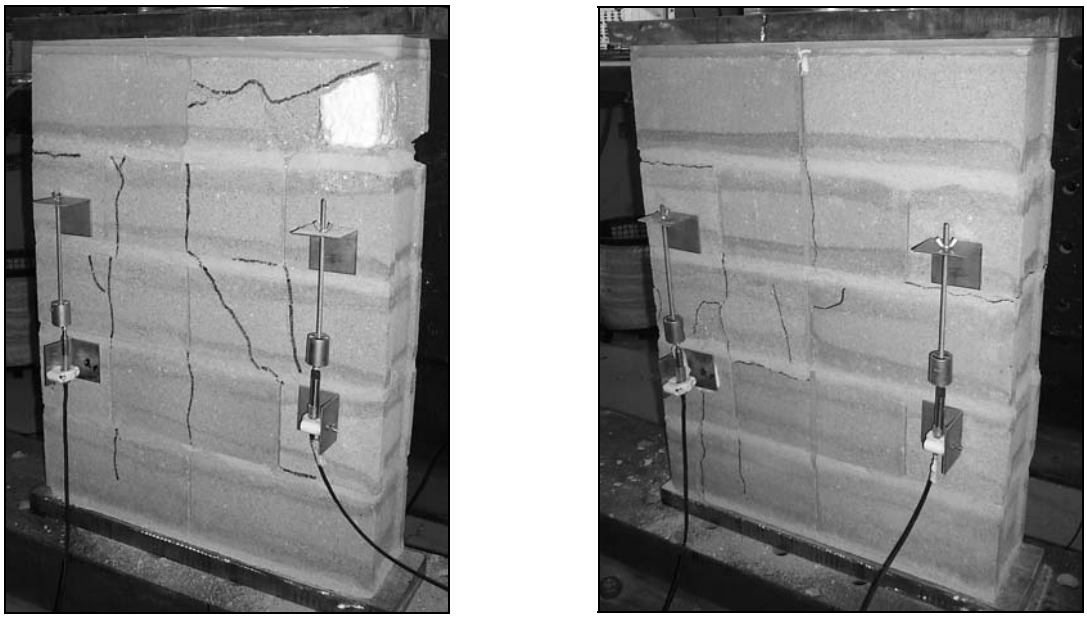

(a) (b)

Figure 3.37 – Cracking pattern on specimens built with 3C-units: (a) specimen 1 and (b) specimen 6.

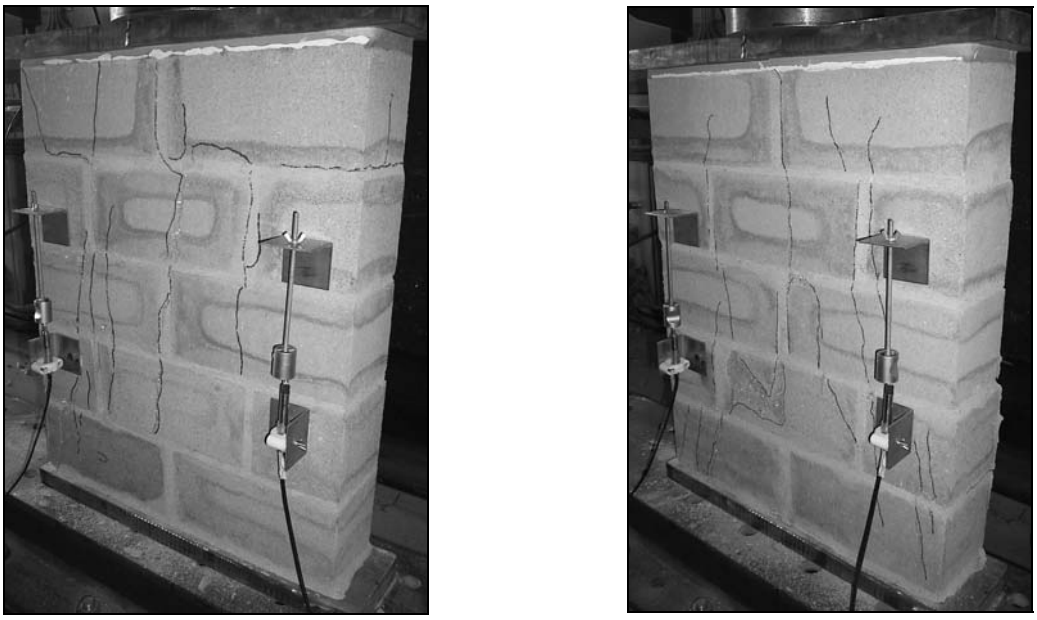

(a) (b)

Figure 3.38 – Cracking patterns on specimens built with 2C-units: specimen 2 and (b) specimen 4.

LVDTs 5 and 6 were used to compare the horizontal deformation at the middle of unit and at the level of a vertical joint. No differences were observed between those deformations, confirming the homogeneous behaviour of the masonry specimens, see Figure 3.39. As expected, specimens built with 3C-units showed higher horizontal deformations and, consequently, a higher Poisson's ratio since there was no contribution of the resistance of mortar in vertical joints. It should be noticed that the values of Poisson's ratios and elastic modulus were very high. This behaviour may be attributed to a possible flexure of the steel plate on the top of specimens. This flexure generated a non-uniform distribution of stresses with higher compressive stresses in the center of specimens and lower stresses in edges where vertical strains were measured.

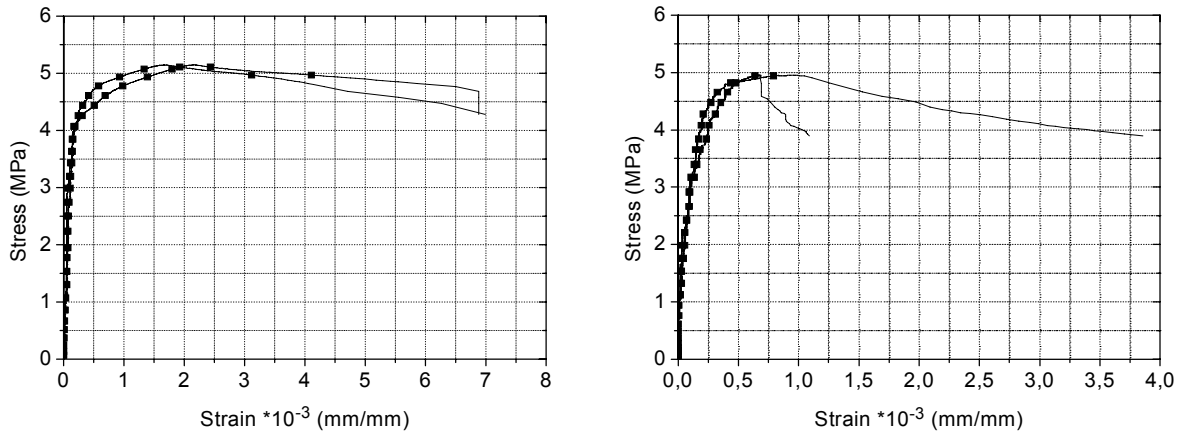

(a) (b)

Figure 3.39 – Horizontal strains: (a) 3C-units and (b) 2C-units.

The relation between stresses and strains suggested by Eurocode 2 (2004) to concrete was also applied to masonry under compression in the perpendicular direction to bed joints according to Eq. 3.5:

$$\sigma_a = f_{ak}\left[1-\left(1-\frac{\varepsilon_a}{\varepsilon_{ay}}\right)^2\right] \qquad \text{Eq. 3.5}$$

Where, σ_a is the stress in masonry, ε_a is the strain in masonry and ε_{ay} is the yield strain of masonry.

From Figure 3.40, it is possible to observe that Eq. 3.5 describes also very well the experimental compressive strength of masonry.

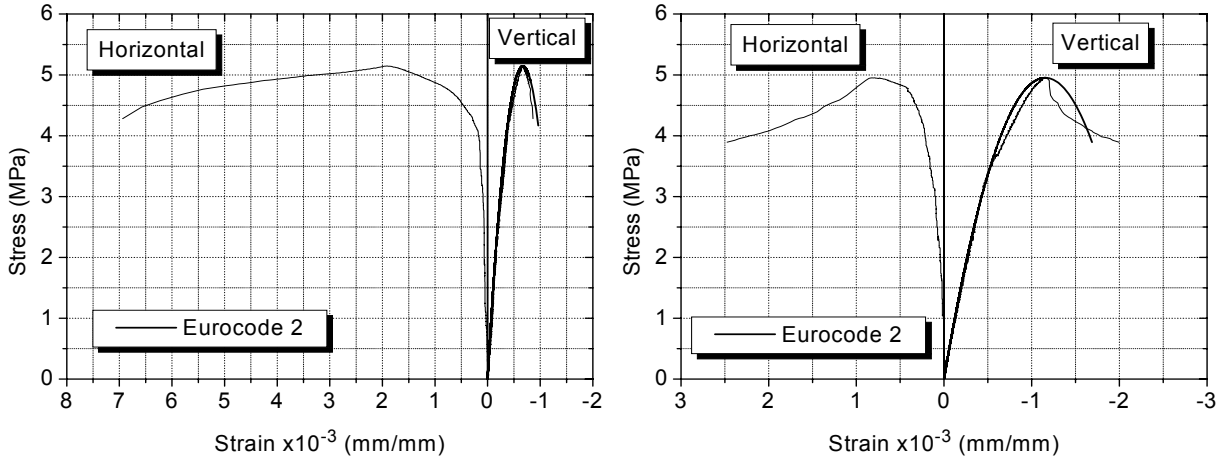

Figure 3.40 – Experimental stress *vs.* strain diagrams and comparison with stress-strain function given by Eurocode 2 (2004): (a) 3C-units and (b) 2C-units.

3.6.2 Compressive tests in direction parallel to bed joints

As aforementioned the compressive tests parallel to bed face were also carried out in order to evaluate the compressive strength of masonry in parallel direction to bed joins since this mechanical property is needed for the design of masonry beams. Six masonry wallets were built with the two geometries of units. Specimens were built with two units of length and three courses height with an 8mm-joint, see Figure 3.a. Six LVDTs were used to measure the vertical and horizontal deformations. Four LVDTs were used to obtain the vertical strains and calculate the elastic modulus of the masonry and two LVDTs were used to evaluate the horizontal strains close of the top and bottom edges of masonry, see Figure 3.b. The mortar

used in the construction of the specimens presented a flexural strength equal to 2.74 MPa and a compressive strength equal to 11.52 MPa.

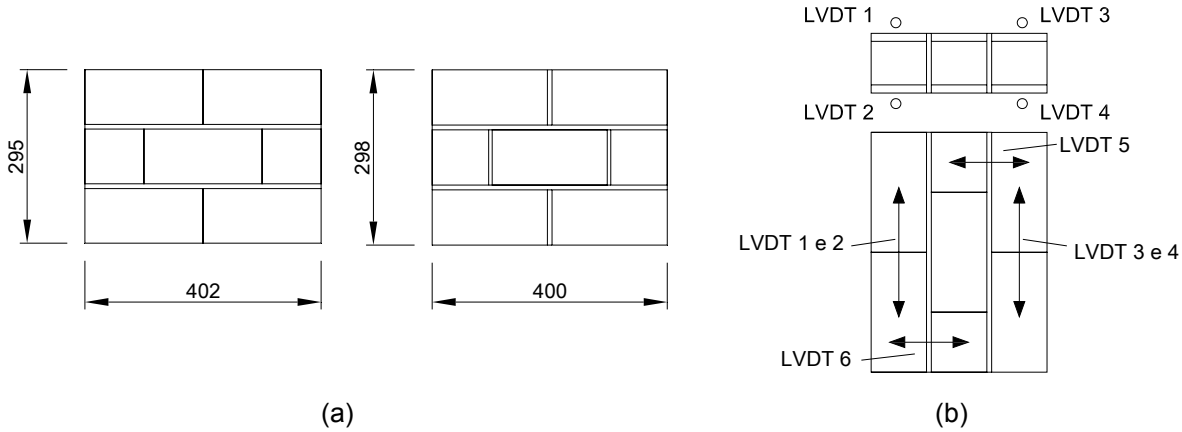

Figure 3.41 – Specimens used in compressive tests in the direction parallel to bed joints: (a) geometry and (b) instrumentation.

A complete summary of the mechanical properties obtained in experimental tests carried out on the direction parallel to bed joints in given in Table 3.10. All properties were calculated in relation to gross area of the specimen. In the Table 3.10, $f_{am//}$ is the mean of compressive strength parallel to the direction of bed joints, $f_{ak//}$ is the characteristic value of compressive strength parallel to the direction of bed joints, $E_{am//}$ is the mean of elastic modulus parallel to the direction of bed joints, $\nu_{am//}$ is the mean of Poisson's ratio parallel to the direction of bed joints, $\varepsilon_{aym//}$ is the mean of yield strain parallel to the direction of bed joints and $f_{ak,Eurocode\ 6\ (2005)//}$ is the characteristic value of compressive strength parallel to the direction of bed joints according to Eurocode 6 (2005). In case of compression parallel to bed joints, Eurocode 6 (2005) suggests the same expression used to calculate the compressive strength in the normal direction to bed joints but considers the normalized compressive strength of the masonry unit obtained in experimental tests carried out on the direction parallel to bed joints. Besides, factor *K* should be also multiplied by 0.5, see Eq. 3.6:

$$f_{ak//} = 0.5\left(0.45 f_{b//}^{0.7} f_m^{0.3}\right) \qquad \text{Eq. 3.6}$$

Where, $f_{b//}$ is the normalized compressive strength of the units parallel to bed face.

The results show that the compressive strength in the direction parallel to bed joints present lower values when compared to the compressive strength of masonry in the direction perpendicular to bed joints, mainly in case of absence of mortar in vertical joints, see Table 3.10. In case of compressive strength in the direction parallel to bed joints, the value of

the characteristic strength suggested by Eurocode 6 (2005) is on the safety side for both geometries of the concrete blocks.

Table 3.10 – Mechanical properties regarding the compressive behaviour of masonry in the direction parallel to bed joints.

Type of unit	$f_{am//}$ *(MPa)*	$f_{ak//}$ *(MPa)*	$E_{am//}$ *(GPa)*	$\nu_{am//}$	$\varepsilon_{aym//}$ (‰)	$f_{ak,Eurocode\ 6\ (2005)//}$ *(MPa)*
2C-units	3.41 (14%)	2.62	7.31 (11%)	0.25 (27%)	1.61 (34%)	1.74
3C-units	2.78 (16%)	2.05	2.50 (29%)	0.17 (41%)	11.26 (28%)	1.94

.

In spite of low strength, the behaviour of specimens in the direction parallel to bed joints was very ductile with ultimate strains higher than 10 ‰. This is related to the failure mode that masonry presented in this direction. The failure mode can be divided in two phases, as in case of compressive tests parallel to bed joints of the concrete blocks, see Figure 3.42.

Figure 3.42 – Behaviour of masonry under compression in the direction parallel to bed joints: (a) 1st phase and (b) 2nd phase.

In the first phase, units and mortar deform in direction of loading due to the compressive loading. On the other hand, compressive loading leads to the lateral deformation of the specimen, which results on the tension of webs of the concrete units up to the opening of tensile cracks when tensile strength of concrete of the units is reached. Tensile stresses also appeared in direction normal to bed joints leading to cracking at the unit-mortar interfaces along bed joints. After this, the second phase begins with the specimen divided in two parts under flexure generated by the eccentricity of loading in relation to shells of the units. After the failure of the webs, the flexure of the two separated parts of the specimen results in cracks at head joints. In some cases, the cracks at head joints propagate to units, see Figure 3.43 and Figure 3.44.

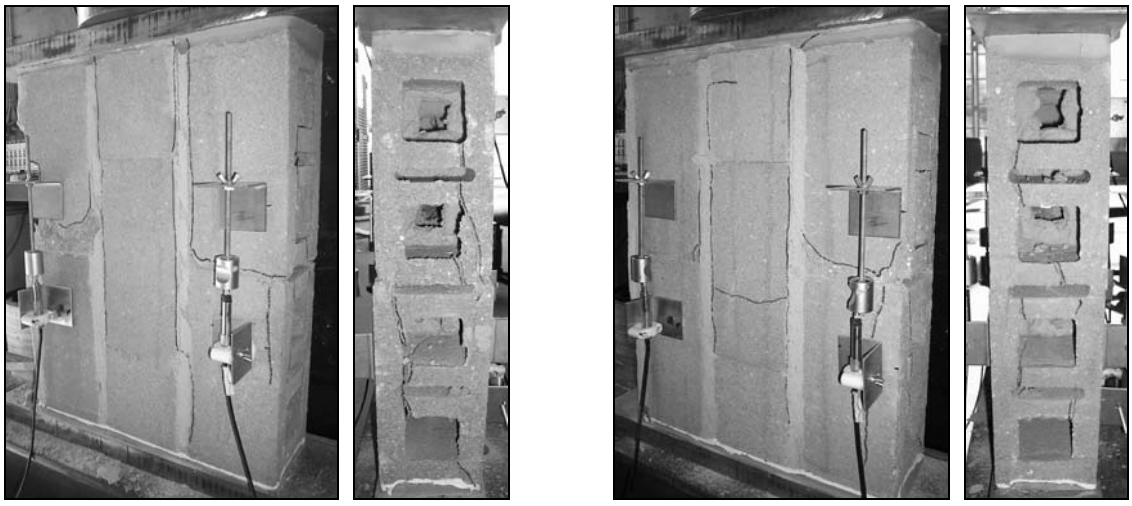

(a) (b)

Figure 3.43 – Cracking patterns of specimens built with 3C-units: (a) specimen 5 and (b) specimen 6.

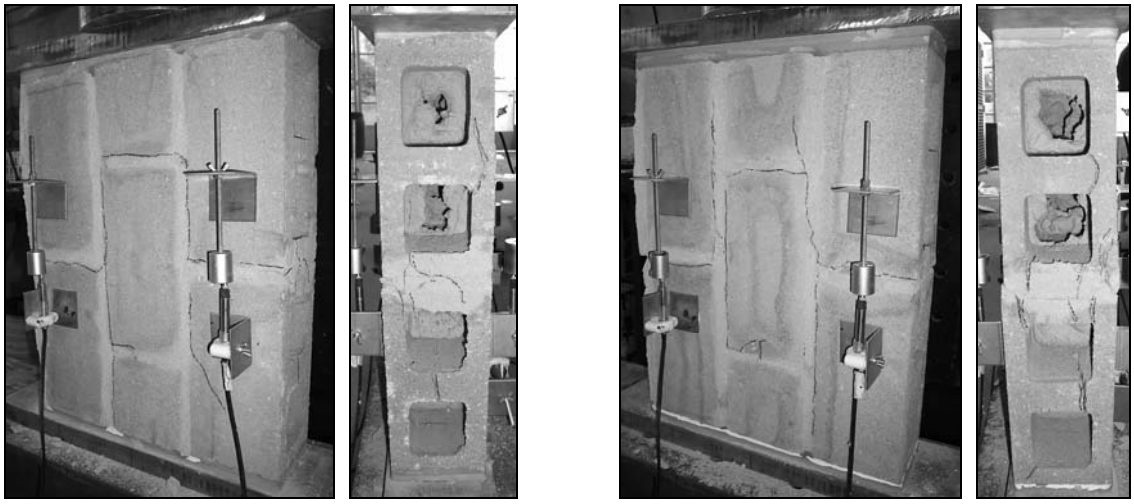

(a) (b)

Figure 3.44 – Cracking patterns of specimens built with 2C-units: (a) specimen 2 and (b) specimen 3.

Specimens built with 2C-units and 3C-units exhibited differences on the complete compressive behaviour in the direction parallel to bed joints. Specimens with 2C-units presented a gradual loss of stiffness up to the maximum load, see Figure 3.45a. On the other hand, specimens built with 3C-units exhibited an increasing of stiffness in the post-peak regime. This behavior is related to the absence of mortar in head joints. It is practically impossible to ensure a total contact between the bands of the 3C-units during the laying of the blocks. Only one grain of sand in this region is sufficient to keep the surfaces separated by some millimetres. The increase on the stiffness and compressive strength is associated to the contact of dry joints and further crushing of the frogged ends, see Figure 3.45b.

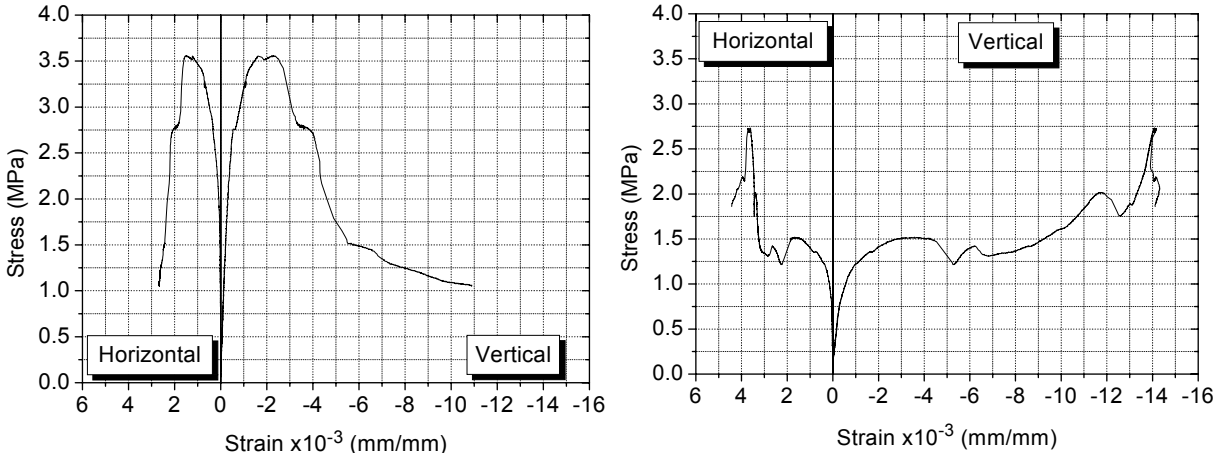

Figure 3.45 – Stress *vs.* strain diagrams obtained in the direction normal to bed joints: (a) 2C-units and (b) 3C-units.

3.6.3 Diagonal tests

Diagonal tests were carried out according to ASTM E519-02 (2000). Six masonry wallets were built with the two geometries of the concrete blocks. Specimens were built with two and a half blocks of length and five courses height with a 8mm-joint aiming at achieving a square-geometry to the specimens, see Figure 3.46a. Four LVDTs were used to measure the deformations of the specimens. Two vertical LVDTs were used to measure the vertical strain and two LVDTs were attached to the specimens to measure the horizontal strains, see Figure 3.46b. The mortar used in the construction of the specimens presented a flexural strength equal to 2.68 MPa and a compressive strength equal to 11.09 MPa.

This test allows the obtainment of the shear strength of the masonry through diagonal compressive loading, which induces an indirect tension with the same value.

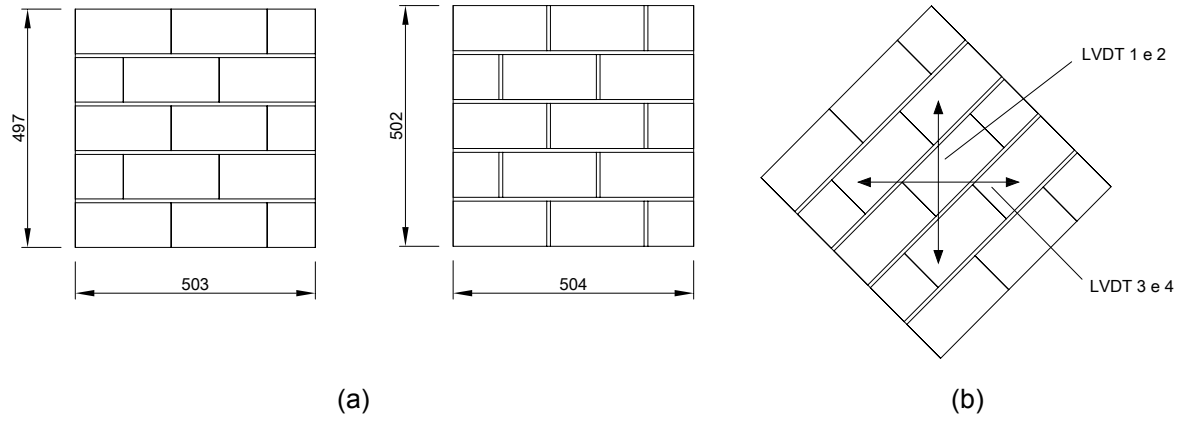

Figure 3.46 – Specimens used in diagonal tests: (a) geometry and (b) instrumentation.

Indirect tension and shear strength are calculated by dividing the applied force by the transversal area of the diagonal section of the specimen, see Eq. 3.7.

$$f_s = f_t = \frac{0.707P}{\left(\frac{b+h}{2}\right)t} \quad \text{Eq. 3.7}$$

Where, f_t is the tensile strength of the masonry, f_s is the shear strength of the masonry P is the applied force, b is the length of the specimen, h is the height of the specimen and t is the width of the specimen.

The shear distortion is calculated based on the displacements measured by the LVDTs through Eq. 3.8. And, the shear elastic modulus of masonry, G, can be calculated from Eq. 3.9.

$$\gamma = \frac{\Delta V + \Delta H}{l_0} \quad \text{Eq. 3.8}$$

$$G = \frac{f_s}{\gamma} \quad \text{Eq. 3.9}$$

Where, γ is the shear distortion of the masonry, ΔV and ΔH are the vertical and horizontal shortening respectively and l_0 is the gage length.

The mechanical properties characterizing the shear and indirect tensile behaviour of masonry are presented in Table 3.11. All properties were calculated in relation to gross area of the specimens. In the Table 3.11, f_{sm} is the mean of shear strength of masonry, f_{tm} is the mean of tensile strength of masonry, f_{sk} is the characteristic value of shear strength of masonry and f_{tk} is the characteristic value of tensile strength of masonry.

Table 3.11 – Mechanical properties from diagonal tests.

Type of unit	***$f_{sm} = f_{tm}$ (MPa)***	***$f_{sk} = f_{tk}$ (MPa)***	***G (GPa)***
2C-units	0.59 (13%)	0.47	2.22 (13%)
3C-units	0.19 (21%)	0.12	1.85 (12%)

It can be observed that specimens built with 3C-units and 2C-units presented distinct shear and tensile properties. The presence of mortar in head joints seems to influence considerably the shear and tensile strength leading to an increasing of strength around to

210%. The filling of vertical joints generated a better distribution of stresses since mortar increase the contact area of the units. On the other hand, the filling of the vertical joints affected in a lower extent the shear stiffness of masonry resulting in a shear modulus 20% higher than in case of masonry built with 3C-units.

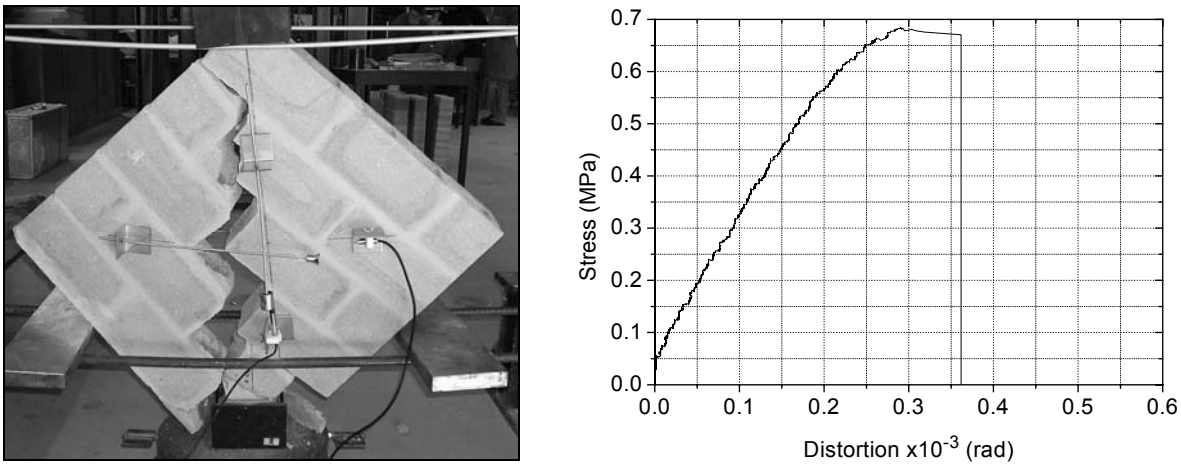

Figure 3.47 – Cracking pattern on specimens built with 2C-units.

The failure of wallets built with 2C-units was very brittle with the sudden cracking of specimens and the projection of the specimen from the testing apparatus, see Figure 3.47. Specimens built with 3C-units exhibited a more ductile behaviour. The cracking was visible and occurred suddenly as in case of specimens built with 2C-units. However, after maximum load was reached, the deformation increased for a load almost constant until the collapse, see Figure 3.48. In fact, the load dropped from the peak to a residual constant stress. The crack pattern is composed of a macro-crack following the unit-mortar interfaces indicating that the units have a tensile strength higher than the shear strength of the unit-mortar interface. The cracking became visible just at the moment of collapse.

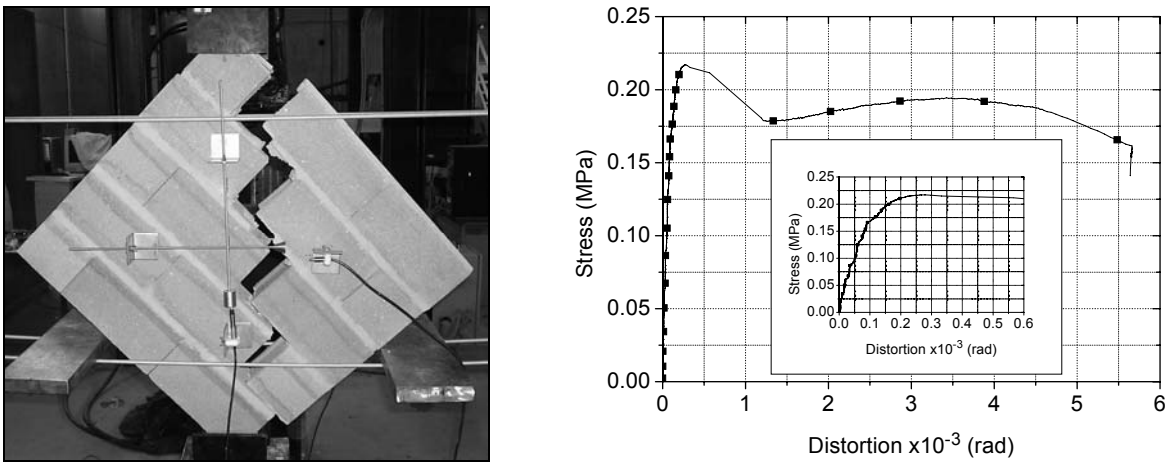

Figure 3.48 – Cracking pattern on specimens built with 3C-units.

3.6.4 Flexural tests

Flexural tests on masonry were carried out according to EN1052-2 (1999). Six masonry wallets were built with the two geometries of concrete blocks. Specimens had two units of length and seven courses height with an 8mm-joint, see Figure 3.49a. Three LVDTs were used to measure the vertical displacements, see Figure 3.49b. The mortar used in the construction of specimens presented a flexural strength equal to 2.50 MPa and a compressive strength equal to 10.15 MPa.

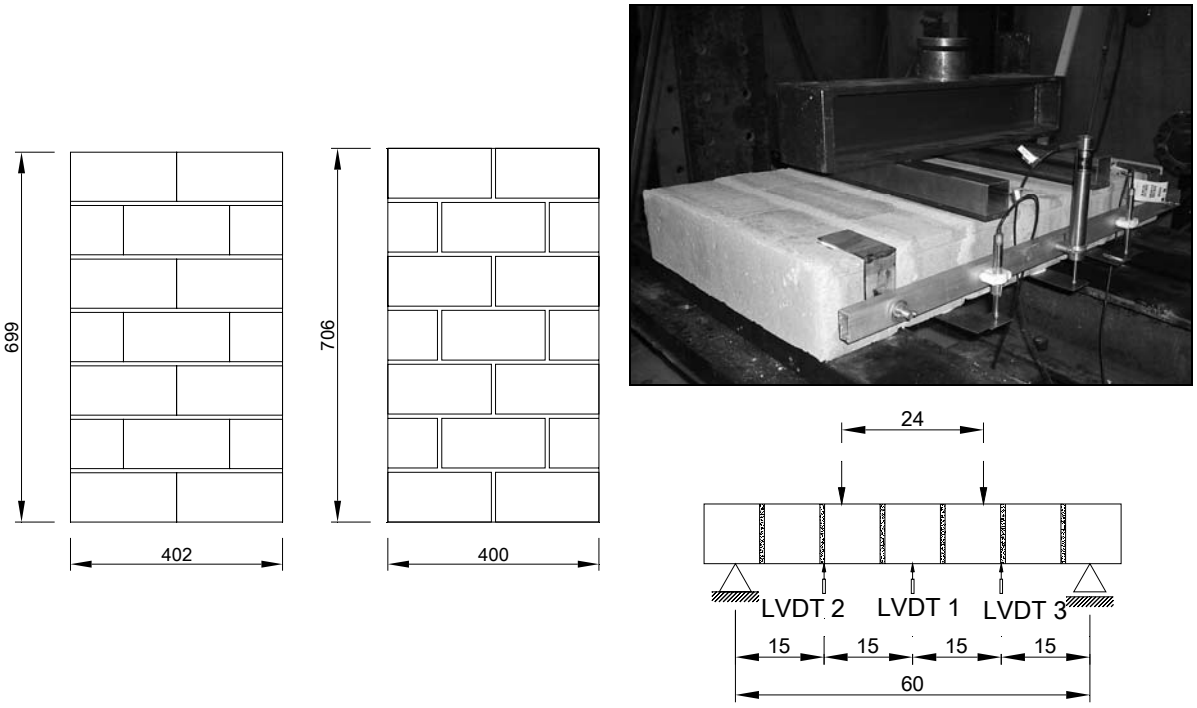

(a) (b)

Figure 3.49 – Flexural tests: (a) Specimens and (b) Test setup.

According to EN 1052-2 (1999) flexural strength is calculated following Eq. 3.10. This value corresponds to the tensile stress in the middle section of the specimen caused by the flexure.

$$f_x = \frac{3P(l_1 - l_2)}{2bt^2} \qquad \text{Eq. 3.10}$$

Where, f_x is the flexural strength, P is the maximum load applied, l_1 is the spacing of the outer bearings, l_2 is the spacing of the inner bearings, b is the length of specimen and t is the width of specimen.

The flexural stiffness of masonry can be calculated based on the moment *vs.* curvature diagram. From the displacements measured by the LVDTs it is possible to define the curvature in the zone of pure flexure, see Figure 3.50. The curvature is given by Eq. 3.11.

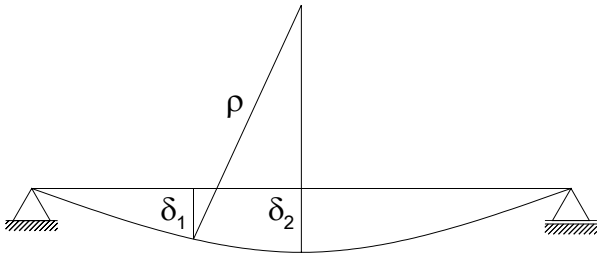

Figure 3.50 – Curvature through the displacements in flexural test.

$$\rho^2 = \left[\rho - \left(\delta_2 - \delta_1\right)\right]^2 + \left(\frac{l_2}{2}\right)^2 \quad \rightarrow \quad \frac{1}{\rho} = \kappa = \frac{2\left(\delta_2 - \delta_1\right)}{\left(\delta_2 - \delta_1\right)^2 + \left(\frac{l_2}{2}\right)^2} \qquad \text{Eq. 3.11}$$

Where, δ_1 is the displacement of the point corresponding to one third length of the specimen and δ_2 is de displacement measured by LVDT1.

LVDTs 2 and 3 were not positioned in the region with constant bending moment and null shear force. So, values of these displacements should be corrected in order to calculate the curvature. Thus, δ_1 was calculated using the mean of displacements of LVDT2 and LVDT3 and using an equation of second order to represents the deformed shape of specimen, see Figure 3.51.

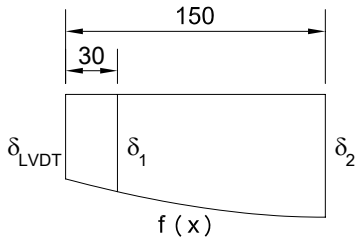

$$f(x) = Ax^2 + Bx + C$$

$$f(0) = \delta_{LVDT},\ f(150) = \delta_2,\ f'(150) = 0$$

$$\delta_1 = 0.64\delta_{LVDT} + 0.36\delta_2$$

$$\delta_2 = \delta_{LVDT1} \qquad \delta_{LVDT} = \frac{\delta_{LVDT2} + \delta_{LVDT3}}{2}$$

Figure 3.51 – Correction of displacements in flexural test.

The value of stiffness was transformed to the gross area to keep consistency with the other results, see Figure 3.52. It is observed that both types of specimens, built with 3C-units and 2C-units, presented negative curvatures at the beginning of the test. It means that displacements of the thirds were higher than displacements in the center of the panel. This

behaviour can be explained by the asymmetric deformation of the rubbers, used in supports to better distribute of the stresses, during the accommodation of the structure.

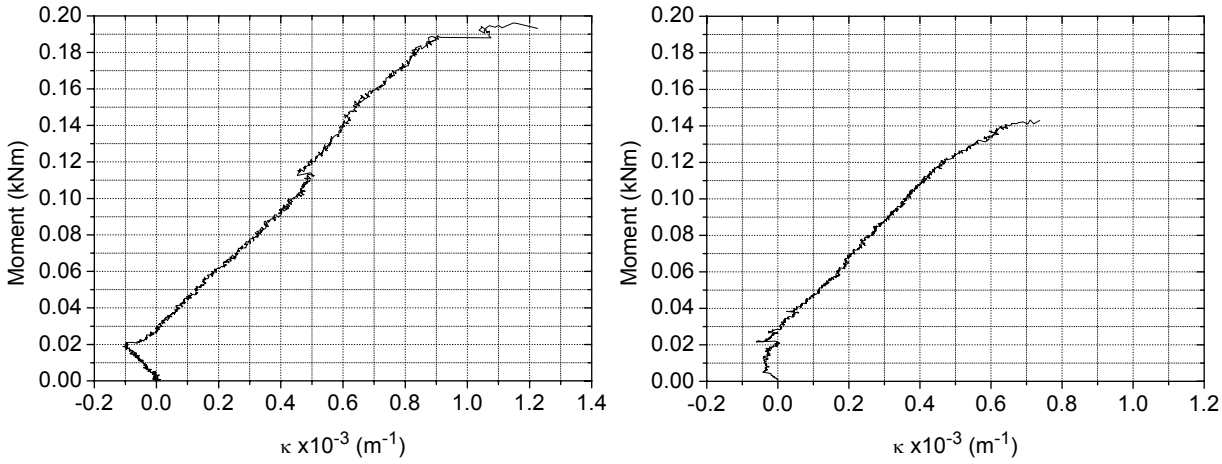

Figure 3.52 – Moment *vs.* curvature diagrams in flexural tests: (a) 3C-units and (b) 2C-units.

The flexural mechanical properties of masonry are presented in Table 3.12, namely the mean, f_{xm}, and the characteristic, f_{xk}, flexural strength and the flexural stiffness, *EI*.

Table 3.12 – Mechanical flexural properties.

Type of unit	***f_{xm} (MPa)***	***f_{xk} (MPa)***	***EI (kNm^2)***
2C-units	0.31 (13%)	0.24	141.80 (7%)
3C-units	0.41 (4%)	0.38	123.44 (16%)

It is seen that specimens built with 3C-units had a higher flexural strength and lower flexural stiffness than the masonry built with 2C-units. The proximity of the internal webs in 3C-units promoted the union of the excess mortar during the laying, providing a better tensile bond strength at the unit-mortar interfaces. On the other hand, the filling of vertical joints in wallets built with 2C-units probably was the responsible by the higher stiffness.

Comparing experimental results with value of flexure strength equal to 0.10 MPa suggested by Eurocode 6 (2005), it can be noticed that the standard underestimates the capacity of masonry under flexion.

3.7 Summary and conclusions

In this chapter a detailed characterization of the mechanical behaviour of masonry components and masonry as a composite material was carried out. Two geometries were considered for the concrete blocks in order to vary the masonry pattern and to obtain different arrangement for the placement of vertical reinforcements on masonry. Tensile and compressive experimental tests were carried out in concrete blocks and flexural and compressive tests were considered to characterize the mortar. The compressive behaviour of masonry in the direction perpendicular and parallel to he bed joints was also characterized based on experimental tests. The shear and indirect tensile strength of masonry was obtained by diagonal tests and the flexural behaviour was analysed based on four point load configuration. Finally the shear behaviour of the unit-mortar interface was characterized from direct shear test of triplet specimens.

From the experimental results the following remarks can be drawn:

(a) Compressive behaviour of units was very similar, meaning that the geometry has no significant influence. Both concrete blocks behaved in a brittle manner under uniaxial compression, being impossible to record the post-peak behaviour.

(b) The compressive strength of units in the parallel direction to the bed joints appears to be a good approximation for the achievement of the tensile strength of concrete units and can replace the direct tensile tests.

(c) The shear strength of unit-mortar interface is higher in 3C-units, possibly due to connection of mortar of the internal webs, avoiding the separation of the blocks. The results showed that shear strength followed the Coulomb's law with a linear relation between shear and normal stresses. Besides, it was observed that dilatancy depends on the normal stresses.

(d) The compressive behaviour of masonry in the perpendicular direction to the bed joints built with the concrete units with distinct geometry appeared to be very brittle. Reasonable approach was finding between experimental compressive strength and the compressive strength calculated according to Eurocode 6 (2005). Besides, the compressive stress-strain diagram obtained for the normal direction to bed joints is well described by the law presented in Eurocode 2 (2004) for concrete structures.

(e) The compressive behaviour of masonry in the parallel direction to the bed joints built with the concrete units with distinct geometry appeared to be more ductile. The geometry of the units influences the ductility of masonry under compression according to the direction of bed joints. The equation recommended by Eurocode 6 (2005) to calculate the

compressive strength of masonry reveals a reasonable approximation but always on the safety side.

(f) The shear and indirect tensile strength of masonry was measured through the diagonal compressive tests. Results revealed that the typology of vertical joints influences the shear and tensile strength of masonry. In case of filled vertical joints the shear and tensile strength presents clearly higher values than in case of unfilled vertical joints. However, when filled vertical joints (2C-units) are used the failure is more brittle than in case of masonry with unfilled vertical joints (3C-units), which in addition presented a residual strength.

Finally, it should be stressed that the knowledge of the mechanical properties and the understanding of the behaviour of masonry and masonry materials is fundamental to analyse the experimental and numerical results of the masonry structural elements under in-plane loading, namely reinforced masonry walls and beams. The mechanical properties are also essential for the design of masonry walls and beams.

4 EXPERIMENTAL PROGRAM II: SHEAR WALLS

4.1 Introduction

In masonry buildings, shear walls are the structural elements responsible for resisting the lateral loads due to wind and earthquakes. These elements are subjected to flexure and shear in conjunction with compression resulting from the gravity loads. Even if the behaviour of masonry walls under flexure is well defined and follows basically the same rules applied to concrete structures, in terms of shear, masonry walls exhibit a more complex behaviour due to the presence of weakness planes along head and bed joints. This means that a research effort has to be made to achieve a better insight on the shear behaviour of masonry walls. This is particularly important in case of reinforced masonry walls as great part of the past and recent investigation is dedicated to the evaluation of unreinforced masonry walls or more recently to strengthen masonry walls with FRPs (Benedetti and Steli, 2006; El Gawady *et al.*, 2006) aiming at improving the strengthening techniques of ancient masonry walls belonging to architectural heritage. The deficit of experimental investigation on reinforced masonry walls is essentially the result of scarce new construction in reinforced masonry, when compared to the reinforced concrete.

The behaviour of masonry structures have been evaluated through different experimental approaches such as quasi-static monotonic or cyclic tests, dynamic shaking table tests and pseudo-dynamic tests. According to Gerardin and Negro (2000) the dynamic shaking table tests are the most realistic way of subjecting a structural model to any particular base motion (Carvalho, 1998; Juhásova *et al.*, 2002; Henderson *et al.*, 2003; Modena *et al.*, 2004; Reneckis *et al.*, 2004; Wight *et al.*, 2004). These tests simulate the seismic action with more accuracy because the tested structure is subjected to real earthquake acceleration records. However, the unavailability of the equipment in most

laboratories and the difficulties in processing the results leads to the preference by other types of tests.

An experimental approach that provides still realistic dynamic results consists of pseudo-dynamic tests. They are, in principle, simpler than shaking table tests. This test is a conjunction of a quasi-static test with a computational model that calibrates the load level to be considered in the dynamic analysis. The masonry structure is submitted to a real earthquake excitation at a relatively slow speed, which enables the observation of the damage evolution. The dynamic characteristics of the structure, equivalent mass and damping are numerically simulated on a computational model, whereas the characteristics of the restoring force are directly measured in the tested specimens.

Still, the quasi-static monotonic/cyclic tests are the most common technique used to evaluate the behaviour of shear walls. They are simple, relatively economical and do not require special apparatus. Static tests are generally carried out in single elements or simple sub-assemblages. The test is performed by controlling the horizontal displacement due to the larger uncertainties in predicting the restoring forces in the nonlinear regime. According to Gerardin and Negro (2000) the main limitation of the static tests concerns the impossibility of simulating the inertial forces. Distinct lateral displacement histories may be used to simulate the seismic loads as shown in Figure 4.1.

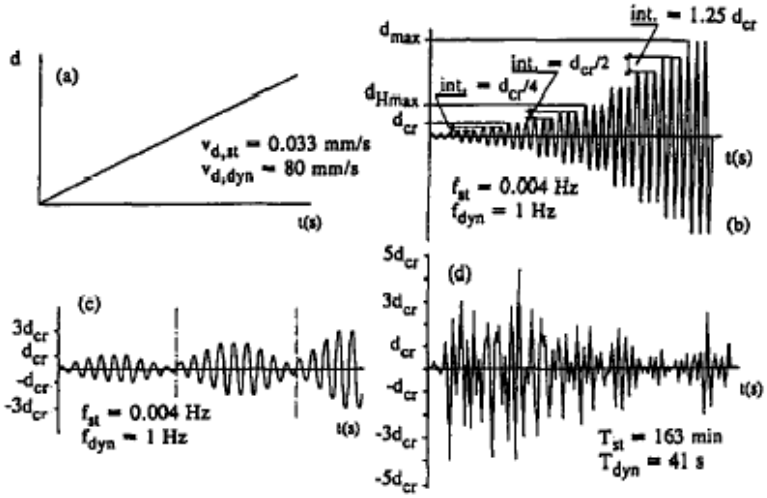

Figure 4.1 – Typical lateral displacement time histories used to simulate seismic loading (Tomaževič, 1999).

Tomaževič *et al.* (1996) investigated the influence of distinct displacement time histories on the in-plane behaviour of masonry walls by comparing the results obtained for each procedure in the same type of specimens. The results showed that in-plane behaviour depends on the displacement time history. Monotonic loading led to the highest lateral

resistance and displacement capacity. Masonry walls exhibited a more brittle behaviour under real earthquake and sinusoidal loading. Figure 4.2 shows the most common configuration for shear walls tested under static monotonic/cyclic loading conditions. Typically, the wall is submitted to combined in-plane horizontal and vertical loading, so that the weight of the upper storeys can be accounted for. According to Tomaževič (1999), in a real situation the axial compression load changes during earthquakes due to restraints that prevent the rotation of the wall at large displacements. However, due to the difficulty of simulating the real boundary conditions, the walls are basically tested with constant vertical load, within the usual limits found in a real building.

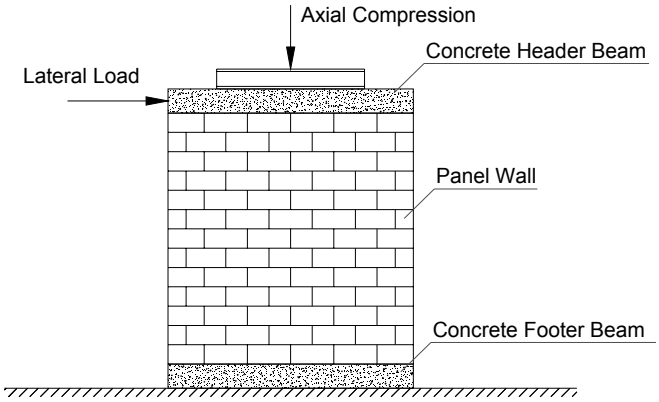

Figure 4.2 - Typical test configuration of shear walls under static monotonic/cyclic lateral loading.

Usually the vertical axial load is applied by means of vertical actuator whose reaction is often given by a steel frame. Keeping a constant value of the axial load during the whole test is a difficult task as the progress of the wall deformation changes the initial characteristics of the test arrangement. Some authors decided to use more than one vertical actuator in order to maintain the force practically constant in the full length of the wall (Vermeltfoort *et al.*, 1993; Anthoine and Magonette, 1995; Kikuchi *et al.*, 1999; Manos *et al.*, 2001; Kikuchi *et al.*, 2003; Yoshimura *et al.*, 2003), see Figure 4.3a. In other cases, horizontal load is applied at the mid-height of the wall, which is equivalent to the application of an in-plane bending moment at the top of the wall (Chai and Yaw,1999; Yoshimura *et al.*, 2003), see Figure 4.3b.

This loading condition means that the wall does not behave as a cantilever wall since the top rotations are partially restrained. In both cases, the diagram of in-plane bending moment is modified, see Figure 4.4. If on one hand the use of the last test setup leads to the preponderance of the shear failure patterns, on the other hand it can lead to the increase on the complexity of the analysis of results as the restraint degree at the top of wall is unknown.

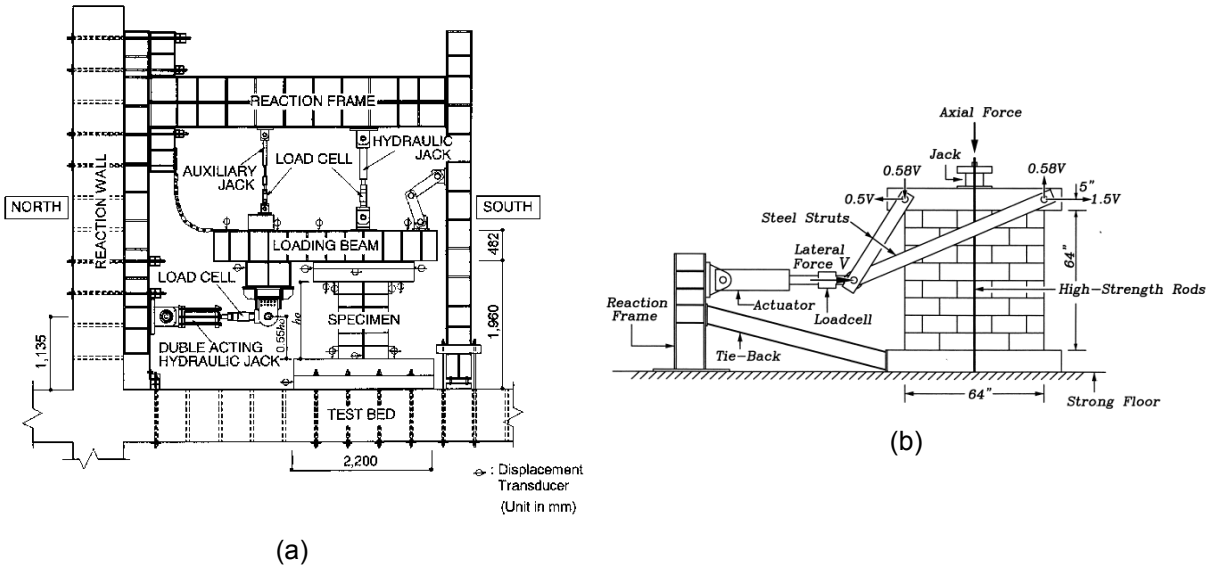

Figure 4.3 – Unusual test setup to shear-walls: (a) Yoshimura *et al.* (2003) (b) Chai and Yaw (1999).

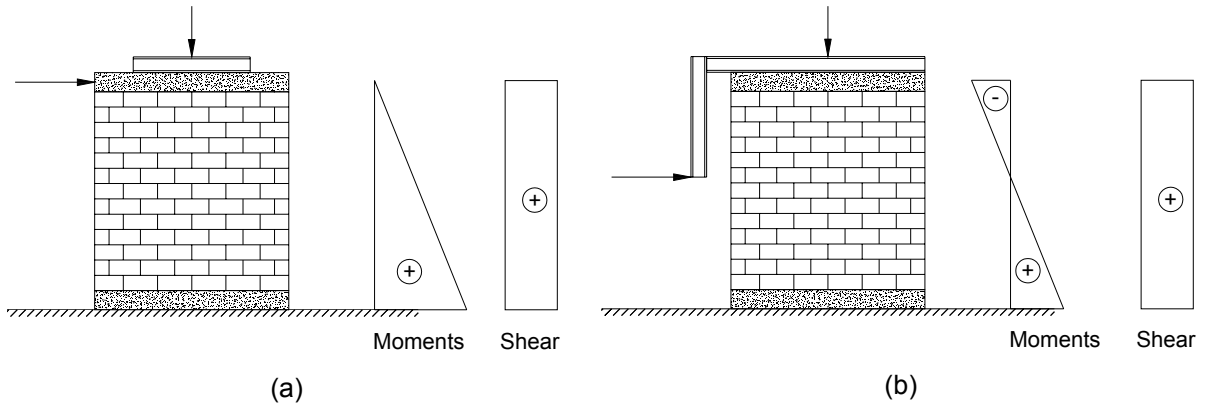

Figure 4.4 – Different boundary conditions of shear walls: (a) cantilever (b) non-cantilever.

This Chapter deals with the mechanical validation of reinforced masonry walls under cyclic in-plane lateral loading. The masonry walls tested correspond to different structural solutions as regards the masonry units, masonry bond pattern and positioning of the vertical and horizontal reinforcement, which can be used in the construction of reinforced masonry buildings in seismic zones. The major aim of the experimental research program is the mechanical validation of concrete block masonry walls and the evaluation of different variables like the masonry bond pattern, presence of vertical reinforcement, horizontal reinforcement ratio and vertical pre-compression on their the in-plane behaviour.

The experimental approach followed in the experimental investigation relies on the static cyclic tests, given the laboratory facilities at University of Minho. Thus, the Chapter is basically divided into three main parts: (a) the presentation of the masonry walls solution and experimental setup; (b) analysis of results based on the experimental data (failure modes and force-displacement diagrams) and evaluation of the seismic performance and, finally; (c)

the comparison between the experimental results in terms of lateral resistance and the values of lateral strength obtained from analytical models available in the literature.

4.2 Experimental Program

As aforementioned, the present experimental program based on static cyclic test on masonry walls aims at validating their mechanical behaviour under cyclic horizontal loads, simulating in a simplified manner the seismic loading. The evaluation of the experimental behaviour is essential when new solutions of masonry walls for masonry construction are envisaged. In this work, the mechanical characterization of the seismic behaviour of reinforced masonry walls is based on static cyclic tests carried out on cantilever panels with geometry that enables them to be tested at the laboratory of the Structural Group of University of Minho.

4.2.1 Masonry specimens

Due to the limited facilities of the laboratory in terms of actuators capacity and space, reduced scale (1:2) concrete masonry units, specifically developed for the research project, were used in the tested masonry panels. Two masonry bond patterns were adopted for the masonry panels built with concrete units of different shape, namely the traditional running bond pattern (B1) and a masonry bond pattern characterized by the existence of continuous reinforced vertical joints (B2), see Figure 4.5.

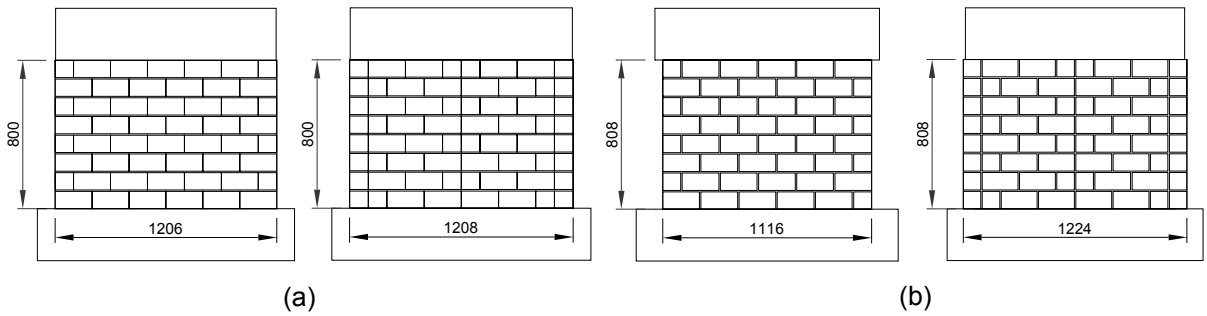

Figure 4.5 - Geometry of in-plane masonry walls with distinct masonry bond patterns: (a) masonry walls built with 3-cell masonry units and (b) masonry walls built with 2-cell masonry units.

Masonry bond pattern B1 corresponds to the traditional running masonry bond pattern (units were overlapped on consecutive courses). This bond patterns enables the positioning of the truss type vertical reinforcement in the frogged ends of the three cell

masonry units and in its internal hollow cell, see Figure 4.6a. In case of masonry walls built with two cell concrete blocks, the vertical reinforcement is positioned in one of the two hollow cells. In the second masonry bond pattern (B2), the vertical reinforcement is placed only in the vertical core defined by the frogged ends of the units in case of the three cell units are used, defining a continuous vertical joint, or in the typical vertical joints in case of masonry built with two cell blocks, see Figure 4.6b. The latter masonry bond pattern has advantages concerning the construction technology, as the masonry units can be laid after the placing of the reinforcement without any change on the traditional technology applied in the construction of unreinforced masonry walls. It is noted that the hollow cell, where the vertical reinforcement was positioned, should be completely filled at each course with the same mortar used to lay the masonry units, in order to avoid an additional material in the building construction. In both bond patterns the horizontal reinforcement is positioned in the bed joints.

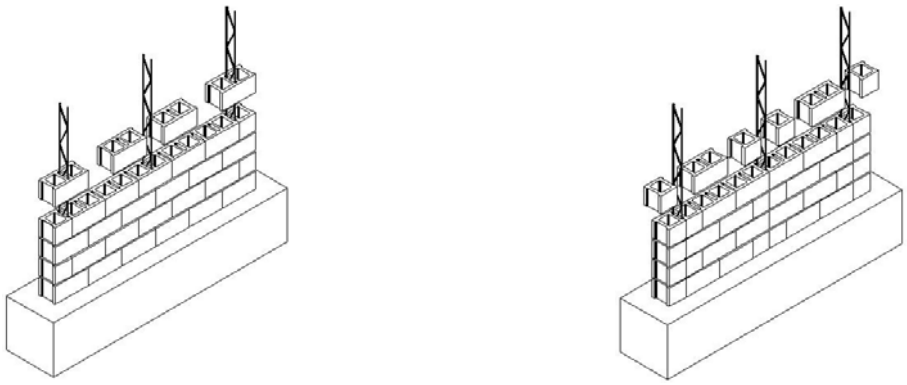

(a) (b)

Figure 4.6 - Masonry bond patterns: (a) running bond pattern, B1 (b) bond pattern with continuous vertical joint, B2.

Besides the different bond patterns other variables were analysed, namely the pre-compression level and the vertical and horizontal reinforcement ratios, see Table 4.1. The specimens are denoted by Nx-y-Bi-z, where *x* indicates the vertical pre-compression force in kN, *y* indicates the geometry of units (3C and 2C for three and two hollow cell units respectively), *i* is the adopted masonry bond pattern and *z* is an optional distinct characteristic concerning the truss type horizontal reinforcement and its ratio (ρ_h). This optional characteristic is UM, for unreinforced masonry, SH, for only horizontal reinforcement, PA, for lower horizontal reinforcement, and MA, for higher horizontal reinforcement. Variation of the horizontal reinforcement ratio is achieved using different diameters for the longitudinal bars (ϕ_h) and by decreasing the vertical spacing, see Table 4.1. In reinforced specimens truss type vertical reinforcements with longitudinal bars with

diameter (ϕ_v) of 5mm were used, to which a certain reinforcement ratio (ρ_v) is associated. The disposition of the horizontal and reinforcements in bed joints and in the vertical internal cores of the concrete units or in the vertical continuous joints is presented in Figure 4.7.

Table 4.1 – Details of shear walls.

Wall	Bond pattern	ϕ_v (mm)	ρ_v (%)	ϕ_h (mm)	ρ_h (%)	Reinf. type	Dimensions (mm)	Pre-compression (MPa)
N60-3C-B1-UM	B1	-	-	-	-	-	1206 x 800 x 100	0,56
N150-3C-B1	B1	5	0.098	4	0.094	R3	1206 x 800 x 100	1.30
N150-3C-B2	B2	5	0.098	4	0.094	R3	1206 x 800 x 100	1.30
N60-3C-B1	B1	5	0.098	4	0.094	R3	1206 x 800 x 100	0.56
N60-3C-B2	B2	5	0.098	4	0.094	R3	1208 x 800 x 100	0.56
N60-2C-B1	B1	5	0.106	4	0.093	R2	1116 x 808 x 94	0.56
N60-2C-B2	B2	5	0.096	4	0.093	R1	1224 x 808 x 94	0.56
N60-3C-B1-SH	B1	-	-	4	0.094	R5	1206 x 800 x 100	0.56
N60-3C-B1-PA	B1	5	0.098	3	0.053	R3	1206 x 800 x 100	0.56
N60-3C-B1-MA	B1	5	0.098	4	0.126	R4	1206 x 800 x 100	0.56

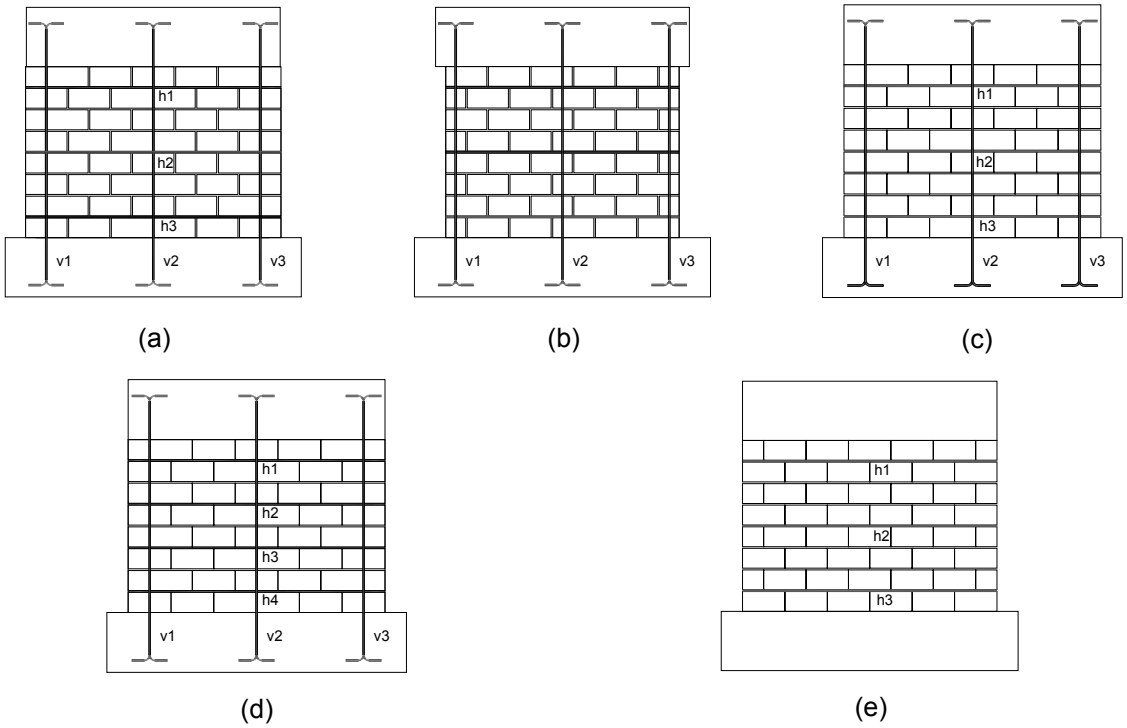

Figure 4.7 - Reinforcement of the in-plane masonry walls: (a) R1, (b) R2, (c) R3, (d) R4 and (e) R5.

In order to obtain lateral responses governed predominantly by shear failure, a height to length ratio lower than 1.0 was considered. The masonry panels built with 3C-units had 1206 mm length and 800 mm height resulting in a height to length ratio of 0.66. The masonry

panels built with 2C-units presented a height to length ratio of 0.66 in case of continuous vertical joint masonry bond pattern (B2 - 1224 mm length and 808 mm height) and a height to length ratio of 0.72 in case of running masonry bond pattern (B1 - 1116 mm length and 808 mm height). A smaller length was used in the last wall to ensure a symmetrical distribution of the vertical reinforcements. Reinforced concrete beams were placed at bottom (280 mm x 280 mm x 1400 mm) and at the top (280 mm x 280 mm x 1200 mm) of the walls in order to anchor the vertical reinforcements and to ensure an uniform distribution of the applied vertical and horizontal loads.

4.2.2 Construction of specimens

The construction of the specimens did not offered special difficulties but particular care had to be taken in the construction of the concrete beams in order to distribute the reinforcement and anchorage of the vertical reinforcements of the walls. The construction of the specimens was carried out in three main steps:

i. Construction of the bottom reinforced concrete beam, where the vertical reinforcements were anchored;
ii. Construction of the wall by an experienced mason;
iii. Construction of the top reinforced concrete beam.

Due to the reduced height of the walls and in order to avoid overlapping of vertical reinforcements, continuous reinforcements were considered. This procedure led to several difficulties in the positioning of these reinforcements. Vertical reinforcement had to be anchored to the stirrups of the concrete bottom beam. Auxiliary timber parts had to be used to guide the reinforcement and the first course of concrete units was placed provisionally to help in the guidance, see Figure 4.8.

Figure 4.8 – Construction of the bottom reinforced concrete beam.

The construction of the wall was made two or three days after casting of the reinforced concrete bottom beam. Firstly, a thin layer of mortar was laid on the base to level the first masonry course. Units were aligned and levelled in their respective position in the course. In case of walls built with 2C-units, all vertical joints were filled with mortar. Bed joints were built by placing mortar in all shells and webs of the concrete units. Even if this is not the procedure recommended by the supplier, mortar was laid in two layers, before and after the positioning of the horizontal reinforcements in order to ensure appropriate bond between reinforcements and masonry, see Figure 4.9.

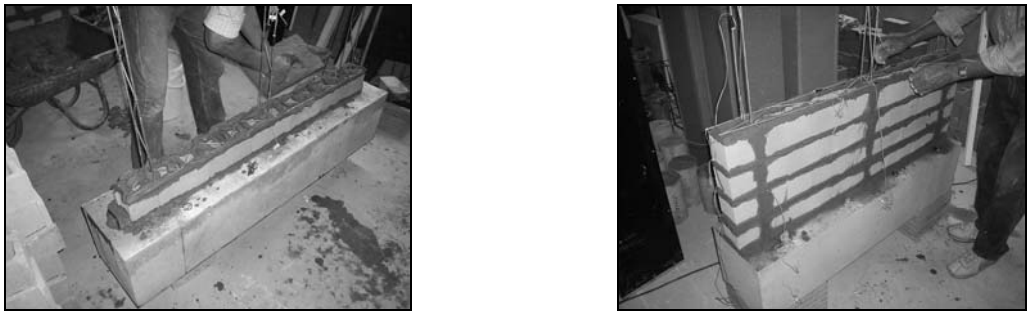

Figure 4.9 – Construction of the walls.

After one week from the construction of the wall, vertical reinforcements were bent and the internal cores of the concrete units of the last course were filled with polyurethane foam to enable the casting of the reinforced concrete top beam without filling the concrete units, see Figure 4.10. After this, the timber mould of the reinforced concrete top beam was positioned with auxiliary timber columns supports and the reinforced concrete top beam was cast, see Figure 4.11. During the construction of the walls, three specimens of mortar (40 mm x 40 mm x 160 mm) were cast aiming at controlling its quality through the compressive strength. The walls were cured in a laboratory environment (underground cave), with approximately relative air humidity of 80%. It should be stressed that the reduced scale of the masonry units required very small errors in the positioning of the vertical reinforcements due to the reduced internal core thickness.

Figure 4.10 – Bending of the vertical bars and filling of the last course of wall with polyurethane foam.

Figure 4.11 – Construction of the reinforced concrete top beam.

4.2.3 Test setup and procedures

The static cyclic tests of the masonry walls were performed following the typical test setup shown in Figure 4.12 used for masonry walls under combined vertical and horizontal load (Vasconcelos, 2005). In order to ensure proper curing of the specimens, the tests were carried out after 28 days from the construction. The mortar specimens were tested simultaneously to the walls.

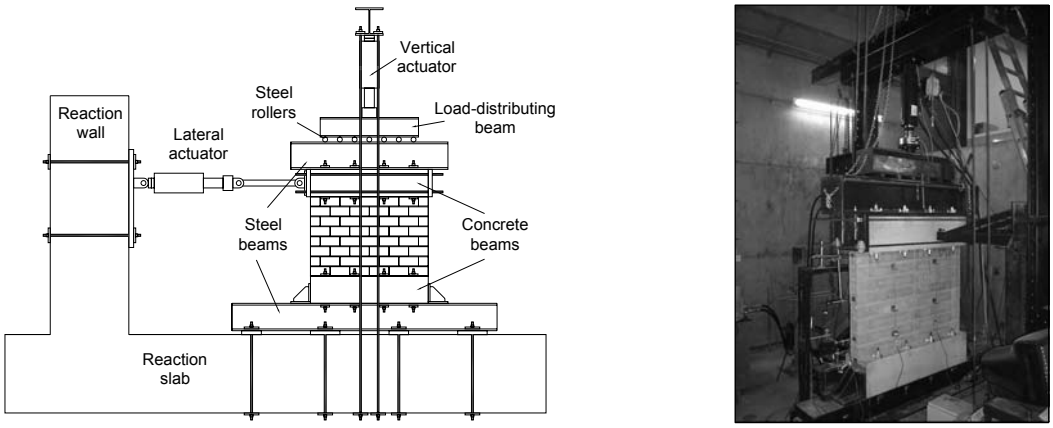

Figure 4.12 - Test setup for in-plane cyclic horizontal load.

The bottom reinforced concrete beam of the wall was fixed to a steel profile through eight steel bolts and two adjustable clamping angles to avoid uplift and slippage of the base. In turn, the steel profile was connected to the strong floor through steel rods. The axial load was applied by using a vertical actuator with vertical steel cables anchored at the strong floor. A stiff steel beam was used for the distribution of the vertical load and a set of steel rollers was placed to allow relative displacement of the wall with respect to the vertical actuator. A rubber layer was placed between the steel profile and the top of the concrete beam to enhance the distribution of stresses. The horizontal load was transferred to the wall

by means of two steel plates fixed at the top concrete beam by using an actuator with two hinges.

The test procedure was divided in two phases. Firstly, a vertical load of 100kN, corresponding approximately to 15% of the compressive strength, was applied at a rate of 0.25kN/s, in order to evaluate the elastic modulus of the wall. Afterwards, the wall was unloaded and reloaded up to a vertical stress equal to 1.30MPa or 0.56MPa depending on the selected level of pre-compression, which was kept constant during the test. The cyclic tests were carried out under displacement control at a rate of 70μm/s by means of an external LVDT connected to the horizontal actuator. The displacement-time history shown in Figure 4.13a was applied in the first test. This displacement-time history did not enable the record of intermediate damage state levels until the collapse of the wall. Thus, other displacement-time histories with lower displacement amplitude steps were performed as indicated in Figure 4.13b, c and d.

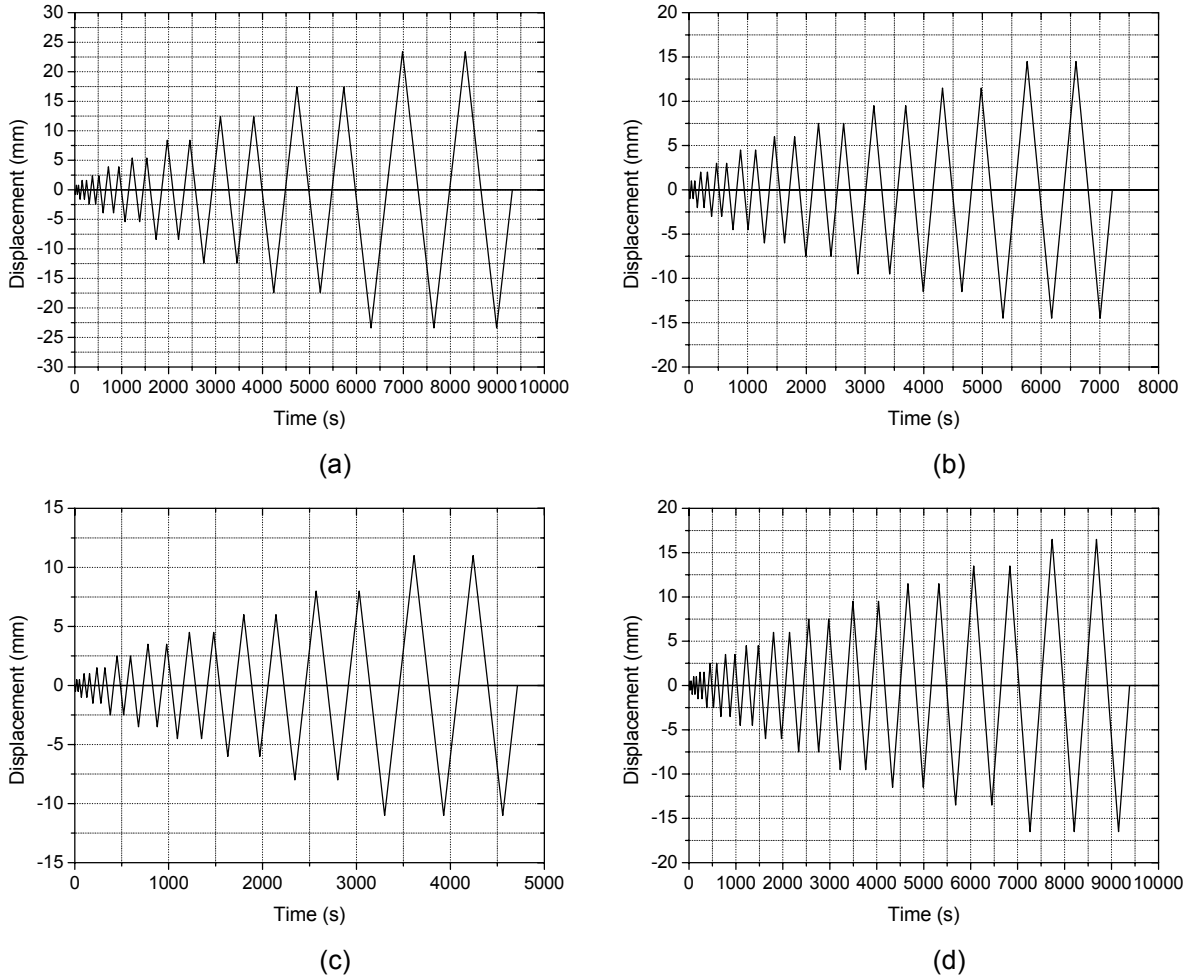

Figure 4.13 – Displacement-time histories: (a) N150-3C-B1, (b) N150-3C-B2 and N60-3C-B1, (c) N60-3C-B1-UM and (d) others walls

4.2.4 Instrumentation

The displacements of the wall under cyclic loading were measured by means of a set of LVDTs arranged according to what is indicated in Figure 4.14a. LVDTs 1, 2 and 3 measured the lateral deformation of the wall. LVDTs 4 and 5 measured the slippage and uplift of the base of the wall respectively, and LVDTs 6 and 7 measured the rotation of the top concrete beam. LVDTs 8 and 9 recorded the diagonal crack openings of the wall indicating also possible rigid body movements along the diagonal cracks. The vertical LVDTs 10, 11, 12 and 13 were fixed to both sides of the wall in order to obtain the elastic modulus of masonry during the first phase of the test as described previously and to evaluate the rotation of the wall during the application of the horizontal load. LVDTs 1, 2, 3, 4 and 5 were fixed to an external steel frame to ensure a fixed reference for measurements. In addition, strain-gauges were glued to the reinforcement at different locations, aiming at evaluating their contribution to the response of the wall, see Figure 4.14b. For specimens N150-3C-B1 and N150-3C-B2, strain gauges were also glued in the top and bottom horizontal reinforcements at the same positions as the ones indicated in Figure 4.14b.

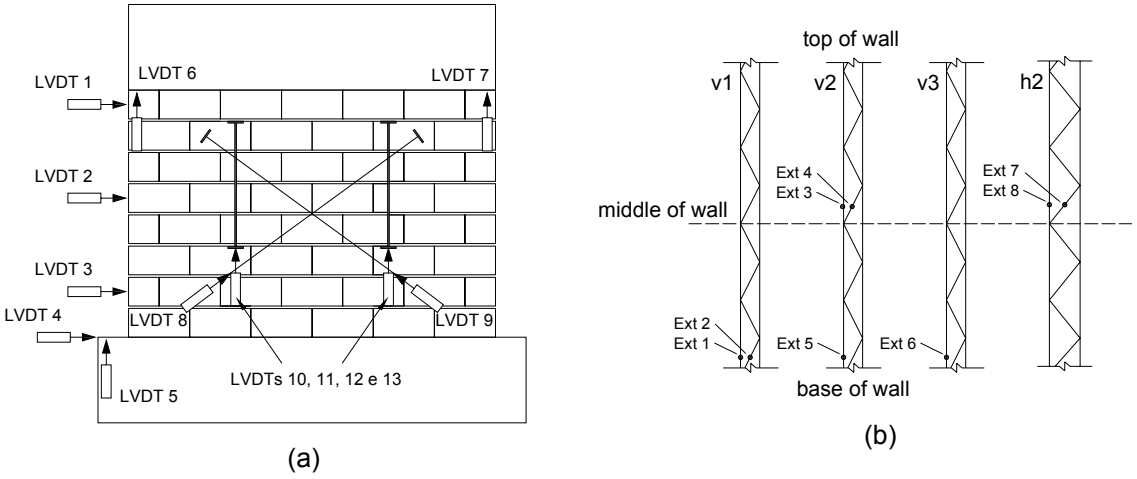

Figure 4.14 - Instrumentation of the in-plane walls: (a) positioning of LVDTs to measure the displacements of the walls: (b) strain-gauges for measurement of the deformation of reinforcements.

4.3 Results

Walls were tested after 28 days of age to ensure the complete curing of the mortar. Three specimens of the mortar used in the construction of each wall with 40mm x 40mm x 160mm were taken during the construction of the walls to be tested under compression and flexure according to EN 1015-11 (1999) to obtain the compressive strength (f_m) and flexural

strength (f_{fl}). These values were intended to be used for controlling the quality of the mortar production. A high variability was observed in these results and none of the mortar specimens reached the expected strength of 10 MPa, see Table 4.2. One reason for this was possibly the different method used for manufacturing the mortar in construction of masonry walls regarding the one that was used in the study of its characterization. Due to the high volumes of mortar produced during the construction of the walls, different equipment was needed to make the mixture leading to the difficulty of ensuring the same properties of the material.

The elastic modulus of the walls ($E_{a,\,exp}$) tested under combined load was also obtained based on the displacements measured by the vertical LVDTs (LVDTs 10, 11, 12 and 13) attached to central part of the wall in the first phase of loading, see Table 4.2. This result was important to control the quality of masonry material and to enable appropriate comparison of results among the different walls.

Table 4.2 – Summary of mortar characterization and elastic modulus of the shear walls.

Wall	f_m (MPa)	f_{fl} (MPa)	$E_{a,\,exp}$ (GPa)
N60-3C-B1-UM	3.58	1.21	5.10
N60-3C-B1-SH	5.16	1.55	9.79
N60-3C-B1	3.82	1.27	7.10
N60-3C-B2	7.11	1.87	8.00
N150-3C-B1	8.62	2.75	7.90
N150-3C-B2	7.72	2.63	8.10
N60-3C-B1-MA	4.82	1.49	13.93
N60-3C-B1-PA	5.16	1.53	9.30
N60-2C-B1	4.82	1.49	10.19
N60-2C-B2	8.84	2.25	7.40

This elastic modulus refers to the wall and not to the masonry material since in most specimens there were vertical reinforcements. The influence of reinforcements can be assessed by considering the elastic homogenization of the cross section based on the equilibrium of forces by Eq. 4.1 to Eq. 4.3 and on compatibility of deformations by Eq. 4.4.

$$N = F_a + F_s \qquad \text{Eq. 4.1}$$

$$\sigma_w A_w = \sigma_a A_a + \sigma_s A_s \qquad \text{Eq. 4.2}$$

$$E_w \varepsilon_w A_w = E_a \varepsilon_a A_a + E_s \varepsilon_s A_s \quad \text{Eq. 4.3}$$

$$\varepsilon_a = \varepsilon_s = \varepsilon_w \quad \& \quad A_a \cong A_w \quad \text{Eq. 4.4}$$

Where, N is the compression force, F_a is the internal force which acts in masonry, F_s is the internal force which act in reinforcement, σ_a is the stress in masonry, σ_s is the stress in reinforcement, σ_w is the stress in wall, A_a is the area of masonry, A_s is the area of reinforcement, A_w is the area of wall, E_a is the elastic modulus of masonry, E_s is the elastic modulus of reinforcement, E_w is the elastic modulus of wall, ε_m is the strain in masonry, ε_s is the strain in reinforcement and ε_w is the strain in wall.

From Eq. 4.5, it is observed that the increase on the stiffness of the walls due to the presence of reinforcements is very small (≈ 20 MPa) and can be negligible since the area of masonry is much higher than the area of reinforcement.

$$E_w = E_a + E_s \frac{A_s}{A_w} \quad \text{Eq. 4.5}$$

From the results displayed in Table 4.2 concerning elastic modulus of the walls, it is seen that the masonry walls had very similar elastic modulus with the exception of specimens N60-3C-B1-UM and N60-3C-B1-MA, which present a very low and very high value respectively. This result indicates that specimen N60-3C-B1-UM probably has a lower compressive strength when compared to the other walls. On the other hand, specimen N60-3C-B1-MA probably had the highest compressive strength compared with the other walls, based on the results of the compressive strength of mortar. These results should be taken in account in the analysis of the masonry walls.

4.3.1 Failure modes

In general, the masonry walls exhibit a mixed shear-flexure failure mode. The behaviour of the walls can be characterized by three critical phases corresponding to the opening of flexural cracking, opening of diagonal cracking and crushing of the bottom corners. Figure 4.15 illustrates the walls cracking patterns at the end of testing for all specimens.

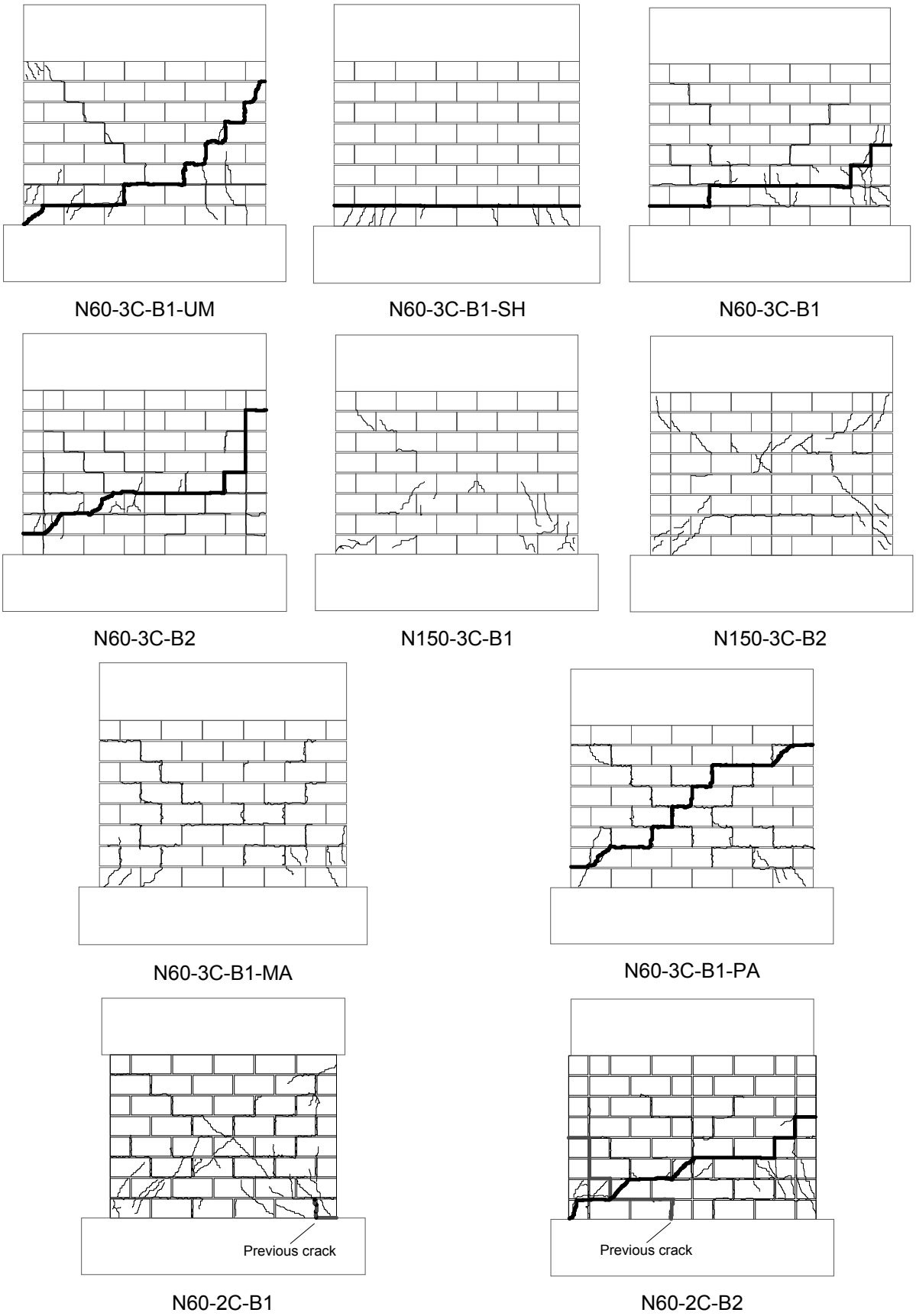

Figure 4.15 – Cracking patterns of masonry walls (thick lines indicate the plane of sliding).

Horizontal flexural cracks appeared at the first or second courses from the bottom, due to increasing tensile stresses resulting from the flexure of the wall. This damage basically depends on the tensile bond strength of the unit-mortar interface and its progress is detected by the vertical LVDTs positioned in the walls and the strain-gauge attached to the central vertical reinforcement at the bottom of the walls, which showed inversion of sign, see Figure 4.16. As the lateral displacement increased, the length of the horizontal cracks tended to increase leading to the shift of the neutral axis and thus to the reduction of the effective resistant shear length. At this stage, strains of the vertical reinforcement increased significantly, demonstrating its effective role in the bearing of the tensile stresses due to flexure by avoiding the uplift of the base of wall.

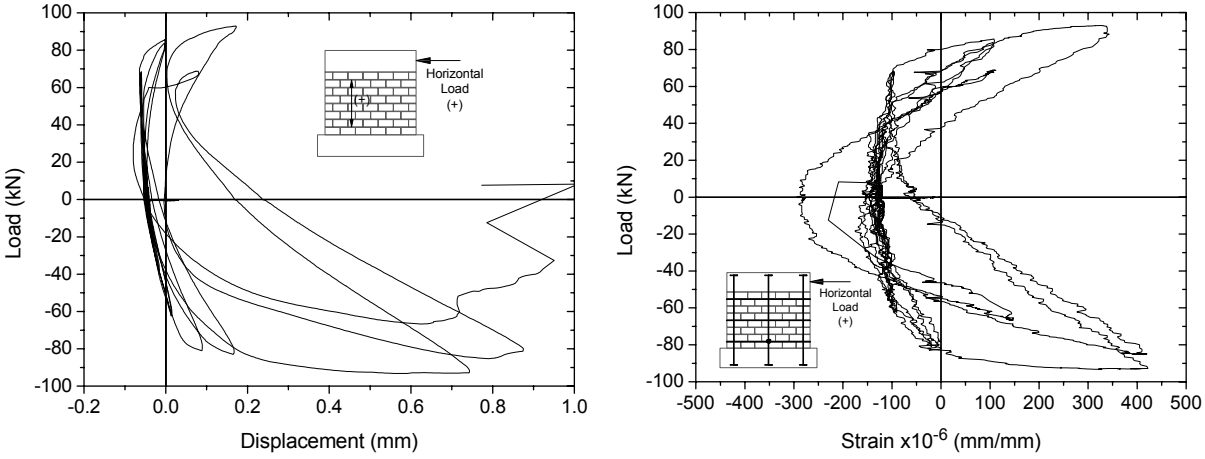

Figure 4.16 – Evaluation of the flexural behaviour of the wall specimen N150-3C-B1 through: (a) Vertical displacement measured by LVDT positioned in the middle of wall (LVDT 11) and (b) vertical strains measured in the central vertical reinforcement (Ext 5).

With the increase of the imposed lateral displacements, diagonal cracks developed mostly in mortar joints and could be clearly detected by the diagonal LVDTs, see Figure 4.17. The opening of the diagonal cracks and the development of horizontal tensile stresses was followed by increasing strains detected on the strain gauges attached at mid length of the horizontal reinforcement in the central region of the wall, see Figure 4.18. The additional strain gauges located in horizontal reinforcement at the top and bottom of specimens N150-3C-B1 and N150-3C-B2 measured no significant strains, meaning that only negligible strains developed in these bars. The diagonal crack width increased for successive imposed lateral displacements and the wall tended to separate itself in two parts. After the opening of diagonal crack, the stress transfer between both parts of the wall occurs mainly at the bottom corners and is improved by the horizontal and vertical reinforcements.

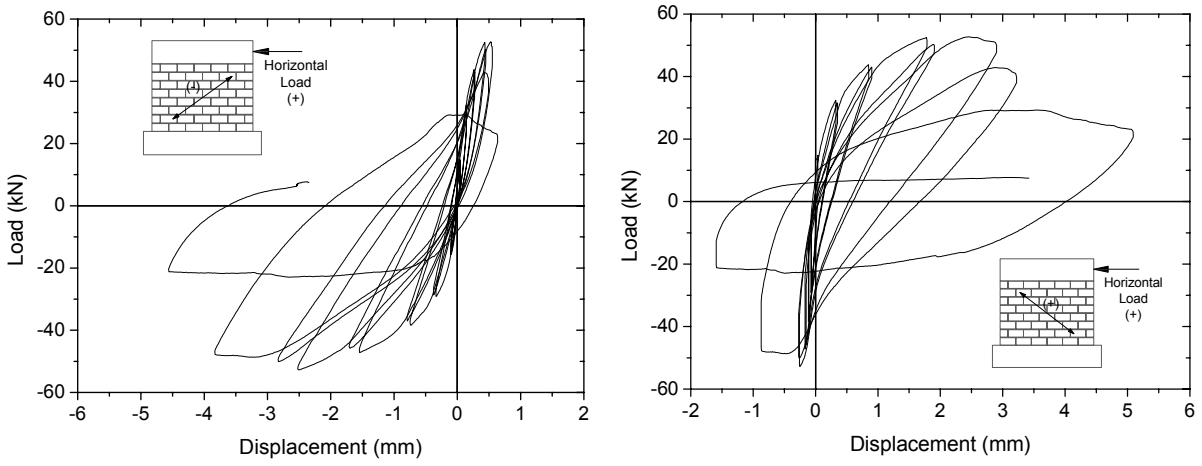

Figure 4.17 – Diagonal displacements in specimen N60-3C-B1: (a) LVDT 8 and (b) LVDT 9.

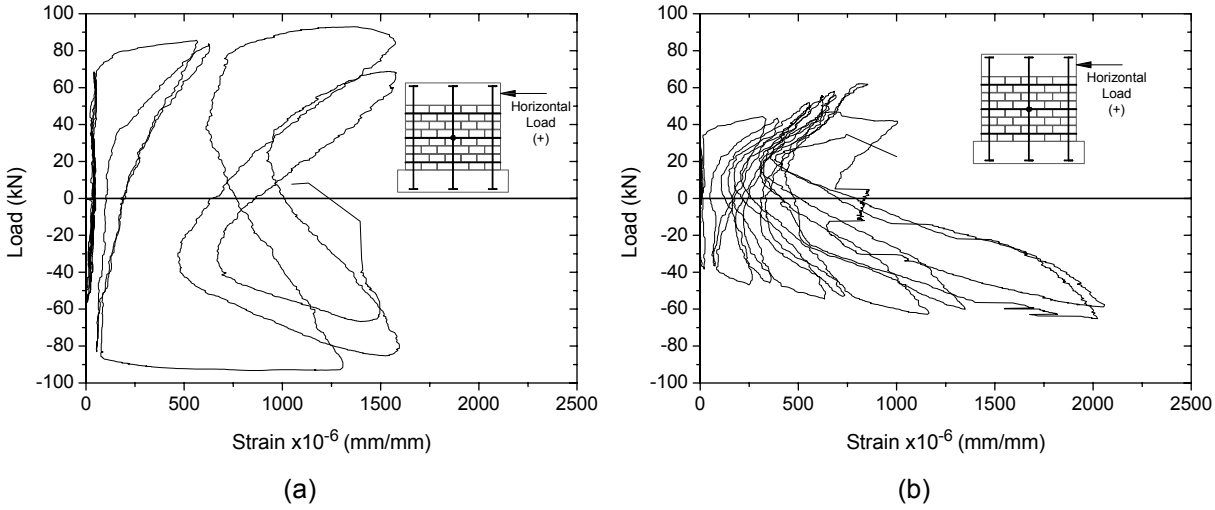

Figure 4.18 – Strains in horizontal reinforcements: (a) specimen N150-3C-B1 and (b) specimen N60-3C-B2.

The concentration of compressive stresses at the base of the wall promoted the toe crushing in all specimens. This failure mode is in part captured by the vertical displacements measured at the central region of the wall, as shown in Figure 4.19. In case of specimens N150-B1 and N150-B2, to which a higher level of vertical compression was applied, this damage was more remarkable and led to a sudden collapse of the walls. In the other specimens, toe crushing was followed by a slight sliding of the upper part of the wall over horizontal and/or diagonal cracks as indicated in Figure 4.20, where horizontal displacement measured by LVDT 3 placed at the basis of the wall is shown.

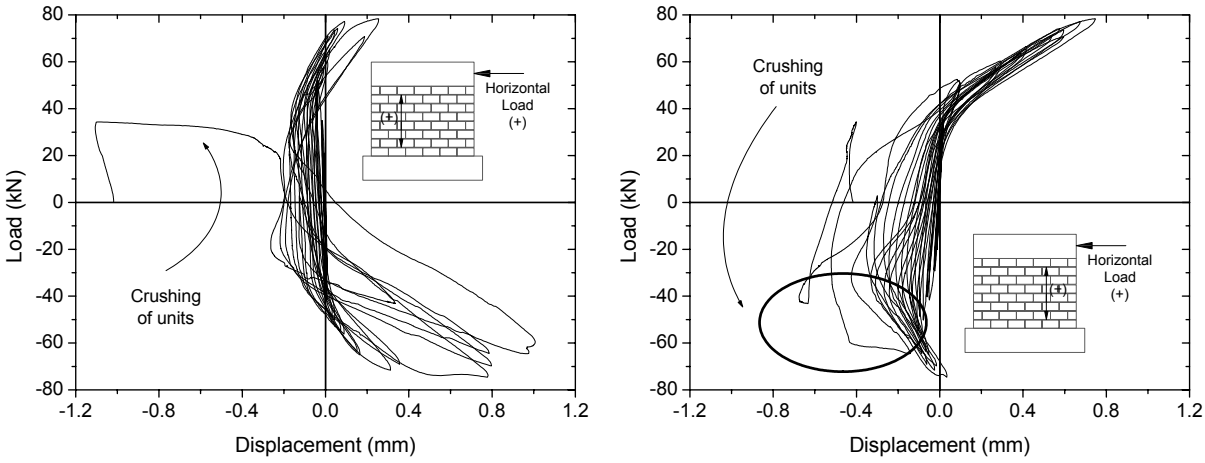

Figure 4.19 – Crushing of the units at the bottom corners of specimen N60-3C-B1-MA: (a) LVDT 10 and (b) LVDT 11.

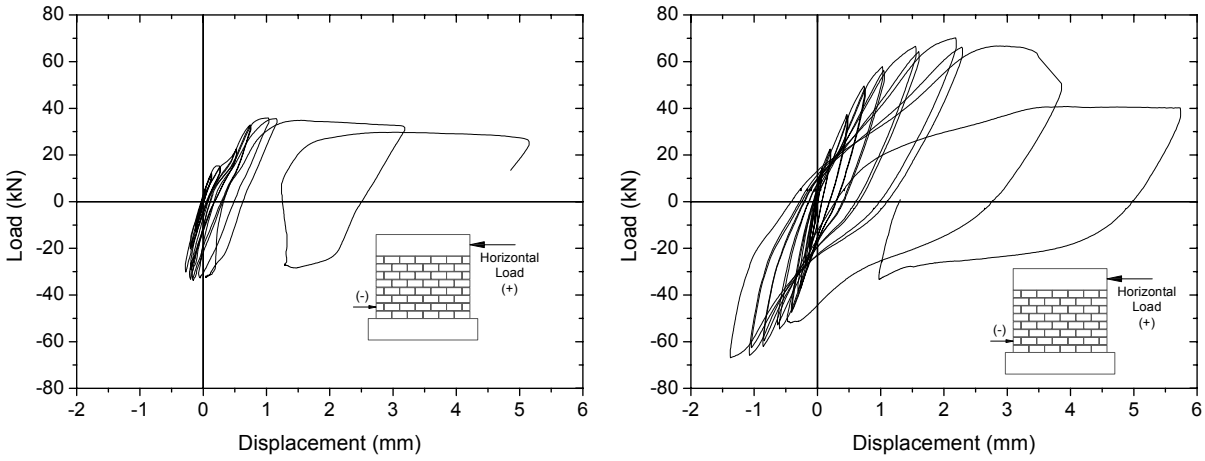

Figure 4.20 – Displacement measured in LVDT 3 (a) N60-3C-B1-UM and (b) N60-3C-B1-PA.

As explained before, in spite of the laboratory mortar production being controlled, a low compressive strength of mortar used in the construction of wall N60-3C-B1 was obtained. This possibly led also to the reduction on the unit-mortar interface adherence, which could be the reason for the detachment of the mortar at the bed joint located near the basis of the wall, see Figure 4.21a. According to Mohamad (2007) the low compressive strength of mortar can be related to a high porosity due to physical phenomenon of exudation. In all specimens, the high compression at the base led to buckling of the vertical reinforcements, see Figure 4.21b. In spite of the higher confinement of the vertical reinforcements in specimen N60-2C-B1, the buckling of vertical reinforcements is attributed to the higher aspect ratio, which increased the flexural effects, increasing also the

compressive stresses at the base of wall, similarly to what was pointed out by Kikuchi *et al.* (2003).

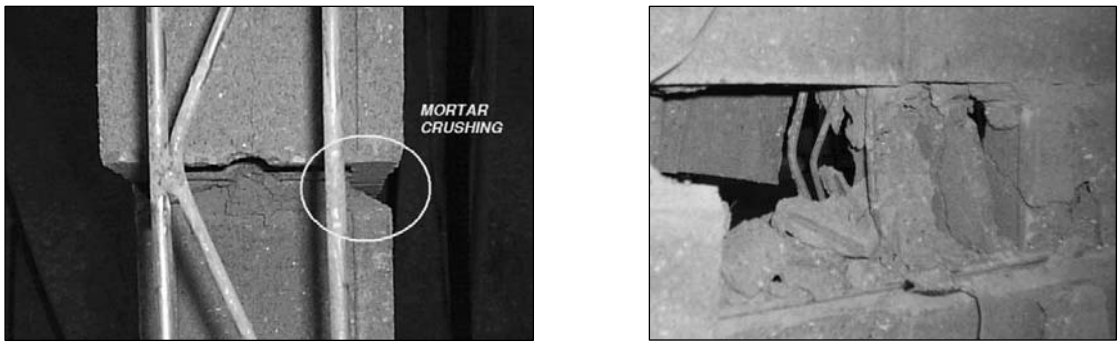

(a) (b)

Figure 4.21 – Characterization of damage: (a) crushing of the mortar in horizontal joint and (b) buckling of vertical reinforcement.

In general, the vertical reinforcement of wall did not reach the yield stress, essentially due to the premature toe crushing. In case of horizontal reinforcement, the yield stress was reached only in specimens N60-3C-B1-MA, N60-3C-B1-PA, N150-3C-B2 and N60-2C-B1 during the post-peak regime, leading to the breakage of the welding between longitudinal and diagonal bars, or to the breakage of longitudinal bars. Strain gauges located in horizontal reinforcement revealed some peak values after the walls have reached the maximum load, which was possibly due to imminent rupture of the bar, see Figure 4.22. It should be stressed that yielding occurs only after peak load and is associated to the increase of lateral displacements.

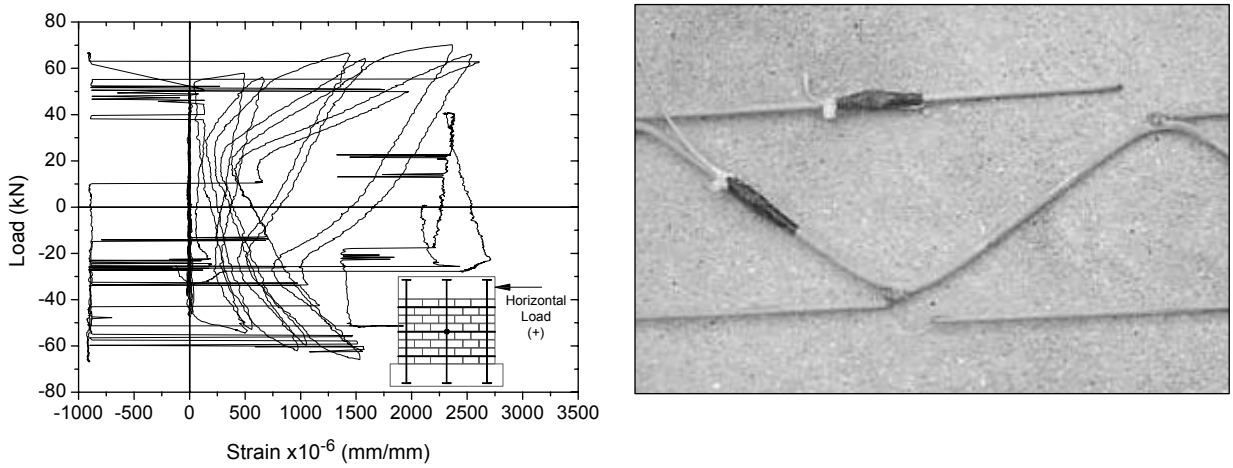

Figure 4.22 – Strains in horizontal reinforcement of specimen N60-3C-B1-PA.

Horizontal reinforcement had a significant effect on cracking, which can be clearly observed by comparing the crack pattern of unreinforced wall (N60-3C-B1-UM) and wall

reinforced at bed joints (N60-3C-B1-SH). In specimen N60-3C-B1-SH, diagonal cracks could not be observed as the horizontal reinforcements prevented their opening. This is also confirmed by the increasing strains measured in the strain gauge attached to the horizontal reinforcement located at the middle of the wall, see Figure 4.23.

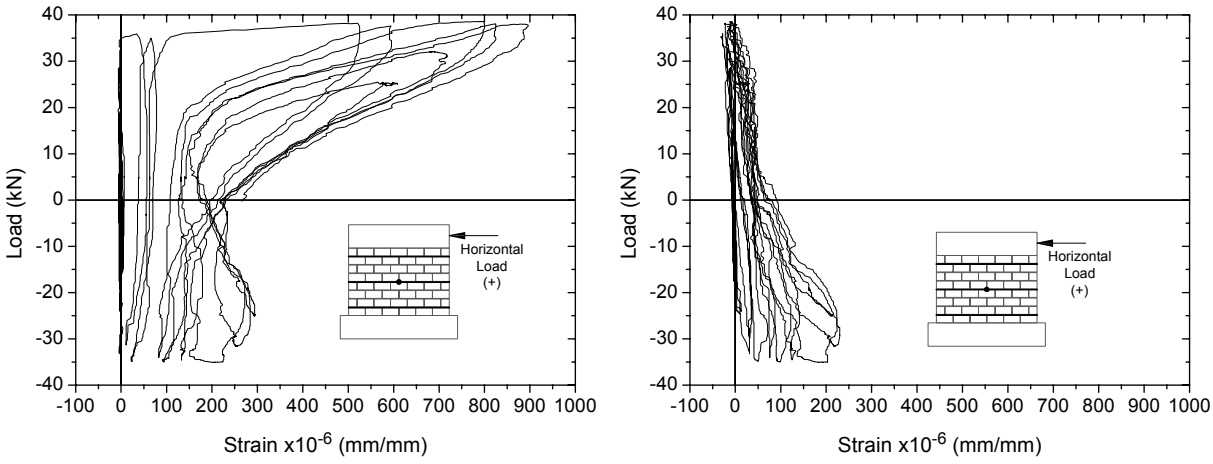

Figure 4.23 – Strains in horizontal reinforcement of specimen N60-3C-B1-SH: (a) longitudinal bar (Ext 7) and (b) diagonal bar (Ext 8).

However, the horizontal reinforcement of wall N60-3C-B1-SH shows the lowest stress level with respect to the yielding strength (about 25%). This is due to the predominant crack pattern developed in this wall, composed by a single horizontal flexural crack located at first course from the bottom, over which some level of sliding develops at the end of the test. This behaviour is confirmed by comparing rotation (θ_i) of the wall measured by vertical LVDTs attached to the wall (LVDTs 10, 11, 12 and 13) and the top global rotation calculated according to Eq. A.1, Eq. 4.7 respectively:

$$\theta_i = \frac{\left(\frac{\delta_{LVDT10} + \delta_{LVDT11}}{2}\right) - \left(\frac{\delta_{LVDT12} + \delta_{LVDT13}}{2}\right)}{l_1} \quad \text{Eq. 4.6}$$

$$\theta_t = \frac{\delta_{LVDT6} - \delta_{LVDT7}}{l_2} \quad \text{Eq. 4.7}$$

Where, δ is the displacement measured by the respective LVDT, l_1 is the distance between the vertical LVDTs attached to the wall and l_2 is the length of wall.

From Figure 4.24 it is observed that the internal rotation (θi) of the wall is negligible when compared with the global rotation (θ_t), which reveals the absence of internal cracking in

the wall. The sliding of the wall occurs after the crushing of the concrete units at the bottom toes due to the high compressive stresses. It should be noticed that the wide horizontal crack occurred due the absence of vertical reinforcement, which in the other walls prevented the progression of the horizontal flexural cracks.

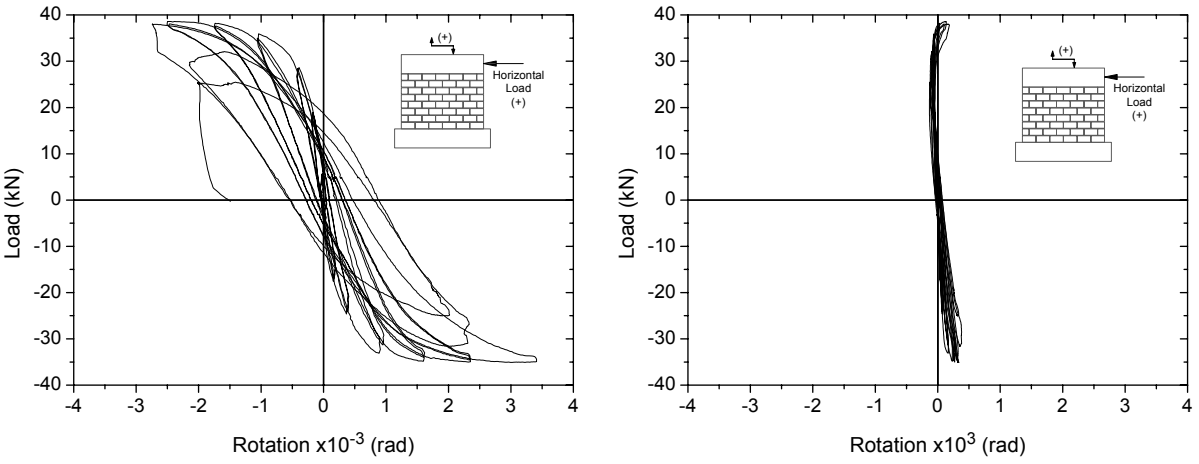

(a) (b)

Figure 4.24 – Rotations of specimen N60-3C-B1-SH: (a) top of the wall (LVDTs 6 and 7) and (b) internal rotation of the wall (LVDTs 10, 11, 12 and 13).

Therefore, the contribution of the horizontal reinforcement to the global lateral response of the walls is low, which is also confirmed by the maximum efficiency of the horizontal reinforcement indicated in Figure 4.25.

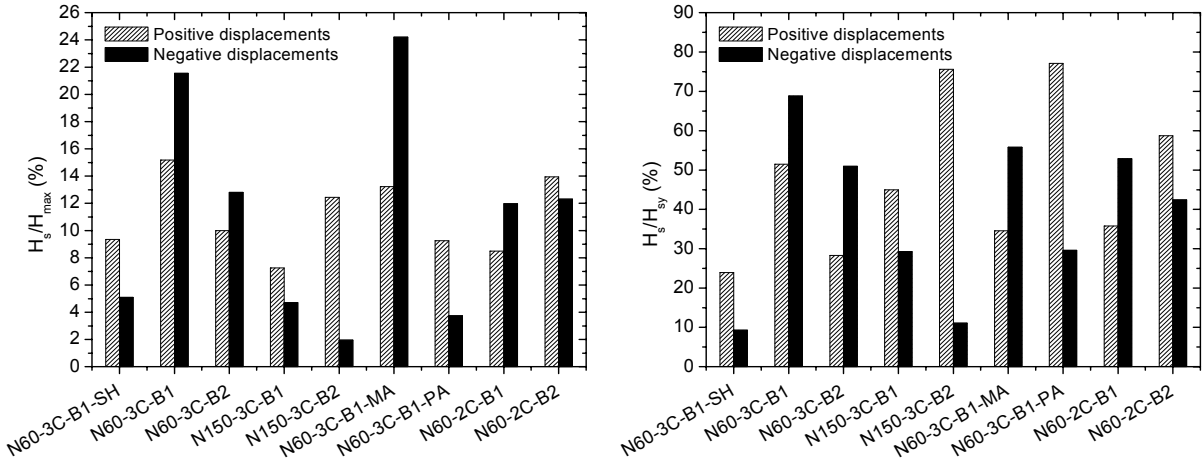

(a) (b)

Figure 4.25 – Efficiency of horizontal reinforcement: (a) percentage of the horizontal lateral load resisted by the horizontal reinforcements and (b) percentage of the yielding force (H_{sy}) resisted by the horizontal reinforcements.

Here, the efficiency of the horizontal reinforcement in the global lateral response of the wall was calculated through two ratios: the ratio between the force carried out by the reinforcement, H_s, and the maximum lateral force of the wall, H_{max}, and the ratio between the force carried out by the reinforcement, H_s, and the yield force of the reinforcements, H_{sy}. The force in the reinforcement is calculated based on the strains measured in the strain gauges. It is observed that apart from walls N60-3C-B1 and N60-3C-B1-MA, whose reinforcements exhibited an efficiency of about 23%, all other walls present efficiency lower than 13%.

After the wall reaches the maximum horizontal load, the strains in horizontal reinforcements continue to increase at the same rate. For specimens that exhibited sliding after crushing, strains in horizontal reinforcements gradually decrease during post-peak, see Figure 4.26.

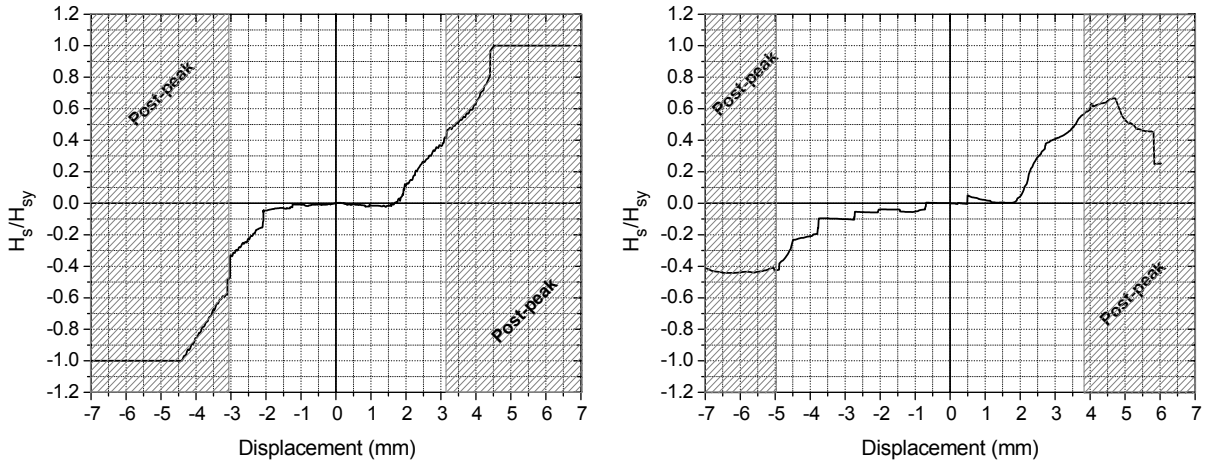

Figure 4.26 – Efficiency of horizontal reinforcement: (a) N150-3C-B2 and (b) N60-2C-B2.

4.3.2 Force *vs.* Displacement diagrams

Force vs. displacement diagrams provides the global behaviour of the masonry walls. Thus, in this section a general discussion about the behaviour of the tested masonry walls will be presented based on the analysis of hysteresis diagrams.

Apart from the unreinforced specimens and the walls built with 2C-units, all the remaining tested masonry walls exhibited a symmetrical force *vs.* displacement diagram with respect to positive and negative displacements. Unreinforced specimens showed a decrease in lateral stiffness due to the premature flexural cracking for positive displacements, as noted in Figure 4.27a. In case of masonry walls built with 2C-units, the asymmetry of the hysteresis diagrams is attributed to cracks developed before the beginning of the test and that were located at the interface between the masonry walls and the concrete beams due to the

unlevelling of the concrete beam. These small cracks opened when the ties used to attach the base of the wall to the reaction slab were tensioned and were the reason for which the masonry walls reached lower lateral resistance in one of the directions.

Specimens N60-3C-B1-UM and N60-3C-B1-SH exhibited a very similar behaviour, see Figure 4.27. Unreinforced wall showed a lower lateral stiffness, which seems to be associated to the low compressive strength of the mortar, as already aforementioned. The sliding mechanism of specimen N60-3C-B1-SH in the end of the test led to a higher ultimate deformation and high energy dissipation.

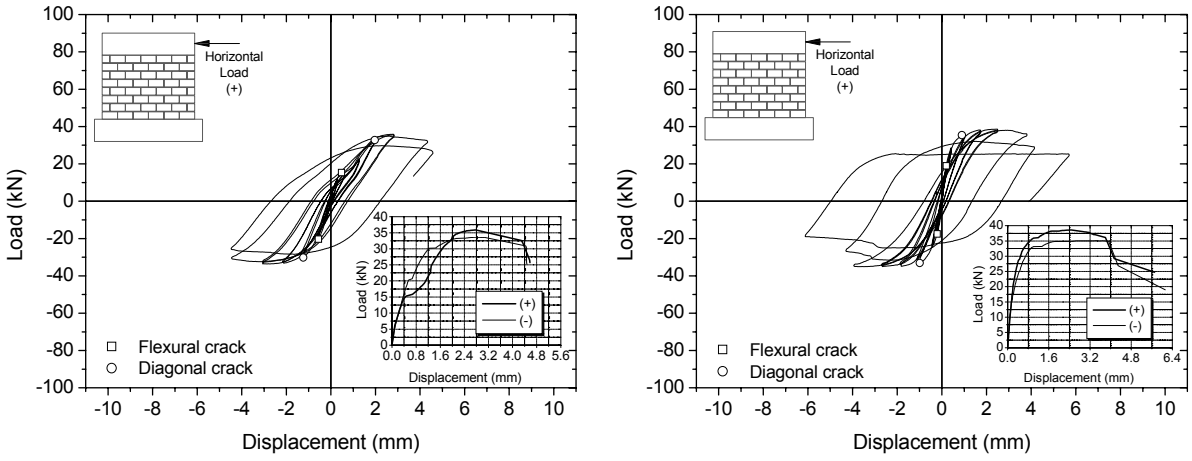

Figure 4.27 – Force *vs.* displacement diagrams: (a) N60-3C-B1-UM and (b) N60-3C-B1-SH.

Specimens with vertical and horizontal reinforcements showed an increase in lateral strength and in deformation capacity, see Figure 4.28. It is observed that masonry bond patterns (B1 and B2) influences only in a minor extent the behaviour of concrete block masonry walls. Specimens N60-3C-B1 and N60-3C-B2 exhibited a similar behaviour, even if a lower lateral strength is achieved by N60-3C-B1 due to weaker mortar used. In case of walls submitted to higher level of pre-compression, no significant differences between masonry bond patterns are detected. An interesting result revealed by the force *vs.* displacement diagrams consists of the higher lateral stiffness of walls with masonry bond pattern B2, in spite of the presence of a continuum vertical joint along the height of the wall. The walls with a higher axial load showed an enhanced lateral strength and stiffness, similarly to pointed out by other researchers (Shing *et al.*, 1989; Zhuge *et al.*, 1996, Vasconcelos, 2005), see Figure 4.28 (c) and (d). Cracking developed for higher values of lateral load in these walls, when compared to the other specimens. This behaviour was also observed by Voon and Ingham (2006), and can be explained by the higher principal tensile stresses needed to originate the collapse of the walls. The higher compressive principal

stresses lead also to the increase of the loads corresponding to flexural and diagonal cracking. However, walls with high pre-compression exhibited a more brittle behaviour with low energy dissipation and deformation capacity.

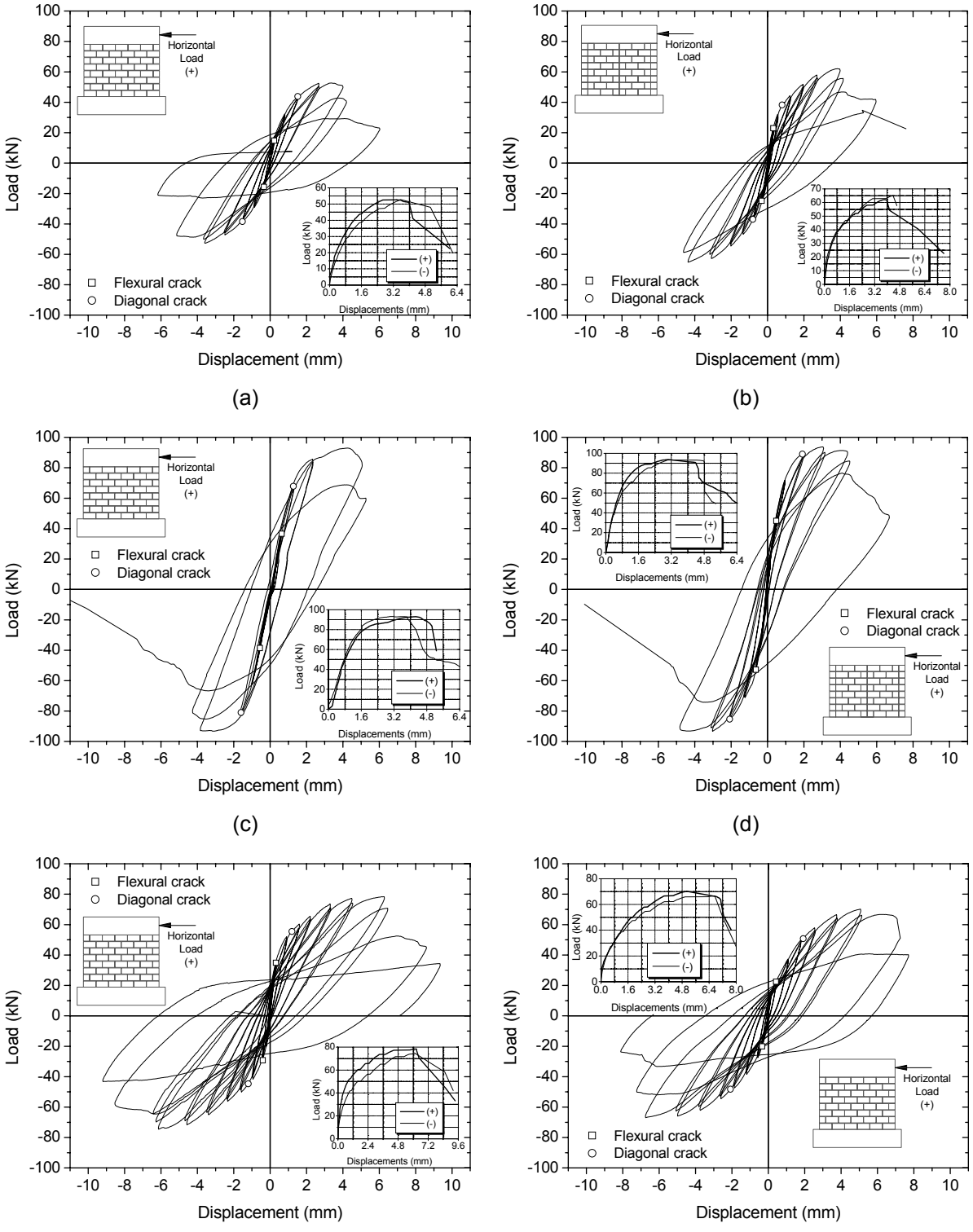

Figure 4.28 – Force *vs.* displacement diagrams: (a) N60-3C-B1, (b) N60-3C-B2, (c) N150-3C-B1, (d) N150-3C-B2, (e) N60-3C-B1-MA and (f) N60-3C-B1-PA.

As observed by Shing *et al.* (1989) an Schultz *et al.* (1998), the influence of the amount of horizontal reinforcement on the lateral response of the concrete block masonry walls appears to be inconsistent, see Figure 4.28 (a), (e) and (f). The wall with the smaller amount of horizontal reinforcement (N60-3C-B1) presented higher lateral strength than the specimen with the intermediate amount of horizontal reinforcement (N60-3C-B1), even if the wall with the maximum horizontal reinforcement ratio presents clearly a higher lateral strength. Thus, it is not possible to state clearly that an increase in the horizontal reinforcement ratio ensures an increase on lateral strength of the walls. However, it is clear that the amount of horizontal reinforcement can significantly improve the post-cracked hysteretic behaviour. The higher horizontal reinforcement ratio used in specimen N60-3C-B1-MA together with the low spacing resulted in a gradual degradation of lateral strength and stiffness after the peak load was reached, as well as on a higher deformation capacity. According to Voon and Ingham (2006), reduced lower spacing of horizontal reinforcement enables the distribution of stresses throughout the wall diagonals after the initiation of the shear cracking. The diagonal crack localization gives place to a more distributed diagonal cracking resulting on higher energy dissipation and on a more ductile behaviour.

As aforementioned, the specimens built with 2C-units showed a non-symmetrical force *vs.* displacement diagrams due to previous cracks developed at the basis of walls during the connection of the concrete beam to the reaction slab. However, this previous and much localized damage influenced only one direction of loading. In spite of the wall with masonry bond pattern B1 having a lower aspect ratio (lower length), it exhibited higher lateral strength than specimens with masonry bond pattern B2, see Figure 4.29. This behaviour is the result of the filling of one of the two hollow cells of the 2C-units with mortar when vertical reinforcement is considered. In this case, the masonry is partially filled with mortar meaning that the ratio of filling is considerably higher than the filling ratio of the 3C-units. This difference leads to higher differences between both masonry bond patterns (N60-2C-B1 and N60-2C-B2) in terms of lateral strength, energy dissipation and ultimate deformation capacity. Comparing specimens N60-2C-B2 and N60-3C-B2, a very similar behaviour can be observed in terms of lateral strength and deformation capacity even if specimens built with 2C-units had lower thickness and all vertical joints filled. As the mechanical properties of 2C-units and 3C-units were very close, the filling of vertical joints maybe improves the lateral behaviour of walls. However, more tests should be carried out in order to clarify this issue.

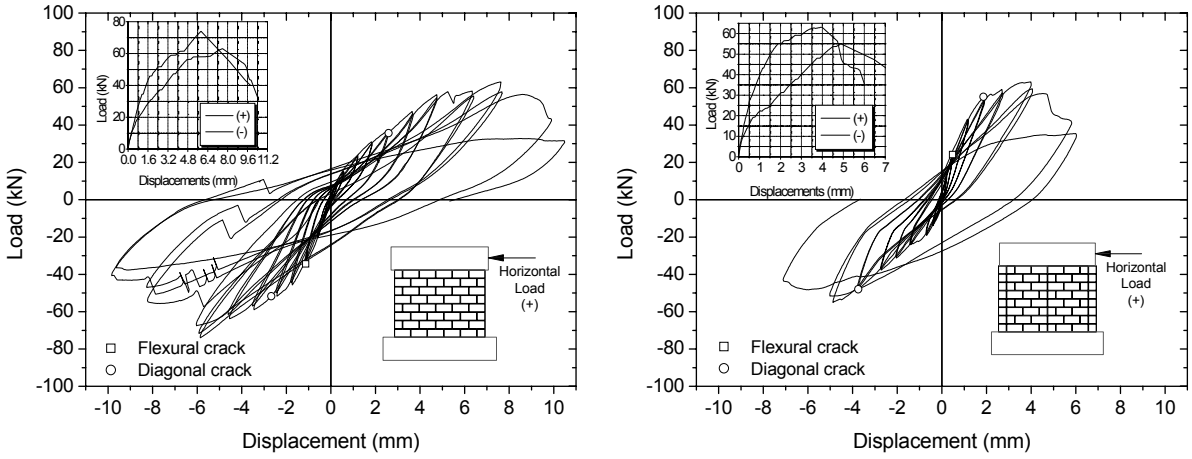

Figure 4.29 – Force *vs.* displacement diagrams: (a) N60-2C-B1 and (b) N60-2C-B2.

4.3.3 Cyclic response of masonry walls

Stiffness degradation and energy dissipation are important parameters within the scope of modelling the cyclic response of masonry walls, as well as of the evaluation of their seismic performance. Unless rocking mechanism prevails in the response of walls submitted to in-plane cyclic loading, it is usual that stiffness degradation occurs during reversed cyclic load. As horizontal forces are distributed among the walls based on their stiffness, it is important to predict the stiffness degradation at the ultimate limit state. Since the degree of stiffness degradation is dependent on the damage of the wall, secant stiffness ($K_{s,i}$) of each cycle was calculated aiming at evaluating the evolution of damage during loading. The secant stiffness at each loading cycle $K_{s,i}$ was calculated according to Eq. 4.8. Figure 4.30a exemplifies the calculation of the secant stiffness. The capacity of the walls to dissipate energy is also an important parameter in the analysis of their cyclic response. This capacity was evaluated through the coefficient of equivalent viscous damping (ξ), calculated as the ratio between the dissipated energy (E_{diss}) and the total energy transferred to the system during the loading process and designated by input potential energy (E_{inp}), see Figure 4.30b.

$$K_{s,i} = \frac{H_{\max,i}}{d_{H\max,i}} \qquad \text{Eq. 4.8}$$

Where, $H_{max,j}$ and $d_{Hmax,i}$ are the maximum load and the maximum displacement at *i* cycle respectively.

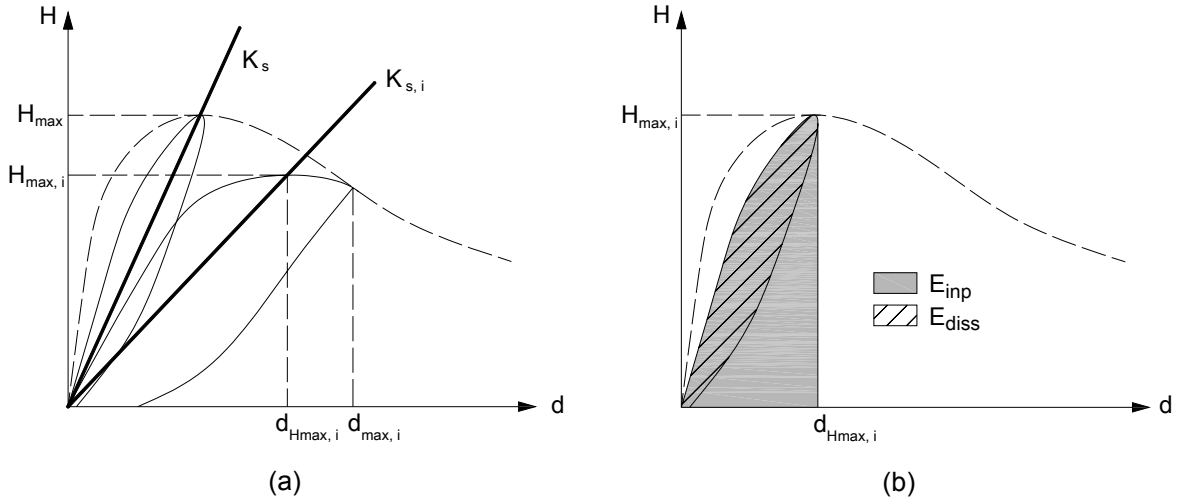

Figure 4.30 – Calculation of the parameters for the evaluation of the in-plane performance: (a) secant stiffness and (b) dissipated and input potential energy.

According to Figure 4.31, where the evolution of the stiffness degradation is shown, it is observed that all walls exhibit decreasing secant stiffness as the lateral displacement increases, following a power function.

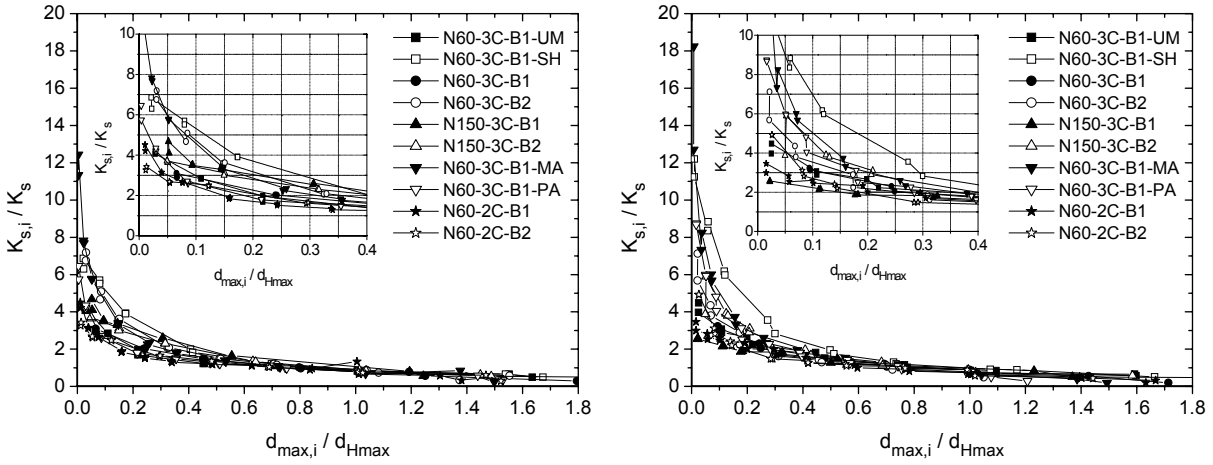

Figure 4.31 – Degradation of stiffness: (a) positive part of diagram and (b) negative part of diagram.

Up to 40 % of the lateral displacement corresponding to the lateral maximum load, it is possible to recognize some differences among the walls. Walls submitted to the highest level of pre-compression and the unreinforced masonry wall presents the lowest stiffness degradation. On the other hand, the walls with horizontal reinforcement, particularly N60-3C-B1-MA and N60-3C-B1-SH, presented the highest stiffness degradation, which, in the latter case, is associated to a sliding failure mechanism. Tomaževič (1999) also pointed out that

stiffness degradation of masonry walls under in-plane cyclic loading follows a power function according to Eq. 4.9:

$$\left(\frac{K_{s,i}}{K_e}\right) = \alpha\left(\frac{d_{H\max,i}}{d_{H\max}}\right)^{\beta} . \qquad \text{Eq. 4.9}$$

The stiffness degradation index is defined as the ratio between the secant stiffness in each cycle $K_{s,i}$ to the elastic stiffness, K_e, as a function of two parameters of degradation α and β and of the relation between the maximum displacements at each cycle, $d_{Hmax,\,i}$, and maximum displacement corresponding to the peak lateral load, d_{Hmax}. A simpler definition is possible if the secant stiffness degradation index is calculated as the ratio between the secant stiffness at each cycle, $K_{s,i}$, and the secant stiffness corresponding to the maximum lateral load, K_s, as only one damage parameter is needed for adjustment, γ:

$$\left(\frac{K_{s,i}}{K_s}\right) = \left(\frac{d_{\max,i}}{d_{H\max}}\right)^{\gamma} \qquad \text{Eq. 4.10}$$

The parameter γ was obtained by regression analysis of experimental curves and in general ranged from 0.41 (N60-3C-B1-UM) to 0.56 (N60-3C-B1-SH), except for specimen N150-3C-B1 and specimens built with 2C-units, where the value of approximately 0.30 indicates low stiffness degradation.

Apart from the specimens with the highest pre-compression level, which practically did not dissipate energy in the first cycles, the other masonry walls exhibited a very similar behaviour in terms of energy dissipation, as observed in Figure 4.32 and Figure 4.33. The coefficient of equivalent viscous damping (ξ) ranged from 40 % to 50 % up to the ultimate load. It should be stressed that a moderate increase of energy dissipation occurs after a displacement of about 50% of the lateral peak load displacement, indicating that moderate damage occurs before peak load is reached. It is immediately after the ultimate load that energy dissipation increases considerably. In particular, specimens N60-3C-B1-SH and N60-3C-B1-PA presented a sudden increase of the viscous damping, ξ, which is associated to the high dissipation of energy due to the tendency of wall N60-3C-B1-SH to slide along the horizontal crack and due to the yielding of the horizontal reinforcement in wall N60-3C-B1-PA.

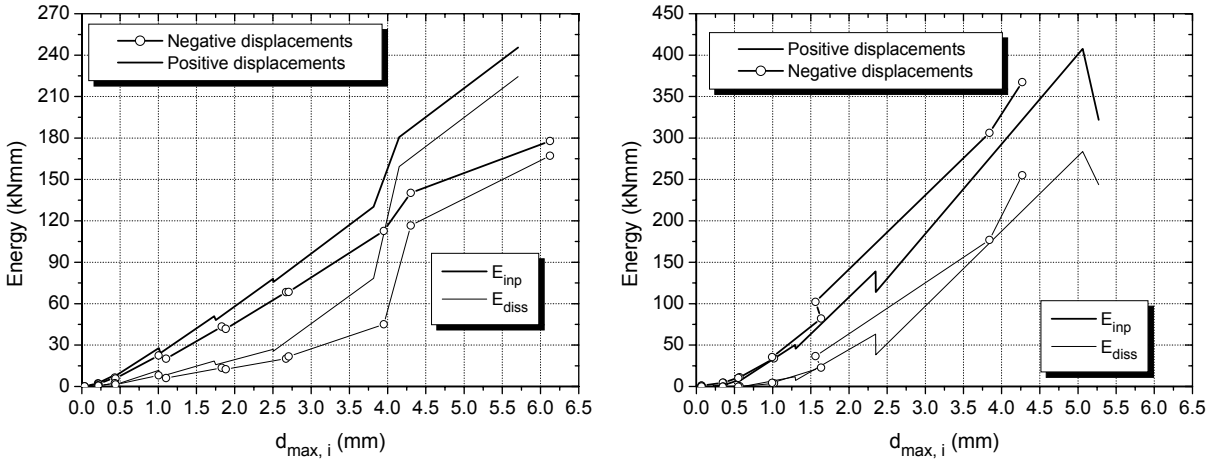

Figure 4.32 – Input and dissipated energy: (a) N60-3C-B1-SH and (b) N150-3C-B1.

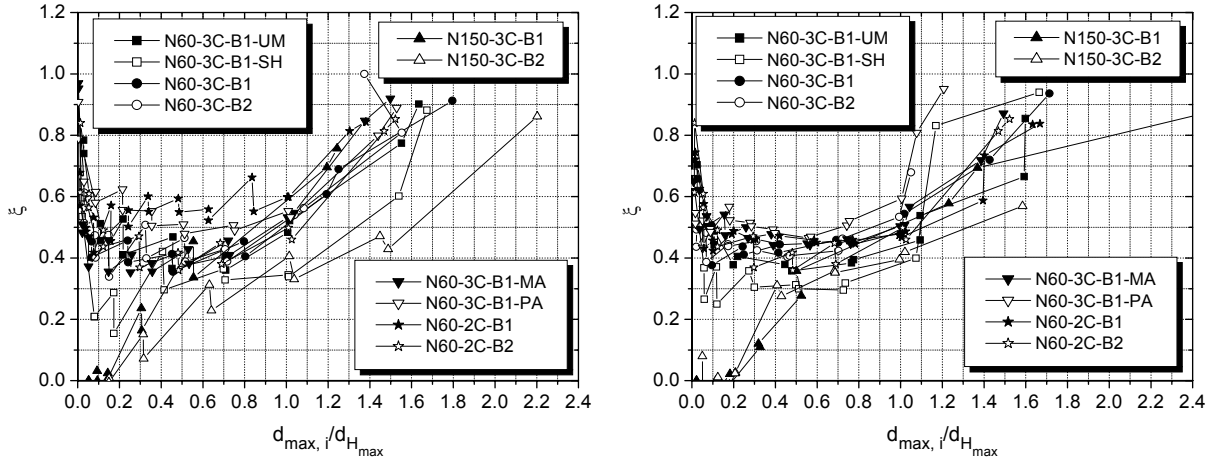

Figure 4.33 – Coefficient of equivalent viscous damping (ξ): (a) positive part of diagram and (b) negative part of diagram.

4.3.4 Evaluation of the seismic performance of masonry walls

Earthquakes are responsible for cyclic horizontal actions, often leading to large bending and shear stresses in structural walls, which exceed the elastic range of masonry materials. In addition to strength, structures subjected to seismic actions should exhibit proper deformation capacity and energy dissipation so that brittle failure is avoided.

In terms of damage evolution and deformation state the behaviour of shear walls is composed by four limit states corresponding to the flexural cracking identified by the point (H_{fc}, d_{fc}), diagonal cracking associated to the point (H_{dc}, d_{fc}), ultimate load corresponding to point (H_{max}, d_{Hmax}) and maximum displacement identified by the point (H_{dmax}, d_{max}), as shown

in Figure 4.34. Table 4.3 presents a summary of the values of the lateral load and corresponding lateral displacement identifying the four distinct limit states.

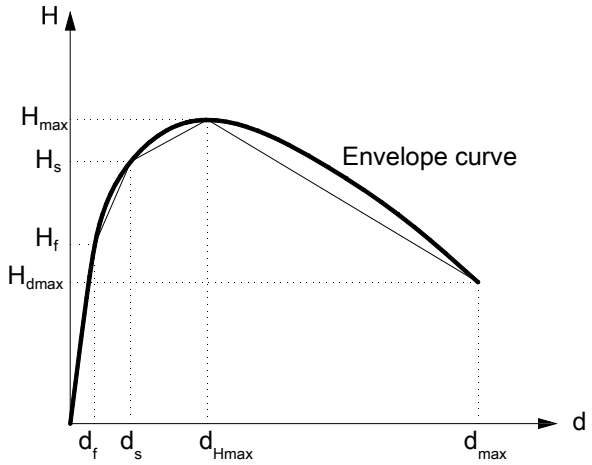

Figure 4.34 – The four limit states identified in the Force *vs.* Displacement experimental envelop.

Table 4.3 – Summary of the lateral loads and corresponding lateral displacements identifying the distinct deformation limit states.

Wall	(+/-)	H_{fc} (kN)	d_{fc} (mm)	H_{dc} (kN)	d_{dc} (mm)	H_{max} (kN)	d_{Hmax} (mm)	H_{dmax} (kN)	d_{max} (mm)
N60-3C-B1-UM	+	15.33	0.48	32.76	1.97	35.88	2.78	25.71	4.58
	-	20.33	0.56	30.20	1.24	33.63	2.78	25.19	4.47
N60-3C-B1-SH	+	18.93	0.20	35.40	0.90	38.61	2.48	24.75	5.71
	-	17.56	0.21	33.13	0.99	35.09	3.68	18.95	6.12
N60-3C-B1	+	14,78	0,22	43,8	1.52	52,73	3.36	22.44	6.03
	-	15.66	0.34	38.42	1.52	52.75	3.60	20.35	6.17
N60-3C-B2	+	22.95	0.32	38.21	0.80	62.09	3.84	22.61	7.61
	-	24.82	0.32	36.97	0.80	65.18	4.40	57.62	4.62
N150-3C-B1	+	36.59	0.64	67.86	1.28	92.98	4.24	58.76	5.27
	-	38.57	0.56	80.98	1.60	93.22	3.12	42.68	6.42
N150-3C-B2	+	45.07	0.48	88.96	1.92	93.80	3.04	47.67	6.69
	-	52.81	0.64	85.35	2.08	93.28	3.04	49.23	5.36
N60-3C-B1-MA	+	34.85	0.32	55.48	1.20	78.36	6.24	33.07	9.35
	-	29.21	0.40	44.68	1.20	74.59	6.16	42.12	9.20
N60-3C-B1-PA	+	22.47	0.42	50.73	1.92	70.22	5.04	40.17	7.70
	-	20.05	0.34	48.26	2.08	66.92	6.72	23.67	8.11
N60-2C-B1	+	-	-	35.65	2.59	63.09	7.52	30.65	10.38
	-	34.37	1.13	51.71	2.67	73.98	5.84	40.02	9.74
N60-2C-B2	+	24.19	0.48	55.09	1.86	63.18	3.92	34.66	5.97
	-	-	-	47.99	3.74	55.05	4.88	42.75	7.04

Flexural cracking loads were defined based on strains measured by strain gauges attached to vertical reinforcement and on rotations of the top of the walls obtained by means of the vertical displacements measured in LVDTs placed at the top concrete beam (LVDTs 6 and LVDT 7). Diagonal cracking loads were defined based on strains measured by strain gauges attached to horizontal reinforcements and on the measurements of diagonal displacements (LVDTs 8 and 9).

From the analysis of results, it seems that vertical reinforcement and mechanical properties of mortar influences the value of the flexural cracking load, even if they are not very significant. In fact, it is observed that the flexural cracking load of specimens N60-3C-B1 and N60-3C-B2 is clearly different and is higher in the latter specimen, which is attributed to the lower strength of the mortar to compressive and flexural loading used in construction of wall N60-3C-B1. In spite of not having available results on tensile bond strength of the unit-mortar interface, it is believed that lower compressive and flexural strength of mortar are associated to lower mechanical resistance of the unit-mortar interface. On the other hand, the presence of vertical reinforcement appears also to have some influence in the response, since by comparing the values of the flexural cracking load in walls N60-3C-B1-SH and N60-3C-B1-PA, it is observed that the specimen with vertical reinforcement presents higher values since the compressive and flexural strength of mortar are similar. It should be stressed that the difference found among the specimens N60-3C-B1, N60-3C-B1-MA and N60-3C-B1-PA is attributed to the differences on the mechanical properties of mortar, see also Table 4.2, where the compressive and flexural strength of mortar are shown together with the elastic modulus of masonry.

As expected, the flexural cracking load is higher for higher pre-compression level. In case of masonry with 2C-units, it is clear that the flexural crack load is higher for masonry bond pattern B1, which is the result of the filling vertical reinforced hollow cell with mortar, leading to higher resisting area.

The diagonal cracking load appears to be positively influenced by the presence of vertical reinforcement. Reinforced specimens at vertical joints present considerable higher diagonal cracking load, when compared to unreinforced specimen or to specimen reinforced only at bed joints. However, it should be noticed that no significant differences were detected among specimen with different ratio of horizontal reinforcement, similarly to what has been pointed out by other authors (Shing *et al.*, 1989; Schultz *et al.*, 1998; Voon and Ingham, 2006). On average the values of the diagonal cracking load obtained in walls built with 2C-units presented higher values. This behaviour is possibly due to the presence of vertical joints, allowing a better distribution of stresses and a higher shear resistance, as already seen in the results of diagonal compressive tests (Chapter 3). In terms of displacement, the values were inconsistent and no relation could be attained among the walls. Parameters like

the combination of vertical and horizontal reinforcement and pre-compression level presented high influence on the lateral strength of the walls. By comparing the lateral strength obtained in the specimens with different horizontal reinforcement ratio, it can be concluded that its contribution is not consistent and the increase on the lateral load should be attributed essentially to the vertical reinforcement and to its contribution to the predominant flexural resistance of the walls. However, it is clear that the horizontal reinforcement enables a better distribution of cracks and a higher deformation capacity.

In order to simplify the analysis and design, many authors consider the definition of idealized curves of the monotonic envelop to experimental force *vs.* displacement hysteresis by taking into account the energy equivalence criterion between the experimental envelop and the idealized diagram. Tomaževič (1999) presented two multilinear idealizations for the Force vs. Displacement diagrams, namely a bilinear and a trilinear relationship, as shown in Figure 4.35. The bilinear idealization seems to be the most common approach used for the evaluation of the in-plane seismic performance in terms of nonlinear deformability (Bosiljkov *et al.*, 2005; Vasconcelos, 2005; Wu, 2004; Magenes and Calvi, 1997), and it was selected in this study.

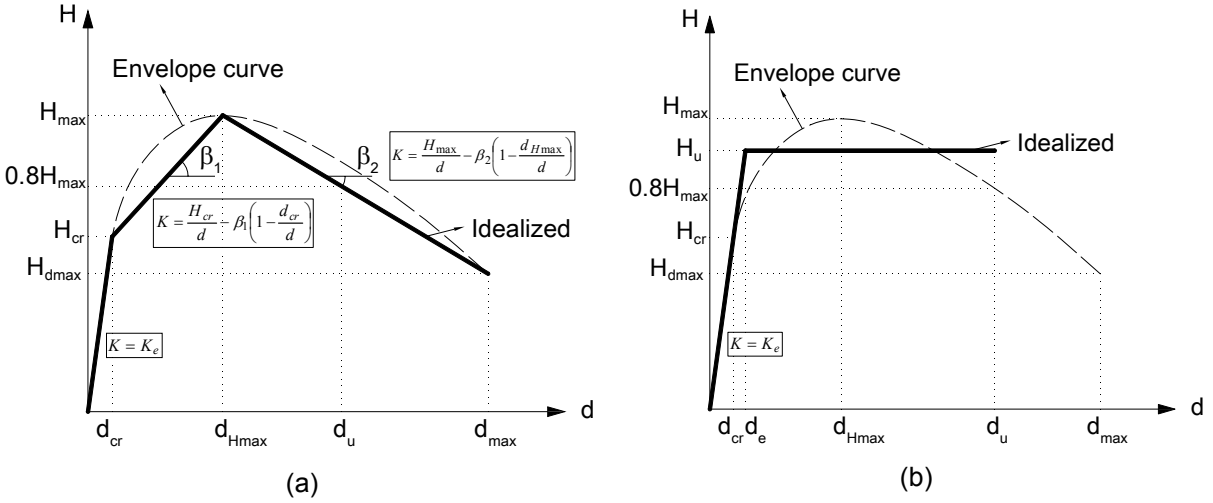

Figure 4.35 – Multilinear idealization of the force *vs.* displacement diagrams suggested byTomaževič (1999): (a) Trilinear idealization and (b) Bilinear idealization.

Firstly, the elastic stiffness, K_e, was calculated by dividing the load corresponding to the first crack (H_{cr}) by the corresponding displacement (d_{cr}). The ultimate load (H_u) was calculated considering that the bilinear idealization encompasses the same energy of deformation as real envelope curve according to Eq. 4.11.

$$H_u = K_e\left(d_{\max} - \sqrt{d_{\max}^2 - \frac{2A_{env}}{K_e}}\right) \quad \text{Eq. 4.11}$$

Where, A_{env} is the area under the experimental envelop diagram.

The elastic displacement (d_e) results from the ratio between the ultimate load, H_u, and the elastic stiffness, K_e. The ultimate displacement, d_u, and the ultimate drift, θ_u, was defined as the displacement measured in the post peak regime corresponding to a lateral load equal to 80% of the maximum experimental load, $H_{máx}$. Through the bilinear idealization of the force-displacement diagram it is possible to define the ductility of the wall which is an essential property of structures subjected to cyclic loads, see Eq. 4.12. The characteristic parameters defining the bilinear diagram for the tested walls are indicated in Table 4.4.

$$\mu = \frac{d_u}{d_e} \quad \text{Eq. 4.12}$$

Table 4.4 – Summary of results of bilinear idealization of masonry walls.

Wall	(+/-)	H_{cr} (kN)	d_{cr} (mm)	K_e (kN/mm)	$K_{e,\,theo}$ (kN/mm)	H_u (kN)	H_u / H_{max}	d_e (mm)	d_u (mm)	θ_u	μ
N60-3C-B1-UM	+	15.33	0.48	31.94	170.16	31.28	0.87	0.98	4.47	0.56	4.56
	-	20.33	0.56	36.62		31.78	0.94	0.87	4.45	0.56	5.13
N60-3C-B1-SH	+	18.93	0.20	95.47	326.63	33.53	0.87	0.35	4.12	0.52	11.73
	-	17.56	0.21	82.29		30.06	0.86	0.37	4.23	0.53	11.58
N60-3C-B1	+	14.78	0.22	66.85	236.88	41.34	0.78	0.62	4.16	0.52	6.73
	-	15.66	0.34	45.50		43.16	0.82	0.95	5.29	0.66	5.58
N60-3C-B2	+	22.95	0.32	71.72	267.70	46.30	0.75	0.65	4.77	0.60	7.39
	-	24.82	0.32	77.56		55.76	0.86	0.72	4.80	0.60	6.68
N150-3C-B1	+	36.59	0.64	57.17	263.57	86.19	0.93	1.51	5.13	0.64	3.40
	-	38.57	0.56	68.88		73.04	0.78	1.06	4.36	0.55	4.11
N150-3C-B2	+	45.07	0.48	93.90	267.70	78.49	0.84	0.84	4.82	0.60	5.77
	-	52.81	0.64	82.52		83.34	0.89	1.01	4.58	0.57	4.53
N60-3C-B1-MA	+	34.85	0.32	108.91	464.76	63.93	0.82	0.59	7.11	0.89	12.11
	-	29.21	0.40	73.03		61.99	0.83	0.85	8.31	1.04	9.79
N60-3C-B1-PA	+	22.47	0.42	53.72	310.28	60.08	0.86	1.12	7.18	0.90	6.42
	-	20.05	0.34	59.23		54.46	0.81	0.92	7.11	0.89	7.73
N60-2C-B1	+	-	-	-	272.52	-	-	-	-	-	-
	-	34.37	1.13	30.38		59.07	0.80	1.94	7.64	0.96	3.93
N60-2C-B2	+	24.19	0.48	50.66	234.09	53.91	0.85	1.06	4.84	0.61	4.55
	-	-	-	-		-	-	-	-	-	-

It is seen that the average value of H_u/H_{max} is 0.84, which is slightly lower than the value of 0.9 given by Tomaževič (1999). It means that during the seismic analysis the horizontal capacity of the walls should be reduced of 16% if the bilinear idealization is adopted. It should be stressed that at this stage the ultimate resistance, H_u, does not represent the design, but the idealized maximum experimental value. By comparing the values of ductility among the walls it is observed that reinforcement clearly increases the ductility of the walls, for low to moderate pre-compression values. For the walls subjected to the highest level of pre-compression (N150-B1 and N150-B2), the ductility found was similar to the ductility recorded in the unreinforced wall with low pre-compression value. The increase in the brittleness of the walls with increasing normal stress has been also reported by Shing *et al.* (1989). The concentration of compressive stresses at the bottom corners leads to the toe crushing, which is followed by buckling of the vertical reinforcement, avoiding the development of tensile stresses in the reinforcement and leading to the lower contribution to the global response of the walls.

An interesting result regarding the masonry bond pattern was the higher stiffness and ductility of masonry specimens built with masonry bond pattern B2. This result appears to confirm the adequate mechanical performance of the continuous vertical masonry joint under in-plane cyclic loading, which demonstrates that the proposed simpler construction technology can be an effective alternative solution for reinforced masonry walls.

Complementary to the ductility, a comparison between the experimental and the theoretical elastic stiffness ($K_{e,\ theo}$) calculated based on the theory of elasticity according to Eq. 4.13 was performed.

$$K_e = \frac{GA_w}{1.2h\left[1 + k'\frac{G}{E}\left(\frac{h}{l}\right)^2\right]} \qquad \text{Eq. 4.13}$$

Where, *k'* related the boundary conditions of the wall (for fixed end walls it is equal to 0.83 and for cantilever walls it is equal to 3.33), *G* is the shear modulus, *E* is the elastic modulus of the wall, A_w is the shear area and *h* and *l* are respectively the height and the length of wall. The elastic modulus used in these calculations was the one obtained in the experimental tests, see Table 4.2, and the shear modulus was calculated considering $\nu = 0.15$.

In fact, the stiffness of structural masonry walls is an important parameter as it is related to the period of the structure and it controls the distribution of the seismic forces in the linear regime. From the results it is observed that the elastic theory gives an important overestimation of the lateral stiffness of the walls, see Table 4.4, which is in accordance to

the results pointed out by Bosiljkov *et al.* (2005). The difference found is likely to be related to the strong anisotropic behaviour of masonry.

4.4 Experimental vs. Theoretical results

4.4.1 Cracking loads

When the experimental analysis of masonry shear walls is performed, different cracking stages can be identified up to the achievement of the peak load, namely flexural and shear cracking. These limit states can be important for the serviceable evaluation of the masonry walls but in general are not associated to the collapse of the reinforced masonry walls as pre-compression and the vertical reinforcement ensure the equilibrium of the wall. As pointed out by Magenes and Calvi (1997), the shear cracking can mean the collapse of the walls when the shear effects are predominant. This has been achieved for example in irregular and unreinforced masonry walls, which exhibited a very brittle behaviour under in-plane cyclic loading (Vasconcelos, 2005).

Flexural cracking develops mainly horizontally at the unit-mortar interface from the vertical edges of the wall. The flexural cracking load (H_{fc}) is essentially related to the tensile strength of the masonry and in particular to tensile bond strength of the unit-mortar interface. The horizontal load corresponding to flexural cracking can be obtained considering the elastic behaviour of the wall and taking into account the contribution of the tensioned masonry, see Figure 4.36, through the definition of the equilibrium equations.

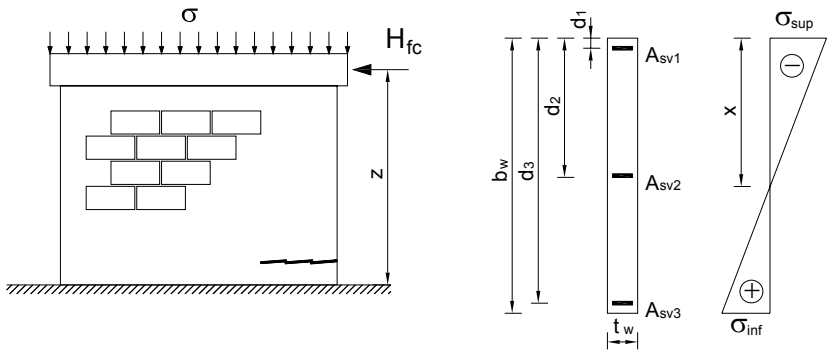

Figure 4.36 – Stress distribution along the section of the wall to calculate the flexural cracking load.

The neutral axis can be derived from the equilibrium of forces, the compatibility of strains and considering that the bottom stress reaches the flexural strength of masonry, see Eq. 4.14. The flexural cracking load is obtained by taking the equilibrium of bending moment in the section, see Eq. 4.15.

$$x = \frac{(f_{fl} + 2\sigma)t_w b_w^2 + 2\alpha_e f_{fl} \sum_i A_{svi} d_i}{(2f_{fl} + 2\sigma)t_w b_w + 2\alpha_e f_{fl} \sum_i A_{svi}} \quad \ldots\ldots \alpha_e = \frac{E_s}{E_m} \qquad \sigma_{\inf} = f_{fl} \qquad \text{Eq. 4.14}$$

$$M_R = H_{fc} z = \frac{f_{fl}}{3(b_w - x)} \left\{ t_w \left[x^3 + (b_w - x)^3 \right] + 6\alpha_e \sum_i A_{svi} (d_i - x)^2 \right\} + \sigma b_w t_w \left(\frac{b_w}{2} - x \right) \qquad \text{Eq. 4.15}$$

Where, f_{fl} is the flexural strength of masonry, E_s is the elastic modulus of the reinforcement, E_m is the elastic modulus of the masonry, F_s is the force resisted by reinforcement and σ is the average normal stress.

A comparison between the theoretical and experimental flexural cracking is presented in Figure 4.37. It is observed that in some cases the theoretical value presented higher values than the experimental ones, which is the result of low tensile bond strength of unit-mortar as already mentioned previously. It is noted that the theoretical values were calculated based on the results obtained in flexural tests of masonry (Chapter 3), in which the specimens were built with a mortar with a higher compressive strength.

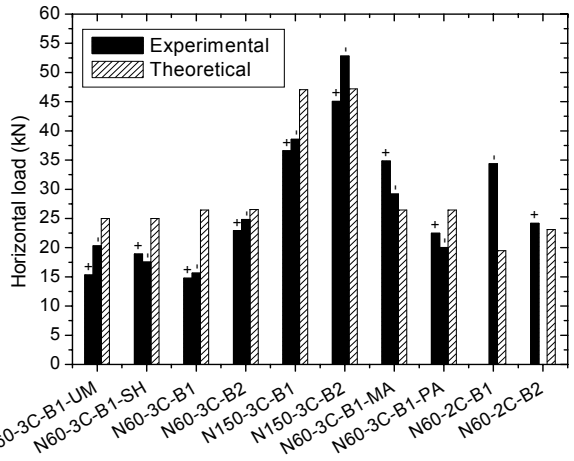

Figure 4.37 – Comparison between theoretical and experimental values of flexural cracking load.

The major difference of about 35% was recorded in walls N60-3C-B1-UM and N60-3C-B1, which were built with the weakest mortar, as previously discussed. The higher theoretical values found in specimens N60-3C-B2 and N60-3C-B1-MA is related to the improved mechanical properties exhibited by these walls and, thus, to the expected higher flexural strength of masonry. In case of wall N60-2C-B1, the difference is associated to the higher effective area due to the filling of the vertical hollow cell, where the reinforcements were positioned leading to higher flexural strength. Note that this was not considered in the calculations as the experimental flexural strength on filled two cell concrete masonry is not available.

Diagonal cracking can be estimated through the principal tensile stresses that develop in walls subjected to a combination of vertical and lateral load (Tomaževič, 1999). These cracks appear as a result of the maximum principal stress being achieved by the tensile strength of masonry. Tomaževič (1999) considers that the opening of diagonal cracking consists of an ultimate state in case of unreinforced masonry, when shear mode predominates. However, in some cases an extra resistance can be achieved after diagonal cracking up to attainment of the maximum lateral force.

Considering the masonry wall as an elastic, homogeneous and isotropic material, the basic equation for the evaluation of the diagonal cracking force of masonry walls can be derived from the definition of the principal stresses and taking into account that diagonal cracking occurs when the tensile stress attains the tensile strength of masonry, see Eq. 4.16.

$$\tau = \frac{H_{dc}}{b_w t_w} = \frac{f_t}{b}\sqrt{\frac{\sigma}{f_t}+1}, \quad b = 1.5 \qquad \text{Eq. 4.16}$$

Where, f_t is the tensile strength of masonry.

The determination of the experimental diagonal cracking is very difficult from visual observation. Hence, in this study the diagonal cracking load was defined from the deformation of the horizontal reinforcement at mid height of the wall. It is clear that a sudden increase on the deformations means the activation of these bars indicating a crack, as discussed in section 4.3.1. The comparison between the experimental and theoretical diagonal cracking forces reveals that there are some differences between predicted and experimental values of diagonal cracking load, see Figure 4.38.

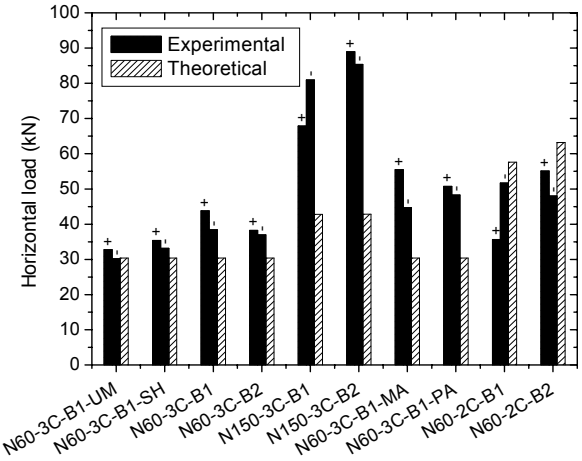

Figure 4.38 – Comparison between theoretical and experimental values of diagonal cracking.

These differences are probably because normal stresses are not uniform. The application of horizontal load generates a diagonal strut which concentrates the stress flow from the top to the bottom of wall. Thus, normal stresses are not uniformly distributed, in opposition to the hypothesis of Eq. 4.16.

4.4.2 Lateral resistance

In this section a comparison between the lateral resistance obtained in static cyclic tests and the lateral strength given by different analytical simplified models is performed. The analytical models used for the comparison have been described in detail in *Chapter 2.* Therefore, only the general procedures and main results are discussed here. The application of the analytical models takes into account the material properties obtained in *Chapter 3*.

4.4.2.1 Eurocode 6 (2005)

The design model proposed by Eurocode 6 (2005) was applied to all masonry walls submitted to combined vertical and horizontal cyclic loading. The values of the flexural and shear strength calculated according to the European standard are summarized in Table 4.5 and a direct comparison with experimental results is shown in Figure 4.39.

Table 4.5 – Theoretical values of maximum force according to Eurocode 6 (2005).

Wall	H_f (kN)	V_{R1} (kN)	V_{R2} (kN)	V (kN)
N60-3C-B1-UM	38.47	17.23	-	17.23
N60-3C-B1-SH	38.47	17.23	39.36	56.59
N60-3C-B1	67.00	83.48	39.36	122.84
N60-3C-B2	67.13	83.57	39.36	122.92
N150-3C-B1	88.82	92.27	39.36	131.62
N150-3C-B2	89.02	92.42	39.36	131.78
N60-3C-B1-MA	67.00	83.48	52.48	135.96
N60-3C-B1-PA	67.00	83.48	22.14	105.63
N60-2C-B1	57.26	51.16	39.36	90.52
N60-2C-B2	64.39	55.77	39.36	95.13

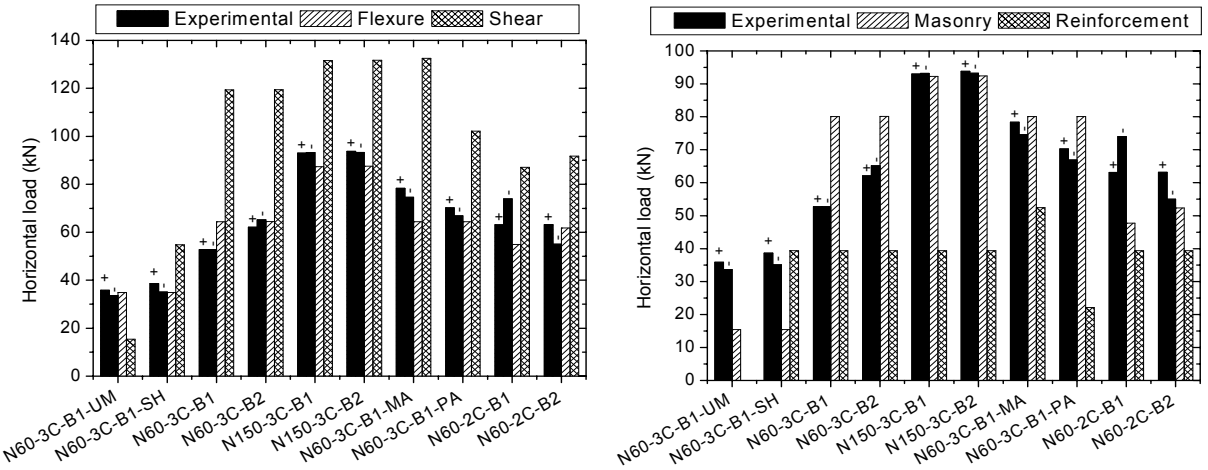

Figure 4.39 – Comparison between theoretical and experimental values of Eurocode 6 (2005): (a) Flexure and shear strength and (b) parcels of shear strength.

It is observed that apart from the unreinforced masonry wall, which presented the shear strength limited by the compressive strength of the unit (Eq. 2.14), the flexural failure ruled the lateral behaviour of the masonry walls. The maximum forces obtained in experimental tests were very similar to theoretical values calculated based on the flexural model proposed by Eurocode 6 (2005), see Figure 4.39a. On the other hand, it is seen that in general the theoretical shear resistance presented considerable high values.

It should be referred that Eurocode 6 (2005) suggests applying a Coulomb type formula to calculate the shear strength irrespectively to the failure mode, which appears to be rather limitative. As already mentioned by other authors (Tomaževič, 1999; Shing *et al.*, 1993; Mann and Muller, 1982), the shear resistance mechanism is very complex and different failure modes may develop depending on distinct factors, namely the vertical pre-compression and height to length ratios. In fact, the shear strength calculated by Eurocode 6 (2005) complies reasonably well with diagonal cracking through unit-mortar interface, where the sliding mechanism along the stair stepped cracks prevails. However, it is not appropriate to describe the diagonal cracking through masonry joints and masonry units, whose onset is due to the achievement of the tensile strength of the masonry material. Thus, the values of shear strength calculated according to Eurocode 6 (2005) may be not representative if the failure mode is different from the stair stepped diagonal cracking.

A comment should also be made concerning the formula presented by Eurocode 6 (2005) to calculate the resisting shear load by considering only the compressed part of the unreinforced wall instead of the total value of the length of the walls, see Eq. 4.17

$$V = f_v l_c t_w \quad \text{Eq. 4.17}$$

Where, f_v is the shear strength of unit-mortar interface and l_c is the compressed length of the wall in flexure.

This appears to be reasonable since the tensioned part of the section of the wall does not influence the sliding effect. On the other hand, in case of reinforced masonry the strength considers two parcels: one related to the masonry resistance and other related to the reinforcement resistance. In case of the masonry resistance parcel, the whole length of the wall is considered to the calculus of shear strength. This leads to high values of shear strength resisted by masonry, see Figure 4.39b. Another issue in the calculation of the shear strength of reinforced masonry walls concerns the contribution of the horizontal reinforcements. In fact, the same amount of force is considered irrespectively of the aspect ratio, which appears not to be reasonable for high height to length ratios, as part of the horizontal reinforcements does not cross the diagonal cracking and thus are not effective. This procedure leads to the overestimation of the shear strength of reinforced masonry walls.

4.4.2.2 MSJC (2002)

The design model proposed by MSJC (2002) was applied to tested masonry walls considering the materials properties obtained by experimental program I – Characterization of materials. Theoretical results exhibited a good approximation to the experimental values, see Table 4.6 and Figure 4.40a. However, all specimens failed by flexure according to MSJC (2002).

None design shear strength reached the limit $0.083\left(6A_n\sqrt{f_a}\right)$ which has the objective of controlling the level of stresses in compressed diagonal. Other interesting consideration of MSJC (2002) is that it does not consider the full capacity of horizontal reinforcements in shear strength of the shear walls as Eurocode 6 (2005). Observing the strength parcels separately in Figure 4.40b, it can be noted that reinforcements are responsible for only about 30% of the shear strength of wall. This consideration is taken due to the fact that the shear stresses are not constant in the height of wall and not all reinforcement will yield in the shear failure.

Table 4.6 – Theoretical values of maximum force according to MSJC (2002).

Wall	H_f (kN)	V_{R1} (kN)	V_{R2} (kN)	V (kN)
N60-3C-B1-UM	38.47	65.61	-	65.61
N60-3C-B1-SH	38.47	60.11	21.87	81.97
N60-3C-B1	67.00	60.23	21.87	81.97
N60-3C-B2	67.13	80.86	21.87	82.09
N150-3C-B1	88.82	80.98	21.87	102.72
N150-3C-B2	89.02	80.98	21.87	102.84
N60-3C-B1-MA	67.00	60.11	29.16	89.26
N60-3C-B1-PA	67.00	60.11	12.30	72.41
N60-2C-B1	57.26	51.88	21.87	73.75
N60-2C-B2	64.39	56.50	21.87	78.37

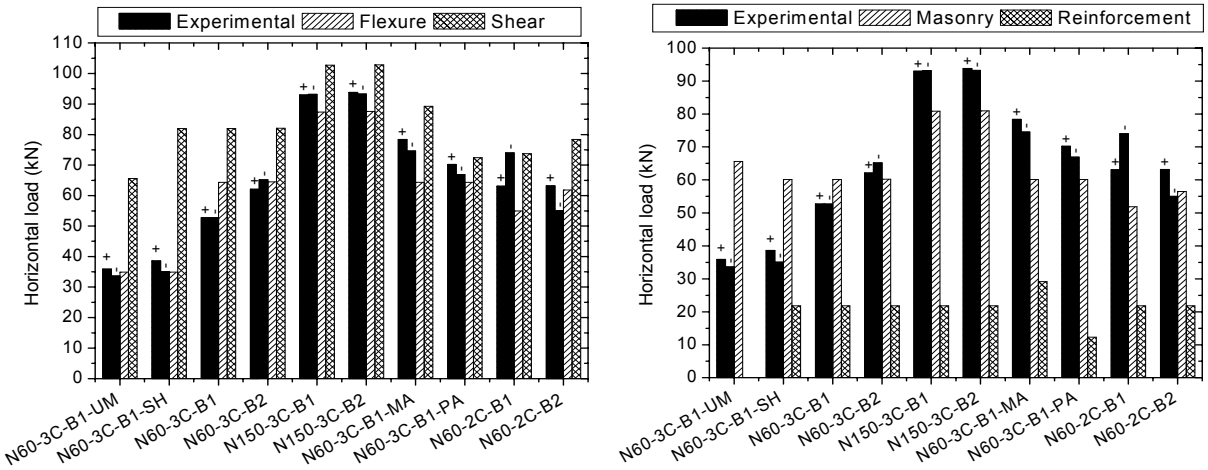

Figure 4.40 – Comparison between theoretical and experimental values of MSJC (2002): (a) Flexure and shear strength and (b) parcels of shear strength.

4.4.2.3 Tomaževič (1999)

In spite of the height to length ratio of the tested walls being lower than 1.0, it was decided to apply the formulation suggested by Tomaževič (1999), where the shear strength of unreinforced masonry is given by the equation pointed out by Turnšek and Čačovič (1971). Flexure strength is presented according to Eurocode 6 (2005) since Tomaževič (1999) presented only a simplification of this formulation according to geometrical conditions of his tested specimens. The summary of the flexural, shear and sliding shear forces are summarized in Table 4.7.

Table 4.7 – Theoretical values of maximum force according to Tomaževič (1999).

Wall	H_f (kN)	V_{R1} (kN)	V_{R2} (kN)	V_{R3} (kN)	V_{sh} (kN)	V_{sl} (kN)
N60-3C-B1-UM	38.47	30.26	-	-	30.26	32.83
N60-3C-B1-SH	38.47	30.26	13.12	-	43.38	32.83
N60-3C-B1	67.00	30.26	13.12	5.65	49.03	38.48
N60-3C-B2	67.13	30.29	13.12	7.71	51.12	40.54
N150-3C-B1	88.82	42.80	13.12	8.49	64.41	85.42
N150-3C-B2	89.02	42.84	13.12	8.03	64.00	84.96
N60-3C-B1-MA	67.00	30.26	17.49	6.35	54.10	39.18
N60-3C-B1-PA	67.00	30.26	7.38	6.57	44.21	39.40
N60-2C-B1	57.26	57.77	13.12	6.35	77.24	35.48
N60-2C-B2	64.39	63.20	13.12	8.60	84.91	40.20

From the results it is seen that the experimental lateral strength is very near the predicted flexural strength. Apart from the specimen N60-3C-B1, specimens presented experimental results always higher than theoretical flexural strength, see Figure 4.41a. Besides, it can be observed that in general the sliding lateral strength presents very low values, even if the dowel action of vertical reinforcements is considered.

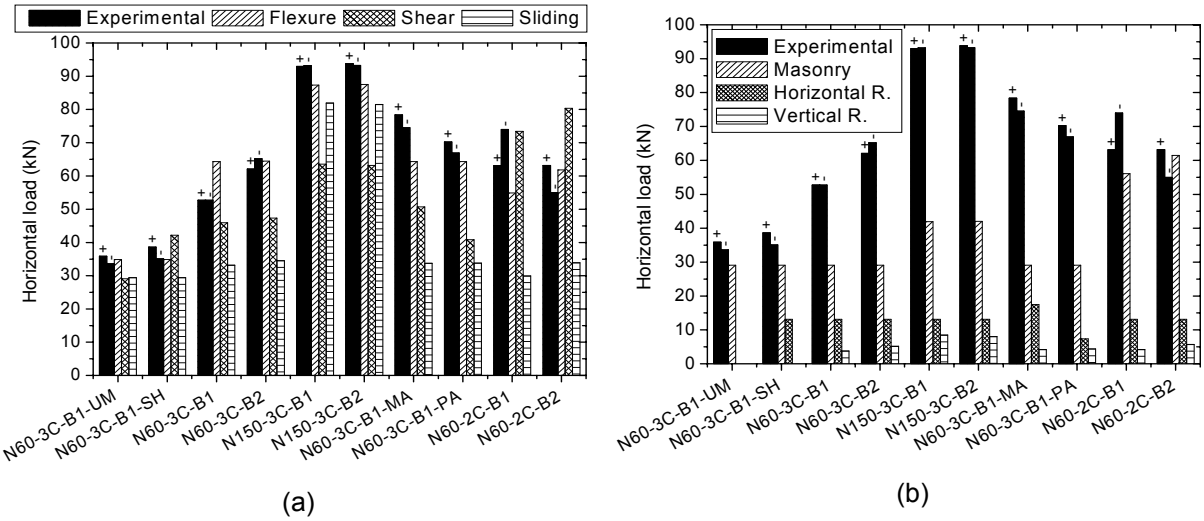

(a) (b)

Figure 4.41 – Comparison between theoretical and experimental values of Tomaževič (1999): (a) Flexure and shear strength and (b) distinct contributions to the shear strength.

Analyzing the contribution of masonry and reinforcements on the lateral strength of the walls, it is observed that masonry is responsible for the higher contribution, with a value not lower than 70 % of resistance in all cases, see Figure 4.41b. On the other hand, dowel action was practically negligible since it is responsible only for 10% of the shear strength.

The contribution of vertical reinforcement in dowel action is directly related to the compressive strength of mortar. In case of this study, mortar had low compressive strength in almost all walls as discussed above.

4.4.2.4 Brunner and Shing (1996)

By applying the model of Brunner and Shing (1996) for the tested walls, it is seen that apart from specimen N60-3C-B1-MA the shear strength is always higher than the experimental lateral strength. Besides, the shear strength is always higher than the flexural strength, which is in general very near the flexural strength, see Table 4.8 and Figure 4.42a. This means that the flexural mode predominates in the response of the walls. According to the Brunner and Shing (1996), when flexural mode is predominant, the equilibrium of the horizontal forces is not achieved, being the shear strength always higher than the flexural strength. Thus, the iterative method proposed was not used. The values of shear strength are calculated from the equilibrated state of the wall, where the horizontal force is equal to H_f. Observing the strength contributions separately in Figure 4.42b, it can be noticed that reinforcements were responsible for a small part of the shear strength of wall, which is the result of only the central horizontal reinforcement being considered in the calculations since the other reinforcement bars did not respect the anchorage length determined by Brunner and Shing's model. In case of specimen N60-3C-B1-MA, none reinforcement presented sufficient anchorage length.

Table 4.8 – Theoretical values of shear strength according to Brunner and Shing (1996).

Wall	H_f (kN)	H_c (kN)	H_i (kN)	H_s (kN)	V (kN)
N60-3C-B1-UM	38.47	50.25	-	-	50.25
N60-3C-B1-SH	38.47	50.25	-	10.93	61.18
N60-3C-B1	67.00	72.34	-	10.93	83.27
N60-3C-B2	67.13	72.37	-	10.93	83.30
N150-3C-B1	88.82	116.53	-	10.93	128.24
N150-3C-B2	89.02	117.65	-	10.93	129.24
N60-3C-B1-MA	67.00	72.34	-	-	72.34
N60-3C-B1-PA	67.00	72.34	-	6.15	78.49
N60-2C-B1	57.26	63.97	-	10.93	74.90
N60-2C-B2	64.39	69.00	-	10.93	79.93

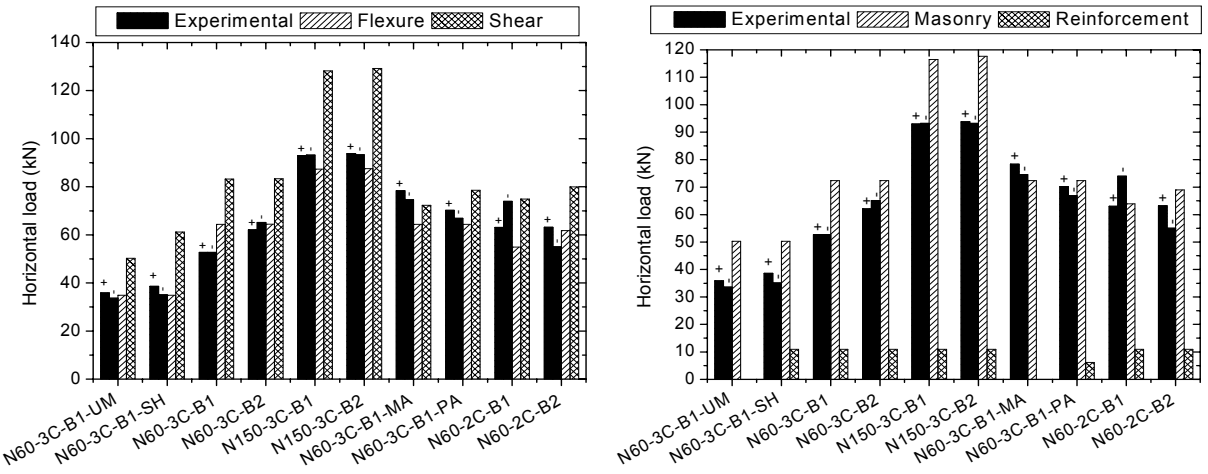

Figure 4.42 – Comparison between theoretical model of Brunner and Shing (1996) and experimental values: (a) Flexure and shear strength and (b) contributions for the shear strength.

4.5 Summary and conclusions

In order to evaluate the in-plane cyclic behaviour of reinforced concrete block masonry walls, an experimental campaign was carried out. Different variables in the experimental analysis were considered, namely the pre-compression level, horizontal reinforcement ratio and masonry bond pattern. Besides the detailed discussion on the failure modes and force-displacement diagrams, an evaluation of the cyclic performance based on ductility obtained from the bilinear idealization of the experimental envelops was presented. Finally a comparison between the experimental lateral resistance and the resistance calculated from different approaches was provided.

From the global analysis of results the following conclusion can be drawn:

(a) the global analysis of the results of the cyclic in-plane tests on concrete block masonry walls allows concluding that the combination of vertical and horizontal reinforcement leads to an improvement on its in-plane cyclic performance. Specimens reinforced simultaneously with vertical and horizontal trussed-bars exhibited an increase on both lateral strength and deformation capacity, with respect to unreinforced masonry walls, even if the efficiency of horizontal reinforcement is low;

(b) The influence of the percentage of horizontal reinforcement in lateral strength appeared to be not clear. The wall with a smaller amount of horizontal reinforcement (N60-3C-B1-PA) presented higher lateral strength than specimen with the intermediate amount of horizontal reinforcement (N60-3C-B1). Additionally, it was possible to observe that the increase of the bed joint reinforcement and the reduction of the vertical spacing in specimen

N60-3C-B1-MA resulted in cracking more distributed, higher strength, gradual stiffness degradation and significant increase on the ductility factor.

(c) concerning the vertical pre-compression, an increase on the lateral strength and a reduction on the lateral deformation with an increase on the brittleness, given by a decrease on the lateral deformation and dissipation of energy, were found in the wall specimens submitted to the highest level of normal stresses.

(d) with respect to the masonry bond pattern, it was seen that no significant differences in the mechanical behaviour were observed for the two adopted bond patterns, even if the non-staggered (reinforced) vertical joint appeared to result in a slight increase on the lateral strength. This means that the best masonry bond pattern in terms of construction technology of reinforced masonry walls, i.e. non-staggered bond pattern, presents similar mechanical performance to traditional running masonry bond pattern.

(e) from the analytical study of the lateral resistance based on distinct approaches, it was seen that a reasonable agreement between the flexural theoretical resistance with the experimental results was achieved, confirming the predominant flexural resisting mechanism governing the in-plane behaviour of the reinforced masonry walls.

5 EXPERIMENTAL PROGRAM III: MASONRY BEAM TESTS

5.1 Introduction

Masonry beams together with shear walls integrate the resistant system of a masonry building responsible to bear the lateral loads. Shear walls are the main components in this structural system, even if masonry beams are the elements that ensure the connection of panels and the distribution of stresses through the masonry piers.

According to Drysdale *et al.* (1999) the design of multi-storey buildings considering simple cantilever shear walls assures ductile response and good energy dissipation. The consideration of masonry beams renders the design too complex. Due to the low span to depth ratio of coupling beams, it is difficult to satisfy the demand of ductility. Therefore, Drysdale *et al.* (1999) suggest the separation of the beams from adjacent walls by movement joints. However, this procedure is rather severe and underestimates the lateral resistance of the structure. The consideration of the coupling beams results in lower flexural efforts at the base of the building than the real capacity of the masonry walls.

Masonry beams are subjected to shear and flexure efforts and according to several authors, the design of masonry beams can be performed using the ultimate strength design method similar to what is used in reinforced concrete beams (Khalaf *et al.*, 1983; Hendry, 1998; Drysdale *et al.*, 1999; Taly, 2001). Nevertheless, the presence of holes in units and the anisotropy of masonry, generated mainly by mortar joints, which are planes of weakness, make the behaviour of masonry beams more complex.

There has been very few works analyzing the behaviour of masonry beams until now. It should be stressed that additional research effort should be given to these masonry structural elements, given the much reduced information available in the literature. Therefore, a large experimental program was developed aiming at improving the understanding on the

behaviour of masonry beams under flexure and shear, for which three and four point load bending tests were considered. The simplicity on the arrangement of these test setups and on the interpretation of results represents important advantages. Horizontal and vertical prefabricated reinforcements were used in bed joints and vertical cores of units, respectively, to evaluate their influence on behaviour of the masonry beams.

5.2 Experimental Program

The experimental program was carried out at Laboratory of Structures of University of Minho (LEST) aiming at evaluating the flexural and shear behaviour of reinforced masonry beams through a three and four point load bending test configuration. Twenty four masonry beams were built with different geometry of units and distinct horizontal reinforcement distribution.

5.2.1 Masonry specimens

Masonry beams were built with three and two hollow cell concrete blocks (3C-units and 2C-units, respectively), 4 courses in height and 7 or 4 blocks in length of horizontal joints. Masonry beams were built with dry vertical joints when 3C-units were used. Common mortar filled vertical joints with 8mm thickness were considered in case of 2C-units. Shape and geometry of masonry beams are shown in Figure 5.1. The distinct geometries considered in the tests were chosen based on the expected flexure or shear failure mode in specimens with 7 or 4 blocks of length respectively. Trussed type reinforcements with yield strength of 700 MPa were used in the construction of the beams.

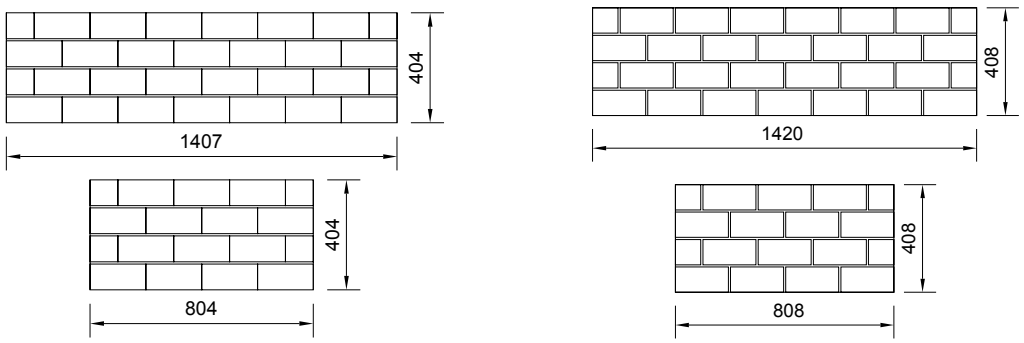

Figure 5.1 - Geometry of masonry beams: (a) masonry beams built with 3C-units and (b) masonry beams built with 2C-units (dimensions in mm).

A summary of the typologies of the masonry beams is indicated in Figure 5.2. Fourteen specimens were tested to evaluate the flexural behaviour. Here, F denotes flexure, 2C and 3C relates the type of unit, D5 and D3 denotes the diameter of bed joint reinforcement (ϕ_h), and UM means unreinforced masonry. In order to avoid shear failure at the supports, two vertical reinforcements of 5mm of diameter were introduced at the vertical cores of the concrete blocks between the supports and the load application points, see Figure 5.2 and Table 5.1. Two vertical reinforcements were added at mid–span (specimens indicated with M) in order to assess its contribution to improve the flexural behaviour of the beams such as the increase on the flexural strength and the prevention of vertical splitting stresses developed at the upper compressive region due to high compressive stresses. The letters C and D indicates if horizontal reinforcement was only placed at the first course or distributed in the three layers of the beam respectively. Bed joint reinforcement ratio, ρ_h, was the main parameter analysed from the results obtained in the tests.

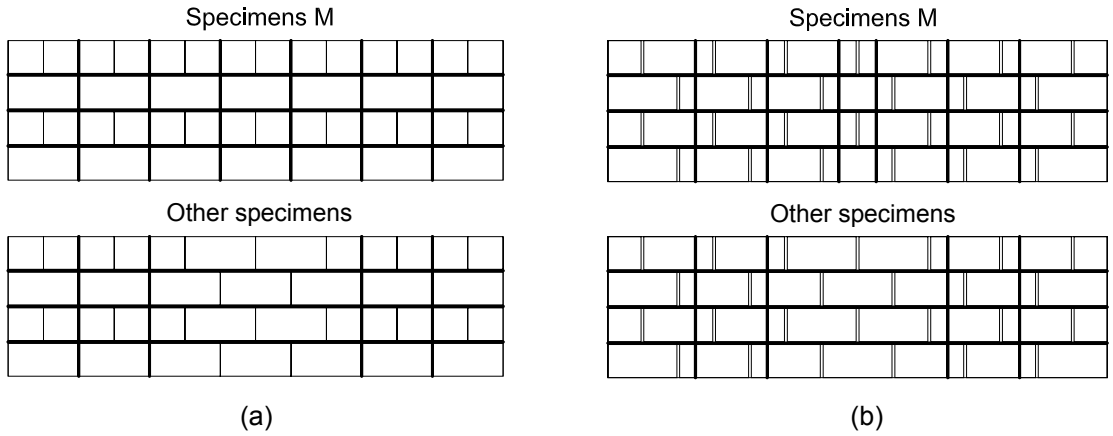

Figure 5.2 - Location of the vertical reinforcements in four point load configuration: (a) masonry beams built with 3C-units and (b) masonry beams built with 2C-units.

Ten masonry beams were built to evaluate the shear behaviour. Here, S denotes shear, 2C and 3C indicates the type of unit, UM means unreinforced masonry, SH means that the masonry beam has only horizontal reinforcements and S1, S2 and S3 indicates different vertical reinforcement ratios. In order to avoid the failure by flexure, traditional steel bars (ρ_h=0.70%) were positioned in a layer of mortar at the base of the beam. Besides, in all reinforced specimens bed joint reinforcements were added at all courses. Table 5.1 shows the location and distribution of vertical shear reinforcements with a diameter of longitudinal bars (ϕ_v) equal to 4mm corresponding to different reinforcement ratios. It should be referred that the position of the vertical reinforcements was to certain extent defined by the geometry of the concrete units, mainly as concerns the vertical perforation. Also in the three point load tests horizontal and vertical reinforcement ratios were the main parameters under analysis.

Table 5.1 – Experimental details of masonry beams.

Beam	$Ø_h$ (mm)	ρ_h (%)	$Ø_v$ (mm)	ρ_v (%)	Dimensions (mm)
F-3C-UM	-	-	5	0.112	1407x404x100
F-3C-D5-C	5	0.097	5	0.112	1407x404x100
F-3C-D5-D	5	0.292	5	0.112	1407x404x100
F-3C-D5-D-M	5	0.292	5	0.167	1407x404x100
F-3C-D3-C	3	0.035	5	0.112	1407x404x100
F-3C-D3-D	3	0.105	5	0.112	1407x404x100
F-3C-D3-D-M	3	0.105	5	0.167	1407x404x100
F-2C-UM	-	-	5	0.118	1420x408x94
F-2C-D5-C	5	0.102	5	0.118	1420x408x94
F-2C-D5-D	5	0.307	5	0.118	1420x408x94
F-2C-D5-D-M	5	0.307	5	0.177	1420x408x94
F-2C-D3-C	3	0.037	5	0.118	1420x408x94
F-2C-D3-D	3	0.111	5	0.118	1420x408x94
F-2C-D3-D-M	3	0.111	5	0.177	1420x408x94
S-3C-UM	-	0.292	-	-	804x404x100
S-3C-SH	5	0.292	4	0.094	804x404x100
S-3C-S1	5	0.292	4	0.125	804x404x100
S-3C-S2	5	0.292	4	0.219	804x404x100
S-3C-S3	5	-	-	-	804x404x100
S-2C-UM	-	0.307	-	-	808x408x94
S-2C-SH	5	0.307	4	0.066	808x408x94
S-2C-S1	5	0.307	4	0.132	808x408x94
S-2C-S2	5	0.307	4	0.199	808x408x94
S-2C-S3	5	0.292	-	-	808x408x94

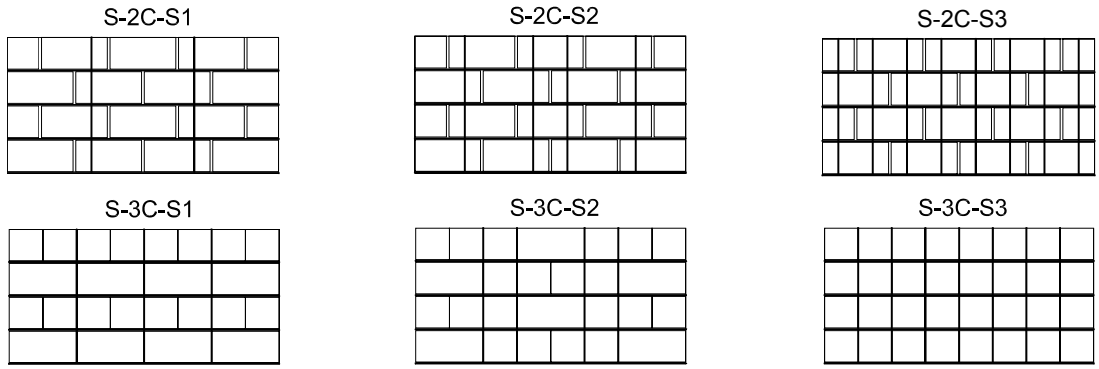

Figure 5.3 – Location of vertical reinforcements in masonry beams with 4 blocks of length.

5.2.2 Test setup and procedures

The static monotonic tests of the masonry beams were performed following two typical test setups (three and four point load configurations) recommended by EN846-9 (2000), as shown in Figure 5.4.

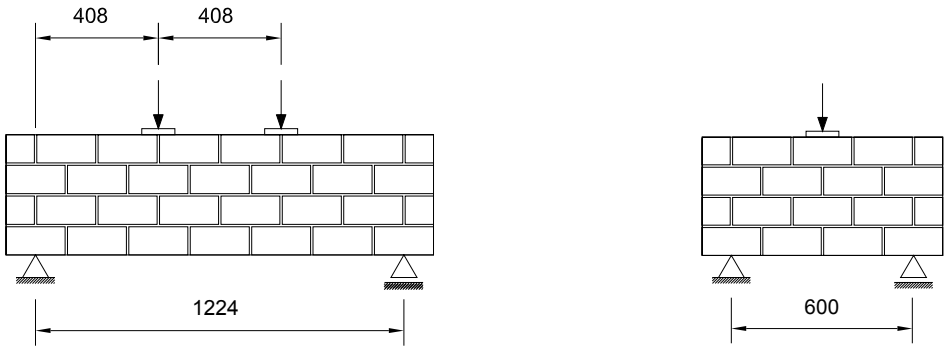

Figure 5.4 – Test setup of masonry beams: (a) four point load test and (b) three point load test (dimensions in mm).

Masonry panels were laid on top of two metallic roller supports with 100 mm x 100 mm in order to avoid stress concentration. One of the supports was fixed to a steel profile anchored to the reaction slab, see Figure 5.5a. The other support was placed above a roller positioned in the direction of the beam to avoid possible torsional stresses. Two Teflon sheets with a layer of grease between them were placed below the steel roller allowing free motion and avoiding possible axial stresses in masonry beam, see Figure 5.5b.

Figure 5.5 – Details of the boundary conditions of masonry beams: (a) fixed support and (b) free support.

Half-rollers were placed at the load application points to avoid axial efforts and a steel beam was used to uniformly distribute the vertical load, as shown in Figure 5.6, which was applied by using a spherical hinge. The monotonic tests were carried out under displacement control at a rate of 5 μm/s by means an external LVDT connected to the actuator.

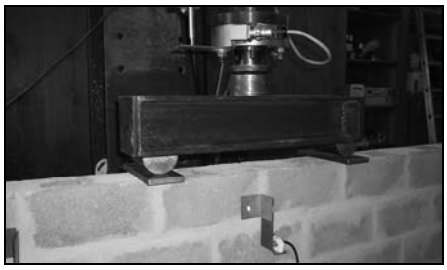

Figure 5.6 – Load configuration for the four point load bending test

During the construction of the beams, three specimens of mortar (40 mm x 40 mm x 160 mm) were cast aiming at controlling its quality through the compressive and flexural strength, see Table 5.2. The masonry beams were cured at laboratory environmental conditions with relative air humidity of approximately 80%. In order to ensure proper curing of the specimens, the tests were carried out after 28 days from the construction. The mortar specimens were tested in the same day of the masonry beams. As can be observed from the results on mortars, no significant variations were obtained for the compressive and flexural strength, meaning that reasonable quality control on the production of the mortar was achieved.

Table 5.2 – Average strength of mortars for masonry beam tests.

Beam	Flexural Strength (MPa)	Compressive Strength (MPa)
F-3C-UM	1.85	6.79
F-3C-D5-C	1.85	6.79
F-3C-D5-D	2.15	8.09
F-3C-D5-D-M	2.15	8.09
F-3C-D3-C	1.92	7.32
F-3C-D3-D	2.15	8.09
F-3C-D3-D-M	2.18	8.54
F-2C-UM	1.65	5.66
F-2C-D5-C	1.89	7.15
F-2C-D5-D	1.92	7.32
F-2C-D5-D-M	2.18	8.54
F-2C-D3-C	1.65	5.66

Beam	Flexural Strength (MPa)	Compressive Strength (MPa)
F-2C-D3-D	1.89	7.15
F-2C-D3-D-M	1.92	7.32
S-3C-UM	1.98	7.56
S-3C-SH	1.98	7.56
S-3C-S1	1.75	6.39
S-3C-S2	1.98	7.56
S-3C-S3	1.75	6.39
S-2C-UM	1.94	7.18
S-2C-SH	1.98	7.56
S-2C-S1	1.94	6.39
S-2C-S2	1.94	7.18
S-2C-S3	1.94	7.18

5.2.3 Instrumentation

The displacements of the masonry beams were measured by means of a set of LVDTs, whose localization is indicated in Figure 5.7. LVDTs 1, 2 and 3 measured the deflections of the beams, whereas LVDTs 4, 5 and 6 intended to measure the slippage of the horizontal joints. The possible opening of vertical flexural crack at vertical joints at mid-span of the beams was detected by LVDT 7. Besides, strain-gauges were glued to reinforcements to evaluate their contribution to the beam response. In four point load bending tests strain-gauges were glued to the horizontal reinforcements at the mid-span of the beam according to the configuration indicated in Figure 5.8a to measure the maximum tensile elongations. In shear tests strain gauges were glued to horizontal reinforcements in the first course and due to the symmetry of the beams, at the mid height of the vertical reinforcements, see Figure 5.8b. Due to the limitation of the acquisition channels, in specimens with vertical reinforcements in the central region of the beam, it was decided not to apply strain gauges in the horizontal reinforcements at the second course.

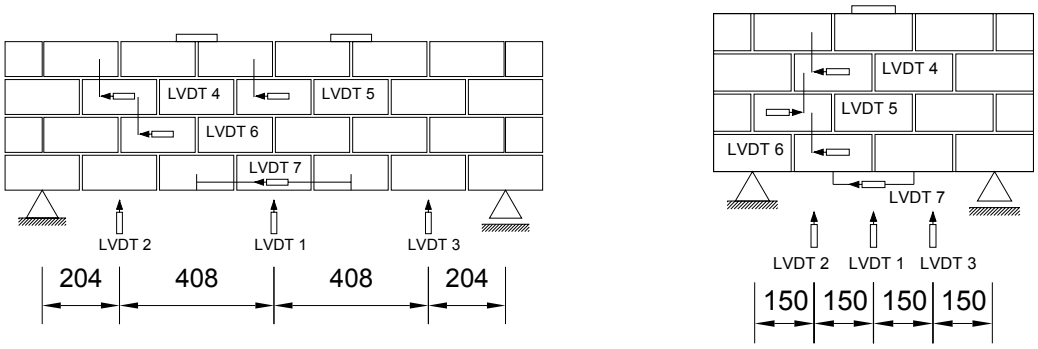

Figure 5.7 – Instrumentation of the masonry beams: (a) four point load tests and (b) three point load tests (dimensions in mm).

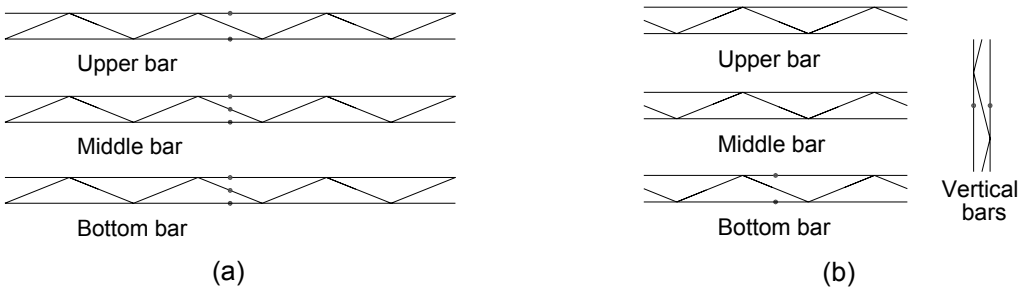

Figure 5.8 – Instrumentation of the reinforcements with strain gauges: (a) four point load tests and (b) three point load tests (dimensions in mm).

5.3 Results

In spite of the care taken with the free support to avoid axial stresses in masonry beam, the results obtained point out that the free support exhibited non-negligible stiffness during the tests. However, experimental tests carried out in masonry beams provided some indicators about their flexure and shear behaviour. The analysis of the results will be presented in terms of failure modes and force–displacements diagrams.

5.3.1 Failure modes

5.3.1.1 Four point load tests

In spite of the presence of vertical reinforcements next to the supports, some beams failed by shear (F-3C-D5-D, F-3C-D5-D-M, F-2C-D5-D and F-2C-D5-D-M) and some specimens exhibited a mixed failure mode (F-3C-D5-C and F-2C-D5-C), see Figure 5.9. However, flexure was the failure mode of the majority of the masonry beams (F-3C-UM, F-2C-UM, F-3C-D3-C, F-2C-D3-C, F-3C-D3-D, F-3C-D3-D-M, F-2C-D3-D and F-2C-D3-D-M), see Figure 5.10.

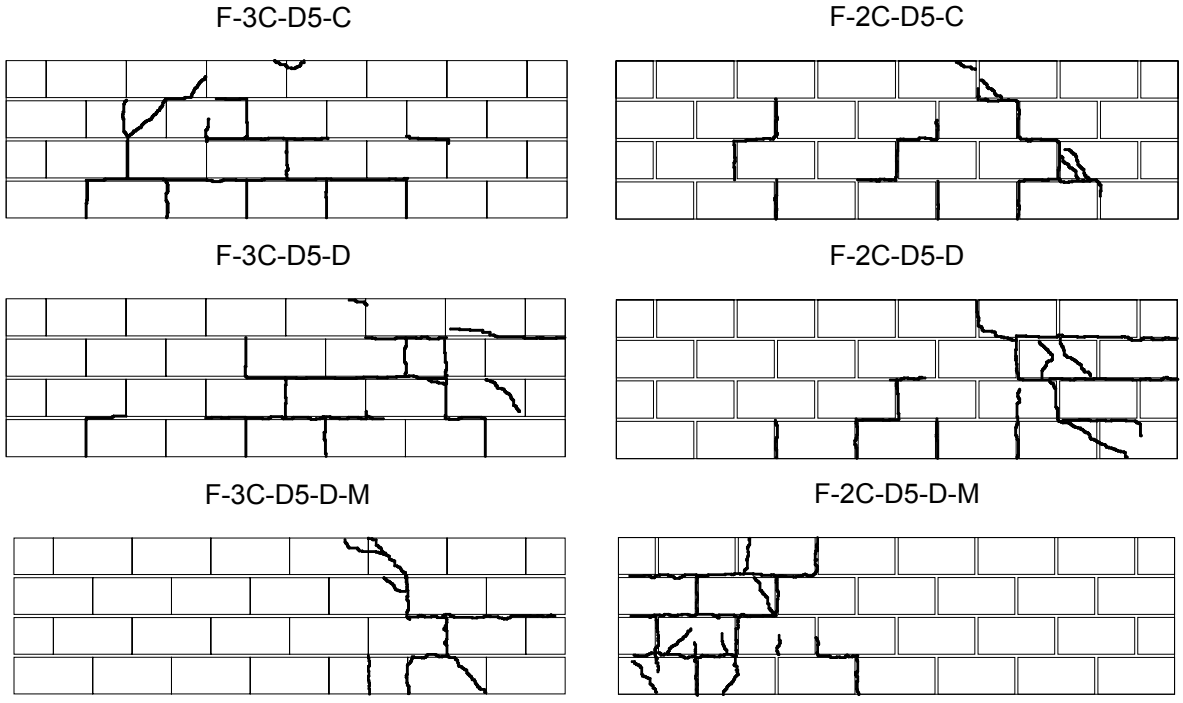

Figure 5.9 – Cracking patterns in four point load tests of masonry beams which presented a shear or a mixed shear-flexure failure.

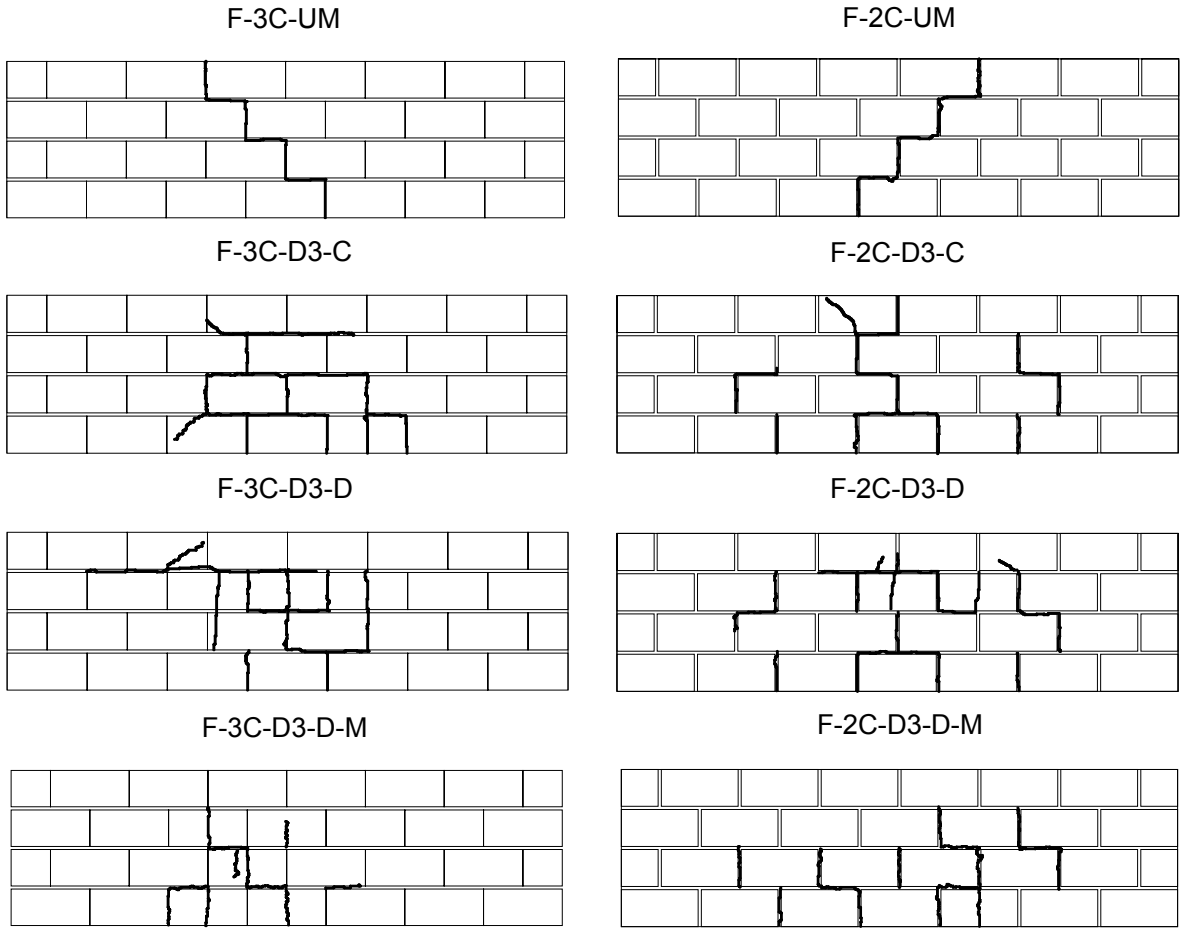

Figure 5.10 - Cracking patterns in four point load tests of masonry beams which presented a flexure failure.

In four point load test, the central region of the beam is under pure flexure without influence of shear stresses. As the vertical load increases, tensile stresses at the bottom region of the masonry beams increases leading to the attainment of the flexural strength of masonry, resulting in the opening of flexural cracks at the vertical joint in the central region of the beam. The opening of this crack could be detected through the results of LVDT 7, which was located at the bottom of the beams, see Figure 5.11. Results showed that flexural crack closed during the post-peak regime in specimens that failed by shear, whereas in specimens failing by flexure this crack remained opened until the end of the test.

In case of unreinforced masonry (F-2C-UM and F-3C-UM), the flexural crack pattern is characterized by a stepped crack along the height of the beam resulting from the sudden propagation of the vertical crack developed at the bottom central region of the beam. However, the resisting mechanism of the masonry beams with or without filled vertical joints was quite different. In case of 2C-units and filled vertical joints, the opening of the flexural crack results from the achievement of the tensile strength of the central vertical unit-mortar interface at the first course. Its propagation up to the top region results from the combination

of the attainment of the tensile and shear strength of the unit-mortar interfaces. In masonry beams built with 3C-units the propagation of the stair stepped flexural crack is essentially due to the achievement of the shear strength of the unit-mortar interface, since the dry vertical joints have no tensile strengths. With the increase of the applied vertical load, vertical joints of the second course exhibit a tendency for opening, which was prevented by the shear stresses on the horizontal unit-mortar interface until the attainment of the corresponding shear strength and by tensile stresses on the unit below the mortar joint. the attainment of the corresponding tensile strength The flexural cracking patterns follows almost exclusively the unit-mortar interfaces due to their low resistance, when compared to the tensile strength of the concrete units, see Figure 5.12.

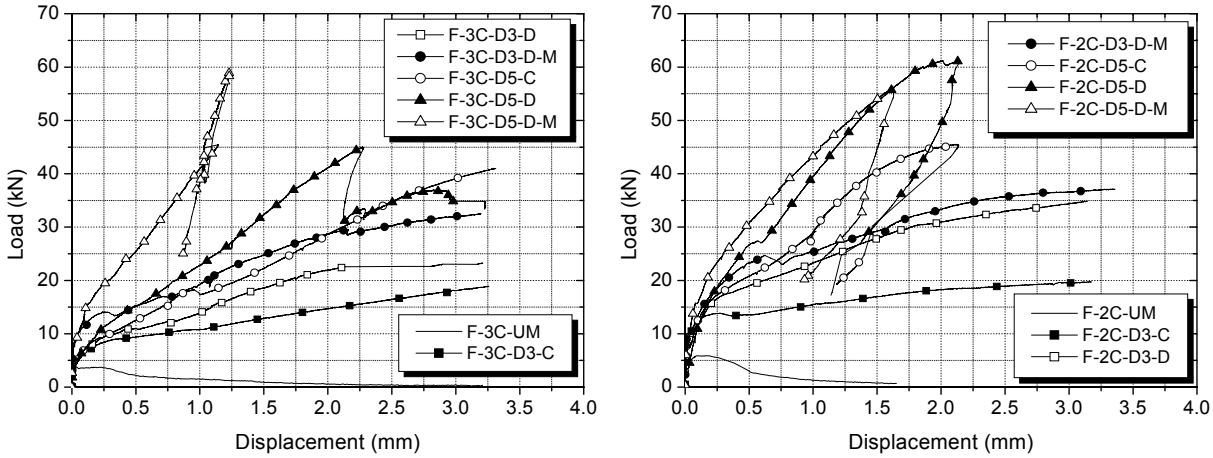

(a) (b)

Figure 5.11 – Results of the LVDT 7 in four point loads tests (opening of flexural cracks): (a) 3C-units and (b) 2C-units.

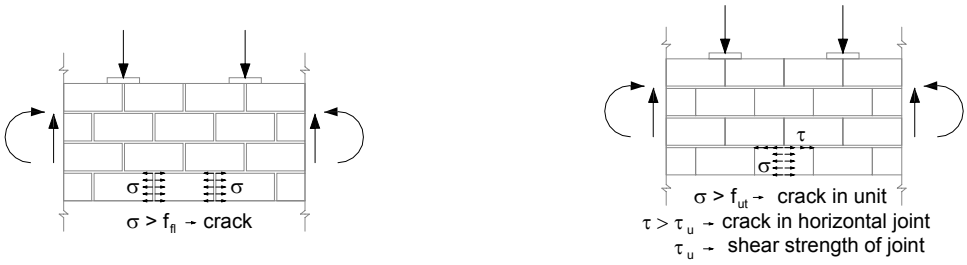

(a) (b)

Figure 5.12 – Resistance mechanisms of unreinforced masonry beams under flexure: (a) F-2C-UM and (b) F-3C-UM.

In case of reinforced specimens, after the opening of the vertical joints in the first course, bed joint horizontal reinforcement contributes considerably to the increase of the shear strength of the mortar-unit interfaces through the development of tensile strains and

thus to the increase of the compressive stresses at the top of the beam. The yielding of these reinforcements is particularly visible in specimens where only a horizontal reinforcement of 3mm diameter is placed at the first course (F-3C-D3-C and F-2C-D3-C), see Figure 5.13. It is observed that horizontal bars exhibited a decrease on strains near failure of the beam, see Figure 5.14, which can be attributed to the unloading of the steel bars after its breakage. The strain-gauges of specimen F-2C-D3-C were probably damaged since the strains measured were very low, in spite of the effective breaking of the bars.

Figure 5.13 – Failure of horizontal reinforcement in four point load tests.

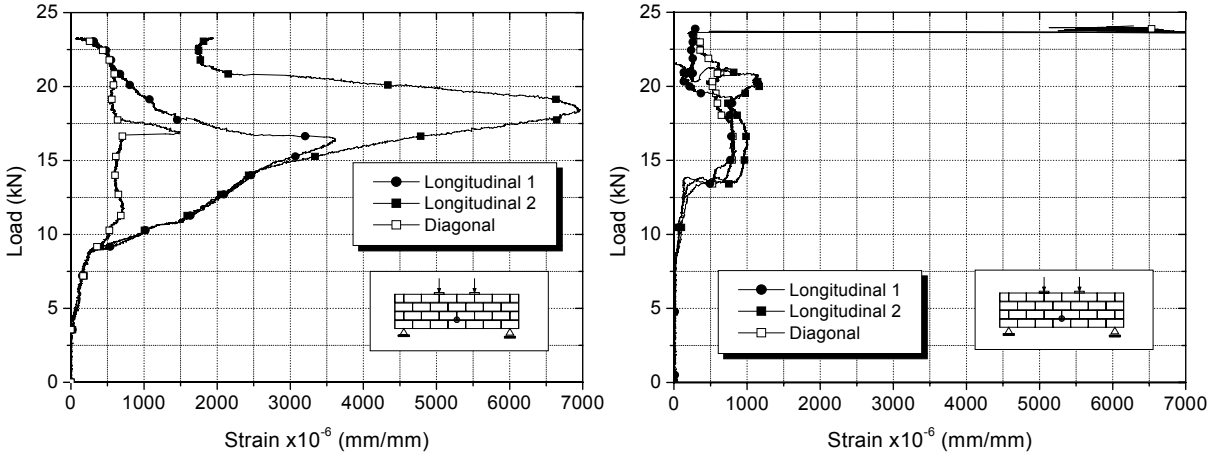

Figure 5.14 – Strains measured in horizontal reinforcements: (a) masonry beam F-3C-D3-C and (b) masonry beam F-2C-D3-C.

Specimens with horizontal reinforcements, F-3C-D3-D, F-3C-D3-D-M, F-2C-D3-D and F-2C-D3-D-M, distributed along the height of the beams exhibited also a typical flexural cracking with the same cracking pattern. Apart from specimen F-3C-D3-D-M, whose horizontal reinforcement broke at first and second courses, all of the abovementioned specimens exhibited breakage of horizontal reinforcements only at the first course. Figure 5.15 shows the vertical load versus the evolution of strains recorded in strain gauges attached to the horizontal reinforcements on the abovementioned specimens. It is observed that in general the horizontal reinforcements placed at first and second courses present tensile strains, whereas the reinforcement of the third course exhibit compressive strains, as

expected. Similarly to specimen F-2C-D3-C, the strain-gauges of specimen F-2C-D3-D were probably damaged at the beginning of test since the strains measured were very low in spite of the breaking of the bars. The introduction of vertical reinforcements at mid-span of the beams increased their flexural strength due to the filling of cells with mortar, which generated a reduction of strains in reinforcements of the first course at mid-span, see Figure 5.15c. The positioning of these reinforcements induced also a change on the cracking pattern, moving the flexural failure for the third part of the beam.

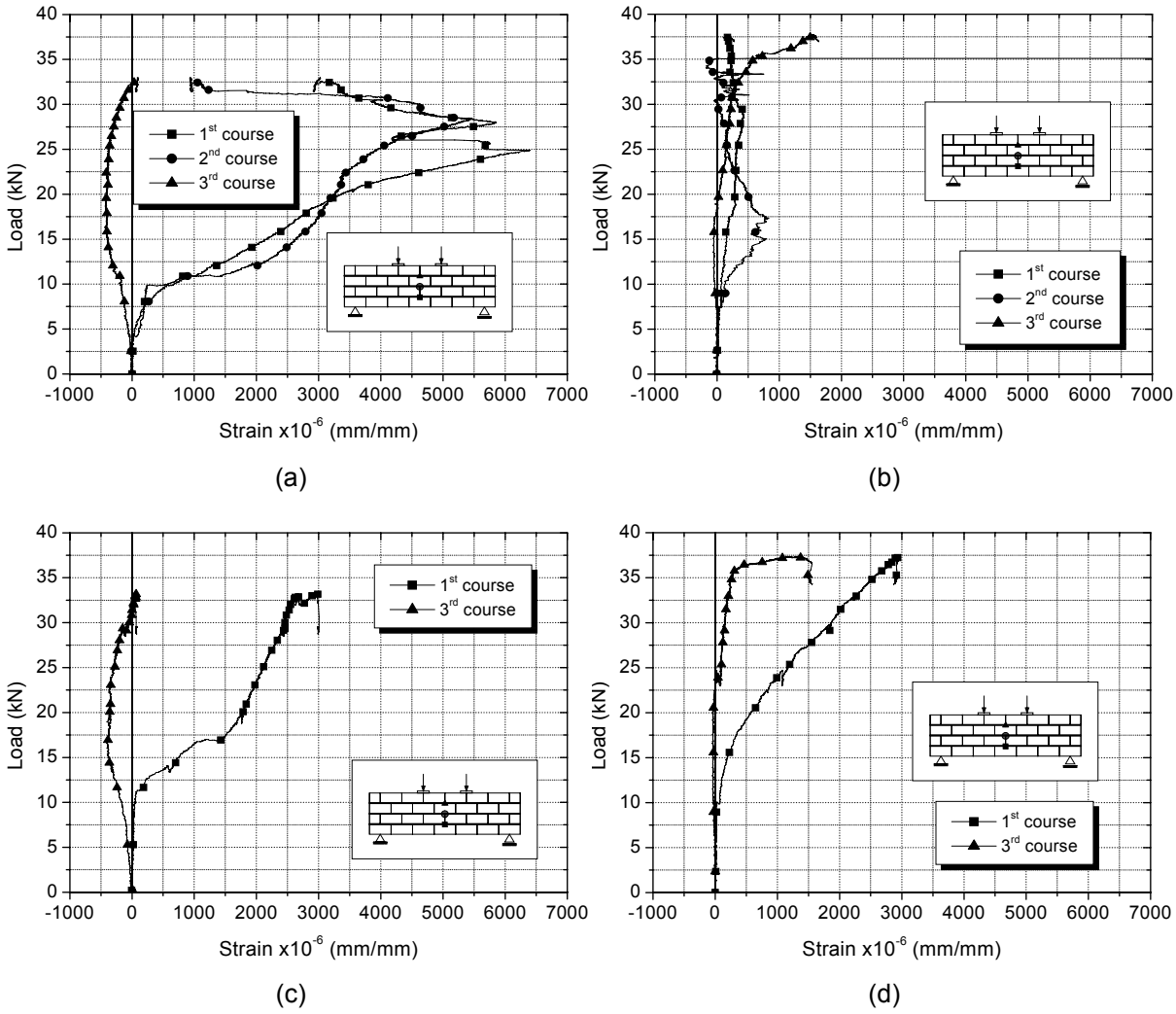

Figure 5.15 – Strains measured in horizontal reinforcements: (a) F-3C-D3-D, (b) F-2C-D3-D, (c) F-3C-D3-D-M and (d) F-2C-D3-D-M.

In specimens reinforced only at the first course (F-3C-D5-C and F-2C-D5-C), shear failure developed associated to diagonal cracking between the point load and the support, even in the presence of vertical reinforcements near the support. The shear cracking pattern develops together the flexural vertical cracks opened at the bottom vertical joint of the central region of the beam. The level of tensile strains developed in the first course's reinforcements

shows that they yield in masonry beams built with 3C-units and dry vertical joints, which confirm its mixed failure mode, see Figure 5.16.

It should be referred that the tensile strains developed in the reinforcements of beams built with the 3C-units present almost always higher values than the tensile strains of reinforcements in beams built with 2C-units, meaning that the 3C-units lead to higher ductility. After the opening of diagonal crack, the vertical reinforcements that connect both edges of the crack ensure the distribution of stresses through the crack. However, it was observed that the contribution of vertical reinforcements located near the support was reduced due to the debonding of vertical joint in case of specimens built with 3C-units, see Figure 5.17.

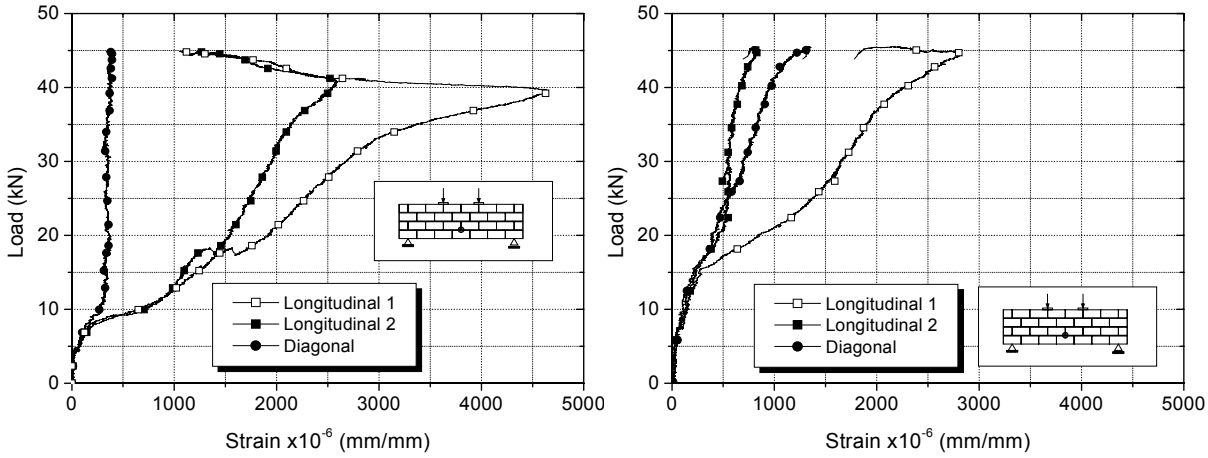

Figure 5.16 – Strains measured in horizontal reinforcements: (a) F-3C-D5-C and (b) F-2C-D5-C.

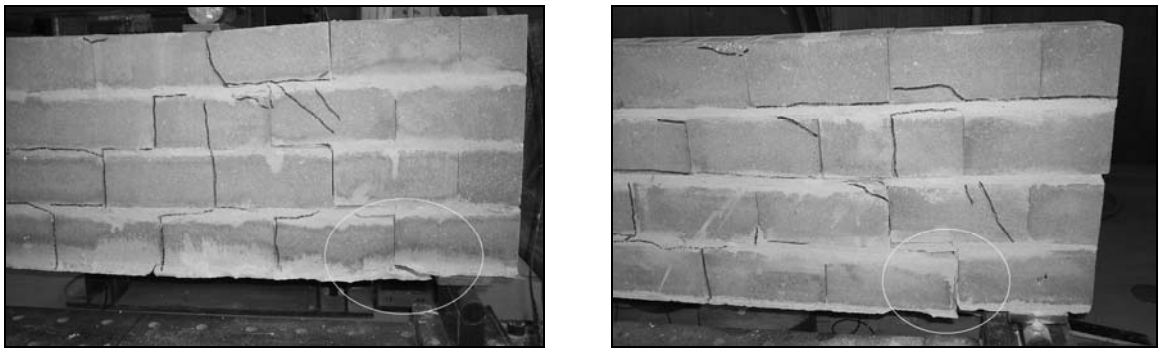

Figure 5.17 – Debonding of vertical joint in specimens built with 3C-units: (a) F-3C-D5-C and (b) F-3C-D5-D.

Specimens with 5mm horizontal reinforcements distributed in all mortar layers failed clearly by shear with the opening of a main diagonal crack between the support and the load

application point. The strains measured in the horizontal reinforcements distributed along the height of the specimen, shown in Figure 5.18, indicates that, as expected, the reinforcement at the first course exhibit the maximum tensile strains for all the specimens.

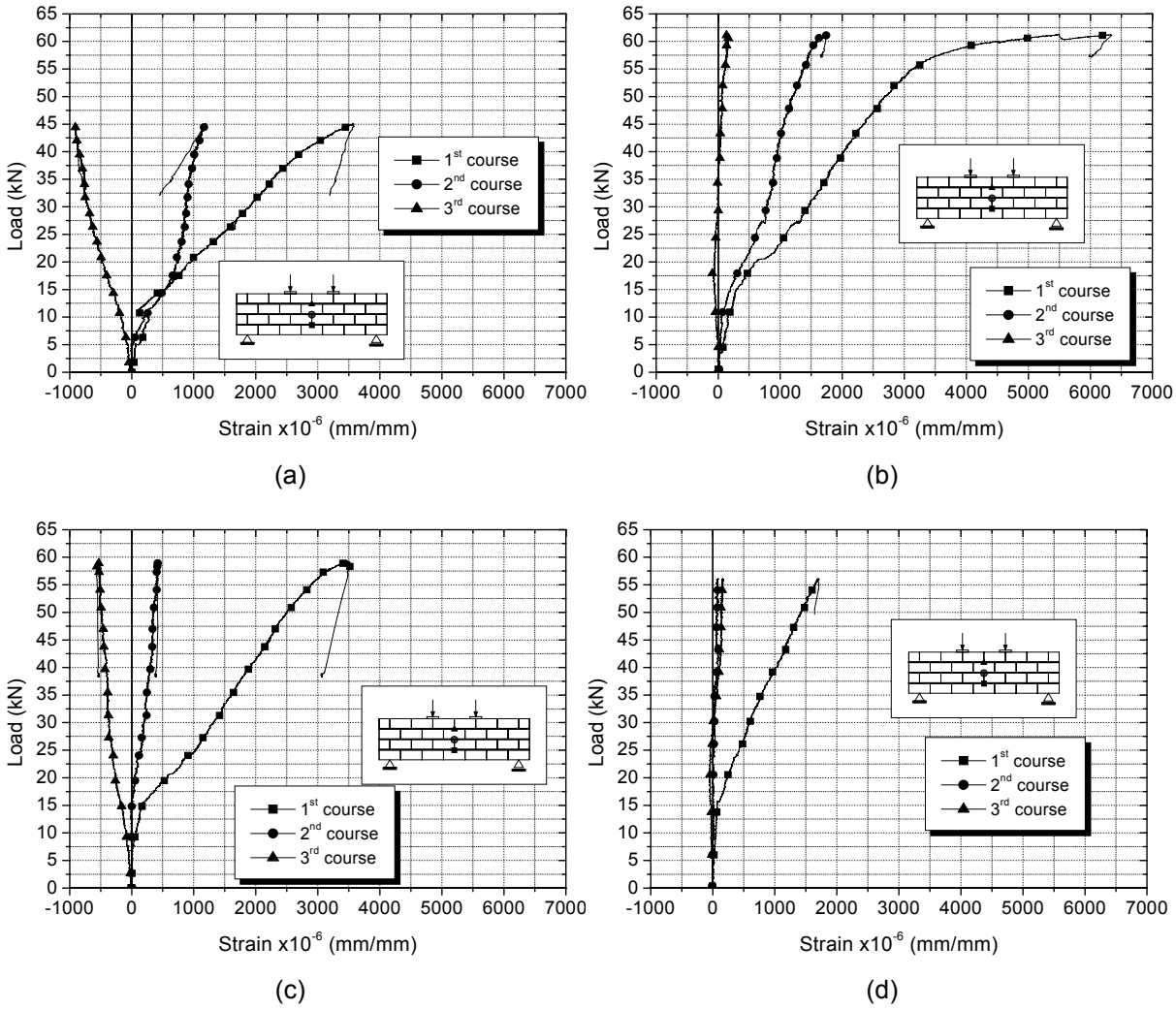

Figure 5.18 – Strains in horizontal reinforcements: (a) F-3C-D5-D, (b) F-2C-D5-D, (c) F-3C-D5-D-M and (d) F-2C-D5-D-M.

In beams with 3C-units the reinforcement positioned at the third course is clearly in compression, whereas in beams with 2C-units the strains are almost zero, meaning that the neutral axis should be at the third course. The decreasing of the strains after the maximum load indicates that total capacity of horizontal reinforcements was not used, confirming the shear failure of the masonry beams. The addition of the central vertical reinforcements seems to improve the resistance of the beam with 3C-units, even if no significant changes occur in the maximum tensile strain, which means that in relative terms the reinforcement present lower strains, as observed in specimens F-3C-D3-D-M and F-2C-D3-D-M. This is also true in specimens built with 2C-units, which exhibit also a slight reduction on the

resistance. The opening of the diagonal crack could be clearly observed through the LVDT 6 positioned near the support measuring the relative displacement between the third and second courses, see Figure 5.19. It is clear that the higher horizontal sliding occurs in specimens where diagonal cracking occurs. In case of specimen F-3C-D5-D-M the low level of sliding is related to localization of the diagonal crack in the opposite side, which was not instrumented. Otherwise LVDT 4 exhibited negligible results.

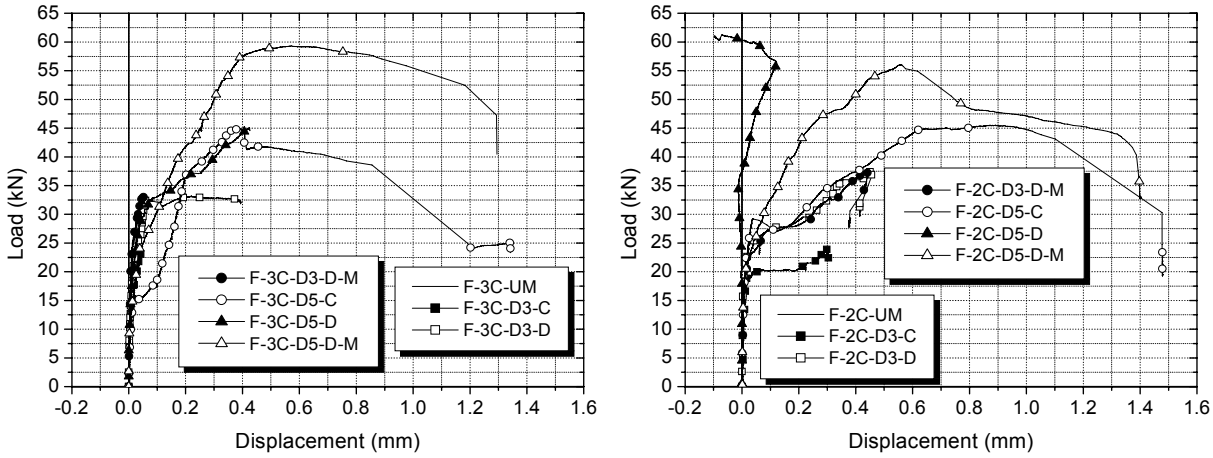

Figure 5.19 – Results of the LVDT 6 of beams measuring the opening of diagonal cracks: (a) 3C-units and (b) 2C-units.

The failure by shear diagonal cracking was also characterized by sliding of the units at the border vertical edges over the bed joint. This behaviour was more remarkable in specimens with horizontal reinforcement distributed along the height of the beams due to the higher ultimate load and thus to higher shear stresses. The sliding at the unit-mortar interface is attributed to the achievement of the shear strength of the unit-mortar interface due to shear stresses in the perpendicular direction to the cross section of the beams due to the symmetry of shear in the cross section and on the perpendicular plan.

The presence of reinforcements distributed along the height of the specimens represents an increase on the resistance of the beam, resulting in a higher resisting moment and, thus, to higher stresses at the upper compressive zone of the beam. This high compressive stresses induces that formation of splitting vertical cracks at the webs of the concrete units according to what is shown in see Figure 5.20. This type of cracking was already detected in the compressive tests carried out on masonry wallets in the direction parallel to bed joints. In fact, note that the compressive stresses in the upper region of the beam develop in the direction parallel to the bed joints.

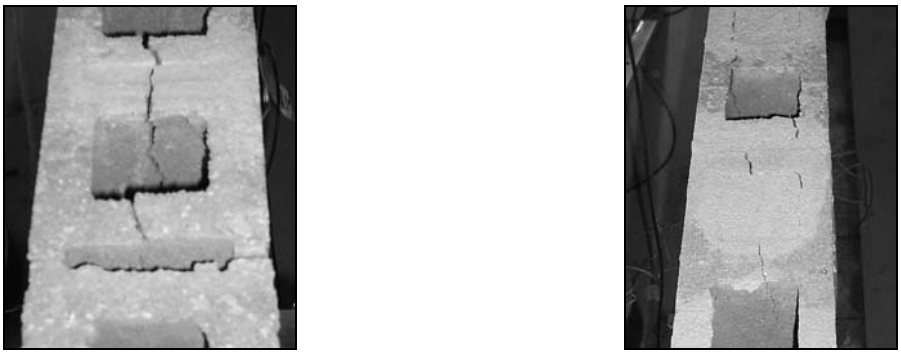

Figure 5.20 – Cracks in webs of blocks due to the high compressive stresses.

The presence of reinforcements in all bed joints also reduced the depth of the neutral axis meaning that the vertical crack at mid-span reached the third course of the beams. Even if LVDT 5 has been positioned at mid-span of beams to record possible slippage between fourth and third courses; it really measured a combined displacement resulting from the opening of vertical crack and the slippage at the upper unit-mortar interface, see Figure 5.21. The vertical reinforcements added at the central region of the beam reduce the slippage at the upper bed joint. As can be seen in Figure 5.10, no debonding of the upper unit-mortar interface developed when the vertical reinforcements are placed in the masonry beams.

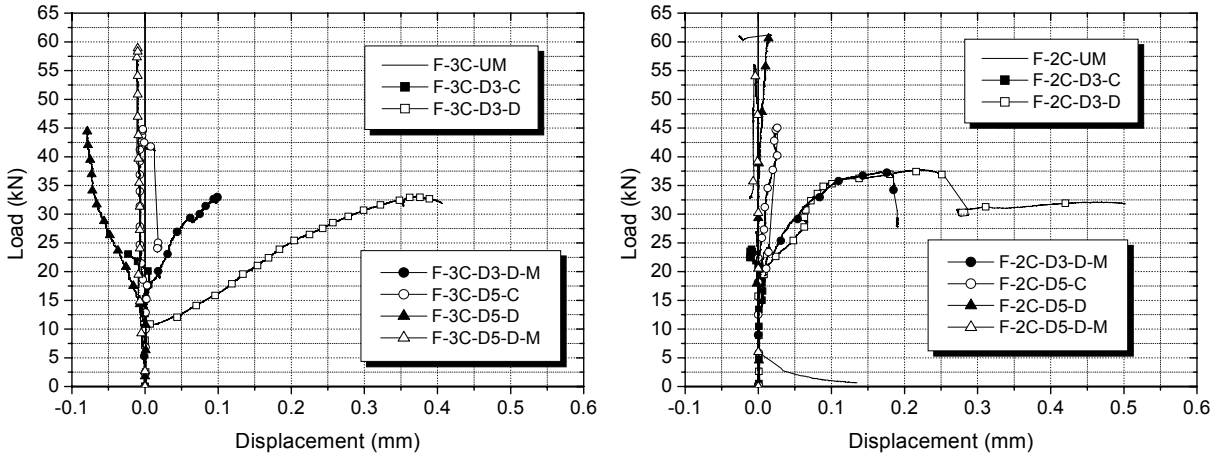

(a) (b)

Figure 5.21 – Results of the LVDT 5 in four point load tests: (a) 3C-units and (b) 2C-units.

The high compression in upper region of the beam led to the splitting of the upper course due to the low tensile strength of the interface unit-mortar. This behaviour is particularly evident when flexural response is predominant, which is associated to high compressive stresses developed in upper region of the beam. The separation of concrete units was also visible in compressive tests in parallel direction to the bed joints carried out on masonry wallets (Chapter 3). The use of vertical reinforcements at the mid-span of the

panels results in a good control of the cracking. It avoids or at least, reduces tensile cracking at the unit-mortar interface. These bars exhibit higher strains in specimens built with 3C-units as the masonry presents lower compressive strength parallel to bed joints and higher ductility, see Figure 5.22. On the other hand, it is clear that the strains are higher in reinforcements with 3mm longitudinal diameter, which is associated to the predominant flexural cracking, conversely to the specimens with 5mm longitudinal diameter that presents a mixed flexural-shear or shear failure.

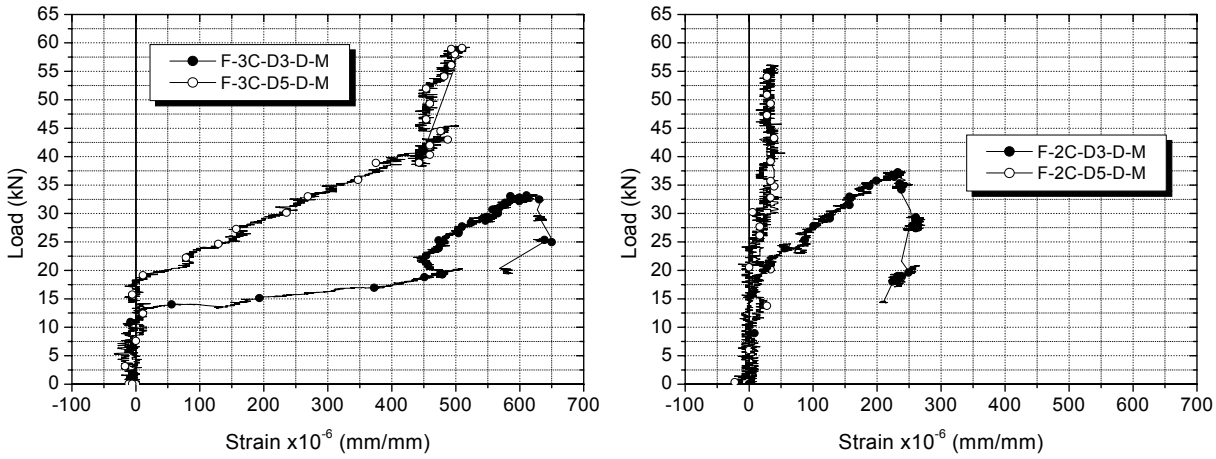

Figure 5.22 – Strains measured at the central vertical reinforcements in four point load tests.

5.3.1.2 Three point load tests

Apart from specimen S-2C-SH, which failed by crushing of the unit located under load application point due to a concentration of stresses, all masonry beams tested under three point load configuration presented a shear failure mode. Specimen S-2C-SH, which was the first to be tested, presented crushing of the unit under the load application point due to stress concentration resulting from the low length of the steel plate placed under the vertical actuator, see Figure 5.23. Higher length of the steel plate, and thus more compatible local compressive stress with strength of the concrete units, was used in the following tests avoiding such local cracking patterns. However, the crushing seemed to occur near the real capacity of the beam since diagonal cracks have been already developed.

It should be stressed that due to the geometry of the specimens and to the horizontal ordinary steel bars placed at the base of the beam no flexural cracking occurred. This is also confirmed by the negligible strains measured in the horizontal truss type reinforcements at the mid-span of specimens as indicated in § 5.2.1 (Figure 5.8b). In this test configuration the load path through the beam is composed by two compressed struts connecting the load application point and the supports. The cracking pattern composed by diagonal cracking is a

consequence of the stress distribution along the compressed struts. Figure 5.24 shows the crack patterns of specimens tested through the three point loading configuration.

Figure 5.23 – Crushing of the concrete block under the load application point in specimen S-2C-SH.

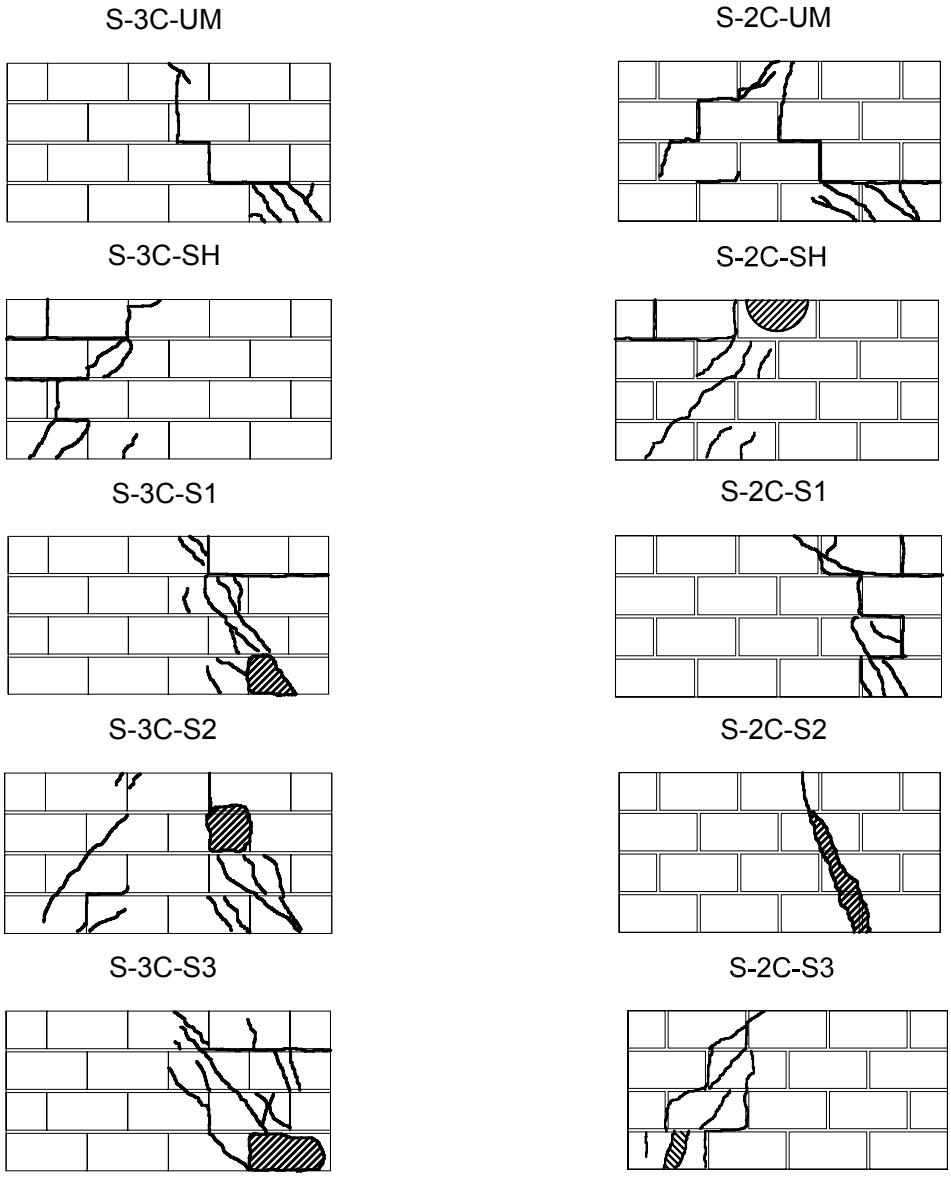

Figure 5.24 – Crack patterns of masonry beams tested according to the three point load configuration.

It is clear that both vertical and horizontal reinforcements had influence on the features of the shear crack patterns. For both types of concrete units, the shear crack developed in unreinforced masonry beams is mainly localized along the vertical and horizontal unit-mortar interfaces. When horizontal reinforcements are placed at the bed joints, the shear crack is more distributed and develops mainly through concrete units. The horizontal reinforcements lead to the increase on the shear strength of the masonry joints and thus to the increase on shear stresses resulting on cracking of the concrete units. The horizontal reinforcements provide a better distribution of shear stresses reducing the masonry anisotropy, leading to a much more homogeneous material. Besides, the horizontal reinforcements improve the shear response of the masonry beams by avoiding the brittle failure due to the dowel action. This effect is particularly visible in specimen S-2C-S2, where the localized shear crack is able to attain a considerable opening, see Figure 5.25a. In case of reinforced specimens the higher vertical load applied to the beam represents an increase on the compressive stresses on the struts and consequently on the compressive stresses at the upper region of the beams in the parallel direction to the bed joints, resulting in the complete splitting of the concrete units of the third course, see Figure 5.25b.

(a) (b)

Figure 5.25 – Damage states on the masonry beams: (a) thick localized shear crack and dowel action effect of the horizontal reinforcements through diagonal crack (S-2C-S2) and (b) splitting of blocks at the upper course (S-3C-SH).

After the opening of the diagonal crack, significant strains are measured in vertical reinforcements as they connect the two edges of the crack and sustain the shear stresses, see Figure 5.26. The presence of vertical reinforcements reduced the horizontal debonding and consequent slippage in mortar joints due to the dowel action effect. In general, vertical reinforcements exhibited very low values of deformation, which can be explained by the premature failure associated to the crushing of units due to the high compressive stresses in the strut connecting the support and the load application point. From the diagrams shown in Figure 5.26 it is clear that the location of vertical bars has a fundamental influence on their contribution to the resisting mechanism to shear stresses.

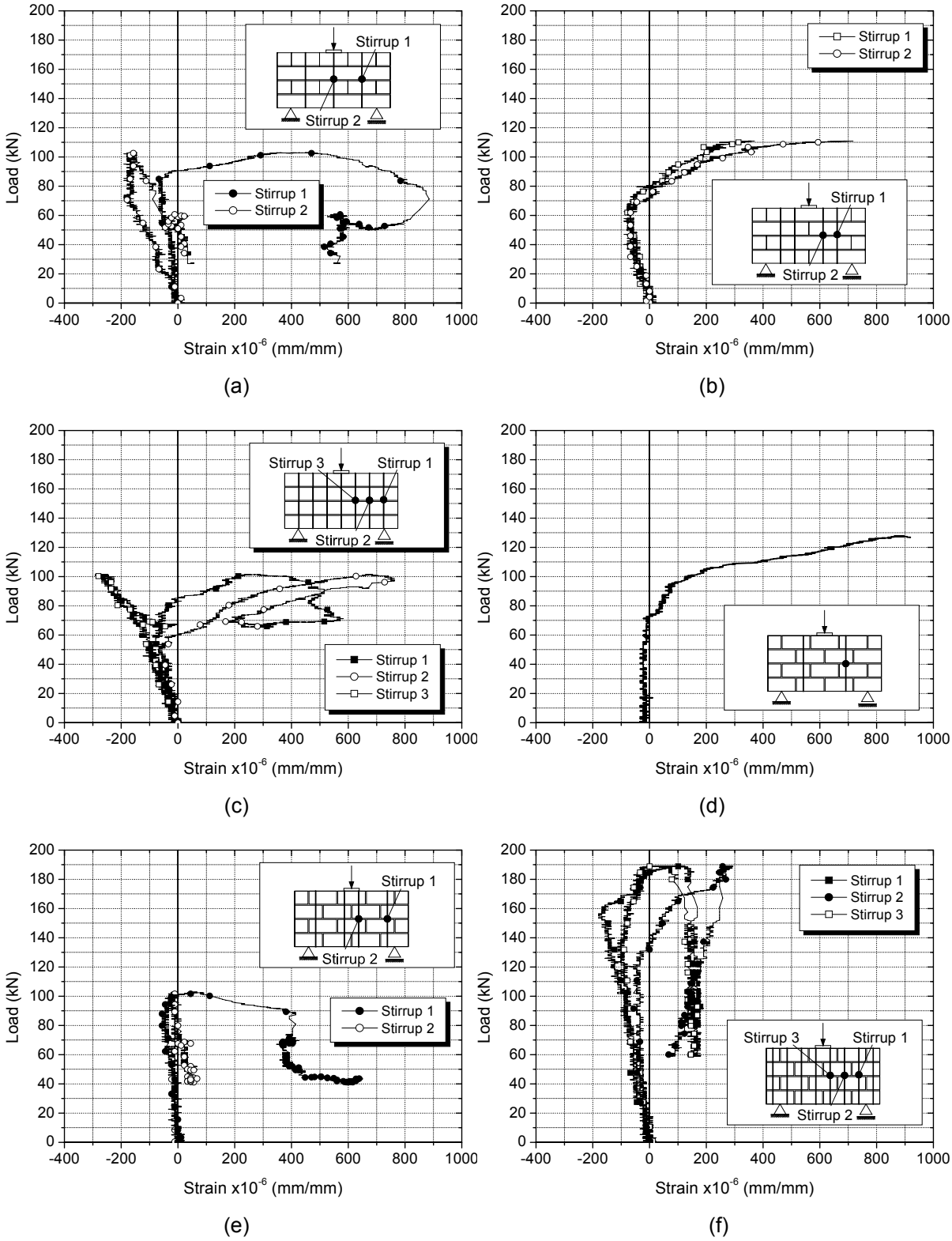

Figure 5.26 – Strains in vertical reinforcements of the masonry beams: (a) S-3C-S1, (b) S-3C-S2, (c) S-3C-S3, (d) S-2C-S1, (e) S-2C-S2 and (f) S-2C-S3.

Reinforcements located out of the diagonal shear band exhibit very low strains, whereas as abovementioned the vertical reinforcements crossing the diagonal crack present

increasing strains after diagonal cracking. An exception should be pointed out to the specimen S-2C-S3, where the negligible strains measured are related to the opening of the diagonal crack at the opposite side, which is not instrumented with strain gauges. Besides, the distribution of stirrups seemed to have a remarkable influence on the shear crack pattern. This is clear if a comparison between the shear crack bands is made between specimen S-2C-S1 and specimen S-2C-S2. Note that in specimen S-2C-S2, two steel truss type bars bound the localized shear crack, meaning that the contribution for the crack distribution is negligible, leading to the failure for a lower external load than the one obtained in specimen S-2C-S1. On the other hand, the vertical reinforcement placed in specimen S-2C-S1 seems to be effective on the crack distribution as it crosses the diagonal shear band. It should be stressed that a more distributed cracking is achieved by decreasing the spacing of vertical reinforcements, which is the case of specimens S-2C-S3 and S-3C-S3.

Similarly to what happened in the four bending tests, the high compressive stresses in upper region of beams generated cracks in webs of the blocks as observed in characterization tests of masonry wallets tested under compression parallel to bed joints. Besides, the sliding of horizontal blocks over the horizontal joints in the extremities of beams also occurred due to the high shear stresses in mortar joint.

5.3.2 Force *vs.* displacement diagrams and crack limits

5.3.2.1 Four point load tests

The force-displacement diagrams exhibiting the global behavior of the tested beams are shown from Figure 5.27 to Figure 5.29.

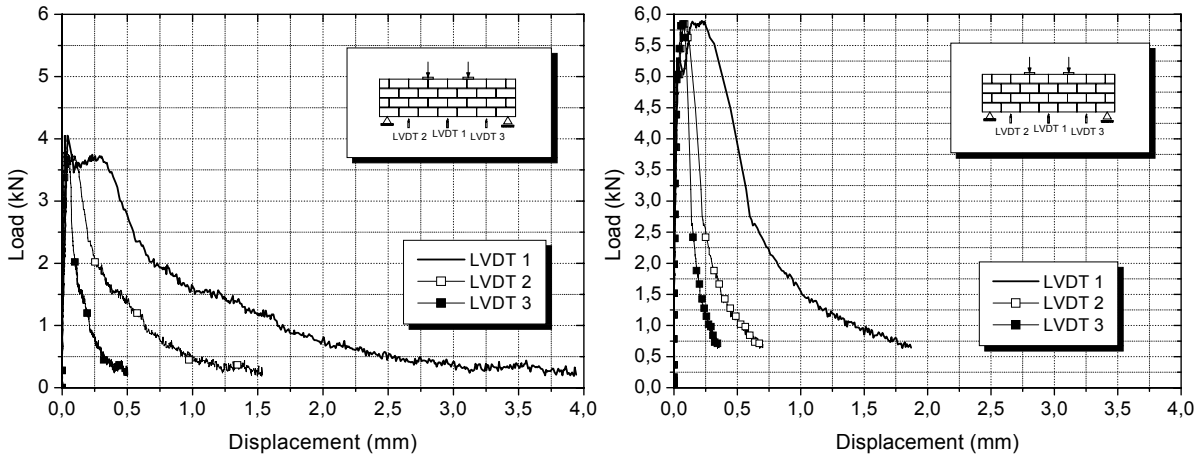

Figure 5.27 – Force–displacement diagrams of the masonry beams: (a) F-3C-UM and (b) F-2C-UM.

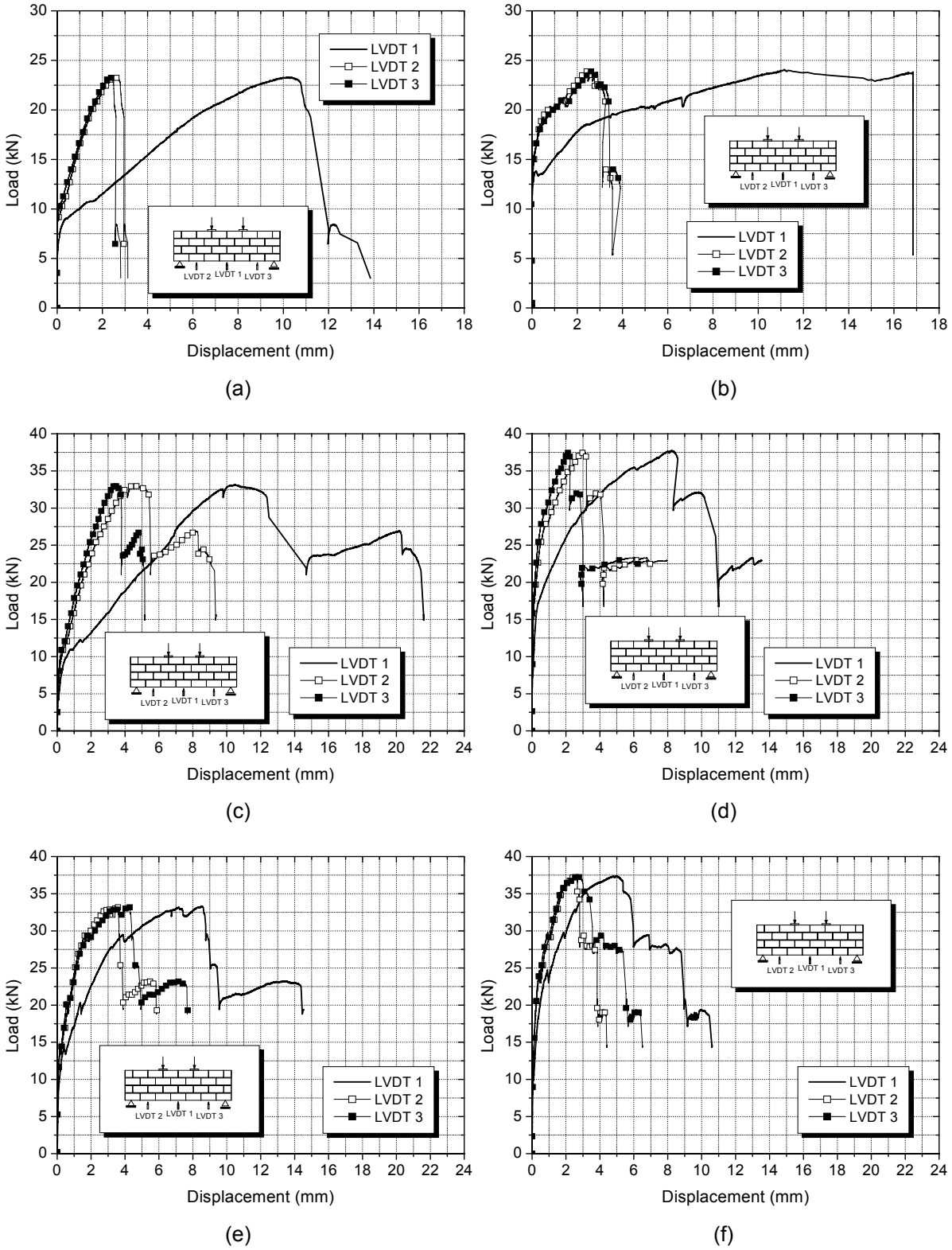

Figure 5.28 – Force-displacements diagrams of the masonry beams: (a) F-3C-D3-C, (b) F-2C-D3-C, (c) F-3C-D3-D, (d) F-2C-D3-D, (e) F-3C-D3-D-M and (f) F-2C-D3-D-M.

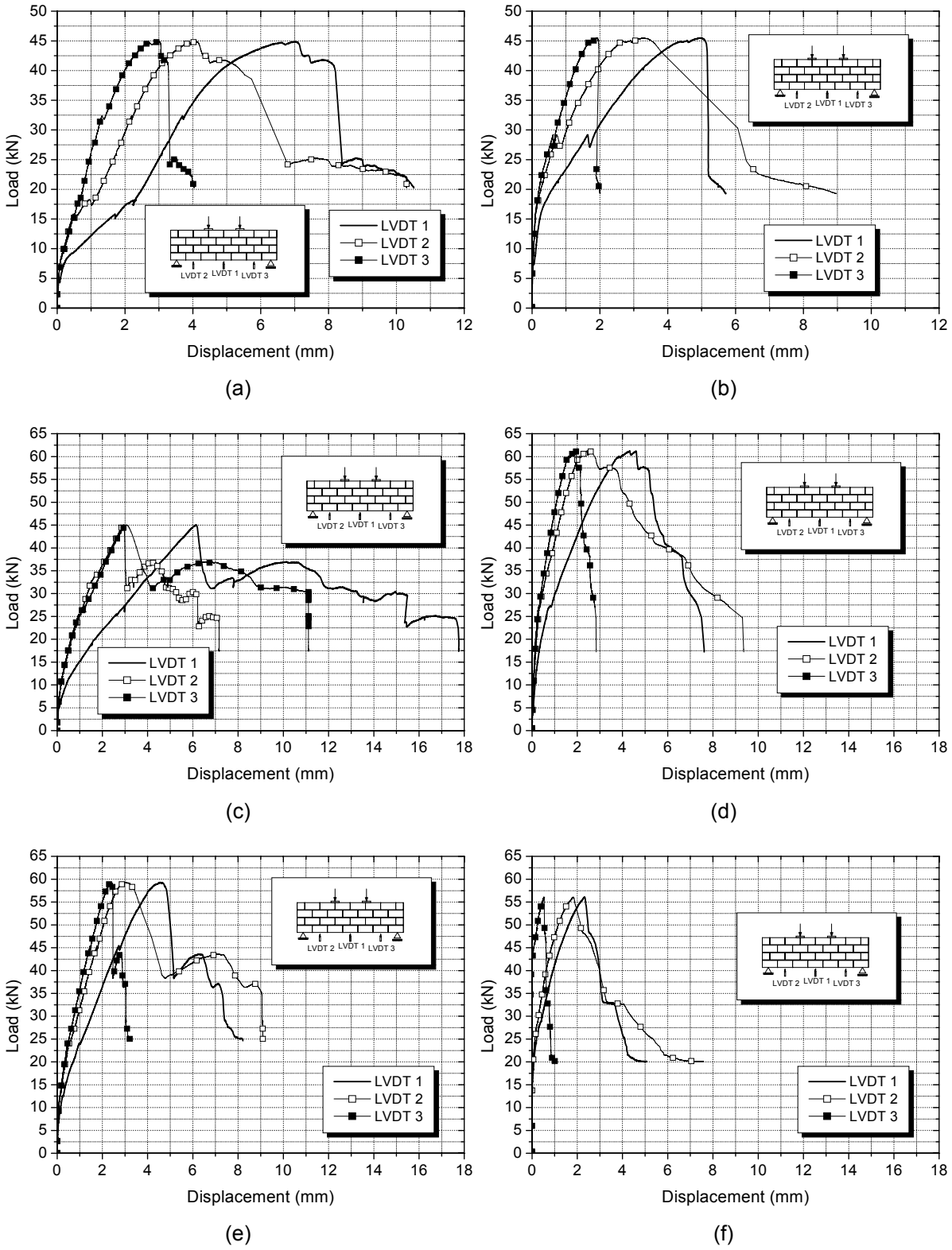

Figure 5.29 – Force-displacement diagrams of the masonry beams: (a) F-3C-D5-C, (b) F-2C-D5-C, (c) F-3C-D5-D, (d) F-2C-D5-D, (e) F-3C-D5-D-M and (f) F-2C-D5-D-M.

Figure 5.30 shows a summary of the force-displacement diagrams of all specimens. In general, three phases characterizes the force-displacement diagrams of masonry beams.

There is an initial elastic behaviour corresponding to a high initial stiffness with very small vertical deflections. The second stage is characterized by the opening of flexural cracks at the unit-mortar interface located at mid-span, which is associated to an abrupt decrease on stiffness and to an increase on the load up to the achievement of the maximum strength of the beam. The decrease on the stiffness is particularly evident on specimens behaving in flexure. The detection of the opening of flexural cracks can be confirmed by the horizontal displacements measured by LVDT 7, as shown previously.

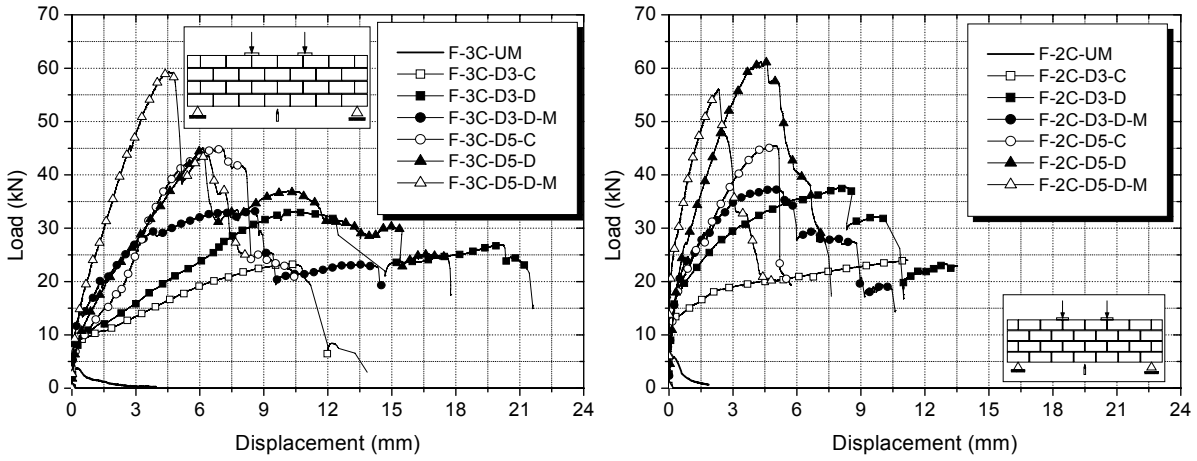

Figure 5.30 – Force-displacement diagrams of the masonry beams in four point loads tests: (a) 3C-units and (b) 2C-units.

On the other hand, diagonal cracking is only identified by the relative displacements measured at the unit-mortar interface near the supports (LVDTs 4, 5 and 6). The stiffness at the second stage depends on the horizontal reinforcement ratio and on the presence of vertical reinforcements at the mid-span, being increasing for increasing horizontal reinforcement ratio and with the placement of vertical reinforcement at mid-span. After flexural cracking, load transfer from the masonry to the horizontal reinforcements occurs, being the resisting mechanism composed by the tensile strength of the reinforcements and compressive strength of masonry. The third stage is characterized by the softening of the masonry beams associated to the reduction on the shear resistance with increasing displacements. The failure of beams can occur by yielding of reinforcement, crushing of the masonry in the upper compressed part or by diagonal cracking. Table 5.3 shows the cracking and maximum loads found in the four point loads tests. Unreinforced masonry beams present very low flexural strength and very brittle behaviour, even if slighter higher strength was obtained in beams with filled vertical joints and 2C-units. After flexural cracking at the bottom course, a sudden stair stepped crack follows up to the compressed edge of the

beams leading to the abrupt failure. It is observed that the introduction of horizontal reinforcement, the increase on its ratio and its distribution along height assumes a central role on the increase of the strength and ductility of the masonry beams. Considerable higher resistance of reinforced beams at bed joints was obtained in comparison with unreinforced masonry beams. Besides, it is clear that higher is the horizontal reinforcement ratio higher is the strength of beams.

Table 5.3 – Cracking and maximum loads in four point load tests.

Beam	Flexural Cracking Load (kN)	Diagonal Cracking Load (kN)	Maximum Load (kN)
F-3C-UM	4.05	-	4.05
F-3C-D3-C	3.84	-	23.32
F-3C-D3-D	4.43	-	33.19
F-3C-D3-D-M	8.69	-	33.30
F-3C-D5-C	4.80	15.70	44.90
F-3C-D5-D	5.15	23.05	45.04
F-3C-D5-D-M	7.60	18.18	59.31
F-2C-UM	5.10	-	5.90
F-2C-D3-C	8.93	18.87	24.09
F-2C-D3-D	7.52	24.41	37.73
F-2C-D3-D-M	10.06	21.88	37.38
F-2C-D5-C	7.43	24.78	45.54
F-2C-D5-D	3.48	41.72	61.24
F-2C-D5-D-M	7.82	22.29	56.10

Specimens predominantly governed by flexure presents considerable higher ductility than the specimens where diagonal shear cracking takes the central role on the behaviour of the beams, with higher deflection corresponding to the maximum resistance, considerable higher ultimate deflection and smoother post-peak branch. It should be stressed that masonry beams built with 3C-units are remarkably more ductile than masonry beams built with 2C-units and filled vertical joints. This appears to be related with the compression in the direction parallel to the bed joints, which is much more ductile for masonry built with 3C- units and dry vertical joints, as already mentioned in Chapter 3.

Results showed that vertical reinforcements placed at mid-span increased the force corresponding to the flexural cracking, which is associated to the mortar filling of the vertical internal cores of the 3C-units, resulting on the increase of the tensile strength of unit-mortar interface in first course at mid span of the beam. However, by analysing the diagonal crack

force, the presence of vertical reinforcements at mid span appears to anticipate the diagonal cracking of the beams, which can be associated to the increasing level of compressive stresses at upper region of beams leading to an increase of compressive stresses on diagonal struts between the load application point and supports.

In case of maximum load of tested masonry beams, by comparing the experimental and flexural and shear theoretical values obtained in masonry beams which failed by flexure calculated according to Eurocode 6 (2005), it is clear an increase of the experimental strength due to the axial stress in the beams provided by the semi-rigid support, see Table 5.4.

Table 5.4 – Comparison between experimental and theoretical loads according to Eurocode 6 (2005) for masonry beams of four point load configuration which failed by flexure.

Beam	Exp. Load (kN)	Theo. Load Flexure (kN)	Theo. Load Shear (kN)
F-3C-D3-C	23.32	13.37	41.28
F-3C-D3-D	33.19	17.98	41.28
F-3C-D3-D-M	33.30	17.98	41.28
F-2C-D3-C	24.09	13.56	49.68
F-2C-D3-D	37.73	19.62	49.68
F-2C-D3-D-M	37.38	19.62	49.68

5.3.2.2 Three point load tests

As expected, shear was the prevailing effect in specimens tested under three point load configuration, being the failure mode governed by diagonal cracking. As no flexural cracking develops, the behaviour is composed by two phases, namely the linear elastic behaviour before diagonal cracking and nonlinear behaviour after diagonal cracking composed by a small stretch of pre-peak nonlinearity and the post-peak descending branch, see Figure 5.31 and Figure 5.32. Figure 5.33 shows a summary of the force-displacement diagrams of all specimens and Table 5.5 shows the cracking and maximum loads for three point load tests.

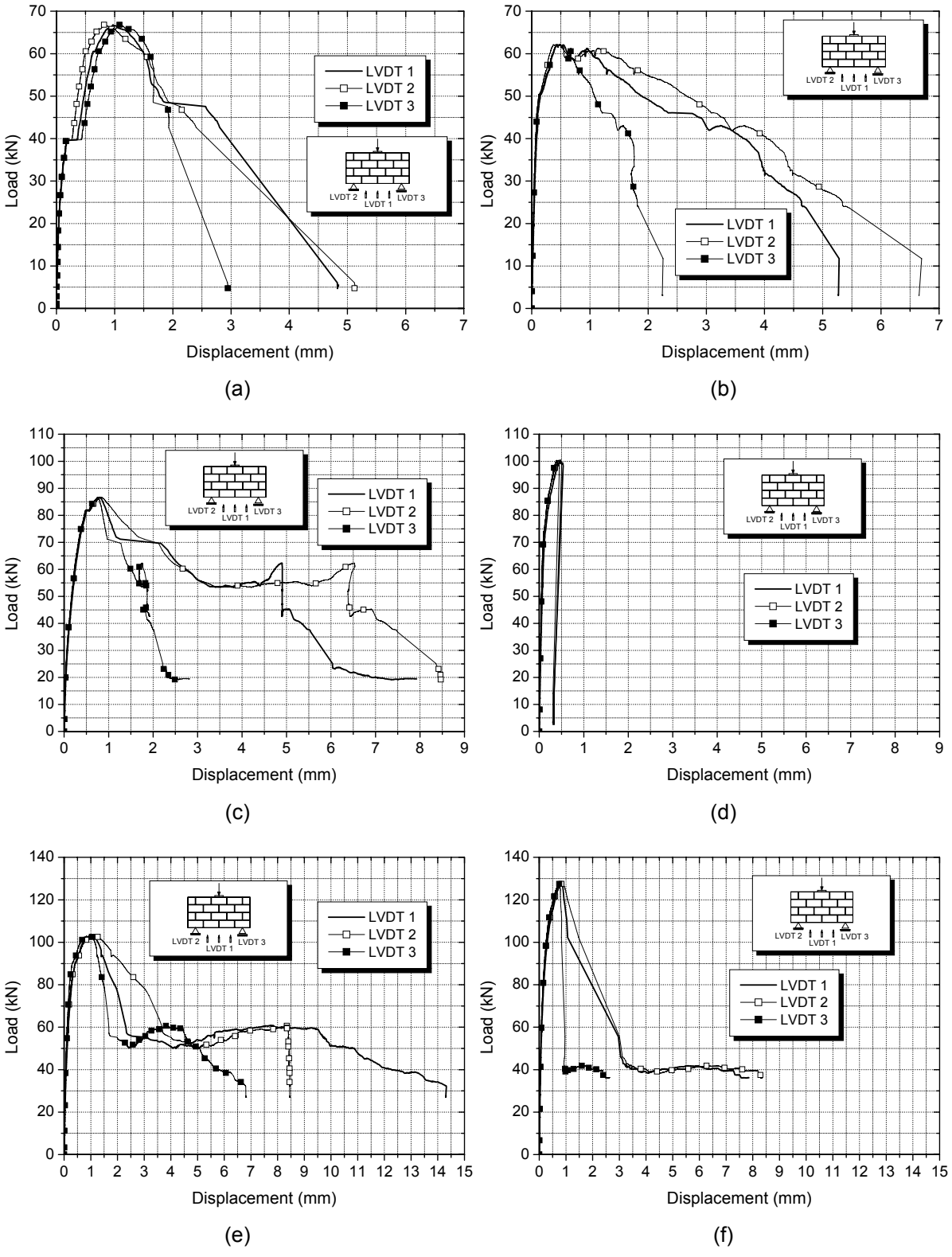

Figure 5.31 – Force-displacements diagrams of the masonry beams: (a) S-3C-UM, (b) S-2C-UM, (c) S-3C-SH, (d) S-2C-SH, (e) S-3C-S1 and (f) S-2C-S1

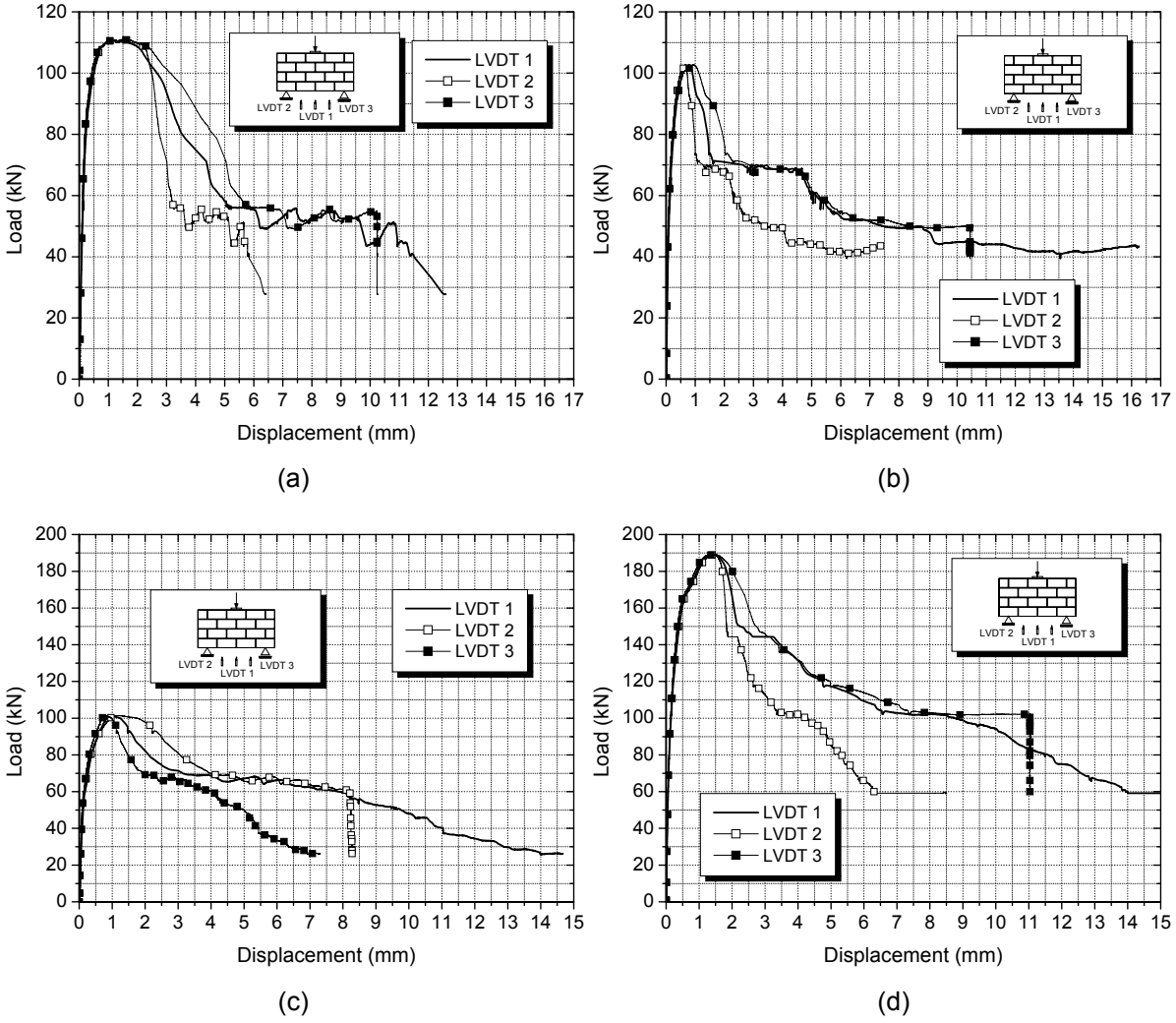

Figure 5.32 – Force–displacements diagrams of the masonry beams: (a) S-3C-S2, (b) S-2C-S2, (c) S-3C-S3 and (d) S-2C-S3.

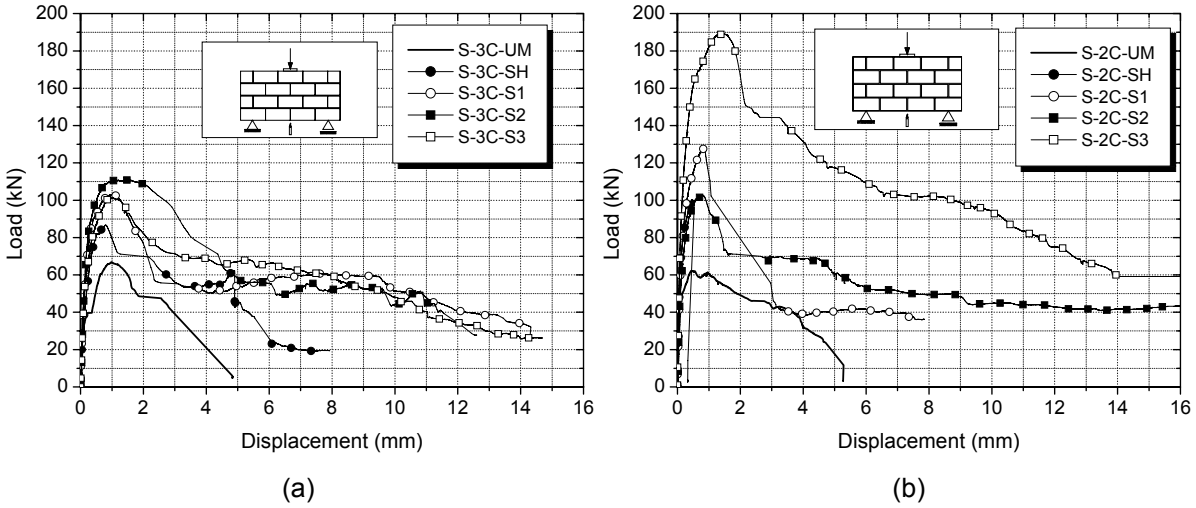

Figure 5.33 – Force-displacement diagrams of the masonry beams of three points loading tests: (a) 3C-units and (b) 2C-units.

Table 5.5 – Cracking and maximum loads in tests of masonry beams for three point loads configuration.

Beam	Diagonal Cracking Load (kN)	Maximum Load (kN)
S-3C-UM	39.80	66.80
S-3C-SH	83.20	86.68
S-3C-S1	86.80	102.91
S-3C-S2	80.00	110.89
S-3C-S3	80.57	101.43
S-2C-UM	49.90	62.11
S-2C-SH	70.00	100.34
S-2C-S1	75.00	127.61
S-2C-S2	102.75	102.75
S-2C-S3	149.60	188.96

Masonry beams exhibited high initial stiffness, being the maximum load attained for very low deflection of the beams. For unreinforced beams built with 3C-units and 2C-units no significant differences were detected in the overall shear behaviour. The maximum strength of beams built with 3C-units is only about 7.5% higher than the strength obtained for beams with 2C-units, being the ultimate deformation approximately the same. It is clear that the presence of reinforcements improved the shear behaviour of beams, increasing the strength and deformation capacity, and, as observed in four point load tests, delaying the diagonal cracking. Horizontal reinforcements influence positively the shear behaviour by enhancing the crack distribution, as already mentioned previously, and by increasing the strength of the beams. Note that the presence of horizontal reinforcements seems also to lead to an improvement of the ultimate deformation capacity for beams with 3C-units, in spite of no conclusions can be pointed out concerning the beam with 2C-units due to the local crushing failure (S-2C-SH). The increase on the global strength results from the improvement of the shear strength of the bed joints as well as from the dowel action effect, which allow additional load transfer between the edges of the shear crack. This effect has been already mentioned for vertical reinforcements in masonry walls subjected to lateral loading. Besides the horizontal reinforcements, vertical reinforcements also contribute for global shear strength by connecting both edges of the shear crack through the development of tensile stresses. An increase on the shear strength of the beams with 3C-units of about 18.7%, 27.9% and of 17% in specimens S-3C-S1, S-3C-S2 and S-3C-S3 was obtained in relation to the specimen with horizontal reinforcement. For beams built with 2C-units increases of 27.2%, 2.4% and of 88.3% were observed in specimens S-2C-S1, S-2C-S2 and S-2C-S3 in relation to the

specimen reinforced in bed joints. Note that the vertical reinforcements in specimen S-2C-S2 are out of the diagonal cracking, appearing that only a slight increase on the strength was obtained.

It should be noticed that apart from specimen S-2C-S2, in the other two beams built with 2C-units the increase on the shear strength due to the addition of vertical reinforcements is considerably higher than in specimens built with 3C-units. In case of beams with 3C-units, the vertical reinforcements are placed in the internal cell of the concrete units and at the frogged ends, where mortar with appropriate plasticity was applied in order to obtain the adequate bond between reinforcements and masonry. In case of beams with 2C-units, the vertical reinforcements are placed in one of the 2C-units being completely filled with mortar. This means that the addition of vertical reinforcements in beams with 2C-units represents a considerable increase on the effective cross section of the beams. For the configuration of uniformly distributed vertical reinforcements (S-2C-S3) the hollow vertical cells are reinforced and completely filled with mortar resulting in much higher shear strength. This means that part of the increase on the shear strength is due to the increase on the effective cross section.

Besides, it should be stressed that the shear capacity of masonry beams depends fundamentally on the position and distribution of vertical reinforcements (stirrups). In specimens built with 3C-units the first two reinforcement ratios increased the shear capacity. However, specimen S-3C-S3 exhibited a reduction of maximum load. This behaviour appears to be related to an increase on the compressive stresses at the struts and thus to the premature crushing of the units in the neighbourhood of the supports. On the other hand, the lower value of the shear strength obtained in specimen S-2C-S2 is attributed to the inadequate positioning of the vertical reinforcements out of the diagonal cracking, leading to its minor contribution to the shear strength. Though, this behaviour was not observed in specimen S-2C-S3 because it was fully filled with mortar, increasing the shear strength in region between the load application and supports.

5.4 Summary and conclusions

This chapter dealt with an extensive experimental program aiming at assessing the mechanical behaviour of masonry beams reinforced with truss type bars positioned at the bed joints and at the vertical cores of the units. Two load configurations were adopted, namely four and three point loads. Geometry of the units and horizontal and vertical reinforcement ratios were the main variables analyzed in the experimental study.

Results point out that bed joint reinforcement improved the flexure behaviour of masonry beams by increasing the capacity of these elements of resist tensile stresses, and the deformation capacity and by providing a better distribution of cracks leading to the delay the opening of diagonal cracking. Shear strength was also increased by the presence of horizontal reinforcement since they promote the connection of both edges of the shear crack allowing the stress transfer between them. Besides, horizontal reinforcement also contributed to shear strength and ductility through the dowel action mechanism.

Vertical reinforcements increased the shear strength of the masonry beams. However, it was observed that more than the reinforcement ratio, the location and distribution of vertical reinforcements take a central role on the shear behaviour of masonry. The distribution of the vertical reinforcements must cross the diagonal cracking for their positive contribution is considered effective for the increase on the shear strength. The correct localization of the vertical reinforcements avoids the localization of the diagonal cracking and improves the cracking distribution.

The increase on the effective cross section by the mortar filling of the hollow cell concrete units leads to the significant improvement on the shear strength of the masonry beams. This behaviour is mainly associated to the significant increase on the compressive strength of the masonry in the parallel direction to the bed joints.

6 NUMERICAL SIMULATION

6.1 Introduction

Masonry elements subjected to in-plane loading exhibit a complex structural behaviour mainly due to the anisotropic nature of masonry material. The prediction of the in-plane behaviour of masonry elements by means of complex numerical methods has been playing a central role in the research effort in the scope of masonry structures (Lourenço, 1996, Sutcliffe *et al.*, 2001, Van Zijl., 2004). It is assumed that experimental analysis is important to understand the behaviour of masonry structures providing the mechanical data for the validation of numerical models, after which more complex analysis like parametric studies can be performed. However, often experimental programs have high costs and a limit number of specimens are tested reducing the analysis of the number of variables that can be evaluated.

Two possible numerical approaches for masonry structures based on macro-modelling and micro-modelling has been presented in Chapter 2. Micro-modelling is suitable for a detailed analysis of small masonry structures, where is it important to describe the local resisting mechanisms. On the other hand, macro-modelling allows an evaluation of large size masonry structures, where the global behaviour is the real concern. Both numerical approaches can be useful on the understanding of the behaviour of masonry elements subjected to in-plane loading.

The numerical approach selected in this work is the micro-modelling due to the need of identifying the real failure mechanisms governing the in-plane cyclic behaviour of reinforced concrete block masonry walls and the flexural and shear behaviour of masonry beams. The micro-model was appropriately calibrated from the experimental results of the tested shear walls and masonry beams, taking into account some material parameters obtained in Chapter 3 and other parameters available in literature. After an initial comparison between experimental and numerical results of shear walls and masonry beams, a detailed

parametric study was carried in order to obtain a better insight on the influence of selected parameters like the filling of vertical joints, variation of pre-compression (in case of walls) and variation of the vertical and horizontal reinforcement ratios on the in-plane behaviour of the masonry structural elements. Besides, numerical models provide important information for the development of the design model of masonry walls and masonry beams.

6.2 Details of numerical modelling

As aforementioned the numerical simulation of masonry walls and beams under in-plane loading was carried out based on the micro-modelling approach by using the software DIANA®. The simplified micro-modelling approach, which represents the masonry as units connected by interface elements, was selected as the main aim is to clarify the resisting mechanisms of shear walls and masonry beams under in-plane loading. In a first phase, the numerical model was defined based on the geometry, boundary and loading conditions of specimens tested during experimental campaign. It should be mentioned that in case of shear walls monotonic loading was considered instead of the cyclic loading due to the compatibility of the interface elements. Newton-Raphson iteration procedure was used with a displacement control and an energetic convergence criterion with a tolerance of 10^{-3}.

6.2.1 Mesh

Mesh was composed by continuum elements representing the units separated by interface elements with zero-thickness representing the joints. Besides head and bed joints, potential vertical cracks were also modelled at the middle of units following the suggestion of Lourenço (1996). In case of units, eight-node isoparametric plane-stress elements with Gauss integration scheme were used in the model, whereas bi-dimensional interface elements with quadratic interpolation were used to represent the unit-mortar interfaces, see Figure 6.1.

In case of masonry beams, in spite of the special care taken to avoid friction forces at free support, results indicated some level of stiffness at this support (Chapter 5). Thus, a one-node translation spring (SP1TR) was introduced in numerical modelling to represent the semi-rigidity of that boundary condition. The stiffness of the spring was calibrated according to experimental results.

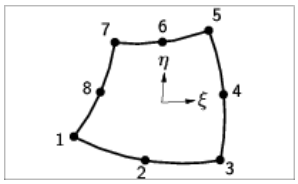

Element CQ16M – DIANA®

(a)

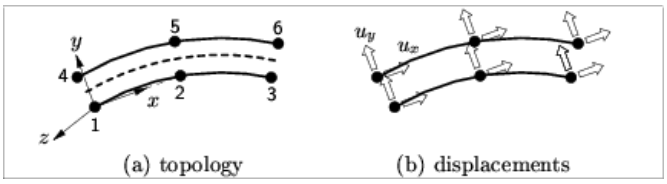

Element CQ16M - DIANA®

(b)

Figure 6.1 – Elements used in numerical modelling; (a) Units and mortar joints; (b) unit-mortar interfaces

Units were modelled with equivalent solid blocks to the actual hollow cell concrete blocks. In order to become the numerical model representative all properties of materials were defined by considering the gross area of the units. For shear walls, units were modelled with two elements, which mean that each half of unit was modelled by one continuum element. For masonry beams, units were modelled by 8 x 4 elements, which mean that each half of unit was modelled by 4 x 4 continuum elements, see Figure 6.2. The level of refinement of masonry beams was higher in order to obtain a representative mesh.

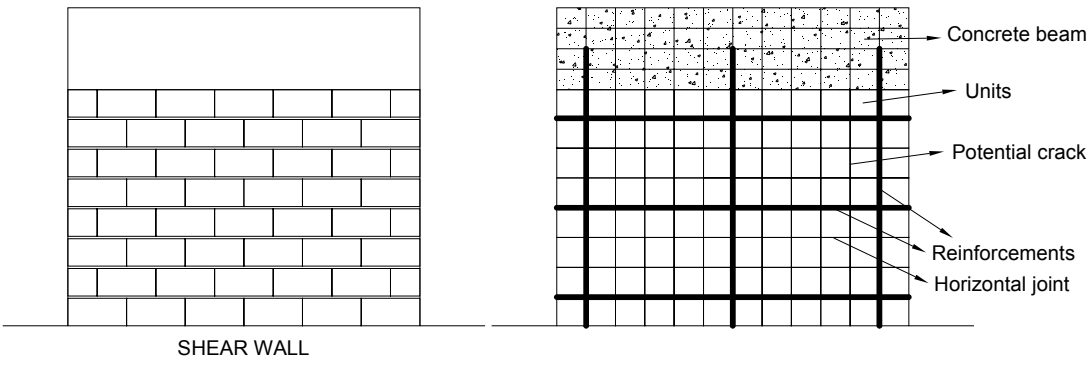

(a)

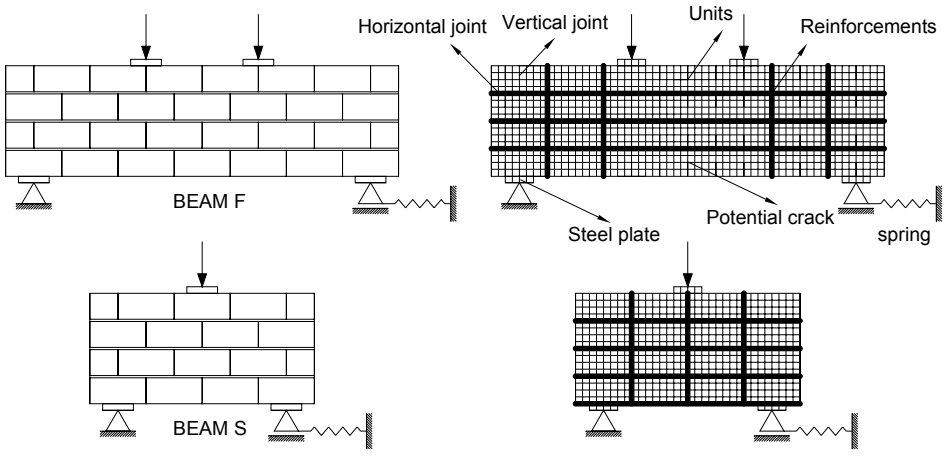

(b)

Figure 6.2 – Example of applied meshes: (a) shear walls and (b) masonry beams.

The upper concrete beam was also considered in the model as in the shear wall tests the horizontal load was applied at mid height of the upper beam. Bottom concrete beam was not modelled since it aims only at anchoring the vertical reinforcements. In case of masonry beams, steel plates used at supports and at points of load application were also simulated in order to avoid the concentration of stresses.

Reinforcements were modelled through embedded bars adding stiffness to the finite element model. Reinforcement strains were computed from the displacement field of the master elements due to the assumption of perfect bond between the reinforcement and the surrounding material.

6.2.2 Material Properties

The material mechanical properties adopted in numerical modelling were obtained through the characterization tests carried out at laboratory and described in Chapter 3. Some properties that were not possible to be measured at laboratory were calibrated by fitting the numerical to the experimental results. The different materials used to model the different structures (masonry beams and walls) in order to suitably represent the experimental behaviour are shown in Table 6.1.

Table 6.1 – Summary of materials used in modelled structures.

Type	Unit	Nº Materials	Description
Shear wall	3C	7	Units, horizontal joint, vertical joint, potential crack, trussed bars, concrete of upper beam and interface between upper beam and shear wall
	2C	9	Units, horizontal joint, vertical joint, potential crack, trussed bars, mortared units, horizontal joints of mortared units, concrete of upper beam and interface between upper beam and shear wall
Beam F	3C	8	Units, horizontal joint, vertical joint, potential crack, trussed bars, spring, steel plates and interface between steel plates and masonry beam
	2C	10	Units, horizontal joint, vertical joint, potential crack, trussed bars, mortared units, horizontal joints of mortared units, spring, steel plates and interface between steel plates and masonry beam
Beam S	3C	9	Units, horizontal joint, vertical joint, potential crack, trussed bars, straight bars, spring, steel plates and interface between steel plates and masonry beam
	2C	11	Units, horizontal joint, vertical joint, potential crack, trussed bars, straight bars, mortared units, horizontal joints of mortared units, spring, steel plates and interface between steel plates and masonry beam

6.2.2.1 Units

The behaviour of the concrete masonry units was represented by a total strain crack model based on a fixed stress-strain concept. The material model describes the tensile and compressive behaviour of a material with one stress-strain relationship in a coordinate system that remains fixed upon crack initiation. An exponential function characterizing the constitutive behaviour of concrete units under tensile loading was adopted, see Figure 6.3a. The results of the mode I fracture energy, G_f^I, of concrete block units obtained by Mohamad (2007) were used for the definition of the exponential model due to the lack of experimental complete tensile stress-strain diagrams of the concrete units used in this research. The compressive fracture energy, G_c, obtained by Mohamad (2007) was also used in order to define the parabolic function for the characterization of the constitutive behaviour in compression, see Figure 6.3b. The shear behavior during cracking was described via a shear retention model defined by a constant, see Figure 6.3c.

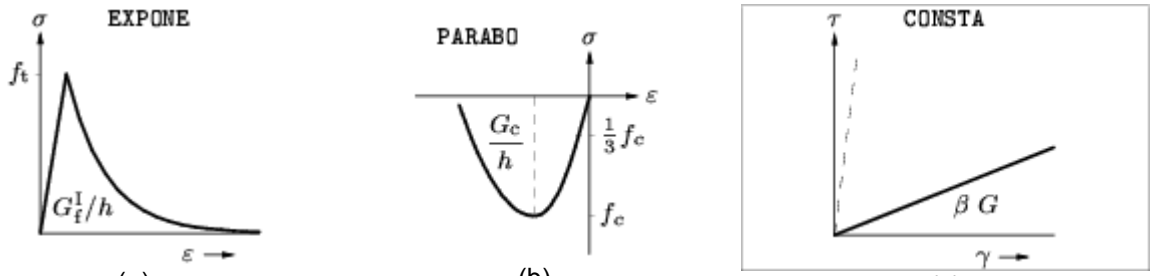

(a) (b) (c)

Figure 6.3 – Constitutive model adopted for concrete units in: (a) tension, (b) compression and (c) shear (DIANA®).

In case of masonry structural elements built with 2C-units, when the masonry bond pattern B1 is adopted, the holes with vertical reinforcement were totally filled with mortar. In numerical modelling these elements had to be represented with different mechanical properties. Therefore, to take into account the mortar filling of the two hollow cell concrete units its strength and stiffness was considered to be the double, even if no experimental values on the mechanical properties were available. The summary of the mechanical properties of 2C- and 3C-units, namely the tensile, f_t, and compressive strength, f_c, elastic modulus, E, Poisson's ratio, υ, the tensile and compressive fracture energies G_f^I and G_c, and the shear retention constant, β, is indicated in Table 6.2. The filled 2C-units are denoted by 2C*.

Table 6.2 – Mechanical properties of units used in numerical modelling.

Units	E (GPa)	ν	f_{bt} (MPa)	G_f^I (N/mm)	f_b (MPa)	G_c (N/mm)	β
3C	9.57	0.20	3.19	0.06	12.13	10.00	0.01
2C	8.80		3.13		9.38		
2C*	20.00	0.20	3.13	1.00	18.80	10.00	0.01

6.2.2.2 Interface elements

The plane stress interface cap model with modern plasticity concepts, capable of capturing all masonry failure mechanisms proposed by Lourenço and Rots (1997) and enhanced by Van Zijl (2004) was used for modelling the unit-mortar interfaces. It is based on multi-surface plasticity, comprising a Coulomb friction model combined with a tension cut-off and an elliptical compression cap, see Figure 6.4. This interface material model, also known as the 'Composite Interface model', is appropriate to simulate tensile fracture, frictional slip as well as crushing along material interfaces, for example at the mortar joints.

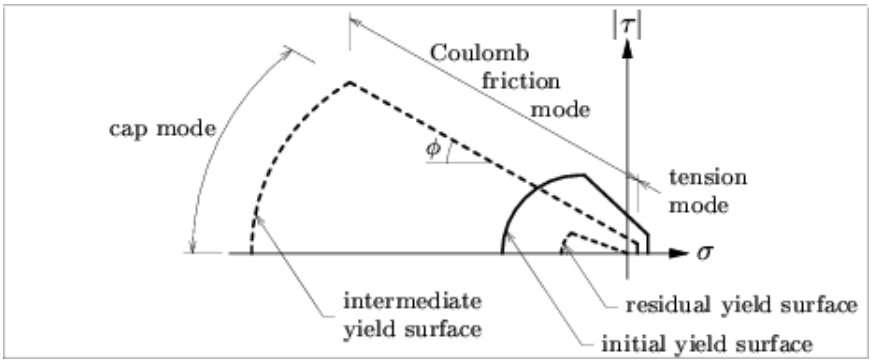

Figure 6.4 – Proposed interface cap model. (Lourenço and Rots, 1997).

The mechanical properties used for the definition of the yield functions in tension, compression and shear of the unit-mortar interfaces are summarized in Table 6.3 for horizontal joints and in Table 6.4 for vertical joints. The shear slipping is described by a Coulomb friction yield function. The definition of this function is made through the knowledge of the cohesion, c, friction coefficient, μ, the dilatancy coefficient, $\tan\psi$, and the shear fracture energy, G_f^{II}. In order to capture adhesion softening and friction softening the residual friction coefficient, μ_{res}.should be known. In the model, the dilatancy is considered to be dependent on the normal confining stress and on the shear slipping. Thus, for the correct definition of the dilatancy, the confining normal stress at which the dilatancy becomes zero, σ_u, and the dilatancy shear slip degradation coefficient, δ, need to be obtained by experimental analysis.

The yield function with exponential softening for the tension cut-off requires the knowledge of the tensile strength and the mode I fracture energy, G_f^I. The yield function for the compression cap, composed of a parabolic hardening rule and a parabolic/exponential softening branch, need the knowledge of the compressive strength, f_c, compressive fracture energy, G_c, and the parameter C_{ss} to take into account the which control the contribution of shear stress to failure.

Table 6.3 – Mechanical properties of horizontal unit-mortar interfaces.

Units	k_n (N/mm^3)	k_s (N/mm^3)	f_t (MPa)	G_f^I (N/mm)	f_a (MPa)	G_c (N/mm)	C_{ss}	c (MPa)	μ	tanψ	G_f^{II} (N/mm)	μ_{res}	σ_u (MPa)	δ
3C	20	48	0.33	0.017	5.95	5.00	5.3	0.42	0.49	0.52	2.0	0.43	1.35	1.64
2C			0.25		5.44			0.35		0.41		0.32	2.14	1.33
2C*	40	96	0.50	0.034	10.88	5.00	5.3	0.70	0.49	0.41	2.0	0.32	2.14	1.33

Table 6.4 – Mechanical properties of vertical joints used in numerical modelling.

Units	k_n (N/mm^3)	k_s (N/mm^3)	f_t (MPa)	G_f^I (N/mm)	f_a (MPa)	G_c (N/mm)	C_{ss}	c (MPa)	μ	tanψ	G_f^{II} (N/mm)	μ_{res}	σ_u (MPa)	δ
3C	2	2	0	0	2.78	5.00	5.3	0	0.65	0	2.0	0	0	0
2C	20	48	0.25	0.034	3.41	5.00	5.3	0.35	0.49	0.41	2.0	0.32	2.14	1.33

For the horizontal joints, apart from the fracture energies and the normal stiffness, all mechanical properties of the interface elements were obtained from experimental testing, on unit-mortar assemblages under shear and compression (Chapter 3). Even if some direct tensile tests have been carried out aiming at measuring the normal stiffness, k_n, of unit-mortar interfaces, the large scatter found led to the need of considering the values pointed out by Vasconcelos *et al.* (2008). The tensile strength of masonry joints was taken as the value corresponding to 80% of the flexural strength of masonry as suggested by Pluijm (1999), see Figure 6.5. The fracture energy under tension and compression were obtained by fitting the numerical to experimental results of the cyclic tests of masonry shear walls.

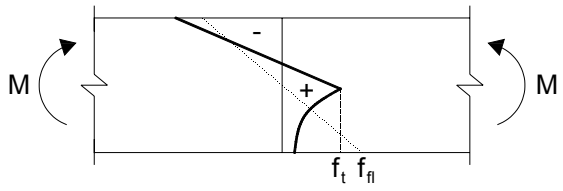

Figure 6.5 – Non-linear stress distribution (solid line) due to bending and the fictitious elastic distribution (dashed line) at the maximum load level.

The shear fracture energy, G_f^{II}, and shear stiffness, k_s, was evaluated through initial shear tests on unreinforced assemblages (triplet specimens, Chapter 3). This value has to be updated to take into account the influence of the vertical reinforcements. From the numerical simulation of the lateral behaviour of masonry shear walls, it was observed that vertical reinforcements provide an increase on the shear fracture energy. Thus, different shear fracture energies were considered to reinforced masonry walls (G_f^{II} = 2.0 N/mm) and unreinforced masonry walls (G_f^{II} = 0.1 N/mm). The parameter C_{ss}, which controls the contribution of shear stress to compression failure was not considered to be 9.0 as suggested by Lourenço and Rots (1997) given that residual compression moves into the tension cut-off, see Table 6.3. According to what was mentioned for 2C-units, also for horizontal joints of two cell concrete block masonry with bond pattern B1 (2C*), the mechanical properties were doubled see Table 6.3.

The mechanical properties adopted for filled vertical joints were the same as the ones considered to horizontal joints in case of masonry walls built with 2C-units (2C*), with the exception of the compressive strength, to which the parallel direction to bed joints was considered. In case of walls built with 3C-units, dry vertical dry-joints characterize the bond patterns B1 and B2. Hence, the tensile strength and fracture energy has to be taken equal to zero and the normal stiffness was very low, only to take into account the influence of the mortar at the bed joints. The stiffness of the vertical joints influences the numerical response only in compression. The normal stiffness was calibrated based on the numerical simulation of he masonry beams as it appears to influence at great extent the compressed region of the beam under flexure. In case of shear walls, the vertical joints are mainly subjected to tensile stresses. The shear behaviour of vertical joints of walls built with 3C-units was described by the Mohr-Coulomb model with a null cohesion and the friction coefficient corresponding to the dry contact between two surfaces of concrete (μ = 0.65).

Potential cracks in the middle of units were modelled through interface elements with a discrete cracking model, see Table 6.5. The constitutive law for discrete cracking in DIANA® is based on a total deformation theory, which expresses the tractions as a function of the total relative displacements. An exponential softening behaviour was adopted to the tensile behaviour of the potential crack.

Table 6.5 – Mechanical properties of potential cracks of concrete units.

Units	k_n (N/mm^3)	k_s (N/mm^3)	f_t (MPa)	G_f^I (N/mm)
3C	10^6	10^6	3.19	0.06
2C			3.13	

According to Lourenço and Rots (1997), it is clear that cracks in units need to be modelled. The authors observed that the lack of potential cracks into the concrete units resulted in an overestimation of the collapse load and a much stiffer response than the one observed in experimental tests.

6.2.2.3 Elastic Elements

Isotropic elasticity was adopted for the upper concrete beam of shear walls and for the steel plates above the supports and under the load application points of masonry beams in order to avoid stress concentration. These elements have no influence on the mechanical behaviour of the masonry structural elements under analysis. These elements were connected to the masonry through elastic interface elements with infinite stiffness to simulate perfect bond connection between these two elements according to what has been observed in experiments.

Table 6.6 – Material properties for elastic elements.

	E (GPa)	ν
Upper beam	30	0.20
Steel plates	210	0.30

6.2.2.4 Reinforcements

An elasto-plastic behaviour was adopted to the reinforcements through Von Mises model. Besides, a 'free length' (thickness of the joints) had to be considered to take into account the crossing of the interface elements, see Figure 6.6.

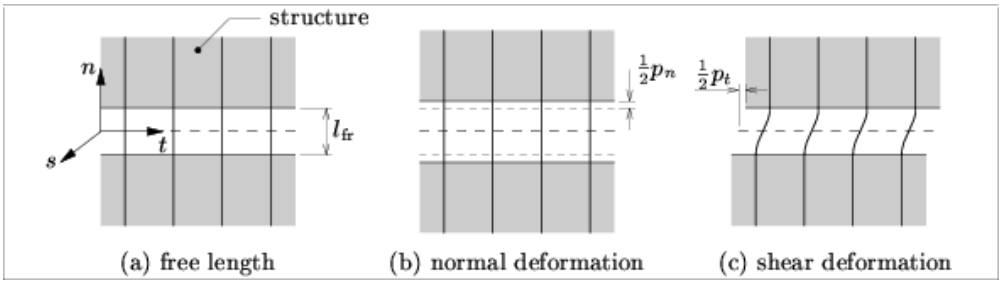

Figure 6.6 – Reinforcement stiffness at the interface (DIANA®).

Vertical reinforcements crossing structural interfaces have displacement and traction components in the same directions as the interface elements: one normal component and one or two shear components. Thus, the definition of a 'free length' is needed to determine the stiffness of the interface crossed by the reinforcement based on Eq. 6.1:

$$k_n = \frac{E_s}{l_{fr}} \quad \text{and} \quad k_s = k_t = \frac{E_s}{2l_{fr}} \qquad \text{Eq. 6.1}$$

Where, k_n and k_s are normal and shear components of the stiffness of the interface, l_{fr} is the free length and E_s is the elastic modulus of the reinforcement.

The considerable increase on the stiffness of interface elements resulting from the crossing of reinforcements leads to an ill-conditioned stiffness matrix. Besides, the introduction of reinforcements in the numerical model increases the number of iterations until the achievement of the convergence and consequently the computational effort.

6.2.2.5 Spring

A spring element was used to represent the partial rigidity of the support of the masonry beam, which was supposed to be completely free. This element was used only to calibrate the numerical model and represent the experimental conditions. In parametrical study this spring was not considered. A stiffness of 400 N/mm was taken from the numerical fitting to the experimental results.

6.3 Numerical *vs.* Experimental results

The first step of the numerical analysis comprises the calibration of the numerical model defined for the masonry shear walls and masonry beams, which is achieved from the comparison between experimental and numerical results. This enables to use a reliable model for the envisaged parametric study and allows obtaining a better insight of the analysis of the experimental results. From numerical simulation it is also possible to correctly understand some issues that experimental analysis becomes difficult like the correct stress distribution along the walls and beams.

6.3.1 Shear walls

As aforementioned, the outcome of numerical modelling of masonry shear walls consists of a numerical monotonic envelop of the experimental results as only monotonic loading was considered. By comparing the maximum lateral resistance obtained in numerical modelling, H_{Num}, with the experimental lateral resistance, H_{Exp}, it is observed that very good approach was achieved, see Table 6.7. A maximum difference on the lateral resistance of 6% was found for specimens built with 3C-units and of 10% for specimens built with 2C-units.

Table 6.7 – Comparison between experimental and numerical lateral resistance of shear walls.

Wall	(+/-)	H_{Exp} (kN)	H_{Num} (kN)	H_{Num} / H_{Exp} (%)	Wall	(+/-)	H_{Exp} (kN)	H_{Num} (kN)	H_{Num} / H_{Exp} (%)
N60-3C-B1-UM	+	35.88	35.28	0.98	N150-3C-B2	+	93.80	90.47	0.96
	-	33.63		1.05		-	93.28		0.97
N60-3C-B1-SH	+	38.61	36.11	0.94	N60-3C-B1-MA	+	78.36	63.13	0.81
	-	35.09		1.03		-	74.59		0.85
N60-3C-B1	+	52.73	52.72	1.00	N60-3C-B1-PA	+	70.22	61.95	0.88
	-	52.75		1.00		-	66.92		0.93
N60-3C-B2	+	62.09	64.29	1.04	N60-2C-B1	+	63.09	59.52	0.94
	-	65.18		0.99		-	73.98		0.80
N150-3C-B1	+	92.98	86.49	0.93	N60-2C-B2	+	63.18	62.30	0.98
	-	93.22		0.93		-	55.05		1.13

The comparison between the cyclic force-displacement diagrams obtained in experimental tests with the numerical monotonic envelop reveals that a reasonable agreement was attained between both approaches in the pre-peak regime in terms of stiffness, pre-peak nonlinear behaviour and lateral resistance, see Figure 6.7 to Figure 6.9. In post-peak behaviour of masonry walls is well represented in unreinforced specimens and in the walls submitted to the highest level of pre-compression but clearly, divergences in the remaining walls. The difference in the elastic stiffness found in specimens N60-2C-B1 and N60-2C-B2 is attributed to the previous damage of the walls observed before testing as already mentioned in Chapter 4.

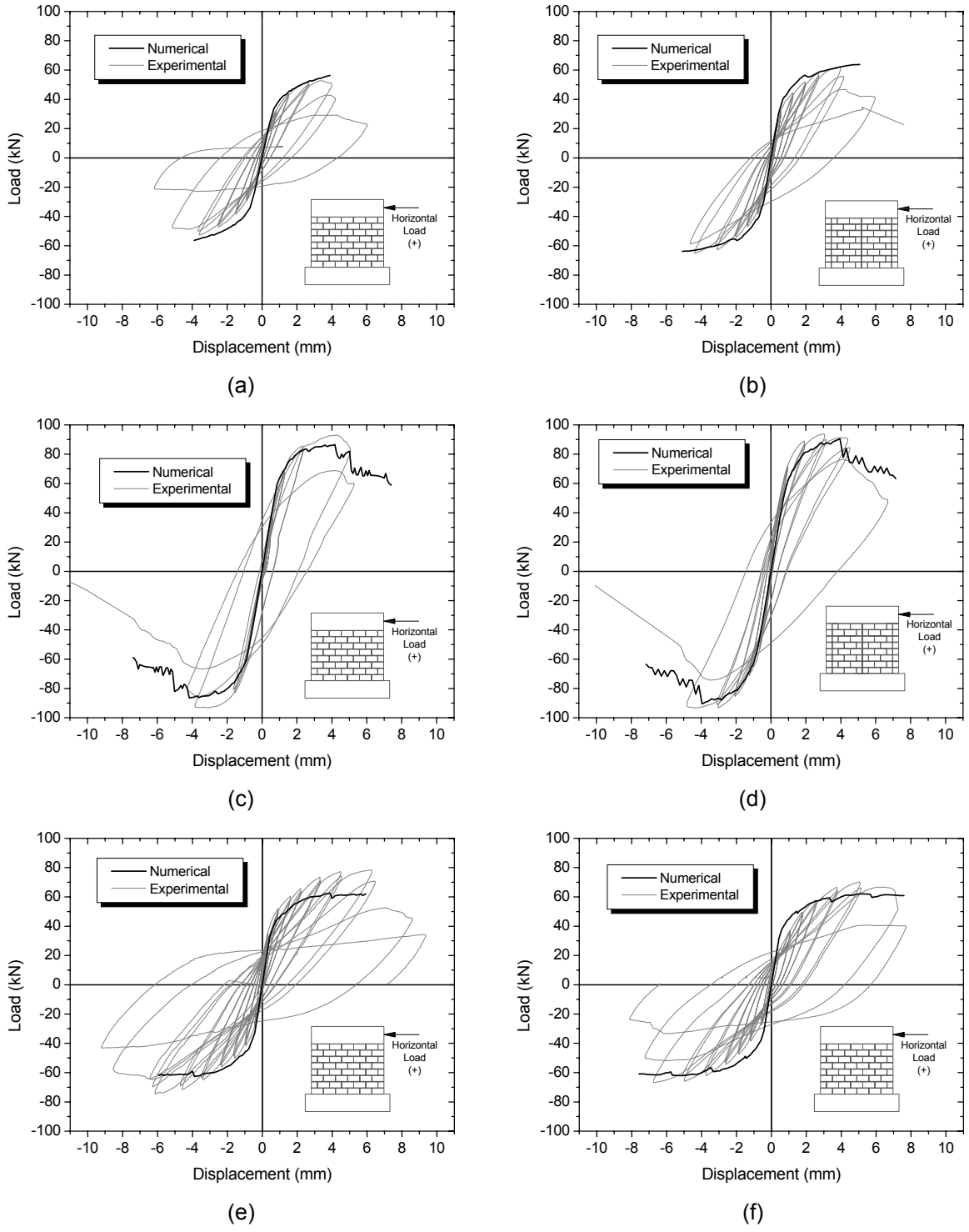

Figure 6.7 – Comparison between numerical and experimental results (Force *vs.* displacement diagrams): (a) IP-N60-3C-B1, (b) IP-N60-3C-B2, (c) IP-N150-3C-B1, (d) IP-N150-3C-B2, (e) IP-N60-3C-B1-MA and (f) IP-N60-3C-B1-PA.

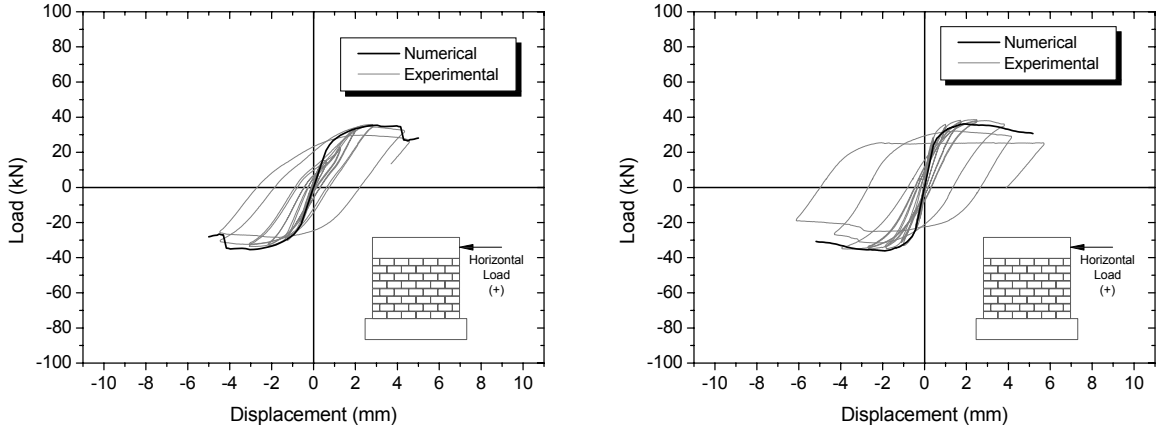

Figure 6.8 – Comparison between numerical and experimental results (Force *vs.* displacement diagrams): (a) N60-3C-B1-UM, (b) N60-3C-B1-SH.

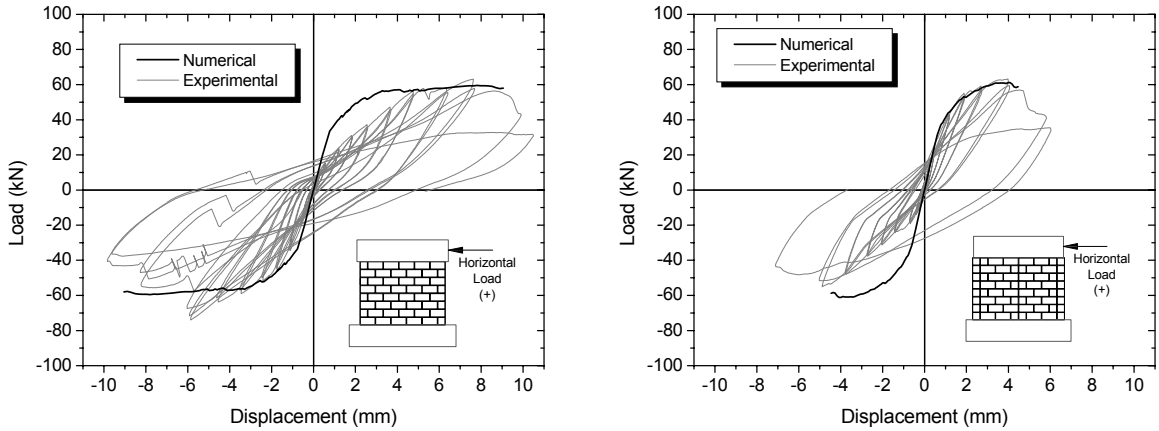

Figure 6.9 – Comparison between numerical and experimental results (Force *vs.* displacement diagrams: (a) N60-2C-B1 and (b) N60-2C-B2.

In terms of failure mode, numerical modelling agrees reasonably well with the experimental results in spite of the monotonic loading considered in numerical modelling. In fact, it is very well known that it is possible that the cyclic horizontal loading can lead to increasing damage accumulation. As shown Figure 6.10a for the unreinforced masonry walls numerical results represented the three main crack patterns developed during experimental behavior of the walls, namely flexural cracking, diagonal cracking and crushing at the bottom of the wall. In the experimental test, after the diagonal crack and crushing at the bottom corner occurred, the upper part of the walls slide over the diagonal crack.

In numerical modeling it was possible to observe some penetrations of the elements in the compressed corner during the sliding. In case of the specimen reinforced at the bed

joints (N60-SH) the horizontal reinforcement controlled the diagonal cracking and only the flexural crack developed similarly to the experimental results, see Figure 6.10b.

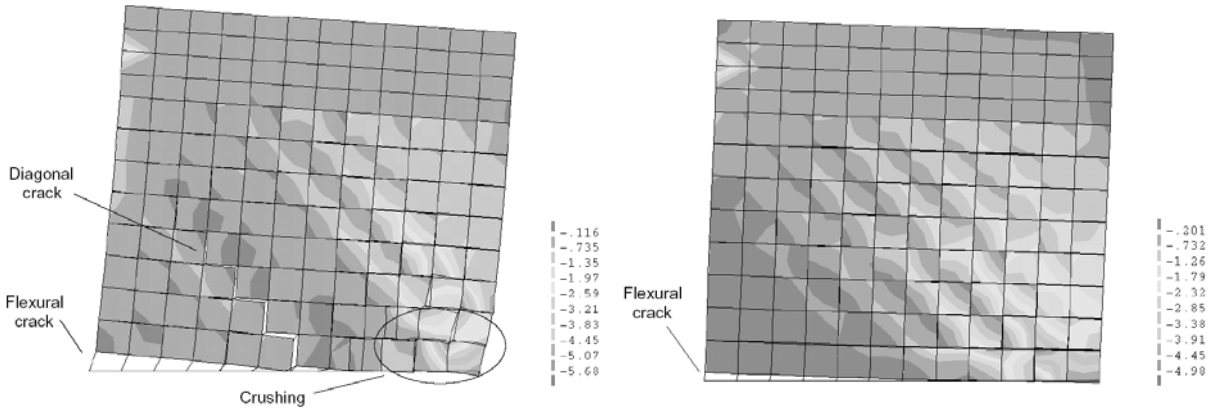

(a) (b)

Figure 6.10 – Deformed mesh with the map of principal stresses at the maximum load: (a) N60-3C-B1-UM and (b) N60-3C-B1-SH.

In case of specimens where vertical and horizontal reinforcements were combined, diagonal cracks were more distributed and flexural crack was controlled by the vertical reinforcement according to the experimental results. However, in the numerical modelling higher damage at the tensile bottom corner of the reinforced walls developed relatively to the experimental crack patterns, see Figure 6.11. Specimens with high pre-compression exhibited almost no cracking as in the experimental tests.

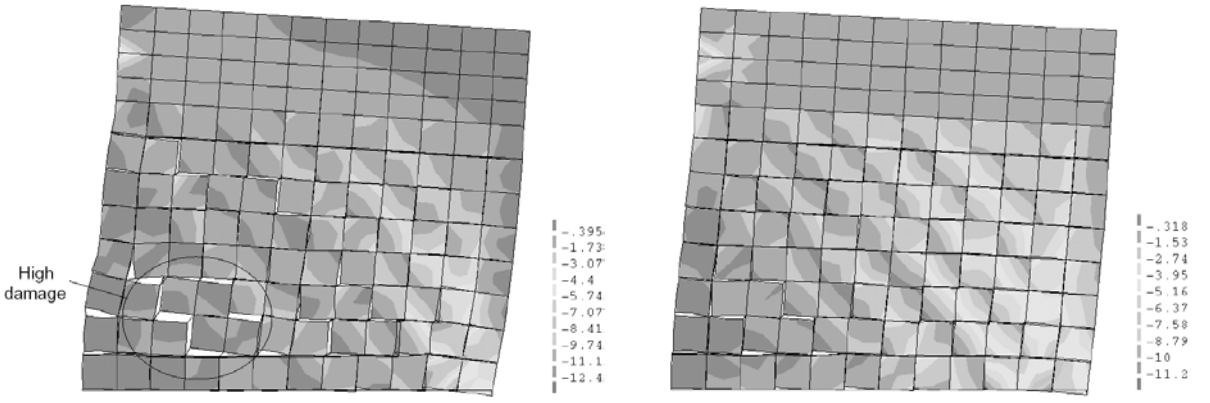

(a) (b)

Figure 6.11 – Deformed mesh with the map of principal stresses at maximum load: (a) N60-3C-B1-PA and (b) N150-3C-B2.

Numerical strains at the reinforcements approach reasonably well the experimental results. Horizontal reinforcements exhibited almost no strains until the diagonal cracking. In this first stage of loading, small compressive strains could be observed in these bars. After

diagonal cracking, the activation of the horizontal reinforcements is revealed by a clear discontinuity on the strain diagram, see Figure 6.12.

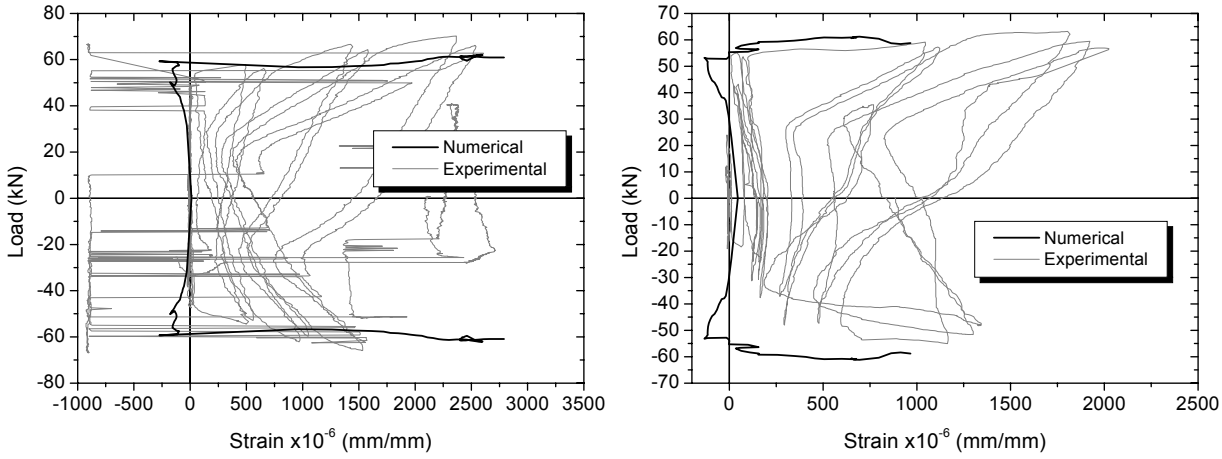

Figure 6.12 – Strains of the horizontal reinforcement at mid-height of the wall in numerical modelling: (a) N60-3C-B1-PA and (b) N60-2C-B2.

In numerical modeling vertical reinforcements behave in a similar manner when compared to experimental results, see Figure 6.13. It is noted that the lower strains obtained in the numerical analysis can be attributed to the permanent plastic deformations accumulated during cyclic loading. However, the comparison between experimental results reveals that the numerical strains approach reasonably well the envelope of the cyclic results.

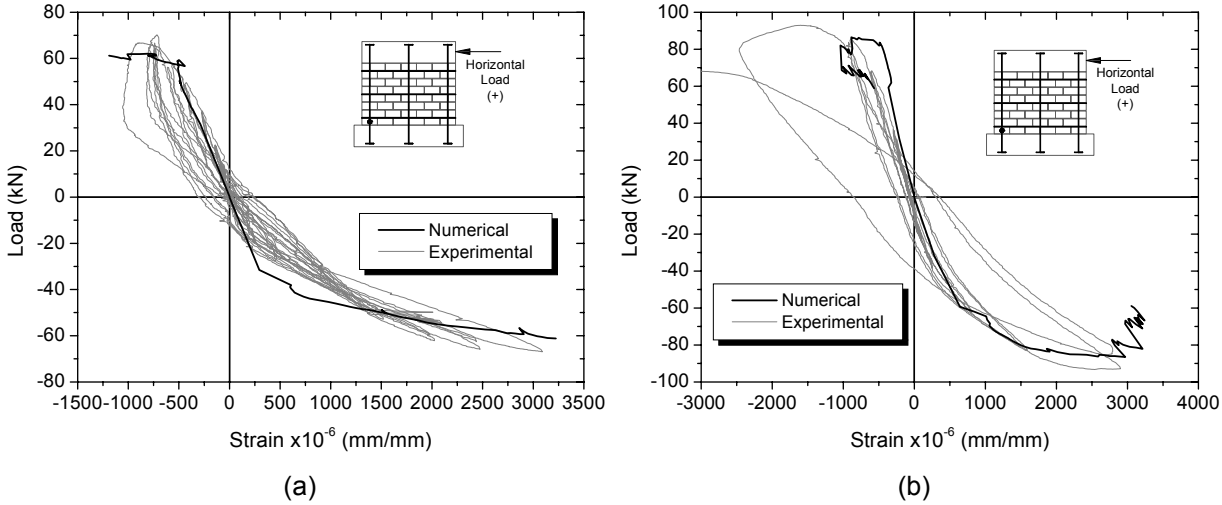

Figure 6.13 – Strains of the vertical reinforcement in numerical modelling: (a) N60-3C-B1-PA and (b) N150-3C-B1.

In general the results of numerical modelling showed a reasonable agreement with experimental results, meaning that it represents satisfactorily well the lateral in-plane behaviour of masonry walls. This indicated that the numerical model is adequate to proceed with the parametric study with accuracy.

6.3.2 Masonry beams

As can be observed in Table 6.7, the numerical modelling of masonry beams provide reasonable results as concerns the ultimate load for the majority of the masonry beams with the difference between experimental and numerical ultimate load lower than 15%.

Table 6.8 – Comparison between experimental and numerical results concerning the ultimate load.

Beam	H_{Exp} (kN)	H_{Num} (kN)	H_{Num} / H_{Exp} (%)	Beam	H_{Exp} (kN)	H_{Num} (kN)	H_{Num} / H_{Exp} (%)
F-3C-UM	4.05	5.48	1.35	F-2C-UM	5.90	8.68	1.47
F-3C-D3-C	23.32	24.90	1.07	F-2C-D3-C	24.09	25.14	1.04
F-3C-D3-D	33.19	29.70	0.89	F-2C-D3-D	37.73	28.79	0.76
F-3C-D3-D-M	33.30	32.75	0.98	F-2C-D3-D-M	37.38	34.59	0.93
F-3C-D5-C	44.90	37.56	0.84	F-2C-D5-C	45.54	40.78	0.90
F-3C-D5-D	45.04	47.66	1.06	F-2C-D5-D	61.24	50.05	0.82
F-3C-D5-D-M	59.31	51.01	0.86	F-2C-D5-D-M	56.10	57.20	1.02
S-3C-UM	66.80	48.72	0.73	S-2C-UM	62.11	59.20	0.95
S-3C-SH	86.68	60.70	0.70	S-2C-SH	100.34	77.72	0.77
S-3C-S1	102.91	94.14	0.91	S-2C-S1	127.61	115.60	0.91
S-3C-S2	110.89	97.08	0.88	S-2C-S2	102.75	125.20	1.22
S-3C-S3	101.43	105.80	1.04	S-2C-S3	188.96	192.20	1.02

Higher differences are obtained for unreinforced specimens (F-3C-UM, F-2C-UM). It is observed that the cohesion of the horizontal joints governed the behaviour of these specimens. The value of cohesion considered in numerical modelling was obtained in triplet specimens, where the production of mortar was more controlled. Besides, the mortar of specimens F-3C-UM and F-2C-UM presented a low compressive strength, which can be an indicative of lower cohesion, leading to a decrease on the ultimate strength of unreinforced masonry beams. It is possible that the influence of cohesion is not so important in case of specimens with a combination of horizontal and vertical reinforcements.

The experimental and numerical load-displacement diagrams for both load configurations and for masonry beams built with 3C- and 2C-units is displayed from Figure 6.14 to Figure 6.19. Apart from the unreinforced masonry beams, the specimens under the four point load configuration and that exhibit a typical flexural behaviour presents reasonable agreement of the pre-peak regime. Worse agreement between experimental and numerical response was observed in specimens governed by shear failure patterns (F-3C-D5-D-M and F-2C-D5-D-M). In case of shear specimens (three point load configuration), there is a very good agreement of numerical and experimental total load-displacement diagram for specimens with shear reinforcements. The specimen with horizontal reinforcement S-2C-SH exhibited the worst agreement both in terms of ultimate load and pre-peak regime, see Figure 6.18, due to the local crushing failure under the load application point.

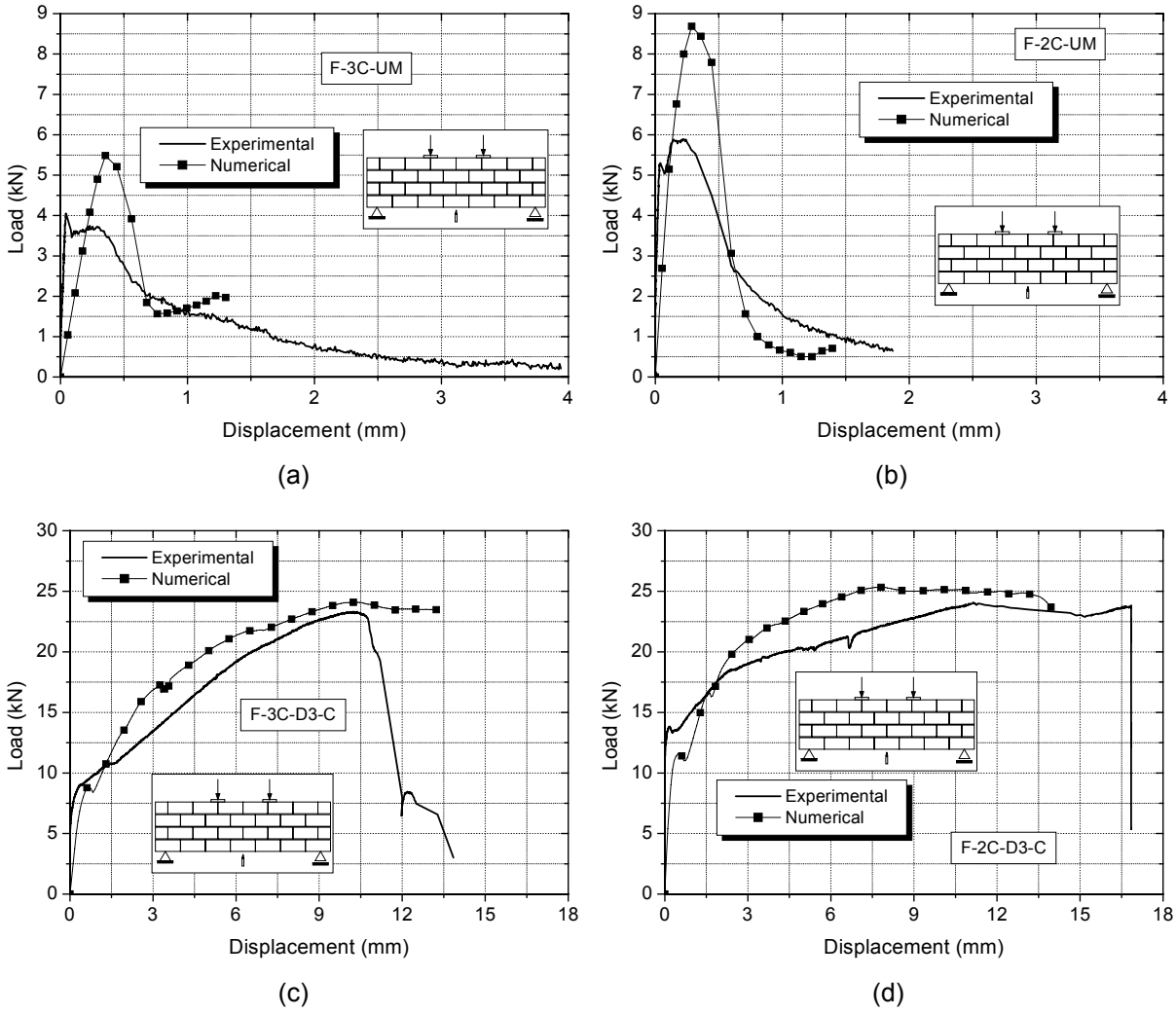

Figure 6.14 – Comparison between numerical and experimental results (Force *vs.* displacement diagrams): (a) F-3C-UM, (b) F-2C-UM, (c)) F-3C-D3-C and (d)) F-2C-D3-C.

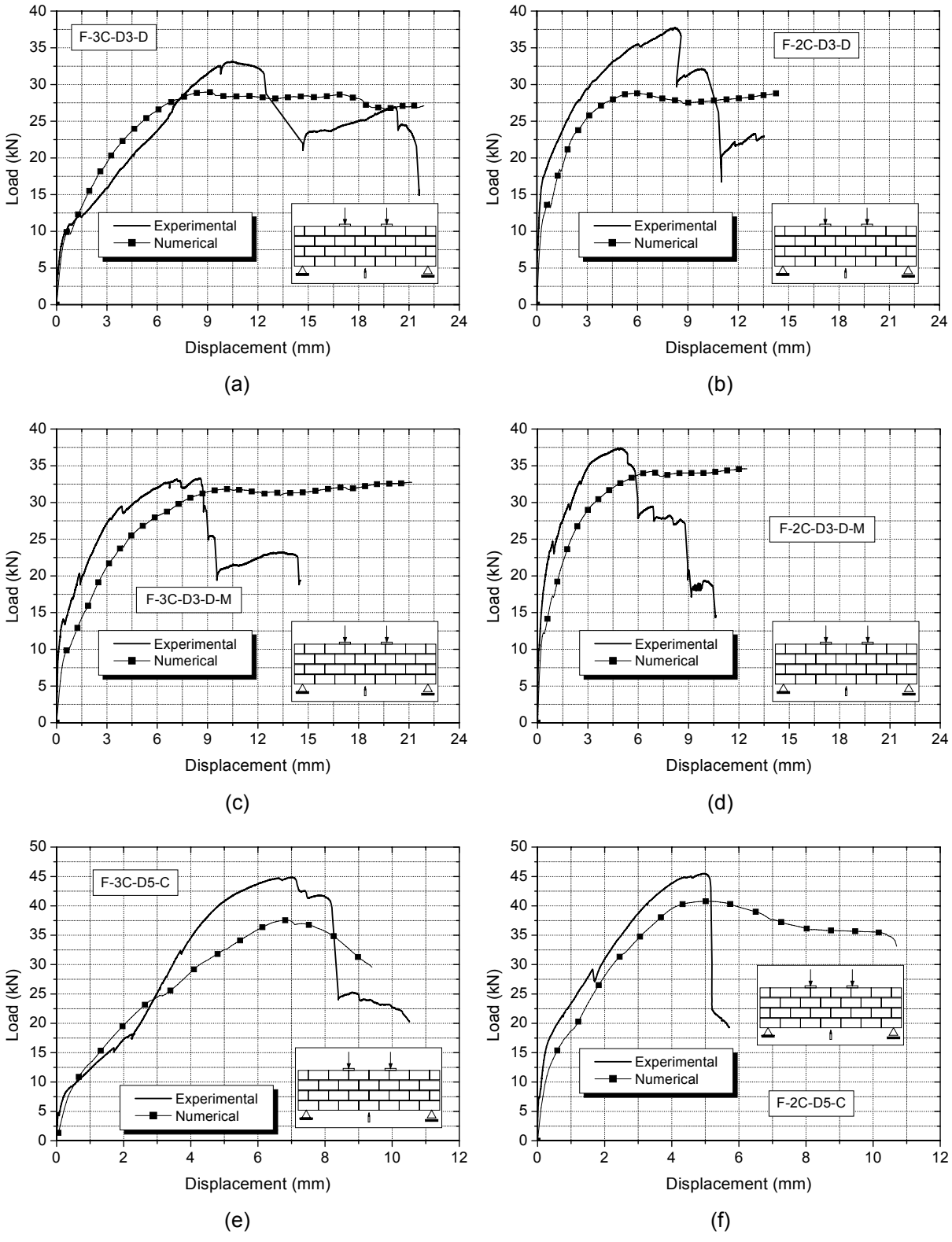

Figure 6.15 – Comparison between numerical and experimental results (Force *vs.* displacement diagrams): (a) F-3C-D3-D, (b) F-2C-D3-D, (c) F-3C-D3-D-M, (d) F-2C-D3-D-M, (e) F-3C-D5-C and (f) F-2C-D5-C.

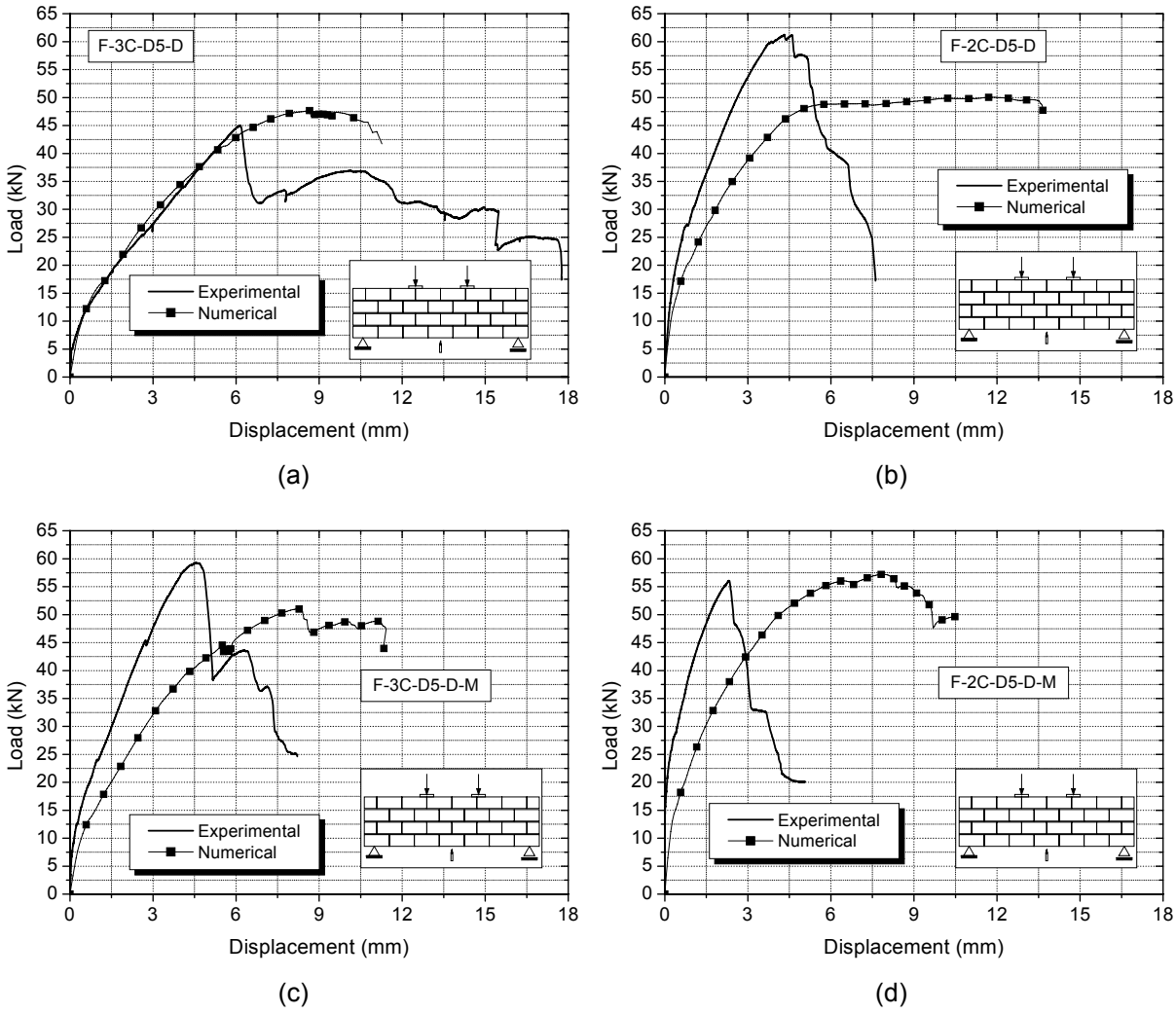

Figure 6.16 – Comparison between numerical and experimental results (Force *vs.* displacement diagrams): (a) F-3C-D5-D, (b) F-2C-D5-D, (c) F-3C-D5-D-M and (d) F-2C-D5-D-M.

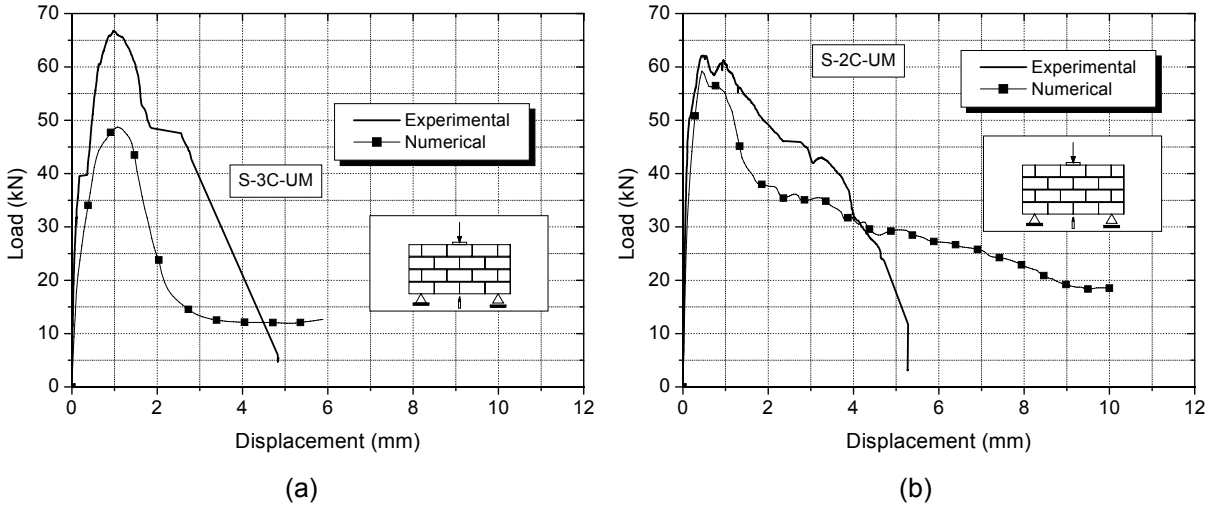

Figure 6.17 – Comparison between numerical and experimental results (Force *vs.* displacement diagrams): (a) S-3C-UM and (b) S-2C-UM.

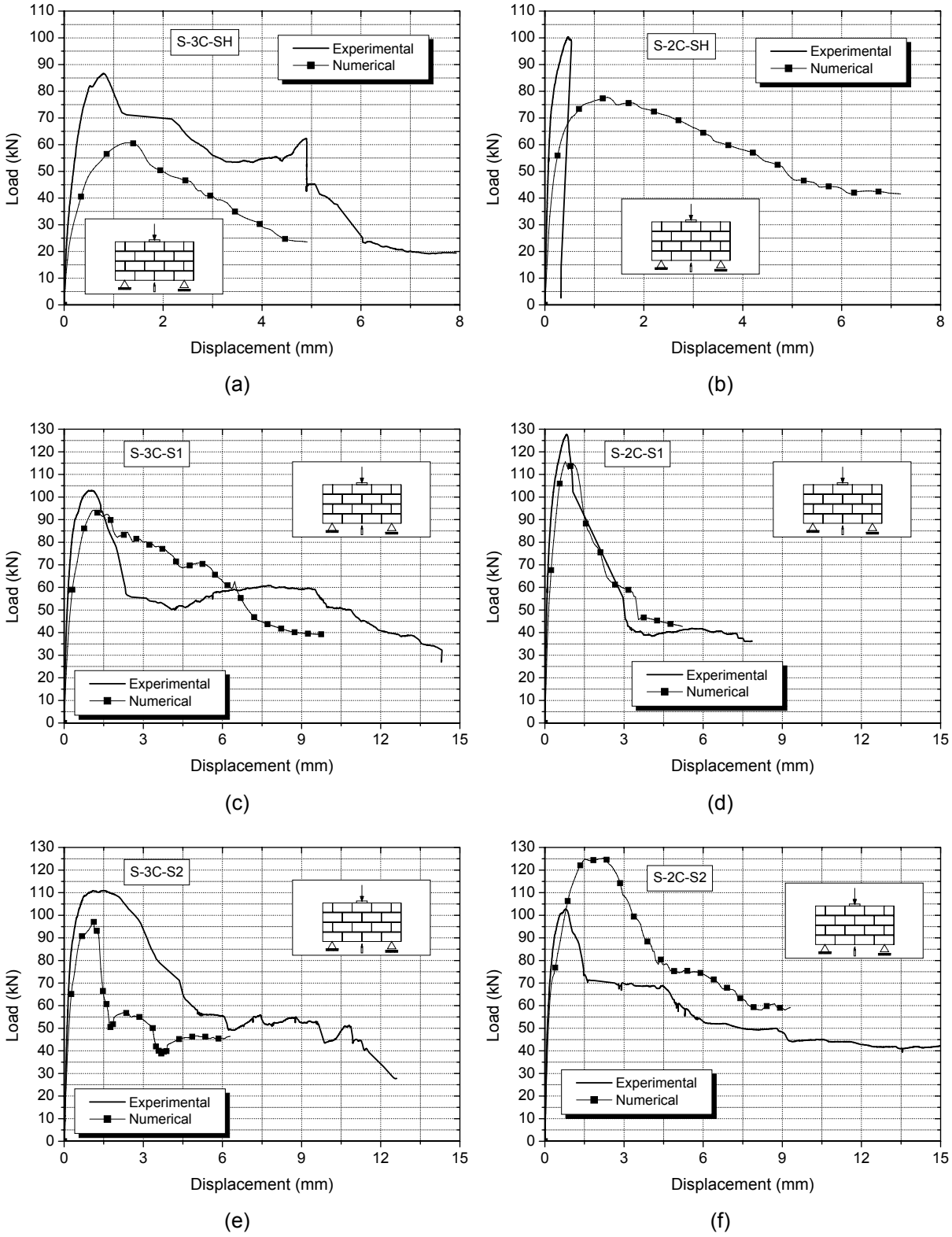

Figure 6.18 – Comparison between numerical and experimental results (Force *vs.* displacement diagrams): (a) S-3C-SH, (b) S-2C-SH, (c) S-3C-S1, (d) S-2C-S1, (e) S-3C-S2 and (e) S-2C-S2.

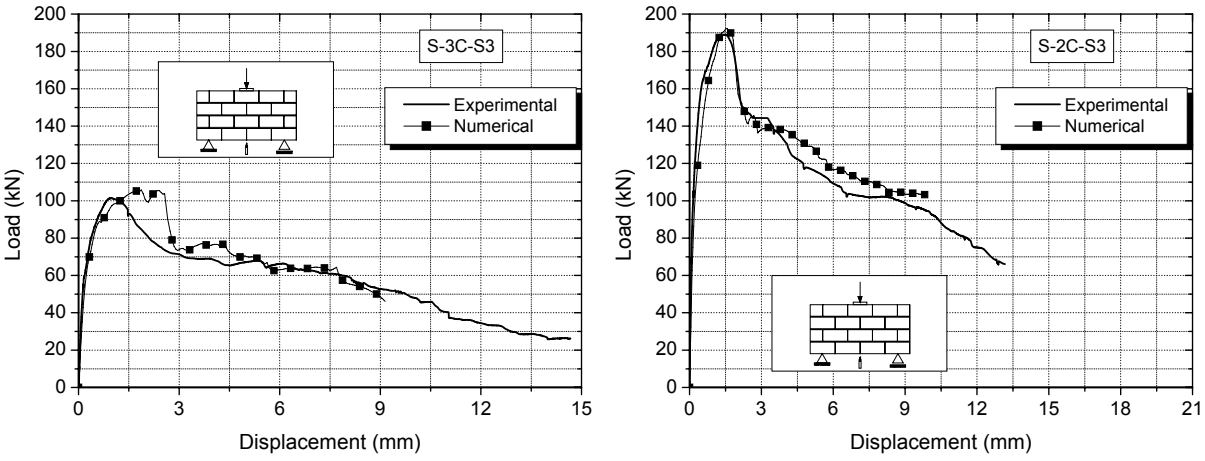

(a) (b)

Figure 6.19 – Comparison between numerical and experimental results (Force *vs.* displacement diagrams): (a) S-3C-S3 and (b) S-2C-S3.

Numerical and experimental results were very similar in terms of cracking patterns and failure modes. Unreinforced beams (F-3C-UM and F-2C-UM) exhibited only one non-symmetrical stair stepped crack located at the mid-span of the beam, see Figure 6.20a. In the calibration of the numerical model it was observed that this non-symmetrical failure mode is influenced by cohesion of the horizontal joints as explained before. If the value of cohesion is slightly higher, cracks developed through a symmetrical pattern from the vertical joints at the bottom edge in the middle of beam up to the points of load application. In case of reinforced specimens, flexural stair stepped cracks growing from the vertical joints at mid-span of the masonry beams up to the upper edge of the beams were also observed in numerical model similarly to the crack pattern developed in experimental specimens, see Figure 6.20b. Diagonal cracks near the supports were also observed in the numerical model in specimens with high longitudinal reinforcement ratio. Besides, it is observed the development of horizontal cracks from the vertical edges of the beams due to shear sliding, similarly to what was seen during the experimental tests, which confirm the good agreement between experimental and numerical results, see Figure 6.20c.

The influence of vertical reinforcements positioned at the middle of the beams could be clearly assessed in numerical model. When the compression stresses increase on the upper course of the beam, the units exhibit the trend to separate from the horizontal joint, which is avoided by the presence of vertical reinforcements. These elements contribute also for the prevention of the horizontal cracks at the horizontal joints. It should be stresses that strains measured in experimental tests were reasonably well described by the ones obtained in numerical modelling, see Figure 6.21. However, these specimens exhibited a lower stiffness in force *vs.* displacements diagram in comparison to experimental results. This fact

occurred probably because the introduction of vertical reinforcements may be change some material properties related to the compressive behaviour of masonry parallel to bed joints such as elastic stiffness of joints, energy of fracture.

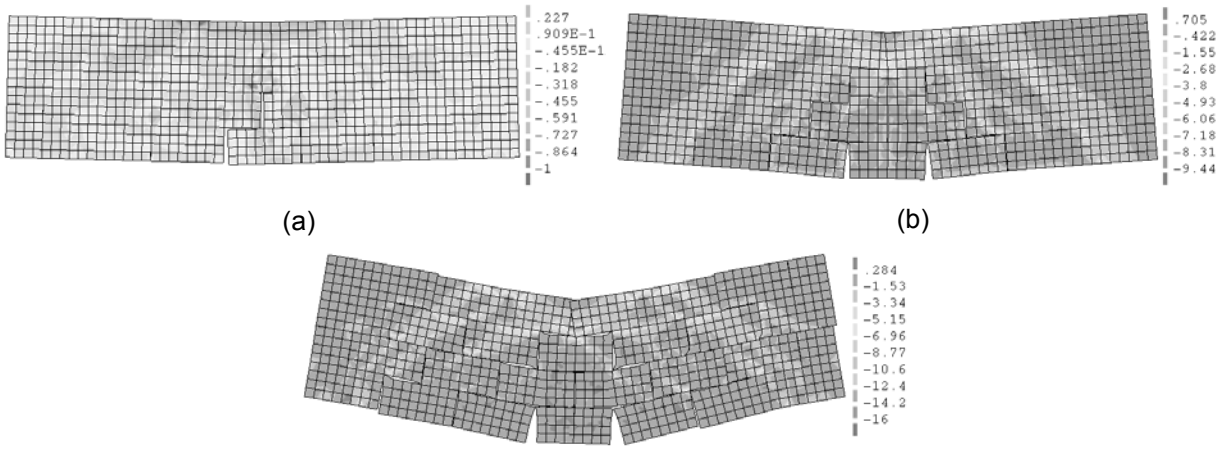

(a) (b)

(c)

Figure 6.20 – Deformed mesh with the map of the principal stresses at the maximum load: (a) F-3C-UM, (b) F-2C-D3-C and (c) F-3C-D5-D.

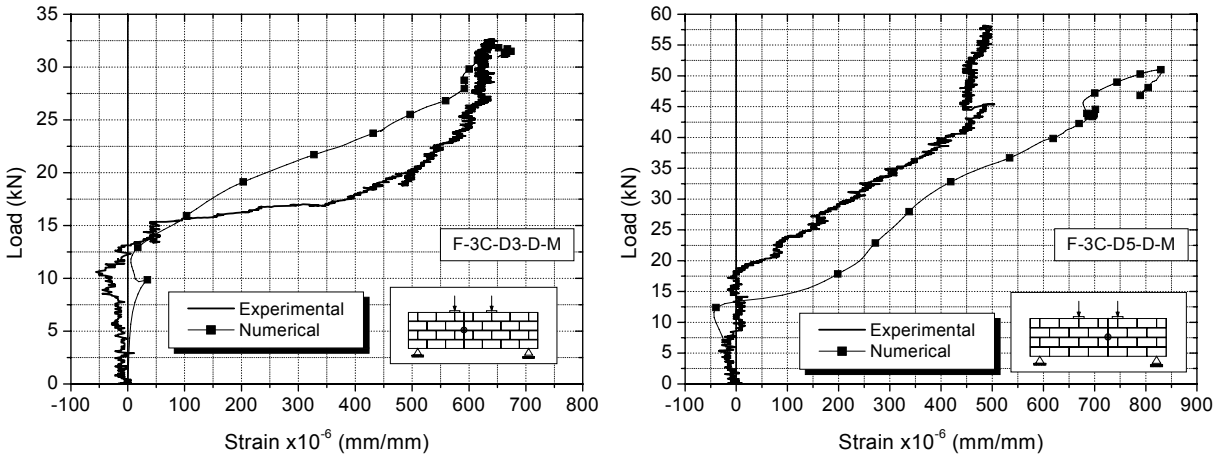

(a) (b)

Figure 6.21 – Strains of the vertical reinforcements located in the mid-span of beams: (a) F-3C-D3-D-M and (b) F-3C-D5-D-M.

In terms of strains of longitudinal reinforcements, the numerical model represents very well the results experimentally observed, see Figure 6.22, which appears to confirm the effectiveness of the numerical model.

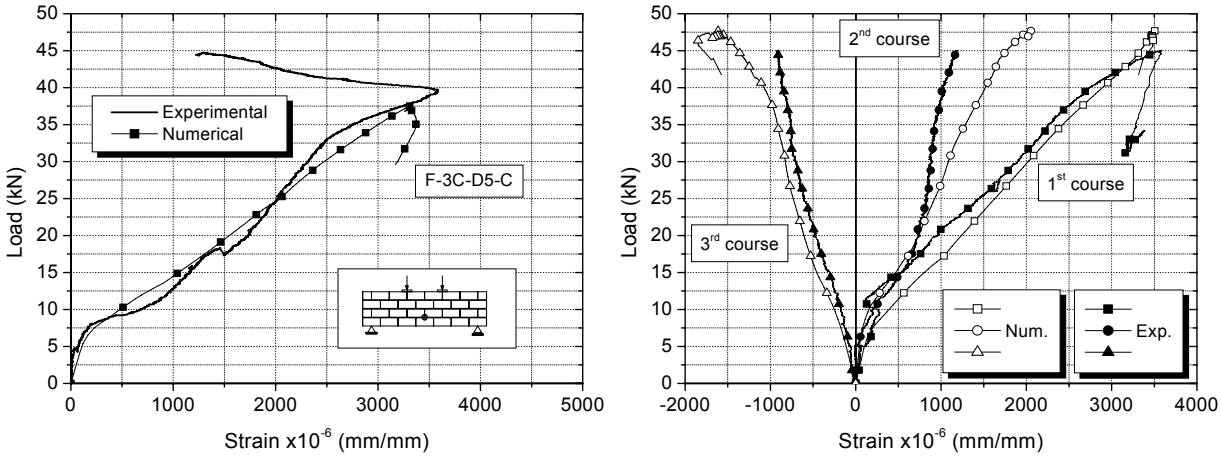

Figure 6.22 – Strains of the horizontal reinforcements: (a) F-3C-D5-C and (b) F-3C-D5-D.

As already mentioned (Chapter 5), in case of beams of type S there were basically two types of failure modes: diagonal cracking and crushing of the diagonal strut connecting the load application point and the supports see Figure 6.23. Numerical model represented both cases, however, in case of diagonal cracking the failure occurred symmetrically with the crack opening in both sides of the specimen, see Figure 6.23a. The numerical modelling reproduces very well the localization of the diagonal strut crushing according to what was observed in experimental tests, see Figure 6.23b.

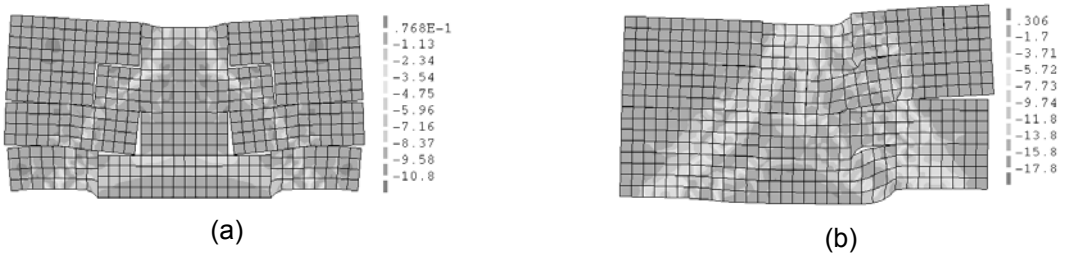

Figure 6.23 – Deformed mesh with the representation of the principal stresses at maximum load: (a) S-2C-UM and (d) S-3C-S1.

Strains of shear vertical reinforcement of masonry beams of type S obtained in numerical modelling did not fit well the experimental results. In some cases the numerical model presents near strains at peak load, but in other cases it deviates from the experimental strains, exhibiting higher strains, see Figure 6.24. It is difficult to determine the reasons for such differences due to the complexity of the behaviour of masonry beams but it is possible that the imperfect bond between the masonry and the steel bars contribute to lower strains as recorded in experimental tests. Besides, it should be mentioned that the diagonal bars of the truss type reinforcements were not modelled.

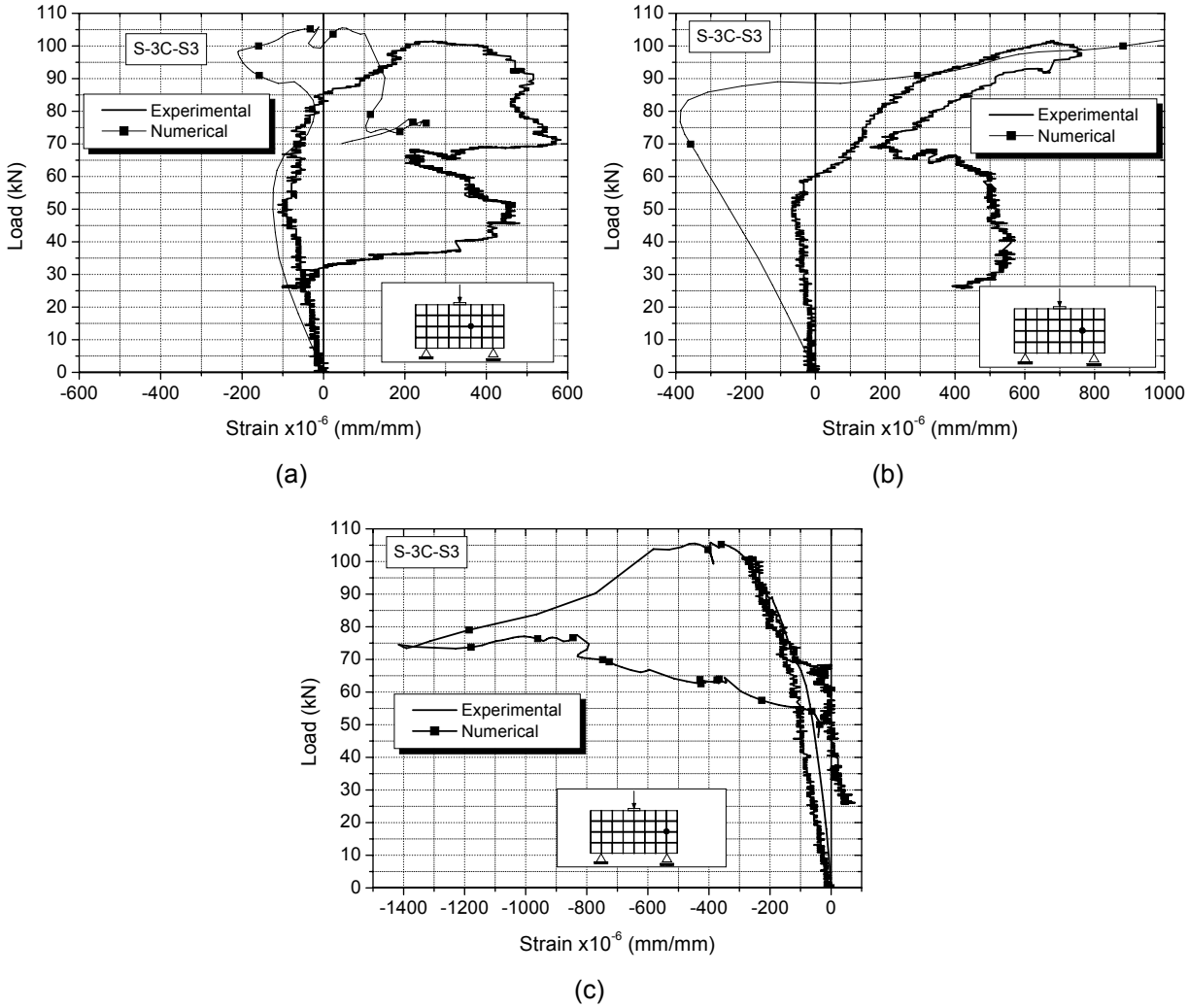

Figure 6.24 – Strains of the vertical reinforcement in numerical modelling of specimen S-3C-S3.

To sum up, it should stressed that in general a reasonable fitting was achieved between numerical and experimental results obtained in masonry beams, even if better results have been obtained in masonry shear walls. In the point of view of the author the major concern about the numerical modelling of the masonry beams was the need of introducing the compressive behaviour of masonry in the direction parallel to bed joints. In fact, the numerical model considers a parabolic function to describe the compressive behaviour but this deviate from the experimental results obtained in Chapter 3. Another aspect that numerical modelling was not able to capture was the cracking of the webs of the units observed in experiments due to the high compression stresses at the upper region of the beams. However, it is considered that numerical model is clearly acceptable for the performance of the parametric study.

6.4 Parametric Study

In order to get a detailed insight on the influence of distinct parameters on the response of masonry shear walls and beams, an extensive parametric study has been performed. Several parameters have been considered taking into account the particularities of each structure analyzed. In this study, the behaviour of unreinforced and reinforced masonry was evaluated in order to define guidelines and recommendations to the design of shear walls and masonry beams. Parametric study was developed considering the material properties used in calibration of experimental walls built with 3C-units.

6.4.1 Shear walls

As aforementioned, several parameters were considered in the parametric study of shear masonry walls, namely (i) pre-compression level; (ii) aspect ratio; (iii) filling of vertical joints; (iv) vertical reinforcement ratio; (v) horizontal reinforcement ratio; (vi) combination between vertical and horizontal reinforcements. Besides, distinct boundary conditions were also analysed (cantilever and fixed end walls) in order to assess the predominance of shear and flexure on the response of masonry shear walls.

Walls with 1400 mm height, which is equivalent a height of 2800 mm in a real scale, was considered in the parametric study as it is a common value used in buildings. Distinct height to length ratios were considered by varying the length of the wall. Five aspect ratios (h/L = 2.33, 1.40, 1.00, 0.78 and 0.64) and five normalized axial stresses with relation to compressive strength of masonry, f_a, (σ/f_a = 0.0, 0.1, 0.2, 0.4 and 0.6) were adopted in the study.

Firstly, two groups of 25 unreinforced masonry walls were used for the assessment of the influence of the aspect ratios and pre-compression levels. A failure surface (aspect ratio, pre-compression and lateral capacity) has been defined to both boundary conditions: cantilever and fixed end. In a second phase, the introduction of horizontal and vertical reinforcement ratios was gradually performed in order to understand the effects in lateral behaviour of masonry walls provided by each type of reinforcement. In addition, the variation of reinforcement ratios was carried out in conjunction with variation of aspect ratio and pre-compression level in order to observe the differences in each case.

6.4.1.1 Unreinforced masonry walls with dry vertical joints

The variation of the lateral resistance for unreinforced masonry walls according to the aspect ratio, for both cantilever and fixed end ended walls, and for varied pre-compression levels is indicated in Figure 6.25. It is observed that the relation between lateral resistance of unreinforced masonry walls and the aspect ratio is well described by a power function independently on the boundary conditions and on the level of pre-compression. As already observed by other authors the lateral resistance of masonry walls increases as the height to length ratio decreases (Anthoine and Magonette, 1995; Schultz *et al.*, 1998 and Kikuchi *et al.*, 2003). It is also seen that pre-compression level improves the lateral strength of the walls for the different values of height to length ratio, similarly to what has been pointed out in literature (Drysdale *et al.*, 1999; Vasconcelos and Lourenço, 2009).

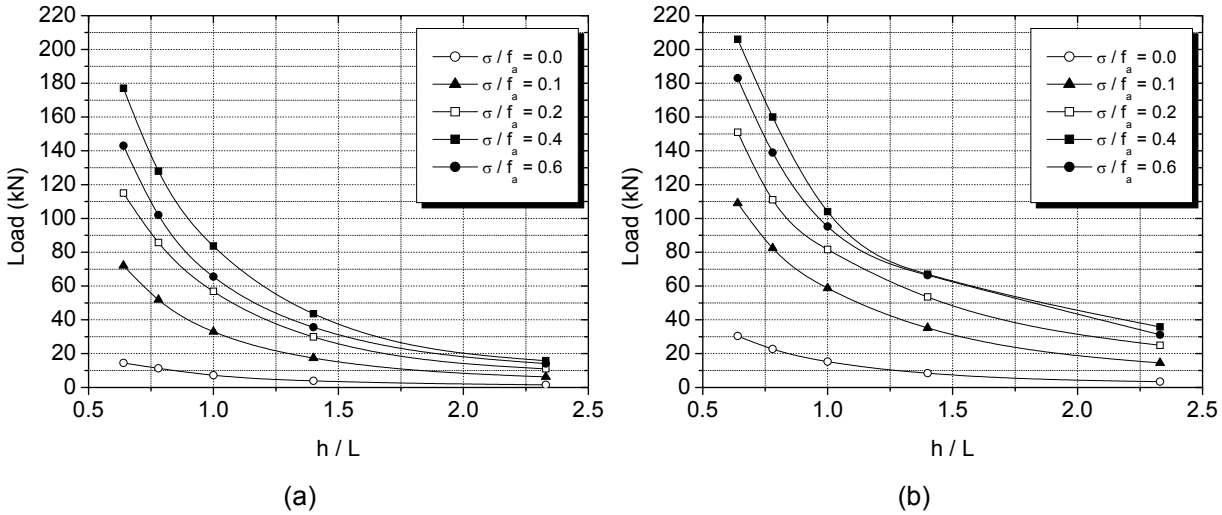

Figure 6.25 – Influence of aspect ratio on lateral capacity of shear-walls: (a) cantilever wall and (b) fixed end wall.

The relation between the lateral resistance and the pre-compression level was seen to be well described by a parabolic function, see Figure 6.26, for the distinct aspect ratios and for both boundary conditions. From numerical analysis it is seen that the lateral strength increases up to approximately 40% of the compressive strength of masonry, after which occurs a progressive decrease on the lateral resistance. In this stage the compressive failure takes a central role on the lateral in-plane behaviour of the masonry walls. This result is valid for both boundary conditions of the walls. Additionally, it is also observed that the compressive failure is more important as the aspect ratio decreases, which is revealed by the higher curvature of the parabolic function.

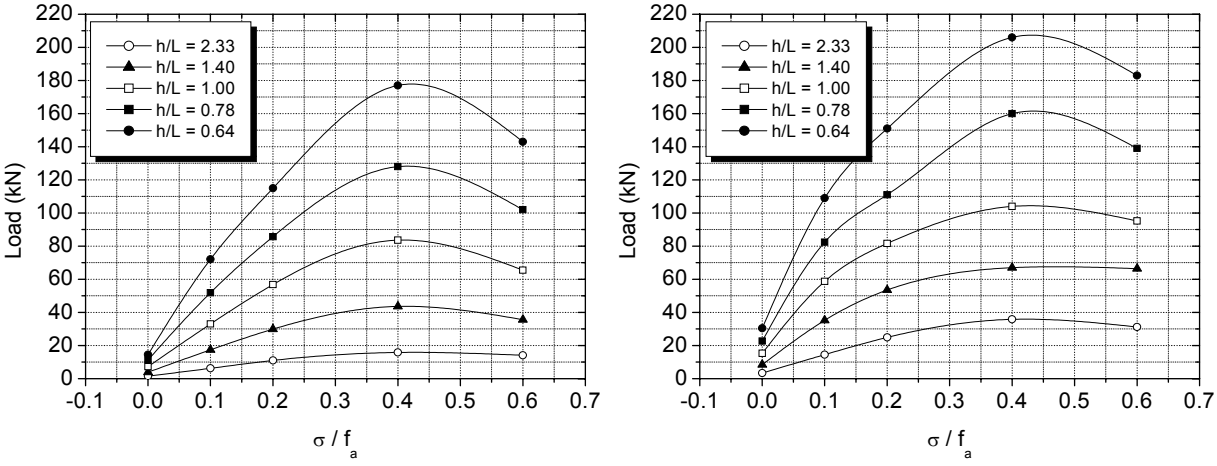

Figure 6.26 – Influence of pre-compression on lateral capacity of shear-walls: (a) cantilever wall and (b) fixed end wall.

The failure surfaces of the walls under in-plane loading were obtained by combining simultaneously the aspect ratio (h/L) and normalized axial stress (σ/f_a) with the lateral resistance, (H), see Figure 6.27. The failure surface presents the same shape for both boundary conditions. The difference between cantilever and fixed end conditions is the level of the lateral resistance of he walls, which is higher in case of walls with both ends fixed due to lower the lever arm. In both cases, the surface curvature presents decreasing values at the aspect ratio increase and as the compressive stress level decreases, which is directly related to the predominant failure mode of the walls. Thus, it seems that the variation of the pre-compression level and aspect ratio play a major role on the lateral strength of walls, where the predominant shear response prevails on their the lateral in-plane behaviour. The influence is not so evident in walls governed essentially by flexure mechanism.

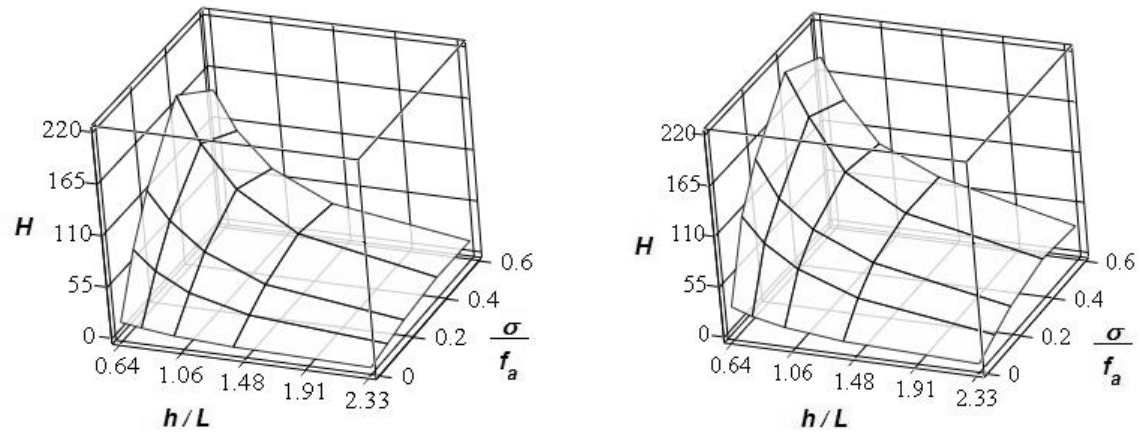

Figure 6.27 – Failure surface of unreinforced shear-walls: (a) cantilever wall and (b) fixed end wall.

An analysis of the failure modes developed on shear walls with distinct boundary conditions and with variable aspect ratio and pre-compression level was also performed. The typical failure modes are defined according to the following description:

1. Flexure (FL)
    a. Rocking (R) – when an horizontal crack opened in base of wall due to the tensile stresses and the wall rotated;
    b. Crushing (C) – when the toe crushing of wall occurred due to the high compressive stresses.
2. Shear (SH) - Diagonal cracking;

The results of numerical modelling concerning the failure modes of the walls are displayed in Table 6.9 and Table 6.10. It is possible to observe that flexure failure modes were predominant in cantilever walls as expected.

Table 6.9 – Failure modes of unreinforced shear walls (cantilever).

h/L \ σ / f_a	0.0	0.1	0.2	0.4	0.6
2.33	FL (R)	FL (R)	FL (R)	FL (R)	FL (R)
1.40	FL (R)	FL (R)	FL (R)	FL (R)	FL (R)
1.00	FL (R)	FL (R)	FL (R)	FL (C)	FL (C)
0.78	FL (R)	SH	SH	SH	FL (C)
0.64	FL (R)	SH	SH	SH	FL (C)

Table 6.10 – Failure modes of unreinforced shear walls (fixed end).

h/L \ σ / f_a	0.0	0.1	0.2	0.4	0.6
2.33	FL (R)	FL (R)	FL (R)	FL (R)	FL (R)
1.40	FL (R)	SH	SH	SH	SH
1.00	FL (R)	SH	SH	SH	SH
0.78	FL (R)	SH	SH	SH	SH
0.64	FL (R)	SH	SH	SH	SH

In case of cantilever slender walls (h/L=2.33 and h/L=1.4), flexural rocking mechanism predominates for all pre-compression levels under analysis. For squared walls toe crushing develops for high pre-compression levels. Shear failures develop only for aspect ratios lower than 1.0 and for medium to high pre-compression levels. When no pre-compression was applied flexural rocking failure mechanism characterized the behaviour of the walls with distinct boundary conditions. In case of fixed end walls, apart from the walls submitted to zero pre-compression level and the highest slender wall, where flexural rocking mechanism prevails, the shear failure mode is predominant on the lateral response of unreinforced masonry walls. Each of the failure modes develop for certain values of aspect ratios and pre-compression levels defining failure regions. The definition of the failure modes of some walls located along the boundaries is difficult because the diagonal cracking or toe crushing develops almost at same time. The understanding of the predominant failure mode of masonry shear walls is important for the analysis of the influence of parameters like

vertical and horizontal reinforcement ratio on the in-plane behaviour as their role depends to great extent on the deformation type exhibited by the walls.

6.4.1.2 Unreinforced masonry walls with the fill of vertical joints

The proposal of a masonry bond pattern with dry joints (masonry built with 3C-units and traditional bond pattern) aims at increasing the productivity during the execution of structural masonry. According to Gouveia and Lourenço (2007), the usage of filled vertical joints promotes only a very moderate difference on the strength of masonry walls subjected to lateral load. However, the results of diagonal compressive tests carried out on concrete block masonry with different bond patterns carried out in Chapter 3, reveal a great difference on the shear resistance of masonry built with 2C-units and filled vertical joints and 3C-units with dry vertical joints. In spite of the wallets built with 2C-units presented a lower width, the diagonal strength was about 3 times higher than specimens built with 3C-units and dry joints.

Therefore, it was decided to evaluate the influence of this parameter on the lateral resistance of masonry walls under in-plane loading through the numerical analysis. Due to the absence of mechanical properties of filled vertical joints (3C-units), the same mechanical properties used for horizontal joints were assumed to vertical joints. Analysis was performed using the same group of 25 walls studied in previous analysis with different aspect ratio and submitted to different pre-compression levels.

According to the results obtained for the lateral resistance of masonry walls with filled and unfilled vertical joints, it is seen that the usage of filled vertical joints play a reduced influence on the lateral strength when the predominant resistant mechanism was flexure see Figure 6.28. No significant differences were found between walls with filled and unfilled vertical joints with the variation of aspect ratio. The differences on the lateral strength are only visible in walls with the aspect ratio lower than 1.0 and for intermediate values of pre-compression level, in which shear response takes the central role. In these cases the lateral strength is slightly higher in walls with filled vertical joints.

In case of fixed end boundary conditions the lateral resistance of walls with filled vertical joints deviates clearly from the lateral resistance found in walls with unfilled vertical joints mainly when the aspect ratio is lower or equal to 1.0, see Figure 6.29. This behaviour is due to the predominant shear resisting mechanisms characterizing the in-plane behaviour of these walls, which is more remarkable than in cantilever walls. It should be noticed that almost no differences were found for slender walls, in which the flexural response predominates.

The higher increasing of lateral strength observed in cantilever walls was equal to 10%, whereas in fixed end walls it was equal to 20%. Thus, it is clear that the influence of filling the vertical joints depends on the predominant shear or flexure resisting mechanism. This result is in agreement with results of the diagonal compression tests (Chapter 3).

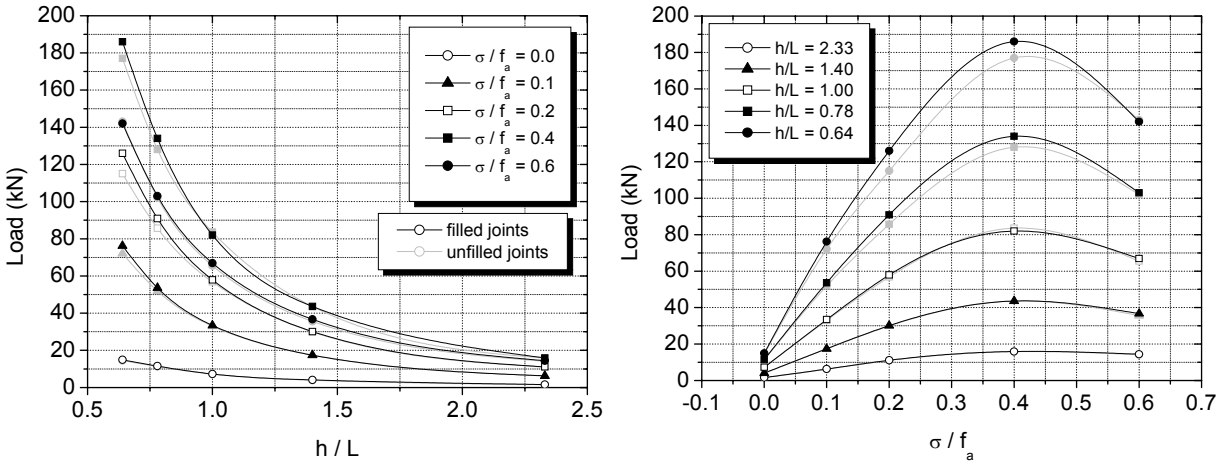

(a) (b)

Figure 6.28 – Influence of the filling of vertical joints on the lateral resistance of cantilever walls: (a) lateral strength *vs.* aspect ratio and (b) lateral strength *vs.* pre-compression.

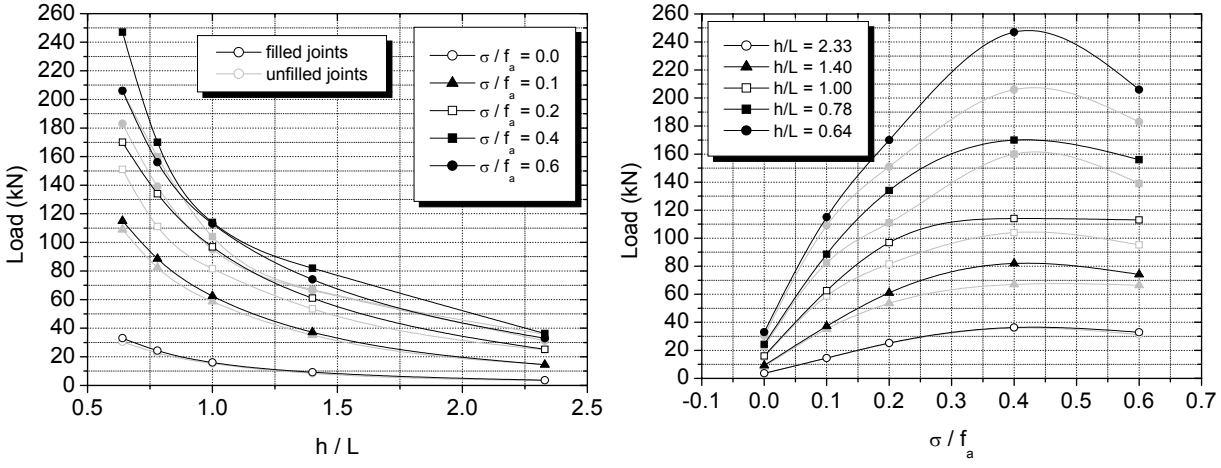

(a) (b)

Figure 6.29 – Influence of the filling of vertical joints on the lateral resistance of fixed end walls: (a) lateral strength *vs.* aspect ratio and (b) lateral strength *vs.* pre-compression.

6.4.1.3 Horizontal reinforcement

In the assessment of the influence of the horizontal reinforcement on the lateral resistance of the concrete block masonry walls, a total of 9 walls were considered for each

type of boundary conditions, namely 5 walls with variable aspect ratios under a pre-compression σ/f_a equal to 0.2 and 4 walls with aspect ratio of 1.0 with variable pre-compression levels adopted in the previous analysis. Three horizontal reinforcement ratios were taken into account: 0.03%, 0.05% and 0.08%. Horizontal reinforcements were uniformly distributed along the height of the walls in five layers. Bars were symmetrically positioned in relation to the mid height at each three courses.

Results clearly show that the boundary conditions have a major influence on the lateral behavior of horizontally reinforced masonry walls. For cantilever walls only an increase on the lateral strength was observed from the unreinforced masonry wall to the remaining reinforced masonry walls in case of an aspect ratio equal to 0.64, see Figure 6.30.

In fact, horizontal reinforcements contribute to the lateral strength of the walls only after the onset of the diagonal crack. In case of cantilever walls diagonal cracking developed before the resistant maximum lateral resistance, only in case of very low aspect ratios, which means that reinforcements are not activated when flexural response is preponderant.

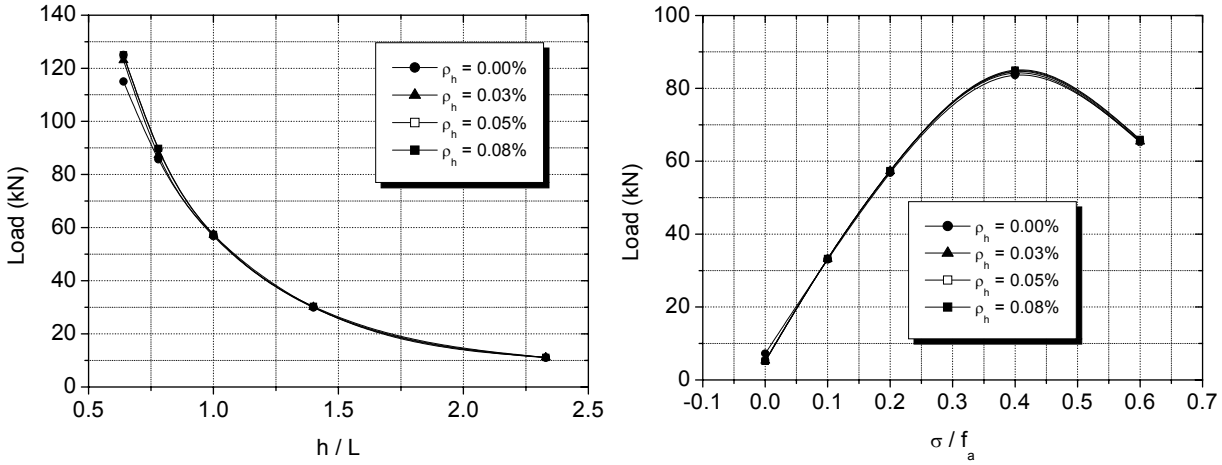

Figure 6.30 – Influence of the horizontal reinforcement on the lateral resistance of cantilever walls: (a) lateral strength vs. aspect ratio and (b) lateral strength vs. pre-compression.

Similar trend was verified in fixed end walls with low values of the vertical pre-compression (σ/f_a = 0.1), after which it is clear that the increase on the horizontal reinforcement ratio leads to increasing values of the lateral strength, see Figure 6.31. After this pre-compression level the shear prevails in the response of the walls, being the horizontal reinforcements activated after opening of the diagonal cracking. In this case the horizontal reinforcements avoid the separation of the walls into two parts and promote the stress transfer between both edges of the diagonal crack. It should be noticed that the trend of overturning of one part of the wall in unreinforced masonry walls is prevented by the

presence of horizontal reinforcements. It is important to stress that a perfect bond between the reinforcements and the mortar of bed joints was considered in the numerical analysis. In design of masonry walls it is mandatory to ensure the required bond length for bed joint reinforcements so that they can be effective in the behavior of the walls.

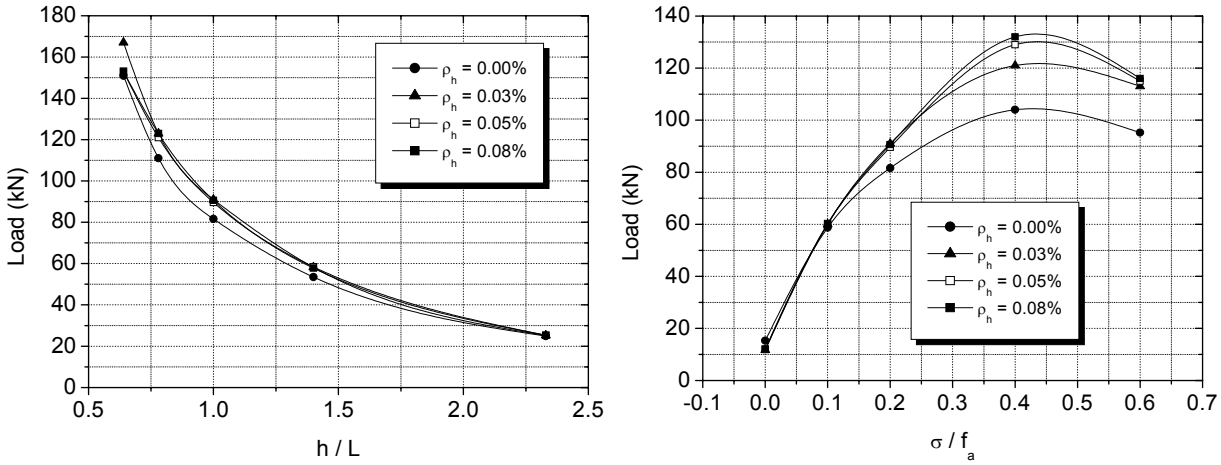

(a) (b)

Figure 6.31 – Influence of the horizontal reinforcement on the lateral resistance of fixed end walls: (a) lateral strength vs. aspect ratio and (b) lateral strength vs. pre-compression.

Independently on the boundary conditions, it becomes clear that the horizontal reinforcement ensures a control of the diagonal cracking, increases the deformation capacity, providing a higher ductility for the masonry wall and enabled a better distribution of the stresses in the wall, see Figure 6.32.

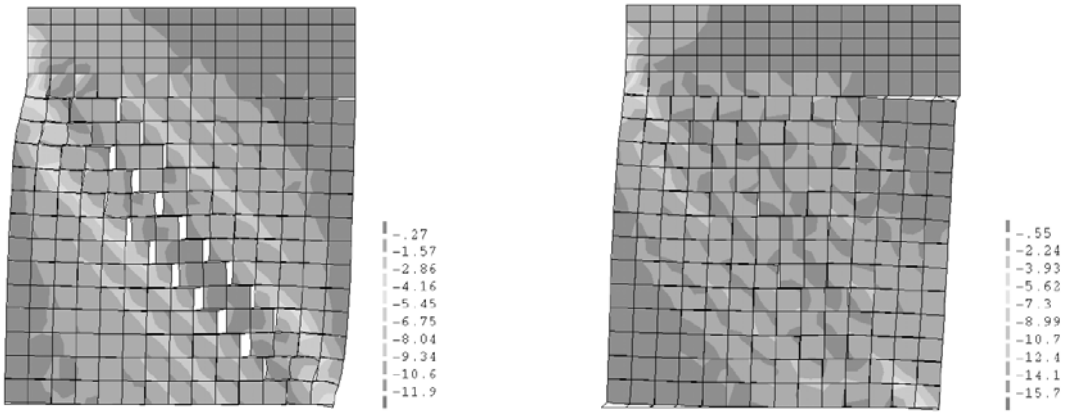

(a) (b)

Figure 6.32 – Deformed mesh with the representation of the principal stresses after the application of a lateral displacement of 5 mm: (a) unreinforced masonry wall (h/L=1.00 - σ/f_a=0.10) and (b) horizontally reinforced masonry wall (h/L=1.00 - σ/f_a=0.10 – ρ_h=0.05%).

6.4.1.4 Vertical reinforcement

In order to obtain a better insight on the influence of the vertical reinforcements on the behavior of concrete block masonry walls under lateral loads, it was decided to consider a parametric analysis on specimens with only vertical reinforcement. Also in this analysis, a total of 9 walls were considered for each type of boundary conditions, namely 5 walls with variable aspect ratios with a pre-compression σ/f_a equal to 0.2 and 4 walls with aspect ratio of 1.0 with variable pre-compression levels from 0 to 0.6. Two different arrangements of reinforcements were applied in shear walls in this study with the bars distributed for length of wall and with reinforcements concentrated in extremities of wall. Three vertical reinforcement ratios were considered in the analysis, namely 0.03%, 0.05% and 0.08%. In case of distributed reinforcements, ρ_v, four vertical reinforcements were uniformly distributed along the length of the walls, except in specimen with h/L=2.33, where only three vertical reinforcements were considered due to its small length. In case of concentrated reinforcement, ρ_{vc}, only vertical reinforcement ratio equal to 0.05% were considered for masonry walls.

From Figure 6.33 and Figure 6.34, it is observed that the presence of vertical reinforcements in masonry walls increased the lateral strength of cantilever and fixed end walls, when the flexural mode predominates in the lateral response. It is common that in unreinforced cantilever walls and especially for high aspect ratios, the horizontal load generates tensile stresses at the base of wall leading to the development of horizontal cracks in first courses and to the uplift until crushing of the bottom corner.

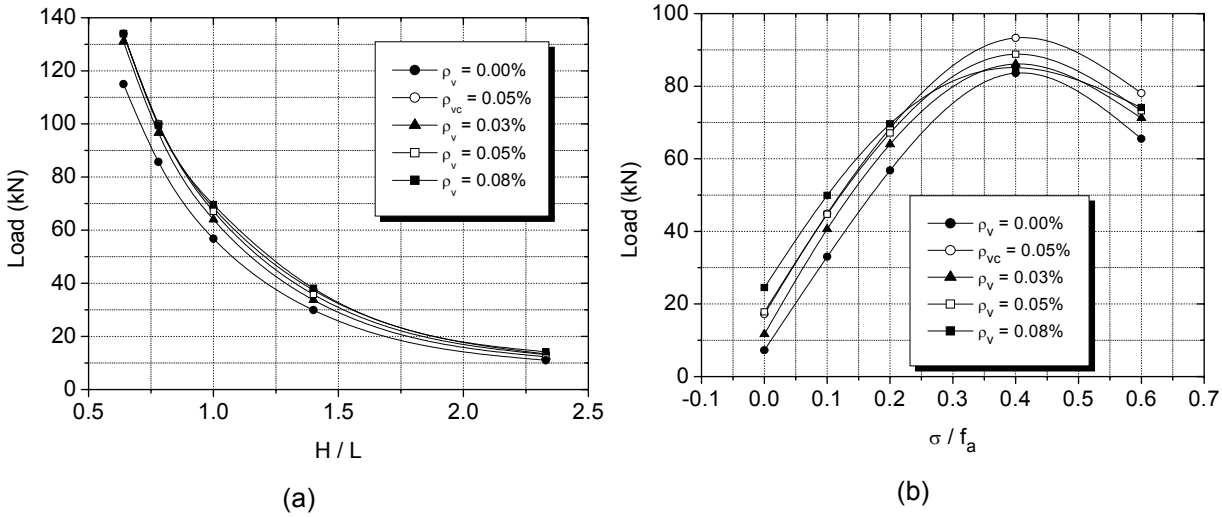

Figure 6.33 – Influence of the vertical reinforcement on the lateral resistance of cantilever walls: (a) lateral strength vs. aspect ratio and (b) lateral strength vs. pre-compression.

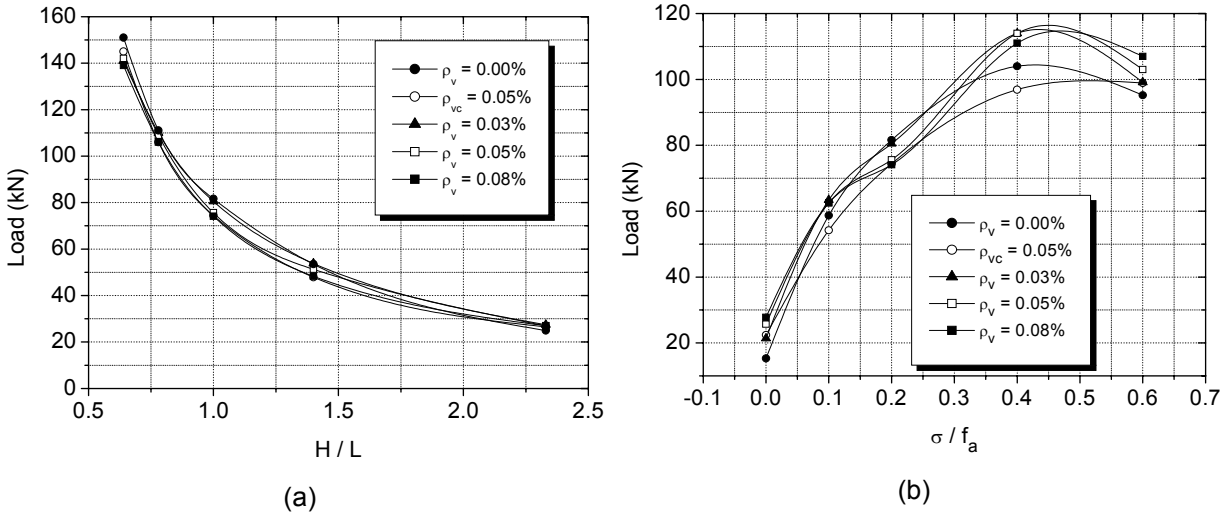

Figure 6.34 – Influence of the vertical reinforcement on the lateral resistance of fixed end walls: (a) lateral strength vs. aspect ratio and (b) lateral strength vs. pre-compression.

In reinforced masonry walls, the vertical reinforcements reduce the uplift and resist the tensile stresses, leading to the increase on the lateral strength. However, this improvement also depends on the level of pre-compression of wall. In fact, the introduction of vertical reinforcements does not mean the increase on the lateral strength for all pre-compression levels. In case of walls with a high pre-compression, vertical reinforcement increased the lateral strength because the failure mode of these walls was governed by the toe crushing. Therefore, vertical reinforcements reduce the uplift of these walls decreasing the compressive stresses at the bottom corner of wall allowing an increasing on the lateral capacity. On the other hand, when an unreinforced masonry walls fails by shear diagonal cracking, the introduction of vertical reinforcements can lead to a reduction on the lateral strength of the wall. The horizontal load applied in a masonry wall generates a diagonal compressive stress flow towards the bottom corner of the wall and, consequently, to a flow of transversal tensile stresses. Vertical reinforcements, bonded to the masonry, by avoiding the uplift of the wall increases the transversal tensile stresses leading to an earlier diagonal cracking. This behaviour can be observed through the principal tensile stresses along the diagonal strut of wall, see Figure 6.35. It should be referred that the presence of vertical reinforcement leads to peak principal tensile stresses mainly localized at the upper and lower regions of the diagonal strut. The evolution of principal stresses is much smoother in unreinforced or lightly reinforced masonry walls. The result found in this work is in agreement with the one pointed out by Tomaževič (1999), which stated that vertical reinforcements alone are not able to contribute to the shear resistance of masonry.

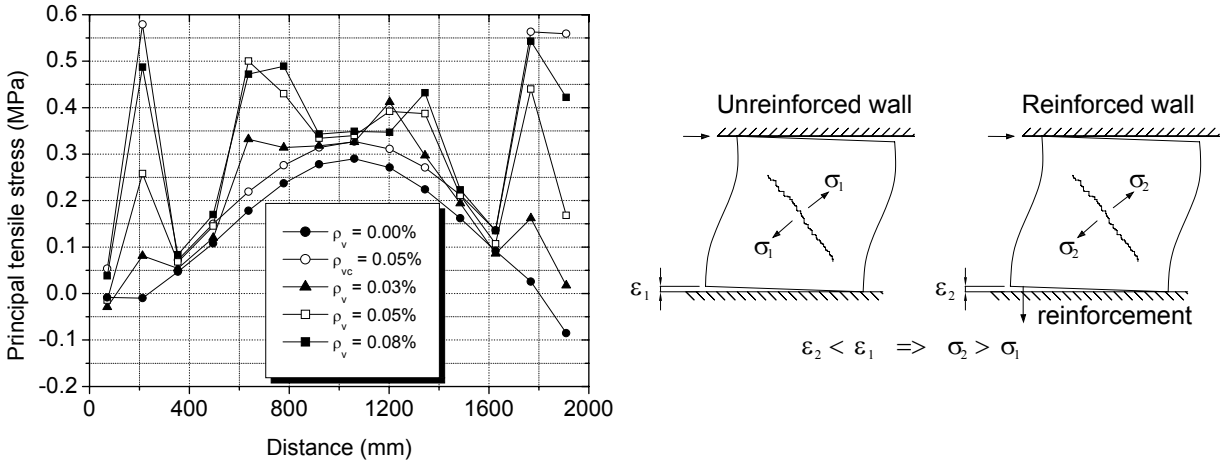

Figure 6.35 – Premature cracking in masonry walls with vertical reinforcements.

6.4.1.5 Vertical and horizontal reinforcement

In order to analyze the influence of combining vertical and horizontal reinforcement on the lateral resistance of masonry walls a last parametric study was carried out. As in other cases, only nine walls from the group of 25 specimens for the evaluation of the effect of the aspect ratio and level of pre-compression were considered. In total 18 walls were used. In nine walls the vertical reinforcement ratio of 0.05% was kept constant and it was combined with three distinct horizontal reinforcement ratios (0.03%, 0.05% and 0.08%). In other nine walls the horizontal reinforcement ratio of 0.05% was kept constant and combined with three different vertical reinforcement ratios (0.03%, 0.05% and 0.08%).

From the results it is possible to observe that in cantilever walls when the vertical reinforcement ratio is kept constant and the horizontal reinforcement ratio varied no changes in lateral strength occurred, which is attributed to the predominant flexural failure mode. On the other hand, in case of fixed end walls, an increase on lateral strength was observed due to the introduction of horizontal reinforcements, see Figure 6.36. However, the increase on the horizontal reinforcement ratio did not lead to the increase on the lateral strength. Shear failure mode developed in the masonry wall with vertical reinforcement ratio equal to 0.05% and without horizontal reinforcement. Thus, when horizontal reinforcements were inserted in the wall, they provided an increase on lateral strength and changed the failure mode from shear to flexure. After this, the increasing on horizontal reinforcement ratio has no influence on the lateral behaviour of masonry walls both in relation to the lateral strength and failure mode.

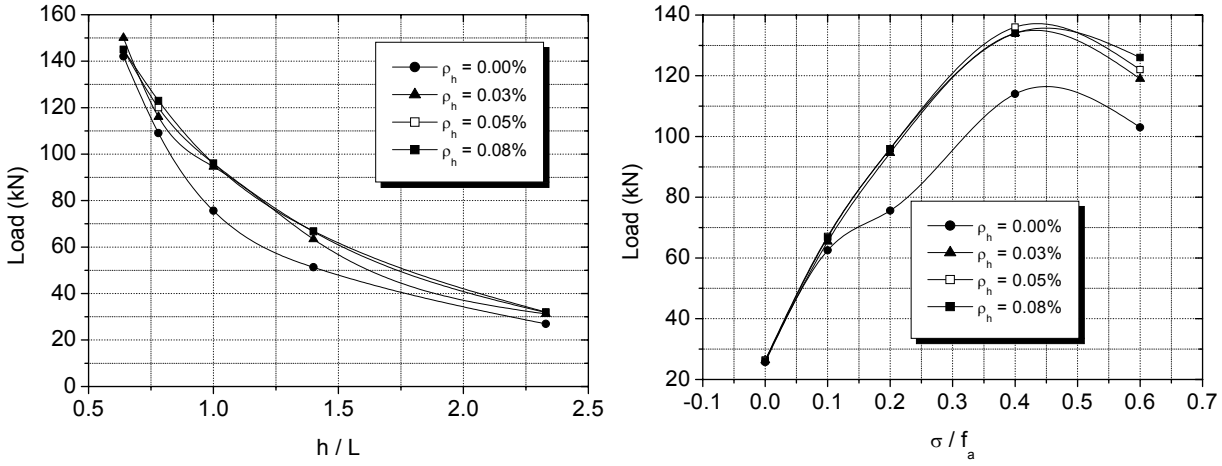

(a) (b)

Figure 6.36 – Influence of the variation of horizontal reinforcement ratio on the lateral resistance of fixed end walls: (a) lateral strength vs. aspect ratio and (b) lateral strength vs. pre-compression.

In masonry walls, where the horizontal reinforcement ratio was kept constant and equal to 0.05% and vertical reinforcement ratios were varied, the increase of the vertical reinforcement ratio improved the lateral strength of cantilever walls since flexure is the preponderant effect in this type of wall, see Figure 6.37. On the other hand, in fixed end walls the variation of vertical reinforcement did not cause any change on the behaviour of masonry walls.

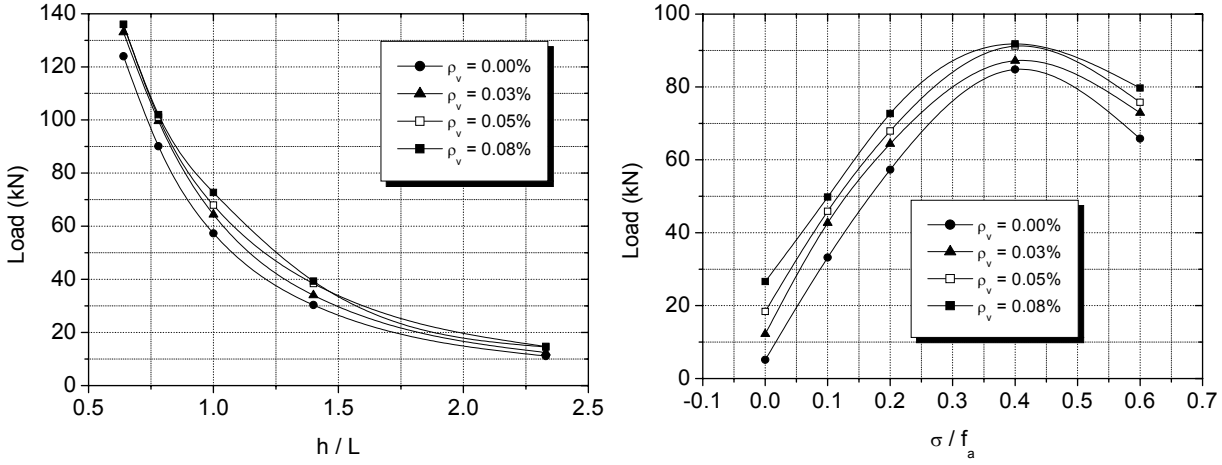

(a) (b)

Figure 6.37 – Influence of the vertical reinforcement ratio on the lateral resistance of cantilever walls: (a) lateral strength vs. aspect ratio and (b) lateral strength vs. pre-compression.

6.4.2 Beams

The parametric study of masonry beams aims at obtaining a better insight on the variables influencing their flexural and shear behaviour. The parameters evaluated were (i) the span to height ratio; (ii) filling of the vertical joints; (iii) horizontal reinforcement ratio and (iv) the combination of vertical and horizontal reinforcements. These parameters were evaluated for different boundary conditions, namely simply supported and fixed end masonry beams in order to assess their influence in flexure and shear respectively. For each boundary condition ten span to height ratios were considered, see Figure 6.38 to Figure 6.41. A three point load configuration is adopted for applying the load through displacement control in order to avoid convergence problems in post-peak regime.

The parametric study was carried out by considering the material properties used in calibration of experimental beams built with 3C-units.

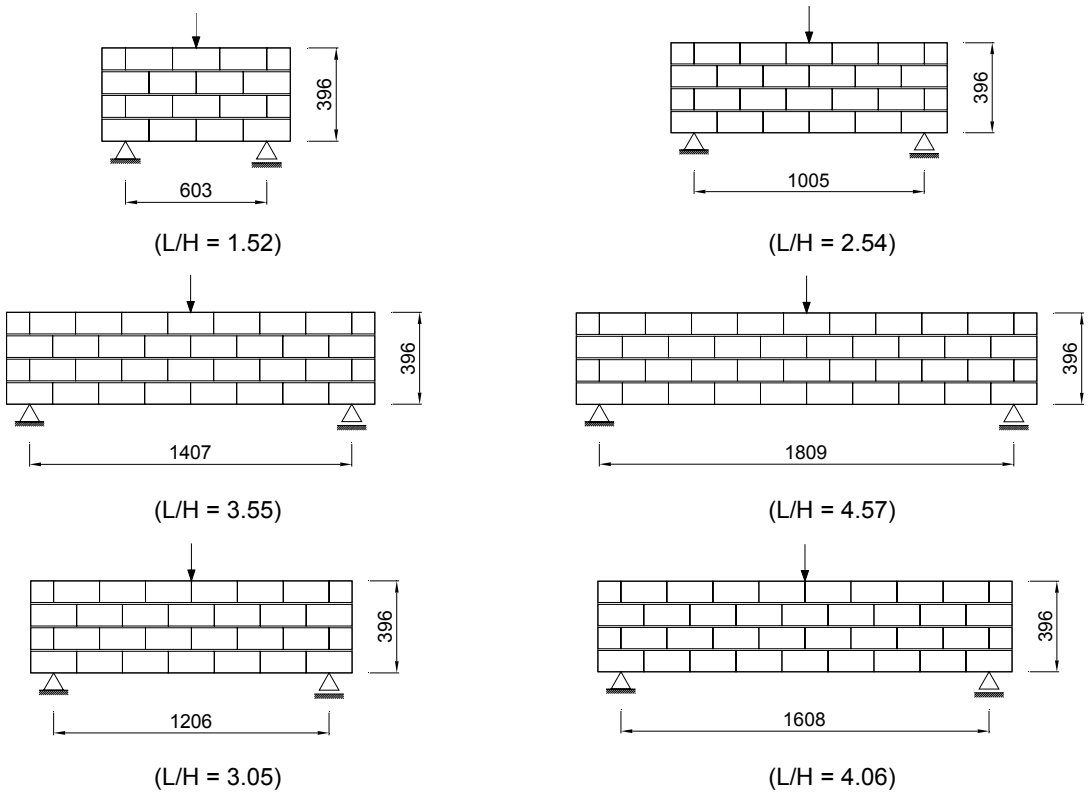

Figure 6.38 – Simply supported masonry beams: variation of span.

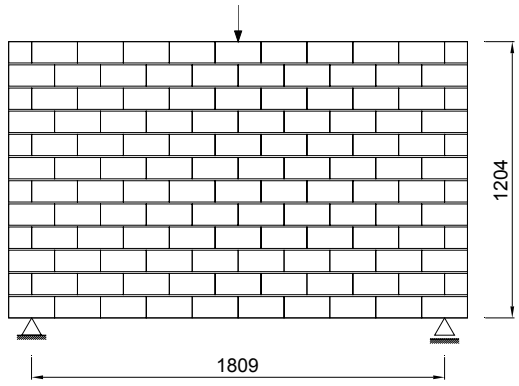

(L/H = 1.50)

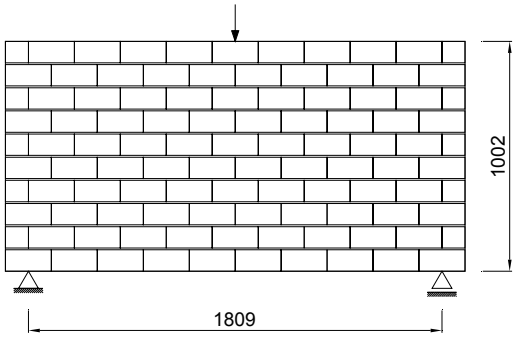

(L/H = 1.81)

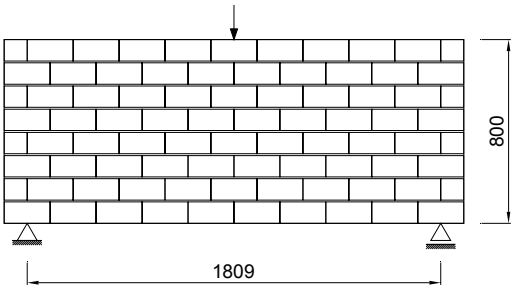

(L/H = 2.26)

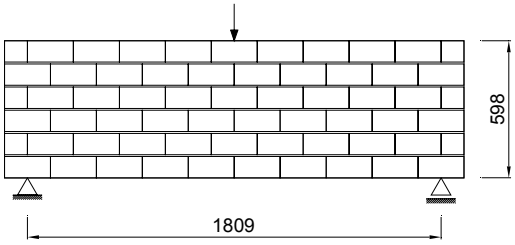

(L/H = 3.03)

Figure 6.39 – Simply supported masonry beams: variation of height.

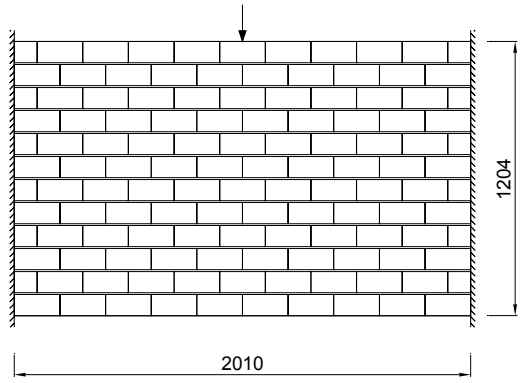

(L/H = 1.67)

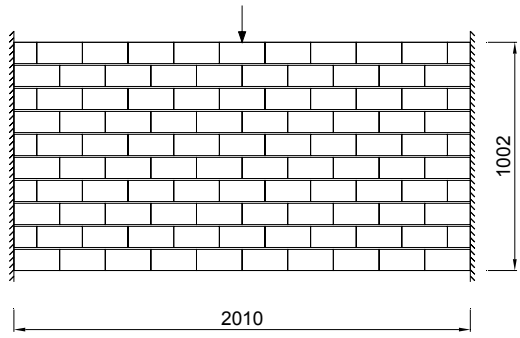

(L/H = 2.00)

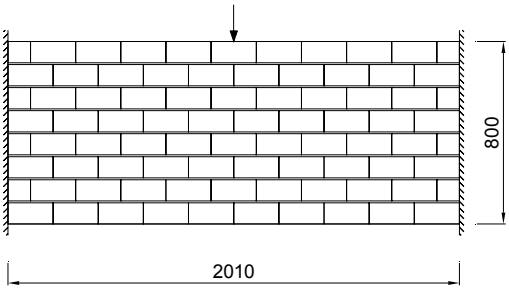

(L/H = 2.51)

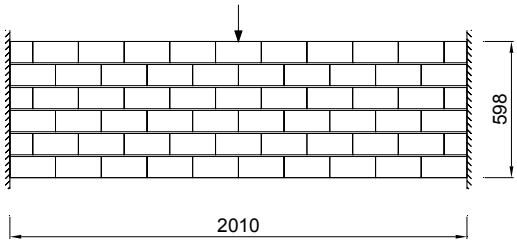

(L/H = 3.36)

Figure 6.40 – Fixed end masonry beams: variation of height.

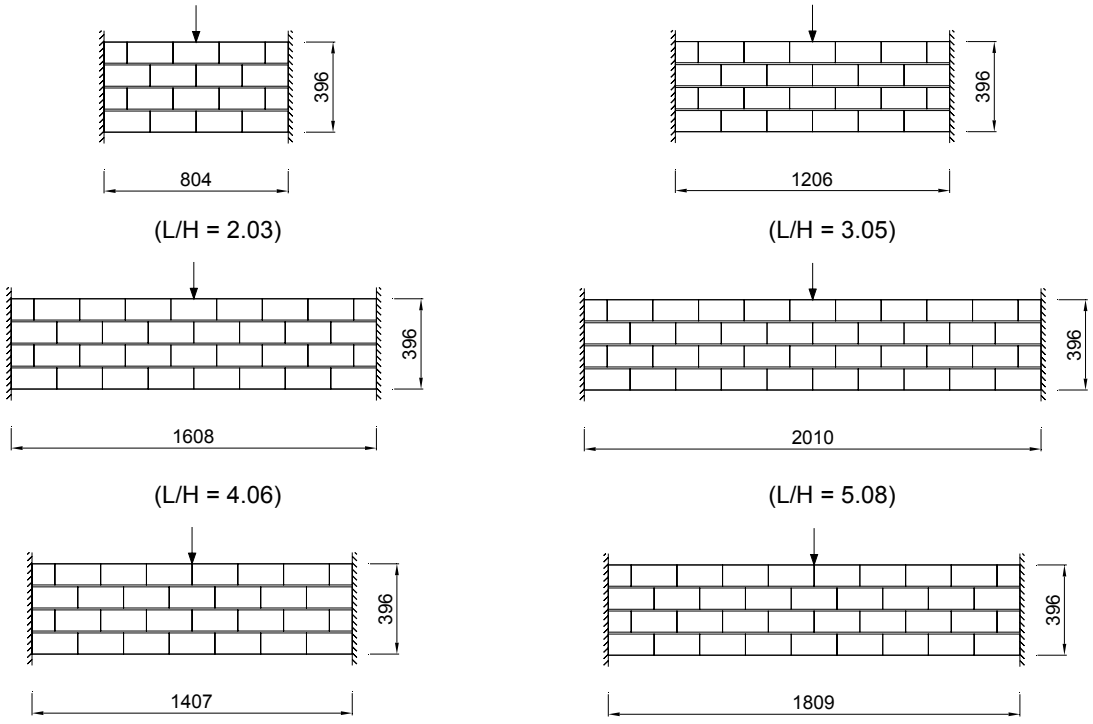

Figure 6.41 – Fixed end masonry beams: variation of span.

6.4.2.1 Unreinforced masonry beams with unfilled vertical joints

Unreinforced masonry beams behave in a very brittle manner due to the low strength of unit-mortar interfaces. The simply supported masonry beams failed by flexure, whereas the fixed end beams failed by shear. Figure 6.42a shows the symmetrical flexural cracking pattern developed in a simply supported beam. The onset of flexural cracking is at bottom vertical joints located at mid span of the beam due to the zero tensile bond strength of the unit-mortar interfaces. In case of failure by shear in fixed end masonry beams, the onset of diagonal cracking takes place when the shear stress is higher than the shear strength of dry vertical joints provided by the friction between the units, see Figure 6.42b. It should be noticed that the shear friction resistance of the vertical joints is enhanced by the compressive stresses in the parallel direction to the bed joints developed in the upper region of the beam due to flexure. The shear sliding of vertical joints induces tensile stresses at the mortar bed joints leading to the definition of the diagonal cracking mostly at the unit-mortar interfaces.

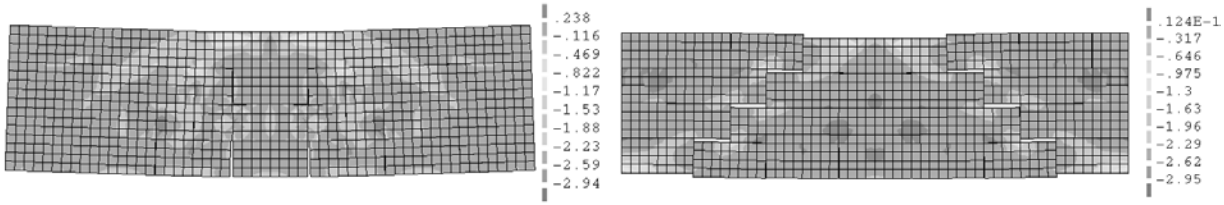

(a) (b)

Figure 6.42 – Deformed mesh with the representation of the principal stresses after the application of a displacement equal to 0.75 mm: (a) simply supported beam (L/H = 3.05) and (b) fixed end beams (L/H = 3.55).

Flexural behaviour of unreinforced masonry beams with unfilled vertical joints is greatly influenced by shear resistance of the bed joints since the flexural strength is provided by the interlocking associated to the traditional running bond pattern and is ensured by the shear strength of bed joints. On the other hand, the shear resistance is dependent on the normal stresses in bed joints. The typical distribution of normal stresses in bed joints along the length of the masonry beams is displayed in Figure 6.43. It is seen that the distribution of normal stresses present an alternation of sign at each half block. The normal stresses profile along the length of the bed joints presents compressive and tensile peaks, which is the result of the no filling of vertical joints. In fact, due to the absence of mortar at the vertical joints, and taking into account the equilibrium of a unit, it is seen that the shear stresses at bed joints have to be balanced with differential normal stresses, see Figure 6.44. The upper mortar joint in the region of unit under the load application point is embraced by the compression struts (with an inclination of approximately 45º) and it is in compression, presenting two peaks in the region of the hollow cell of the units and a minimum at the region of internal webs. For the highest level of the load applied, the normal stresses in the region of the internal webs can even be tensile stresses, which can be associated to tensile stresses developed in the unit. The concentration of stresses reduces gradually in the first and second bed joints.

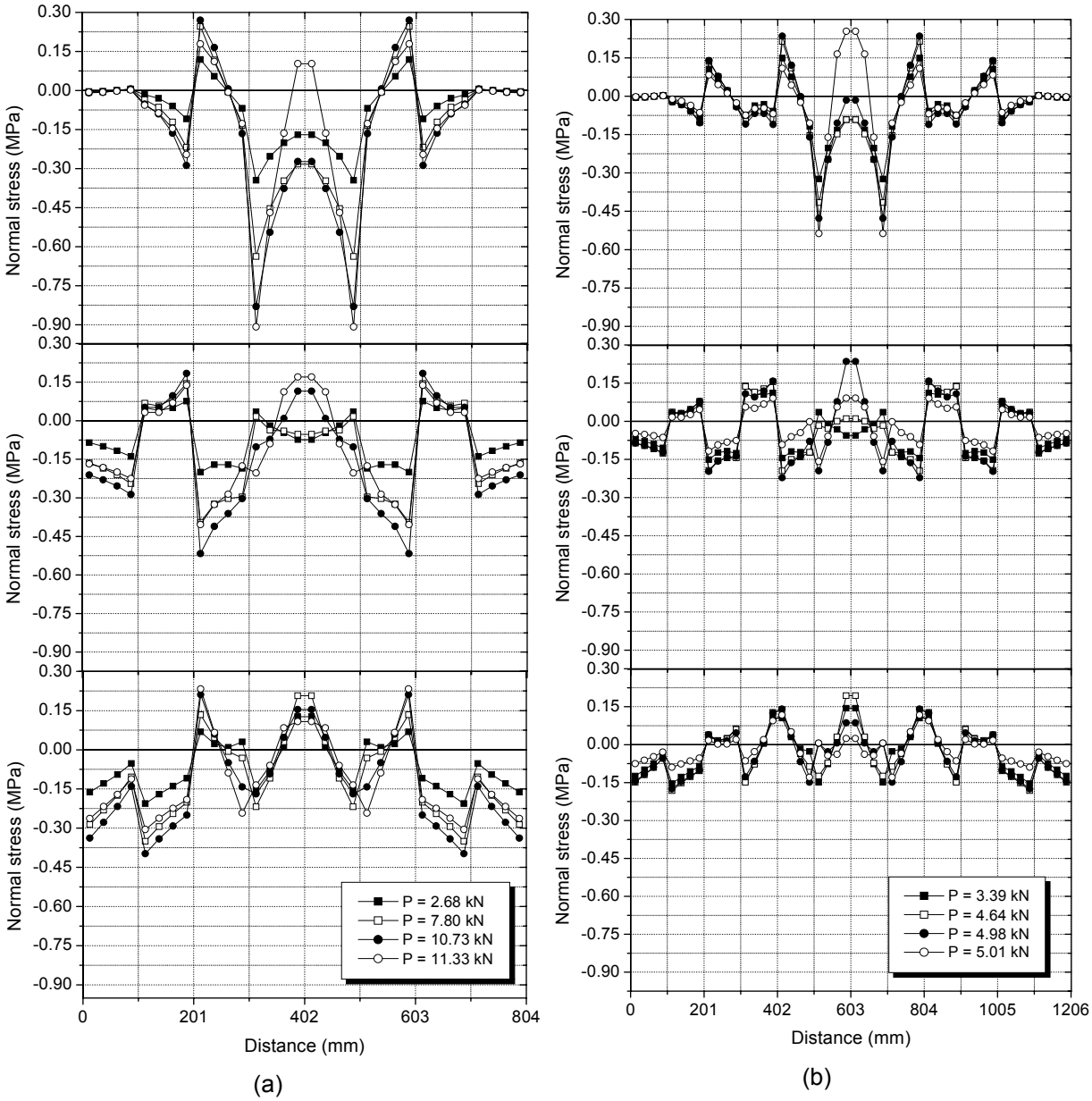

Figure 6.43 – Normal stress in bed joints of simply supported beams with unfilled of vertical joints: (a) L/H=1.52 and (b) L/H=2.54.

Figure 6.44 – The way of stresses from the point of application to the supports through the bed joints.

By comparing the profile of the normal stresses at bed joints for distinct geometry ratios, it is seen the span to height influences the distribution of the normal stresses at bed joints, see Figure 6.45. For the same height and increasing span length corresponding to a higher span to height ratio, the normal stresses present higher amplitude. This means that

normal stresses in bed joints increase with the higher flexural deformed shape resulting in the higher interlocking between units. This behaviour is also valid in case of the height increases and the span length is kept constant, where the interlocking between units progressively decreases as a result of the lower flexural deformation of the beams.

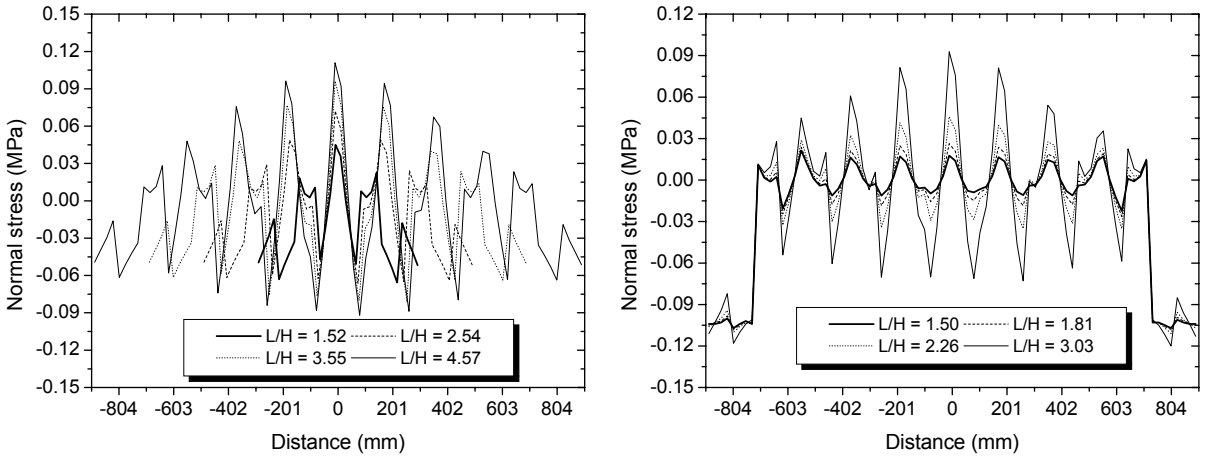

Figure 6.45 – Normal stress distribution in first bed joint of simply supported beams with unfilled vertical joints in the same level of loading: (a) variation of span length (P=2kN) and (b) variation of height (P=5kN).

All fixed end masonry beams failed by shear through the development of a diagonal cracking resulting from sliding of vertical joints and tensile bond failure of the horizontal joints, see Figure 6.46.

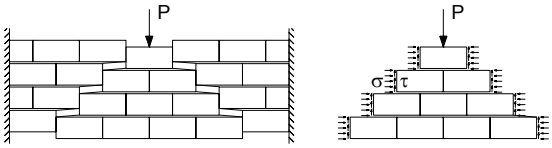

Figure 6.46 – Normal and shear stresses in diagonal crack.

This typical failure mode is the result of having dry vertical joints. As aforementioned, the low shear and tensile strength of the unit-mortar interface lead that diagonal crack mostly develops along the unit-mortar interfaces. This means that the shear behaviour of masonry beams is very dependent on the normal stresses in vertical and horizontal joints, since it is assumed that their shear resistance follows a typical Mohr-Coulomb criterion. From Figure 6.47, where the distribution of normal and shear stresses along the diagonal crack is indicated (vertical interfaces), it is observed that the normal stresses presents higher values at the extremities of the diagonal crack line (DCL) resulting from the typical normal stresses

diagram due to bending moments. In middle of DCL normal stresses presents low values which leads to a minimum shear strength, from which the diagonal cracking..

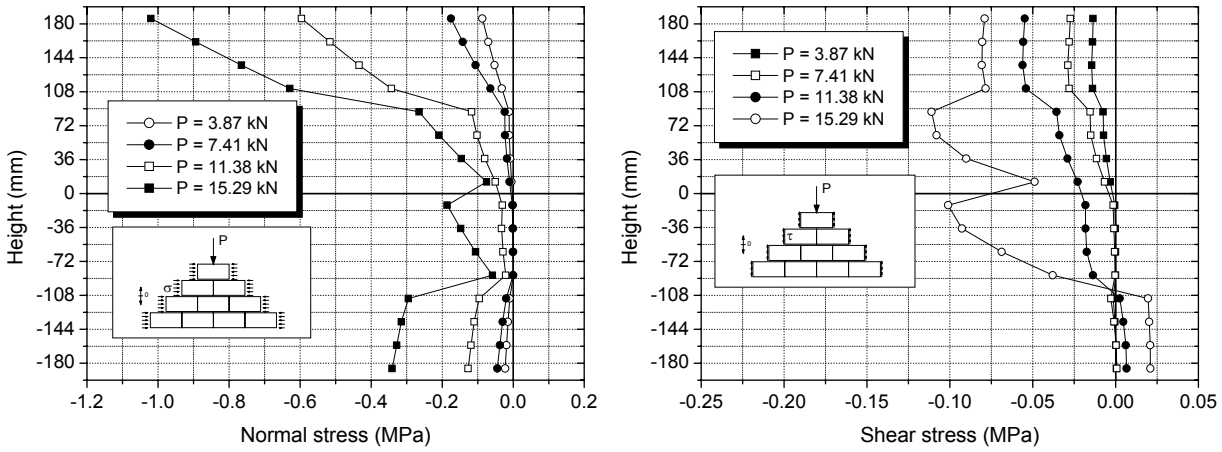

Figure 6.47 – Profile of normal stresses in vertical joints along the diagonal crack of fixed end beam with unfilled of vertical joints (L/H = 4.06): (a) normal stresses and (b) shear stresses.

By comparing the normal stresses through the DCL among the masonry beams with distinct heights and spans for a same load level it can be concluded that they increase with the reduction of height of the beam and with the increase of the span of the beam, see Figure 6.48

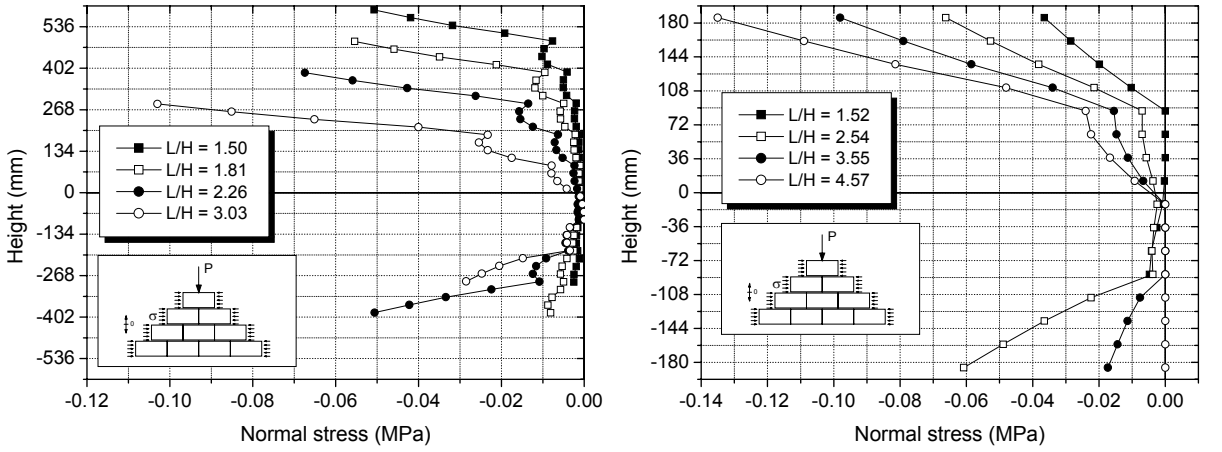

Figure 6.48 – Normal stresses in vertical joints along the DCL of fixed end beams with unfilled vertical joints for the same level of vertical load: (a) influence of the variation of the height (P= 10kN) and (b) influence of the variation of span (P= 5kN).

The normal stresses along the height of the masonry beams can be the result of axial forces and bending moments. In this case, the normal stresses along the DCL increases for increasing span lengths due to the increase on the bending moments. The increase on the normal stresses as the height decreases of the beams can be explained by the decrease of the inertia properties of the cross section of the beams.

The results obtained on the distribution of shear stresses along the DCL reveals that they also increase with the reduction of beam height and with the increase of the beam span, see Figure 6.49. In first case it is expected that the shear stresses decrease with the increase of the beam height since the length on which the shear stresses develop for the same load level increases. The increasing shear stresses with increasing beam span lengths can be explained in a similar manner. In case of high spans, it is possible that the damages at the bottom of the beam due to the flexure, associated to higher bending moments, reduce the height for the development of shear stresses leading to the higher shear concentration stresses on the remaining effective cross section.

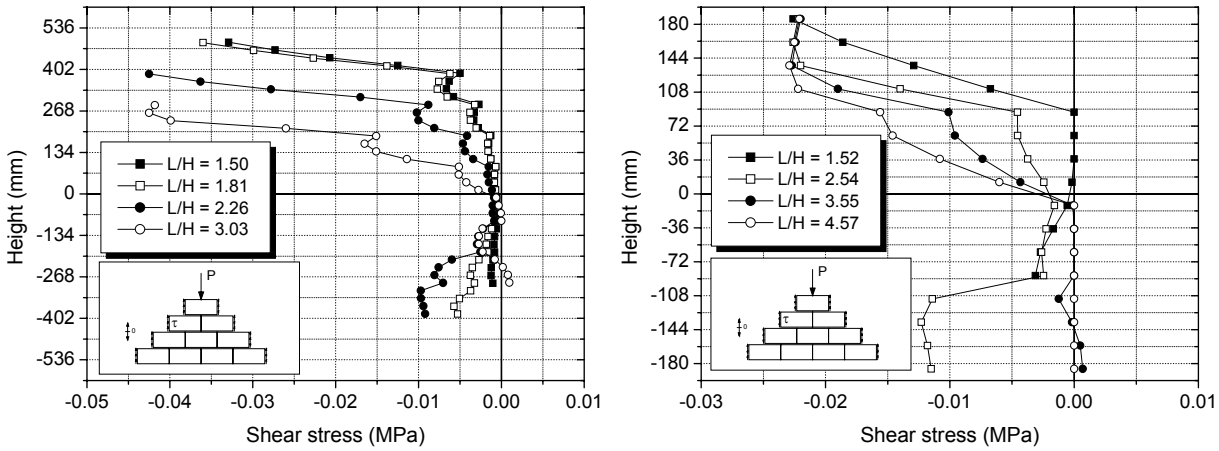

Figure 6.49 – Shear stresses along vertical joints of the DCL of fixed end beams with unfilled vertical joints in the same level of vertical load: (a) influence of the variation of the height (P= 10kN) and (b) influence of the variation of span (P= 5kN).

The results also indicated that the capacity of masonry beams to resist vertical loads is influenced by the location of vertical joints in relation to the critical section. From Figure 6.50, where the load-displacement diagrams obtained in numerical modelling are shown, it is observed that masonry beams with distinct height to span ratios present similar behaviour.

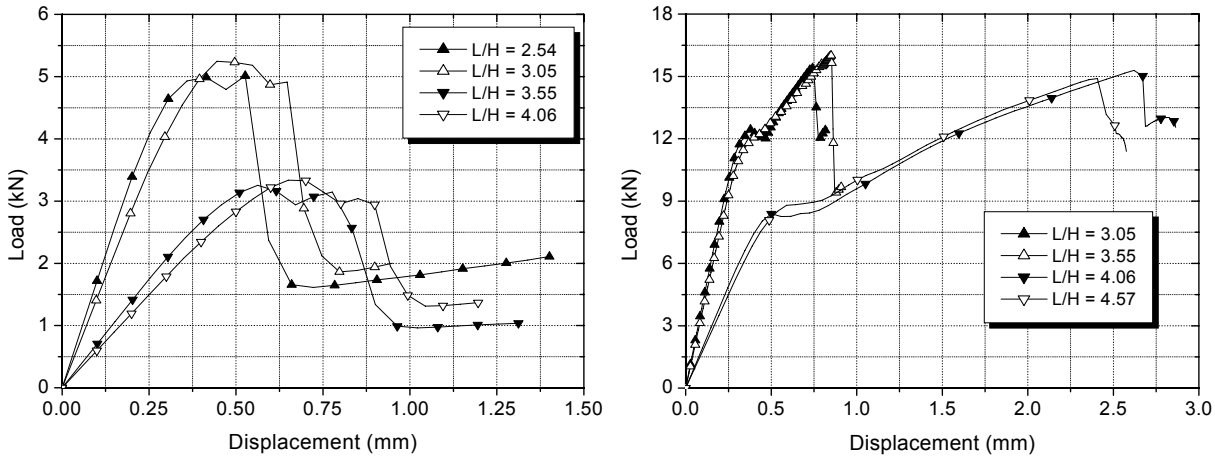

(a) (b)

Figure 6.50 – Influence of bond pattern on the strength of masonry beams with unfilled vertical joints: (a) simply supported beams and (b) fixed end beams.

In effect, in spite of the specimen with L/H equal to 2.54 presents lower span than specimen with L/H equal to 3.05, the potential flexural crack develops from the vertical joint at equal distance from the support. It is in line with the vertical load in case of beam L/H equal to 2.54 and immediately to the left or to the right of load line in case of specimen with L/H equal to 3.05. This behaviour could also be observed in specimens with L/H equal to 3.55 and 4.05. The same behaviour was observed in case of shear failure indicating that the arrangement of units has a high influence in failure mode of masonry beams.

The maximum capacity of the masonry beams for the distinct boundary conditions is clearly influenced by the variation of their height and span length, see Figure 6.51.

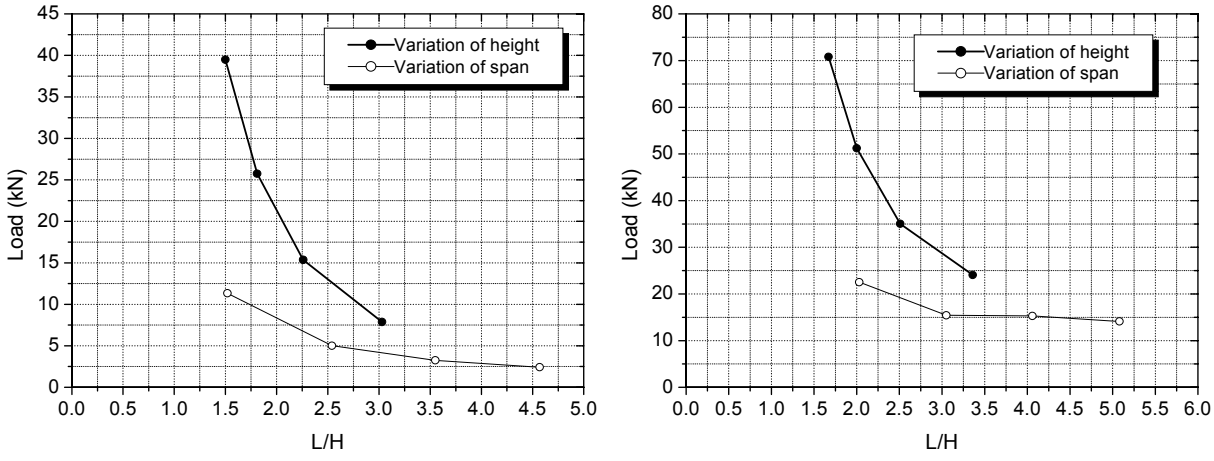

(a) (b)

Figure 6.51 – Variation of load capacity of beams with unfilled vertical joints in relation to the span to height ratio: (a) simply supported beams and (b) fixed end beams.

It is seen that the major parameter that influences the flexural and shear behaviour of masonry beams is the variation of the section. Both flexural and shear strength decreases significantly with the reduction of the height of the beams. Similar trend was recorded for the increase on the span length, even if a much smoother manner. In case of fixed end masonry beams the shear strength only decreases slightly with the increase of span length.

In terms of flexure, considering an elastic behaviour of the unreinforced masonry beams a higher influence of the variation of the height of the beam was expected since the flexural strength is proportional to inertia of the cross section beam, which depends on the height of beam section. Otherwise, by keeping the height of the beam constant, and thus the same resisting cross section, and by varying the span length of the beam, it was expected that the vertical load decreased given that the bending moment acting on the beam depends directly on the span length. Besides, it was expected that the applied load should increase linearly with the span length it in fact was nonlinear. As seen previously from the normal stresses profile along the bed joints (Figure 6.45), the normal stresses increases for increasing span length of the beams, leading to the increase of shear strength of bed joints and thus to the nonlinear increase of flexural strength.

In terms of shear, as expected the strength of masonry beams increase with the height. It was seen that for the same load acting on the beam the shear stresses are minimal for the highest height of the beam (Figure 6.49), meaning that an extra load level can be applied until the failure is reached. The shear resistance of the masonry beams is influenced by the span length in a much lower ratio. In the particular case, the higher shear resistance of the beam with L/H = 2.03 is explained by its geometry, which avoids the completely sliding of the central region over the diagonal crack of the beam according what was shown in Figure 6.42, as the progress of diagonal crack from the top of the beam is restrained by the supports. Apart from this particular case, almost no differences are observed in shear strength as the span length increases. Note that as is shown in Figure 6.44 the increase on the normal stresses on the dry vertical joints appear to be counterbalanced with increase on the shear stress, resulting on the maintenance of the shear strength.

6.4.2.2 Unreinforced masonry beams with filling of vertical joints

Similarly to shear walls, the parametric study on masonry beams included the analysis of the influence of the filling of vertical joints on the overall mechanical behaviour of masonry beams. As no mechanical characterization was carried out for vertical joints, the same mechanical properties used for horizontal joints were assumed to vertical joints in

numerical modelling. In this analysis the same geometry, loading and boundary conditions of the previously study were used.

Contrarily to unreinforced masonry beams with unfilled vertical joints, in case of masonry beams with filled vertical joints, all specimens failed by flexure. The usage of filled vertical joints improves the shear strength of the beams avoiding the diagonal cracking. From Figure 6., where the profile of the normal stress along the bed joints is displayed, it is observed that the usage of filled vertical joints also provides a better distribution of normal stresses in bed joints, becoming the masonry a more homogeneous material.

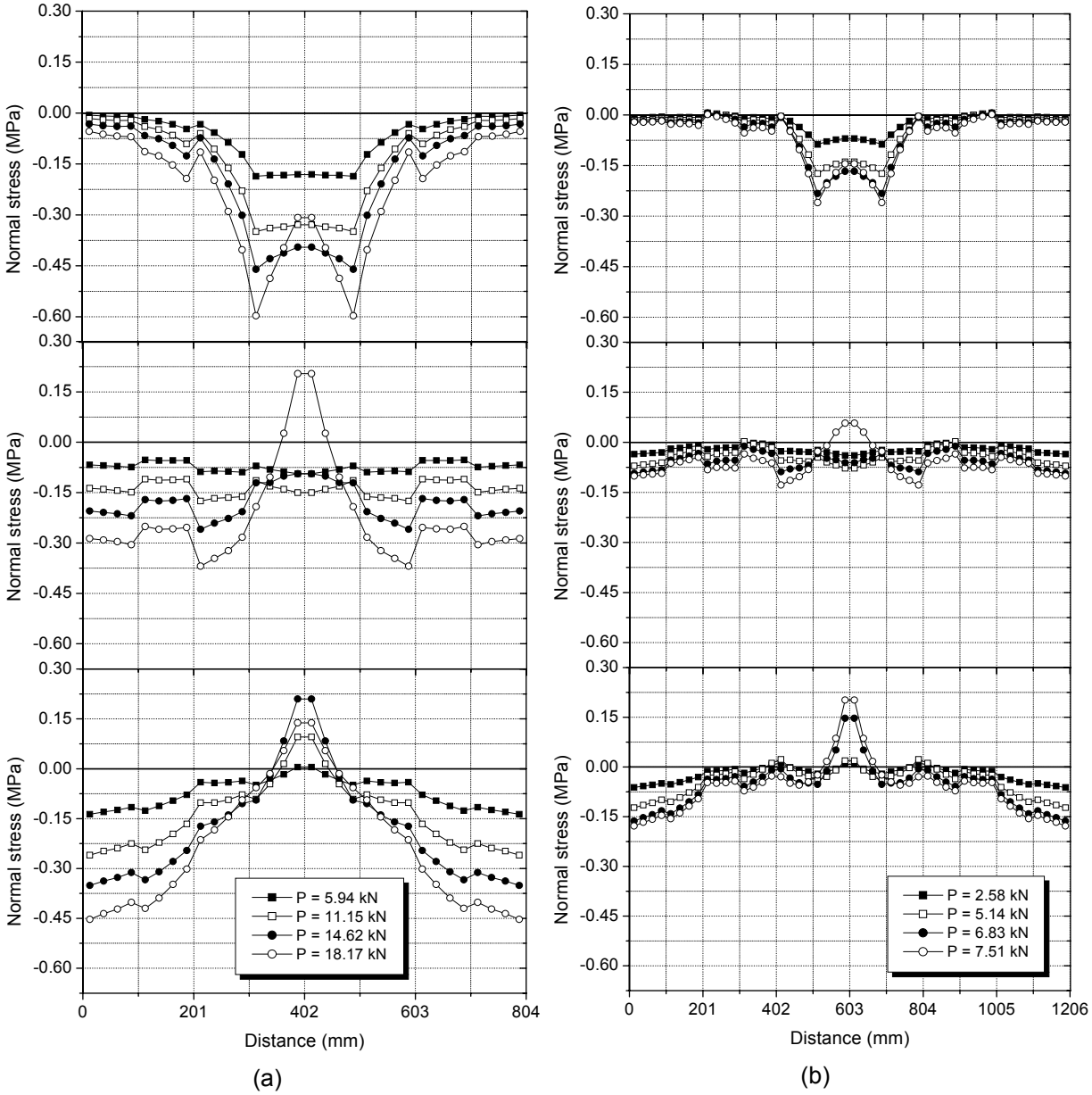

Figure 6.52 – Normal stress in bed joints of simply supported beams with filling of vertical joints: (a) L/H=1.52 and (b) L/H=2.54.

In case of masonry beams with filled vertical joints, the distribution of stresses is much smoother, without the inversion of the stress sign. Only two smoother stress peaks are identified in the region of the load application being dissipated in lower bed joints, as in case of beam without filling in vertical joints.

Contrarily to the shear walls the filling of vertical joints had a great influence on the behaviour of masonry walls leading to the preponderance of flexure. This is the result of the enhancement of the compressive strength in the parallel direction to bed joints, which consists of the primary direction for the development of normal stresses. Thus, it can be concluded that the filling of vertical joints on masonry beams improves behaviour of them under flexure due to improvement of the compressive strength of masonry material.

As in case of masonry beams with unfilled vertical joints, normal stresses in bed joints are influenced by the variation of the height and the span length. However, the level of stresses is much lower reaching values of approximately 16% of the normal stresses in bed joints of the masonry beams with unfilled vertical joints, which confirms the better distribution of stresses provided by the filling of vertical joints, see Figure 6.53.

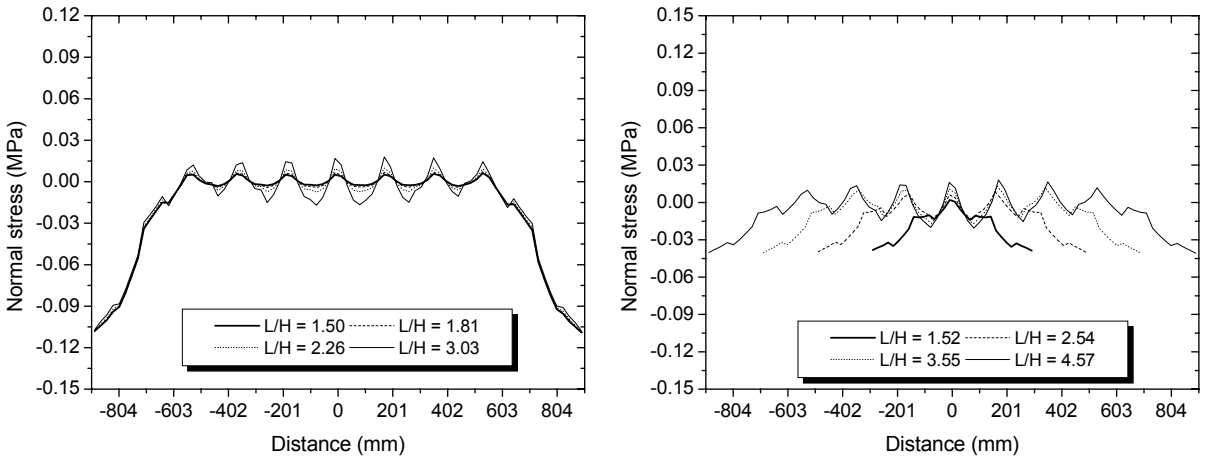

Figure 6.53 – Distribution of normal stresses at first bed joint of simply supported beams with filled vertical joints in the same level of loading: (a) variation of height (P= 5kN) and (b) variation of span (P=2kN).

The distribution of normal stresses along the height of vertical joints is very similar to that observed in masonry beams with unfilled vertical joints, even if their value is much higher due to the increasing of the masonry beam capacity, see Figure 6.54a. Distribution of shear stresses in first steps of loading are also very similar to that observed in masonry beams with unfilled vertical joints, see Figure 6.54b. However, in the maximum load resisted by the beam, the peak of shear stresses did not occur in middle of beam probably because these specimen failed by flexure and they did not reached the maximum shear capacity.

Some discontinuities can be observed in normal and shear stresses along the height of beam in the ultimate load promoted by the sliding of courses due to the high compressive stresses.

It is observed that the filling of vertical joints results on the significant enhancement of the load capacity of the masonry beams for both boundary conditions see Figure 6.55. Simply supported beams exhibited increases on the flexural capacity up to 60%, whereas the fixed end masonry beams the increase on the capacity was up to 200%, see Figure 6.55. As observed in shear walls, the filling of vertical joints had a higher influence on the elements where of shear resisting mechanism predominates.

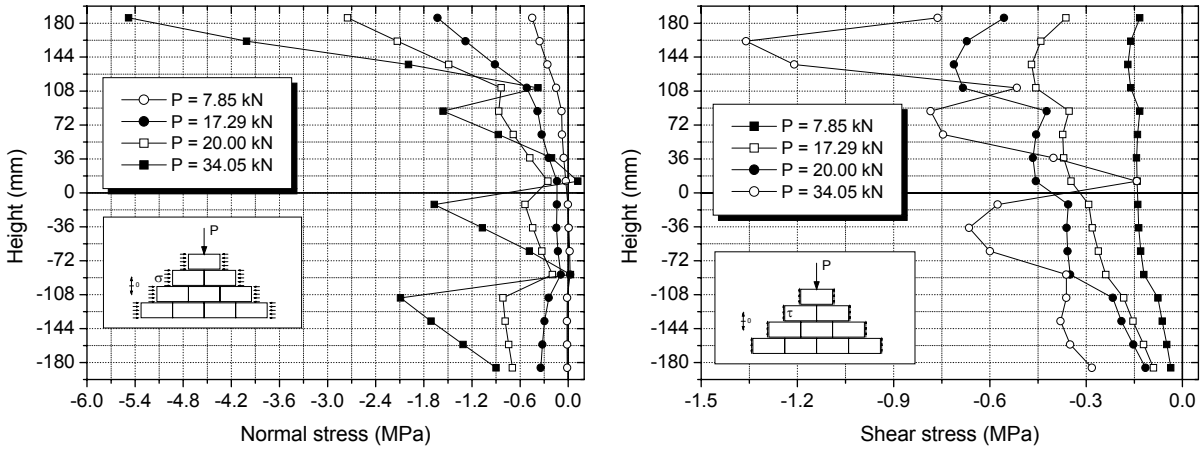

(a) (b)

Figure 6.54 – Stresses in vertical joints of the diagonal crack of fixed end masonry beam (L/H = 4.06): (a) normal stresses and (b) shear stresses.

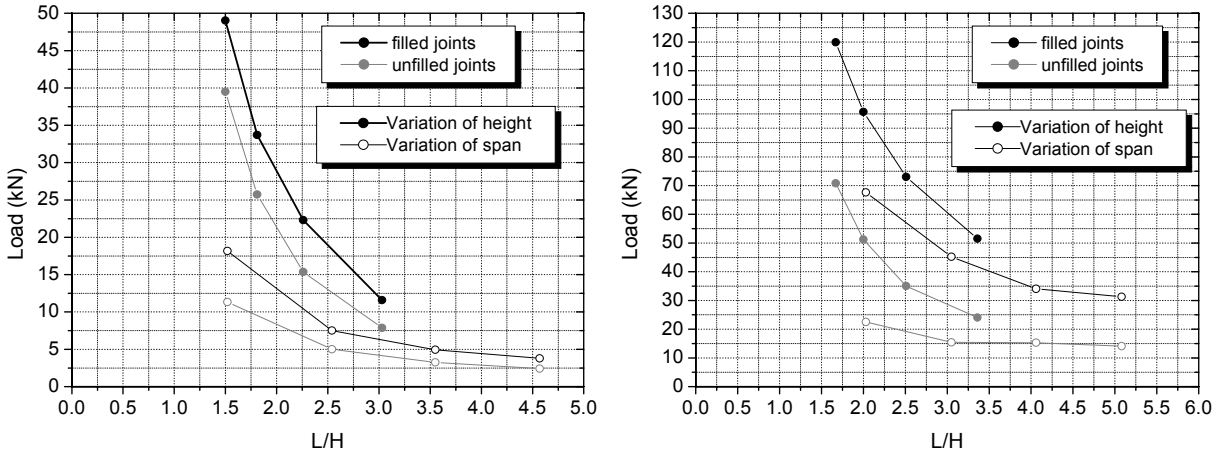

(a) (b)

Figure 6.55 – Variation of load capacity in beams with filled vertical joints in relation to the span to height ratio and comparison with beams with unfilled vertical joints: (a) simply supported beams and (b) fixed end beams.

6.4.2.3 Horizontal reinforcement

The influence of horizontal reinforcements on the flexural and shear behaviour of masonry beams was analysed by considering distinct arrangement of bed joint reinforcements for both boundary conditions. Two distinct arrangements of reinforcements were considered: (i) reinforcements uniformly distributed bars along the height; (ii) reinforcements concentrated in first bed joint. Three horizontal reinforcement ratios, ρ_h, were considered: 0.10%, 0.20% and 0.30%. Only horizontal reinforcement ratio equal to 0.10% was considered in masonry beams with reinforcements concentrated in the first bed joint. Results can be seen in Table 6.11.

Table 6.11 – Ultimate load and failure modes of masonry beams with bed joint reinforcement.

Boundary condition	Variation of	H/L	ρ_h				
			0.00%	0.10%	0.20%	0.30%	0.10% concentrated
Simply supported	height	1.50	39.49 (FL)	65.23 (SH)	70.33 (SH)	71.00 (SH)	70.26 (SH)
		1.81	25.74 (FL)	42.38 (SH)	46.94 (SH)	50.22 (SH)	49.49 (SH)
		2.26	15.36 (FL)	30.98 (SH)	31.27 (SH)	33.31 (SH)	33.34 (SH)
		3.03	7.87 (FL)	18.37 (FL)	21.01 (SH)	21.22 (SH)	18.24 (SH)
	span	1.52	11.33 (FL)	33.29 (FL)	35.38 (SH)	37.29 (SH)	34.95 (SH)
		2.54	5.01 (FL)	16.45 (FL)	17.04 (SH)	18.24 (SH)	11.86 (SH)
		3.55	3.25 (FL)	10.36 (FL)	11.31 (SH)	11.44 (SH)	10.74 (SH)
		4.57	2.42 (FL)	8.37 (FL)	9.48 (SH)	10.32 (SH)	9.68 (SH)
Fixed end	height	1.67	70.81 (SH)	79.14 (SH)	79.99 (SH)	80.69 (SH)	72.03 (SH)
		2.00	51.23 (SH)	58.45 (SH)	59.04 (SH)	59.40 (SH)	50.70 (SH)
		2.51	35.03 (SH)	42.45 (SH)	40.65 (SH)	43.61 (SH)	34.65 (SH)
		3.36	24.07 (SH)	28.05 (SH)	27.19 (SH)	28.30 (SH)	20.65 (SH)
	span	2.03	22.52 (SH)	43.87 (SH)	45.60 (SH)	46.61 (SH)	36.81 (SH)
		3.05	15.42 (SH)	16.60 (SH)	16.19 (SH)	15.98 (SH)	12.53 (SH)
		4.06	15.29 (SH)	15.05 (SH)	14.99 (SH)	15.00 (SH)	12.48 (SH)
		5.08	14.11 (SH)	14.06 (SH)	13.95 (SH)	13.98 (SH)	12.03 (SH)

The variation of the load capacity of simply supported and fixed end masonry beams for different height to span length ratio is displayed in Figure 6.56 and Figure 6.57. As expected, flexural capacity was improved by the application of horizontal reinforcements since they provide the increase of tensile strength of masonry beam, avoiding their premature and brittle failure.

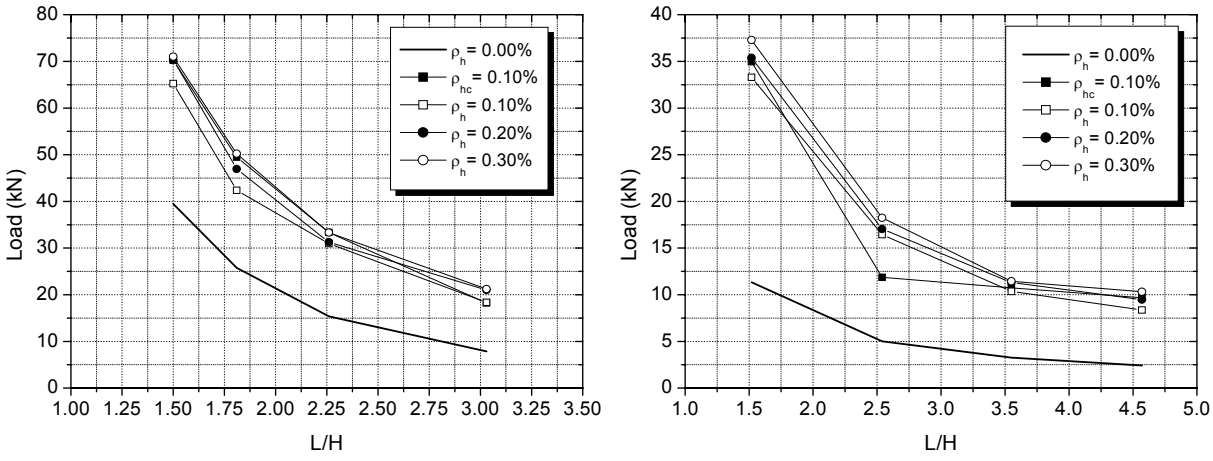

(a) (b)

Figure 6.56 – Variation of load capacity of simply supported beams with variation of horizontal reinforcement ratio: (a) variation of H in L/H ratio and (b) variation of L in L/H ratio.

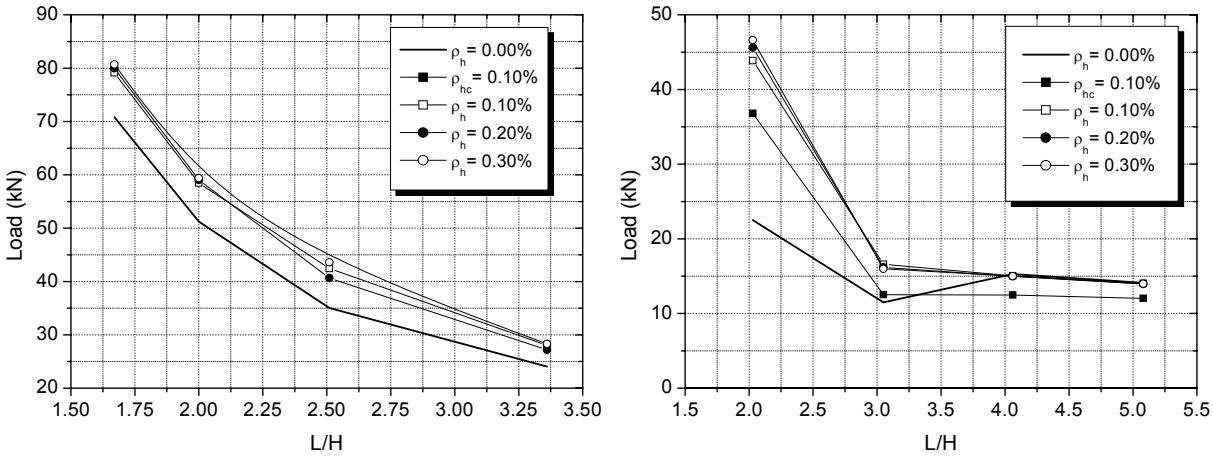

(a) (b)

Figure 6.57 – Variation of load capacity of fixed end beams with variation of horizontal reinforcement ratio: (a) variation of H in L/H ratio and (b) variation of L in L/H ratio.

Simply supported masonry beams with horizontal reinforcement concentrated at the first bed joint exhibited higher flexural strength, as expected, since the contribution to increase tensile strength is higher due to the higher reinforcement area with higher lever arm. However, the improvement of flexural strength is not very significant if a comparison with the

ultimate load obtained in masonry beams with the same reinforcement ratio but distributed along the height of the beam. On the other hand, the horizontal reinforcement changed the failure mode of the majority of specimens from flexure (FL) to shear (SH). Exceptions to this trend are beams with span to height ratios equal to 1.52, 2.54, 3.05, 3.55 and 4.57, corresponding to specimens with height kept constant and span length variable, when the reinforcement ratio is 0.10%. These beams failed by flexure due to yield of the reinforcement positioned at first bed joint.

In general, load capacity of beams was clearly improved by the introduction of horizontal reinforcements, but the variation of horizontal reinforcement ratio seemed not to influence the strength of masonry beams. The increase of the load capacity was more remarkable in simply supported beams, achieving in average 50% higher values than unreinforced masonry beams, probably due to change of the failure mode. In case of fixed end beams, shear failure mode with diagonal cracking is maintained and an increase on the load capacity of 15% is attained.

In case of fixed end masonry beams, whose predominant shear behaviour is shear diagonal cracking, it should be noticed that the concentration of bed joint reinforcement at first course appears to be harmful. This means that the concentration of bed joint reinforcement should be avoided. As seen in Figure 6.58, the concentrated reinforcement at the first curse is not effective on the distribution of cracking, even if it avoids flexural cracking at bottom edge of the beam. A more distributed crack pattern is only achieved through the distribution of reinforcement along the height of the beam. The increase on the reinforcement ratio improves also the cracking distribution.

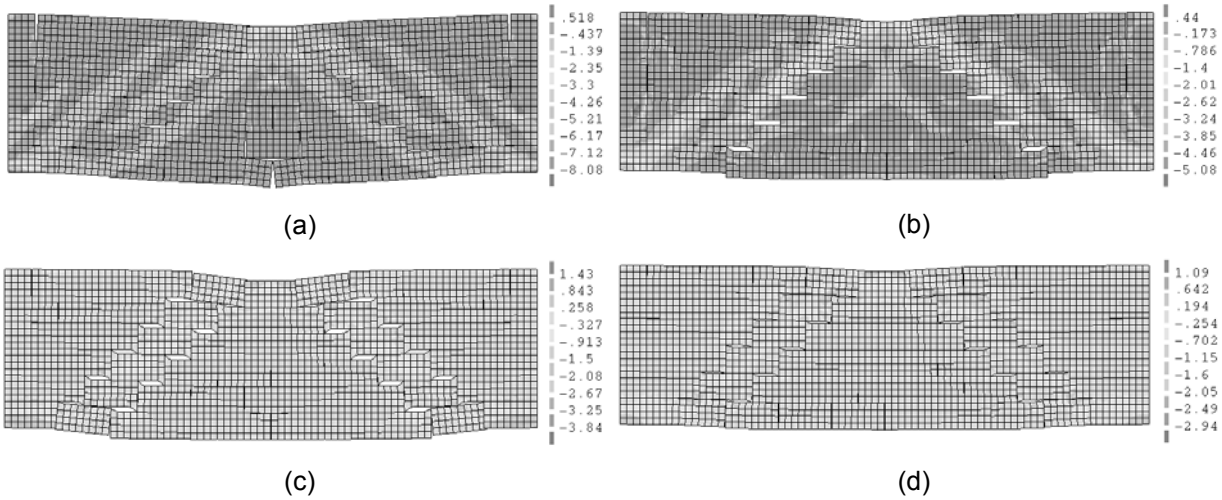

Figure 6.58 – Deformed mesh with indication of cracking patterns and principal stresses in reinforced fixed end masonry beams with L/H = 3.36: (a) ρ_h = 0.00%, (b) ρ_h = 0.10% concentrated, (c) ρ_h = 0.10% and (d) ρ_h = 0.30%.

From the distribution of normal and shear stresses along DCL for the same load level it can be concluded that the introduction of horizontal reinforcements reduces the level of stresses in DCL independent on the boundary condition, see Figure 6.59 and Figure 6.60.

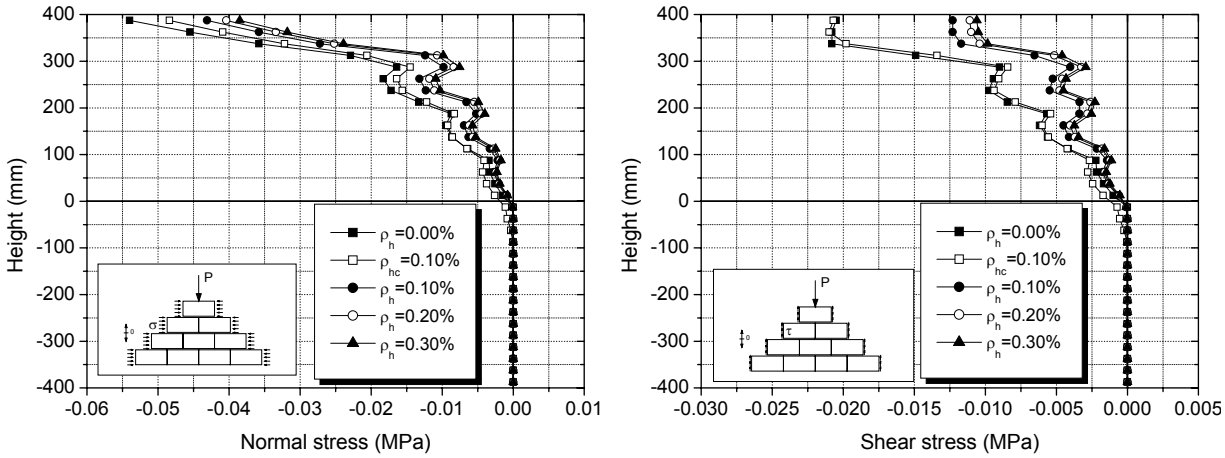

(a) (b)

Figure 6.59 – Variation of stresses in vertical joints along DCL of simply supported beam (L/H = 2.26) for distinct reinforcement ratios (P= 5kN): (a) normal stresses and (b) shear stresses.

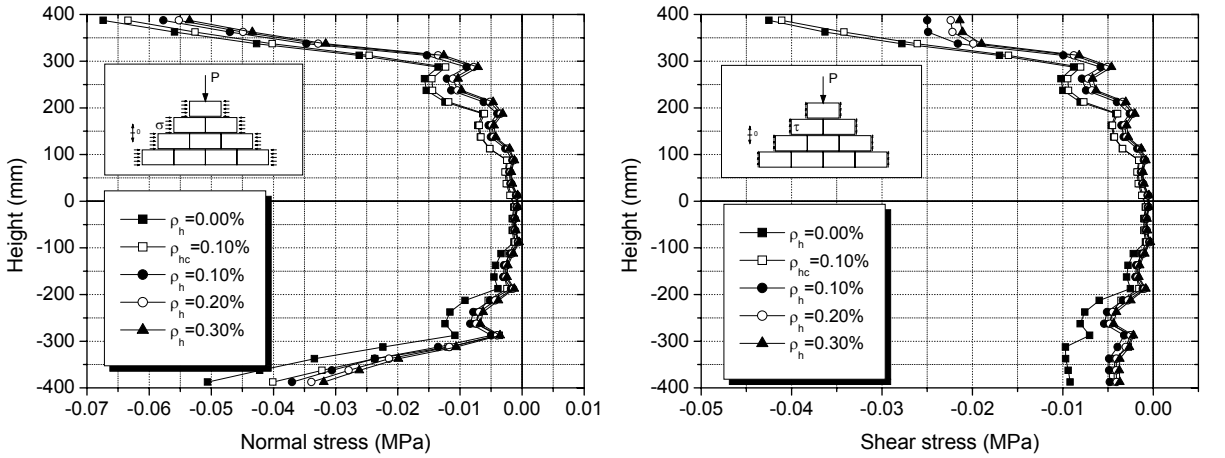

(a) (b)

Figure 6.60 – Variation of stresses in vertical joints along DCL of fixed end beam (L/H = 2.51) for distinct reinforcement ratios (P= 10kN): (a) normal stresses and (b) shear stresses.

The lowering of the stresses along the DCL is the result of the stress transfer between the masonry to reinforcements. The reduction of normal and shear stresses is related to the arrangement of the steel bars along the height of the masonry beam. The shear stress distribution profile shows that the level of stresses in unreinforced and reinforced masonry beams with concentration of bed joint reinforcement at first course is practically coincident. This behavior confirms that the concentrated reinforcement is not

effective on the redistribution of shear stresses between masonry and reinforcement, meaning that horizontal reinforcements did not provided increase in shear capacity of masonry beams.

6.4.2.4 Vertical and horizontal reinforcement

In order to evaluate the influence of vertical reinforcements on the mechanical behaviour of masonry beams, a constant horizontal reinforcement ratio of 0.20% was considered, being adopted three vertical reinforcement ratios, namely 0.05%, 0.15% and 0.25%. Two different spacing were considered for vertical reinforcement ratio of 0.05%, namely 200mm and 300mm, whereas only the spacing of 200mm was taken for the other reinforcement ratios. In this analysis the same geometry, loading and boundary conditions of the previously studies were used. Results can be seen in Table 6.12.

Table 6.12 – Ultimate load of masonry beams horizontally and vertically reinforced in numerical modelling.

Boundary condition	Variation of	H/L	ρ_v				
			0.00%	0.05%	0.15%	0.25%	0.05% s=300mm
Simply supported	height	1.50	70.33	120.50	121.50	120.30	132.20
		1.81	46.94	103.90	107.00	106.80	99.58
		2.26	31.27	75.24	80.17	80.86	70.09
		3.03	21.01	43.51	45.92	46.15	44.84
	span	1.52	35.38	58.45	58.90	59.62	56.08
		2.54	17.04	33.28	33.45	34.11	34.86
		3.55	11.31	23.05	24.04	24.32	22.23
		4.57	9.48	17.73	18.18	17.99	17.77
Fixed end	height	1.67	79.99	125.80	125.60	124.70	137.20
		2.00	59.04	123.80	123.90	122.65	113.10
		2.51	40.65	97.99	116.80	116.40	82.91
		3.36	27.19	66.05	81.33	82.65	57.45
	span	2.03	45.60	49.95	59.98	59.50	60.45
		3.05	16.19	45.63	55.35	56.86	45.63
		4.06	14.99	37.69	46.43	49.43	32.01
		5.08	13.95	34.63	43.51	46.00	30.55

From the analysis of results, relating the ultimate load found for the beams with different geometries, boundary conditions and for distinct reinforcement ratios, it can be

concluded that the use of vertical reinforcement results in a considerable additional resistance. Besides, vertical reinforcements control the opening of diagonal cracking.

In case of simply supported beams, all specimens had their strength limited by the crushing of masonry at mid span upper edge, which explains the non variation of the ultimate loads by increasing the vertical reinforcement ratio. On the other hand, in case of fixed end masonry beams, the variation of vertical reinforcement led to the increasing of beam capacity in case of resisting mechanism is controlled by shear.

Simply supported beams with large span length to height ratios such as the beam with L/H = 4.57 reached the crushing of masonry before the yield of reinforcements. Decreasing the span to height ratio, the strength of beams increased and the crushing takes place after the yielding of reinforcements, In fact, with the increase of the applied vertical load some vertical reinforcements reached the yield stress becoming the beam more deformable enabling the yielding of horizontal reinforcements, contributing to the increase of the ultimate load.

As previously mentioned, in fixed end beams shear behaviour is preponderant. Thus; the failure mode of these masonry beams was quite different. All specimens failed by masonry crushing on upper edge at middle span. However, before achieving this limit state all vertical reinforcement reached the yield stress. As in case of simply supported beams, the yield of vertical reinforcements became the beam more deformable leading to the yielding of horizontal reinforcements and finally to crushing of masonry. Therefore, the increase of vertical reinforcement ratio delayed the crushing of masonry and improved the behaviour of beam.

Variation in spacing of vertical reinforcements did not influence the behaviour of simply supported masonry beams. On the other hand, in case of fixed end specimens, higher spacing in general seemed to reduce the strength of beams. This behaviour occurred possibly due to fact that lower spacing represents higher capacity of control the opening of diagonal cracks, see Figure 6.61.

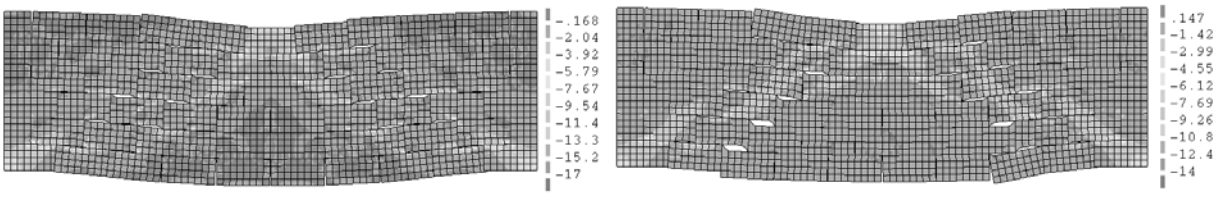

(a) (b)

Figure 6.61 – Deformed mesh with the representation of the principal stresses after the application of a displacement equal to 3.00 mm in a fixed end beam with L/H = 3.36: (a) spacing equal to 200 mm and (b) spacing equal to 300 mm.

In order to evaluate the influence of horizontal reinforcements on the mechanical behaviour of masonry beams, a constant vertical reinforcement ratio of 0.05% was considered, being adopted three horizontal reinforcement ratios, namely 0.10%, 0.20%, 0.30% and 0.10% concentrated in the first bed joint. A spacing of 200 mm was considered for vertical reinforcements. In this analysis the same geometry, loading and boundary conditions of the previously studies were used. Results can be seen in Table 6.13.

Table 6.13 – Ultimate load of masonry beams horizontally and vertically reinforced in numerical modelling with variation of horizontal reinforcement ratio.

Boundary condition	Variation of	H/L	ρ_h			
			0.10%	0.20%	0.30%	0.10% concentrated
Simply supported	height	1.50	105.20	120.50	123.40	108.90
		1.81	77.13	103.90	112.70	89.52
		2.26	52.10	75.24	82.13	65.88
		3.03	27.83	43.51	52.42	46.82
	span	1.52	42.11	58.45	65.91	51.47
		2.54	22.56	33.28	40.20	34.60
		3.55	15.17	23.05	28.64	24.26
		4.57	11.26	17.73	22.13	18.38
Fixed end	height	1.67	123.50	125.80	126.50	118.90
		2.00	121.10	123.80	125.40	113.90
		2.51	101.90	97.99	96.36	93.46
		3.36	69.51	66.05	63.35	62.95
	span	2.03	49.95	49.95	49.95	49.95
		3.05	45.44	45.63	46.79	46.20
		4.06	40.35	37.69	38.38	39.17
		5.08	37.54	34.63	33.79	33.19

As expected, the variation of horizontal reinforcement ratio increase the flexural strength of simply supported masonry beams since tensile stresses generated by the loading can be resisted by the reinforcements. On the other hand, as in case of vertical reinforcements for shear walls, the variation of horizontal reinforcement ratio did not cause any change on the behaviour of fixed end masonry beams. The behaviour of these beams is governed by shear; so, the horizontal reinforcements seem not increase the shear strength of masonry beams.

6.5 Summary and conclusions

For the numerical simulation of masonry walls under in-plane lateral load and of masonry beams under flexure and shear micro-modelling approach was selected due to the need of understanding in detail the resisting mechanisms of masonry walls and beams. The mechanical properties of materials used in the model were obtained from experimental tests, even if few of them had to be obtained by fitting the numerical and the experimental results. In a first phase the numerical model has been calibrated based on the experimental results of masonry walls and beams. Very reasonable agreement was found between the numerical force-displacement diagrams and the monotonic experimental envelop describing the in-plane behaviour of masonry walls and beams. In a second phase, an extensive parametric study has been performed aiming at evaluating the influence of the aspect ratio, vertical pre-compression, filling of vertical joints, horizontal and vertical reinforcement ratio on the in-plane behaviour of masonry walls. The parameters selected for the parametric study relating masonry beams included the span to height ratio, the filling of vertical joints and the variation of the horizontal and vertical reinforcement ratio.

Concerning the results of numerical modelling of masonry walls the following conclusions can be drawn:

(a) A failure surface defined based on the pre-compression and aspect ratio has been found indicating that walls with low aspect ratio and moderate pre-compression levels are more favourable to develop shear failure, whereas walls with high aspect ratios and low pre-compression levels are more favourable to develop flexure failure. On the other hand, it was observed that in cantilever walls flexure is preponderant, whereas in fixed end walls shear failure prevails on the in-plane response of the masonry walls.

(b) the influence of vertical reinforcements depends on the predominant resisting mechanism. They exhibited a small influence on the lateral resistance of walls when shear is the preponderant effect but they provide an enhancement on lateral strength when flexural govern the behaviour of the walls since they resist tensile stresses due to the uplift of the wall.

(c) in case of horizontal reinforcement, its influence on the behaviour of shear walls depends on the preponderance of the resisting shear mechanisms. It was observed that horizontal reinforcements act only after the diagonal cracking as observed in experiments. Besides, horizontal reinforcements provided a better distribution of stresses in the walls leading to a more distributed diagonal cracking. It was noticed that it is very difficult to observe the influence of horizontal reinforcements on the lateral resistance of cantilever walls due to the preponderant flexure effect.

(d) the filling of vertical joints influences the lateral resistance in case on shear resisting mechanism prevails. as regards the filling of vertical joints, it was seen that in cantilever walls a maximum increase of 10 % on the lateral resistance was achieved, whereas in fixed end masonry walls the increase reached a maximum of 20%.

The parametric study carried out on masonry beams revealed that:

(a) the usage of filled vertical joints increased the shear strength of masonry beams, particularly in case of shear resisting mechanisms control the ultimate load. The increase on the flexural strength is attributed to the higher compressive strength of masonry in the parallel direction when compared the compressive resistance in dry masonry. Besides, it was clear that the filling of vertical joints provide a better distribution of stresses becoming the masonry a more homogeneous material.

(b) horizontal reinforcements in masonry beams can be compared with vertical reinforcements in shear walls because they are longitudinal bars in relation to the applied efforts. Horizontal reinforcement increased the flexural strength of masonry beams, since resist the tensile stresses. Besides, the horizontal reinforcements increased shear strength of masonry beams relatively to unreinforced beams due to the prevention of sliding and thus of the progress of diagonal cracking. However, the variation on reinforcement ratio has no influence on the shear resistance of masonry beams.

(c) the introduction of vertical reinforcements improved the shear resistance of masonry beams. The vertical reinforcements control the crack opening and generated a change on the failure mode of beams leading flexure failure by crushing of masonry. As in case of shear walls, the combination of horizontal and vertical reinforcements reveal to enhance the flexural and shear behaviour of masonry beams.

7 DEVELOPMENT OF A NEW ANALYTICAL DESING METHOD

7.1 Introduction

Masonry structures subjected to in-plane lateral loads are basically designed to resist flexural and shear efforts. Flexural behaviour is well understood and the existent design methods give reliable previsions for the maximum flexural capacity of structures. Flexural design of masonry structures follows the same methodology used for concrete structures. On the other hand, shear behaviour is more complex and it is not still very well explained. In case of masonry structures, mortar joints generate weakness planes and concentrate the majority of nonlinear behavior of masonry.

In general, design methods evaluate the shear behaviour separately from flexure behavior. However, it is clear that both mechanisms occur simultaneously and interact for the different levels of horizontal loading. For example, shear strength depends on the level of normal stresses, which are directly related to the flexure of the wall.

Thus, based on the results of in-plane experimental tests carried out on shear walls and masonry beams and on the parametric study carried out through the finite element modelling presented in Chapter 6, a design method is proposed by considering the coupling between flexure and shear behavior. The design method proposed in this research uses an iterative method to calculate the maximum lateral capacity of masonry elements subjected to in-plane loading and may be considered as an improvement of the design model proposed by Brunner and Shing (1996). The design methodology is systematized in a Windows® application and practical examples are presented to clarify the use of the software.

7.2 General assumptions about the behaviour of masonry structural elements subjected to in-plane loading

Experimental and parametric numerical analysis provided relevant information on the resisting mechanisms developed in masonry walls and beams subjected to in-plane loading. Apart from the arrangement of masonry units in relation to normal stresses, shear walls and masonry beams develop similar flexural and shear resisting mechanisms. In shear walls, flexure leads to flexural cracking predominantly at bed joints and compressive stresses perpendicular to the bed joints. On the other hand in case of masonry beams, flexural efforts lead to compressive stresses in the parallel direction to bed joints and the flexural cracking occurs mainly at the vertical joints due the horizontal tensile stresses. For example, a simply supported beam can be simplified by symmetry through a half of beam with a support A which restricts displacements and a support B which restrict displacements in direction of the axis of beam and rotations and with half of loading applied over the support B as showed in Figure 7.1. The applied loading generates a reaction force of equal value in support A. This structural scheme is equivalent to the scheme of a shear wall since the reaction in support A can be admitted as the loading and the loading as the reaction force. The same analogy can be made between a fixed end wall and a fixed end beam with a load applied in the middle of beam.

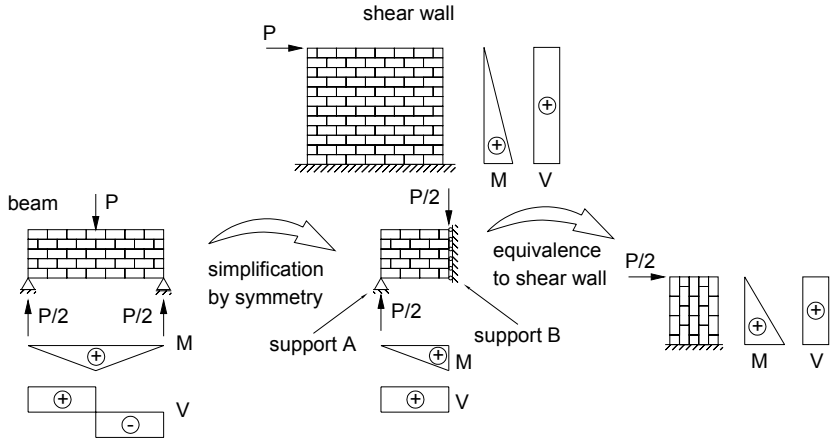

Figure 7.1 – Equivalence between shear walls and masonry beams subjected to a concentrated load.

In general, concentrated loads are not common in masonry beams in a real building. In this case, masonry beams are partially restricted at the extremities where moments and shear forces act as a result of rotations and displacements caused by lateral loading. The same analogy with shear walls can be performed in this configuration of masonry beams.

However, the whole length of beam should be considered instead of the half of beam as in previous case, see Figure 7.2.

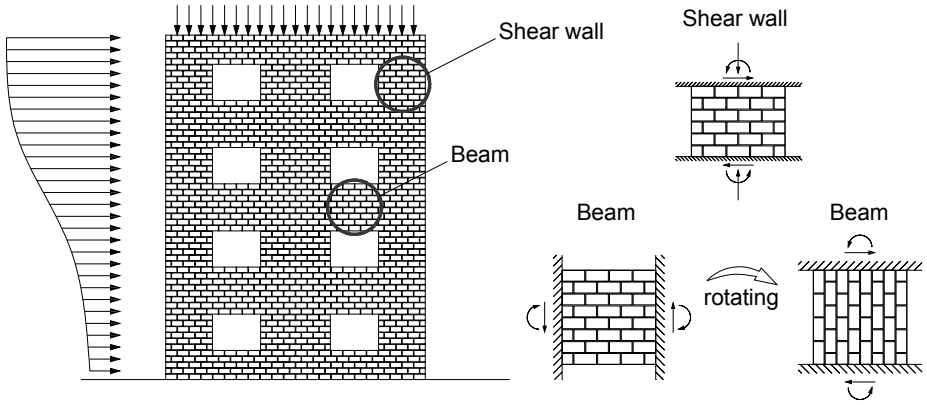

Figure 7.2 – Equivalence between shear walls and masonry beams in real buildings

As seen in Chapter 6 from the parametric analysis, the behaviour of masonry elements under in-plane loading depends on the boundary conditions. As seen from Figure 7.3, the deformation patterns are quite different, leading to the distinct preponderance of flexure or shear effects. In cantilever walls, the lateral load leads to generation of a diagonal flow of compressive stresses from the load application point up to the opposite bottom corner. The concentration of compressive stresses at bottom corners results in most cases in the crushing of this region. Diagonal tensile cracks can occur in the alignment of the compressive strut associated to the tensile stresses developed in the perpendicular direction. Flexure can leads to horizontal cracks mainly at the bed joints associated to the tensile stresses and to uplift of the base of the wall, which can be prevented or minimized by the introduction of vertical reinforcements. Fixed end walls present also the diagonal flow of compressive stresses, but here the stresses concentration can occur at the top and bottom corners of the wall, resulting in the possible crushing. However, it should be mentioned that the level of concentration of compressive stress at the corners reach a lower level than in case of cantilever walls. On the other hand, this configuration of stresses results in more common diagonal tensile cracks, meaning that for this boundary condition the shear behaviour is more predominant. For fixed end walls tensile stresses due to flexure can also occur leading to horizontal cracking, even if this crack patterns is much rarer than in case of cantilever walls, see Figure 7.3b.

Apart the normal stresses direction, the same configuration of stresses can be observed in masonry beams and shear walls. Simply supported beams can be compared with cantilever walls whereas fixed end beams can be compared with fixed end walls.

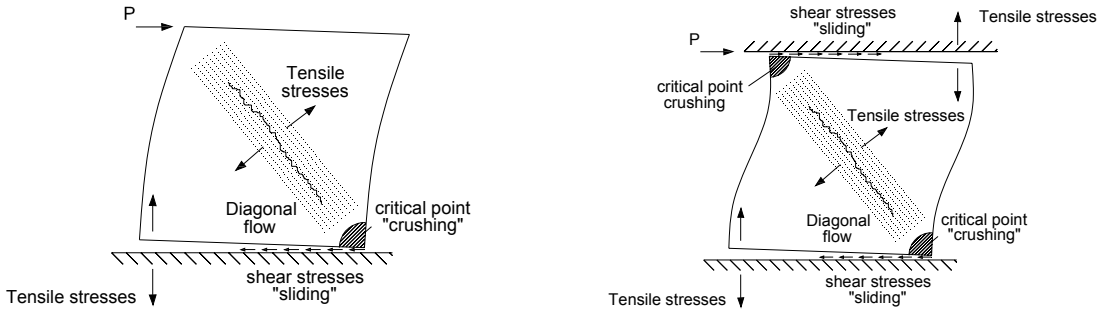

Figure 7.3 – Possible crack patterns due to in-plane horizontal loading (a) cantilever shear walls and (b) fixed-fixed end shear walls.

In simply supported beams under the four point load configuration point, as defined in experimental program and numerical analysis, the vertical loading leads to a diagonal flow of compressive stresses connecting the supports to the load application points, see Figure 7.4a. Tensile stresses appear transversally to the diagonal flow of compressive stresses and at the mid span of bottom edge resulting in diagonal and vertical cracking. In case of fixed end beams, tensile cracks can develop at mid span of the beams and at the interface between the beams and the supports at the upper region due to the flexure and diagonal tensile cracks develop along the diagonal flow of compressive stresses, see Figure 7.4b. For both boundary conditions the compressive crushing occurs at the upper edge of the beams and in case of fixed end, the beams present also crushing at the bottom corners. It is seen also that the diagonal cracks follows predominantly the horizontal and vertical joints but can pass through the concrete units. The onset of flexural cracks take place at the vertical joint from the bottom edge but their progress up to the upper edge encompasses also the bed joints.

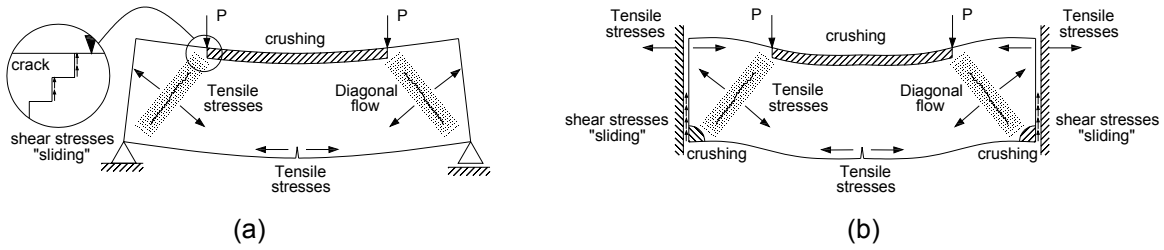

Figure 7.4 – Possible crack patterns in masonry beams: (a) simply supported and (b) fixed end.

It is seen that either in shear walls or masonry beams, flexural and shear resisting mechanisms characterizes their global resistance under in-plane loading. Besides the boundary conditions, the behaviour of structural masonry elements subjected to in-plane loading depends on the pre-compression level, aspect ratio and on the presence of vertical and horizontal reinforcement (Chapter 6). Different combinations of these variables lead to

distinct failure modes of the masonry elements. In general terms, the failure modes developed in the masonry structural elements can be classified as follows:

1. failure by flexure;
    a. Flexural cracking;
    b. Yielding of longitudinal reinforcements;
    c. Crushing of masonry;
2. failure by shear;
    a. Diagonal cracking;
    b. Yielding of transversal reinforcements;
    c. Sliding.
3. Mixed flexure-shear failure mode;

The flexural failure mode prevails in case of low compression load levels and for high aspect ratios. Flexural cracking is a failure mode only by unreinforced elements and develops when tensile stresses due to flexure reach the tensile bond strength of unit-mortar interface. In addition, if the masonry element is reinforced with longitudinal bars, the opening of the flexural cracking is minimized or prevented due the contribution of reinforcement to resist the tensile stresses. The increase of lateral loading can promote the yielding of vertical reinforcements or crushing of masonry, which represent other two possible flexural type failure modes.

As shown in Figure 7.3 and Figure 7.4, diagonal flow of compressive stresses appears in masonry elements subjected to in-plane loading and consequently tensile stresses develop in the perpendicular direction to the diagonal flow. When the tensile stresses reach the tensile strength of masonry, diagonal cracks open and the masonry element can fail by diagonal cracking if no transversal reinforcement exists. In fact, tensile diagonal cracking is considered to promote the brittle collapse of unreinforced masonry elements. If the masonry element has transversal reinforcements, the shear failure is much more ductile and can occur by yielding of the transversal reinforcements. In fact, the shear reinforcement aims at promoting the load transfer between the edges of the diagonal crack, contributing to the resisting load by the development of tensile stresses. The shear sliding failure over the diagonal crack can occur when deficient anchorage length of transversal reinforcements. In case of walls, the shear sliding failure can develop along a horizontal bed joint, mostly positioned at the base of the wall.

Masonry elements subjected to in-plane loading can also fail by mixed flexure-shear mode. This mixed failure happens when both flexural and shear resisting mechanism contribute to the final resistance of the masonry element. The typical shear-flexure failure mode is characterized in a first phase by diagonal cracking due to the tensile stresses

perpendicular to the diagonal flow of compressive stresses. Due to the presence of transversal reinforcement, the failure by diagonal cracking is prevented and the increase on the lateral load lead to the yielding of longitudinal reinforcements or to the crushing of masonry due to high compressive stresses. The mixed failure mode can also occur in unreinforced elements after diagonal cracking and further stress concentration at the bottom corners resulting in the crushing of masonry. In this case, the load limits for each failure mode are very close.

7.3 Design methodology

Flexure and shear resisting mechanisms are usually considered separately in design. However, flexural and shear efforts occur simultaneously leading often to the simultaneous development of flexural and shear resisting mechanism. Sometimes it is very difficult to define the failure mode during experimental tests. Shear is function of normal stresses and distribution of normal stresses depends on flexure.

Besides, the shear resistance depends on the effective cross section of the structural element, which is a function of the tensile and compressive stresses developed due to flexural efforts. Thus, the main goal of the analysis of structural masonry under in-plane load presented in this work is the design of masonry cross sections taking into account the coupling between shear and flexural behavior. For the effect, an iterative design model considering the coupling of flexure and shear has been developed following the general flow chart given in Figure 7.5.

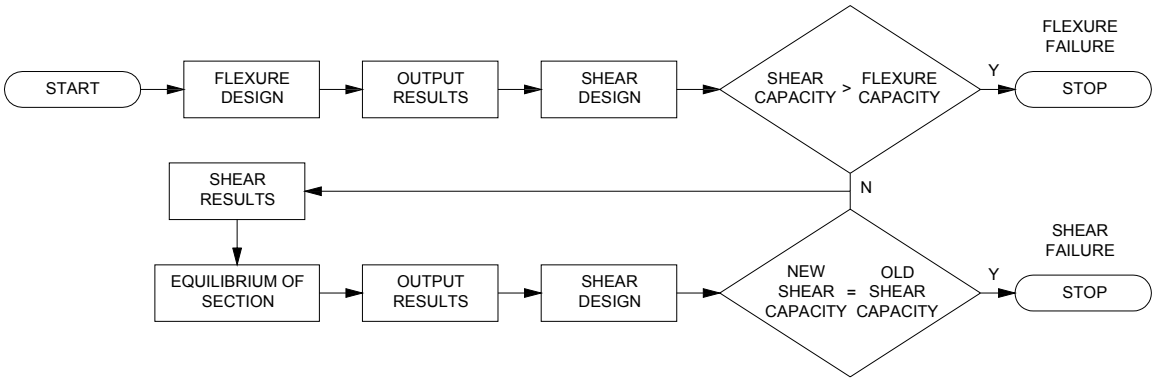

Figure 7.5 – Simplified flow chart of design model considering coupling of flexure and shear.

The shear resistance of a masonry element is calculated after the flexural strength of masonry elements is obtained based on the classical design approach used in reinforced concrete sections. If the shear resistance is higher than the flexural resistance, then the

resistance of the structural masonry element is determined by the flexural resistance and flexural failure mode can be attributed to the collapse. If shear resistance is lower than flexural resistance, an iterative method should be applied. A loading which promotes a shear force equal to the previous calculated shear resistance should be applied and the masonry element section should be re-equilibrated. A new shear resistance is calculated using the output results of the section equilibrium and it is compared to the previous shear resistance. If both results are equal, the shear resistance of the masonry element was found. On the contrary, a new iteration should be carried out.

7.3.1 Flexural resisting mechanism

7.3.1.1 Unreinforced Masonry

Early flexural cracking develop frequently in masonry due to its low tensile bond strength. Flexural cracks develop mainly at bed joints in walls and at the vertical joints in case of beams reducing the effective section area of these elements. The flexural cracking load can be calculated considering the elastic behaviour of masonry element and taking into account the contribution of the tensile strength masonry, see Figure 7.6.

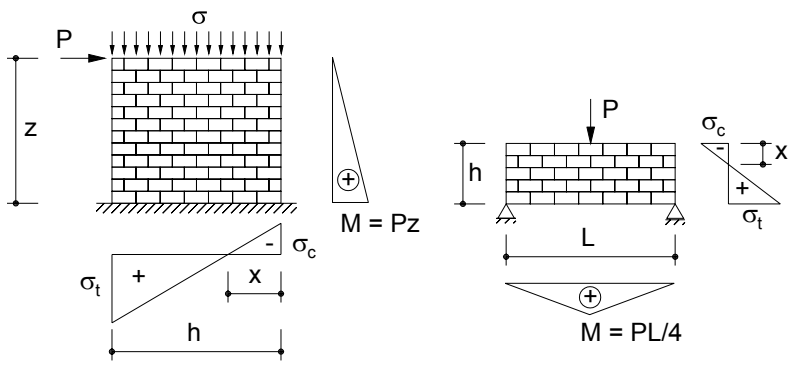

Figure 7.6 – Normal stresses distribution in masonry for the calculation of flexural cracking for unreinforced elements.

As seen in Chapter 4, the neutral axis can be derived from the equilibrium of forces (Eq. 7.1), the compatibility of strains (Eq. 7.3) and considering that tensile stresses (σ_t) reaches the tensile bond strength of masonry (f_{fl}), see Eq. 7.4.

$$\frac{\sigma_c xt}{2} = \sigma xt + \frac{\sigma_t xt}{2} \qquad \text{Eq. 7.1}$$

$$\sigma_c = E_m \varepsilon_m \text{ and } \sigma_t = E_m \varepsilon_t \quad \text{Eq. 7.2}$$

$$\frac{\varepsilon_m}{x} = \frac{\varepsilon_t}{h - x} \quad \text{Eq. 7.3}$$

$$x = \frac{(f_{fl} + 2\sigma)h}{(2f_{fl} + 2\sigma)} \quad \text{Eq. 7.4}$$

Where, x is position of neutral axis, t is the thickness of masonry element, E_m is the elastic modulus of masonry, ε_m and ε_t are the strains of compressed and tensioned masonry, f_{fl} is the tensile bond strength of masonry and σ is the pre-compression for shear walls. In case of masonry beams σ = 0.

The flexural cracking moment, M_{fc}, is obtained by taking the equilibrium of bending moments, see Eq. 4.15.

$$M_{fc} = \frac{f_{fl}}{3(h-x)}\left\{t\left[x^3 + (h-x)^3\right]\right\} + \sigma h t\left(\frac{h}{2} - x\right) \quad \text{Eq. 7.5}$$

7.3.1.2 Reinforced masonry

In case of masonry reinforced with longitudinal bars, the influence of reinforcements should be considered in the calculation of the flexural cracking moment. As in case of unreinforced elements, the loading that produces the flexural cracking can be calculated considering the elastic behaviour of the masonry element and taking into account the contribution of the tensioned masonry, see Figure 7.7.

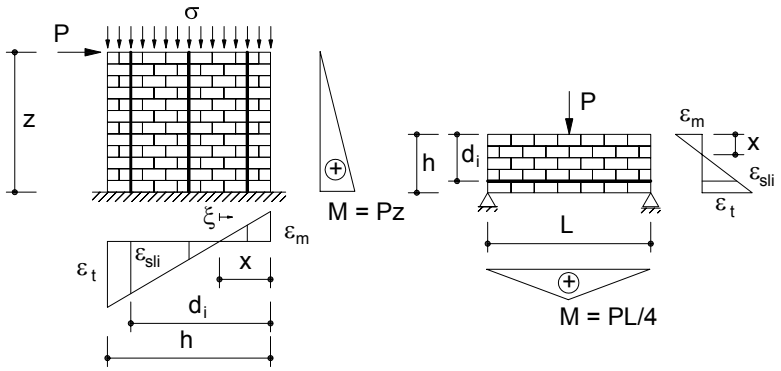

Figure 7.7 – Strain distribution in masonry and reinforcements in reinforced masonry elements.

A parcel is added to previous equations in order to consider the influence of longitudinal reinforcements, see Eq. 7.6 to Eq. 7.11.

$$\frac{\sigma_c xt}{2} = \sigma xt + \frac{\sigma_t xt}{2} + \Sigma \sigma_{sli} A_{sli} \quad \text{Eq. 7.6}$$

$$\sigma_c = E_m \varepsilon_m,\ \sigma_t = E_m \varepsilon_t \text{ and } \sigma_{sli} = E_s \varepsilon_{sli} \quad \text{Eq. 7.7}$$

$$\alpha_e = \frac{E_s}{E_m} \quad \text{Eq. 7.8}$$

$$\frac{\varepsilon_c}{x} = \frac{\varepsilon_t}{h-x} = \frac{\varepsilon_{sli}}{d_i - x} \quad \text{Eq. 7.9}$$

$$x = \frac{(f_{fl} + 2\sigma)th^2 + 2\alpha_e f_{fl} \sum_i A_{sli} d_i}{(2f_{fl} + 2\sigma)th + 2\alpha_e f_{fl} \sum_i A_{sli}} \quad \text{Eq. 7.10}$$

$$M_{fc} = \frac{f_{fl}}{3(h-x)} \left\{ t\left[x^3 + (h-x)^3\right] + 6\alpha_e \sum_i A_{sli}(d_i - x)^2 \right\} + \sigma ht\left(\frac{h}{2} - x\right) \quad \text{Eq. 7.11}$$

Where A_{sli} is the area of longitudinal reinforcements, E_s is the elastic modulus of reinforcements, σ_{sli} and ε_{sli} are the stress and strain of longitudinal reinforcements respectively.

In case of reinforced masonry, after the opening of flexural cracks, longitudinal steel bars begin to resist the tensile stresses increasing the flexural strength of the walls. When flexural behaviour governs the lateral behaviour of masonry walls, they can fail either by breaking of reinforcements or by crushing of the masonry. In this case the maximum capacity of the masonry element can be calculated by means of the classic flexural theory based on the plane-section assumption. The evaluation of masonry elements subjected to flexure shall be based on the following assumptions:

- the reinforcement is considered to be completely adherent to masonry leading that masonry and reinforcements have the same strain at the level of the reinforcements.
- the tensile strength of the masonry is taken to be zero;
- the tensile strain of the reinforcement should be limited by 0.01;
- the maximum compressive strain of the masonry is chosen according to compressive behaviour of masonry;
- the maximum tensile strain in the reinforcement depends on the material;
- the stress-strain relationship of masonry is taken to be linear, parabolic, parabolic rectangular or rectangular ($\lambda = 0.8x$);

- for cross-sections not fully in compression, the limiting compressive strain is taken to be not greater than ε_{mu} = -0.0035 or ε_{mu} = -0.002 depending on the geometry of units according to Eurocode 6 (2005).

The resistant moment (M_R) should be calculated considering the constitutive laws for masonry in compression (Eq. 7.12 and Eq. 7.13), compatibility of strains (Eq. 7.14), and equilibrium of forces and moments (Eq. 7.15 and Eq. 7.16 respectively).

$$\sigma_c = f(\varepsilon) \text{ and } \varepsilon = f(\xi) \quad \text{Eq. 7.12}$$

$$\begin{cases} \sigma_{sli} = E_s \varepsilon_{sli} & \varepsilon_{sli} \le \varepsilon_{sly} \\ \sigma_{sli} = f_{sly} & \varepsilon_{sli} > \varepsilon_{sly} \end{cases} \quad \text{Eq. 7.13}$$

$$\frac{\varepsilon_m}{x} = \frac{\varepsilon_{sli}}{d_i - x} \quad \text{Eq. 7.14}$$

$$\int_0^x \sigma_c t d\xi = \sigma x t + \Sigma \sigma_{sli} A_{sli} \quad \text{Eq. 7.15}$$

$$M_R = \int_0^x \sigma_c t \xi d\xi + \sum_i \sigma_{sli} A_{sli} \left(d_i - \frac{h}{2} \right) + \sigma h t \left(\frac{h}{2} - x \right) \quad \text{Eq. 7.16}$$

Where, ξ is a local coordinate, f_{sly} *and* ε_{sly} is the yield stress and strain of longitudinal reinforcements respectively.

7.3.2 Shear resisting mechanism

7.3.2.1 Unreinforced Masonry

As aforementioned, in case of unreinforced masonry under in-plane load the diagonal cracking means the global collapse of the masonry walls and beams as there are no resisting mechanisms able to perform the stress transfer between both edges of the crack, being the masonry element divided into two parts. This means that the calculus of the diagonal cracking shear force, V_{dc}, represents the shear resistance of the unreinforced masonry elements, V_s. From the parametric study carried out in Chapter 6, it was also seen that masonry beams reinforced only with horizontal bars and shear walls reinforced only with vertical bars also fail by tensile diagonal cracking since only dowel action is not able to improve the shear strength of those masonry elements.

Considering the masonry as an elastic, homogeneous and isotropic structural material, the basic equation for the evaluation of the diagonal cracking shear force can be derived by the equation of principal stresses provided by the elementary theory of elasticity:

$$V_s = V_{dc} = t\int_0^x f_t \sqrt{\frac{\sigma(\varepsilon(\xi))}{f_t} + 1}\, d\xi \qquad \text{Eq. 7.17}$$

$$\sigma = f(\varepsilon) \qquad \varepsilon(\xi) = \frac{\varepsilon_m}{x}\xi \qquad \text{Eq. 7.18}$$

Where, V_s is the shear resistance, V_{dc} is the diagonal cracking shear force, f_t is the tensile strength of masonry, $\sigma(\varepsilon(\xi))$ is the normal stress along the compressive length of the wall, ε_m is the maximum strain of masonry, $\varepsilon(\xi)$ is the strain of masonry at ξ distance from the zero normal stress and x is the depth of the neutral axis.

This equation is similar to the equation presented by Tomaževič (1999) for the calculation of shear strength of unreinforced masonry walls, see Eq. 7.19.

$$V_s = ht\frac{f_t}{b}\sqrt{\frac{\sigma}{f_t} + 1} \qquad \text{Eq. 7.19}$$

Where h and t are respectively the length and thickness of the wall and σ is the average normal stress calculated by dividing the pre-compression load by the area of the cross section. The variable b is a shear stress distribution factor and is taken to be equal to 1.5.

The major difference between the proposed formulation and the equation pointed out by Tomaževič (1999) is the consideration of variable normal stresses along the cross section of the wall instead of the average constant normal stresses. It appears that the distribution of normal stresses along the length of the diagonal strut is not constant due to the flexure of the wall. Thus, the distribution of compressive stresses in the section with the higher moment seems to be a more realistic and it was considered for the calculation of the diagonal cracking shear force. The calculation of the diagonal cracking shear force requires an iterative process since the position of neutral axis and the compressive stresses due to flexure are necessary, see Figure 7.8.

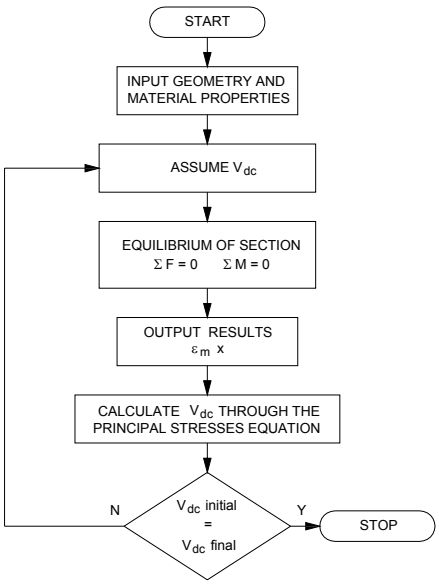

Figure 7.8 - Flow chart for the calculation of the diagonal cracking shear force.

7.3.2.2 Reinforced masonry

In case of reinforced walls, diagonal cracking determines the contribution of transversal reinforcements for the shear resistance. If diagonal cracks do not open, horizontal reinforcements have no contribution for the shear resistance as they do not work. This is the case of shear reinforced masonry walls fail by shear sliding over a bed joint, see Figure 7.9a. This behaviour does not occur in masonry beams as the running bond pattern prevents the sliding over a vertical joint without a diagonal crack. However, if diagonal crack opens, as already seen in Chapters 4 and 6, the transversal reinforcement increases the shear strength of masonry walls since it connects both edges of the diagonal crack allowing the stress transfer between them by conducting tensile stresses see Figure 7.9b.

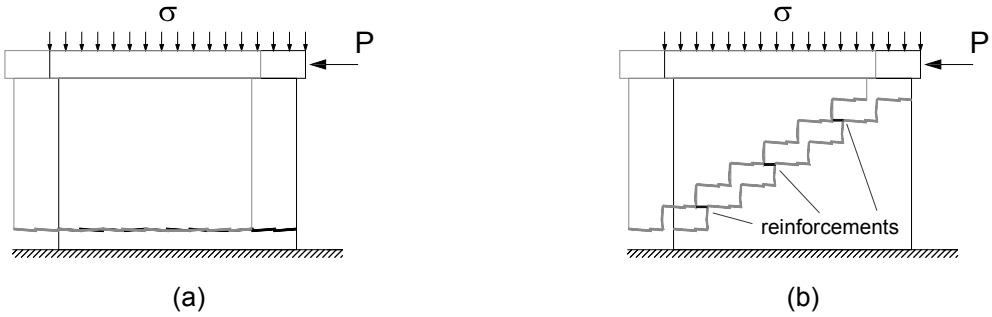

Figure 7.9 – Failure by sliding: (a) horizontally and (b) diagonally.

Longitudinal reinforcements also increase the shear strength of reinforced elements through the dowel action effect according to Tomaževič (1999) and Shing *et al.* (1990a, b).

However, as seen in Chapter 6 and according to Tomaževič (1999) longitudinal reinforcements without the presence of transversal reinforcements is not effective for the contribution of the shear strength of masonry elements. Therefore, in case of shear walls and beams being reinforced with longitudinal and transversal steel bars, the shear resistance should be calculated by considering the contribution of masonry and the contribution of vertical and horizontal reinforcements see Figure 7.10. Thus, the shear strength of reinforced shear masonry elements is calculated through Eq. 7.20.

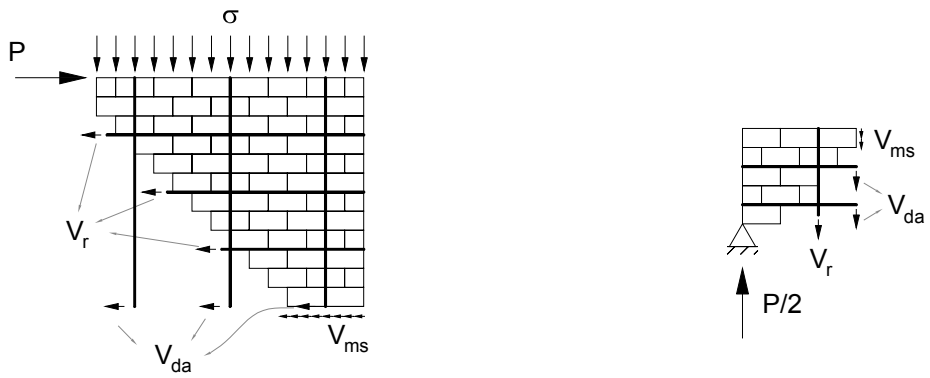

Figure 7.10 – Shear resisting mechanisms of reinforced masonry elements: (a) shear wall and (b) masonry beam.

$$V_s = V_{ms} + V_{da} + V_r \qquad \text{Eq. 7.20}$$

Where V_s is the shear resistance, V_{ms} is the shear resistance of masonry and V_{da} and V_r are the resistance of longitudinal and transversal reinforcement respectively.

In the proposed model, the contribution of masonry to the shear resistance is limited to the compressed part of the wall and it is a function of the normal stresses in the section of masonry element. The Mohr-Coulomb law is a very well known failure criterion for the description of the shear failure of brittle materials, see Figure 7.11.

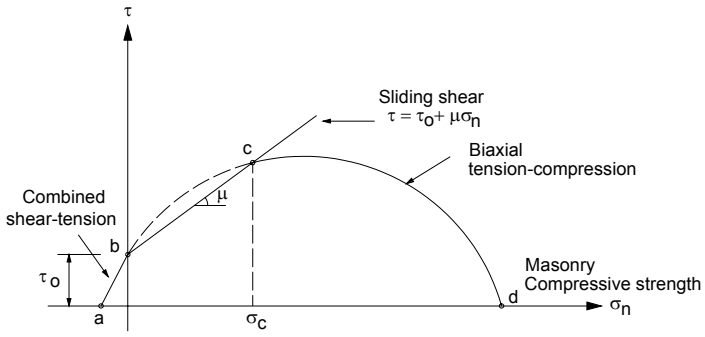

Figure 7.11 – Mohr-Coulomb's failure criterion.

The Mohr-Coulomb criterion is composed of two parts: the Coulomb's linear relation describing the sliding shear resistance and Mohr's circle describing the biaxial tension-compression behavior. The classic Coulomb criterion defines the relation between the shear strength, τ, and the normal stresses, σ, according to Eq. 7.21.

$$\tau = \tau_0 + \mu\sigma \quad \rightarrow \quad 0 \le \sigma \le \sigma_c \qquad \text{Eq. 7.21}$$

Where, τ_0 and μ are the cohesion and friction coefficient of bed joints for shear walls or vertical joints for masonry beams respectively. This criterion is valid only for low levels of normal stresses, being defined the limit of σ_c, after which the shear behaviour of masonry structural elements is describe by the Mohr criterion, in which the relation between shear and normal stresses is given by Eq. 7.22.

$$\tau = f_a\sqrt{1-\frac{\sigma}{f_a}} \quad \rightarrow \quad \sigma_c \le \sigma \le f_a \qquad \text{Eq. 7.22}$$

Where, f_a is compressive strength of masonry perpendicular to bed joints in case of shear walls and parallel to bed joints in case of masonry beams and σ is the normal stress.

The normal stress, σ_c, corresponding to the intersection point *c,* between the Coulomb criterion (Eq. 7.21) and Mohr criterion (Eq. 7.22), can be calculated through Eq. 7.23.

$$\sigma_c = \frac{\sqrt{f_a^2 + 4\mu\tau_0 f_a + 4\mu^2 f_a^2} - (2\mu\tau_0 + f_a)}{2\mu^2} \qquad \text{Eq. 7.23}$$

Thus, considering that the normal stresses present a variation through the length and height of section in shear walls and masonry beams respectively, the shear strength may be calculated through the integration of Mohr-Coulomb criterion as a function of normal stresses through the length or height of section, see Figure 7.12.

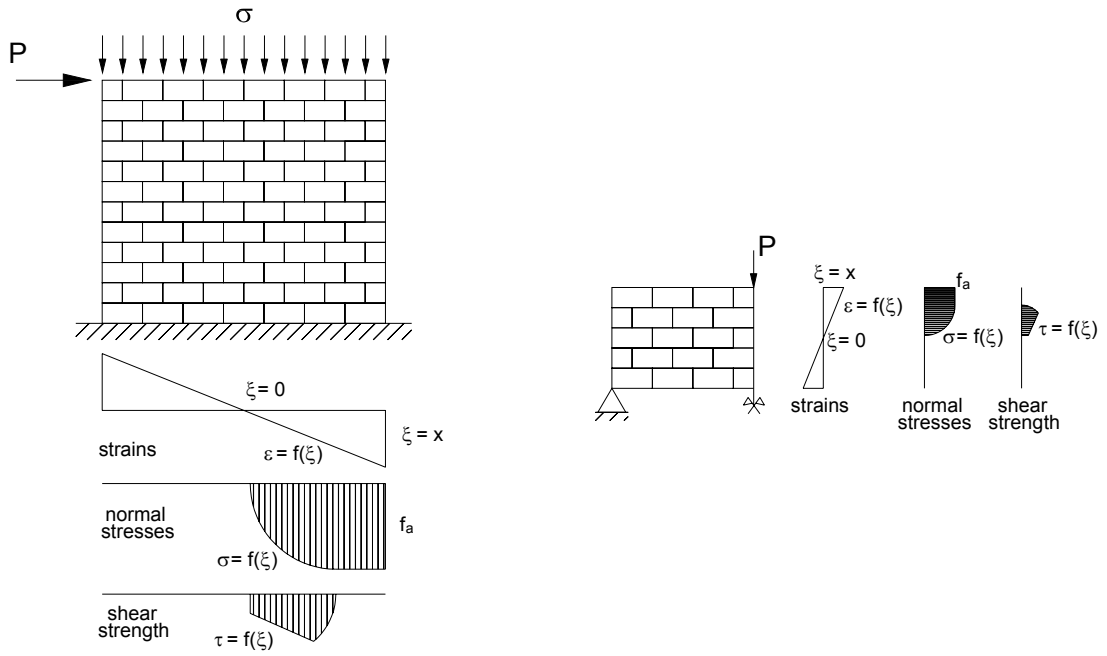

Figure 7.12 – Variation of normal stresses and shear strength envelop through the height of section (a) shear wall and (b) masonry beam.

Therefore, the contribution of masonry for the shear strength of masonry shear walls and masonry beams is given by Eq. 7.24.

$$V_{ms} = \int_0^{x_c} [\tau_0 + \mu\sigma(\varepsilon(\xi))]d\xi + \int_{x_c}^{x} f_a \sqrt{1 - \frac{\sigma(\varepsilon(\xi))}{f_a}}d\xi \qquad \text{Eq. 7.24}$$

Where, x_c is the value of ξ corresponding to the normal stress σ_c.

As aforementioned, the contribution of longitudinal reinforcements to the shear strength due to the dowel action is taken into account in the proposed model and it is defined according to the equation presented by Tomaževič (1999), see Eq. 7.25.

$$V_{da} = 1.026\Sigma A_{sli}\sqrt{f_m f_{sly}} \qquad \text{Eq. 7.25}$$

Where, A_{sli} is the area of longitudinal reinforcements (vertical bars for shear walls and horizontal bars for masonry beams), f_m is the compressive strength of mortar and f_{sly} is yield stress of longitudinal reinforcements.

Finally, the contribution of the transversal reinforcement (V_r) for the shear resistance of the masonry structural elements is calculated through Eq. 7.26.

$$V_r = \Sigma A_{sti} f_{sty}$$ Eq. 7.26

Where, A_{sti} is the area of transversal reinforcements (horizontal bars for shear walls and vertical bars for beams) and f_{sty} is yield stress of transversal reinforcements

Effectiveness of horizontal reinforcements depends on the aspect ratio of the walls and also on their anchorage length. This means that, after diagonal crack, the length of horizontal reinforcement to both sides of the crack should be higher than the anchorage length. Thus, considering that the diagonal cracking develops according to an orientation of 45º as shown in Figure 7.13 (Brunner and Shing, 1996), only reinforcements positioned in a central region of the wall are effective in resisting shear strength. In case of masonry beams, the same evaluation should be performed. This means that the percentage of effective reinforcements has to be calculated based on the anchorage length.

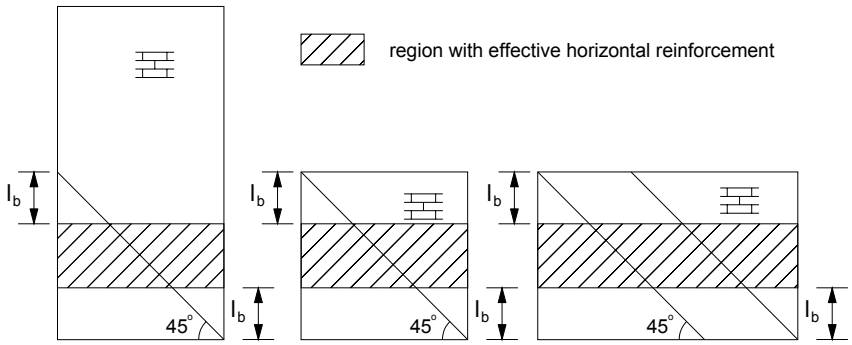

Figure 7.13 – Region of the wall where horizontal reinforcements are effective.

The complete procedure to be followed for the calculation of the lateral resistance of masonry shear walls and beams is given in the flow chart of Figure 7.14. By using input data of geometry and material properties, diagonal cracking shear force, V_{dc}, is calculated through Eq. 7.17 following the iterative procedure pointed out in the flow chart of Figure 7.8. After this, the flexural design is performed in order to obtain the maximum compressive strain of masonry, ε_m, the position of neutral axis, x, and resistant moment of the masonry element, M_R. Admitting that the diagrams of moments and shear forces of the masonry element is known, the shear force, V_{fl}, equivalent to the resistant bending moment considered in section of the maximum moment, should be calculated. In case of unreinforced masonry elements or masonry elements reinforced only with longitudinal bars, if diagonal cracking shear force, V_{dc}, is higher than the shear force, V_{fl}, the masonry element fails by flexure. If the shear force, V_{fl}, is higher than diagonal cracking shear force, V_{dc}, the masonry element fails by shear.

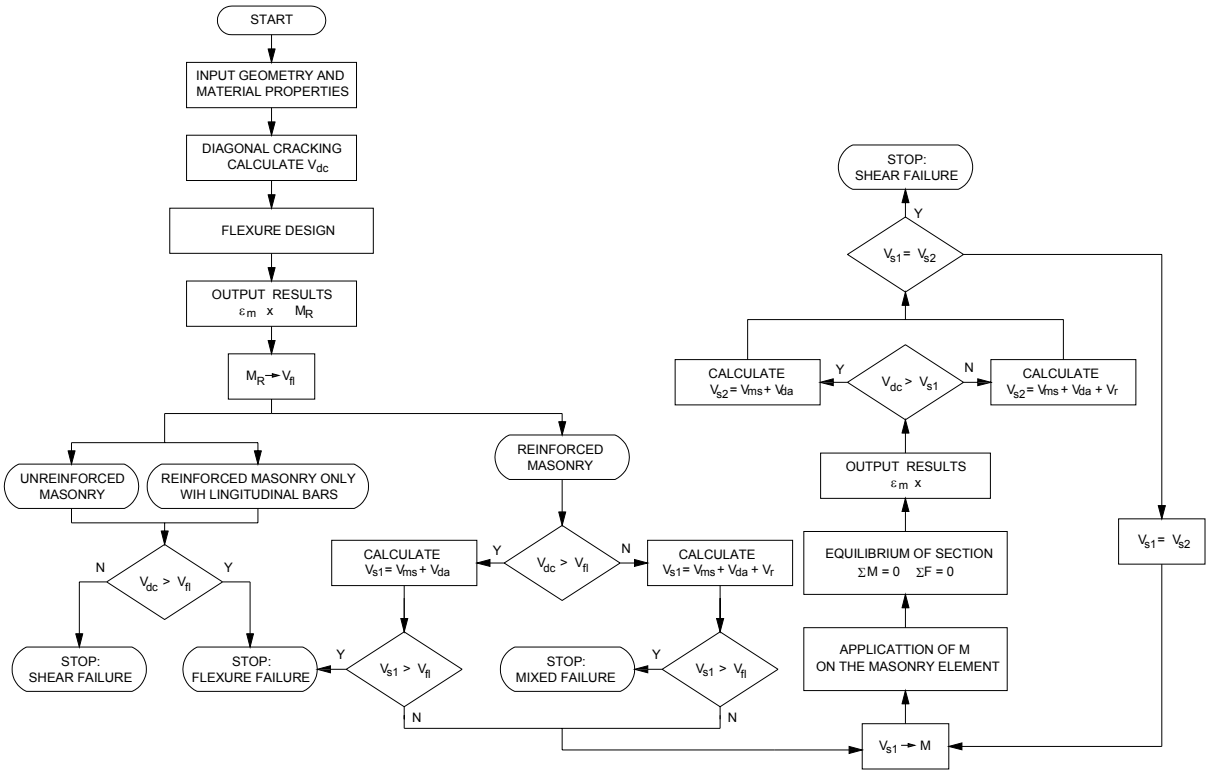

Figure 7.14 – Methodology proposed for defining the load capacity of masonry elements under in-plane loading.

In case of reinforced masonry elements, the diagonal cracking shear force, V_{dc}, is not considered as an ultimate state but it is important for the assessment of the contribution of horizontal reinforcements to the shear resistance. If diagonal cracking shear force is higher than the shear force, V_{fl},, equivalent to the resistant bending moment, M_R, the diagonal cracking does not open and the shear resistance, V_{s1}, is calculated by considering the contribution of masonry, V_{ms}, and the contribution of longitudinal bars, V_{da}. If diagonal cracking shear force is lower than the shear force, V_{fl}, equivalent to the resistant bending moment, M_R, it is considered that diagonal cracking develops and the contribution of the transversal bars, V_r, is taken into account in the shear resistance, according to Eq. 7.20. The reinforced masonry elements fail by flexure if the shear resistance, V_{s1}, and diagonal cracking shear force is higher than the shear force, V_{fl}. In case of diagonal cracking shear force is lower and shear resistance, V_{s1}, is higher than the shear force, V_{fl}, equivalent to the resistant bending moment, M_R, the masonry element fails in a mixed flexural-shear mode. If diagonal cracking develops and shear resistance, V_{s1}, is lower than the shear force, V_{fl}, an iterative procedure is followed to calculate the actual shear resistance. In the iterative process the cross section of the masonry element should be re-equilibrated by considering a moment, M, which is equivalent to the shear resistance, V_1. Considering the new maximum compressive strain of masonry, ε_m, and the position of neutral axis, x, a new shear

resistance, V_{s2}, should be calculated through Eq. 7.20 and compared to the previous shear resistance, V_{s1}. If both results are equal, the shear resistance of the masonry element was found and shear failure mode is attributed to the wall. On the contrary, a new iteration should be carried out. Note that the contribution of the masonry for the shear resistance, V_{ms}, is calculated in a first phase based on the normal stress configuration used for the flexural ultimate state.

7.3.3 Comparison of the design models with experimental results

In order to evaluate the accuracy of the proposed model and to compare its performance with other analytical approaches described in Chapter 2, a database composed of approximately 100 walls tested under in-plane load was organized. For the database various types of walls were selected, namely with distinct geometry, masonry materials, vertical and horizontal reinforcement ratios and pre-compression levels. The main aim was to find a wide range of specimens ensuring the occurrence of distinct failure modes. The major concern on the definition of the database was the obtainment of the mechanical properties of masonry materials of the tested walls, namely from units and mortar, due to the absence of this information in the literature. Mechanical properties like friction coefficient, cohesion and tensile strength were almost never reported in most of the researches about in-plane behaviour of masonry walls in spite of these are basic properties for the assessment of the lateral resistance of the walls. Thus, according to the characteristics of the units and mortar, friction coefficient and cohesion were estimated from Eurocode 6 (2005), when no information was given. When tensile strength was not reported in literature, a value of approximately 67% of the average bed joint sliding strength was taken into account as suggested by Steelman and Abrams (2007). The geometrical features (z/h), vertical and horizontal reinforcement ratios (ρ_v and ρ_h) and the mechanical properties considered for each wall are summarized in Table 7.1. Here, f_{yv} is the yielding strength of vertical reinforcements, f_{yh} is the yielding strength of horizontal reinforcements, f_b is the compressive resistance of units, f_m is the compressive strength of mortar, f_a is the compressive strength of masonry, f_t is the tensile strength of masonry, f_{x1} is the flexural strength of masonry and f_{v0} is the initial shear strength of interface unit-mortar. In Table 7.2, information about the literature sources from which the walls were taken for the analytical study is presented.

Table 7.1 – Database used to comparing the design models of shear-walls.

Nº	Dimensions (mm)	Area (cm^2)	z/h	ρ_v (%)	f_{yv} (MPa)	ρ_h (%)	f_{yh} (MPa)	f_b (MPa)	f_m (MPa)	f_a (MPa)	f_t (MPa)	f_{x1} (MPa)	f_{v0} (MPa)	μ	σ (MPa)	Material
1	1206 x 800 x 100	1206	1.18	0.00	580.00	0.00	580.00	11.77	3.58	5.95	0.19	0.41	0.42	0.49	0.56	concrete
2	1206 x 800 x 100	1206	1.18	0.00	580.00	0.09	580.00	11.77	5.16	5.95	0.19	0.41	0.42	0.49	0.56	concrete
3	1206 x 800 x 100	1206	1.18	0.10	580.00	0.09	580.00	11.77	3.82	5.95	0.19	0.41	0.42	0.49	0.56	concrete
4	1208 x 800 x 100	1208	1.18	0.10	580.00	0.09	580.00	11.77	7.11	5.95	0.19	0.41	0.42	0.49	0.55	concrete
5	1206 x 800 x 100	1206	1.18	0.10	580.00	0.09	580.00	11.77	8.62	5.95	0.19	0.41	0.42	0.49	1.30	concrete
6	1208 x 800 x 100	1208	1.18	0.10	580.00	0.09	580.00	11.77	7.72	5.95	0.19	0.41	0.42	0.49	1.30	concrete
7	1206 x 800 x 100	1206	1.18	0.10	580.00	0.13	580.00	11.77	4.82	5.95	0.19	0.41	0.42	0.49	0.56	concrete
8	1206 x 800 x 100	1206	1.18	0.10	580.00	0.05	580.00	11.77	5.16	5.95	0.19	0.41	0.42	0.49	0.56	concrete
9	1116 x 808 x 94	1049.04	1.17	0.11	580.00	0.10	580.00	9.29	4.82	5.44	0.59	0.31	0.21	0.49	0.57	concrete
10	1224 x 808 x 94	1150.56	1.17	0.10	580.00	0.10	580.00	9.29	8.84	5.44	0.59	0.31	0.21	0.49	0.56	concrete
11	1829 x 1829 x 143	2612.9	1.00	0.38	440.96	0.24	461.63	16.54	24.12	19.98	0.50	0.20	0.20	0.40	1.38	concrete
12	1829 x 1829 x 143	2612.9	1.00	0.38	440.96	0.24	385.84	16.54	24.12	19.98	0.63	0.20	0.20	0.40	1.86	concrete
13	1829 x 1829 x 143	2612.9	1.00	0.74	496.08	0.13	385.84	16.54	27.56	20.67	0.63	0.20	0.20	0.40	1.86	concrete
14	1829 x 1829 x 143	2612.9	1.00	0.74	496.08	0.13	385.84	16.54	20.67	17.91	0.13	0.20	0.20	0.40	0.00	concrete
15	1829 x 1829 x 143	2612.9	1.00	0.74	496.08	0.13	385.84	16.54	20.67	17.91	0.32	0.20	0.20	0.40	0.69	concrete
16	1829 x 1829 x 143	2612.9	1.00	0.38	440.96	0.13	385.84	16.54	20.67	17.91	0.13	0.20	0.20	0.40	0.00	concrete
17	1829 x 1829 x 143	2612.9	1.00	0.74	496.08	0.13	385.84	16.54	20.67	20.67	0.32	0.20	0.20	0.40	0.69	concrete
18	1829 x 1829 x 143	2612.9	1.00	0.38	440.96	0.24	461.63	16.54	20.67	20.67	0.13	0.20	0.20	0.40	0.00	concrete
19	1829 x 1829 x 143	2612.9	1.00	0.38	440.96	0.13	385.84	16.54	20.67	20.67	0.63	0.20	0.20	0.40	1.86	concrete
20	1829 x 1829 x 143	2612.9	1.00	0.38	440.96	0.13	385.84	17.91	18.60	22.05	0.32	0.20	0.20	0.40	0.69	concrete
21	1829 x 1829 x 143	2612.9	1.00	0.74	496.08	0.24	385.84	17.91	18.60	22.05	0.13	0.20	0.20	0.40	0.00	concrete
22	1829 x 1829 x 143	2612.9	1.00	0.38	440.96	0.24	461.63	17.91	18.60	22.05	0.32	0.20	0.20	0.40	0.69	concrete
23	1829 x 1829 x 143	2612.9	1.00	0.54	440.96	0.24	461.63	17.91	20.67	22.74	0.63	0.20	0.20	0.40	1.86	concrete
24	1829 x 1829 x 143	2612.9	1.00	0.54	440.96	0.13	385.84	17.91	20.67	22.74	0.63	0.20	0.20	0.40	1.86	concrete
25	1829 x 1829 x 143	2612.9	1.00	0.54	440.96	0.24	461.63	17.91	20.67	22.74	0.32	0.20	0.20	0.40	0.69	concrete
26	1829 x 1829 x 143	2612.9	1.00	0.74	496.08	0.24	385.84	17.91	16.54	17.23	0.63	0.20	0.20	0.40	1.86	concrete
27	1422 x 1321 x 137	1941.93	1.00	0.58	451.30	0.15	427.18	45.47	20.67	22.46	0.86	0.20	0.20	0.40	2.73	clay
28	1829 x 1321 x 137	2496.77	1.00	0.56	444.41	0.15	444.41	45.47	20.67	23.08	0.63	0.20	0.20	0.40	1.86	clay
29	2235 x 1321 x 137	3051.06	1.00	0.55	444.41	0.15	444.41	45.47	20.67	23.08	0.54	0.20	0.20	0.40	1.52	clay
30	610 x 760 x 100	610	1.13	0.26	522.00	0.22	253.00	10.00	10.00	5.20	0.45	0.20	0.20	0.40	1.00	concrete
31	610 x 760 x 100	610	1.13	0.26	522.00	0.22	253.00	10.00	10.00	5.20	0.45	0.20	0.20	0.40	2.00	concrete
32	790 x 1200 x 190	1501	0.55	1.15	370.00	0.17	351.00	50.80	45.80	33.40	0.34	0.20	0.20	0.40	0.79	concrete
33	790 x 1200 x 190	1501	0.55	0.67	353.00	0.35	347.00	50.80	48.70	29.20	0.34	0.20	0.20	0.40	0.79	concrete
34	793 x 1200 x 133	1054.69	0.55	0.53	342.00	0.83	370.00	33.60	48.70	28.30	0.34	0.20	0.20	0.40	0.79	concrete
35	1060 x 1200 x 133	1409.8	0.55	0.45	342.00	0.83	370.00	33.60	43.70	26.50	0.34	0.20	0.20	0.40	0.79	concrete
36	1326 x 1200 x 133	1763.58	0.55	0.41	342.00	0.83	370.00	33.60	51.00	32.50	0.34	0.20	0.20	0.40	0.78	concrete
37	793 x 1200 x 133	1054.69	0.55	0.87	336.00	0.25	339.00	33.60	49.20	27.20	0.34	0.20	0.20	0.40	0.79	concrete
38	1060 x 1200 x 133	1409.8	0.55	0.58	336.00	0.25	339.00	33.60	50.70	33.60	0.34	0.20	0.20	0.40	0.79	concrete
39	1326 x 1200 x 133	1763.58	0.55	0.51	336.00	0.25	339.00	33.60	47.10	30.20	0.34	0.20	0.20	0.40	0.78	concrete
40	1626 x 1626 x 152	2477.41	0.58	0.44	514.00	0.34	414.00	19.20	57.00	12.00	0.32	0.20	0.20	0.40	0.69	concrete
41	1100 x 1700 x 190	2095.12	0.50	1.16	360.07	0.00	0.00	28.12	45.46	26.35	0.18	0.20	0.20	0.40	0.19	concrete
42	1100 x 1700 x 190	2095.12	0.50	1.16	360.07	0.16	354.08	28.12	45.46	26.35	0.18	0.20	0.20	0.40	0.19	concrete
43	1100 x 1700 x 190	2095.12	0.50	1.16	360.07	0.32	354.08	28.12	45.46	26.35	0.18	0.20	0.20	0.40	0.19	concrete
44	1100 x 1700 x 190	2095.12	0.50	1.16	360.07	0.64	354.08	28.12	45.46	26.35	0.18	0.20	0.20	0.40	0.19	concrete
45	1100 x 1700 x 190	2095.12	0.50	0.56	388.87	0.32	354.08	28.12	45.46	26.35	0.18	0.20	0.20	0.40	0.19	concrete
46	1100 x 1700 x 190	2095.12	0.50	0.73	369.44	0.00	0.00	26.62	33.11	28.61	0.18	0.20	0.20	0.40	0.19	concrete
47	1100 x 1700 x 190	2095.12	0.50	0.73	369.44	0.16	354.08	26.62	33.11	28.61	0.18	0.20	0.20	0.40	0.19	concrete
48	1100 x 1700 x 190	2095.12	0.50	0.73	369.44	0.32	354.08	26.62	33.11	28.61	0.18	0.20	0.20	0.40	0.19	concrete
49	1100 x 1700 x 190	2095.12	0.50	0.73	369.44	0.64	354.08	26.62	33.11	28.61	0.18	0.20	0.20	0.40	0.19	concrete
50	2240 x 1450 x 240	5376	0.50	0.00	0.00	0.00	0.00	7.36	2.26	2.84	0.13	0.20	0.15	0.40	0.12	clay
51	2240 x 1450 x 240	5376	0.50	0.00	0.00	0.00	0.00	7.36	4.91	3.58	0.17	0.20	0.15	0.40	0.28	clay
52	2240 x 1450 x 240	5376	0.50	0.00	0.00	0.00	0.00	7.36	4.41	3.47	0.17	0.20	0.15	0.40	0.28	clay
53	1120 x 1500 x 240	2688	0.50	0.00	0.00	0.00	0.00	7.36	1.11	2.29	0.21	0.20	0.15	0.40	0.41	clay
54	1120 x 1480 x 240	2688	0.50	0.00	0.00	0.00	0.00	7.36	1.81	2.66	0.18	0.20	0.15	0.40	0.31	clay
55	1120 x 1480 x 240	2688	0.50	0.00	0.00	0.00	0.00	7.36	1.81	2.66	0.24	0.20	0.15	0.40	0.51	clay
56	1250 x 1500 x 240	3000	0.50	0.00	0.00	0.03	258.00	7.36	1.67	2.59	0.28	0.20	0.15	0.40	0.66	clay
57	1250 x 1500 x 240	3000	0.50	0.00	0.00	0.03	258.00	7.36	4.09	3.39	0.28	0.20	0.15	0.40	0.66	clay
58	1250 x 1500 x 240	3000	0.50	0.00	0.00	0.08	258.00	7.36	7.30	4.04	0.22	0.20	0.15	0.40	0.46	clay
59	1250 x 1500 x 240	3000	0.50	0.00	0.00	0.08	258.00	7.36	7.10	4.00	0.22	0.20	0.15	0.40	0.46	clay
60	1250 x 1500 x 240	3000	0.50	0.00	0.00	0.17	258.00	7.36	4.09	3.39	0.28	0.20	0.15	0.40	0.66	clay
61	1250 x 1500 x 240	3000	0.50	0.00	0.00	0.17	258.00	7.36	5.79	3.77	0.26	0.20	0.15	0.40	0.59	clay
62	400 x 607 x 63	252	0.50	0.00	0.00	0.00	0.00	12.10	12.40	5.43	0.58	0.20	0.20	0.40	1.66	concrete
63	400 x 607 x 63	252	0.50	0.00	0.00	0.00	0.00	12.10	17.80	6.15	0.58	0.20	0.20	0.40	1.66	concrete
64	400 x 607 x 63	252	0.50	0.00	0.00	0.16	314.00	12.10	12.40	5.43	0.58	0.20	0.20	0.40	1.66	concrete
65	400 x 607 x 63	252	0.50	0.00	0.00	0.16	314.00	12.10	17.80	6.15	0.58	0.20	0.20	0.40	1.66	concrete
66	400 x 607 x 63	252	0.50	0.00	0.00	0.29	302.00	12.10	12.40	5.43	0.58	0.20	0.20	0.40	1.66	concrete
67	400 x 607 x 63	252	0.50	0.00	0.00	0.29	302.00	12.10	17.80	6.15	0.58	0.20	0.20	0.40	1.66	concrete
68	400 x 607 x 63	252	0.50	0.00	0.00	0.37	302.00	12.10	12.40	5.43	0.58	0.20	0.20	0.40	1.66	concrete
69	400 x 607 x 63	252	0.50	0.00	0.00	0.37	302.00	12.10	17.80	6.15	0.58	0.20	0.20	0.40	1.66	concrete
70	374 x 569 x 65	243.1	0.50	0.00	0.00	0.00	0.00	17.80	7.80	9.78	0.57	0.20	0.15	0.40	1.78	clay
71	374 x 569 x 65	243.1	0.50	0.00	0.00	0.00	0.00	17.80	12.30	9.18	0.57	0.20	0.15	0.40	1.78	clay
72	374 x 569 x 65	243.1	0.50	0.00	0.00	0.16	314.00	17.80	7.80	9.78	0.57	0.20	0.15	0.40	1.78	clay
73	374 x 569 x 65	243.1	0.50	0.00	0.00	0.16	314.00	17.80	12.30	9.18	0.57	0.20	0.15	0.40	1.78	clay
74	374 x 569 x 65	243.1	0.50	0.00	0.00	0.30	302.00	17.80	7.80	9.78	0.57	0.20	0.15	0.40	1.78	clay
75	374 x 569 x 65	243.1	0.50	0.00	0.00	0.30	302.00	17.80	12.30	9.18	0.57	0.20	0.15	0.40	1.78	clay
76	374 x 569 x 65	243.1	0.50	0.00	0.00	0.38	302.00	17.80	7.80	9.78	0.57	0.20	0.15	0.40	1.78	clay
77	374 x 569 x 65	243.1	0.50	0.00	0.00	0.38	302.00	17.80	12.30	9.18	0.57	0.20	0.15	0.40	1.78	clay

Nº	Dimensions (mm)	Area (cm^2)	z/h	ρ_v (%)	f_{yv} (MPa)	ρ_h (%)	f_{yh} (MPa)	f_b (MPa)	f_m (MPa)	f_a (MPa)	f_t (MPa)	f_{x1} (MPa)	f_{v0} (MPa)	μ	σ (MPa)	Material
78	978 x 521 x 51	496.77	0.70	0.00	0.00	0.00	0.00	27.73	15.85	18.36	0.50	0.20	0.20	0.40	1.38	concrete
79	978 x 952 x 51	496.77	0.62	0.00	0.00	0.00	0.00	27.73	15.85	18.36	0.32	0.20	0.20	0.40	0.69	concrete
80	978 x 952 x 51	496.77	0.62	0.00	0.00	0.00	0.00	13.87	15.85	9.30	0.32	0.20	0.20	0.40	0.69	concrete
81	940 x 940 x 48	448.77	0.62	0.12	446.47	0.12	446.47	19.29	15.50	15.85	0.13	0.20	0.20	0.40	0.00	concrete
82	940 x 940 x 48	448.77	0.62	0.12	446.47	0.12	446.47	19.29	15.50	15.85	0.32	0.20	0.20	0.40	0.69	concrete
83	940 x 940 x 48	448.77	0.62	0.12	446.47	0.12	446.47	19.29	15.50	15.85	0.50	0.20	0.20	0.40	1.38	concrete
84	1000 x 1000 x 100	1000	0.50	0.00	0.00	0.00	0.00	50.00	10.00	8.95	0.36	0.13	0.15	0.40	0.98	clay
85	1000 x 1000 x 100	1000	0.50	0.00	0.00	0.00	0.00	50.00	10.00	8.95	0.39	0.13	0.15	0.40	1.07	clay
86	1000 x 1000 x 100	1000	0.50	0.00	0.00	0.00	0.00	50.00	10.00	8.95	0.35	0.13	0.15	0.40	0.95	clay
87	1000 x 1000 x 100	1000	0.50	0.00	0.00	0.00	0.00	50.00	10.00	11.73	0.42	0.13	0.15	0.40	1.20	clay
88	1000 x 1000 x 100	1000	0.50	0.00	0.00	0.00	0.00	50.00	10.00	11.73	0.31	0.13	0.15	0.40	0.78	clay
89	1000 x 1000 x 100	1000	0.50	0.00	0.00	0.00	0.00	50.00	10.00	11.73	0.38	0.13	0.15	0.40	1.06	clay
90	1800 x 1800 x 140	2520	1.00	0.62	318.00	0.06	325.00	30.00	10.00	17.60	0.13	0.20	0.20	0.40	0.00	concrete
91	1800 x 1800 x 140	2520	1.00	0.62	318.00	0.01	325.00	30.00	10.00	17.60	0.13	0.20	0.20	0.40	0.00	concrete
92	1800 x 1800 x 140	2520	1.00	0.62	318.00	0.16	320.00	30.00	10.00	17.00	0.13	0.20	0.20	0.40	0.00	concrete
93	1800 x 1800 x 140	2520	1.00	0.62	318.00	0.06	320.00	30.00	10.00	17.00	0.13	0.20	0.20	0.40	0.00	concrete
94	1800 x 1800 x 60	1080	1.00	1.45	318.00	0.00	0.00	30.00	10.00	18.50	0.13	0.20	0.20	0.40	0.00	concrete
95	1800 x 1800 x 60	1080	1.00	0.87	318.00	0.00	0.00	30.00	10.00	18.50	0.13	0.20	0.20	0.40	0.00	concrete
96	1800 x 1800 x 140	2520	1.00	0.62	318.00	0.06	325.00	30.00	10.00	18.80	0.27	0.20	0.20	0.40	0.50	concrete
97	1800 x 1800 x 140	2520	1.00	0.62	318.00	0.06	325.00	30.00	10.00	18.80	0.20	0.20	0.20	0.40	0.25	concrete
98	1800 x 1800 x 140	2520	1.00	0.97	318.00	0.05	325.00	30.00	10.00	24.30	0.20	0.20	0.20	0.40	0.25	concrete
99	3000x1800x140	4200	1.00	0.60	318.00	0.06	325.00	30.00	10.00	24.30	0.17	0.20	0.20	0.40	0.15	concrete
100	1020 x 1150 x 143	1458.6	0.50	0.00	0.00	0.00	0.00	5.70	10.00	3.20	0.37	0.20	0.20	0.40	0.90	AAC
101	1020 x 1150 x 143	1458.6	0.50	0.00	0.00	0.07	580.00	5.70	10.00	3.20	0.37	0.20	0.20	0.40	0.90	AAC

Table 7.2 – Authors of researches used to create the database.

Nº of walls	Author
1 – 10	This work
11 – 26	Shing *et al.* (1989)
27 – 29	Brunner and Shing (1996)
30 – 31	Tomaževič (1996)
32 – 39	Yoshimura *et al.* (2003)
40	Chai and Yaw (1999)
41 – 49	Matsumura (1990)

Nº of walls	Author
50 – 61	Jingqian *et al.* (1986)
62 – 77	Tomaževič and Zarnic (1986)
78 – 80	Mahmoud *et al.* (1995)
81 – 83	Ghanem *et al.* (1993)
84 – 89	Vermeltfoort *et al.* (1993)
90 – 99	Voon and Ingham (2006)
100 – 101	Gouveia and Lourenço (2007)

The comparison between experimental and analytical lateral resistance predicted by Eurocode 6 (2005) is shown in Figure 7.15a. It is observed that the European code provides in general lower values of the lateral resistance than the ones obtained in experimental tests, meaning that it gives very safe values of the lateral capacity of masonry walls. It is seen that the predicted values of maximum horizontal load was higher than the experimental lateral resistance only in 15% of the walls. In addition, only in 2% of the walls the analytical lateral resistance exceeds in more than 10% the experimental values. Approximately 40% of the analysed walls presented an analytical lateral strength 30% lower than experimental result.

In average, Tomaževič's model predicted an analytical lateral resistance of approximately 64% the experimental maximum horizontal load, being the scatter reasonably low. This model only predicted higher lateral resistance than experimental results in 2% of the walls of the database, see Figure 7.15b. A reason that explains the lower analytical values is related to the evaluation of the sliding resistance, which does not consider the initial cohesion. If the cohesion is considered in evaluation of sliding, the relation between

predicted and experimental horizontal load increases to 0.80 and the coefficient of variation of the results shows also a small reduction.

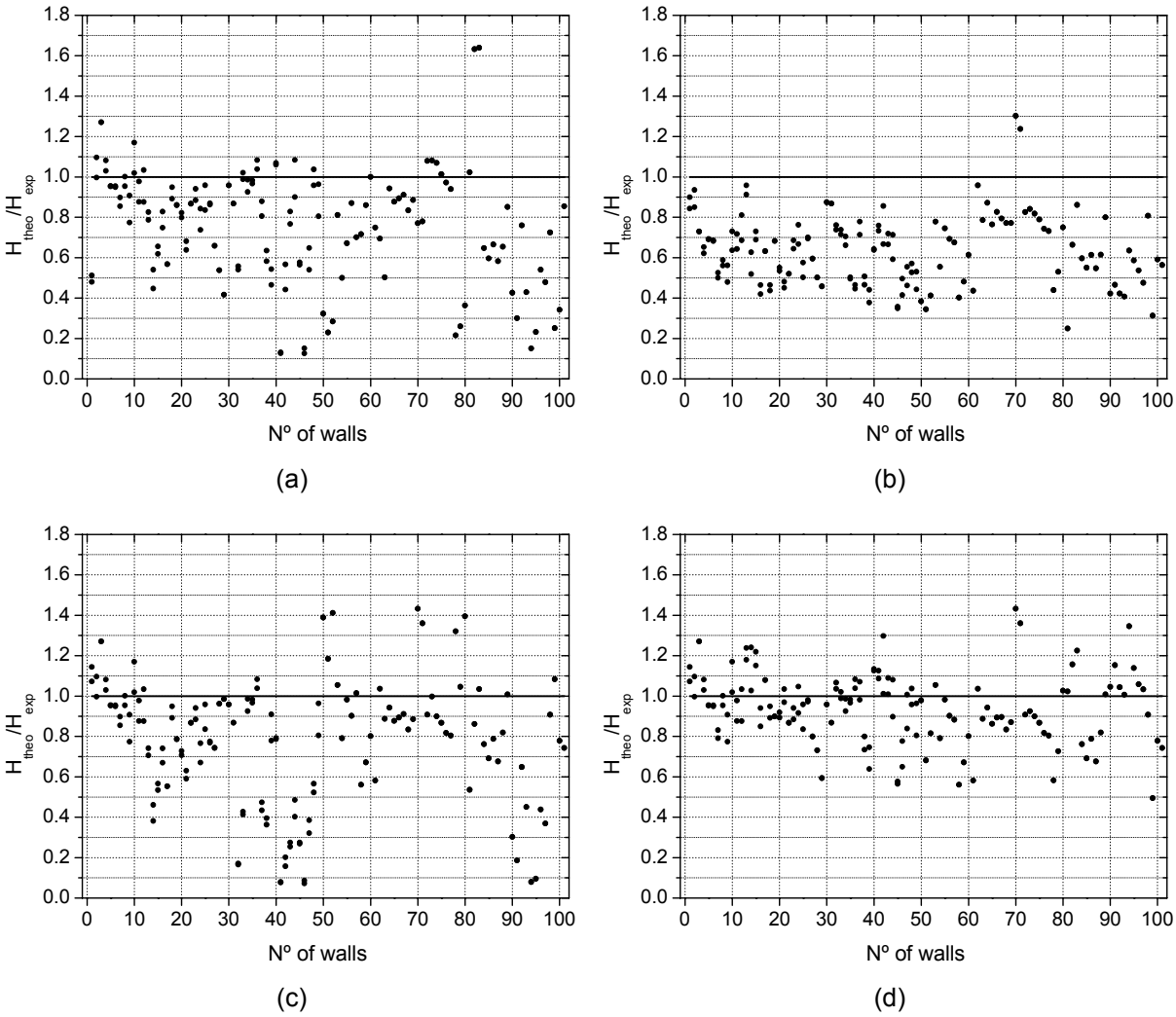

Figure 7.15 – Comparison of the design models for shear walls: (a) Eurocode 6 (2005), (b) Tomaževič's model, (c) Brunner and Shing's model and (d) proposed model.

The great innovation of the Brunner and Shing's model is the consideration of coupling between the flexure and shear in the proposed design model. The ratio between the analytical lateral resistance provided by the Brunner and Shing's model and the experimental values is about 0.78 with a coefficient of variation around to 35%, see Figure 7.15c. The Brunner and Shing's model defines integration bounds for the calculation of shear strength based on the inclination of diagonal crack, which is assumed to develop at an orientation of 45º. The distribution of compressive stresses acting at the bottom edge of walls is considered effective only between the intersection point between the diagonal crack and the base of the wall and the bottom corner of the wall. This means that the model considers only part of the compressed length of the wall for the calculation of the shear strength. Consequently, in case

of walls with aspect ratio greater or equal than 1.0, diagonal crack is considered to develop from the bottom corner of the wall resulting in the null compressed length. In Figure 7.15c this fact can be really seen from the underestimation of the lateral strength in walls with aspect ratio equal to 1.0 (walls from nº 30 to nº 50 and from nº 90 to nº 98).

The proposed design model in this work is considered to be an improvement of the Brunner and Shing's model by considering the Mohr-Coulomb criterion for the calculation of the shear strength of masonry walls. In fact, all extent of the compressed part is considered for the calculation of the shear strength of masonry. However, different stretches of the failure criterion are considered depending on the level of normal stresses along the compressed length of the wall. By comparing the proposed model and the other ones presented in literature, it is seen that a better approximation is achieved between experimental and analytical lateral resistance of the walls, see Figure 7.15d. In average, the analytical to experimental lateral resistance ratio is about 0.92 with a coefficient of variation of approximately 20%. This result confirms the better accuracy of this model to predict the lateral resistance of walls, when a comparison, in average terms, among the analytical models is performed, see Table 7.3.

Table 7.3 – Comparison of the accuracy of the design models to predict the lateral resistance of shear walls

	Eurocode 6 (2005)	Tomaževič	Brunner & Shing	Proposed
Average of H_{theo}/H_{exp}	0.74	0.64	0.78	0.92
C. V. (%)	32.88	23.28	34.85	18.45

Due to the unavailability of experimental results on the behaviour of masonry beams in literature, it was not possible to compare the performance of the distinct analytical models to obtain an estimation of the load capacity. Concerning the experimental results on beams available in this work, it was decided not to apply the model given the uncertainty on the stiffness of the elastic support aiming at representing the effect of axial force generated by the friction resistance.

7.4 Software to design masonry elements under in-plane loading

Some sophisticated computer programs for structural design of masonry structures have been recently developed aiming at analysing the complete behaviour of masonry

buildings under different load conditions. Structural engineers can insert all geometrical details of the structural elements to be designed, material properties and boundary conditions and the software gives almost the final structural design. However, the complexity of these programs requires the critical analysis of results, which sometimes is hardly carried out by the civil engineers. In this scope, it is important provide the structural engineer with simple tools in order to be able to proceed with initial localized structural verifications before accepting the results of the sophisticated structural programs. Simple design methods can be also useful for the individual structural verification of masonry sections given the internal efforts for a specific load combination.

Therefore, aiming at providing a tool for the design of masonry elements subjected to in-plane loading considering the coupling shear and flexural behaviour, a Windows® application called *RMW (Reinforced Masonry Walls)* was developed by using the compiler Borland Delphi 7 which uses Pascal language. Software *RMW* allows designing reinforced masonry walls and beams using the Eurocode 6 (2005), Tomaževič's model, Brunner and Shing's model and the design method proposed in this study. Besides, a prediction of the flexural and diagonal cracking can be performed through the methodology presented in section 7.3. Besides, software *RMW* provides the interaction diagrams Bending moment *vs.* Normal compressive force and Shear force *vs.* Normal compressive force for a given reinforced masonry element section. Software *RMW* presents a friendly interface divided in two parts: region of data entrance and cascade menus, see Figure 7.16.

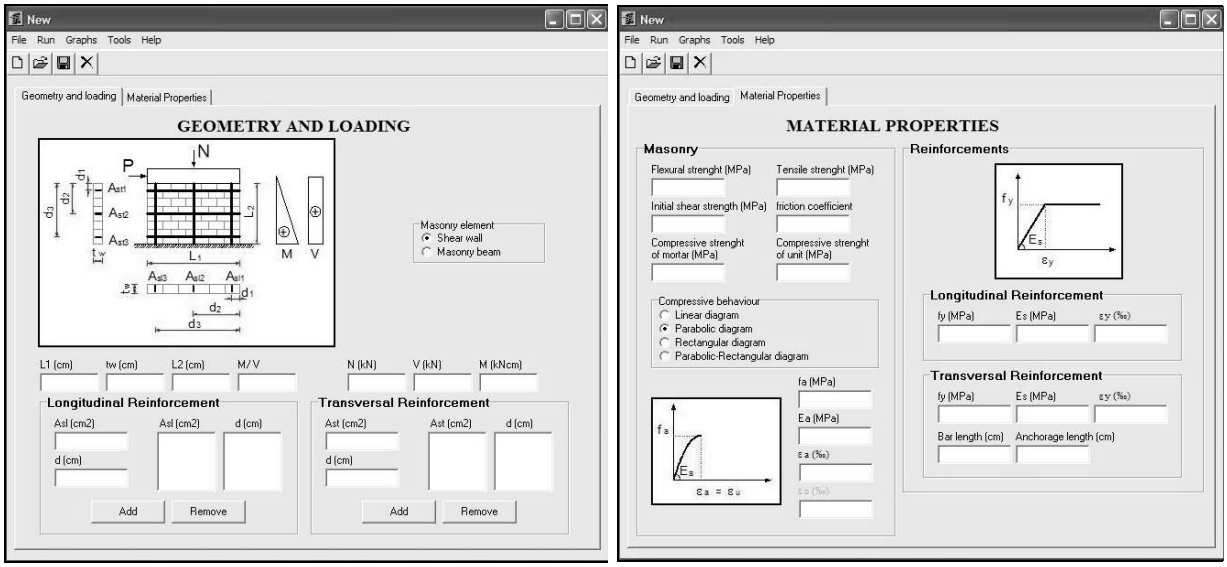

Figure 7.16 – Interface of the software *RMW*.

7.4.1 Data entrance

The entrance of data in the automatic program is divided in three parts: geometry, material properties and internal forces resulting from the load combinations. The geometry data includes the height, length, width and lever arm of the masonry wall or beam. In addition, the type, amount and position of vertical and horizontal reinforcements should be indicated. The material properties of units, mortar, reinforcements and of masonry as a composite should be indicated (flexural strength of masonry, tensile strength of masonry, initial shear strength of the interface unit-mortar, friction coefficient the interface unit-mortar, compressive strength of mortar, compressive strength of units, yield stress of reinforcements and elastic modulus of reinforcements). In case of compressive behaviour of masonry, software *RMW* allows the user to choose between the linear, parabolic, rectangular and parabolic-rectangular diagrams describing the distribution of normal stresses, see Figure 7.17.

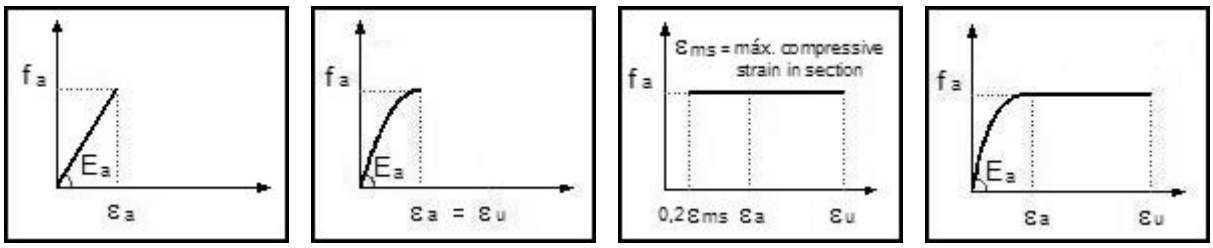

Figure 7.17 – Optional diagrams for compressive behaviour of masonry.

It is needed to define the anchorage length and the total length for horizontal reinforcements in order the program is able to identify which horizontal bars can be considered in the calculation of the shear strength. Finally, internal efforts (normal force, moment and shear force) acting in masonry structural element should be defined in order to identify the state of the structural element in relation to the interaction diagrams.

7.4.2 Main menus

There are five cascade menus in software RMW, namely the menus File, Run, Graphs, Tools and Help. In menu “File” the user can decide to save the inserted data in a text file and open a new file or a previously saved data file, see Figure 7.18.

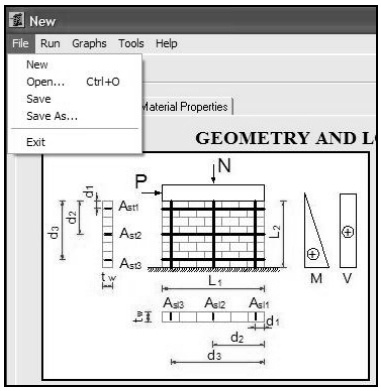

Figure 7.18 – Menu "File" of the software *RMW*.

In the menu "Tools" the user can configure the maximum number of iterations and the convergence interval of the Newton's iterative method for the coupling shear-flexure design. In this menu the user can still choose the number of points that will be plotted in the interaction diagrams and the values of safety factors, see Figure 7.19. In menu "Help" the user can access the manual describing the software and check additional information about the software, see Figure 7.20.

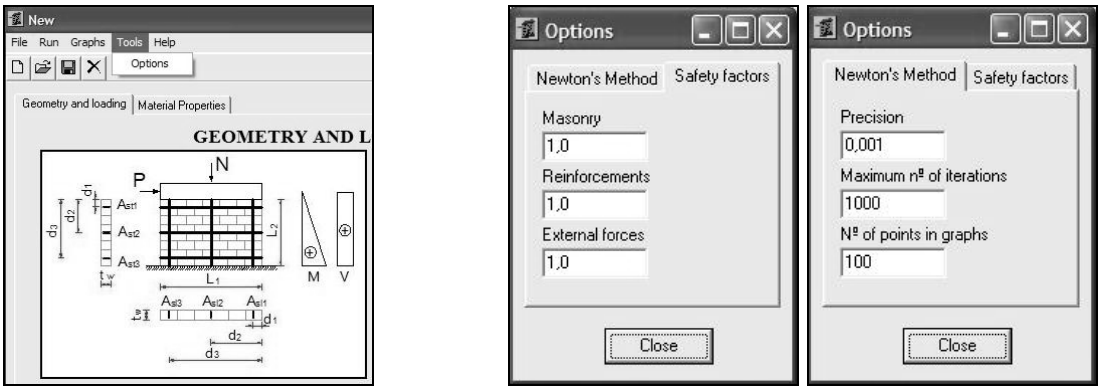

Figure 7.19 – Menu "Tools" of the software *RMW*.

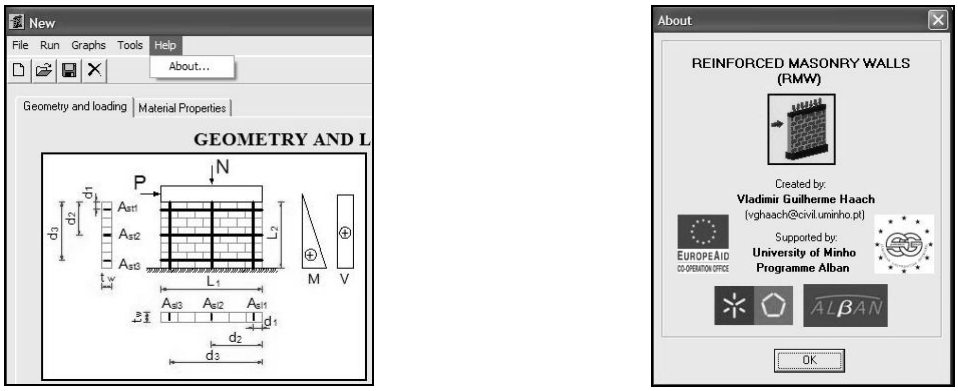

Figure 7.20 – Menu "Help" of the software *RMW*.

In menu “Run” the user can choose to obtain the prediction of cracking loads and the design resistance of the masonry structural element according to the distinct selected design methods, see Figure 7.21a. In the menu “Graphs” the user can create the interaction diagrams according to the design models presented in this study, see Figure 7.21b. The software provides a message box with the information about the flexural and shear diagonal cracking loads. Besides, information about the intermediate calculation such as the depth of neutral axis, distance of the application point of the resultant compressive force to the neutral axis, strains in reinforcements and maximum strain in masonry, the maximum bending moment resisted by the wall or beam section, the maximum shear force resisted by the wall or beam, the separated contribution of each resisting mechanism for the shear strength and finally the failure mode, see Figure 7.22. It is still possible to evaluate the equilibrated condition of a section with a given applied bending moment lower than its flexural capacity.

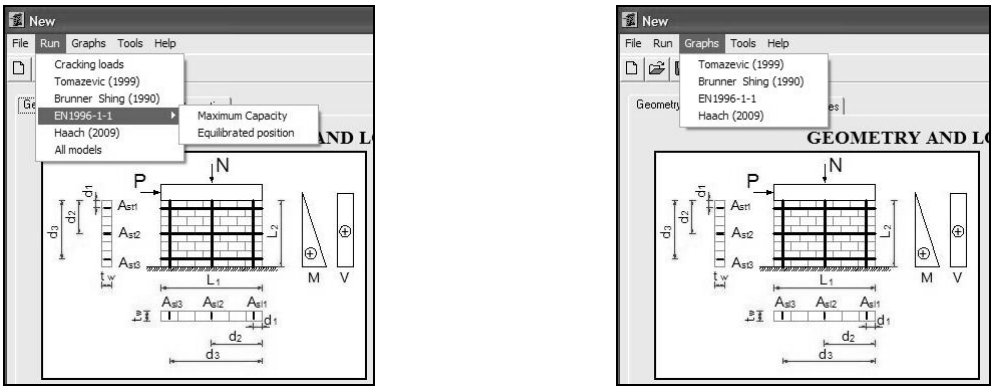

Figure 7.21 – Menus “Run” and “Graphs” of the software *RMW*.

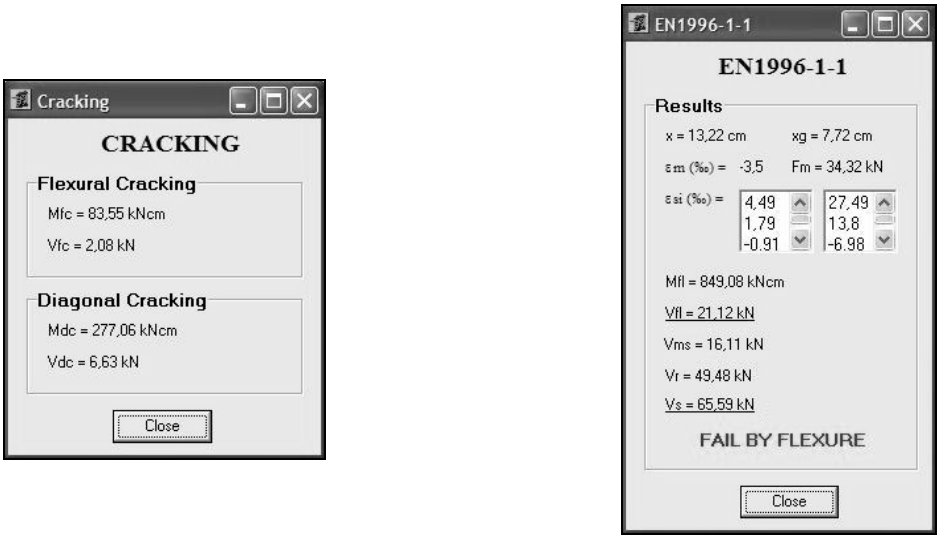

Figure 7.22 – Message boxes with the results of the software *RMW*.

Finally, the software provides also interaction diagrams, see Figure 7.23, which define a line representing the maximum capacities of the reinforced masonry wall or beams in terms of bending moments and shear forces for different levels of normal forces. They are envelop diagrams of all possible combination of bending moments and axial forces and of shear resistance and normal forces. The point represented in Figure 7.23 represents the internal forces acting on the structural masonry element as defined in the entrance data. If the point is inside the region delimited by the interaction diagrams the reinforced masonry wall is in safe state. The doted interaction diagram V x N results by dividing the interaction diagram M x N by the lever arm of the concentrated load, *z*, and represents the lateral resistance of the masonry walls associated to the flexural resisting mechanism. The continuous line represents the interaction diagram V x N corresponding to the shear resisting mechanism.

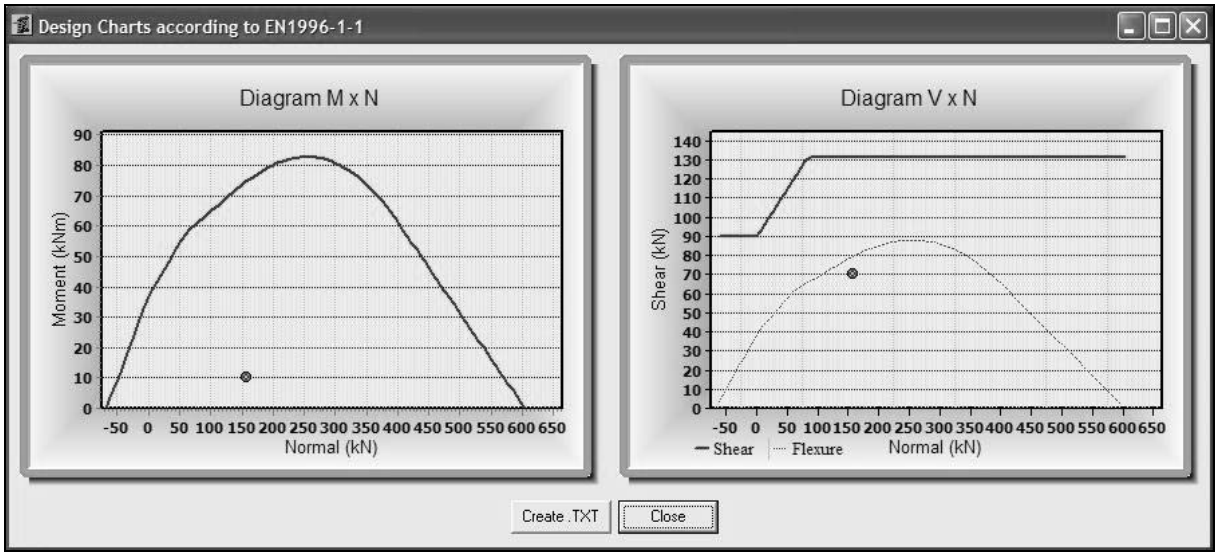

Figure 7.23 – Interaction diagrams calculated by the software *RMW*.

7.5 Design of Masonry walls and beams

In order to exemplify the application of the software *RMW* and design method proposed in this research an elastic and linear structural analysis and design of a masonry building is presented.

A building with seven floors, roof, elevator room and water reservoir was considered by adapting the example presented in Ramalho and Côrrea (2003) to the structural solution of masonry walls and beams with the traditional masonry bond pattern and real scale three cell concrete units, see Figure 7.24 and Figure 7.25.

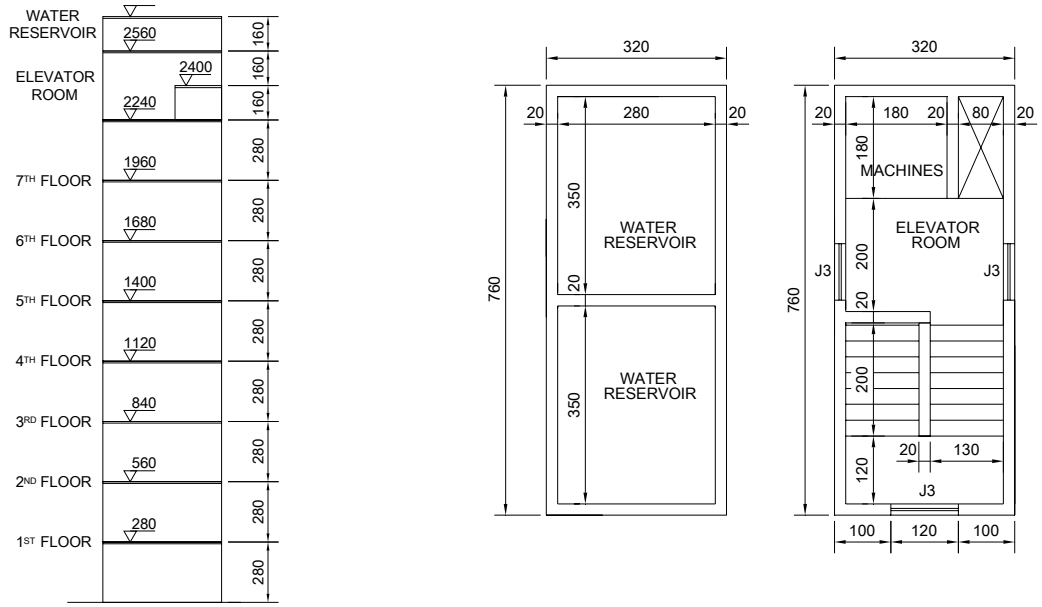

Figure 7.24 – Vertical layout and plan view of water reservoir and elevator room of the building (Ramalho and Côrrea, 2003 - dimensions in cm).

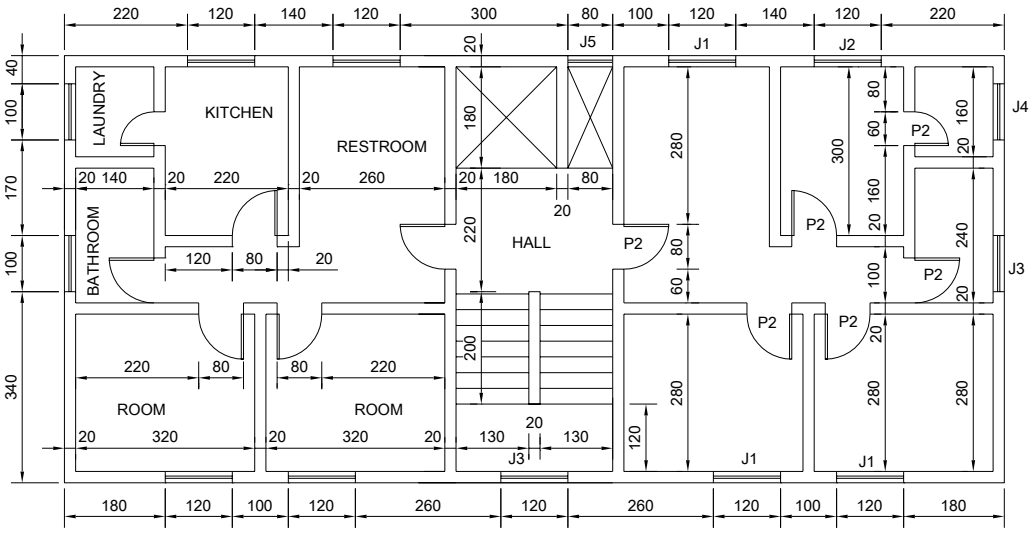

	Length	Height	Sill
J1	120	120	100
J2	120	100	120
J3	100	60	160
J4	100	120	100
J5	60	120	100
P1	60	220	-
P2	80	220	-

Figure 7.25 – Plan view of typical floor of the building (Ramalho and Côrrea, 2003 - dimensions in cm)

The methodology for the design is composed of two phases: (1) obtaining the internal efforts of masonry walls and beams based on the global analysis of the building; (2) design of masonry walls and beams through the software *RMW*. The obtaining of the internal efforts requires the calculation of the load combinations and the numerical modelling of the building.

For the structural design all walls defined in the architecture were considered to be in structural masonry.

7.5.1 Calculation of the external loading

7.5.2 Vertical loading

The vertical loading in general use buildings encompasses mainly dead and live loads. The dead load assumes a permanent character and refers essentially to the weight of the structural and non-structural elements such as walls, floors, roofs and finishing materials. The calculation of the dead loads can be made by using information about the density of construction materials (concrete, mortar, masonry), which is available in technical documents. In this work, the vertical loading was defined according to Eurocode 1 – Part 1 (2001). Concrete slabs reinforced in two directions casted in place were considered in design with density equal to 25kN/m^3 and with a covering layer corresponding to a permanent vertical load of 1.0kN/m^2. Stairs were considered to be supported on the lateral walls corresponding to a vertical load of 2.0kN/m^2. The concrete blocks of the structural masonry walls have a self weight of 20kg. Considering a mortar covering of 5mm on both sides of wall a total self weight for the walls of 8.0kN/m was taken into account. Besides, live loading was also considered according to the Portuguese Standard RSA (1983). Vertical loading was distributed from slabs to the structural walls through the yield lines method, see Figure 7.26. Table 7.4 and Table 7.5 summarize the geometry and vertical loads on each slab.

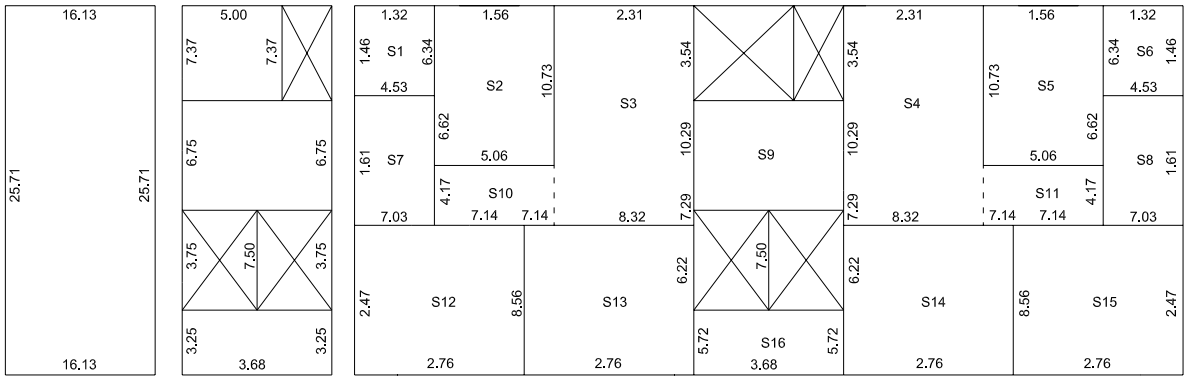

(a) (b)

Figure 7.26 – Reactions of slabs in walls: (a) typical floor and (b) elevator room and water reservoir.

Table 7.4 – Loading and geometrical properties of elevator room and water reservoir.

Slab	Geometry			Loading (kN/m^2)				
	Lx (cm)	Ly (cm)	Thick. (cm)	Self-weight	Live loading	Covering	Non-load-bearing masonry	Total
Machines	200.0	190.0	10.0	2.5	5.5	1.0	-	10.0
Elevator room	300.0	220.0	8.0	2.0	1.5	1.0	-	4.5
Bottom of water reservoir	300.0	740.0	10.0	2.5	14.0	1.0	0.5	18.0
Cover of water reservoir	300.0	740.0	8.0	2.0	0.5	1.0	0.0	3.5

Table 7.5 – Loading and geometrical properties of typical floors.

Slab	Geometry			Loading (kN/m^2)				
	Lx (cm)	Ly cm)	Thick. (cm)	Self-weight	Live loading	Covering	Non-load-bearing masonry	Total
S1 = S6	160.0	180.0	8.0	2.0	1.5	1.0	-	4.5
S2 = S5	240.0	320.0	8.0	2.0	1.5	1.0	-	4.5
S3 = S4	280.0	440.0	8.0	2.0	1.5	1.0	-	4.5
S7 = S8	160.0	260.0	8.0	2.0	1.5	1.0	-	4.5
S9	300.0	220.0	8.0	2.0	1.5	1.0	-	4.5
S10 = S11	240.0	120.0	8.0	2.0	1.5	1.0	-	4.5
S12 = S13 S14 =S15	340.0	300.0	8.0	2.0	1.5	1.0	-	4.5
S16	300.0	130.0	8.0	2.0	2.0	1.0	-	5.0
stairs	150.0	200.0	-	2.0	2.0	1.0	-	5.0

7.5.3 Horizontal loading

The main horizontal loading acting in a building is wind and seismic forces. Eurocode 1 – Part 4 (2004) and Eurocode 8 (2003) were the European standards used to evaluate wind and seismic actions on masonry buildings respectively. Besides, the Portuguese Standard RSA (1983) was also considered to obtain wind and seismic national parameters.

7.5.3.1 Wind actions

Wind actions act directly as pressures on the external surfaces of enclosure walls, resulting in forces normal to the surface of the structure. In general, the wind action is simply represented by pressures or forces whose effects are equivalent to the extreme winds. Wind forces act on the building were calculated according to the national code for calculation of building actions (Portuguese Standard RSA, 1983) through Eq. 7.27.

$$F_w = \delta_f h_1 d_k p_w \quad \text{Eq. 7.27}$$

Where, δ_f is the force coefficient which depends on the shape of building, h_1 is the height of the building, d_k is the dimension of building perpendicular to the wind load direction to be considered and p_w is the dynamic pressure of wind.

According to RSA (1983), the building under study is considered to be in zone B, with soil roughness of type I, which lead to calculus of dynamic pressure through Eq. 7.28.

$$p_w = 0.7356 v^2 \quad \text{Eq. 7.28}$$

$$v = 18\left(\frac{h}{10}\right)^{0.28} + 14 \quad \text{Eq. 7.29}$$

Where, v is the wind velocity and *h* is the height above ground.

Table 7.6 presents the resultant of wind forces to be applied at each floor of the building. Here, F_{wx} and F_{wy} are the wind forces acting according to the axis presented in Figure 7.25 and results from dynamic pressure applied to the surface multiplied by the effective area. The area is calculated by multiplying the storey height by the length of the building. The force coefficient was considered equal to 1.35, in case of wind acting in the direction perpendicular to the biggest side of building and equal to 1.00, in case of wind acting in direction perpendicular to the smallest side of building.

Table 7.6 – Wind forces acting at each floor of building.

Height (cm)	F_{wx} (kN)	F_{wy} (kN)
280	11.08	33.06
560	13.44	40.11
840	15.18	45.30
1120	16.62	49.59
1400	17.86	53.30
1680	18.97	56.62
1960	19.99	59.64
2240	22.42	31.22
2560	18.79	10.01
2720	6.40	3.41

7.5.3.2 Seismic loading

The seismic loading is the result of horizontal and vertical ground movements due to earthquake inducing inertial forces in the structure, which are related to the distributions of

mass and rigidity. For simplicity, earthquake loading can be represented by equivalent static forces if the response to seismic actions is not affected significantly by the contribution of vibration modes other than the first mode of vibration. According to Eurocode 8 (2003) the seismic action can be represented by the response spectrum defined in terms of ground acceleration designated by elastic response spectrum. The horizontal static forces equivalent to the seismic action is described by two independent orthogonal components represented by the same response spectrum. This simplified approach requires that the building fulfil the requirements of geometric regularity both in side and plan views (Eurocode 8, 2003).

The elastic response spectrum is a plot of the peak response (displacement, velocity or acceleration) of a series of single degree of freedom systems of variable natural frequency, which are forced to vibrate by the same base vibration. The elastic response spectra given by the codes are obtained from different accelerograms, and are differentiated on the basis of the soil characteristics and structural damping. Thus, the response spectrum depends on the localization of the building, type of soil and of the damping coefficient of the structure. Each seismic region has associated a certain local seismic hazard, which is described by the peak ground acceleration (PGA). The Portuguese territory is divided in different seismic zones. The new version of the national annex of the European code presents a novel seismic region distribution according to the two types of seismic action corresponding to near and distant seismic sources, see Figure 7.27. For near seismic action, three seismic zones are considered with a maximum peak ground acceleration of 0.17g (seismic zone 1), of 0.11g for seismic zone 2 and of 0.08g for seismic zone 3, Table 7.7. For distant seismic zones, five zones are considered, being the peak ground acceleration in Zone 1 of 0.25g, 0.20g for the seismic zone 2, of 0.15 for the seismic zone 3, 0.10g for the seismic zone 4 and finally for the seismic zone 5 of 0.05g, see Table 7.8.

(a) (b)

Figure 7.27 – Zoning for seismic action with a return period of 475 years: (a) near action and (b) distant action.

Table 7.7 – Peak ground acceleration for near seismic action.

Zones	a_g (cm/s^2)	T_B (s)	T_C (s)	T_D (s)
1	170	0.10	0.25	2.00
2	110			
3	80			

Table 7.8 – Peak ground acceleration for distant seismic action.

Zones	a_g (cm/s^2)	T_B (s)	T_C (s)	T_D (s)
1	250	0.10	0.60	2.00
2	200			
3	150			
4	100			
5	50			

For the horizontal components of the seismic action the design spectrum, $S_d(T)$, is defined by the following expressions:

$$0 \le T \le T_B \rightarrow S_d(T) = a_g S\left[\frac{2}{3} + \frac{T}{T_B}\left(\frac{2.5}{q} - \frac{2}{3}\right)\right] \quad \text{Eq. 7.30}$$

$$T_B \le T \le T_C \rightarrow S_d(T) = a_g S \frac{2.5}{q} \quad \text{Eq. 7.31}$$

$$T_C \le T \le T_D \rightarrow S_d(T) = a_g S \frac{2.5}{q}\left[\frac{T_C}{T}\right] \ge \beta a_g \quad \text{Eq. 7.32}$$

$$T_D \le T \rightarrow S_d(T) = a_g S \frac{2.5}{q}\left[\frac{T_C T_D}{T^2}\right] \ge \beta a_g \quad \text{Eq. 7.33}$$

Where, T is the vibration period of a linear single-degree-of freedom system, a_g is the design ground acceleration on type A ground ($a_g = \gamma a_{gr}$), S is the soil factor, a_{gR} is the reference peak ground acceleration, γ is the importance factor, q is the behaviour factor and β is the lower bound factor for the horizontal design spectrum, recommended to be equal to 0.2, T_B and T_C, are the lower and upper limits of the period of the constant spectral acceleration branch and T_D is the period defining the beginning of the constant displacement response range of the spectrum.

The fundamental period of vibration of the building can be calculated based on the Rayleigh method, by considering the first mode shape, or in buildings with total height up to 40m, it can be approximated by the following expression:

$$T = 0.05H^{3/4} \quad \text{Eq. 7.34}$$

Where, H is the height of the building, in m, from the foundation or from the top of a rigid basement.

The use of the behaviour factor, q, aims at considering in a simplified manner the material non-linear behaviour. Note that all the ordinate of the response spectra are reduced by the behaviour factor, leading to the obtaining of the design response spectra.

After the definition of the response spectrum, the base shear forces to perform an elastic structural analysis are calculated from Eq. 7.35.

$$F_{sa} = S_d(T)m\lambda \quad \text{Eq. 7.35}$$

Where, $S_d(T)$ is the ordinate of the design spectrum at period T, m is the total mass of the building above the foundation, λ is the correction factor to takes into account the lesser effective modal mass of the 1st fundamental mode (on average by 15% than the total building mass).

The weight considered to calculate the seismic actions should be calculated by the combination of permanent, $G_{k,j}$, and variable actions, $Q_{k,i}$ see Eq. 7.36.

$$\sum G_{k,j} + \sum \psi_{E,i} Q_{k,i} \quad \text{Eq. 7.36}$$

Where, $\psi_{E,I}$ is the combination coefficient for variable action i.

When the fundamental shape is approximated by horizontal displacements increasing linearly along the height of the building, the horizontal forces F_{sai} should be taken as being given by Eq. 7.37.

$$F_{sai} = F_{sa} \frac{w_i z_i}{\sum w_i z_i} \quad \text{Eq. 7.37}$$

Where, w_i is the weigth in i-storey and z_i is the height of the i-storey.

The horizontal forces calculated according to Eq. 7.37 shall be distributed to the lateral load resisting system assuming that the floors are rigid in their plane. In this study the building was considered to be localized at North of Portugal, in zone 3 and 5 for near and distant seismic actions respectively. A correction factor, λ, of 0.85 is considered. A behaviour factor of 2.5 is adopted as reinforced masonry system is foreseen. The soil factor S is

considered to be equal to 1.0. The masonry building in analysis presents a fundamental period equal to 0.60, which leads to values of S_d equal to 33.33 cm/s^2 and 50 cm/s^2 for near and distant seismic actions. Table 7.9 presents the seismic forces acting at the distinct levels of building.

Table 7.9 – Seismic forces acting in different levels of building.

Height (cm)	Weigth (kN)	Close action (kN)	Distant action (kN)
280	1272.82	7.63	11.44
560	1272.82	15.26	22.89
840	1272.82	22.89	34.33
1120	1272.82	30.51	45.78
1400	1272.82	38.14	57.22
1680	1272.82	45.77	68.66
1960	1272.82	53.40	80.11
2240	1010.98	48.47	72.72
2560	582.51	31.92	47.89
2720	119.14	6.94	10.41

7.5.4 Actions combinations

For the calculation of the internal efforts in masonry structural elements three load combinations were considered according to RSA (1983). The first load combination considered the live load as the as the main variable action, see Eq. 7.38. The second combination considered wind load as the main variable action, see Eq. 7.39. Finally, the last combination considered seismic forces as the main variable action, see Eq. 7.40. Only seismic forces for the distant action were considered in analysis since it was the more unfavourable.

$$S_d = 1.5S_{Gk} + 1.5\left(S_{Qk} + 0.6S_{Wk}\right) \quad \text{Eq. 7.38}$$

$$S_d = 1.5S_{Gk} + 1.5\left(S_{Wk} + 0.7S_{Qk}\right) \quad \text{Eq. 7.39}$$

$$S_d = S_{Gk} + 1.5S_{Ek} + 0.4S_{Qk} \quad \text{Eq. 7.40}$$

Where, S_d is design action, S_{Gk} is the characteristic value of permanent actions, S_{Qk} is the characteristic value of live load, S_{Wk} is the characteristic value of wind actions and S_{Ek} is the characteristic value of seismic actions.

Each actions combination was considered in direction *x* and in direction *y*. In direction y, horizontal loads were applied with positive and negative sign since in this axis the analyzed building is not symmetrical.

7.5.5 Structural analysis

Structural analysis was performed through the representation of the building by a 3D-frame, see Figure 7.28. In this type of analysis masonry walls are represented by 3D bars positioned at gravity center of the wall. Rigid bars connect the walls that intersect themselves in the plane of each floor in order to ensure the interaction between them. Masonry beams are also represented by simple bars connecting the groups of walls, see Figure 7.29.

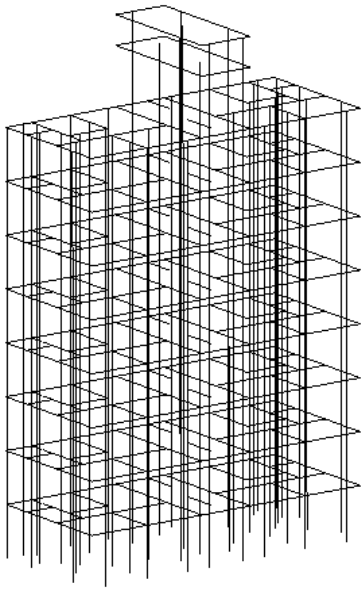

Figure 7.28 – 3D-frame representing the masonry building.

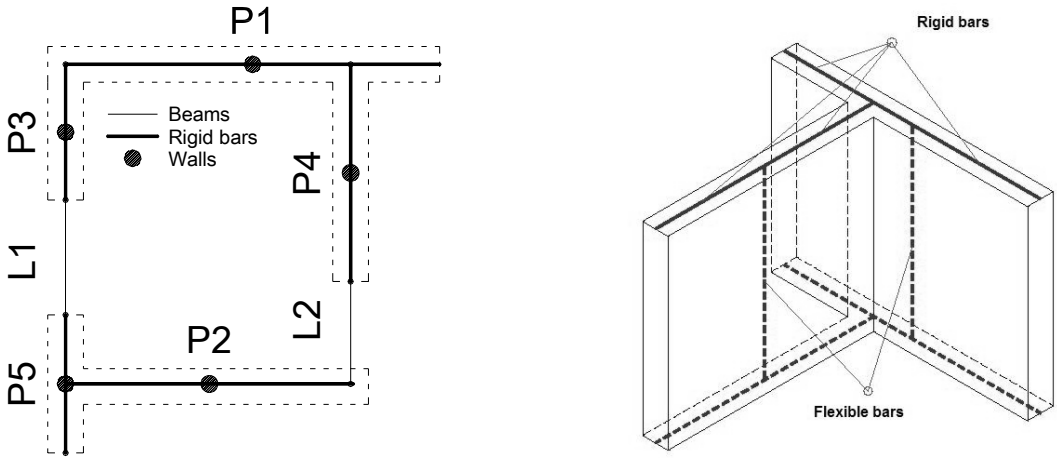

Figure 7.29 – Representation of rigid and flexible bars. (Nascimento, 1999).

All bars were represented by beam elements with 6 degree of freedom per node. The transverse displacement for these elements is a cubic Hermite shape function expressed in the nodal displacements and rotations. It is assumed that the cross sections remain plane and perpendicular to the slope of the beam axis. Therefore these beam elements may be viewed as based on the Bernoulli theory. Shear deformation was taken into account according to the theory of Timoshenko, assuming a constant shear stress distribution along a cross-section. In order to consider the slab as a rigid diaphragm, all nodes in each floor were tied to a master node located in the geometrical center of the building. Horizontal forces were applied in the master node at the level of each floor.

Bars representing walls and masonry beams were considered with the real geometrical properties. Transversal section of rigid bars was considered with the thickness of the walls and with the ceiling height as suggested by Ramalho and Corrêa (2003). The elastic modulus of 2.77GPa was considered for all bars since according to Eurocode 6 (2005) this value corresponds to a masonry composed of units with compressive strength of 5.0MPa and mortar with a compressive strength of 10.0 MPa.

7.5.6 Internal forces

The numerical modelling of the 3D-frame of the building provides the normal, shear forces and bending moments in all bars of the building for the three load combinations. The walls and beams of the masonry building were named as shown in Figure 7.30.

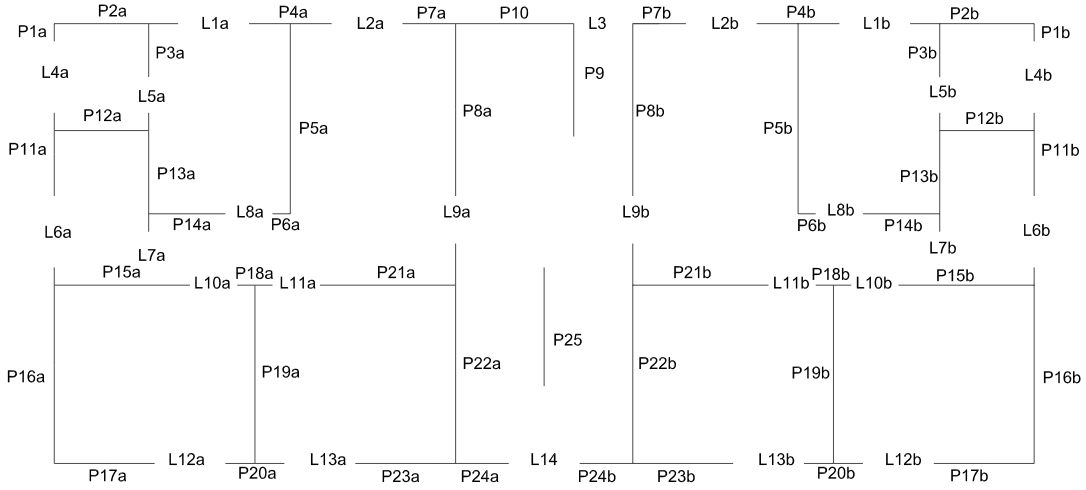

Figure 7.30 – Name of the walls and beams of masonry building.

The complete results of the walls and beams are presented in Appendix B. After the attainment of the internal forces, namely the axial force, *N*, the bending moment, *M*, and the

shear force, *V*, structural masonry walls and beams can be designed by considering the three combinations previously presented.

As the design of the masonry structural elements is repetitive, it was decided to present the example of only one wall and one beam in order to exemplify the design procedure. For the design of the masonry elements the following mechanical material properties were admitted:

- Compressive strength of unit: 5.0 MPa.
- Compressive strength of mortar: 10.0 MPa.
- Compressive strength of masonry perpendicular to bed joints: 2.77 MPa.
- Compressive strength of masonry parallel to bed joints: 1.39 MPa.
- Tensile strength of masonry: 0.40 MPa.
- Flexural strength of masonry: 0.10 MPa
- Friction coefficient of joints: 0.40.
- Cohesion of joints: 0.20 MPa.
- Yield strength of reinforcements: 700 MPa
- Safety factor for masonry: 2.0
- Safety factor for reinforcements: 1.15

7.5.6.1 Design of a masonry wall

Wall P16 was chosen to exemplify the design procedure for shear walls since it is in general, one of the walls with the highest moment, normal and shear forces. The internal forces considered more unfavourable were obtained for the load combination where the seismic action was the main variable load, see

Table 7.10 to Table 7.12.

Table 7.10 – Axial forces in wall P16 for lateral load applied in y-direction (kN).

Wall	BASEMENT	1ST FLOOR	2ND FLOOR	3RD FLOOR	4TH FLOOR	5TH FLOOR	6TH FLOOR	7TH FLOOR
P16a	-246	-219.6	-194.8	-169	-140.8	-109.2	-73.76	-34.29
P16b	-244.7	-218.5	-193.8	-168.2	-140.2	-108.8	-73.46	-34.17

Table 7.11 – Shear forces in wall P16 for lateral load applied in negative y-direction (kN).

Wall	BASEMENT	1ST FLOOR	2ND FLOOR	3RD FLOOR	4TH FLOOR	5TH FLOOR	6TH FLOOR	7TH FLOOR
P16a	-57.55	-58.95	-56.7	-52.24	-45.81	-37.43	-26.79	-12.82
P16b	-57.55	-58.94	-56.68	-52.22	-45.78	-37.39	-26.75	-12.77

Table 7.12 – Bending moments in wall P16 for lateral load applied in negative y-direction (kNcm).

Wall	BASEMENT	1ST FLOOR	2ND FLOOR	3RD FLOOR	4TH FLOOR	5TH FLOOR	6TH FLOOR	7TH FLOOR
P16a	-19250	-14800	-12020	-9654	-7418	-5258	4326	2346
P16b	-19250	-14800	-12020	-9652	-7414	-5254	4321	2336

The entrance of data in software *RMW* regarding wall P16, corresponding to the section of the basement, is presented in Figure 7.31.

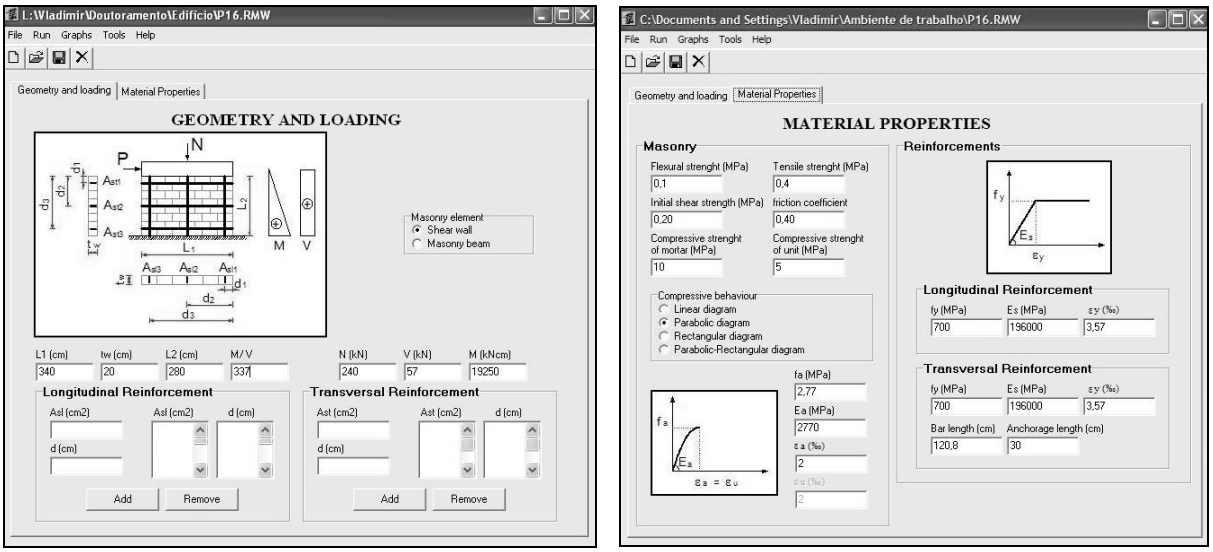

(a) (b)

Figure 7.31 – Entrance of data of wall P16 in software *RMW*; (a) geometry data; (b) mechanical properties of materials

The flexural cracking bending moments calculated from Eq. 4.15. for wall P16 are indicated in Table 7.13. Results indicate that at the basement and 1st floor acting moments are higher than resisting bending moments, meaning that flexural cracking occur. This result indicated that vertical reinforcement can be added in order to avoid this type of cracking.

Table 7.13 – Flexural cracking moments for lateral load applied in negative y-direction (kN.cm).

Wall	BASEMENT	1ST FLOOR	2ND FLOOR	3RD FLOOR	4TH FLOOR	5TH FLOOR	6TH FLOOR	7TH FLOOR
P16a	15345	13893	12529	11110	9559	7821	5872	3701
P16b	15274	13833	12474	11066	9526	7799	5855	3694

If the minimum vertical reinforcement ratio suggested by Eurocode 8 (2003) to be used in seismic regions of 0.08%, which is equivalent to a reinforcement area of 5.44cm^2, is applied in the wall, the flexural cracking can be avoided. Considering the pre-fabricated reinforcements used in this study, 15 trussed-bars with 5mm-diamater should be applied in wall P16 according to Figure 7.32. The flexural strength of the reinforced wall can be calculated through Eq. 7.12 to Eq. 7.16 according to the flexure theory. In Figure 7.33 information on the position of neutral line (x), the compressive force in masonry (F_m) and its position in masonry section (x_g) and strains and forces in reinforcements is indicated. It is observed that by adding the minimum vertical reinforcement to the wall, its flexural resisting moment increases considerably.

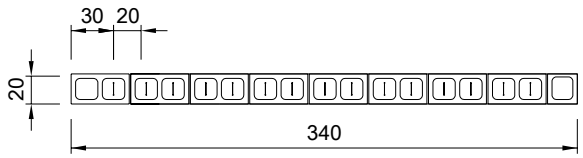

Figure 7.32 – Vertical reinforcements in wall P16.

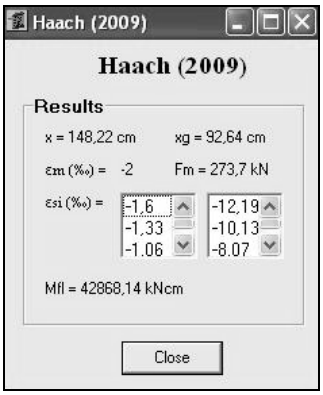

Figure 7.33 – Results of software *RMW* for the flexural design of wall P16 at the basement.

The interaction diagrams NxM and VxN given by software *RMW* for the wall P16 with the vertical reinforcement previously considered are indicated in Figure 7.34.

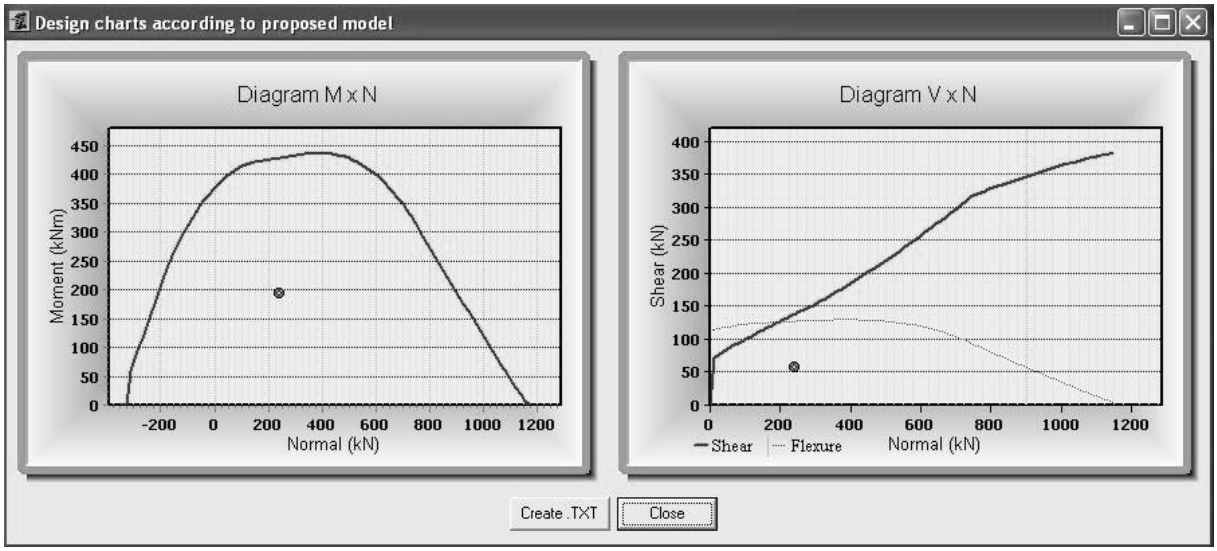

Figure 7.34 – Interaction diagrams M x N and V x N of wall P16

It can be seen that lateral resistance is ruled by shear up to a normal force of approximately 200kN, after which the lateral resistance is governed by flexure resisting mechanism. The results indicate also that no horizontal reinforcement is needed for the global stability of the walls as the shear internal force is considerably lower than the shear resistance. These results indicate that maybe unreinforced masonry can also be a structural solution in regions with moderate to low seismic hazard.

The interaction diagrams MxN and VxN for wall P16 reinforced at bed joints with the minimum horizontal reinforcement suggested by Eurocode 8 (2003) and Eurocode 6 (2005) of 0.05% for masonry walls in seismic areas are presented in Figure 7.35 . This horizontal reinforcement ratio is equivalent to an area of 2.80cm^2 .Considering the pre-fabricated

reinforcements used in this study, 7 trussed-bars with 5mm diameter with vertical spacing of two courses should be applied in wall P16. In this case, the lateral resistance of the wall is always controlled by the flexural resisting mechanism. It is seen that the shear envelop is always above the flexural envelop. This is the result of the increase on the shear resistance of the wall by the addition of the horizontal reinforcement.

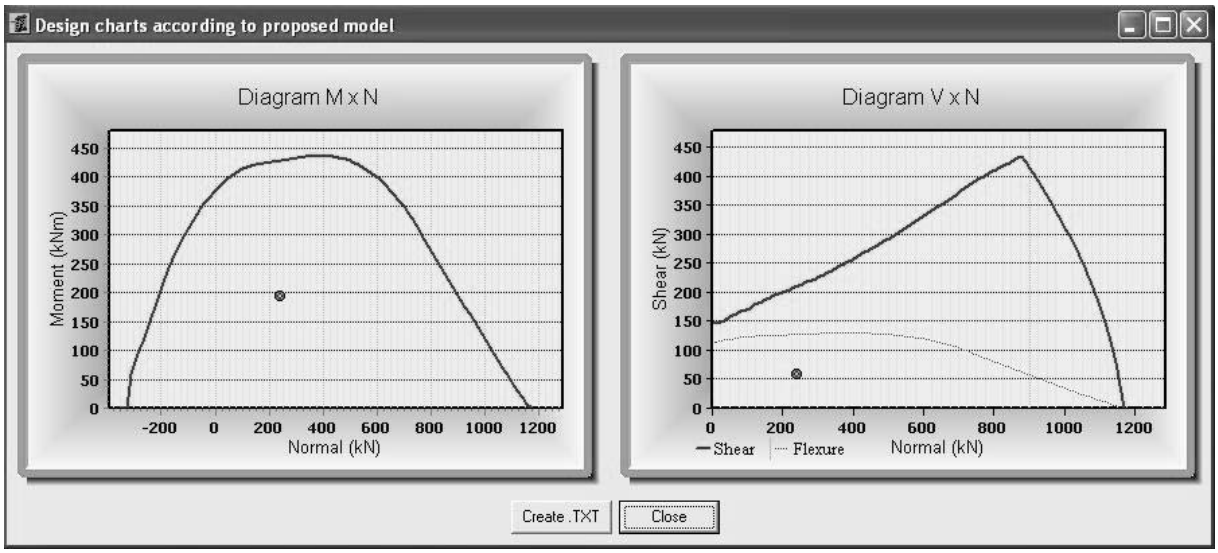

Figure 7.35 – Interaction diagrams M x N and V x N of masonry wall P16 with horizontal reinforcement provided by software RMW.

7.5.6.2 Beam

Masonry beam L2 was chosen to exemplify the design procedure for masonry beams. As in case of shear walls, the more unfavourable internal forces were associated to load combination which the seismic action was the main variable action. For masonry beam L2, the horizontal load acting in x-direction is predominant. Under this load combination the beam L2 is subjected to the internal forces presented in Table 7.14. Masonry beams are not subjected to axial forces since all nodes at level of each floor was considered with the same x- and y- displacements in order to ensure the consideration of rigid diaphragm to slabs.

Table 7.14 – Shear forces and moments in beam L2 for lateral load applied in x-direction with seismic forces as the main action.

Beam	1ST FLOOR		2ND FLOOR		3RD FLOOR		4TH FLOOR		5TH FLOOR		6TH FLOOR		7TH FLOOR		ROOF	
	M (kNcm)	V (kN)	M (kNcm)	V (kN)	M (kNcm)	V (kN)	M (kNcm)	V (kN)	M (kNcm)	V (kN)	M (kNcm)	V (kN)	M (kNcm)	V (kN)	M (kNcm)	V (kN)
L2a	-3449	-42.17	-2484	-33.99	-2530	-34.78	-2464	-33.9	-2372	-32.44	-2316	-31.33	-2415	-32.37	-565.7	-11.68
L2b	4259	-49.43	5169	-60.2	5127	-61.04	4679	-57.15	3983	-50.25	3132	-41.43	2311	-32.53	445.6	-8.56

Entrance of data in software *RMW* of beam L2 regarding the internal forces recorded in 1st floor is presented in Figure 7.36. Considering that this window has a height equal to 120 cm and the ceiling height of the building is 280 cm, the height of beam L2 is the difference between these two values. Thus, the beam L2 has a section with 160 cm x 20 cm. Considering the material properties, the bending moment which generates the flexural cracking can be calculated through Eq. 4.15. As no axial force acts in beam, the bending moment that generates the flexural cracking is the same for all floors and equal to 426.67 kNcm.

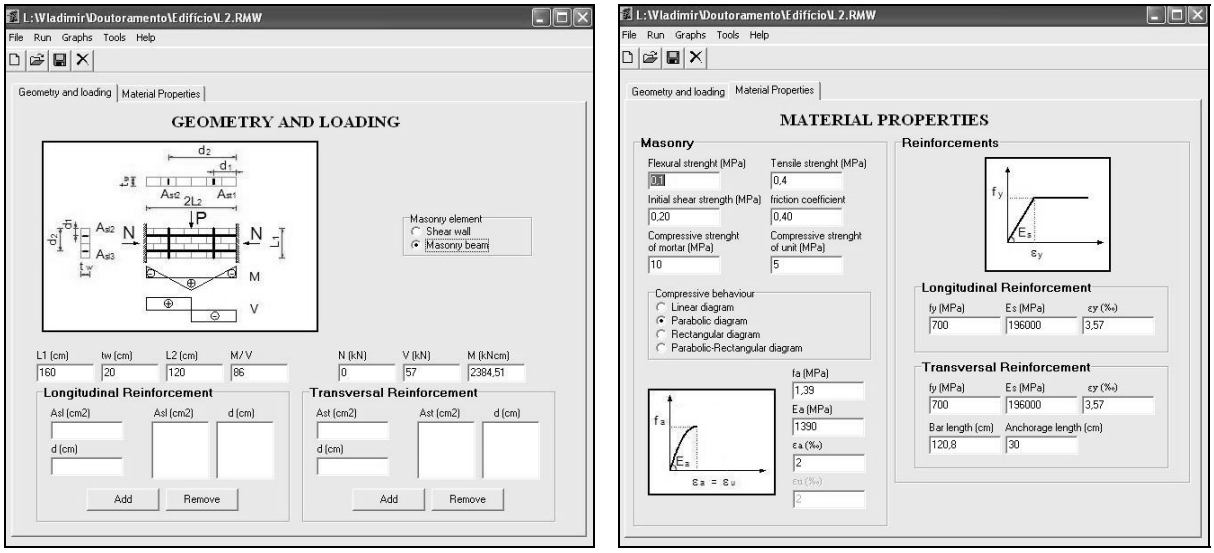

Figure 7.36 – Entrance of data of beam L2 in software *RMW*.

Observing the acting bending moments in beam L2 in all floors presented in Table 7.14 it is seen that moment of flexural cracking is very low and the beams should be reinforced. Considering the minimum reinforcement suggested by Eurocode 8 (2003), 1.6cm^2 of horizontal reinforcement should be applied in beam L2. Considering the pre-fabricated reinforcements used in this study, 4 trussed bars with 5mm diameter with spacing of two courses should be applied. The flexural strength of the masonry beam may be simply calculated through the classic theory of flexure through Eq. 7.12 to Eq. 7.16. Reinforced masonry beam resist to a bending moment equal to 5756.53 kNcm. On the other hand, the diagonal shear cracking load and thus the shear resistance of unreinforced masonry beam calculated by Eq. 7.17 and the flow chart of Figure 7.8 is equal to 7.69 kN, which is lower to the internal shear forces. Thus, vertical reinforcement should be added to the beam L2 to resist the shear forces. Shear generates diagonal cracking in beams as shown in Figure 7.37. The introduction of vertical reinforcements provides the control of diagonal cracks and allows the development of shear strength in vertical joints. Thus, low vertical reinforcement ratios generate a high increasing in shear strength. Considering the pre-fabricated

reinforcements used in this study, 2 trussed-bars with 3mm-diamater with spacing showed in Figure 7.37 increased the resisted shear force to 143.53 kN, see Figure 7.38.

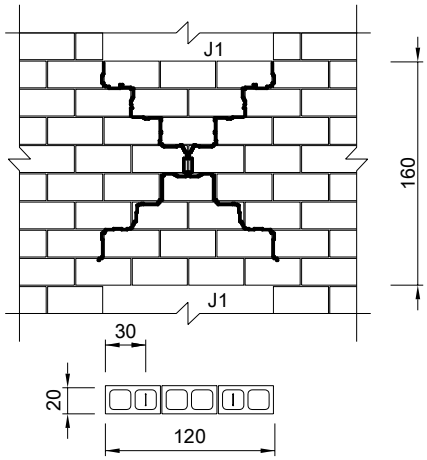

Figure 7.37 – Diagonal cracking in beam L2 and reinforcement to be applied.

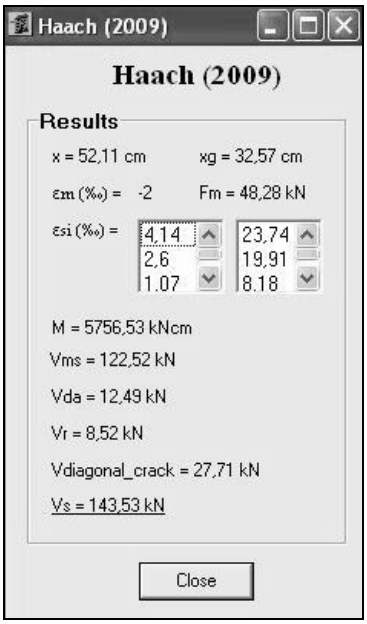

Figure 7.38 – Design of beam L2 through software *RMW*.

7.6 Summary and conclusions

Based on experimental and numerical analysis a new design method for masonry elements subjected to in-plane loading was proposed. This model is considered to be an adaptation of the Brunner and Shing's model (Brunner and Shing, 1996). The design method considers the coupling behaviour between flexure and shear in masonry elements. Flexure is evaluated through the classic theory of flexure. In case of unreinforced masonry walls, the shear resistance is assumed to be equal to the diagonal cracking shear force assuming masonry as a homogeneous and isotropic material and calculated based on the theory of elasticity. For reinforced masonry walls and beams a Mohr-Coulomb criterion is adopted to describe the shear resisting mechanism and only the compressed part of the walls and beams is considered for the calculation of the contribution of masonry the shear resistance. The compressed part of masonry is calculated based on the equilibrium of the section through the classic theory of flexure.

The analytical method proposed was compared with three other analytical methods presented in literature review. The accuracy of three design models for masonry walls was evaluated and compared through the application of the models to a database composed of

101 walls. The proposed model presents a better performance than the other analytical models when a comparison is made between the experimental and analytical lateral resistance.

A Windows® application was developed to verify in a fast simple manner the capacity of sections of unreinforced and reinforced masonry walls. The software evaluates sections of reinforced masonry elements subjected to in-plane loading through four different analytical models: Tomaževič's analytical model (Tomaževič, 1999), Eurocode 6 (2005), Brunner and Shing's model (Brunner and Shing, 1996) and the analytical model proposed in this research. Besides, software provides also the shear and flexural cracking loads and interaction diagrams MxN and VxN. Finally, an example of design of a masonry building is presented in order to exemplify the use of the software *RMW*.

8 CONCLUSION AND FINAL REMARKS

8.1 Conclusion

The very complex behaviour of masonry structures under in-plane loading observed by other researchers could be confirmed in the present work. Besides the anisotropic behaviour of masonry, the bi-axial stress state to which they are subjected becomes shear walls and beams structures an object for scientific research in the field of civil engineering. This work aimed at contributing to the advance on the understanding of reinforced masonry structures subjected to lateral loading. In the author's point of view, this work contributed to achieve a better insight on the in-plane behaviour of masonry walls and beams and to clarify the influence of distinct parameters such as the presence of vertical and horizontal reinforcements, reinforcement ratios, boundary conditions, pre-compression level and masonry bond pattern. The work was divided in an enlarged experimental and numerical analysis of shear walls and masonry beams aiming at combining the main results for the development of a new analytical method for the design of reinforced masonry walls and beams.

8.1.1 Characterization of materials

The characterization of materials plays an important role on the accurate analysis of experimental results of masonry walls and beams. Besides, the results of this chapter are fundamental for the numerical analysis as the mechanical properties of masonry and masonry materials are mandatory. Finally, the mechanical properties of materials are the fundamental data if the design of the structural masonry elements under in-plane loading is required. Regarding the characterization of materials it was possible to formulate the following conclusions:

a) The compressive test carried out on masonry wallets in the direction parallel to shells of the concrete blocks appeared to be an interesting alternative experimental method to obtain the tensile strength of the units. When the unit is under this type of compressive loading, tensile stresses develop in the central web of units. The diagram stress *vs.* strain in this tests presented two distinct phases. In first phase webs and shells resist the stresses as a conjunct. When the central web reaches the tensile strength of unit, a peak of deformation occurs and after that only the shells of unit resist the stresses;
b) The equal displacements measured in the middle of a concrete unit and in one vertical joint in compressive tests normal to bed joints confirmed the homogeneous behaviour of masonry. Results of these tests indicated that the compressive behaviour of masonry normal to bed joints follows a parabolic behaviour as in case of concrete under compression;
c) In case of compressive strength of masonry parallel to bed joints the parabolic behaviour was not observed. In these tests a very ductile behaviour was observed mainly in specimens built with three cell concrete blocks since in this case the masonry was built without filling of vertical joints. Compressive strength of masonry parallel to bed joints presented lower values when compared with compressive strength perpendicular to bed joints;
d) The equation proposed for Eurocode 6 (2005) to determine the compressive strength of masonry as a function the compressive strength of unit and mortar presented good correlation with the experimental results for both loading directions;
e) In case of diagonal tests it could be concluded that the filling of vertical joints has a great influence on the tensile and shear strength of masonry. Specimens built with 2C-units and consequently with filled vertical joints presented an increase higher than 100%.

8.1.2 Experimental analysis of reinforced masonry shear walls

In experimental campaign carried out for the analysis of reinforced masonry walls under in-plane cyclic loading, geometry of units, masonry bond pattern, pre-compression level and horizontal reinforcement ratio were the variables analyzed. With the results of these tests it was possible to formulate the following conclusions:

a) Masonry bond pattern has no significant influence on the overall behavior of the reinforced walls, which means that the easier construction technology through bond pattern B2 can be a reasonable solution;
b) The vertical pre-compression influences the behavior of the reinforced concrete block masonry walls. Higher values of normal stresses are associated to higher values of lateral strength but more fragile behaviour, leading to the reduction of the reinforcement efficiency;
c) The effectiveness of the horizontal reinforcement appears to be related with the presence of vertical reinforcement. If vertical reinforcement is present, initial flexural cracking is limited, which enables the progression and development of diagonal cracking. On the other hand, it is demonstrated that the variation of the percentage of horizontal reinforcement seems not to improve the lateral strength. However, crack localization appears to be avoided by the presence of horizontal reinforcement, enabling a more smeared crack distribution and larger nonlinear lateral deformations.
d) The use of filled vertical joints seemed to improved the lateral behaviour of masonry walls. Comparing specimens N60-2C-B2 and N60-3C-B2, a very similar behaviour can be observed in terms of lateral strength and deformation capacity. However, specimens built with 2C-units have lower thickness. More researches should be carried out to confirm this hypothesis.

8.1.3 Tests in masonry beams

In masonry buildings subjected to horizontal loads masonry beams are the elements responsible for the transference of load between masonry piers in case of the existence of openings. Thus, an experimental program was defined in order to better understand the behaviour of masonry beams. With the results of these tests it was possible to formulate the following conclusions:

a) Unreinforced masonry beams present very low tensile strength and very brittle failure.
b) Horizontal reinforcement clearly improved the flexural behaviour of masonry beams by increasing its tensile strength, the ductility through remarkable increasing deformation capacity and by providing a control of cracks opening. Besides, horizontal reinforcement seems to contribute to shear strength through the dowel action mechanism, delaying the opening of diagonal cracking.

c) Vertical reinforcements increase the shear strength and provide a better distribution of cracks. However, the location of vertical bars had a fundamental influence in its contribution to resist the shear stresses.
d) Vertical reinforcement also improved the flexural behaviour of masonry beams in compressed area, producing a good control of the cracking and avoiding the splitting of units.
e) The filling of vertical mortar joints had a great influence in behaviour of masonry beams. Masonry beams built with 2C-units and consequently with the fill of vertical joints presented higher strength than similar masonry beams built with 3C-units and consequently without filling of vertical joints.

8.1.4 Numerical modelling

Based on the experimental results a numerical model using the micro-modelling approach was calibrated and a parametric analysis was carried out for shear walls and masonry beams using the software DIANA®. Aspect ratio, vertical and horizontal reinforcement ratios and masonry bond pattern were the variables analyzed. In case of shear walls, pre-compression level was also varied. With the results of these studies it was possible to formulate the following conclusions:

a) The mechanical behaviour of masonry shear walls and beams under in-plane loading appeared to be described by the same flexural and shear resisting mechanisms;
b) Failure mode of shear walls and masonry beams is highly influenced by boundary conditions. In cantilever walls and simply supported beams the flexural behaviour is preponderant flexural behaviour, whereas in fixed end walls and fixed end beams the shear behaviour takes the major role on the in-plane behavior.
c) Filling of the vertical joints has no influence in flexural behaviour of shear masonry walls. However, in case of walls with preponderance of shear behaviour the filling of vertical joints can increase the lateral strength in 20%. In case of masonry beams the filling of vertical joints improve flexural and shear behaviour.
d) Lateral strength of shear walls potentially increased with the reduction of the aspect ratio and with the increasing of pre-compression. However, when compressive stresses increase beyond 40% of the compressive strength of masonry, compressive failure takes a central role, being the lateral strength decreased considerably for higher values of the pre-compression;

e) Horizontal reinforcements increase the lateral strength of shear walls when diagonal cracks open by avoiding the separation of the wall into two parts and promoting the stress transfer between both edges of the diagonal crack. Besides, horizontal reinforcement ensures a control of the diagonal cracking and increases the deformation capacity, providing a higher ductility for the masonry wall and enables a better distribution of the stresses in the wall;
f) Vertical reinforcement increases the flexural capacity of walls. However, if shear failure predominates the introduction of vertical reinforcements can reduce the lateral strength of the wall since they increase the tensile stresses at the middle of wall. This behaviour does not occur if the walls are reinforced with horizontal bars.
g) Flexural strength of masonry beams without filled vertical joints is very influenced by the interlocking between the units.
h) In case of masonry beams, horizontal reinforcements improve the flexural behaviour by increasing the tensile strength of masonry, avoiding the premature failure though the sudden propagation of flexural cracks from the bottom edge to the top edge of the beam. As in case of shear walls, horizontal reinforcements provide the control of cracking. However, horizontal reinforcement seemed not to influence the shear strength of beams.
i) Vertical reinforcement provides an additional resistance in masonry beams after the appearance of diagonal crack and controls its opening.

8.1.5 Development of a new design method

Based on experimental and numerical results a new design method was developed considering the coupling behaviour between flexure and shear. In this proposed model, flexure is evaluated through the classic theory of flexure, whereas shear behaviour is described by a Mohr-Coulomb's failure criterion and the shear strength is obtained by an iterative method. The new proposed model can be considered as an update of the Brunner and Shing's model combined with Tomaževič's model for unreinforced masonry walls. The proposed model was validated by using it on the prediction of the lateral strength of masonry walls from a database composed of 101 masonry walls. The database was built with the results of in-plane tests available in literature. In case of masonry beams the same procedure could not be carried out due to the absence of results in literature.

8.2 Further Works

In the scope of mechanical characterization of masonry some aspects that deserve further attention are highlighted:

a) Assessment of the influence of the mortar composition on the compressive strength of masonry parallel to bed joints, in tensile strength of masonry (through diagonal tests) and in tensile and shear strength of unit-mortar interface;
b) Evaluation of the influence of reinforcements in compressive strength of masonry parallel to bed joints;
c) Evaluation of bi-axial behaviour of masonry with concrete units mainly in tension-compression;
d) Evaluation of the bond strength of pre-fabricated trussed bars used as vertical and horizontal reinforcement;
e) Detailed study for further clarification of the influence of the filling of vertical joints on the shear behaviour of masonry;
f) Evaluation of the influence of reinforcements on the shear strength of masonry by means of diagonal compressive tests.

In the scope of masonry shear wall some research orientations are highlighted:

a) Study of masonry walls reinforced only with horizontal bars;
b) Experimental assessment of the dowel action of longitudinal reinforcements on the shear behaviour of masonry walls;
c) Study of masonry walls wit H section in order to verify the influence of the transversal walls in shear behaviour;
d) Study of bond beams in behaviour of shear walls;
e) Evaluation of the in-plane behaviour of masonry walls with openings.

In the scope of masonry beams some aspects that deserve further attention are highlighted:

a) Study of masonry beams using the units with U-shape (lintel blocks) in the base of specimens;
b) Detailed of the dowel action effect provided by horizontal reinforcements;
c) Evaluation of masonry beams with low span to height ratios since they are more common in masonry buildings;
d) Study of the anchorage of vertical bars in beams;

REFERENCES

Abdou, L., Ami Saad, R., Meftah, F., Mebarki, A. (2006). “Experimental investigations of the joint-mortar behaviour”, *Mechanics research communications*, V.33, 370-384.

Abrams, D.P. (1986). “Lateral resistance of a two-story block building”, *ASCE Structures Congress*, New Orleans, USA, 41-57.

Adell, J. M.; Garcia-Santos, A.; Lauret, B.; López, C.; Martín, H.; Peña, J.; Pol, M.; Timperman, P.; Veja, S. (2008). “6m span lintels tests on a new wall PI-brackets type”, *Proceedings of 14th International Brick/block Masonry Conference*, Austin, Australia, 10pp.

Andreaus, U. (1996). “Failure criteria for masonry panels under in-plane loading”, *Journal of Structural Engineering*, V.122(1), 37-46.

Anthoine, A., Magonette, G. (1995). “Shear-compression testing and analysis of brick masonry walls”, *Proceedings of 10th European Conference on Earthquake Engineering*, Balkema, Rotterdam, Netherlands, 1657-1662.

ASSOCIAÇÃO BRASILEIRA DE NORMAS TÉCNICAS (ABNT). NBR 13279, Argamassa para assentamento de paredes e revestimentos de paredes e tetos. Determinação da resistência à compressão. Rio de Janeiro, 1995. (in Portuguese)

Asteris, P.G.; Tzamtzis, A.D. (2003). “On the Use of a Regular Yield Surface for the Analysis of Unreinforced Masonry Walls”, *Electronic Journal Of Structural Engineering*, V.3, pp.23-42.

ASTM E519-02 - Standard Test Method for Diagonal Tension (Shear) in Masonry Assemblages, 2000.

Benedetti, A.; Steli, E. (2006). “Analytical models for shear–displacement curves of unreinforced and FRP reinforced masonry panels”, *Construction and building materials*, V.22(3), 175-185.

Biggs, D. T. (2005). "Grouting masonry using Portland cement-lime mortars", Proceedings of the International Building Lime Symposium, Orlando, USA, pp. 1-16.

Bosiljkov, V.; Page, A., Bokan-Bosiljkov, V., Žarnić, R. (2003). “Performance based studies of in-plane loaded unreinforced masonry walls”, *Masonry International*, V.16(2), 39-50.

Bosiljkov, V.; Totoev, Y. Z., Nichols, J. M. (2005). “Shear modulus and stiffness of brickwork masonry: An experimental perspective”, *Structural Engineering & Mechanics*, V.20(1), 21-43.

Brunner, J. D; Shing, P. B. (1996). “Shear strength of reinforced masonry walls”, *TMS Journal*, V.14(1), 65-77.

BS 5628-1. (1992). Code of practice for use of masonry. British Standard Institution.

Calvi, G.M., Kingsley, G.R., Magenes, G. (1996). “Testing masonry structures for seismic assessment”, *Earthquake Spectra*, Journal of Earthquake Engineering Research Institute, 12 (1), 145-162.

Carvalho, E.C. (1998). “Seismic testing of structures”, *Proceedings of 11th European Conference on Earthquake Engineering*, Rotterdam, Netherlands, 13pp.

Carvalho, M.C.R.; Santos, F.A.; Roman, H.R. (2001). “Architectural and structural design requirements for constructability in structural masonry”, *Proceedings of 9th Canadian Masonry Symposium*, Fredericton, NB, Canada, 10pp.

Chaimoon, K.; Attard, M.M. (2007). “Modelling of unreinforced masonry walls under shear and compression”, *Engineering structures*, V.29(3), 2056-2068.

Chai, Y.H.; Yaw, L.L. (1999). “Reversed cyclic response of monolithic and slitted reinforced concrete masonry wall-piers”, *Engineering Structures*, V.21(2), 99-111.

Chen, Y.; Ashour, A. F.; Garrity, S. W. (2008). “Moment/thrust interaction diagrams for reinforced masonry sections”, *Construction and Building Materials*, V.22(5), 763-770.

Dhanasekar, M., Haider, W. (2004). “Behaviour of wide spaced reinforced masonry walls under in-plane cyclic loading”, *Proceedings of 13th International Brick and Block Masonry Conference*, Amsterdam, Netherlands, 535-544.

Drysdale, R.G., Hamid, A.A., Baker, L.R. (1999). “Masonry structures: behaviour and design”, The Masonry Society, Boulder, Colorado, USA.

Edgell, G., Haseltine, B.A. (2005). "Building mortar for low rise housing recommendations, problems and solutions", *British Masonry Society Publication*, pp.29.

El-Dakhakhni, W.W., Drysdale, R.G.; Khattab, M.M. (2006). "Multilaminate Macromodel for Concrete Masonry: Formulation and Verification", *Journal of Structural Engineering*, V.132(12), 1984-1996.

ElGawady, M. A.; Lestuzzi, P., Badoux, M. (2006). “Shear strength of URM walls retrofitted using FRP”, *Engineering structures*, V.28(12), 1658-1670.

EUROPEAN STANDARD. EN 197-1, Cement. Compositions, specifications and conformity criteria for common cement, 2000.

EUROPEAN STANDARD. EN 772-1, Methods of tests for masonry units – Part1: Determination of compressive strength, 2000.

EUROPEAN STANDARD. EN 772-2, Methods of tests for masonry units – Part2: Determination of percentage area of voids in aggregate concrete masonry units (by paper indentation), 1998.

EUROPEAN STANDARD. EN 772-11, Methods of tests for masonry units – Part11: Determination of water absorption of aggregate concrete, manufactured stone and natural stone masonry units due to capillary action and the initial rate of water absorption of clay masonry units, 2000.

EUROPEAN STANDARD. EN 772-16, Methods of tests for masonry units – Part16: Determination of dimensions, 2000.

EUROPEAN STANDARD. EN 846-9, Methods of tests for ancillary components for masonry – Part 9: Determination of flexural resistance and shear resistance of lintels, 2000.

EUROPEAN STANDARD. prEN 1991-1-1, Eurocode 1: Actions on structures - Part 1-1: General actions - Densities, self-weight, imposed loads for buildings, 2001.

EUROPEAN STANDARD. prEN 1991-1-1, Eurocode 1: Actions on structures - General actions - Part 1-4: Wind actions, 2004.

EUROPEAN STANDARD. EN 1992-1-1, Eurocode 2. Design of concrete structures. General rules and rules for buildings, 2004.

EUROPEAN STANDARD. EN 1996-1-1, Eurocode 6: Design of masonry structures, 2005.

EUROPEAN STANDARD. prEN 1998-1, Eurocode 8: Design of structures for earthquake resistance, Part 1: General rules, seismic actions and rules for buildings, 2003.

EUROPEAN STANDARD. EN 1015-3, Methods of test for mortar for masonry: Part 3: Determination of consistence of fresh mortar (by flow table), 1999.

EUROPEAN STANDARD. EN 1015-11, Methods of test for mortar for masonry: Part 11: Determination of flexure and compressive strength of hardened mortar, 1999.

EUROPEAN STANDARD. EN 1052-1, Methods of test for masonry: Part 1 – Determination of compressive strength, 1999.

EUROPEAN STANDARD. EN 1052-2, Methods of test for masonry: Part 2 - Determination of flexural strength, 1999.

EUROPEAN STANDARD. EN 1052-3, Methods of test for masonry: Part 3 - Determination of initial shear strength, 2002.

Fereig, S. M. (1994). “Shear strength of reinforced concrete masonry beams without Web reinforcement”, *TMS Journal*, V.12(2), 8-15.

Gambarota, L.; Lagomarsino, S. (1997). “Damage models for the seismic response of brick masonry shear walls. Part II: The continuum model and its applications”, *Earthquake engineering and structural dynamics*, V.26, 441-462.

Gerardin, M., Negro, P. (2000). “The European Laboratory for Structural Assessment(ELSA) and its Role for the Validation of European Seismic Codes”, *Proceedings of EuroConference on Global Change and Catastrophe Risk Management: Earthquake Risks in Europe*, Laxenburg, Austria, 10pp.

Ghanem, G. M.; Salama, A. M.; Elmagd, S. A.; Hamid, A. A. (1993). “Effect of axial compression on the behaviour of partially reinforced masonry shear walls”, *Proceedings of 6th North American Masonry Conference*, Philadelphia, Pensylvania, USA, 1145-1157.

Gouveia, J.P.; Lourenço, P. B. (2007). “Masonry shear walls subjected to cyclic loading: Influence of confinement and horizontal reinforcement”, *Proceedings of 10th North American Masonry Conference*, St. Louis, Missouri, USA, 838-848.

Haach, V.G.; Vasconcelos, G.; Lourenço, P. B.; Mohamad, G. (2007). “Study of a mortar to use as infill and embedding”, *Proceedings of 10th North American Masonry Conference*, St. Louis, Missouri, USA, 530-541.

Haller P. (1969). “Load capacity of brick masonry”, In.:Johnson FB (ed.) Designing, Engineering and Constructing with Masonry Products. Houston: Gulf Publishing Co., p.129-149.

Haseltine, B. A.; Moore, J.F.A. (1981). “Handbook to BS-5628: structural use of masonry. Part1: Unreinforced masonry”, *The Brick Development Association*.

Henderson, R.C.; Fricke, K.E.; Jones, W.D.; Beavers, J. E.; Bennett, R.M. (2003). “Summary of a large- and small-scale unreinforced masonry infill test program”, *Journal of Structural Engineering*, V.129(12), 1667-1675.

Hendry, A.W. (1998). “Structural Masonry”, *MacMillan Press LTDA*, London, UK.

Hendry, A.W. (2002). “Engineered design of masonry buildings: fifty years development in Europe”, *Prog. Struct. Eng. Mater.*, V.4, University of Edinburgh, Scotland, p.291–300.

Jang, J. J.; Hart, G. C. (1995). “Analysis of concrete masonry beams”, *Journal of structural engineering*, 121(11), 1598-1602.

Jingqian, X., Sijun, Z., Shiwen, D. (1986). “Experimental study on behaviour of earthquake resistance of brick masonry under cyclic loading”, *Proceedings of 8th European Conference on Earthquake Engineering*, Lisbon, Portugal, V.4, 8pp.

Juhásova, E., Hurák, M., Zembaty, Z. (2002). “Assessment of seismic resistance of masonry structures including boundary conditions”, *Soil Dynamics and Earthquake Engineering*, V.22(9), 1193-1197.

Khalaf, F. M., Glanville, J. I., El Shahawi, M. (1983). “A study of flexure in reinforced masonry beams”, *Concrete International*, V.5(6), 46-53.

Kikuchi, J.; Yoshimura, K.; Tanaka, A. (1999). “Effect of the presence of masonry units on the seismic behaviour of reinforced fully grouted concrete masonry walls”, *Proceedings of 8th North American Masonry Conference*, Austin, Texas, USA, paper nº 19.

Kikuchi, K., Yoshimura, K., Tanaka, A., Yoshida, K. (2003). “Effect of wall aspect ratio on seismic behaviour of reinforced fully grouted concrete masonry walls”, *Proceedings of 9th North American Masonry Conference*, Clemson, South Carolina, USA, 214-225.

Li, D.; Neis, V. V. (1986). “Performance of reinforced masonry beams subjected to reversed cyclic loadings”, Proceedings of 4th Canadian Masonry Symposium, V.1, Fredericton, N.B., 351-365.

Limón, T. G.; Hortelano, A. M., Fernández, B. M. (2000). “Vertical flexural behaviour of bed joint reinforced brick masonry”, *Proceeding of 12th International Brick and Block Masonry Conference*, Madrid, Spain, 10pp.

Lourenço, P.B. (1996). “Computational strategies for masonry structures”, PhD Thesis, Delft University of technology, Delft, The Netherlands. ISBN 90-407-1221-2. Available from www.civil.uminho.pt/masonry.

Lourenço, P.B. (2004). "Design of large size non-loadbearing masonry walls: case studies in Portugal. Technical and economical benefits", *Proceedings of 13th International Brick/block Masonry Conference*, Amsterdam, Netherlands, 8pp.

Lourenço, P.B. (2006). "Reinforced masonry walls I: Possibilities and Applications", Ingenium 91, p. 80-84. (in Portuguese)

Lourenço, P.B.; Rots, J.G. (2000). “An anisotropic failure criterion for masonry suitable for numerical implementation”, *TMS Journal*, V.18(1), 11-18.

Lourenço, P.B.; Rots, J.G. (1997). “Multisurface interface model for analysis of masonry structures”, *Journal of engineering mechanics*, V.123(7), 660-668.

Lourenço, P.B.; Vasconcelos, G.; Gouveia, J.; Haach, V.G. (2006) “Current experimental investigation on modern masonry”, In: 43rd Meeting of the CIB Commission W023-Masonry walls, Lisboa, 10pp.

Magenes, G.; Calvi, G. M. (1997). “In-Plane seismic response of brick masonry walls”, *Earthquake engineering and structural dynamics*, V.26(11), 1091-1112.

Mahmoud, A.D.S.; Hamid, A.A.; El Mags, S. A. (1995). “Lateral response of unreinforced solid masonry shear walls: an experimental study”, *Proceedings of 7th Canadian Masonry Symposium*, Hamilton, Ontario, Canada, 110-125.

Mann, W.; Müller, H. (1982). “Failure shear-stressed masonry – an enlarged theory, tests and application to shear walls”, Proc. British Ceramic Society, V.30, 223-235.

Manos, G.C.; Yasin, M.; Thawabteh, J.; Kourtides, V. (2001). “The earthquake performance of partially reinforced masonry piers subjected to in-plane cyclic loading”, *Proceedings of 9th Canadian Masonry Symposium*, Fredericton, New Brunswick, Canada.

Matsumura, A. (1990). “Planar shear loading test on reinforced fully grouted hollow clay masonry walls”, *Proceedings of 5th North American Masonry Conference*, Urbana-Champaign, Illinois, USA, 347-358.

Modena, C., Porto, F., Valluzzi, M.R. (2004). “Reinforced and rectified clay block masonry”, *Proceedings of 6th National Congress of Seismology and Seismic engineering*, Guimarães, Portugal, 155-177.

Mohamad, G. (2007). “Mechanism failure of concrete block masonry under compression”, PhD Thesis, University of Minho, Guimarães, Portugal. Available from www.civil.uminho.pt/masonry. (in Portuguese)

MSJC (2002). Building code requirements for masonry structures. ACI530-02 / ASCE 5-02 / TMS 402-02. USA: Masonry Standards Joint Committee.

Nascimento, J. A. (1999). “Investigação das solicitações de cisalhamento em edifícios de alvenaria estrutural submetidos a ações horizontais”, Msc Thesis, University of São Paulo, Engineering School of São Carlos, São Carlos, São Paulo, Brazil. (in Portuguese)

Noson, L.L; Qamar, A.; Thorsen, G.W. (1988). Washington State Earthquake Hazards. Washington division of geology and earth resources Information circular 85.

Page, A.W.; Kleeman, P.W. (1991). “The influence of capping material and platen restraint on the failure of hollow masonry units and prisms”. *Proceeding of 9th International Brick/block Masonry Conference*, Berlin, Germany, p.662-70.

Paes, M. S. (2008). “Interação entre edifício de alvenaria estrutural e pavimento em concreto armado considerando-se o efeito arco com a atuação de cargas verticais e ações horizontais”, MsC Thesis, São Carlos Engineering School, University of São Paulo, São Carlos-SP, Brazil, 163pp. (in Portuguese)

Panarese, W. C., Kosmatka, S. H., Randall, F. A. (1991). "Concrete masonry handbook for architects, engineers, builders”, Portland Cement Association, 5th ed., USA.

Pluijm, R.V.D. (1999). “Out-of-Plane bending of masonry, behavior and strength”, PhD Thesis, Eindhoven University of Technology.

Ramalho, M.A.; Corrêa.M.R.S. (2003), “Projetos de edifícios de alvenaria estrutural”. São Paulo, Pini. (in Portuguese).

Rauber, F.K. (2005). “Contribuições Ao Projeto Arquitetônico De Edifícios Em Alvenaria Estrutural”, Msc. Thesis, University Federal of Santa Maria, Rio Grande do Sul, Brazil, 111pp. (in Portuguese).

Reneckis, D., Lafave, J.M., Clarke, W.M. (2004). “Out-of-plane performance of brick veneer walls on wood frame construction”, *Engineering Structures*, V.26(8), 1027-1042.

RSA - Regulamento de segurança e acções para estruturas de edifícios e pontes, 1983. (in Portuguese)

Sabbatini, F. H. (1984). "O processo construtivo de edifícios de alvenaria estrutural sílico-calcário", Thesis of Master of Science, University of São Paulo, São Paulo, Brazil, 298pp. (in Portuguese)

Schultz, A.E., Hutchinson, R.S., Cheok, G.C. (1998). "Seismic performance of masonry walls with bed joint reinforcement", *Proceedings of Structural Engineers World Congress*, San Francisco, California, USA, paper nº 40.

Shing, P. B.; Noland, J. L.; Klamerus, E., Spaeh, H. (1989). "Inelastic behaviour of concrete masonry shear walls", *Journal of Structural Engineering*, V.115(9), 2204-2225.

Shing, P. B.; Schuller, M.; Hoskere, V. S. (1990a). "In-Plane resistance of reinforced masonry shear walls", *Journal of Structural Engineering*, V.116(3), 619-640.

Shing, P. B.; Schuller, M.; Hoskere, V. S.; Carter, E. (1990b). "Flexural and shear response of reinforced masonry walls", *ACI Structural Journal*, V.87(6), 646-656.

Shing, P. B.; Brunner, J. D.; Lofti, H. R. (1993). "Evaluation of shear strength of reinforced masonry walls", *TMS Journal*, V.12(1), 1993, 61-76.

Sorić, Z. (1994). "Masonry lintels – Shear failure analysis", *TMS Journal*, V.12(2), 60-71.

Stafford Smith, B.; Riddington, J.R. (1977). "The composite behavior of elastic wall-beam systems" *Proceedings of the Institution of Civil Engineers*, V.63(2), 377-391.

Steelman, J.; Abrams, D. P. (2007). "Effect of axial stress and aspect ratio on lateral strength of URM shear walls", *Proceedings of 10th North American Masonry Conference*, St. Louis, Lissouri, USA, 849-859.

Sutcliffe, D. J.; Yu, H. S.; Page, A. W. (2001). "Lower bound limit analysis of unreinforced masonry shear walls", *Computers & Structures*, 79(14), 1295-1312.

Suter, G. T.; Keller, H.; Fenton, G. A.. "Summary of a Decade of reinforced masonry research at Carleton University", Department of Civil Engineering, Carleton University, Ottawa, 1984.

Taly, N. (2001). “Design of reinforced masonry structures”, McGraw-Hill, New York, USA.

Tomazela, C. A. (1995) “Ação conjunta parede-viga na alvenaria estrutural”, MsC Thesis, São Carlos Engineering School, University of São Paulo, São Carlos-SP, Brazil, 249pp. (in Portuguese)

Tomaževič, M., Zarnic, R. (1986). “The behaviour of horizontally reinforced masonry walls subjected to cyclic lateral in-plane loads reversals”, *Proceedings of 8th European Conference on Earthquake Engineering*, Lisbon, Portugal, V.4, 9pp.

Tomaževič, M.; Lutman, M.; Petkovič, L. (1996). “Seismic behaviour of masonry walls: experimental simulation”, *Journal of Structural Engineering*, V.122(9), 1040-1047.

Tomaževič, M. (1999). “Earthquake-resistant design of masonry buildings”, Imperial College Press, London.

Turnšek, V., Čačovič, F. (1971). “Some experimental results on the strength of brick masonry walls”, SIBMAC Proceedings, 149-156.

Van Zijl, G.P.A.G. (2004). “Modeling masonry shear-compression: Role of Dilatancy highlighted”, *Journal of engineering mechanics*, V.30(11), 1289-1296.

Vasconcelos, G. (2005). “Experimental investigations on the mechanics of stone masonry: Characterization of granites and behaviour of ancient masonry shear walls”, PhD Thesis, University of Minho, Guimarães, Portugal. Available from www.civil.uminho.pt/masonry.

Vasconcelos, G., Lourenço, P.B., Haach, V.G. (2008). “Avaliação experimental da aderência de juntas de alvenaria de blocos de betão”, *Proceedings of 7º Congresso Nacional de Mecânica Experimental*, Vila Real, Portugal, 101-103. (in Portuguese)

Vasconcelos, G., Lourenço, P.B. (2009), “In-plane experimental behaviour of stone masonry walls under cyclic loading”, ASCE, Journal of Structural Engineering. (in press).

Vermeltfoort, A.Th., Raijmakers, Th.M.J., Janssen, H.J.M. (1993). “Shear tests on masonry walls”, *Proceedings of 6th North American Masonry Conference*, Philadelphia, USA, 1183-1193.

Voon, K.C., Ingham, J.M. (2006). “Experimental In-Plane shear strength investigation of reinforced concrete masonry walls”, *Journal of Structural Engineering*, V.132(3), 400-408.

Wight, G.D.; Igham, J.M.; Kowalsky, M.J. (2004). “Shake table testing of port-tensioned concrete masonry walls”, *Proceedings of 13th International Brick and Block Masonry Conference*, Amsterdam, Netherlands, 1059-1068.

Wittmann, F.H., Slowik, V., Alvaredo, A. M. (1994). “Probabilistic aspects of fracture energy of concrete”, *Materials and Structures*, V.27, 499-504.

Wood, R. H. (1952) “Studies in composite construction. Part 1: The composite action of brick panels supported on reinforced concrete beams”, *National Building Studies*, Research Paper n.13.

Wu, Y. (2004). “The effect of longitudinal reinforcement on the cyclic shear behaviour of glass fiber reinforced gypsum wall panels: tests”, *Engineering Structures*, V.26(11), 1633-1646.

Yoshimura, K., Kikuchi, K., Kuroki, M., Nonaka, H., Kim, K.T., Matsumoto, Y. Itai, T., Reeznag, W., Ma, L. (2003). “Experimental study on reinforcing methods for confined masonry walls subjected to seismic forces”, *Proceedings of 9th North American Masonry Conference*, Clemson, South Carolina, USA, 89-100.

Zhang, X.D.; Singh, S.S.; Bull, D.K.; Cooke, N. (2001). “Out-of-plane performance of reinforced masonry walls with openings”, *Journal of Structural Engineering*, V.127(1), 51-57.

Zhuge, Y.; Corderoy, J.; Thambiratnam, D. (1996). “Behavior of unreinforced brick masonry under lateral (cyclic) loading”, *TMS Journal*, V.14(2), 55-62.

APPENDIX A – SHEAR WALLS

A.1 Lateral displacements

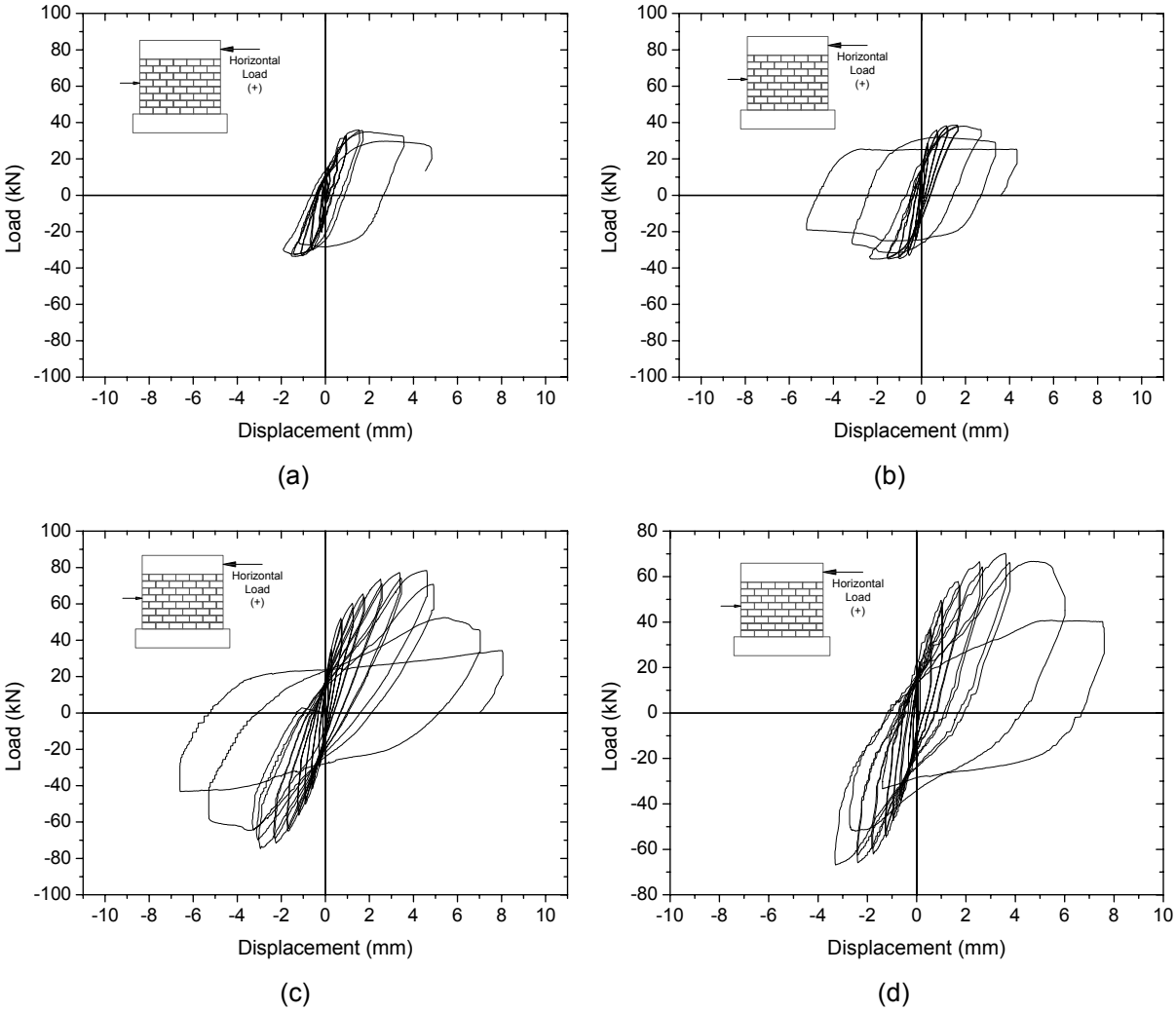

Figure A.1 – Displacements of LVDT 2: (a) N60-3C-B1-UM, (b) N60-3C-B1-SH, (c) N60-3C-B1-MA and (d) N60-3C-B1-PA.

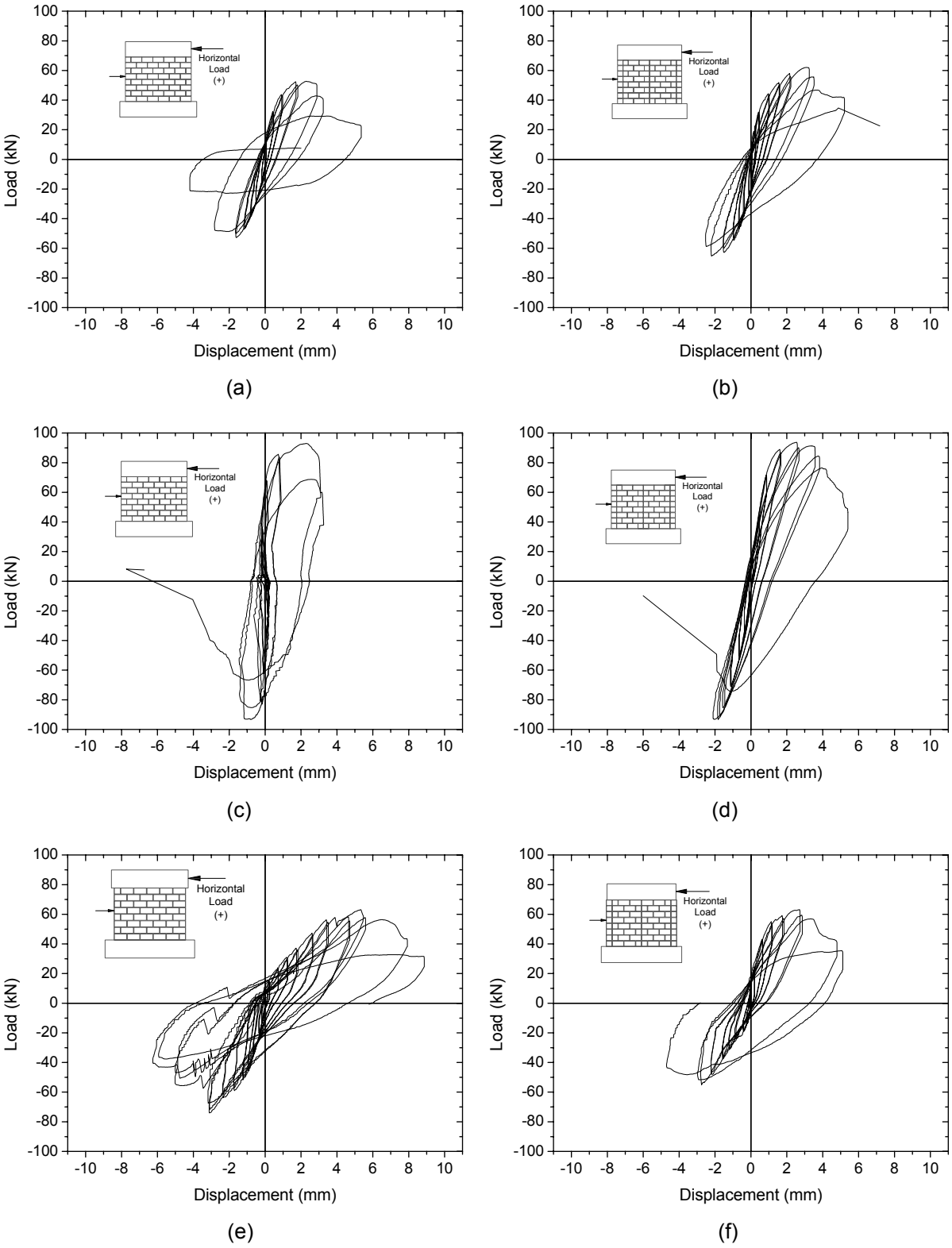

Figure A.2 – Displacements of LVDT 2: (a) N60-3C-B1, (b) N60-3C-B2, (c) N150-3C-B1, (d) N150-3C-B2, (e) N60-2C-B1 and (f) N60-2C-B2.

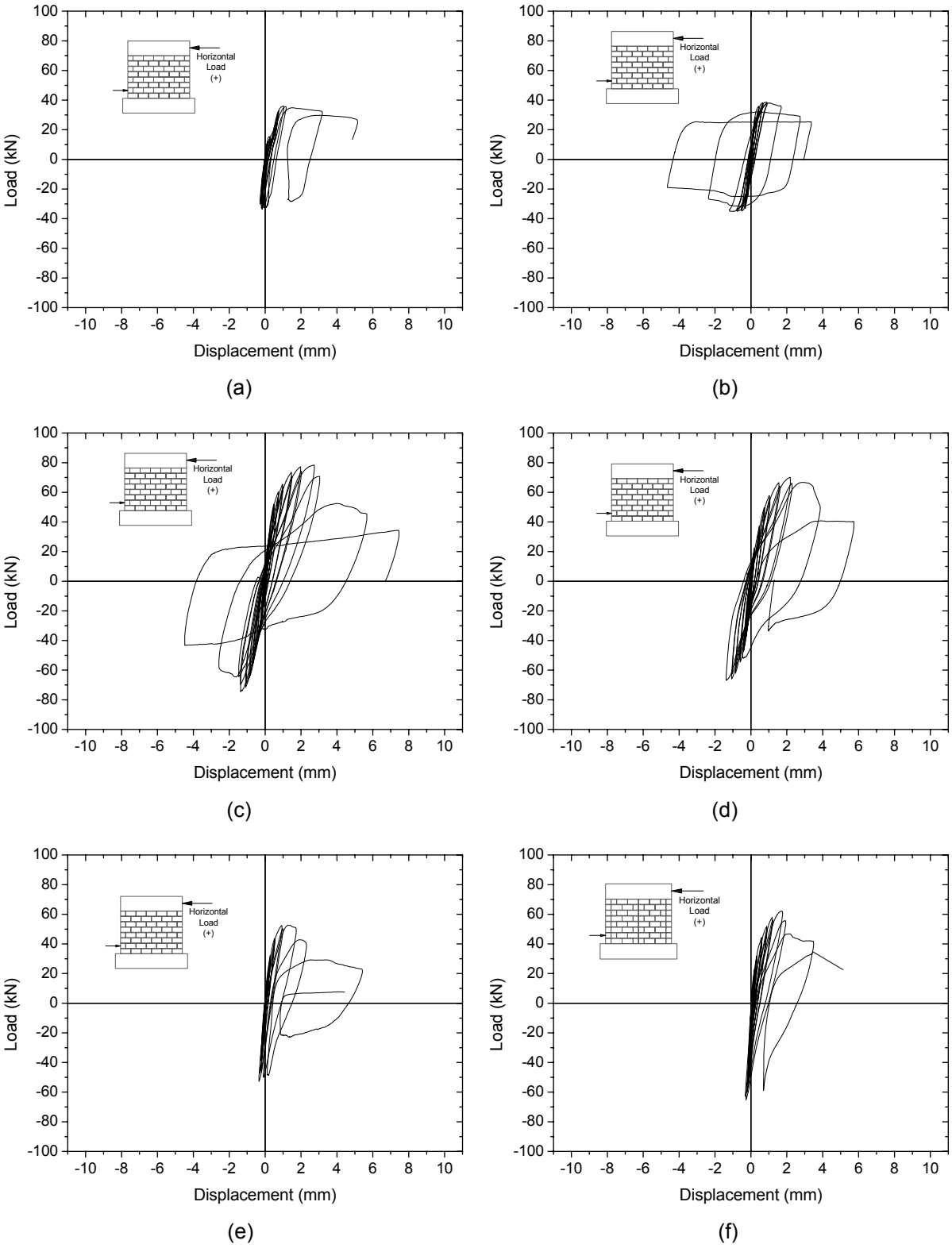

Figure A.3 – Displacements of LVDT 3: (a) N60-3C-B1-UM, (b) N60-3C-B1-SH, (c) N60-3C-B1-MA, (d) N60-3C-B1-PA, (e) N60-3C-B1 and (f) N60-3C-B2.

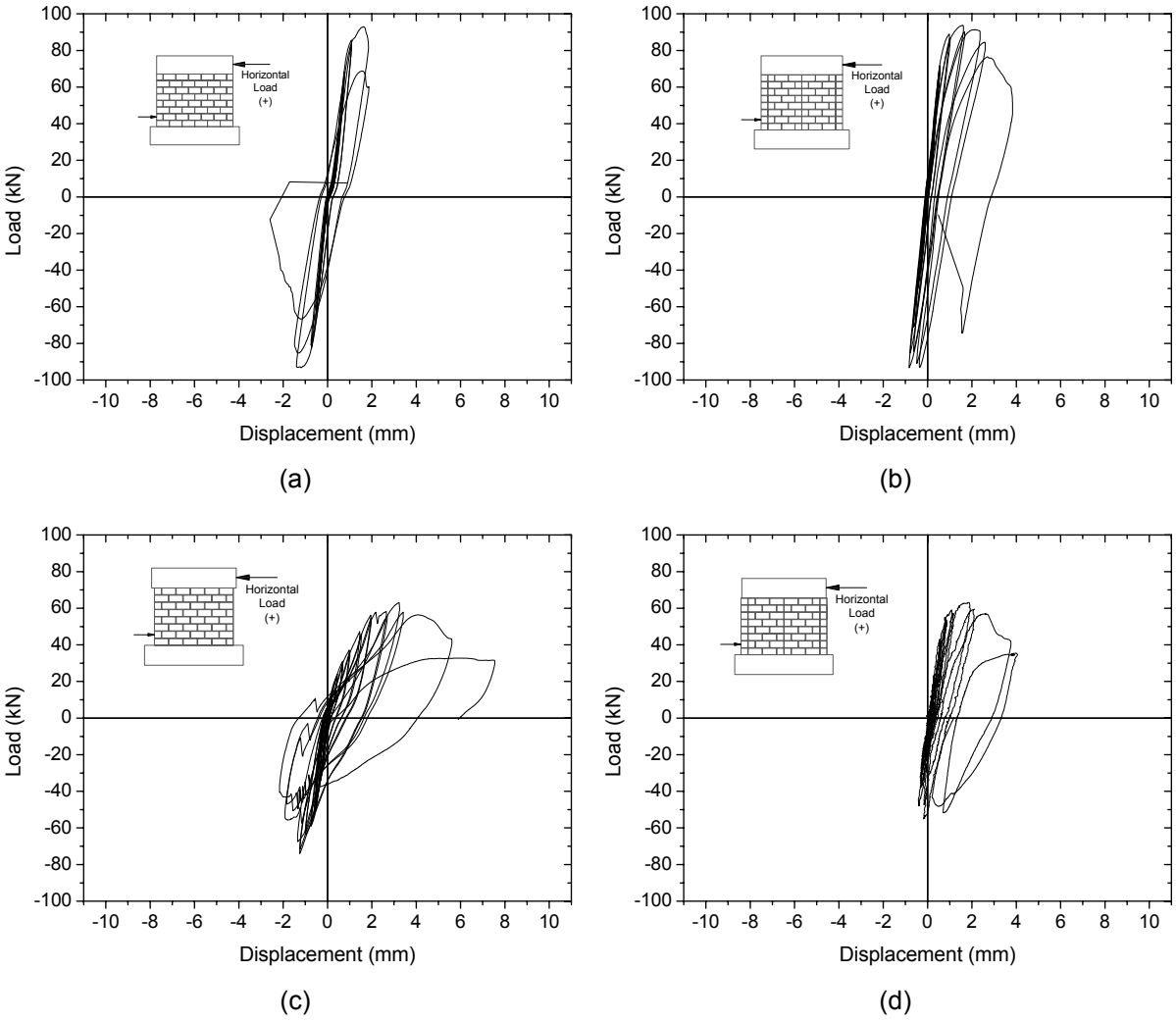

Figure A.4 – Displacements of LVDT 3: (a) N150-3C-B1, (b) N150-3C-B2, (c) N60-2C-B1 and (d) N60-2C-B2.

A.2 Diagonal displacements

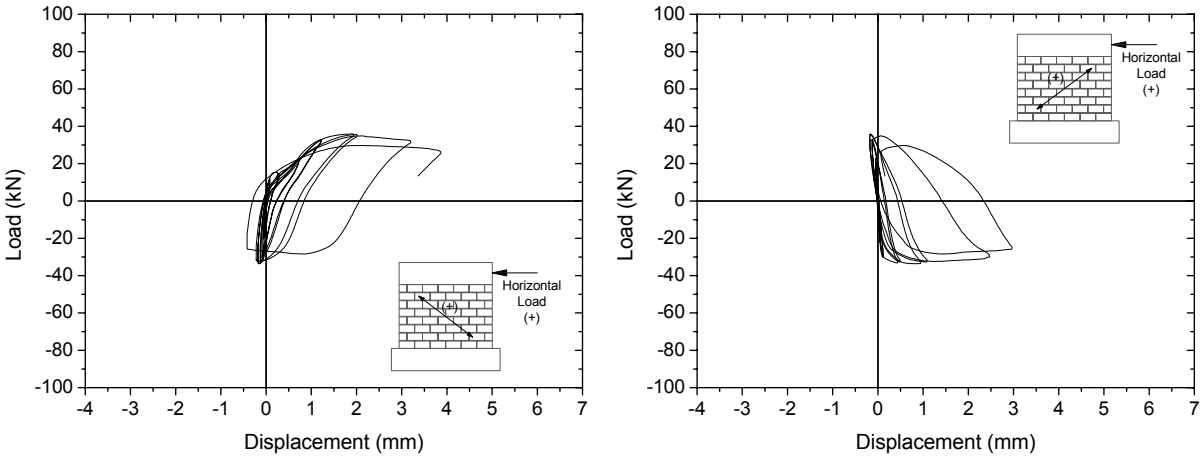

Figure A.5 – Diagonal displacements of specimen N60-3C-B1-UM.

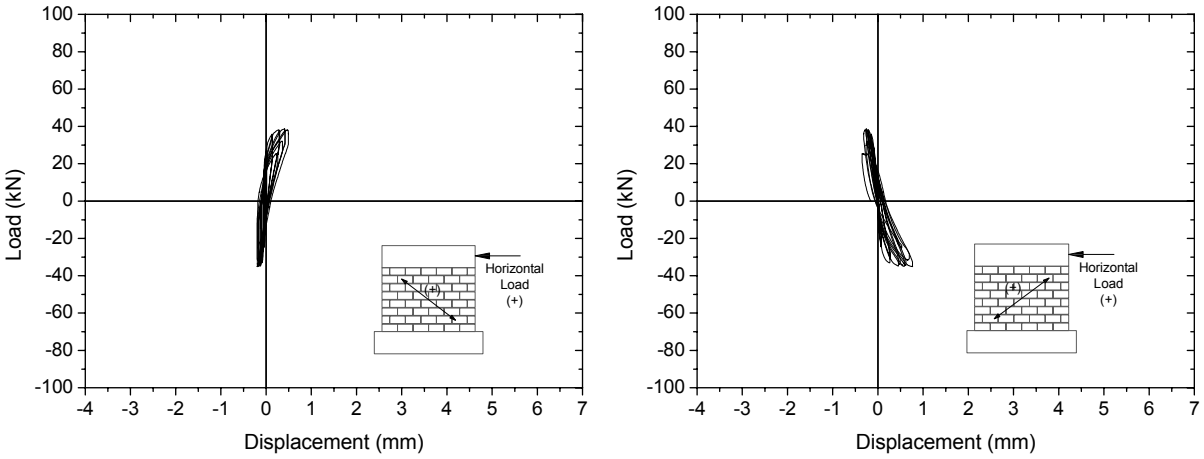

Figure A.6 – Diagonal displacements of specimen N60-3C-B1-SH.

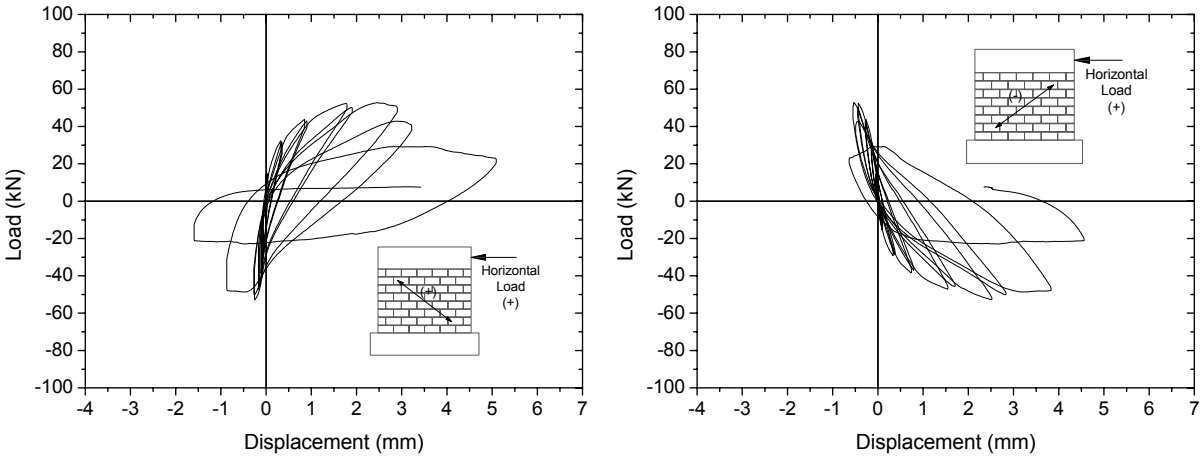

Figure A.7 – Diagonal displacements of specimen N60-3C-B1.

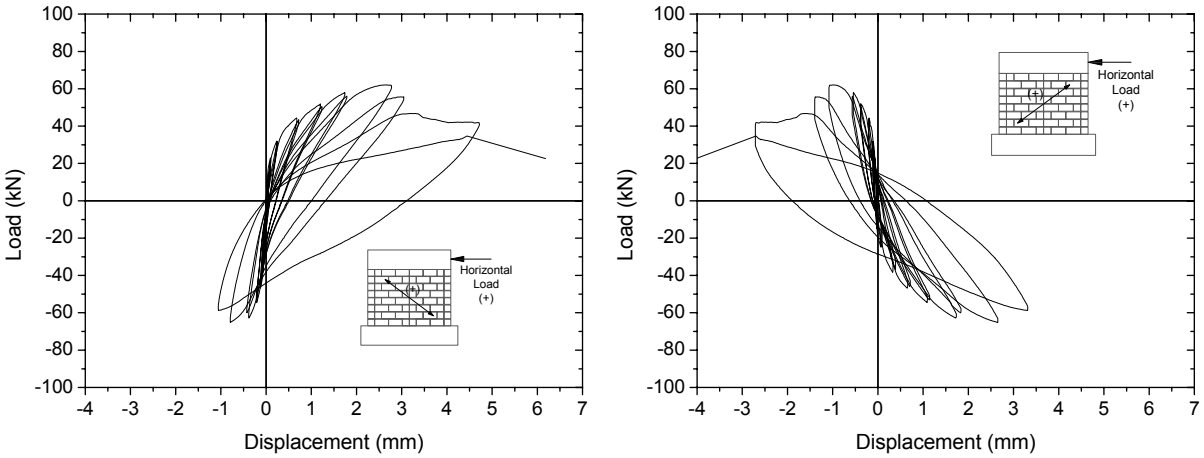

Figure A.8 – Diagonal displacements of specimen N60-3C-B2.

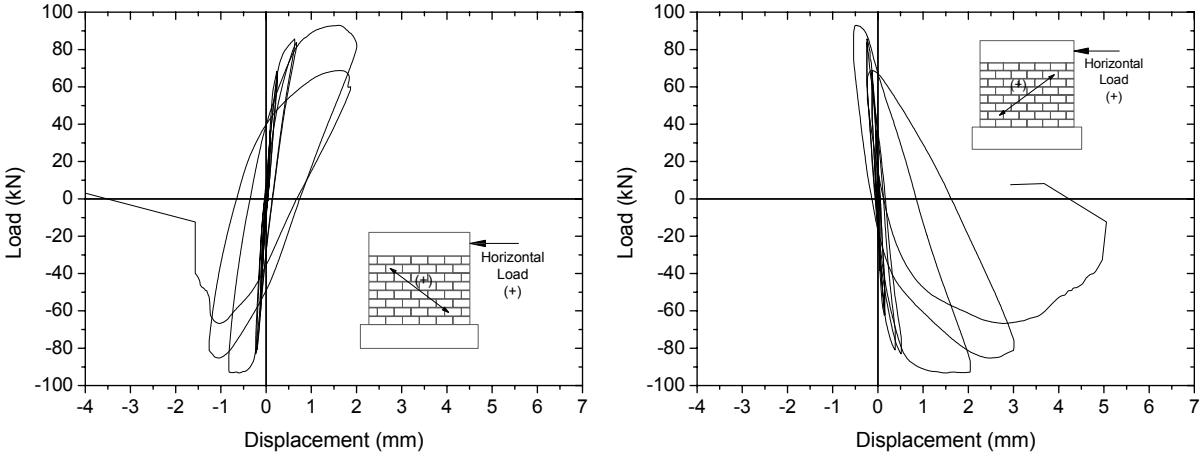

Figure A.9 – Diagonal displacements of specimen N150-3C-B1.

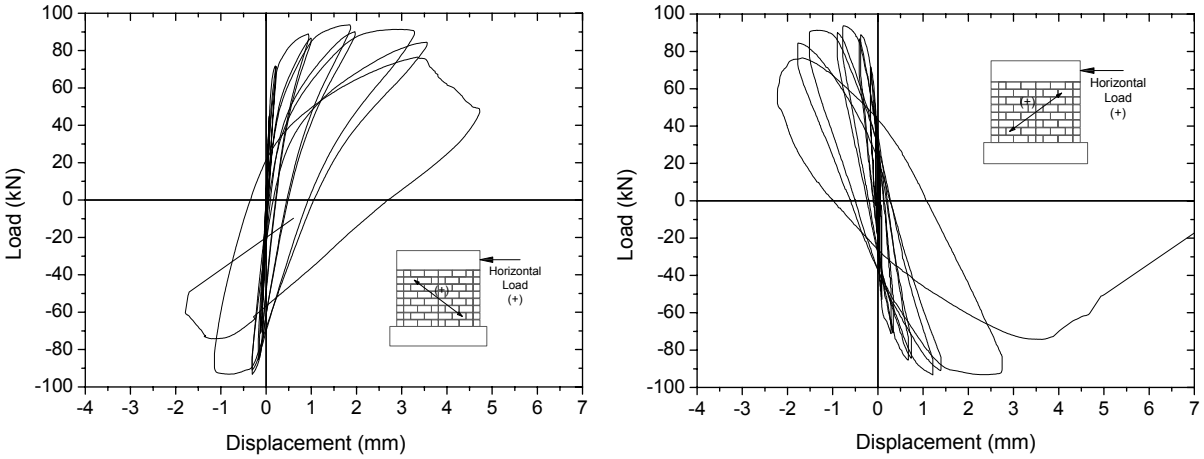

Figure A.10 – Diagonal displacements of specimen N150-3C-B2.

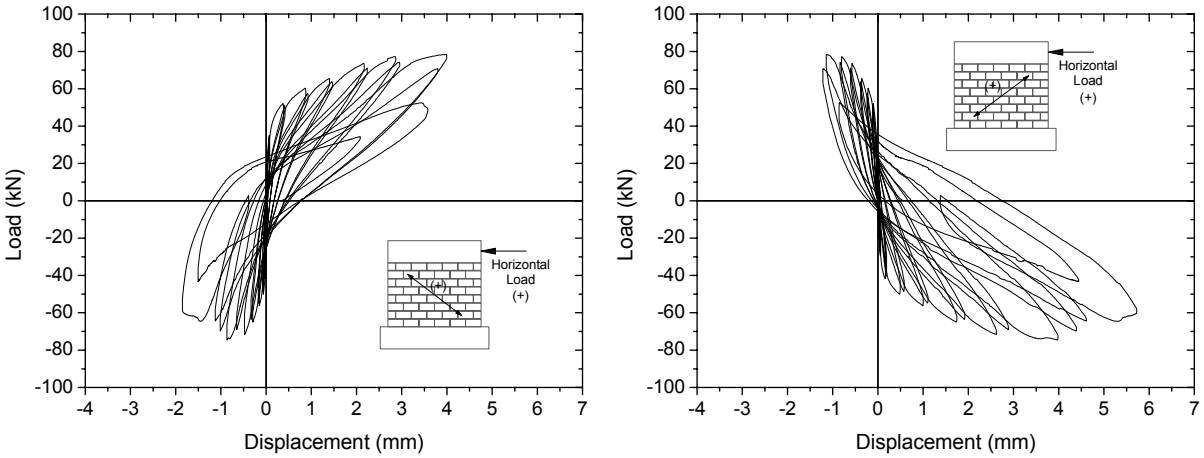

Figure A.11 – Diagonal displacements of specimen N60-3C-B1-MA.

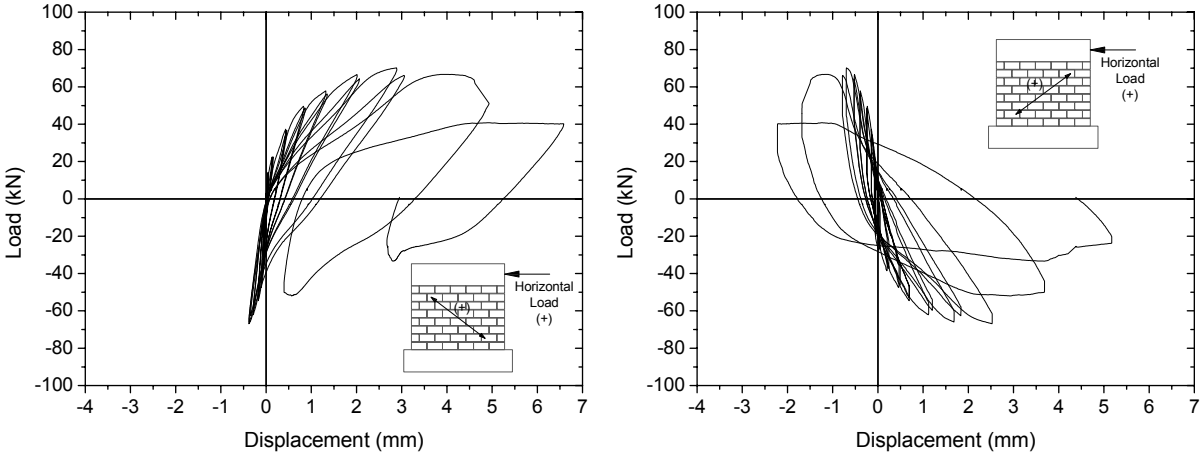

Figure A.12 – Diagonal displacements of specimen N60-3C-B1-PA.

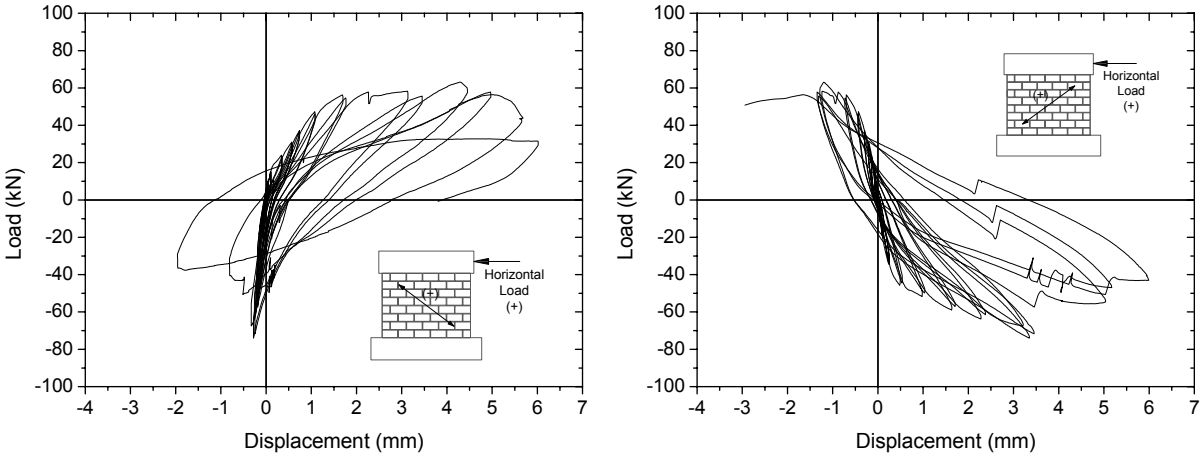

Figure A.13 – Diagonal displacements of specimen N60-2C-B1.

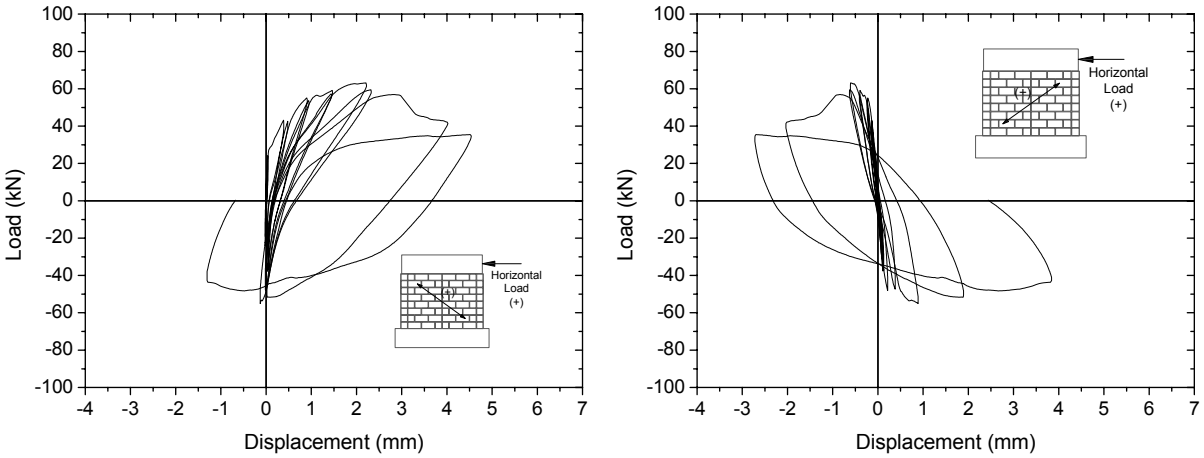

Figure A.14 – Diagonal displacements of specimen N60-2C-B2.

A.3 Vertical displacements

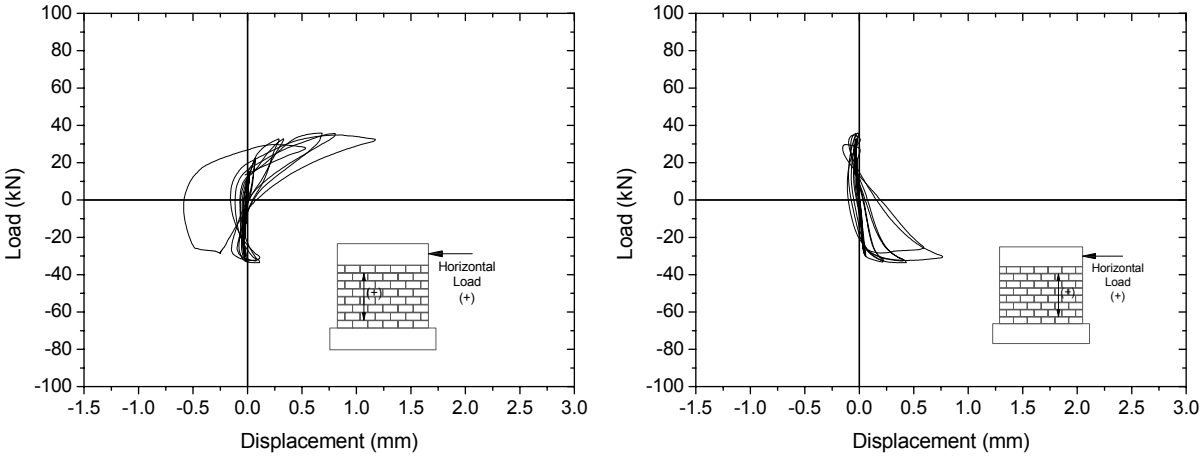

Figure A.15 – Vertical displacements of specimen N60-3C-B1-UM.

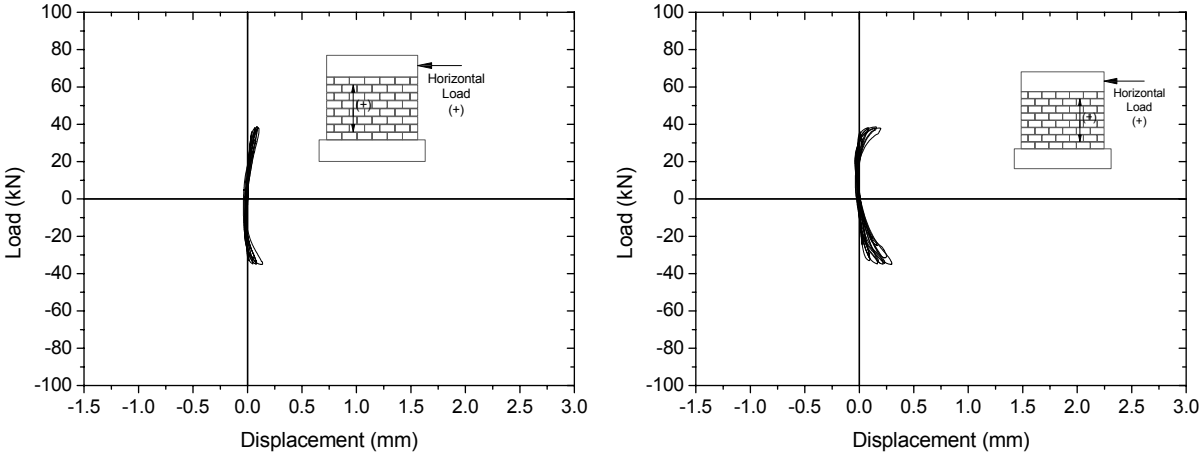

Figure A.16 – Vertical displacements of specimen N60-3C-B1-SH.

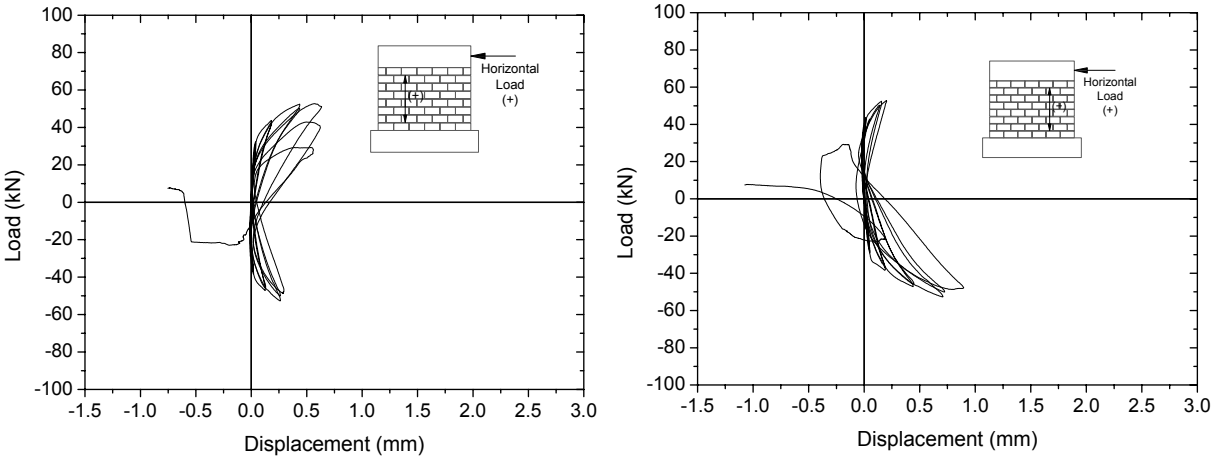

Figure A.17 – Vertical displacements of specimen N60-3C-B1.

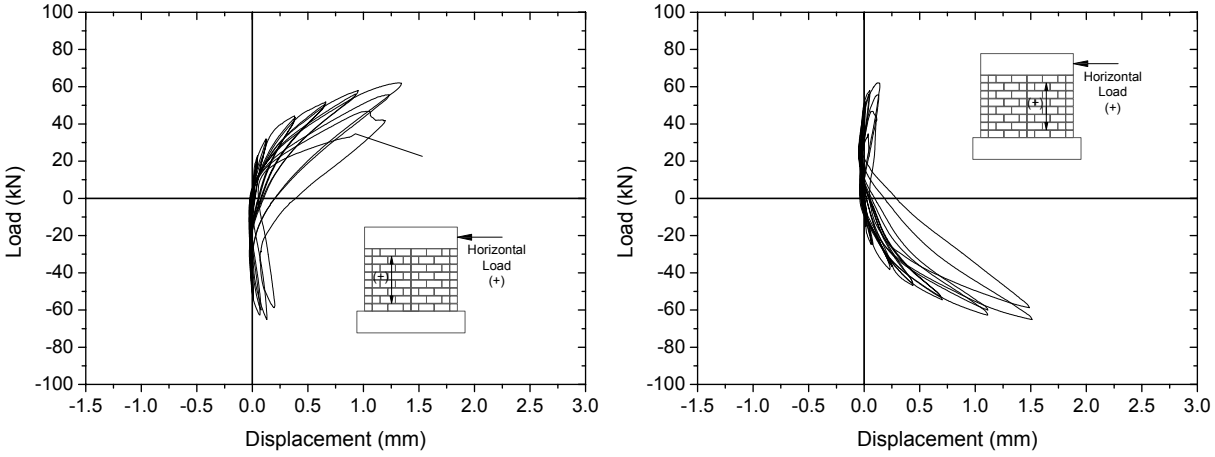

Figure A.18 – Vertical displacements of specimen N60-3C-B2.

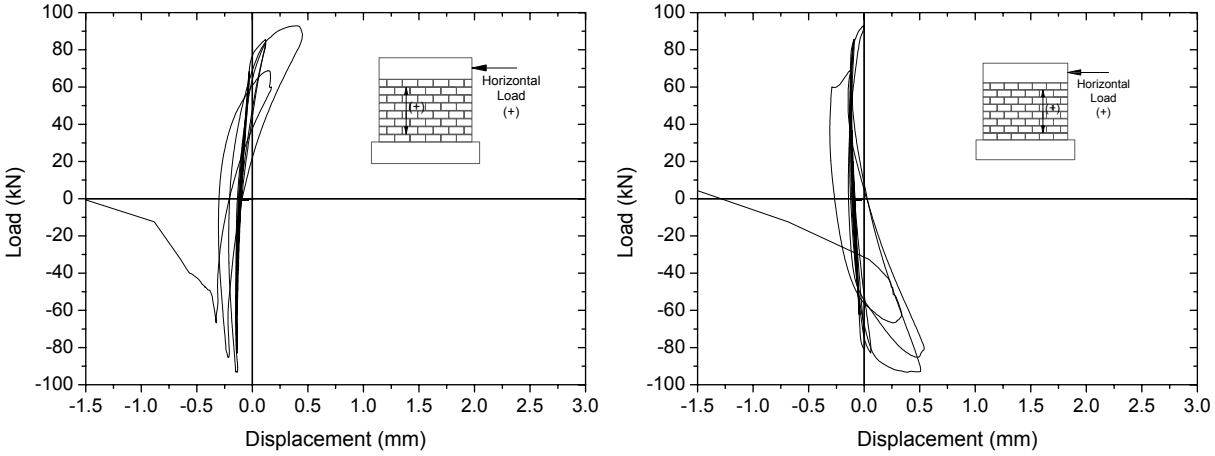

Figure A.19 – Vertical displacements of specimen N150-3C-B1.

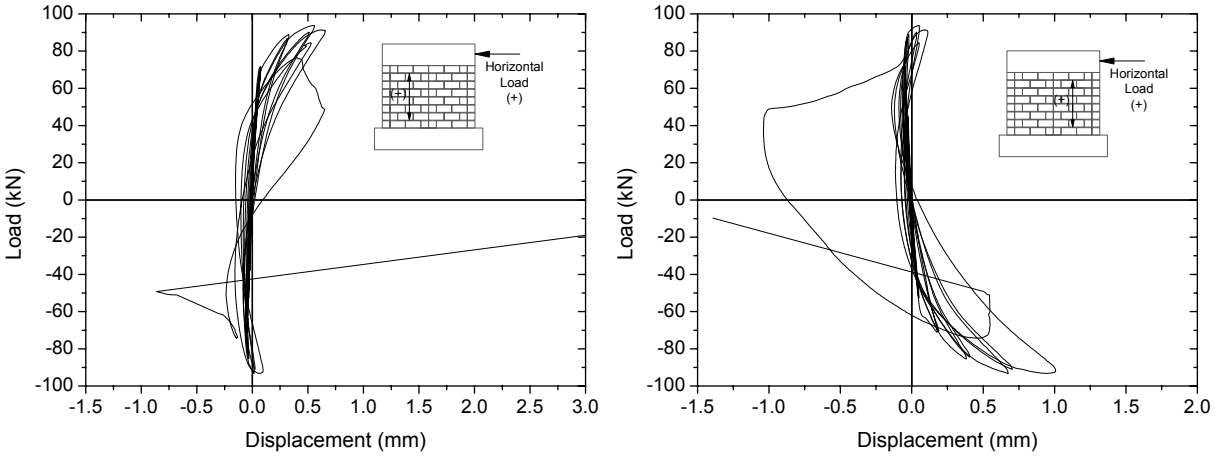

Figure A.20 – Vertical displacements of specimen N150-3C-B2.

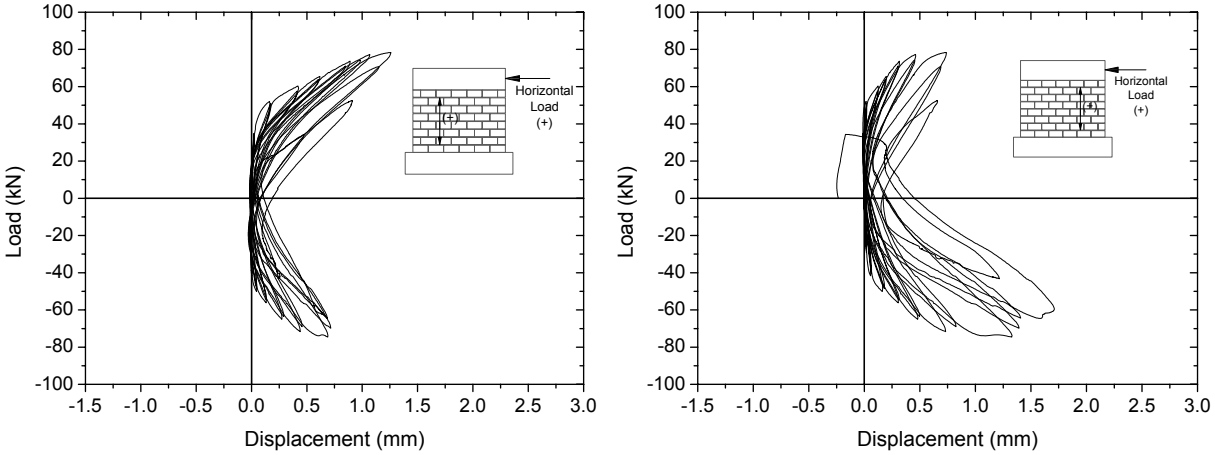

Figure A.21 – Vertical displacements of specimen N60-3C-B1-MA.

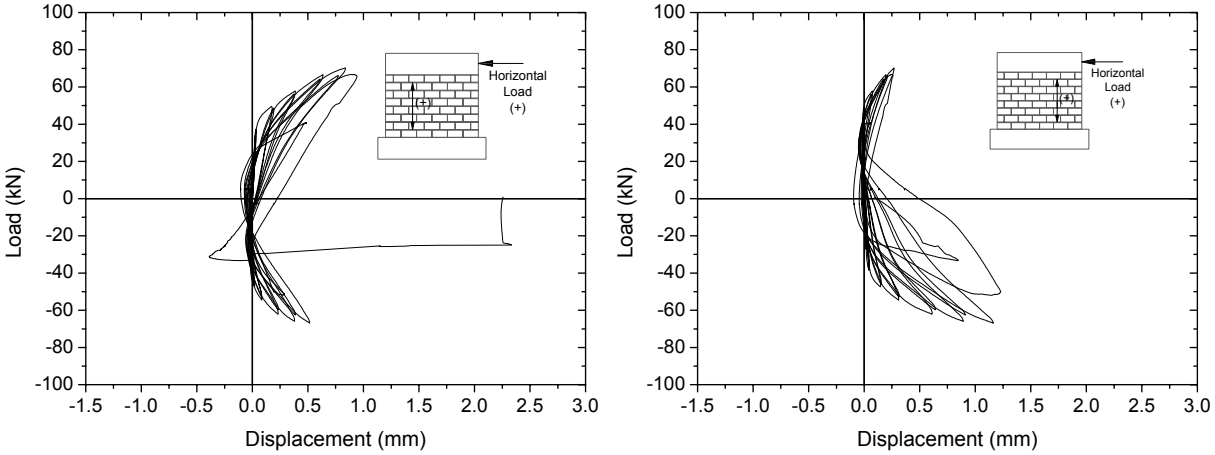

Figure A.22 – Vertical displacements of specimen N60-3C-B1-PA.

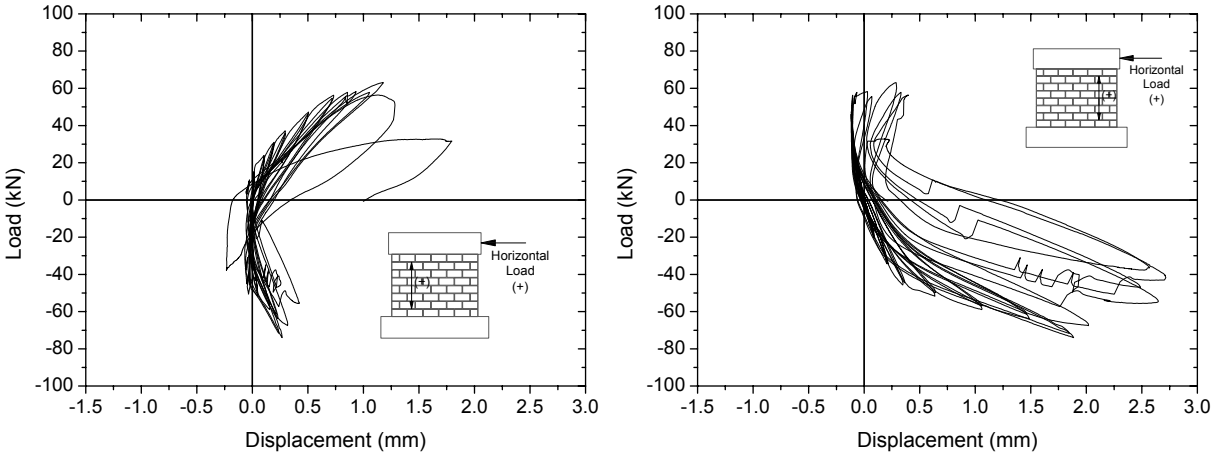

Figure A.23 – Vertical displacements of specimen N60-2C-B1.

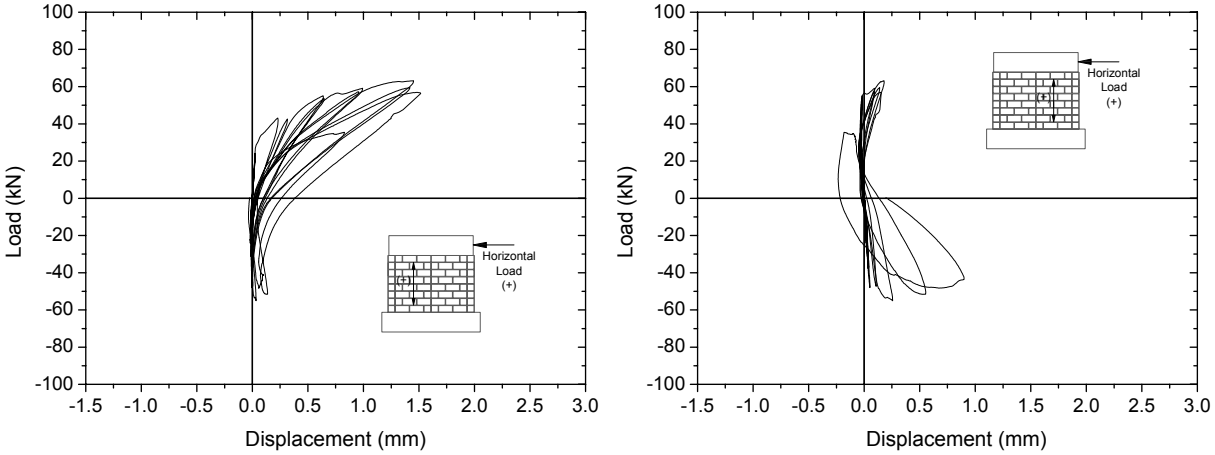

Figure A.24 – Vertical displacements of specimen N60-2C-B2.

Obs.: Diagrams results represent the medium values of LVDTs positioned in extremities of the wall.

A.4 Interior rotation of the walls

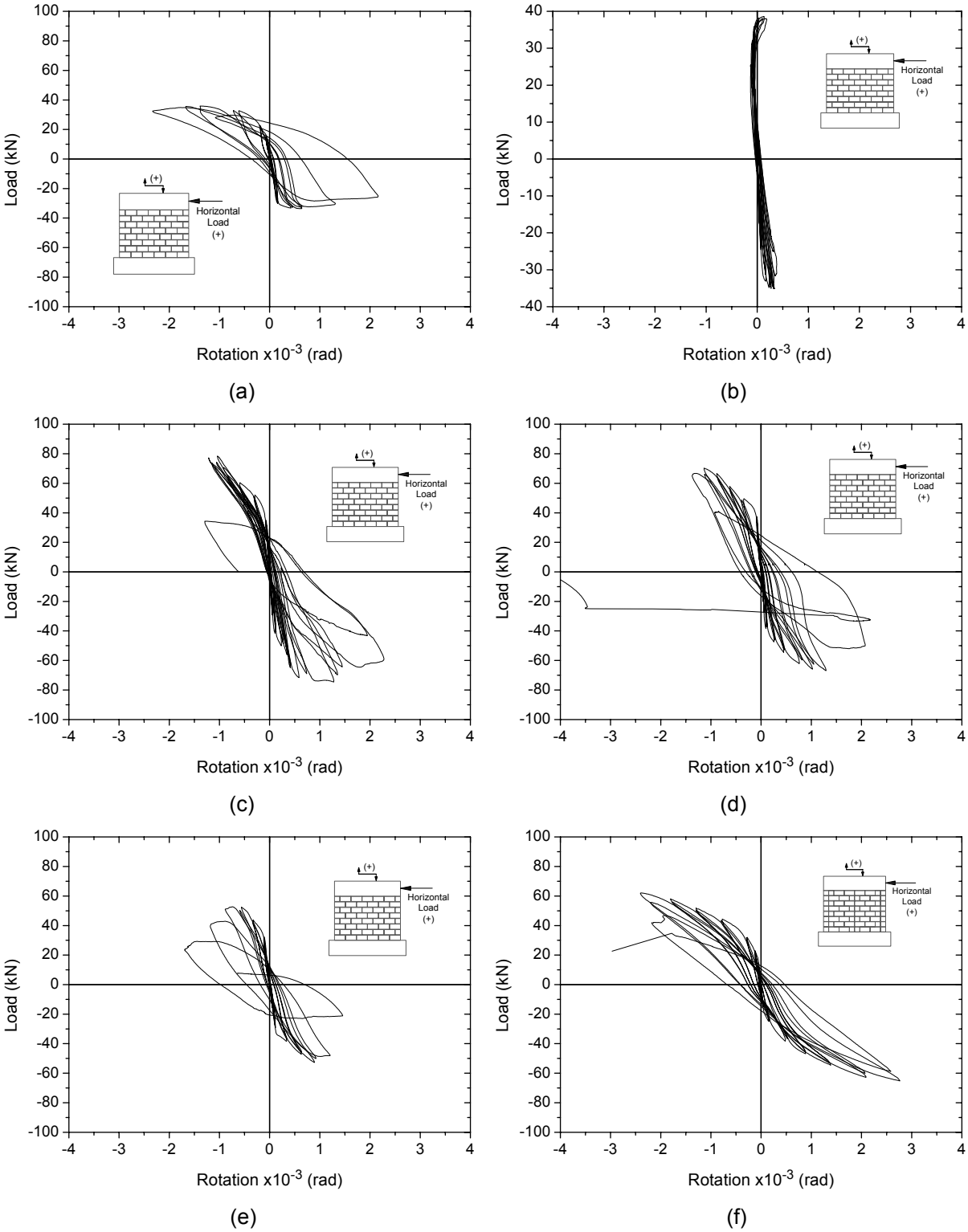

Figure A.25 – Interior rotation: (a) N60-3C-B1-UM, (b) N60-3C-B1-SH, (c) N60-3C-B1-MA, (d) N60-3C-B1-PA, (e) N60-3C-B1 and (f) N60-3C-B2.

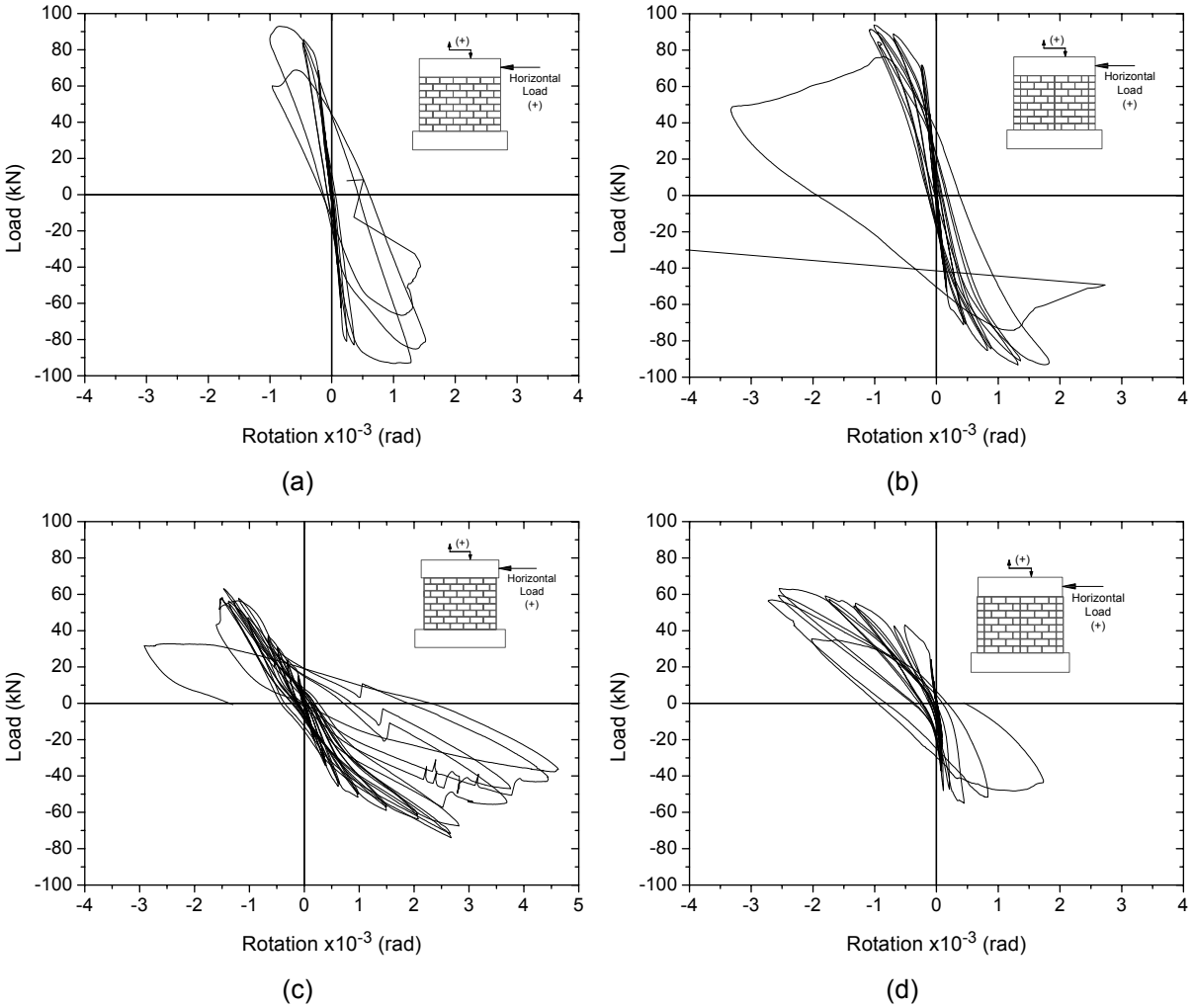

Figure A.26 – Interior rotation: (a) N150-3C-B1, (b) N150-3C-B2, (c) N60-2C-B1 and (d) N60-2C-B2.

Obs.: interior rotation (θ_i) of the walls was measured by vertical LVDTs attached to the wall (LVDTs 10, 11, 12 and 13) and calculated as follows:

$$\theta_i = \frac{\left(\frac{\delta_{LVDT10} + \delta_{LVDT11}}{2}\right) - \left(\frac{\delta_{LVDT12} + \delta_{LVDT13}}{2}\right)}{l_1} \qquad \text{Eq. A.1}$$

Where, δ is the displacement measured by the respective LVDT and l_1 is the distance between the vertical LVDTs attached to the side of wall.

A.5 Rotation of the top of the walls

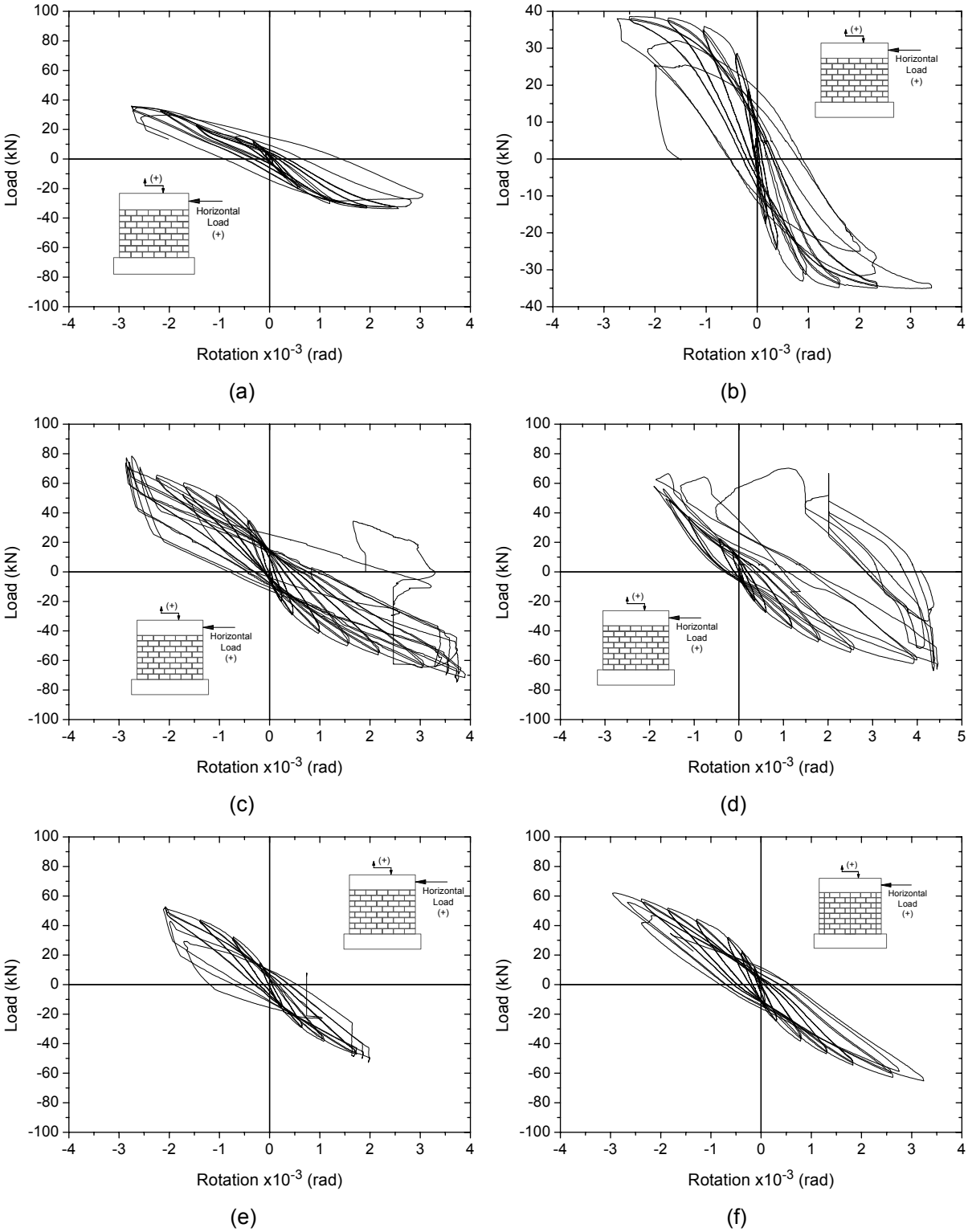

Figure A.27 – Rotation of the top of the wall: (a) N60-3C-B1-UM, (b) N60-3C-B1-SH, (c) N60-3C-B1-MA, (d) N60-3C-B1-PA, (e) N60-3C-B1 and (f) N60-3C-B2.

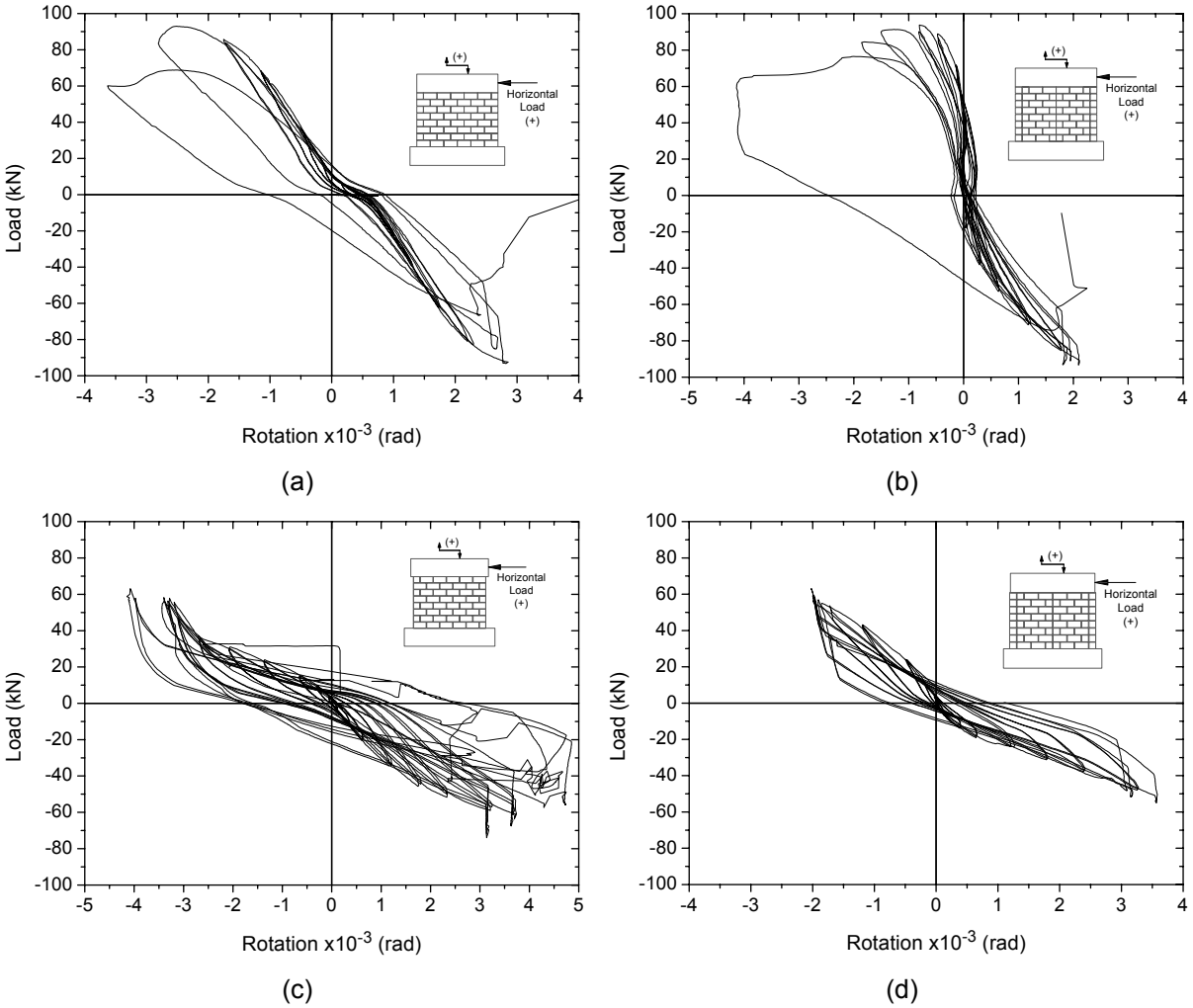

Figure A.28 – Rotation of the top of the wall: (a) N150-3C-B1, (b) N150-3C-B2, (c) N60-2C-B1 and (d) N60-2C-B2.

Obs.: rotation of the top of the wall (θ_t) was measured by vertical LVDTs attached to the top of wall (LVDTs 6 and 7) and calculated as follows:

$$\theta_t = \frac{\delta_{LVDT6} - \delta_{LVDT7}}{l_2} \qquad \text{Eq. A.2}$$

Where, δ is the displacement measured by the respective LVDT and l_2 is the length of wall.

In some specimens, the measurements of LVDTs which measured the rotation of the top of the wall reached values higher than the length of the field of them.

A.6 Strain-gauges in horizontal reinforcements

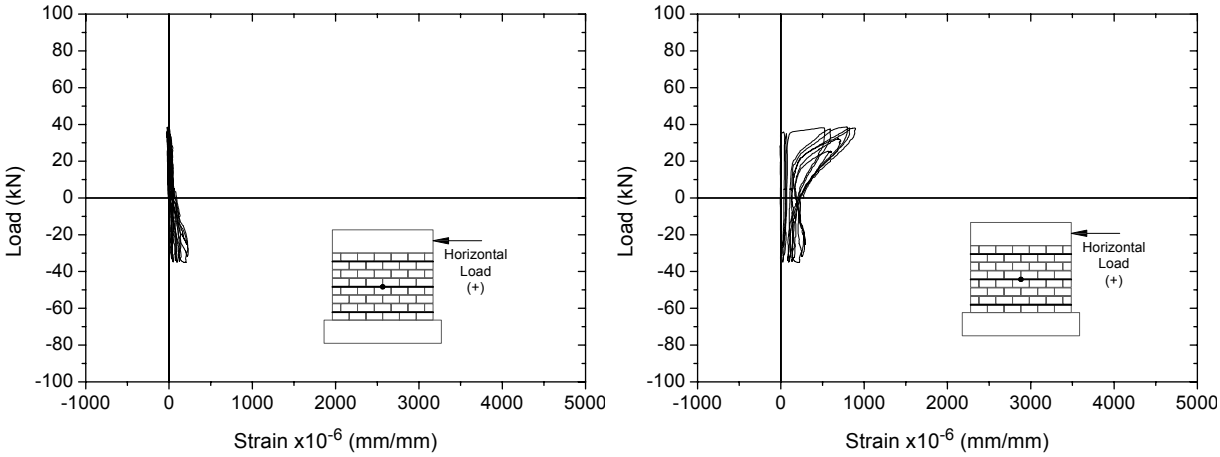

Figure A.29 – Strains in horizontal reinforcement (N60-3C-B1-SH): (a) Ext. 7 and (b) Ext. 8.

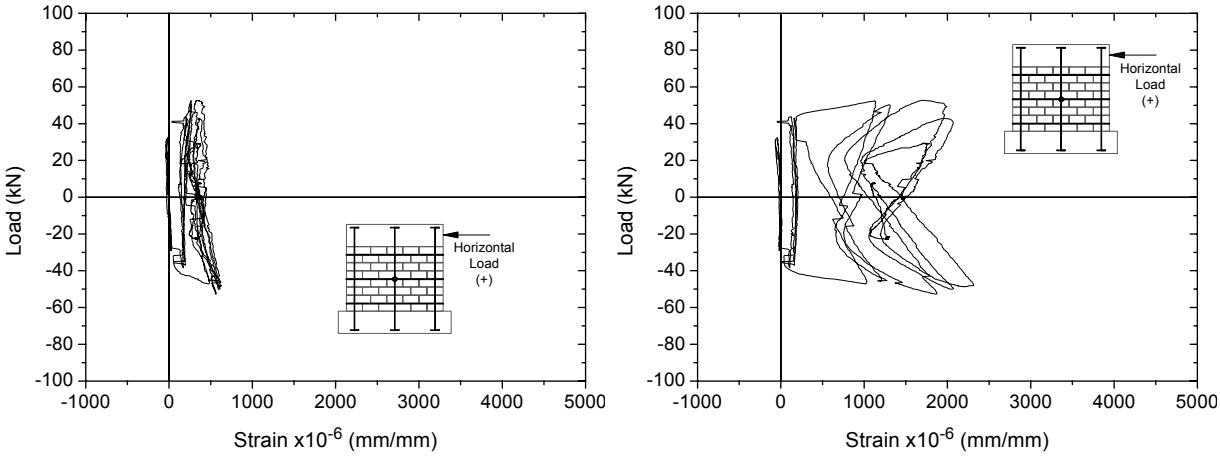

Figure A.30 – Strains in horizontal reinforcement (N60-3C-B1): (a) Ext. 7 and (b) Ext. 8.

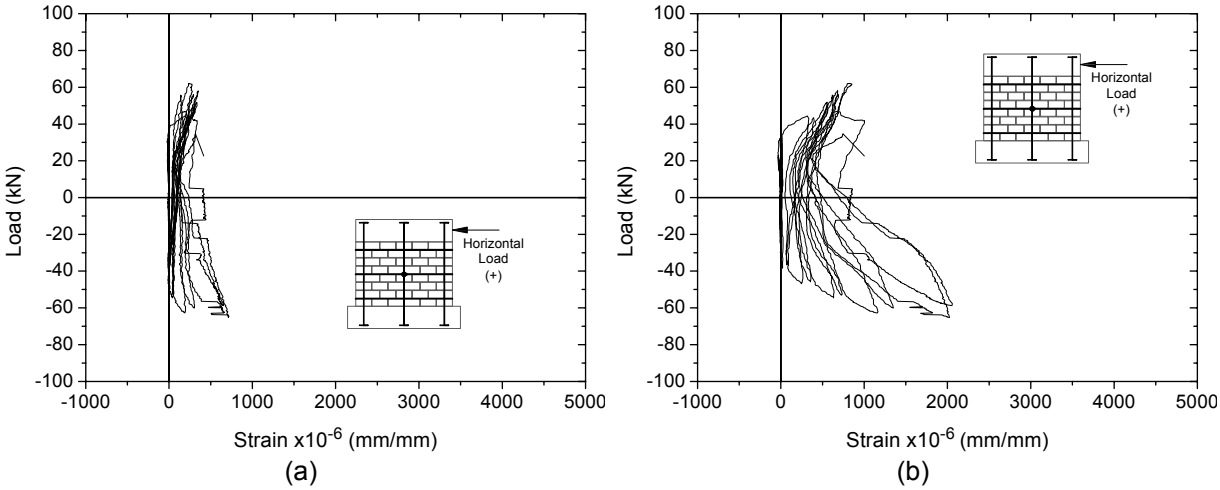

Figure A.31 – Strains in horizontal reinforcement (N60-3C-B2): (a) Ext. 7 and (b) Ext. 8.

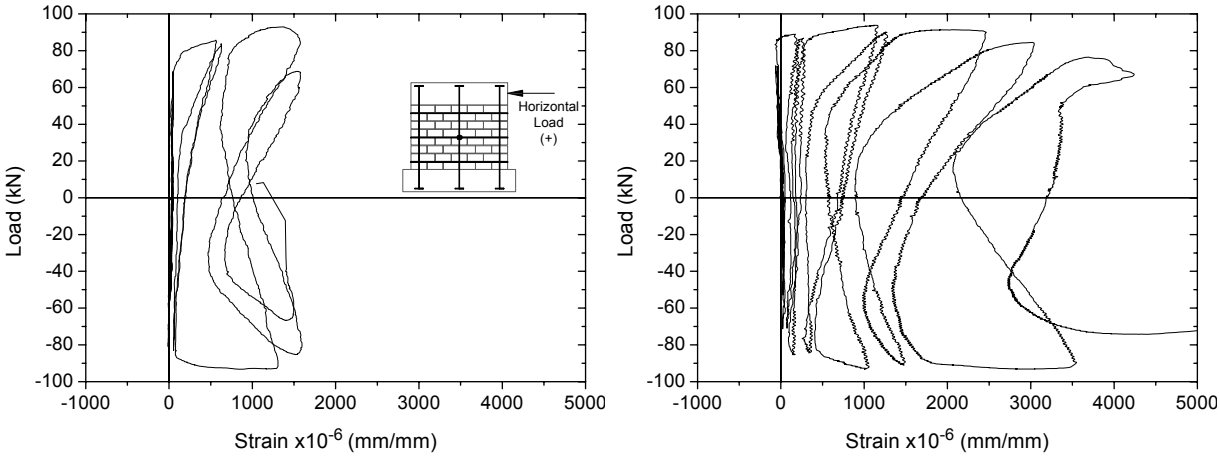

Figure A.32 – Strains in horizontal reinforcement (Ext. 8): (a) specimen N150-3C-B1 and (b) specimen N150-3C-B2.

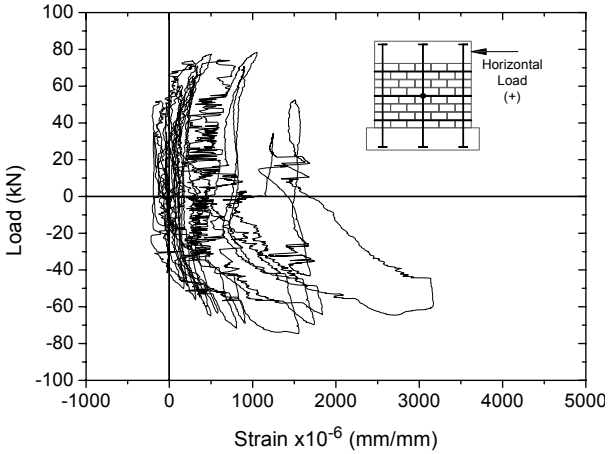

Figure A.33 – Strains in horizontal reinforcements of specimen N60-3C-B1-MA (Ext. 8).

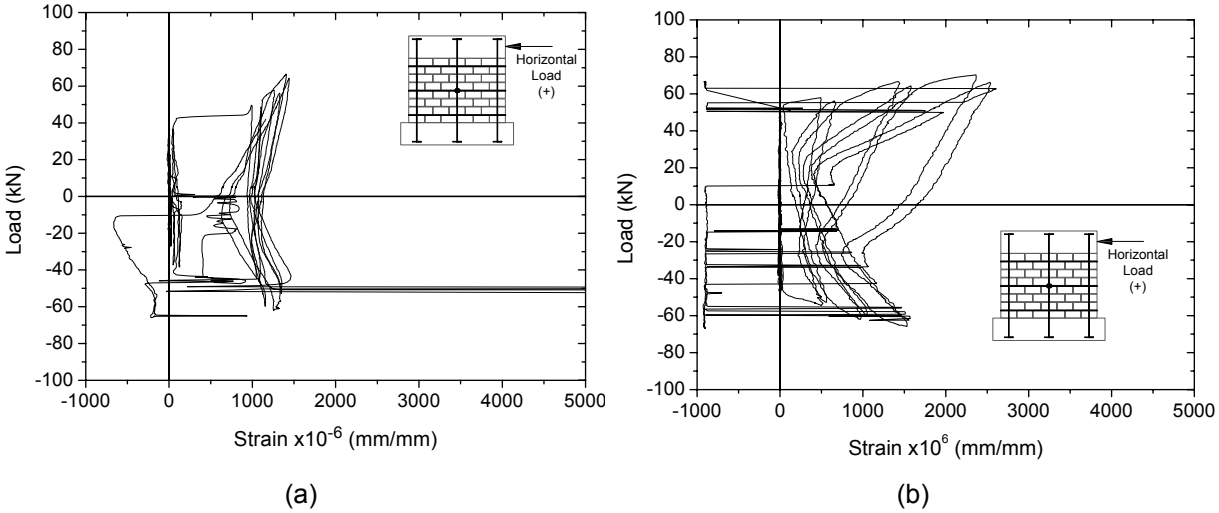

Figure A.34 – Strains in horizontal reinforcement (N60-3C-B1-PA): (a) Ext. 7 and (b) Ext. 8.

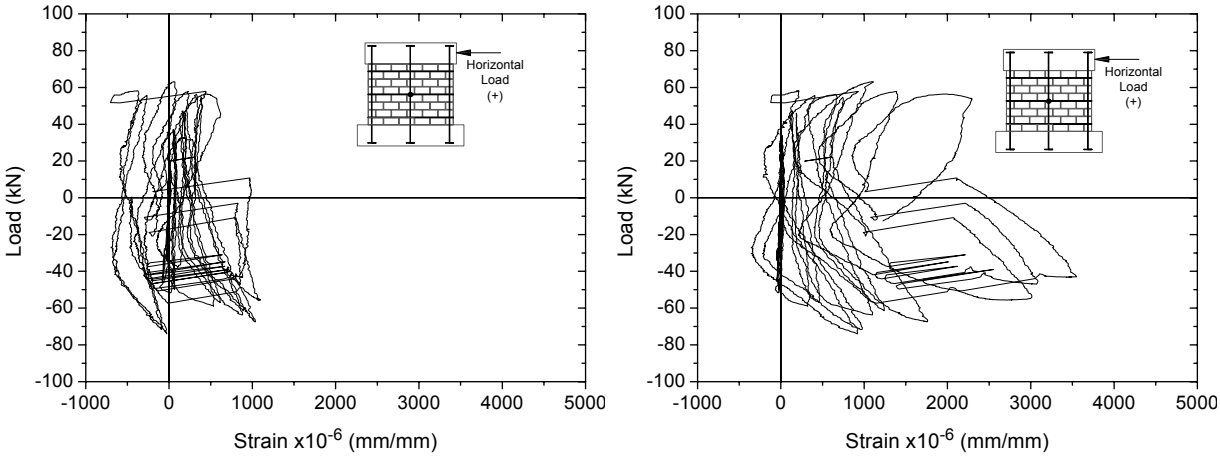

Figure A.35 – Strains in horizontal reinforcement (N60-2C-B1): (a) Ext. 7 and (b) Ext. 8.

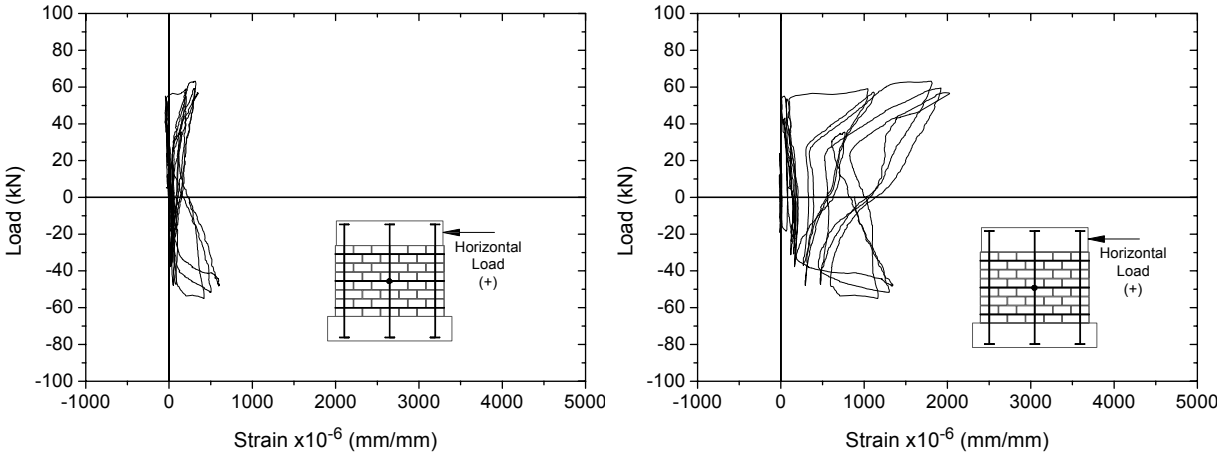

Figure A.36 – Strains in horizontal reinforcement (N60-2C-B2): (a) Ext. 7 and (b) Ext. 8.

A.7 Strain-gauges in vertical reinforcements

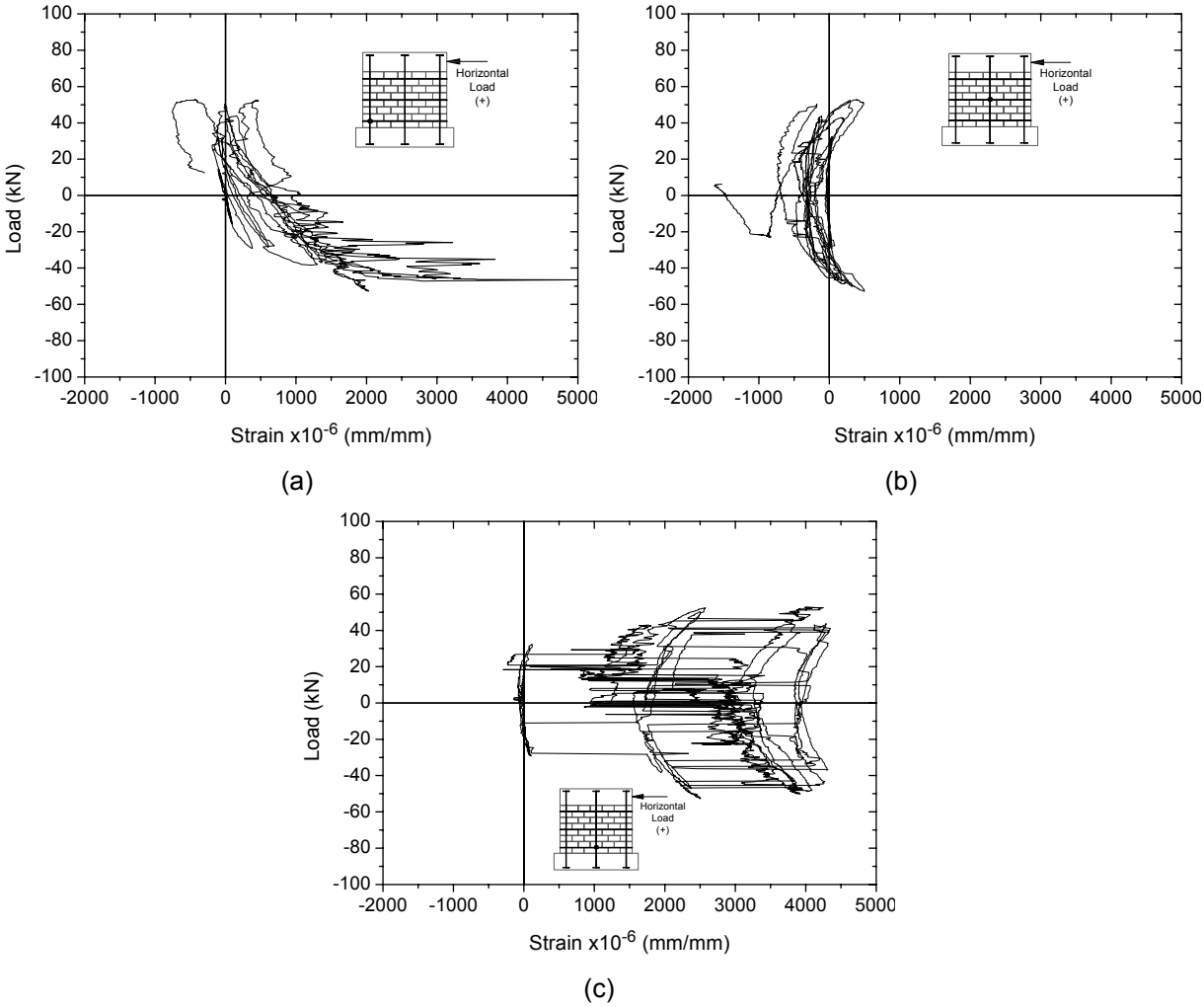

Figure A.37 – Strains in vertical reinforcement (N60-3C-B1): (a) Ext. 1, (b) Ext. 3 and (c) Ext. 5.

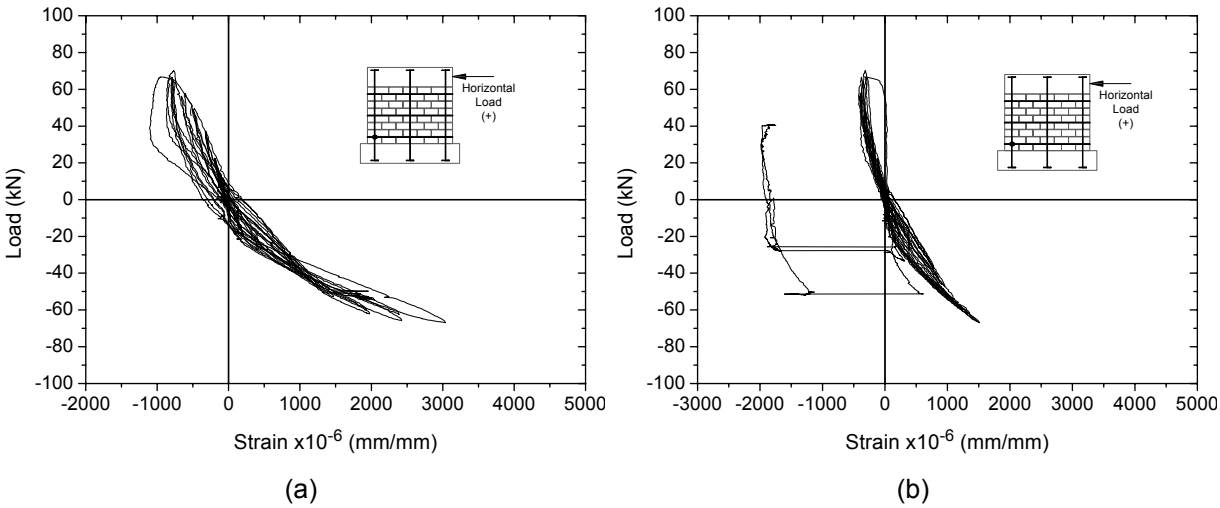

Figure A.38 – Strains in vertical reinforcement (N60-3C-B1-PA): (a) Ext. 1 and (c) Ext. 2.

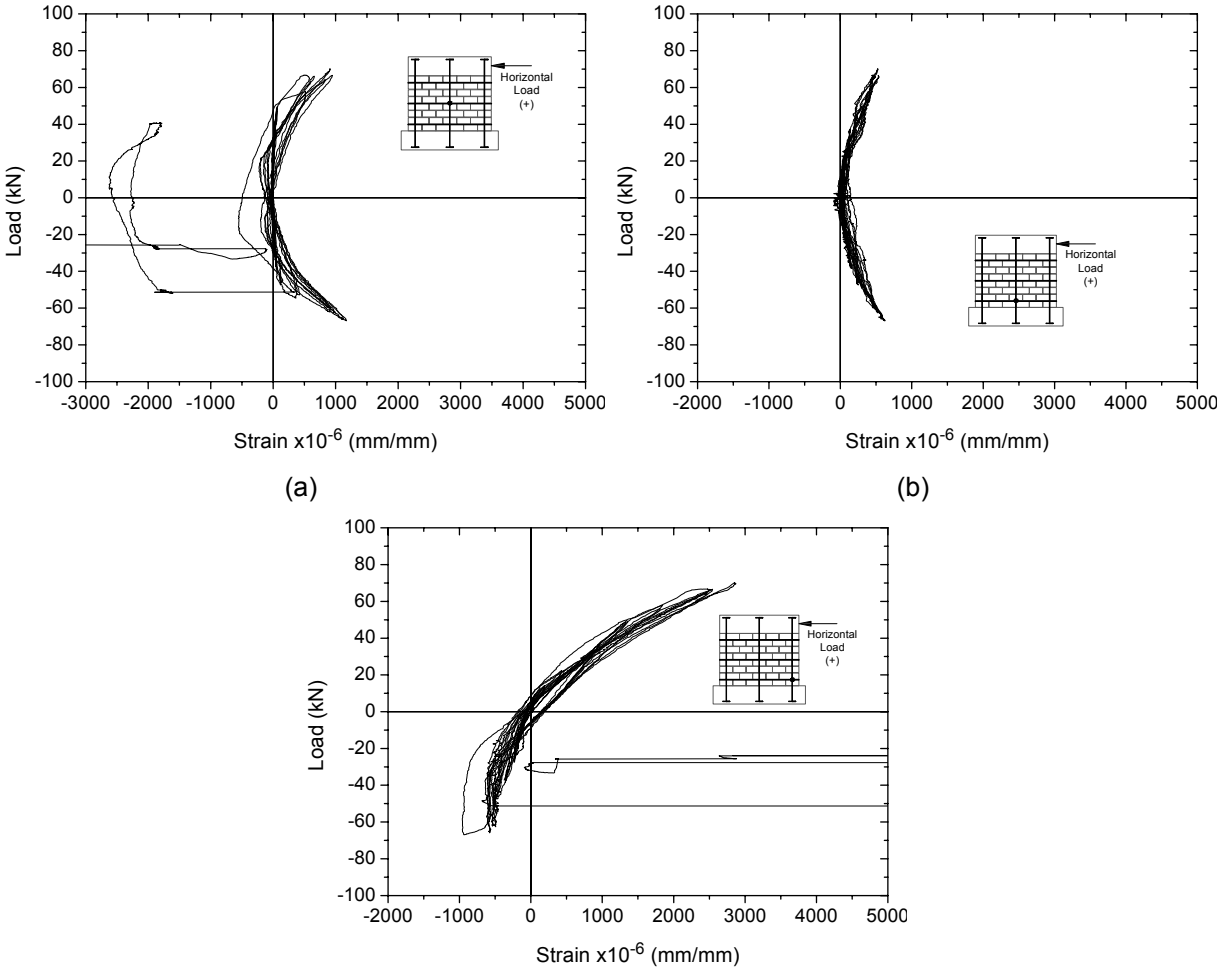

Figure A.39 – Strains in vertical reinforcement (N60-3C-B1-PA): (a) Ext. 4, (b) Ext. 5 and (c) Ext. 6.

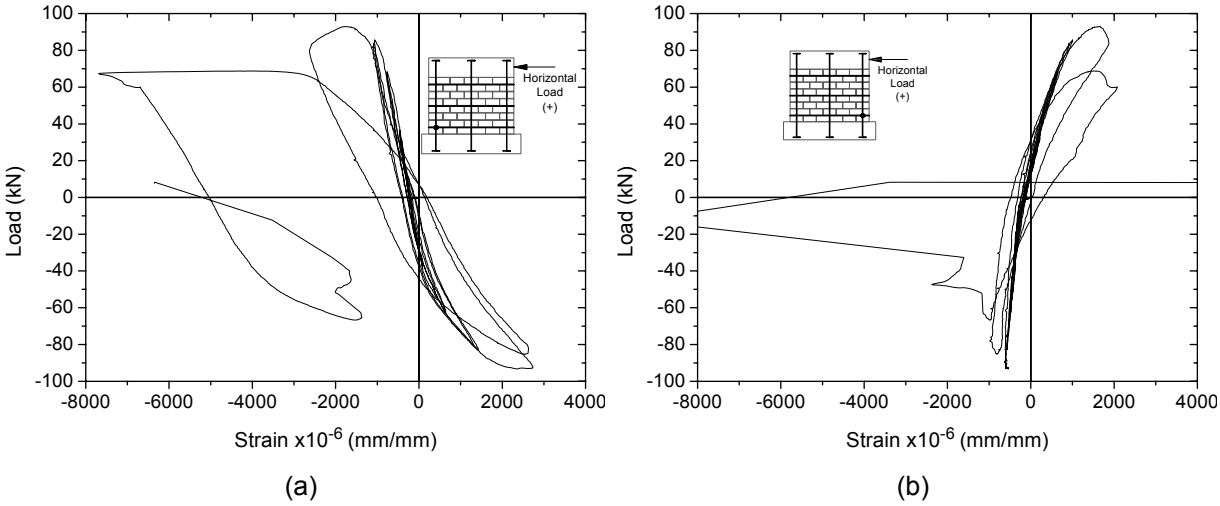

Figure A.40 – Strains in vertical reinforcement (N150-3C-B1): (a) Ext. 1 and (c) Ext. 6.

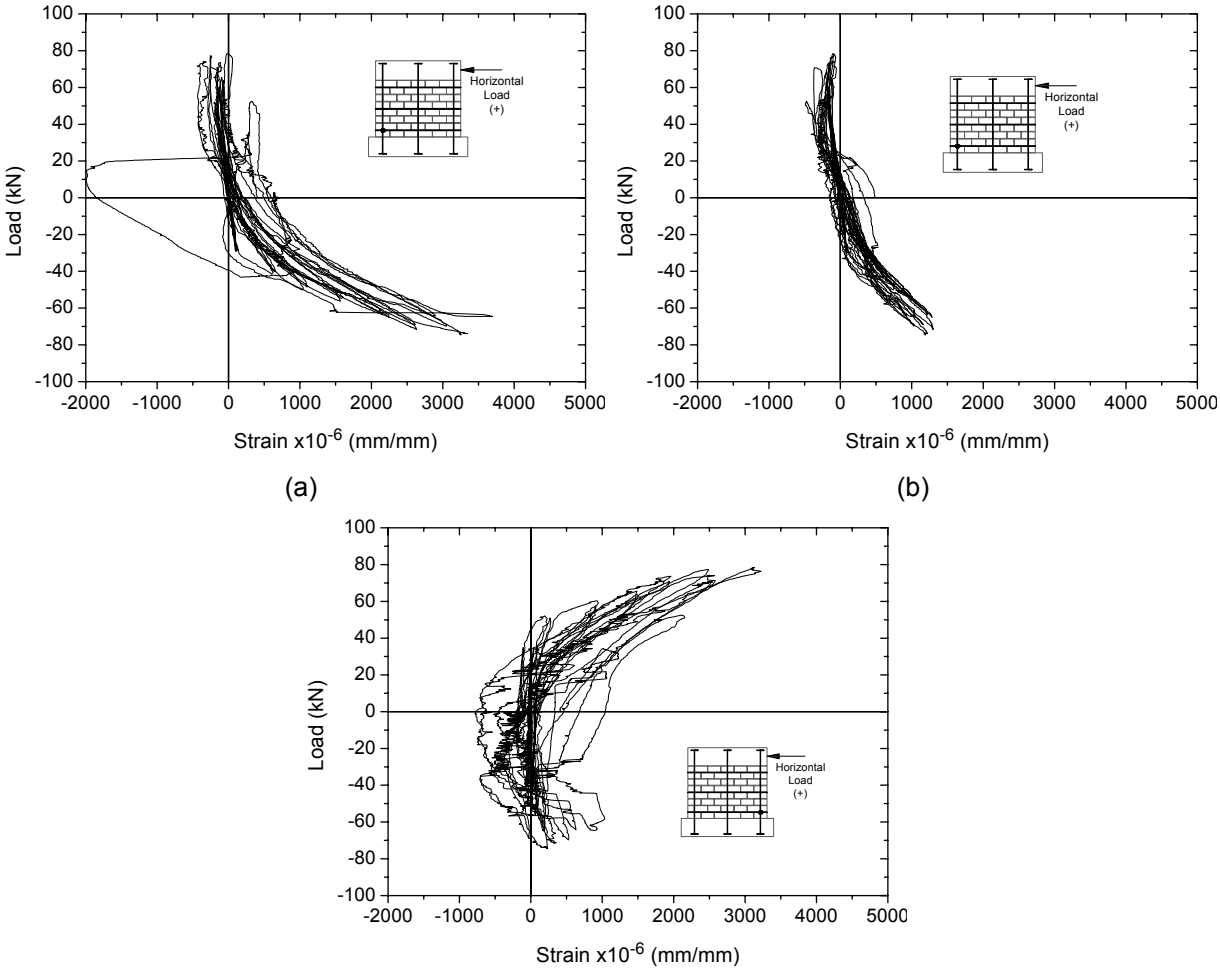

Figure A.41 – Strains in vertical reinforcement (N60-3C-B1-MA): (a) Ext. 1, (b) Ext. 2 and (c) Ext. 5.

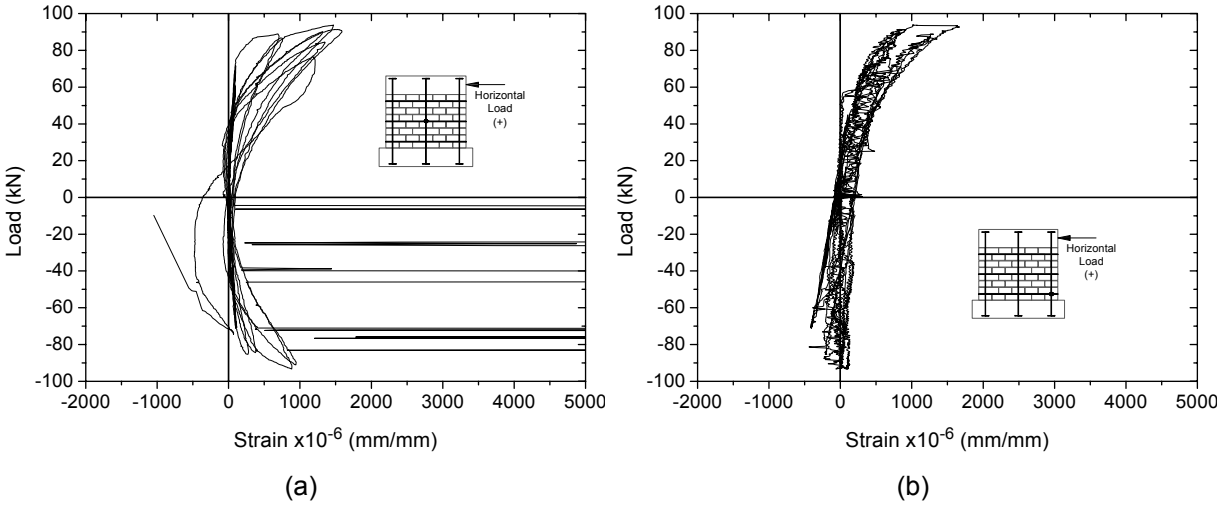

Figure A.42 – Strains in vertical reinforcement (N150-3C-B2): (a) Ext. 3 and (c) Ext. 6.

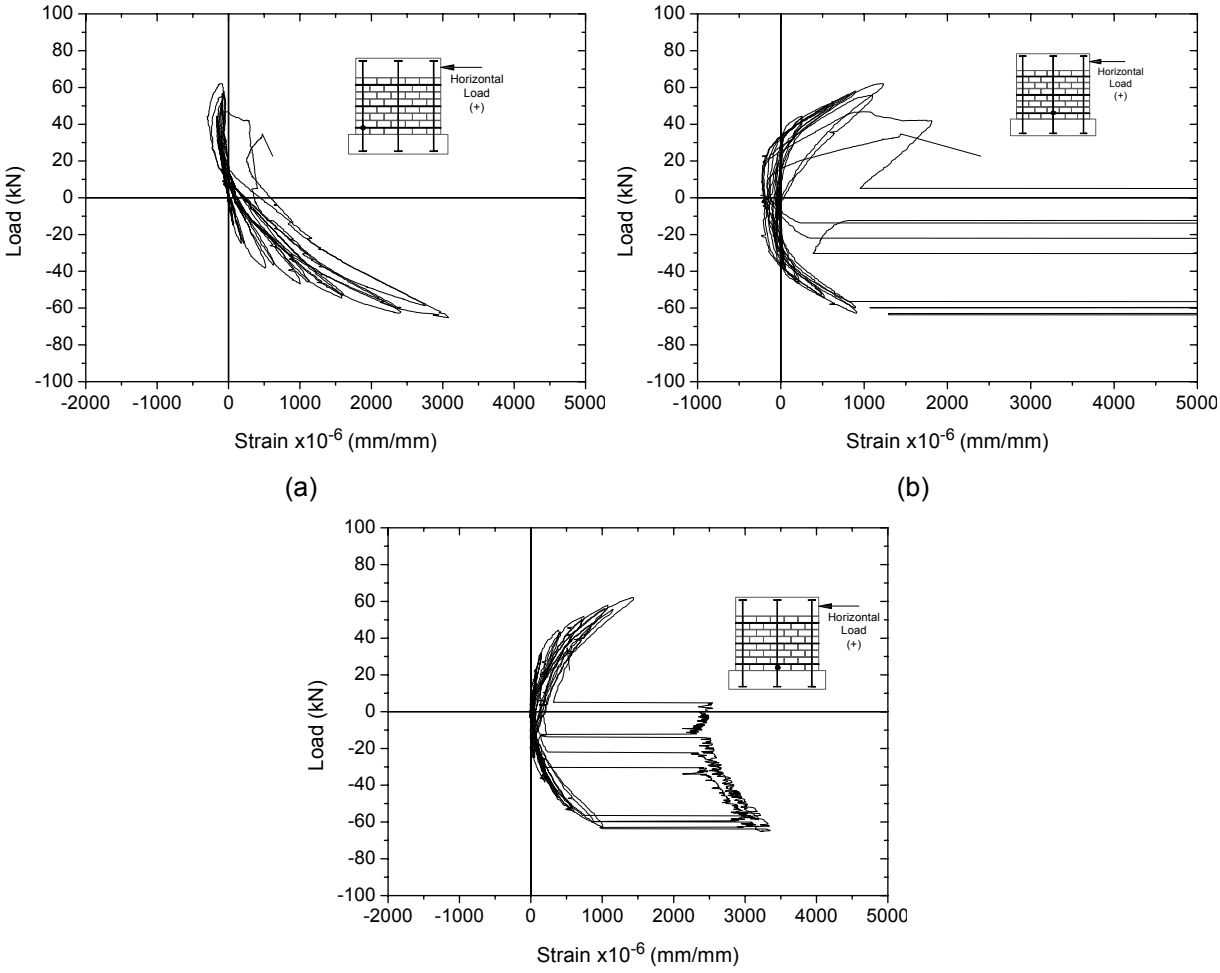

Figure A.43 – Strains in vertical reinforcement (N60-3C-B2): (a) Ext. 1, (b) Ext. 3 and (c) Ext. 5.

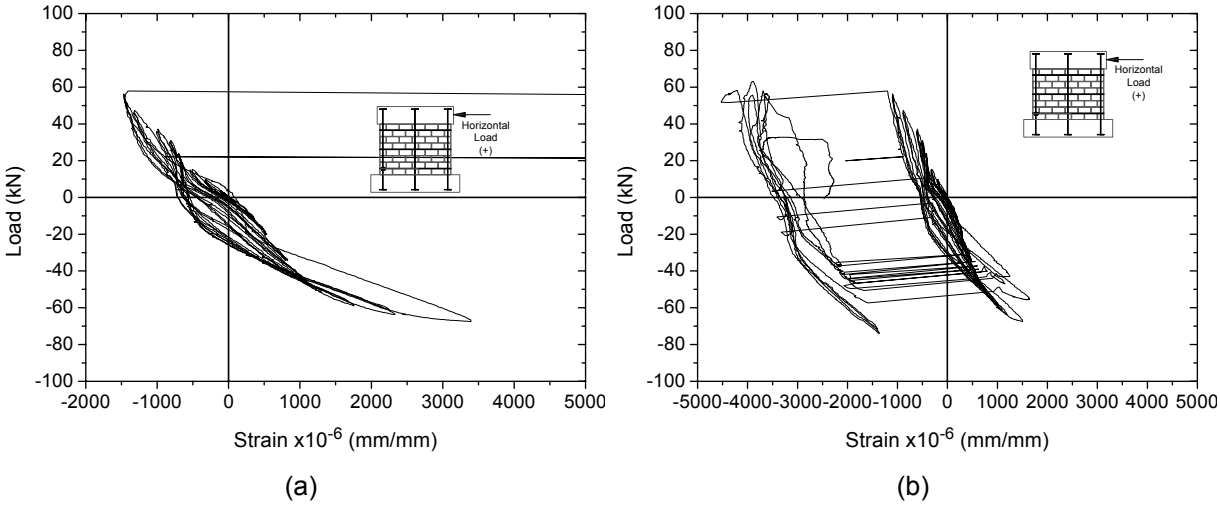

Figure A.44 – Strains in vertical reinforcement (N60-2C-B1): (a) Ext. 1 and (c) Ext. 2.

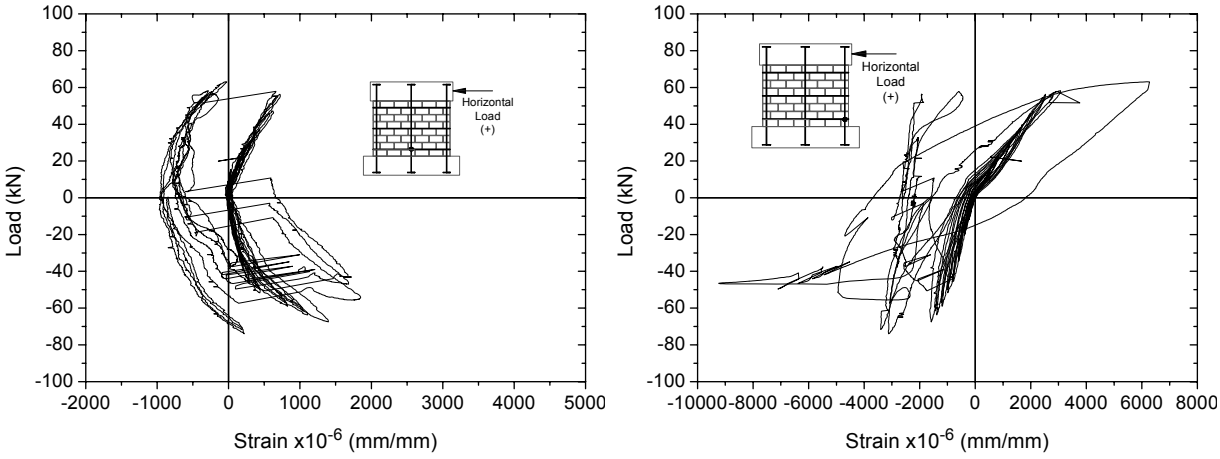

Figure A.45 – Strains in vertical reinforcement (N60-2C-B1): (a) Ext. 5 and (c) Ext. 6.

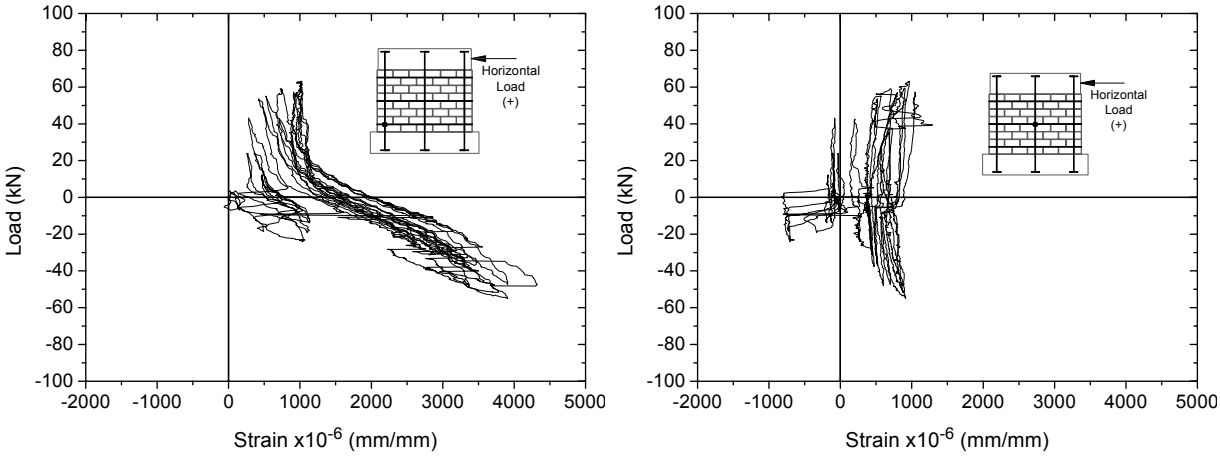

Figure A.46 – Strains in vertical reinforcement (N60-2C-B2): (a) Ext. 1 and (c) Ext. 3.

Obs.: Some strain-gauges exhibited damages and did not show measurements.

APPENDIX B – INTERNAL FORCES ON WALLS AND BEAMS OF MASONRY BUILDING

B.1 Load Combination I - Live load as the main action

Table B.1 – Bending moments and shear forces in beams for lateral load applied in x-direction with live load as the main action.

Beam	1ST FLOOR		2ND FLOOR		3RD FLOOR		4TH FLOOR		5TH FLOOR		6TH FLOOR		7TH FLOOR		ROOF	
	M (kNcm)	V (kN)	M (kNcm)	V (kN)	M (kNcm)	V (kN)	M (kNcm)	V (kN)	M (kNcm)	V (kN)	M (kNcm)	V (kN)	M (kNcm)	V (kN)	M (kNcm)	V (kN)
L1a	799.5	-17.3	1043.0	-20.6	1160.0	-22.1	1260.0	-22.9	1383.0	-23.6	1550.0	-23.9	1781.0	-23.4	432.6	-8.3
L1b	-717.9	-9.4	-781.5	-7.0	-764.5	7.9	-751.5	10.7	-740.7	13.4	-663.8	15.8	899.9	17.4	296.8	6.6
L2a	-482.0	-9.5	-823.4	-12.5	-1046.0	-13.9	-1282.0	-15.8	-1561.0	-18.5	-1915.0	-22.5	-2364.0	-28.5	471.3	-11.5
L2b	1123.0	-19.9	1269.0	-22.8	1107.0	-21.9	782.1	-19.0	-645.1	-14.3	-546.3	-7.9	-889.9	12.5	259.8	7.1
L3	-1008.0	-16.8	-1298.0	-21.8	-1369.0	-23.1	-1359.0	-22.5	-1315.0	-20.8	-1266.0	-18.3	-1247.0	-15.0	-1317.0	-6.5
L4a	-234.4	-5.8	-252.7	-5.7	-249.1	-5.7	-242.6	-5.9	-243.9	-5.9	-259.2	-5.7	-296.2	5.4	79.8	-3.7
L4b	-328.7	5.6	-360.8	6.2	-365.7	6.3	-362.0	6.2	-359.7	6.2	-367.3	6.3	-394.9	6.6	-78.2	-3.5
L5a	140.4	-6.7	170.7	-7.3	193.8	-7.8	211.4	-8.2	223.2	-8.5	228.1	-8.6	225.0	-8.3	145.8	-7.7
L5b	-68.9	-3.7	-64.2	-3.9	-55.4	-4.3	-47.3	-4.8	74.6	-5.3	99.8	-5.8	118.1	-6.0	-85.7	-6.2
L6a	-652.5	8.6	-683.5	7.3	-677.7	-7.7	-669.0	-8.2	-670.8	-8.7	-696.5	-9.2	-748.9	-9.9	180.5	-5.0
L6b	-623.6	-8.0	-744.4	-7.8	-782.3	-7.9	-787.7	-8.3	-788.4	-8.8	-806.0	-9.3	-851.6	-10.0	165.3	-4.9
L7a	88.0	4.6	89.9	4.7	88.5	4.7	88.2	4.7	90.9	4.8	98.5	5.0	119.8	5.6	0.0	4.6
L7b	-136.1	-5.6	-86.8	-4.9	61.7	-4.3	74.1	4.2	88.3	4.7	108.4	5.3	144.2	6.1	0.0	-5.6
L8a	310.0	-8.6	-101.5	5.5	122.8	7.5	243.1	9.4	362.0	11.2	470.4	12.6	556.5	13.6	484.9	11.9
L8b	-103.1	-4.2	407.8	-9.9	463.3	-10.7	498.5	-11.1	521.8	-11.4	534.9	-11.6	542.1	-11.7	423.1	-9.8
L9a	-125.8	7.6	-152.1	9.3	-182.8	10.7	-210.5	11.7	-225.7	12.1	-217.0	11.5	-177.3	9.1	-2213.0	-15.3
L9b	-177.8	10.4	-229.1	12.0	-267.6	13.0	-292.4	13.7	-295.9	13.7	-267.8	12.8	-204.0	9.9	-2659.0	-16.1
L10a	376.2	-10.8	542.0	-13.7	644.9	-15.5	718.6	-16.6	775.2	-17.4	816.4	-17.7	842.3	-17.8	713.0	-14.6
L10b	-115.5	-6.7	-395.6	-8.7	-485.0	-7.4	-562.1	-7.8	-644.0	-9.2	-732.6	-11.0	-790.2	-12.5	-495.5	-6.7
L11a	-256.5	-10.3	-304.6	-12.3	-356.3	-13.5	-397.0	-14.8	-435.0	-16.2	-470.2	-18.0	-482.1	-19.5	-363.7	-13.7
L11b	206.2	-8.8	-95.6	4.6	-78.5	5.4	133.5	6.3	203.7	7.3	269.3	8.1	325.9	8.9	265.1	7.9
L12a	795.6	-16.4	1128.0	-20.6	1336.0	-23.1	1506.0	-24.8	1678.0	-26.0	1883.0	-26.8	2136.0	-26.8	571.6	-10.7
L12b	-558.2	-7.5	-651.8	-13.0	-742.5	-11.2	-819.8	-8.3	-975.7	8.9	-1323.0	13.9	-1776.0	20.2	315.1	8.7
L13a	-565.6	-11.0	-611.9	9.5	-682.6	12.9	-740.6	16.0	-732.7	18.6	1072.0	20.9	1456.0	22.4	455.2	9.4
L13b	-441.9	-12.7	-623.2	-9.9	-728.8	-10.6	-888.0	-12.1	-1161.0	-14.9	-1583.0	-19.6	-2208.0	-27.1	498.9	-11.4
L14	-740.2	-16.3	-980.9	-17.9	-1187.0	-18.0	-1409.0	-17.3	-1684.0	-16.3	-2077.0	-14.9	-2769.0	-13.2	-5046.0	-14.8

Table B.2 – Axial forces in walls for lateral load applied in x-direction with live load as the main action.

Wall	BASEMENT	1ST FLOOR	2ND FLOOR	3RD FLOOR	4TH FLOOR	5TH FLOOR	6TH FLOOR	7TH FLOOR
	N (kN)	N (kN)	N (kN)	N (kN)	N (kN)	N (kN)	N (kN)	N (kN)
P1a	-48.7	-49.8	-42.2	-34.7	-27.3	-19.9	-12.6	-6.3
P1b	-58.0	-44.6	-39.1	-32.9	-26.5	-19.7	-12.8	-6.1
P2a	-358.7	-346.1	-295.7	-244.8	-193.8	-142.5	-91.1	-39.1
P2b	-394.0	-319.2	-276.7	-232.2	-186.2	-138.6	-89.8	-39.0
P3a	-168.1	-148.2	-127.3	-105.9	-84.2	-62.4	-40.2	-17.6
P3b	-161.0	-139.6	-120.0	-100.4	-80.3	-59.8	-38.8	-18.0
P4a	-261.2	-234.2	-202.2	-170.4	-138.6	-106.2	-72.2	-33.5
P4b	-267.5	-228.2	-197.0	-166.1	-135.1	-103.4	-70.3	-33.9
P5a	-621.9	-549.7	-472.9	-397.1	-321.4	-244.4	-165.0	-82.3
P5b	-628.5	-541.5	-463.7	-388.1	-313.2	-237.8	-160.8	-81.3
P6a	-61.5	-52.4	-45.0	-37.8	-30.5	-23.1	-15.7	-8.3
P6b	-60.8	-52.2	-44.3	-36.8	-29.5	-22.3	-15.1	-8.1
P7a	-527.8	-480.8	-423.6	-366.2	-309.3	-253.4	-198.8	-141.7
P7b	-536.0	-476.1	-420.6	-363.7	-306.6	-249.5	-191.2	-125.4
P8a	-566.3	-497.5	-437.9	-379.6	-322.8	-268.9	-220.8	-189.2
P8b	-559.6	-499.4	-436.9	-376.8	-318.7	-263.6	-214.4	-194.2
P9	-338.0	-309.8	-277.5	-242.8	-207.3	-171.6	-136.2	-22.8
P10	-160.8	-147.1	-130.9	-114.0	-96.9	-80.0	-63.7	-80.3
P11a	-239.5	-236.8	-200.6	-165.4	-130.6	-96.1	-62.0	-27.5
P11b	-274.9	-214.0	-186.2	-156.6	-125.8	-94.2	-61.8	-28.0
P12a	-283.1	-267.1	-228.0	-189.0	-150.0	-111.2	-72.5	-35.2
P12b	-305.7	-248.9	-214.4	-179.2	-143.4	-107.1	-70.4	-34.6
P13a	-370.0	-333.4	-286.9	-239.4	-191.4	-143.2	-95.2	-46.8
P13b	-378.8	-322.4	-274.8	-228.1	-181.9	-135.9	-90.4	-45.0
P14a	-251.5	-218.5	-188.6	-158.0	-126.9	-95.6	-64.4	-34.1
P14b	-247.7	-215.7	-182.7	-151.1	-120.3	-90.0	-60.2	-31.8
P15a	-431.8	-392.0	-337.1	-280.9	-223.7	-166.0	-108.0	-50.1
P15b	-445.9	-372.3	-317.9	-264.6	-211.1	-156.7	-102.0	-47.5
P16a	-645.3	-568.8	-487.9	-405.0	-321.0	-236.1	-150.8	-66.5
P16b	-573.9	-518.0	-452.5	-381.3	-306.3	-228.4	-147.8	-65.5
P17a	-338.5	-300.5	-259.5	-216.7	-172.7	-127.6	-81.3	-32.6
P17b	-315.4	-279.9	-243.1	-204.6	-164.4	-122.5	-78.8	-32.8
P18a	-124.2	-109.7	-93.9	-78.6	-63.4	-47.9	-32.1	-16.2
P18b	-127.7	-106.5	-91.0	-76.1	-61.4	-46.5	-31.2	-15.8
P19a	-632.8	-554.7	-477.2	-400.7	-324.1	-246.0	-165.1	-80.7
P19b	-616.2	-538.6	-462.6	-388.2	-313.8	-238.3	-160.1	-78.9
P20a	-213.0	-186.8	-161.5	-136.2	-110.7	-84.7	-57.4	-26.0
P20b	-207.7	-181.3	-156.5	-131.9	-107.2	-82.0	-55.5	-25.7
P21a	-481.7	-435.2	-376.2	-321.0	-267.9	-215.3	-160.3	-93.0
P21b	-501.6	-425.1	-370.7	-317.6	-265.5	-213.4	-158.7	-91.7
P22a	-773.0	-694.3	-611.2	-527.8	-446.0	-367.4	-295.3	-218.5
P22b	-788.7	-697.7	-608.3	-521.8	-438.2	-358.4	-285.2	-224.8
P23a	-367.2	-325.8	-285.2	-245.1	-205.7	-167.4	-130.3	-91.5
P23b	-359.5	-321.6	-282.0	-242.2	-203.0	-164.5	-126.4	-83.9
P24a	-192.7	-172.3	-151.6	-130.9	-110.5	-91.0	-72.8	-65.2
P24b	-194.2	-172.1	-150.9	-129.9	-109.4	-89.6	-71.0	-66.7
P25	-399.4	-352.9	-306.4	-259.9	-213.4	-166.9	-120.4	-24.0

Table B.3 – Shear forces in walls for lateral load applied in x-direction with live load as the main action.

Wall	BASEMENT		1ST FLOOR		2ND FLOOR		3RD FLOOR		4TH FLOOR		5TH FLOOR		6TH FLOOR		7TH FLOOR	
	Vx (kN)	Vy (kN)	Vx (kN)	Vy (kN)	Vx (kN)	Vy (kN)	Vx (kN)	Vy (kN)	Vx (kN)	Vy (kN)	Vx (kN)	Vy (kN)	Vx (kN)	Vy (kN)	Vx (kN)	Vy (kN)
P2a	-6.5	0.0	-10.4	0.0	-11.0	0.0	-11.5	0.1	-12.0	0.1	-12.5	0.1	-12.8	0.1	-11.0	0.0
P2b	-9.4	0.0	-3.2	-0.1	-0.9	-0.1	1.1	-0.1	3.2	0.0	5.3	0.0	7.3	0.0	8.3	0.0
P4a	-4.7	0.0	-6.4	0.0	-7.1	0.0	-7.6	0.0	-8.3	0.0	-9.4	0.0	-10.9	0.0	-11.9	0.0
P4b	-5.0	0.0	-5.3	-0.1	-4.4	-0.1	-2.9	-0.1	-0.9	-0.1	1.6	-0.1	4.4	0.0	6.6	0.0
P6a	-0.1	0.0	-0.2	0.0	-0.3	0.0	-0.3	0.0	-0.4	0.0	-0.4	0.0	-0.4	0.0	-0.4	0.0
P6b	-0.1	0.0	-0.1	0.0	-0.1	0.0	0.0	0.0	0.1	0.0	0.1	0.0	0.2	0.0	0.2	0.0
P7a	-14.8	-0.1	-12.5	-0.1	-11.7	-0.2	-11.3	-0.2	-11.3	-0.2	-11.8	-0.2	-13.3	-0.3	-20.2	-0.5
P7b	-13.8	-0.1	-14.7	-0.1	-13.9	-0.2	-12.0	-0.2	-9.1	-0.2	-5.1	-0.2	0.7	-0.3	11.4	-0.6
P10	-1.7	0.0	-2.1	0.0	-2.0	0.0	-1.9	0.0	-1.7	0.0	-1.6	0.0	-1.4	-0.1	-7.0	0.0
P12a	-4.0	0.0	-4.7	0.0	-4.3	0.0	-4.2	0.0	-4.2	0.0	-4.3	0.0	-4.4	0.0	-5.2	0.1
P12b	-5.1	0.0	-1.8	0.0	-0.1	0.0	1.1	0.0	2.1	0.0	3.0	0.0	4.0	0.0	5.6	0.0
P14a	-2.0	0.0	-4.8	0.0	-5.2	0.0	-5.5	0.0	-5.6	0.0	-5.8	0.0	-5.8	0.0	-7.0	0.0
P14b	-3.9	0.0	-0.2	0.0	0.8	0.0	1.7	0.0	2.5	0.0	3.3	0.0	4.0	0.0	5.6	0.0
P15a	-5.2	0.0	-14.4	0.1	-15.6	0.1	-16.4	0.2	-17.1	0.2	-17.6	0.2	-17.9	0.2	-21.8	0.2
P15b	-11.9	0.1	2.2	0.0	6.3	0.1	9.0	0.1	11.1	0.1	12.9	0.2	14.7	0.2	19.8	0.3
P17a	-8.1	0.0	-11.5	0.0	-13.4	0.0	-14.8	0.0	-15.9	0.0	-16.8	0.0	-17.4	0.0	-15.3	0.0
P17b	-3.4	0.0	0.6	0.0	3.4	0.0	5.9	0.0	8.2	0.0	10.5	0.0	12.5	0.0	12.3	0.0
P18a	-0.6	0.0	-2.1	0.0	-2.6	0.1	-3.0	0.1	-3.3	0.1	-3.7	0.1	-4.0	0.1	-4.3	0.1
P18b	-1.1	0.0	-0.6	0.0	-0.1	0.1	0.4	0.1	1.0	0.1	1.7	0.1	2.3	0.1	2.8	0.1
P20a	-2.9	0.0	-4.5	0.0	-5.5	0.0	-6.2	0.0	-6.9	0.0	-7.7	0.0	-8.7	0.0	-9.6	0.0
P20b	-1.9	0.0	-1.5	0.0	-0.5	0.0	0.8	0.0	2.2	0.0	3.7	0.0	5.4	0.0	6.8	0.0
P21a	-9.8	0.0	-4.7	0.1	-3.4	0.1	-3.3	0.1	-4.1	0.1	-6.0	0.1	-10.5	0.0	-24.6	0.0
P21b	-7.9	0.0	-9.2	0.1	-8.4	0.1	-7.0	0.1	-4.9	0.1	-1.6	0.1	4.2	0.1	18.5	0.0
P23a	-7.1	0.0	-8.8	0.0	-9.6	0.0	-10.2	0.0	-10.7	0.0	-11.6	0.0	-13.2	0.0	-17.4	0.1
P23b	-6.8	0.0	-7.5	0.0	-6.5	0.0	-4.9	0.0	-2.6	0.1	0.2	0.1	4.0	0.1	10.4	0.1
P24a	-1.9	0.0	-2.6	0.0	-2.7	0.0	-2.7	0.0	-2.7	0.0	-2.7	0.0	-2.7	0.0	-7.4	0.0
P24b	-1.7	0.0	-2.0	0.0	-1.9	0.0	-1.6	0.0	-1.2	0.0	-0.6	0.0	0.1	0.1	-7.4	0.1

Table B.4 – Bending moments in walls for lateral load applied in x-direction with live load as the main action.

Wall	BASEMENT		1ST FLOOR		2ND FLOOR		3RD FLOOR		4TH FLOOR		5TH FLOOR		6TH FLOOR		7TH FLOOR	
	Mx (kNcm)	My (kNcm)	Mx (kNcm)	My (kNcm)	Mx (kNcm)	My (kNcm)	Mx (kNcm)	My (kNcm)	Mx (kNcm)	My (kNcm)	Mx (kNcm)	My (kNcm)	Mx (kNcm)	My (kNcm)	Mx (kNcm)	My (kNcm)
P2a	8.7	-1638.0	2.5	-1527.0	5.8	1574.0	8.0	1696.0	9.5	1800.0	10.3	1887.0	11.2	1910.0	8.5	-1694.0
P2b	2.1	-1689.0	11.9	-697.1	10.6	-253.8	8.3	-224.2	5.6	-485.7	3.2	-761.8	0.5	-1035.0	9.3	1236.0
P4a	6.0	-732.3	4.8	-900.2	5.5	1010.0	4.8	1106.0	3.0	1227.0	0.2	1396.0	-4.1	1639.0	6.7	1691.0
P4b	2.9	-748.6	11.7	-787.2	14.6	-667.6	14.9	-457.5	13.3	-185.1	10.1	-291.8	-6.3	-700.6	3.5	-957.1
P6a	1.9	13.4	1.7	35.8	1.6	43.8	1.4	48.8	1.2	52.1	0.8	54.3	0.4	55.3	0.2	-54.1
P6b	1.2	21.1	3.2	-16.3	3.5	-10.1	3.4	-1.8	3.1	-9.8	2.6	-18.5	2.1	-26.3	1.8	-30.3
P7a	11.4	-3254.0	19.1	-2115.0	23.3	-1682.0	26.4	1707.0	29.5	1819.0	33.9	1995.0	37.9	2380.0	82.2	4098.0
P7b	11.2	-3305.0	21.0	-2383.0	26.4	-2061.0	29.7	-1762.0	32.4	-1374.0	36.4	-881.2	40.2	-476.0	94.2	-2787.0
P10	2.0	-258.2	2.9	-302.4	3.3	-288.9	3.8	-266.7	4.6	244.0	5.8	219.0	7.8	192.2	-2.3	1125.0
P12a	1.9	-869.9	2.1	-729.1	3.1	-615.8	3.9	607.4	4.4	625.4	4.7	650.3	5.0	670.9	-8.0	835.4
P12b	1.5	-924.3	2.7	-384.7	2.3	-72.6	2.4	-181.6	2.7	-294.4	3.1	422.0	3.4	554.2	-6.3	-853.2
P14a	1.2	-492.6	4.7	-671.9	4.1	741.0	3.7	784.5	3.3	814.8	3.0	838.0	3.1	840.2	-0.6	1092.0
P14b	3.8	-612.8	2.0	-95.4	3.0	-147.8	3.3	-256.7	3.4	-362.5	3.4	-466.8	3.7	563.7	-1.6	-856.4
P15a	2.4	-2013.0	20.9	-2052.0	21.2	2253.0	21.7	2424.0	22.2	2541.0	23.5	2620.0	26.8	2666.0	31.6	3679.0
P15b	-10.7	-2031.0	5.0	-798.7	10.7	-1094.0	15.6	-1344.0	19.6	-1568.0	23.7	1822.0	-29.7	2072.0	-38.6	-3249.0
P17a	1.7	-1163.0	1.2	1661.0	1.6	1950.0	1.6	2153.0	1.4	2315.0	1.4	2442.0	2.1	2521.0	3.2	-2329.0
P17b	2.3	-955.3	3.9	-276.7	3.9	-593.3	3.8	-909.3	3.5	-1218.0	3.2	-1513.0	3.6	-1780.0	4.7	1872.0
P18a	-2.9	-88.0	6.2	304.8	7.1	376.5	7.3	429.6	7.3	477.3	7.2	524.6	7.4	565.3	8.0	603.6
P18b	-3.1	178.3	5.9	-90.8	6.8	-33.6	7.0	-72.3	7.1	-160.4	7.1	-253.6	7.4	-341.0	8.2	-400.1
P20a	1.5	425.5	3.4	658.7	5.1	790.4	5.7	895.1	5.4	998.7	4.5	1118.0	3.5	1270.0	-4.6	1378.0
P20b	1.4	-307.3	3.3	-250.2	5.3	-101.6	6.2	-144.4	6.1	-337.2	5.5	-553.1	4.8	-796.3	-5.8	-970.9
P21a	5.6	-2025.0	8.8	-934.6	8.5	-505.0	8.3	563.1	7.9	768.6	7.5	1160.0	7.2	2034.0	4.9	5045.0
P21b	4.3	-2020.0	12.6	-1459.0	11.9	-1253.0	11.5	-1031.0	10.8	-746.1	10.1	-364.1	9.5	-956.5	7.3	-3931.0
P23a	2.0	-1116.0	1.8	-1231.0	1.2	1372.0	1.8	1475.0	2.4	1580.0	3.3	1732.0	4.5	2013.0	-14.6	2762.0
P23b	2.3	-1104.0	4.5	-1120.0	6.3	-980.9	7.1	-748.4	7.4	-443.6	7.7	-127.0	8.3	-711.2	-19.6	-1830.0
P24a	1.3	-272.6	1.2	-362.7	0.6	382.8	1.0	386.0	1.7	382.3	2.7	380.2	-4.3	394.2	8.1	1092.0
P24b	1.4	-253.4	3.1	-287.0	4.4	-273.2	5.1	-232.4	5.6	-173.4	6.1	-98.5	7.3	-31.6	9.6	-1276.0

Table B.5 – Axial forces in walls for lateral load applied in positive y-direction with live load as the main action.

Wall	BASEMENT	1ST FLOOR	2ND FLOOR	3RD FLOOR	4TH FLOOR	5TH FLOOR	6TH FLOOR	7TH FLOOR
	N (kN)	N (kN)	N (kN)	N (kN)	N (kN)	N (kN)	N (kN)	N (kN)
P1a	-45.9	-41.1	-36.0	-30.6	-24.9	-18.8	-12.3	-6.2
P1b	-45.9	-41.0	-36.0	-30.6	-24.9	-18.8	-12.3	-6.2
P2a	-322.0	-288.5	-253.2	-215.9	-175.9	-133.2	-87.5	-38.4
P2b	-322.0	-288.5	-253.2	-215.8	-175.8	-133.1	-87.4	-38.4
P3a	-145.5	-127.9	-111.5	-94.6	-76.9	-58.1	-38.1	-17.1
P3b	-145.6	-127.9	-111.6	-94.6	-76.9	-58.1	-38.1	-17.2
P4a	-224.7	-202.3	-179.7	-155.2	-129.2	-101.3	-70.8	-34.9
P4b	-224.1	-202.8	-180.1	-155.5	-129.3	-101.2	-70.4	-34.7
P5a	-624.0	-535.3	-452.9	-375.4	-300.8	-227.2	-153.3	-77.9
P5b	-623.0	-536.3	-453.7	-376.0	-301.0	-227.2	-153.0	-77.7
P6a	-69.1	-56.1	-45.7	-36.7	-28.6	-20.9	-13.7	-7.4
P6b	-69.0	-56.2	-45.8	-36.8	-28.6	-20.9	-13.7	-7.4
P7a	-451.7	-416.3	-377.7	-334.8	-289.1	-241.5	-191.6	-134.9
P7b	-449.5	-418.9	-379.9	-336.5	-290.2	-241.4	-189.2	-127.6
P8a	-540.3	-470.4	-411.4	-356.6	-303.8	-253.2	-207.1	-180.6
P8b	-538.2	-472.5	-413.3	-358.2	-305.1	-254.2	-208.1	-192.4
P9	-330.1	-294.2	-259.9	-226.2	-192.9	-160.0	-127.7	-22.8
P10	-137.0	-129.3	-117.6	-104.5	-90.6	-76.2	-61.6	-77.5
P11a	-239.2	-211.5	-184.2	-155.6	-125.7	-94.6	-62.3	-28.5
P11b	-239.4	-211.4	-184.1	-155.5	-125.6	-94.4	-62.2	-28.5
P12a	-269.1	-240.4	-209.1	-176.5	-142.6	-107.5	-71.5	-35.4
P12b	-269.2	-240.4	-209.1	-176.4	-142.5	-107.5	-71.4	-35.4
P13a	-367.8	-320.5	-273.8	-227.6	-181.6	-135.8	-90.2	-44.2
P13b	-367.8	-320.6	-273.8	-227.6	-181.6	-135.8	-90.3	-44.2
P14a	-261.2	-222.2	-186.3	-152.7	-120.5	-89.2	-59.1	-31.6
P14b	-261.1	-222.3	-186.4	-152.8	-120.5	-89.3	-59.2	-31.6
P15a	-437.7	-385.7	-334.1	-280.5	-224.8	-167.6	-109.2	-49.5
P15b	-437.8	-385.6	-334.1	-280.4	-224.8	-167.6	-109.1	-49.5
P16a	-659.3	-586.1	-503.8	-417.7	-330.1	-242.1	-154.3	-67.7
P16b	-658.9	-585.8	-503.5	-417.4	-329.8	-241.9	-154.2	-67.7
P17a	-387.9	-336.1	-282.9	-230.7	-179.6	-129.7	-80.9	-32.9
P17b	-387.8	-336.0	-282.9	-230.6	-179.5	-129.7	-80.9	-32.9
P18a	-117.7	-105.4	-93.1	-79.8	-65.6	-50.6	-34.4	-17.4
P18b	-117.6	-105.4	-93.2	-79.9	-65.7	-50.6	-34.5	-17.4
P19a	-655.4	-577.0	-497.2	-417.1	-336.5	-254.6	-170.3	-83.0
P19b	-655.7	-577.3	-497.5	-417.4	-336.8	-254.9	-170.5	-83.1
P20a	-245.1	-209.4	-176.4	-145.2	-115.2	-86.0	-56.8	-25.3
P20b	-245.1	-209.5	-176.5	-145.3	-115.3	-86.1	-56.9	-25.4
P21a	-479.8	-426.0	-375.8	-325.7	-274.9	-222.9	-167.2	-97.7
P21b	-479.3	-426.5	-376.4	-326.3	-275.6	-223.8	-168.2	-98.7
P22a	-815.1	-728.3	-637.9	-547.7	-459.8	-375.9	-299.7	-217.2
P22b	-816.0	-729.2	-638.8	-548.7	-460.9	-377.3	-301.6	-223.6
P23a	-418.0	-366.2	-313.7	-263.4	-215.8	-171.4	-129.7	-86.8
P23b	-418.1	-366.4	-314.0	-263.6	-216.1	-171.7	-130.2	-87.7
P24a	-222.9	-194.8	-167.2	-140.8	-116.0	-93.1	-72.6	-61.2
P24b	-223.0	-194.9	-167.3	-140.9	-116.1	-93.3	-72.7	-62.8
P25	-399.4	-352.9	-306.4	-259.9	-213.4	-166.9	-120.4	-24.0

Table B.6 – Shear forces in walls for lateral load applied in positive y-direction with live load as the main action.

Wall	BASEMENT		1ST FLOOR		2ND FLOOR		3RD FLOOR		4TH FLOOR		5TH FLOOR		6TH FLOOR		7TH FLOOR	
	Vx (kN)	Vy (kN)	Vx (kN)	Vy (kN)	Vx (kN)	Vy (kN)	Vx (kN)	Vy (kN)	Vx (kN)	Vy (kN)	Vx (kN)	Vy (kN)	Vx (kN)	Vy (kN)	Vx (kN)	Vy (kN)
P1a	0.0	0.2	0.0	0.2	0.0	0.2	0.0	0.2	0.0	0.2	0.0	0.2	0.0	0.1	0.0	0.1
P1b	0.0	0.2	0.0	0.2	0.0	0.2	0.0	0.2	0.0	0.2	0.0	0.2	0.0	0.1	0.0	0.1
P3a	0.0	2.6	0.0	3.1	-0.1	3.3	-0.1	3.2	-0.1	2.9	-0.1	2.6	-0.1	2.1	-0.1	1.2
P3b	0.0	2.6	0.0	3.1	0.1	3.3	0.1	3.2	0.1	2.9	0.1	2.5	0.1	2.1	0.1	1.2
P5a	0.1	22.2	-0.2	12.6	-0.3	6.3	-0.3	2.6	-0.4	0.4	-0.4	-1.0	-0.4	-2.1	-0.6	-5.1
P5b	-0.1	22.2	0.2	12.6	0.3	6.4	0.3	2.8	0.4	0.6	0.4	-0.9	0.4	-2.1	0.5	-5.3
P8a	0.0	19.5	0.0	12.7	0.0	8.6	0.0	4.6	0.0	-0.1	0.0	-5.6	0.0	-12.3	-0.1	-8.7
P8b	0.0	19.5	0.0	12.9	0.0	9.0	0.0	5.0	0.0	0.4	0.0	-5.2	0.0	-12.4	0.1	-8.7
P9	0.0	9.0	0.0	5.4	0.0	4.5	0.0	4.1	0.0	3.8	0.0	3.4	0.0	3.1	0.0	3.3
P11a	0.0	8.6	-0.1	11.5	-0.1	12.2	-0.1	11.7	-0.1	10.5	-0.1	9.1	-0.1	7.6	-0.2	5.9
P11b	0.0	8.6	0.1	11.5	0.1	12.2	0.1	11.7	0.1	10.5	0.1	9.1	0.1	7.6	0.2	5.9
P13a	0.0	12.3	-0.1	11.0	-0.1	9.8	-0.2	8.3	-0.2	6.6	-0.2	4.7	-0.2	2.6	-0.3	2.1
P13b	0.0	12.3	0.1	11.0	0.1	9.8	0.2	8.3	0.2	6.6	0.2	4.7	0.2	2.6	0.3	2.1
P16a	0.0	31.7	-0.1	34.0	-0.1	32.5	-0.1	29.6	-0.2	25.9	-0.2	21.9	-0.2	18.0	-0.3	12.2
P16b	0.0	31.7	0.1	34.0	0.1	32.5	0.1	29.6	0.2	25.9	0.2	21.9	0.2	18.0	0.3	12.2
P19a	0.0	25.9	-0.1	25.0	-0.2	22.2	-0.2	19.2	-0.3	16.1	-0.4	12.8	-0.5	9.5	-0.7	7.3
P19b	0.0	25.9	0.1	25.0	0.2	22.2	0.2	19.2	0.3	16.1	0.4	12.8	0.4	9.5	0.7	7.3
P22a	0.0	37.8	0.0	40.7	0.0	38.2	0.0	34.0	-0.1	29.1	-0.1	23.7	-0.1	18.2	-0.2	11.4
P22b	0.0	37.8	0.0	40.9	0.0	38.5	0.0	34.5	0.0	29.7	0.1	24.5	0.1	19.1	0.2	12.8
P25	0.0	7.4	0.0	1.4	0.0	0.9	0.0	0.6	0.0	0.4	0.0	0.3	0.0	0.1	0.0	0.1

Table B.7 – Bending moments in walls for lateral load applied in positive y-direction with live load as the main action.

Wall	BASEMENT		1ST FLOOR		2ND FLOOR		3RD FLOOR		4TH FLOOR		5TH FLOOR		6TH FLOOR		7TH FLOOR	
	Mx (kNcm)	My (kNcm)	Mx (kNcm)	My (kNcm)	Mx (kNcm)	My (kNcm)	Mx (kNcm)	My (kNcm)	Mx (kNcm)	My (kNcm)	Mx (kNcm)	My (kNcm)	Mx (kNcm)	My (kNcm)	Mx (kNcm)	My (kNcm)
P1a	23.1	-0.7	30.5	1.6	32.3	2.4	30.7	3.2	27.1	3.9	22.3	4.5	17.1	5.0	11.0	-4.9
P1b	23.1	0.7	30.5	-1.6	32.3	-2.4	30.6	-3.2	27.0	-3.9	22.2	-4.5	17.0	-5.0	10.9	4.9
P3a	463.1	2.2	487.2	5.0	492.2	7.4	465.4	9.6	419.4	11.8	361.3	13.9	298.3	15.9	197.6	-15.7
P3b	463.2	-2.2	487.5	-5.0	492.7	-7.5	466.0	-9.7	419.7	-11.9	361.1	-13.9	297.3	-15.8	196.5	15.6
P5a	9660.0	-17.0	5403.0	32.4	2907.0	41.1	1331.0	47.2	290.5	51.5	-374.0	55.8	-718.1	-56.4	-768.4	84.4
P5b	9661.0	16.9	5407.0	-32.5	2920.0	-41.4	1353.0	-47.6	317.9	-51.9	-345.3	-56.1	-697.3	56.3	-771.8	-83.5
P8a	7556.0	1.8	4237.0	2.6	2695.0	2.0	1548.0	1.4	534.0	0.4	1090.0	2.0	2004.0	-2.4	-2864.0	-12.5
P8b	7559.0	-1.9	4248.0	-2.7	2734.0	-2.2	1603.0	-1.5	575.2	-0.5	1056.0	-2.4	2105.0	-3.3	-3214.0	17.0
P9	2688.0	-1.1	1410.0	1.3	979.6	0.6	732.8	0.2	559.7	0.3	-532.6	0.7	-527.5	-0.9	925.3	2.6
P11a	1476.0	-3.6	1779.0	8.9	1833.0	12.7	1727.0	14.9	1535.0	16.1	1302.0	16.9	1069.0	17.5	851.7	24.4
P11b	1476.0	3.6	1779.0	-8.9	1832.0	-12.7	1726.0	-14.9	1534.0	-16.1	1301.0	-16.9	1068.0	-17.4	850.5	-24.4
P13a	3109.0	-5.1	2267.0	14.0	1816.0	20.7	1413.0	24.4	1037.0	26.5	683.1	28.0	-360.9	-28.3	-519.8	44.9
P13b	3109.0	5.1	2268.0	-14.0	1817.0	-20.7	1414.0	-24.4	1037.0	-26.5	683.4	-28.0	-362.8	28.2	-520.7	-44.8
P16a	9638.0	6.0	7859.0	11.9	6495.0	15.6	5271.0	18.7	4141.0	21.6	3141.0	24.7	-2702.0	-25.4	2001.0	41.7
P16b	9638.0	-6.0	7858.0	-11.9	6495.0	-15.6	5270.0	-18.8	4139.0	-21.6	3139.0	-24.7	-2701.0	25.2	2000.0	-41.5
P19a	7888.0	5.3	6046.0	13.9	4643.0	22.9	3533.0	32.5	2613.0	43.1	1839.0	55.7	-1469.0	63.2	-1385.0	107.2
P19b	7888.0	-5.3	6046.0	-13.7	4645.0	-22.7	3536.0	-32.4	2617.0	-42.9	1844.0	-55.5	-1468.0	-62.9	-1376.0	-107.2
P22a	12420.0	-0.1	10190.0	0.6	8192.0	2.3	6442.0	4.5	4886.0	7.1	3549.0	11.8	-2612.0	16.3	1913.0	-28.5
P22b	12410.0	-0.1	10200.0	-0.5	8223.0	-2.1	6492.0	-4.2	4955.0	-6.8	3636.0	-11.3	-2779.0	-16.5	2369.0	-34.4
P25	2988.0	-0.1	908.7	0.0	516.6	0.0	262.1	0.0	84.8	-0.1	-112.7	0.1	-147.4	-0.6	15.6	2.1

Table B.8 – Bending moments and shear forces in beams for lateral load applied in positive y-direction with live load as the main action.

Beam	1ST FLOOR		2ND FLOOR		3RD FLOOR		4TH FLOOR		5TH FLOOR		6TH FLOOR		7TH FLOOR		ROOF	
	M (kNcm)	V (kN)	M (kNcm)	V (kN)	M (kNcm)	V (kN)	M (kNcm)	V (kN)	M (kNcm)	V (kN)	M (kNcm)	V (kN)	M (kNcm)	V (kN)	M (kNcm)	V (kN)
L1a	-352.6	-8.8	-542.1	-11.9	-721.6	-14.8	-834.1	-17.5	-877.3	-19.9	1065.0	-21.9	1395.0	-23.1	411.9	-8.3
L1b	-350.4	8.8	-534.4	11.9	-710.1	14.8	-818.8	17.5	-857.4	19.8	1074.0	21.8	1389.0	22.9	412.0	8.3
L2a	-290.6	9.5	-517.2	8.9	-636.3	6.8	-805.6	-9.3	-1095.0	-13.1	-1517.0	-18.0	-1992.0	-24.6	405.8	-10.2
L2b	-290.6	-9.5	-425.0	-11.1	-526.2	-11.3	-582.9	-9.9	-649.7	-7.1	-856.2	9.9	-1340.0	16.2	304.3	7.9
L3	592.3	-8.6	578.3	-9.0	529.0	-9.3	449.3	-9.4	322.1	-9.2	-391.9	-8.6	-572.8	-7.1	-1331.0	8.5
L4a	421.0	-9.9	505.9	-10.5	505.2	-10.5	451.4	-10.1	357.4	-9.3	229.5	-8.3	-211.8	-7.1	116.4	-4.2
L4b	420.6	-9.9	505.1	-10.5	503.9	-10.5	449.6	-10.0	355.2	-9.3	227.3	-8.3	-212.2	-7.0	116.1	-4.2
L5a	375.5	-14.1	448.7	-15.9	460.7	-15.9	445.2	-15.3	413.2	-14.2	369.2	-12.7	318.2	-11.0	176.4	-8.6
L5b	375.5	-14.1	448.9	-15.9	461.0	-15.9	445.4	-15.3	413.1	-14.2	368.5	-12.7	317.3	-11.0	176.0	-8.6
L6a	-1094.0	-20.1	-1198.0	-23.5	-1151.0	-23.8	-1065.0	-22.7	-973.1	-20.8	-897.0	-18.7	-831.8	-16.8	292.2	-6.8
L6b	-1094.0	-20.1	-1199.0	-23.5	-1152.0	-23.8	-1065.0	-22.7	-973.8	-20.8	-897.7	-18.7	-831.9	-16.9	292.1	-6.8
L7a	372.9	10.1	554.4	12.8	612.8	13.7	596.5	13.4	542.1	12.6	479.5	11.6	444.5	11.0	0.0	10.1
L7b	372.6	10.1	554.3	12.8	612.8	13.7	596.6	13.4	542.1	12.6	479.1	11.6	444.0	11.0	0.0	10.1
L8a	361.1	-8.6	187.9	-7.8	151.9	-6.1	204.5	6.6	329.2	8.7	449.8	10.6	553.5	12.2	479.4	10.7
L8b	361.2	8.6	489.0	-10.6	561.8	-11.8	601.1	-12.4	618.8	-12.7	621.1	-12.8	617.8	-12.9	461.7	-10.5
L9a	-514.7	-19.8	-664.0	-23.2	-647.6	-22.7	-557.4	-20.5	-439.3	-17.5	-330.9	-14.8	-284.6	-13.7	-2537.0	-24.3
L9b	-518.0	-19.8	-669.8	-23.3	-656.0	-22.9	-567.7	-20.7	-450.4	-17.8	-343.0	-15.1	-303.6	-14.1	-2856.0	-26.8
L10a	185.2	8.3	187.4	7.8	151.3	6.1	206.3	-6.6	331.3	-8.7	452.3	-10.7	556.3	-12.3	481.7	-10.7
L10b	185.5	-8.3	-270.6	8.5	-346.6	9.6	-422.0	10.6	-508.7	11.8	-605.8	13.4	-672.6	14.7	-360.0	8.7
L11a	230.8	-10.5	278.6	-12.5	290.7	-13.6	295.4	-14.6	-312.6	-15.8	-363.0	17.4	-390.5	18.7	-256.3	-12.7
L11b	230.5	10.5	489.5	10.6	562.8	11.8	602.0	12.4	619.1	12.7	620.3	12.8	616.3	12.9	460.6	10.5
L12a	469.9	-13.7	692.2	-17.0	872.2	-19.0	1056.0	-20.7	1260.0	-22.1	1495.0	-23.2	1754.0	-23.3	484.7	-9.6
L12b	465.8	13.6	-522.8	-9.0	-643.7	-6.9	-814.8	9.3	-1106.0	13.0	-1535.0	18.0	-2021.0	24.7	408.7	10.3
L13a	-373.0	9.7	685.9	16.9	864.9	19.0	1048.0	20.7	1250.0	22.1	1485.0	23.2	1745.0	23.3	482.5	9.5
L13b	-376.1	-9.7	-429.4	11.4	-533.5	11.7	-587.9	10.5	-647.4	7.6	-857.5	-9.5	-1419.0	-16.6	322.2	-8.3
L14	-632.3	-9.1	-794.8	-9.1	-992.9	-9.2	-1243.0	-9.3	-1565.0	-9.4	-2012.0	-9.5	-2751.0	-9.7	-4914.0	-9.5

Table B.9 – Bending moments and shear forces in beams for lateral load applied in negative y-direction with live load as the main action.

Beam	1ST FLOOR		2ND FLOOR		3RD FLOOR		4TH FLOOR		5TH FLOOR		6TH FLOOR		7TH FLOOR		ROOF	
	M (kNcm)	V (kN)	M (kNcm)	V (kN)	M (kNcm)	V (kN)	M (kNcm)	V (kN)	M (kNcm)	V (kN)	M (kNcm)	V (kN)	M (kNcm)	V (kN)	M (kNcm)	V (kN)
L1a	-567.3	-11.3	-740.8	-13.9	-762.0	-15.3	-717.9	-16.3	720.0	-17.2	981.9	-18.0	1289.0	-17.9	317.4	-6.6
L1b	-537.1	11.2	-706.0	13.9	-727.9	15.2	-684.8	16.2	742.0	17.2	991.8	17.9	1278.0	17.7	317.0	6.6
L2a	471.8	13.4	-655.6	-8.5	-849.9	-9.7	-1060.0	-11.6	-1343.0	-14.4	-1701.0	-18.5	-2114.0	-24.1	377.8	-9.9
L2b	419.7	-12.6	-484.4	-13.4	-479.2	-11.7	-469.1	-8.5	-595.8	8.4	-1039.0	14.6	-1674.0	22.8	428.5	10.0
L3	-205.0	-6.4	444.3	-11.5	571.7	-13.9	-560.3	-14.5	-646.3	-14.1	-753.6	-13.0	-912.3	-11.5	-1167.0	3.5
L4a	-651.3	9.7	-815.2	11.0	-813.9	11.0	-742.9	10.4	-654.8	9.6	-578.5	8.8	-525.7	8.2	-85.3	-3.1
L4b	-653.6	9.7	-819.2	11.0	-818.3	11.0	-747.2	10.4	-658.7	9.6	-581.6	8.9	-527.2	8.2	-85.6	-3.1
L5a	-247.6	11.0	-276.7	11.9	-245.0	11.0	-185.3	9.5	122.1	7.6	77.8	5.6	41.0	3.9	-74.0	-5.3
L5b	-247.9	11.0	-277.1	11.9	-245.3	11.1	-185.7	9.5	122.2	7.6	77.9	5.6	40.7	3.9	-73.9	-5.3
L6a	-1337.0	20.7	-1736.0	23.0	-1793.0	22.4	-1679.0	20.3	-1483.0	17.6	-1270.0	14.4	-1142.0	11.2	54.5	-3.1
L6b	-1337.0	20.7	-1736.0	23.0	-1793.0	22.3	-1679.0	20.3	-1483.0	17.5	-1269.0	14.4	-1141.0	11.2	54.6	-3.1
L7a	-482.5	-11.1	-609.4	-13.0	-624.6	-13.3	-572.1	-12.5	-478.3	-11.0	-359.9	-9.2	-229.7	-7.3	0.0	-11.1
L7b	-482.8	-11.1	-609.7	-13.0	-624.6	-13.3	-571.7	-12.5	-477.6	-11.0	-359.2	-9.2	-229.0	-7.2	0.0	-11.1
L8a	-154.4	4.2	559.1	16.3	674.2	18.4	750.4	19.4	800.9	19.8	829.6	19.5	837.9	19.0	712.1	15.7
L8b	-154.3	-4.2	-148.0	4.2	-124.5	-4.3	-95.8	-5.1	107.5	-6.0	184.8	-7.0	252.6	-7.8	228.3	-7.2
L9a	676.2	23.6	932.5	30.4	-1022.0	32.6	-1007.0	32.0	-913.0	29.4	-751.7	25.2	-500.3	18.8	-2332.0	11.3
L9b	670.7	23.4	917.8	30.0	-999.2	32.0	-982.2	31.3	-889.6	28.8	-731.5	24.7	-480.2	18.2	-2546.0	8.4
L10a	377.6	-12.5	565.1	-16.4	681.8	-18.5	758.4	-19.5	808.9	-19.9	837.7	-19.7	846.0	-19.2	718.9	-15.8
L10b	374.2	12.5	-205.6	-8.9	-239.2	-7.5	-272.7	-5.4	-343.1	4.9	-468.6	8.0	-578.6	10.7	-391.1	6.8
L11a	-152.2	8.9	-213.1	4.3	-240.8	-4.1	-274.5	-6.3	-330.9	-8.9	-385.5	-12.0	-414.4	-14.7	-341.3	-10.9
L11b	-151.9	-9.0	-147.8	-4.2	-124.1	4.3	-95.5	5.1	107.2	6.0	183.4	6.9	250.5	7.7	226.6	7.2
L12a	-406.3	-8.6	-549.6	-13.2	-698.9	-17.1	845.5	-20.1	1144.0	-22.6	1475.0	-24.6	1851.0	-26.0	545.1	-10.6
L12b	-411.4	8.5	-658.4	8.4	-853.7	9.5	-1064.0	11.4	-1350.0	14.2	-1716.0	18.3	-2143.0	24.0	378.9	10.0
L13a	-428.1	-8.0	-554.4	13.1	-706.1	16.9	821.3	20.0	1119.0	22.4	1450.0	24.5	1828.0	25.9	540.1	10.5
L13b	-429.6	7.9	-527.5	14.2	-522.2	12.5	-489.3	9.3	-592.9	-7.7	-1053.0	-14.3	-1797.0	-23.4	451.9	-10.5
L14	-492.2	-9.1	-630.4	-9.3	-837.6	-9.4	-1105.0	-9.5	-1446.0	-9.6	-1909.0	-9.8	-2669.0	-9.9	-4946.0	-9.8

Table B.10 – Axial forces in walls for lateral load applied in negative y-direction with live load as the main action.

Wall	BASEMENT	1ST FLOOR	2ND FLOOR	3RD FLOOR	4TH FLOOR	5TH FLOOR	6TH FLOOR	7TH FLOOR
	N (kN)	N (kN)	N (kN)	N (kN)	N (kN)	N (kN)	N (kN)	N (kN)
P1a	-60.7	-53.4	-45.3	-37.0	-28.8	-20.9	-13.1	-6.2
P1b	-60.9	-53.3	-45.2	-37.0	-28.8	-20.8	-13.1	-6.2
P2a	-430.6	-376.9	-319.2	-261.2	-204.1	-148.1	-93.4	-39.7
P2b	-430.9	-376.6	-319.0	-261.0	-203.9	-147.9	-93.3	-39.7
P3a	-183.5	-159.9	-135.8	-111.6	-87.7	-64.1	-40.9	-18.4
P3b	-183.5	-159.9	-135.8	-111.6	-87.6	-64.1	-40.9	-18.4
P4a	-305.0	-259.3	-218.9	-181.0	-144.4	-108.5	-72.1	-32.7
P4b	-303.6	-260.2	-219.5	-181.3	-144.4	-108.2	-71.5	-32.4
P5a	-628.2	-554.5	-482.6	-409.1	-333.4	-255.0	-172.8	-85.8
P5b	-625.9	-556.3	-483.9	-409.8	-333.7	-254.8	-172.4	-85.5
P6a	-53.3	-48.4	-43.5	-37.8	-31.4	-24.5	-17.0	-8.9
P6b	-53.2	-48.6	-43.7	-37.9	-31.5	-24.5	-17.0	-8.9
P7a	-614.7	-536.1	-464.1	-394.0	-326.6	-262.5	-201.7	-139.8
P7b	-606.0	-540.6	-466.6	-395.2	-326.8	-261.4	-198.0	-130.8
P8a	-587.1	-521.9	-460.6	-398.2	-337.0	-279.2	-228.2	-189.7
P8b	-580.8	-526.5	-463.5	-400.0	-337.9	-279.5	-228.3	-202.1
P9	-354.0	-330.1	-297.2	-260.0	-221.4	-182.8	-144.5	-22.8
P10	-187.9	-165.3	-143.8	-122.7	-102.2	-82.8	-64.6	-80.8
P11a	-274.8	-239.6	-202.8	-166.5	-130.9	-95.9	-61.6	-27.0
P11b	-275.3	-239.2	-202.5	-166.3	-130.7	-95.7	-61.5	-27.0
P12a	-319.5	-275.7	-233.4	-191.8	-151.0	-110.8	-71.5	-34.4
P12b	-319.8	-275.4	-233.2	-191.7	-150.8	-110.7	-71.5	-34.3
P13a	-381.0	-335.3	-287.9	-239.9	-191.7	-143.4	-95.4	-47.6
P13b	-381.0	-335.3	-287.9	-239.9	-191.6	-143.3	-95.4	-47.5
P14a	-238.1	-211.9	-184.9	-156.3	-126.7	-96.3	-65.4	-34.4
P14b	-237.9	-212.1	-185.0	-156.4	-126.7	-96.3	-65.4	-34.4
P15a	-439.8	-378.7	-321.0	-265.2	-210.1	-155.2	-100.8	-48.1
P15b	-440.1	-378.5	-320.8	-265.0	-209.9	-155.1	-100.8	-48.0
P16a	-560.7	-501.5	-437.3	-369.2	-297.6	-222.7	-144.6	-64.3
P16b	-559.6	-500.5	-436.4	-368.5	-297.1	-222.2	-144.3	-64.2
P17a	-266.3	-244.5	-219.9	-190.8	-157.6	-120.6	-79.2	-32.5
P17b	-266.0	-244.2	-219.6	-190.6	-157.5	-120.5	-79.2	-32.5
P18a	-134.2	-110.7	-91.7	-74.9	-59.1	-43.8	-28.7	-14.6
P18b	-134.1	-110.8	-91.8	-74.9	-59.2	-43.9	-28.8	-14.6
P19a	-593.2	-516.0	-442.3	-371.5	-301.1	-229.3	-154.6	-76.5
P19b	-593.5	-516.2	-442.6	-371.8	-301.4	-229.7	-154.9	-76.6
P20a	-175.6	-158.7	-141.5	-122.8	-102.5	-80.5	-56.0	-26.4
P20b	-175.7	-158.7	-141.6	-122.9	-102.7	-80.7	-56.1	-26.5
P21a	-503.8	-433.4	-370.2	-312.2	-257.6	-204.8	-150.7	-86.0
P21b	-503.1	-434.2	-371.0	-312.9	-258.4	-205.7	-151.8	-87.1
P22a	-745.1	-662.2	-580.3	-500.6	-423.1	-348.3	-278.7	-204.0
P22b	-746.7	-663.7	-581.7	-501.9	-424.5	-349.9	-280.8	-210.3
P23a	-308.6	-281.0	-253.2	-223.6	-192.5	-160.1	-126.4	-87.5
P23b	-308.8	-281.3	-253.5	-223.9	-192.8	-160.6	-127.0	-88.5
P24a	-163.9	-149.5	-135.2	-119.9	-103.8	-87.3	-71.0	-63.1
P24b	-164.0	-149.7	-135.3	-120.0	-103.9	-87.5	-71.2	-64.7
P25	-399.4	-352.9	-306.4	-259.9	-213.4	-166.9	-120.4	-24.0

Table B.11 – Shear forces in walls for lateral load applied in negative y-direction with live load as the main action.

Wall	BASEMENT		1ST FLOOR		2ND FLOOR		3RD FLOOR		4TH FLOOR		5TH FLOOR		6TH FLOOR		7TH FLOOR	
	Vx (kN)	Vy (kN)	Vx (kN)	Vy (kN)	Vx (kN)	Vy (kN)	Vx (kN)	Vy (kN)	Vx (kN)	Vy (kN)	Vx (kN)	Vy (kN)	Vx (kN)	Vy (kN)	Vx (kN)	Vy (kN)
P1a	0.0	-0.2	0.0	-0.2	0.0	-0.3	0.0	-0.2	0.0	-0.2	0.0	-0.2	0.0	-0.1	0.0	-0.1
P1b	0.0	-0.2	0.0	-0.2	0.0	-0.3	0.0	-0.2	0.0	-0.2	0.0	-0.2	0.0	-0.1	0.0	-0.1
P3a	0.0	-3.0	0.0	-3.8	-0.1	-3.6	-0.1	-3.1	-0.1	-2.5	-0.1	-1.8	-0.1	-1.0	-0.1	-0.9
P3b	0.0	-3.0	0.0	-3.8	0.1	-3.6	0.1	-3.1	0.1	-2.5	0.1	-1.8	0.1	-1.1	0.1	-0.9
P5a	-0.1	-26.1	0.1	-22.3	0.1	-18.2	0.0	-14.4	0.0	-10.7	-0.1	-6.6	-0.2	-1.9	-0.3	3.8
P5b	0.1	-26.3	-0.1	-22.1	-0.1	-17.8	0.0	-14.1	0.0	-10.4	0.1	-6.4	0.2	-1.9	0.3	3.6
P8a	0.0	-29.6	0.0	-37.9	0.0	-40.2	0.0	-40.4	0.0	-39.2	0.0	-37.6	0.0	-36.6	-0.1	-17.8
P8b	0.0	-30.1	0.0	-36.8	0.0	-39.0	0.0	-39.2	0.0	-38.2	0.0	-36.8	0.0	-36.4	0.1	-17.8
P9	0.0	-6.6	0.0	0.6	0.0	3.2	0.0	4.3	0.0	4.7	0.0	4.7	0.0	4.8	0.0	5.9
P11a	0.0	-8.3	0.0	-10.3	0.0	-10.1	0.0	-8.9	0.0	-7.1	0.0	-5.1	-0.1	-2.8	-0.1	-0.1
P11b	0.0	-8.3	0.0	-10.3	0.0	-10.1	0.0	-8.9	0.0	-7.1	0.0	-5.1	0.1	-2.8	0.1	-0.1
P13a	0.0	-12.7	0.0	-12.2	0.0	-11.6	0.0	-10.3	0.0	-8.7	-0.1	-6.9	-0.1	-5.1	-0.1	-2.4
P13b	0.0	-12.7	0.0	-12.2	0.0	-11.6	0.0	-10.3	0.0	-8.7	0.1	-6.9	0.1	-5.1	0.1	-2.4
P16a	0.0	-27.7	-0.1	-24.4	-0.2	-20.7	-0.2	-16.5	-0.2	-11.9	-0.2	-6.8	-0.2	-0.6	-0.3	5.8
P16b	0.0	-27.7	0.1	-24.4	0.2	-20.7	0.2	-16.5	0.2	-11.9	0.2	-6.8	0.2	-0.6	0.3	5.8
P19a	-0.1	-21.8	-0.1	-15.0	-0.2	-9.8	-0.3	-6.0	-0.4	-3.0	-0.5	-0.3	-0.5	2.9	-0.8	9.0
P19b	0.1	-21.8	0.1	-15.0	0.2	-9.8	0.3	-6.0	0.4	-3.0	0.5	-0.3	0.5	2.9	0.8	9.0
P22a	0.0	-32.5	0.0	-28.7	0.0	-24.4	0.0	-19.7	0.0	-14.6	0.0	-9.2	-0.1	-4.0	-0.1	6.1
P22b	0.0	-32.3	0.0	-28.3	0.0	-23.7	0.0	-18.7	0.0	-13.5	0.0	-8.0	0.1	-2.5	0.2	7.9
P25	0.0	-7.4	0.0	-1.3	0.0	-0.8	0.0	-0.5	0.0	-0.3	0.0	-0.2	0.0	0.0	0.0	1.5

Table B.12 – Bending moments in walls for lateral load applied in negative y-direction with live load as the main action.

Wall	BASEMENT		1ST FLOOR		2ND FLOOR		3RD FLOOR		4TH FLOOR		5TH FLOOR		6TH FLOOR		7TH FLOOR	
	Mx (kNcm)	My (kNcm)	Mx (kNcm)	My (kNcm)	Mx (kNcm)	My (kNcm)	Mx (kNcm)	My (kNcm)	Mx (kNcm)	My (kNcm)	Mx (kNcm)	My (kNcm)	Mx (kNcm)	My (kNcm)	Mx (kNcm)	My (kNcm)
P1a	-23.8	-0.7	-34.5	1.4	-35.0	1.8	-31.7	2.2	-26.5	2.6	-20.6	3.1	14.6	3.6	14.0	-3.6
P1b	-23.8	0.7	-34.6	-1.4	-35.1	-1.8	-31.8	-2.2	-26.6	-2.6	-20.7	-3.1	14.7	-3.5	14.0	3.6
P3a	-462.9	3.4	-557.7	6.0	-522.3	7.1	-444.7	8.2	-347.3	9.5	247.7	11.0	152.7	12.5	156.8	-12.1
P3b	-462.9	-3.5	-557.7	-6.1	-522.1	-7.2	-444.5	-8.3	-347.4	-9.6	248.8	-11.0	154.7	-12.4	157.4	12.1
P5a	-7930.0	11.2	-5139.0	16.2	-3360.0	12.6	-2110.0	7.0	1856.0	4.3	1537.0	14.7	966.4	23.3	1082.0	45.1
P5b	-7921.0	-11.7	-5112.0	-16.1	-3316.0	-12.5	-2061.0	-6.7	1824.0	-4.8	1528.0	-15.0	992.3	-23.2	1072.0	-44.0
P8a	-5998.0	-0.2	-6065.0	-1.2	-5833.0	-1.8	5816.0	1.5	5917.0	0.8	5912.0	1.7	6035.0	-2.3	-3725.0	-9.1
P8b	-5972.0	-0.1	-5929.0	0.7	-5663.0	-1.3	5661.0	-1.1	5784.0	-0.3	5832.0	-2.6	6112.0	-4.3	-4438.0	15.3
P9	-2318.0	1.2	-590.6	-1.5	-617.0	-0.6	635.3	-0.5	813.2	0.7	890.6	1.0	925.2	-1.0	1643.0	3.4
P11a	-1337.0	-0.9	-1544.0	-1.2	-1479.0	1.2	-1279.0	2.0	-1009.0	3.5	713.3	5.4	412.3	7.7	-35.5	11.3
P11b	-1337.0	0.8	-1546.0	1.1	-1481.0	-1.1	-1281.0	-2.0	-1011.0	-3.5	714.4	-5.4	412.9	-7.6	-36.0	-11.2
P13a	-2775.0	-4.3	-2084.0	-5.3	-1781.0	-3.2	-1452.0	3.8	1311.0	5.8	1135.0	8.4	926.8	10.6	422.2	18.7
P13b	-2775.0	4.1	-2082.0	5.1	-1778.0	-3.0	-1449.0	-3.8	1309.0	-5.8	1132.0	-8.4	923.3	-10.4	418.9	-18.6
P16a	-8468.0	8.2	-5500.0	16.6	-3784.0	21.7	-2475.0	25.4	1970.0	28.1	1500.0	30.7	689.0	-31.2	1478.0	47.1
P16b	-8468.0	-8.4	-5500.0	-16.6	-3784.0	-21.6	-2475.0	-25.2	1969.0	-27.9	1499.0	-30.6	687.3	30.8	1479.0	-46.7
P19a	-6978.0	9.0	-3968.0	21.8	-2130.0	33.1	-914.9	43.6	793.6	53.7	675.5	65.4	1083.0	70.1	1414.0	119.9
P19b	-6978.0	-9.0	-3966.0	-21.4	-2126.0	-32.4	-908.2	-42.8	784.6	-52.9	668.0	-64.6	1092.0	-69.3	1419.0	-119.1
P22a	-10990.0	-0.4	-6945.0	-1.7	-4655.0	-2.8	-2966.0	2.2	2515.0	0.6	2222.0	5.5	1799.0	11.1	2699.0	-20.5
P22b	-11020.0	-0.4	-6923.0	1.9	-4588.0	-3.4	-2861.0	-3.1	2339.0	-1.2	2024.0	-4.5	1566.0	-10.9	2942.0	25.9
P25	-2643.0	-0.1	-582.4	-0.1	-226.3	-0.1	136.0	0.0	230.9	-0.1	291.4	0.2	299.2	-0.7	427.9	2.3

B.2 Load combination II - Wind as the main action

Table B.13 – Axial forces in walls for lateral load applied in x-direction with wind as the main action.

Wall	BASEMENT	1ST FLOOR	2ND FLOOR	3RD FLOOR	4TH FLOOR	5TH FLOOR	6TH FLOOR	7TH FLOOR
	N (kN)	N (kN)	N (kN)	N (kN)	N (kN)	N (kN)	N (kN)	N (kN)
P1a	-43.8	-49.7	-41.6	-34.0	-26.5	-19.2	-12.1	-6.2
P1b	-59.1	-41.2	-36.5	-31.1	-25.2	-19.0	-12.4	-5.8
P2a	-333.2	-342.5	-291.1	-239.8	-189.0	-138.4	-88.2	-37.9
P2b	-391.9	-297.8	-259.6	-219.0	-176.4	-132.0	-86.0	-37.7
P3a	-164.2	-145.5	-124.9	-103.7	-82.3	-60.9	-39.1	-16.9
P3b	-152.3	-131.3	-112.9	-94.5	-75.8	-56.6	-36.9	-17.5
P4a	-248.1	-227.0	-195.9	-165.0	-133.9	-102.4	-69.3	-31.6
P4b	-259.2	-216.6	-186.9	-157.6	-128.1	-98.0	-66.6	-32.6
P5a	-591.9	-529.3	-456.0	-383.3	-310.1	-235.7	-158.8	-78.6
P5b	-603.9	-514.6	-440.1	-367.8	-296.4	-224.9	-152.1	-77.1
P6a	-58.8	-50.2	-43.3	-36.4	-29.5	-22.4	-15.1	-7.9
P6b	-57.7	-49.7	-42.0	-34.8	-27.9	-21.0	-14.2	-7.6
P7a	-503.3	-464.3	-407.5	-351.3	-295.8	-241.6	-188.8	-134.8
P7b	-520.7	-454.0	-400.9	-346.1	-291.0	-235.6	-178.8	-114.4
P8a	-543.5	-476.6	-419.6	-363.5	-308.7	-256.7	-210.3	-164.5
P8b	-535.3	-477.4	-416.2	-357.6	-301.2	-247.5	-199.3	-169.5
P9	-322.0	-295.4	-264.7	-231.6	-197.3	-162.8	-128.0	-22.8
P10	-153.5	-141.0	-125.5	-109.1	-92.6	-76.3	-60.4	-70.5
P11a	-218.0	-235.5	-197.7	-161.9	-127.1	-93.0	-59.6	-26.4
P11b	-276.8	-197.8	-173.9	-147.4	-119.2	-89.9	-59.4	-27.1
P12a	-264.3	-263.0	-223.7	-184.9	-146.4	-108.2	-70.3	-33.9
P12b	-301.6	-232.8	-201.3	-168.7	-135.4	-101.5	-67.0	-33.0
P13a	-351.7	-323.7	-279.4	-233.6	-186.9	-139.9	-93.0	-45.5
P13b	-366.3	-305.3	-259.4	-214.9	-171.1	-127.8	-85.0	-42.5
P14a	-242.0	-210.2	-182.8	-153.8	-123.9	-93.6	-63.1	-33.4
P14b	-235.8	-205.5	-172.9	-142.3	-112.8	-84.2	-56.2	-29.5
P15a	-408.7	-382.5	-329.7	-274.8	-218.8	-162.3	-105.6	-49.0
P15b	-432.0	-349.8	-297.8	-247.8	-197.7	-146.9	-95.7	-44.8
P16a	-643.8	-562.7	-479.5	-395.9	-312.3	-228.7	-145.6	-64.4
P16b	-525.5	-478.6	-421.0	-356.8	-288.2	-216.1	-140.8	-62.7
P17a	-331.9	-294.4	-253.6	-211.1	-167.7	-123.7	-78.6	-31.4
P17b	-293.6	-260.2	-226.5	-191.1	-154.0	-115.2	-74.5	-31.7
P18a	-117.0	-105.8	-90.6	-75.9	-61.2	-46.2	-30.9	-15.5
P18b	-122.9	-100.4	-85.7	-71.7	-57.8	-43.7	-29.3	-14.9
P19a	-609.0	-534.4	-460.0	-386.3	-312.3	-236.9	-158.8	-77.3
P19b	-581.1	-507.4	-435.4	-365.1	-294.9	-223.7	-150.3	-74.2
P20a	-204.9	-179.9	-155.5	-131.1	-106.5	-81.5	-55.1	-24.9
P20b	-196.0	-170.6	-147.0	-123.8	-100.5	-76.8	-51.9	-24.3
P21a	-450.5	-417.7	-359.9	-306.5	-255.3	-204.9	-152.5	-88.9
P21b	-484.3	-400.5	-350.4	-300.4	-250.7	-201.0	-149.0	-85.8
P22a	-729.9	-659.2	-582.1	-503.4	-425.7	-350.9	-281.9	-194.1
P22b	-755.3	-664.0	-576.4	-492.6	-411.9	-334.7	-263.6	-200.5
P23a	-352.1	-311.1	-271.9	-233.4	-195.8	-159.2	-124.0	-88.2
P23b	-339.1	-304.0	-266.5	-228.5	-190.9	-153.9	-116.9	-74.8
P24a	-182.6	-163.8	-144.1	-124.4	-105.0	-86.3	-68.9	-58.8
P24b	-185.1	-163.3	-142.9	-122.7	-103.0	-83.9	-65.8	-60.4
P25	-377.8	-334.0	-290.2	-246.4	-202.6	-158.8	-115.0	-24.0

Table B.14 – Shear forces in walls for lateral load applied in x-direction with wind as the main action.

Wall	BASEMENT		1ST FLOOR		2ND FLOOR		3RD FLOOR		4TH FLOOR		5TH FLOOR		6TH FLOOR		7TH FLOOR	
	Vx (kN)	Vy (kN)	Vx (kN)	Vy (kN)	Vx (kN)	Vy (kN)	Vx (kN)	Vy (kN)	Vx (kN)	Vy (kN)	Vx (kN)	Vy (kN)	Vx (kN)	Vy (kN)	Vx (kN)	Vy (kN)
P2a	-12.0	-0.1	-14.6	0.0	-14.5	0.1	-14.3	0.1	-14.2	0.1	-14.0	0.1	-13.6	0.1	-10.9	0.1
P2b	-14.6	0.0	-8.1	-0.1	-5.5	-0.1	-3.0	-0.1	-0.6	-0.1	1.9	-0.1	4.5	0.0	6.4	-0.1
P4a	-8.0	0.0	-10.3	0.0	-10.8	0.0	-10.9	0.0	-11.1	0.0	-11.5	0.0	-12.4	0.1	-12.7	0.1
P4b	-8.2	0.0	-9.3	-0.1	-8.4	-0.1	-6.7	-0.1	-4.4	-0.1	-1.7	-0.1	1.4	-0.1	4.0	0.0
P6a	-0.2	0.0	-0.4	0.0	-0.4	0.0	-0.4	0.0	-0.4	0.0	-0.4	0.0	-0.4	0.0	-0.4	0.0
P6b	-0.2	0.0	-0.2	0.0	-0.2	0.0	-0.1	0.0	-0.1	0.0	0.0	0.0	0.1	0.0	0.1	0.0
P7a	-23.9	0.0	-22.7	-0.1	-21.4	-0.1	-20.1	-0.1	-18.9	-0.2	-18.0	-0.2	-17.8	-0.2	-22.3	-0.5
P7b	-23.9	0.0	-22.9	-0.1	-21.6	-0.2	-19.2	-0.2	-15.6	-0.2	-10.9	-0.2	-4.4	-0.3	6.3	-0.5
P10	-3.0	0.0	-3.6	0.0	-3.6	0.0	-3.3	0.0	-3.0	0.0	-2.6	0.0	-2.1	0.0	-11.3	0.0
P12a	-7.1	0.0	-6.5	0.0	-5.4	0.0	-4.7	0.0	-4.3	0.0	-4.1	0.0	-3.9	0.0	-4.4	0.1
P12b	-8.0	0.0	-4.2	0.0	-2.0	0.0	-0.4	0.0	0.9	0.0	2.0	0.0	3.2	0.0	5.0	0.0
P14a	-4.1	0.0	-6.2	0.0	-6.4	0.0	-6.3	0.0	-6.2	0.0	-6.1	0.0	-5.9	0.0	-6.8	0.0
P14b	-5.8	0.0	-2.1	0.0	-1.0	0.0	0.1	0.0	1.1	0.0	2.0	0.0	2.9	0.0	4.5	0.0
P15a	-11.3	0.0	-17.5	0.2	-17.5	0.2	-17.6	0.1	-17.6	0.1	-17.5	0.1	-17.2	0.2	-20.4	0.2
P15b	-17.3	0.1	-2.7	0.0	2.1	0.0	5.2	0.1	7.7	0.1	9.8	0.2	12.0	0.2	17.1	0.3
P17a	-11.8	0.0	-14.6	0.0	-16.0	0.0	-16.8	0.0	-17.4	0.0	-17.7	0.0	-17.7	0.0	-15.0	0.0
P17b	-7.4	0.0	-3.5	0.0	-0.6	0.0	2.1	0.0	4.7	0.0	7.2	0.0	9.6	0.0	10.2	0.0
P18a	-1.2	0.0	-2.9	0.0	-3.4	0.0	-3.7	0.0	-3.9	0.0	-4.1	0.0	-4.2	0.1	-4.4	0.1
P18b	-1.7	0.0	-1.5	0.0	-1.2	0.0	-0.6	0.0	0.1	0.0	0.8	0.0	1.5	0.1	2.0	0.1
P20a	-4.4	0.0	-6.4	0.0	-7.2	0.0	-7.6	0.0	-8.0	0.0	-8.5	0.0	-9.1	0.0	-9.8	0.0
P20b	-3.5	0.0	-3.7	0.0	-2.7	0.0	-1.4	0.0	0.2	0.0	1.8	0.0	3.6	0.0	5.0	0.0
P21a	-15.6	0.0	-9.5	0.0	-7.5	0.0	-6.9	0.0	-7.1	0.0	-8.3	0.0	-11.8	0.0	-25.1	0.0
P21b	-13.9	0.0	-13.6	0.1	-12.2	0.1	-10.3	0.1	-7.9	0.1	-4.4	0.1	1.4	0.1	14.6	0.0
P23a	-11.6	0.0	-13.9	0.0	-14.6	0.0	-14.7	0.0	-14.6	0.0	-14.6	0.0	-15.2	0.0	-18.0	0.1
P23b	-11.4	0.0	-12.9	0.0	-12.1	0.0	-10.1	0.1	-7.4	0.1	-4.0	0.1	0.2	0.1	7.0	0.1
P24a	-3.1	0.0	-4.1	0.0	-4.2	0.0	-4.1	0.0	-3.9	0.0	-3.6	0.0	-3.4	0.0	-11.6	0.0
P24b	-2.9	0.0	-3.5	0.0	-3.5	0.0	-3.1	0.0	-2.5	0.0	-1.8	0.0	-0.8	0.1	-11.6	0.1

Table B.15 – Bending moments in walls for lateral load applied in x-direction with wind as the main action.

Wall	BASEMENT		1ST FLOOR		2ND FLOOR		3RD FLOOR		4TH FLOOR		5TH FLOOR		6TH FLOOR		7TH FLOOR	
	Mx (kNcm)	My (kNcm)	Mx (kNcm)	My (kNcm)	Mx (kNcm)	My (kNcm)	Mx (kNcm)	My (kNcm)	Mx (kNcm)	My (kNcm)	Mx (kNcm)	My (kNcm)	Mx (kNcm)	My (kNcm)	Mx (kNcm)	My (kNcm)
P2a	10.3	-2743.0	6.5	-2222.0	10.6	-2025.0	12.7	2089.0	13.7	2121.0	14.0	2124.0	14.1	2045.0	11.8	-1692.0
P2b	2.7	-2789.0	15.5	-1476.0	15.1	-904.5	13.0	-480.1	10.1	-89.4	7.3	290.4	4.0	657.8	13.1	939.1
P4a	6.4	-1227.0	1.0	-1458.0	0.9	1518.0	1.5	1557.0	2.7	1601.0	4.9	1682.0	-8.3	1831.0	10.4	1790.0
P4b	1.1	-1240.0	12.8	-1361.0	16.3	-1237.0	16.9	-991.4	15.4	-673.5	12.4	-298.8	-8.9	-274.8	5.7	-604.8
P6a	2.0	25.5	0.9	50.8	0.7	58.5	0.5	61.7	0.2	62.6	0.2	62.0	0.5	60.3	0.7	-57.3
P6b	0.7	31.9	3.5	-33.8	3.8	-29.4	3.8	-20.9	3.4	-10.7	3.0	-2.5	2.4	-12.1	2.2	-17.9
P7a	10.0	-5448.0	15.2	-3749.0	18.6	-3092.0	21.5	2944.0	24.6	2921.0	29.2	2908.0	33.5	3028.0	75.3	4249.0
P7b	9.1	-5450.0	19.3	-3749.0	24.9	-3170.0	28.1	-2721.0	30.4	-2196.0	33.9	-1573.0	37.3	-849.7	86.8	-1899.0
P10	1.8	-434.0	2.4	-520.0	2.6	-502.8	3.0	-463.6	3.7	414.5	4.9	360.1	6.8	298.8	-2.3	1796.0
P12a	1.9	-1472.0	1.6	-1058.0	3.1	-787.9	4.1	679.9	4.6	659.8	4.9	647.0	5.1	619.2	-7.9	719.9
P12b	1.3	-1513.0	2.7	-791.8	1.7	-354.0	1.6	-67.7	1.8	135.9	2.2	303.9	2.6	469.6	-5.2	-752.6
P14a	1.5	-865.4	5.2	-897.4	4.1	892.4	3.4	905.7	2.9	903.7	2.4	893.2	2.5	858.7	-0.5	1069.0
P14b	4.5	-974.0	1.8	-377.8	2.2	-175.1	2.8	-26.4	3.1	-150.5	3.2	287.8	3.6	420.4	-1.7	-680.3
P15a	5.5	-3355.0	24.8	-2684.0	23.0	2465.0	21.6	2590.0	20.8	2655.0	20.9	2672.0	22.9	2631.0	26.3	3484.0
P15b	-14.3	-3370.0	2.2	-1006.0	5.5	-535.1	11.4	-790.9	16.4	1111.0	21.3	1461.0	-27.8	1767.0	-37.6	-2779.0
P17a	2.3	-1858.0	2.0	-2055.0	1.5	2295.0	1.3	2437.0	1.1	2527.0	0.9	2579.0	1.2	2576.0	2.3	-2295.0
P17b	2.4	-1665.0	4.4	-721.3	4.2	-219.8	4.1	-370.5	3.8	-706.6	3.5	-1037.0	3.7	-1353.0	4.8	1542.0
P18a	-2.5	171.9	5.6	415.8	6.4	483.8	6.5	521.9	6.5	550.0	6.4	575.9	6.5	596.2	7.1	622.3
P18b	-2.8	259.1	5.1	-221.8	5.8	-178.5	6.1	-100.6	6.1	-24.0	6.3	-126.3	6.6	-223.9	7.3	-284.8
P20a	1.2	628.8	2.7	908.0	4.1	1022.0	4.5	1091.0	4.1	1150.0	3.2	1222.0	2.2	1326.0	-3.3	1402.0
P20b	1.1	-540.8	2.5	-553.0	4.4	-410.7	5.3	-223.6	5.3	-55.8	4.9	-288.5	4.4	-544.0	-5.4	-725.0
P21a	-5.9	-3366.0	6.4	-1743.0	6.4	-1112.0	6.3	1072.0	6.1	1216.0	5.9	1519.0	5.7	2254.0	4.3	5135.0
P21b	3.3	-3362.0	12.6	-2229.0	11.7	-1801.0	11.2	-1465.0	10.5	-1103.0	9.8	-665.7	9.1	-456.8	7.6	-3202.0
P23a	2.8	-1850.0	3.5	-1989.0	3.1	2060.0	2.2	2099.0	1.1	2107.0	1.1	2140.0	2.6	2277.0	-12.4	2798.0
P23b	2.3	-1842.0	5.1	-1908.0	7.1	-1757.0	7.8	-1477.0	7.9	-1105.0	8.0	-651.5	8.3	-169.7	-19.3	-1328.0
P24a	1.9	-446.0	2.6	-572.2	2.3	-586.4	1.6	572.2	0.5	542.7	1.1	508.3	-3.0	482.8	7.1	1755.0
P24b	1.5	-428.6	3.6	-504.1	5.0	-491.4	5.7	-437.5	6.0	-357.4	6.3	-256.8	7.2	-132.6	8.4	-1940.0

Table B.16 – Bending moments and shear forces in beams for lateral load applied in x-direction with wind as the main action.

Beam	1ST FLOOR		2ND FLOOR		3RD FLOOR		4TH FLOOR		5TH FLOOR		6TH FLOOR		7TH FLOOR		ROOF	
	M (kNcm)	V (kN)	M (kNcm)	V (kN)	M (kNcm)	V (kN)	M (kNcm)	V (kN)	M (kNcm)	V (kN)	M (kNcm)	V (kN)	M (kNcm)	V (kN)	M (kNcm)	V (kN)
L1a	1288.0	-21.6	1591.0	-24.9	1664.0	-25.6	1688.0	-25.7	1721.0	-25.4	1791.0	-24.9	1933.0	-23.6	441.7	-8.3
L1b	-1190.0	-14.6	-1251.0	-12.8	-1062.0	-9.7	-873.3	-6.5	-729.8	8.6	-626.0	11.6	-478.8	13.9	216.3	5.3
L2a	-956.6	-15.3	-1093.0	-16.2	-1274.0	-17.4	-1450.0	-18.7	-1667.0	-20.7	-1962.0	-23.9	-2374.0	-29.3	490.1	-11.7
L2b	1667.0	-25.1	1919.0	-29.1	1756.0	-28.3	1400.0	-25.1	910.1	-20.0	-582.2	-13.4	-491.9	6.4	159.4	5.1
L3	-1631.0	-22.6	-2031.0	-28.8	-2080.0	-30.0	-1998.0	-28.9	-1854.0	-26.4	-1683.0	-22.9	-1531.0	-18.6	-1519.0	-11.4
L4a	-194.5	-5.8	-209.1	-5.9	-204.0	-6.0	-197.7	-6.2	-200.3	-6.2	-216.8	-6.0	-253.0	-5.7	86.3	-3.6
L4b	-350.6	5.6	-387.1	6.3	-395.6	6.5	-393.9	6.5	-390.4	6.5	-393.9	6.5	-415.3	6.8	-78.6	-3.3
L5a	187.5	-7.3	221.3	-8.0	243.1	-8.5	255.6	-8.9	259.9	-9.0	256.2	-8.9	245.4	-8.5	162.1	-7.6
L5b	-91.2	4.5	-88.7	4.3	-76.4	4.1	-60.9	3.6	-47.4	-3.7	43.9	-4.3	68.8	-4.7	-78.6	-5.1
L6a	-642.5	9.2	-628.8	7.4	-606.5	-7.6	-593.7	-8.1	-595.7	-8.5	-622.0	-8.9	-671.6	-9.6	173.6	-4.8
L6b	-597.3	-8.7	-730.5	-8.0	-780.1	-7.9	-790.2	-8.2	-790.5	-8.6	-803.3	-9.1	-842.3	-9.7	148.5	-4.5
L7a	112.8	5.1	103.7	4.9	91.9	4.6	84.5	4.4	81.7	4.3	84.2	4.4	98.5	4.8	0.0	5.1
L7b	-188.4	-6.1	-128.3	-5.2	-69.7	-4.4	62.0	-3.7	77.7	4.2	100.1	4.9	137.8	5.8	0.0	-6.1
L8a	407.4	-9.6	-204.3	-7.8	-145.6	-5.9	-100.7	5.9	172.6	7.9	296.7	9.5	397.5	10.8	353.1	9.8
L8b	-171.7	-5.6	519.1	-11.1	568.0	-11.7	587.0	-12.0	589.7	-12.0	580.8	-11.8	568.3	-11.7	439.1	-9.6
L9a	-105.5	-7.4	-117.2	7.3	-136.5	8.6	-159.4	9.7	-176.3	10.2	-176.1	9.9	-152.0	7.7	-2290.0	-17.0
L9b	-192.2	10.6	-246.4	12.0	-282.7	12.8	-302.2	13.2	-299.4	13.1	-265.2	12.2	-196.2	9.4	-2757.0	-16.2
L10a	504.9	-12.5	691.2	-15.6	781.0	-17.1	829.9	-17.9	857.7	-18.2	869.6	-18.0	870.1	-17.7	730.4	-14.3
L10b	-218.4	-8.7	-568.8	-11.6	-648.1	-10.5	-700.9	-10.2	-752.2	-11.2	-808.8	-12.4	-841.1	-13.5	-532.5	-7.4
L11a	-399.6	-12.3	-382.5	-14.7	-428.2	-15.8	-456.1	-16.7	-478.7	-17.6	-498.1	-18.9	-497.5	-20.0	-374.2	-13.8
L11b	363.0	-11.0	-171.7	-5.3	-140.6	-4.6	-104.2	4.0	-75.4	5.1	140.2	6.1	210.4	7.1	177.6	6.5
L12a	1167.0	-19.2	1515.0	-23.3	1674.0	-25.1	1776.0	-26.1	1872.0	-26.7	1998.0	-26.9	2180.0	-26.3	562.1	-10.3
L12b	-843.3	-11.2	-794.1	-16.8	-867.3	-15.1	-845.7	-12.1	-847.1	-8.1	-1006.0	9.7	-1371.0	15.5	227.9	6.9
L13a	-804.1	-14.2	-801.3	-8.0	-734.5	8.2	-709.1	11.5	-700.7	14.5	660.4	17.1	1058.0	19.0	370.6	8.1
L13b	583.2	-15.9	-1211.0	-17.1	-1308.0	-17.7	-1410.0	-18.6	-1588.0	-20.3	-1905.0	-23.8	-2439.0	-30.2	539.8	-12.0
L14	-984.3	-20.6	-1277.0	-23.3	-1460.0	-23.3	-1625.0	-22.2	-1814.0	-20.3	-2081.0	-17.9	-2602.0	-15.0	-4730.0	-17.8

Table B.17 – Bending moments and shear forces in beams for lateral load applied in positive y-direction with wind as the main action.

Beam	1ST FLOOR		2ND FLOOR		3RD FLOOR		4TH FLOOR		5TH FLOOR		6TH FLOOR		7TH FLOOR		ROOF	
	M (kNcm)	V (kN)	M (kNcm)	V (kN)	M (kNcm)	V (kN)	M (kNcm)	V (kN)	M (kNcm)	V (kN)	M (kNcm)	V (kN)	M (kNcm)	V (kN)	M (kNcm)	V (kN)
L1a	-269.8	-7.4	-425.5	-10.3	-634.6	-13.5	-794.5	-16.6	-883.8	-19.2	982.3	-21.5	1290.0	-23.1	407.3	-8.2
L1b	-276.0	7.4	-427.6	10.3	-633.0	13.6	-788.0	16.7	-871.4	19.3	995.2	21.5	1291.0	23.0	408.2	8.3
L2a	-267.0	7.6	-469.9	10.2	-532.9	7.9	-653.9	-7.9	-896.4	-11.6	-1299.0	-16.5	-1754.0	-22.8	380.9	-9.6
L2b	-271.1	-7.8	-376.9	-9.6	-495.1	-10.5	-577.1	-10.0	-636.5	-8.0	-758.0	7.5	-1085.0	12.7	233.5	6.6
L3	730.7	-8.9	580.4	-7.6	469.7	-7.1	377.7	-7.0	264.1	-6.9	-227.1	-6.6	-424.1	-5.4	-1250.0	9.0
L4a	783.9	-12.7	957.1	-14.0	955.6	-14.0	858.9	-13.2	701.5	-11.9	502.5	-10.3	261.2	-8.5	147.3	-4.3
L4b	784.5	-12.7	957.9	-14.0	956.1	-14.0	859.0	-13.2	701.1	-11.9	501.9	-10.3	261.3	-8.5	147.2	-4.3
L5a	579.2	-19.7	684.6	-22.3	687.9	-22.0	645.2	-20.6	576.5	-18.4	491.4	-15.8	400.7	-13.0	213.1	-9.1
L5b	579.4	-19.7	685.3	-22.3	688.9	-22.1	646.2	-20.6	577.2	-18.4	491.6	-15.9	400.7	-13.0	213.3	-9.1
L6a	-1539.0	-28.9	1641.0	-34.2	1775.0	-34.4	1666.0	-32.2	1419.0	-28.7	1114.0	-24.8	-860.3	-21.2	359.7	-7.7
L6b	-1538.0	-28.9	1642.0	-34.2	1776.0	-34.4	1666.0	-32.2	1420.0	-28.7	1114.0	-24.8	-860.0	-21.2	359.8	-7.7
L7a	659.7	14.3	940.0	18.5	1020.0	19.7	978.7	19.0	873.0	17.3	747.6	15.4	653.6	13.9	0.0	14.3
L7b	659.6	14.3	940.1	18.5	1020.0	19.7	979.1	19.0	873.2	17.3	747.3	15.4	653.1	13.9	0.0	14.3
L8a	492.5	-9.6	363.8	-12.3	336.1	-10.9	278.1	-8.7	211.5	-6.1	262.4	6.3	392.5	8.5	344.1	7.8
L8b	493.1	9.6	654.4	-12.2	732.3	-13.6	757.9	-14.1	751.3	-14.1	724.6	-13.9	694.4	-13.6	503.4	-10.8
L9a	-918.6	-29.0	-1208.0	-36.0	-1215.0	-36.2	-1085.0	-33.1	-891.6	-28.3	-686.0	-23.2	-527.9	-19.4	-2824.0	-32.1
L9b	-921.0	-29.0	-1210.0	-36.0	-1219.0	-36.3	-1091.0	-33.2	-898.6	-28.5	-694.6	-23.4	-543.7	-19.7	-3074.0	-34.1
L10a	314.6	11.5	363.8	12.3	336.2	10.9	278.1	8.7	211.2	6.1	262.8	-6.3	393.4	-8.5	344.8	-7.9
L10b	314.6	-11.5	-360.8	11.3	-418.3	12.2	-468.6	12.7	-528.3	13.3	-599.0	14.1	-645.1	14.8	-306.7	8.5
L11a	345.2	-12.6	427.8	-15.0	439.8	15.9	428.1	16.3	414.8	16.9	413.4	17.8	422.2	18.5	261.8	-12.2
L11b	345.1	12.6	655.7	12.3	734.2	13.6	760.1	14.1	753.0	14.1	725.3	13.9	694.4	13.6	503.4	10.8
L12a	624.6	-14.7	788.3	-17.1	901.3	-18.4	1026.0	-19.4	1175.0	-20.2	1352.0	-20.8	1543.0	-20.4	417.3	-8.4
L12b	623.2	14.7	-474.1	-10.2	-539.2	-7.9	-662.8	7.9	-908.5	11.6	-1315.0	16.5	-1780.0	22.9	384.0	9.7
L13a	-371.3	10.9	787.1	17.2	900.8	18.4	1025.0	19.4	1172.0	20.3	1348.0	20.8	1539.0	20.4	416.0	8.4
L13b	-373.5	-10.9	-367.3	9.7	-487.2	10.8	-571.2	10.5	-628.0	8.5	-749.4	-7.1	-1123.0	-12.8	245.3	-6.9
L14	-634.1	-8.6	-785.3	-8.7	-959.0	-8.7	-1178.0	-8.8	-1464.0	-8.9	-1865.0	-9.0	-2527.0	-9.1	-4403.0	-9.0

Table B.18 – Axial forces in walls for lateral load applied in positive y-direction with wind as the main action.

Wall	BASEMENT	1ST FLOOR	2ND FLOOR	3RD FLOOR	4TH FLOOR	5TH FLOOR	6TH FLOOR	7TH FLOOR
	N (kN)	N (kN)	N (kN)	N (kN)	N (kN)	N (kN)	N (kN)	N (kN)
P1a	-39.0	-35.2	-31.4	-27.2	-22.6	-17.3	-11.6	-5.9
P1b	-39.0	-35.2	-31.4	-27.2	-22.6	-17.3	-11.6	-5.9
P2a	-272.0	-246.6	-220.3	-191.6	-159.3	-122.8	-82.1	-36.7
P2b	-271.9	-246.6	-220.4	-191.6	-159.2	-122.8	-82.1	-36.7
P3a	-126.6	-111.7	-98.7	-85.0	-70.0	-53.7	-35.7	-16.1
P3b	-126.6	-111.7	-98.7	-85.0	-70.1	-53.7	-35.7	-16.1
P4a	-187.3	-173.9	-158.4	-139.6	-118.2	-94.3	-67.0	-34.0
P4b	-187.0	-174.3	-158.8	-139.9	-118.4	-94.3	-66.7	-33.8
P5a	-595.3	-505.3	-422.7	-347.1	-275.9	-207.1	-139.2	-71.3
P5b	-594.6	-506.0	-423.4	-347.6	-276.2	-207.2	-139.1	-71.2
P6a	-71.4	-56.3	-44.5	-34.7	-26.2	-18.7	-11.9	-6.5
P6b	-71.4	-56.3	-44.5	-34.8	-26.3	-18.7	-11.9	-6.6
P7a	-376.4	-356.9	-331.0	-298.9	-262.2	-221.6	-176.8	-123.5
P7b	-376.5	-358.7	-333.0	-300.7	-263.6	-222.2	-175.5	-118.1
P8a	-500.1	-431.4	-375.4	-325.1	-277.1	-230.6	-187.5	-150.1
P8b	-499.6	-432.6	-376.9	-326.7	-278.5	-231.9	-188.8	-158.7
P9	-308.7	-269.3	-235.4	-203.9	-173.4	-143.4	-113.9	-22.8
P10	-113.7	-111.2	-103.3	-93.4	-82.2	-69.9	-56.9	-65.9
P11a	-217.6	-193.4	-170.4	-145.6	-118.9	-90.3	-60.1	-27.9
P11b	-217.6	-193.3	-170.4	-145.6	-118.8	-90.3	-60.1	-27.9
P12a	-240.8	-218.5	-192.3	-164.0	-133.9	-102.1	-68.6	-34.3
P12b	-240.8	-218.6	-192.3	-164.0	-133.9	-102.1	-68.6	-34.3
P13a	-348.1	-302.2	-257.7	-213.9	-170.6	-127.5	-84.7	-41.2
P13b	-348.0	-302.3	-257.7	-214.0	-170.7	-127.6	-84.7	-41.2
P14a	-258.3	-216.4	-179.0	-145.0	-113.2	-83.0	-54.4	-29.1
P14b	-258.2	-216.5	-179.1	-145.1	-113.3	-83.0	-54.4	-29.1
P15a	-418.6	-372.0	-324.7	-274.1	-220.6	-165.0	-107.6	-48.1
P15b	-418.5	-372.0	-324.8	-274.1	-220.6	-165.0	-107.6	-48.1
P16a	-667.2	-591.5	-506.0	-417.0	-327.5	-238.7	-151.4	-66.4
P16b	-667.1	-591.5	-505.9	-416.9	-327.4	-238.6	-151.3	-66.4
P17a	-414.2	-353.8	-292.7	-234.4	-179.3	-127.1	-78.0	-31.9
P17b	-414.3	-353.8	-292.7	-234.5	-179.3	-127.1	-78.0	-31.9
P18a	-106.1	-98.6	-89.3	-77.8	-64.9	-50.6	-34.8	-17.6
P18b	-106.1	-98.7	-89.3	-77.9	-65.0	-50.6	-34.9	-17.6
P19a	-646.7	-571.6	-493.3	-413.5	-332.9	-251.2	-167.4	-81.1
P19b	-647.0	-571.9	-493.6	-413.9	-333.3	-251.5	-167.7	-81.2
P20a	-258.3	-217.5	-180.3	-146.1	-114.1	-83.6	-54.1	-23.7
P20b	-258.4	-217.6	-180.4	-146.2	-114.2	-83.7	-54.2	-23.7
P21a	-447.5	-402.4	-359.4	-314.3	-267.1	-217.7	-164.0	-96.6
P21b	-447.1	-402.8	-359.8	-314.8	-267.7	-218.4	-164.9	-97.5
P22a	-800.1	-716.0	-626.5	-536.6	-448.7	-365.0	-289.4	-192.0
P22b	-800.7	-716.6	-627.2	-537.4	-449.7	-366.3	-290.9	-198.4
P23a	-436.6	-378.5	-319.5	-264.0	-212.7	-165.7	-122.8	-80.5
P23b	-436.8	-378.7	-319.7	-264.2	-212.9	-166.1	-123.3	-81.2
P24a	-233.0	-201.2	-170.1	-140.9	-114.1	-89.9	-68.5	-52.2
P24b	-233.0	-201.3	-170.1	-141.0	-114.2	-90.0	-68.7	-53.7
P25	-377.8	-334.0	-290.2	-246.4	-202.6	-158.8	-115.0	-24.0

Table B.19 – Shear forces in walls for lateral load applied in positive y-direction with wind as the main action.

Wall	BASEMENT		1ST FLOOR		2ND FLOOR		3RD FLOOR		4TH FLOOR		5TH FLOOR		6TH FLOOR		7TH FLOOR	
	Vx (kN)	Vy (kN)	Vx (kN)	Vy (kN)	Vx (kN)	Vy (kN)	Vx (kN)	Vy (kN)	Vx (kN)	Vy (kN)	Vx (kN)	Vy (kN)	Vx (kN)	Vy (kN)	Vx (kN)	Vy (kN)
P1a	0.0	0.3	0.0	0.4	0.0	0.4	0.0	0.4	0.0	0.3	0.0	0.3	0.0	0.2	0.0	0.1
P1b	0.0	0.3	0.0	0.4	0.0	0.4	0.0	0.4	0.0	0.3	0.0	0.3	0.0	0.2	0.0	0.1
P3a	0.0	4.5	0.0	5.5	0.0	5.6	-0.1	5.3	-0.1	4.7	-0.1	4.0	-0.1	3.2	-0.1	1.9
P3b	0.0	4.5	0.0	5.5	0.1	5.6	0.1	5.3	0.1	4.7	0.1	4.0	0.1	3.2	0.1	1.9
P5a	0.1	38.6	-0.3	24.8	-0.4	15.3	-0.4	9.1	-0.5	4.9	-0.5	1.5	-0.5	-1.8	-0.6	-7.7
P5b	-0.1	38.6	0.3	24.9	0.4	15.3	0.4	9.2	0.5	5.0	0.5	1.7	0.5	-1.7	0.6	-7.8
P8a	0.0	36.4	0.0	30.8	0.0	26.6	0.0	21.4	0.0	14.9	0.0	7.1	0.0	-2.0	-0.1	-5.0
P8b	0.0	36.5	0.0	30.7	0.0	26.6	0.0	21.6	0.0	15.2	0.0	7.4	0.0	-2.1	0.1	-5.0
P9	0.0	14.1	0.0	6.8	0.0	4.7	0.0	3.7	0.0	3.2	0.0	2.7	0.0	2.2	0.0	2.0
P11a	0.0	14.2	-0.1	18.7	-0.1	19.5	-0.1	18.4	-0.1	16.3	-0.1	13.6	-0.1	10.8	-0.2	7.6
P11b	0.0	14.2	0.1	18.7	0.1	19.5	0.1	18.4	0.1	16.3	0.1	13.6	0.1	10.8	0.2	7.6
P13a	0.0	20.7	-0.1	18.8	-0.2	17.0	-0.2	14.6	-0.2	11.8	-0.2	8.7	-0.2	5.3	-0.3	3.7
P13b	0.0	20.7	0.1	18.8	0.2	17.0	0.2	14.6	0.2	11.8	0.2	8.8	0.2	5.3	0.3	3.7
P16a	0.0	51.4	-0.1	53.1	-0.1	49.8	-0.1	44.4	-0.1	37.9	-0.1	30.8	-0.2	23.5	-0.2	13.6
P16b	0.0	51.4	0.1	53.1	0.1	49.8	0.1	44.4	0.1	37.9	0.1	30.8	0.2	23.5	0.2	13.6
P19a	0.0	41.4	-0.1	37.6	-0.1	31.9	-0.2	26.7	-0.2	21.5	-0.3	16.3	-0.4	10.9	-0.6	5.8
P19b	0.0	41.4	0.1	37.6	0.1	31.9	0.2	26.7	0.2	21.6	0.3	16.3	0.4	10.9	0.6	5.7
P22a	0.0	60.8	0.0	63.0	0.0	58.0	0.0	50.9	-0.1	42.6	-0.1	33.7	-0.1	24.7	-0.2	12.9
P22b	0.0	60.8	0.0	63.2	0.0	58.2	0.0	51.2	0.1	43.0	0.1	34.3	0.1	25.4	0.2	14.1
P25	0.0	12.4	0.0	2.3	0.0	1.5	0.0	1.0	0.0	0.7	0.0	0.4	0.0	0.2	0.0	-0.5

Table B.20 – Bending moments in walls for lateral load applied in positive y-direction with wind as the main action.

Wall	BASEMENT		1ST FLOOR		2ND FLOOR		3RD FLOOR		4TH FLOOR		5TH FLOOR		6TH FLOOR		7TH FLOOR	
	Mx (kNcm)	My (kNcm)	Mx (kNcm)	My (kNcm)	Mx (kNcm)	My (kNcm)	Mx (kNcm)	My (kNcm)	Mx (kNcm)	My (kNcm)	Mx (kNcm)	My (kNcm)	Mx (kNcm)	My (kNcm)	Mx (kNcm)	My (kNcm)
P1a	38.7	-0.6	52.1	1.5	54.6	2.4	51.3	3.2	44.6	3.9	36.3	4.5	27.2	5.0	18.1	-4.9
P1b	38.7	0.6	52.1	-1.5	54.6	-2.4	51.3	-3.2	44.6	-3.9	36.3	-4.6	27.2	-5.0	18.1	4.9
P3a	772.2	1.6	841.7	4.1	834.9	6.7	771.0	9.1	674.7	11.4	559.9	13.5	-443.3	15.6	288.2	-15.4
P3b	772.3	-1.6	842.3	-4.1	835.9	-6.8	772.3	-9.3	675.9	-11.5	560.8	-13.6	-443.2	-15.6	288.3	15.4
P5a	15410.0	-26.0	8910.0	47.0	5037.0	56.5	2542.0	61.8	838.1	64.0	-755.1	65.5	-1052.0	-63.9	-1354.0	90.3
P5b	15410.0	26.0	8907.0	-47.1	5040.0	-56.8	2555.0	-62.2	859.0	-64.4	-770.9	-65.9	-1029.0	64.0	-1349.0	-89.9
P8a	11980.0	2.5	7756.0	3.2	5693.0	2.1	4091.0	1.2	2594.0	0.3	1144.0	2.0	329.3	-2.2	-2419.0	-12.8
P8b	11980.0	-2.4	7723.0	-3.4	5685.0	-2.4	4103.0	-1.6	2623.0	-0.6	1186.0	-2.0	401.5	2.6	-2736.0	16.1
P9	4336.0	-1.8	1984.0	2.1	1161.0	0.8	707.6	0.3	-470.1	0.3	-537.7	0.7	-533.1	-0.9	559.0	1.9
P11a	2405.0	-4.0	2873.0	10.6	2917.0	15.4	2706.0	17.8	2357.0	18.8	1941.0	19.1	1519.0	-19.2	1109.0	26.6
P11b	2405.0	4.1	2873.0	-10.6	2918.0	-15.4	2706.0	-17.9	2357.0	-18.8	1941.0	-19.2	1519.0	19.1	1109.0	-26.5
P13a	5050.0	-4.7	3708.0	16.1	3017.0	25.0	2376.0	29.4	1769.0	31.3	-1254.0	32.3	-825.0	-32.1	-837.4	50.1
P13b	5050.0	4.7	3709.0	-16.1	3017.0	-25.1	2376.0	-29.5	1769.0	-31.5	-1256.0	-32.4	-827.0	32.0	-839.1	-50.0
P16a	15590.0	4.6	12190.0	9.0	9793.0	11.8	7723.0	14.4	5852.0	17.1	-4427.0	20.1	-3753.0	-20.8	2033.0	35.8
P16b	15590.0	-4.6	12190.0	-9.0	9793.0	-11.9	7723.0	-14.5	5851.0	-17.2	-4426.0	-20.1	-3751.0	20.6	2032.0	-35.7
P19a	12790.0	3.4	9246.0	9.4	6733.0	16.5	4841.0	24.9	3331.0	34.7	-2467.0	46.5	-1961.0	54.5	-1326.0	92.0
P19b	12790.0	-3.3	9246.0	-9.3	6734.0	-16.6	4843.0	-25.0	3334.0	-34.8	-2469.0	-46.6	-1960.0	-54.5	-1319.0	-92.2
P22a	20140.0	-0.2	15700.0	1.4	12250.0	3.9	9348.0	6.4	6815.0	8.8	-4797.0	13.1	-4053.0	16.7	-1963.0	-29.4
P22b	20140.0	0.2	15700.0	-1.3	12260.0	-3.8	9376.0	-6.2	6857.0	-8.7	-4895.0	-12.7	-4183.0	-16.9	2162.0	-35.5
P25	4844.0	0.0	1386.0	0.0	747.1	0.0	336.8	0.0	-140.1	-0.1	-256.6	0.1	-302.6	-0.5	-133.8	1.7

Table B.21 – Axial forces in walls for lateral load applied in negative y-direction with wind as the main action.

Wall	BASEMENT	1ST FLOOR	2ND FLOOR	3RD FLOOR	4TH FLOOR	5TH FLOOR	6TH FLOOR	7TH FLOOR
	N (kN)	N (kN)	N (kN)	N (kN)	N (kN)	N (kN)	N (kN)	N (kN)
P1a	-63.8	-55.8	-46.8	-37.9	-29.1	-20.8	-13.0	-6.0
P1b	-63.9	-55.7	-46.8	-37.8	-29.1	-20.8	-12.9	-6.0
P2a	-453.1	-393.8	-330.3	-267.2	-206.1	-147.6	-92.0	-38.9
P2b	-453.4	-393.6	-330.1	-267.0	-206.0	-147.5	-91.9	-38.9
P3a	-189.9	-165.0	-139.1	-113.2	-88.0	-63.7	-40.3	-18.2
P3b	-189.9	-165.1	-139.1	-113.2	-88.0	-63.7	-40.3	-18.2
P4a	-321.2	-268.9	-223.7	-182.5	-143.6	-106.2	-69.2	-30.3
P4b	-319.5	-270.0	-224.4	-182.8	-143.7	-105.9	-68.7	-30.0
P5a	-602.3	-537.2	-472.2	-403.2	-330.2	-253.4	-171.7	-84.5
P5b	-599.6	-539.4	-473.7	-404.0	-330.6	-253.2	-171.3	-84.2
P6a	-45.2	-43.5	-40.8	-36.5	-31.1	-24.7	-17.4	-9.0
P6b	-45.0	-43.7	-40.9	-36.6	-31.1	-24.7	-17.4	-9.0
P7a	-648.0	-556.5	-475.0	-397.5	-324.6	-256.7	-193.7	-131.6
P7b	-637.3	-561.5	-477.5	-398.6	-324.7	-255.5	-190.2	-123.5
P8a	-578.2	-517.3	-457.4	-394.6	-332.5	-273.9	-222.5	-165.4
P8b	-570.7	-522.5	-460.6	-396.4	-333.3	-274.0	-222.4	-174.7
P9	-348.6	-329.2	-297.5	-260.2	-220.8	-181.3	-142.0	-22.8
P10	-198.5	-171.3	-147.0	-123.7	-101.6	-80.9	-61.9	-71.3
P11a	-276.9	-240.1	-201.4	-163.8	-127.5	-92.6	-58.9	-25.5
P11b	-277.4	-239.7	-201.0	-163.5	-127.3	-92.4	-58.8	-25.5
P12a	-324.9	-277.3	-232.7	-189.7	-147.9	-107.6	-68.7	-32.6
P12b	-325.2	-277.0	-232.5	-189.5	-147.8	-107.5	-68.7	-32.6
P13a	-370.0	-326.8	-281.1	-234.5	-187.4	-140.2	-93.3	-46.8
P13b	-369.9	-326.8	-281.1	-234.5	-187.4	-140.1	-93.2	-46.8
P14a	-219.7	-199.3	-176.5	-151.0	-123.5	-94.7	-64.8	-33.8
P14b	-219.5	-199.5	-176.7	-151.1	-123.6	-94.8	-64.8	-33.8
P15a	-422.1	-360.4	-302.9	-248.6	-196.0	-144.3	-93.7	-45.7
P15b	-422.4	-360.1	-302.6	-248.4	-195.8	-144.1	-93.6	-45.7
P16a	-502.9	-450.5	-395.1	-336.2	-273.4	-206.3	-135.2	-60.8
P16b	-501.7	-449.4	-394.2	-335.5	-272.8	-205.9	-134.9	-60.7
P17a	-211.6	-201.2	-187.6	-168.0	-142.7	-111.9	-75.2	-31.2
P17b	-211.3	-200.9	-187.3	-167.7	-142.5	-111.8	-75.1	-31.2
P18a	-133.7	-107.5	-87.0	-69.6	-54.0	-39.3	-25.3	-12.8
P18b	-133.6	-107.5	-87.0	-69.7	-54.1	-39.4	-25.4	-12.8
P19a	-543.1	-469.8	-401.8	-337.4	-273.9	-209.0	-141.3	-70.3
P19b	-543.3	-470.1	-402.1	-337.7	-274.2	-209.4	-141.6	-70.5
P20a	-142.6	-133.0	-122.2	-108.7	-92.9	-74.5	-52.8	-25.4
P20b	-142.6	-133.0	-122.3	-108.8	-93.0	-74.6	-52.9	-25.5
P21a	-487.5	-414.8	-349.9	-291.8	-238.2	-187.5	-136.6	-77.2
P21b	-486.7	-415.6	-350.8	-292.5	-239.0	-188.3	-137.5	-78.2
P22a	-683.5	-605.7	-530.6	-458.1	-387.6	-319.1	-254.4	-170.0
P22b	-685.2	-607.3	-532.0	-459.5	-389.0	-320.6	-256.3	-176.3
P23a	-254.4	-236.5	-218.6	-197.7	-173.7	-147.0	-117.4	-81.6
P23b	-254.6	-236.7	-218.9	-198.0	-174.1	-147.4	-118.0	-82.5
P24a	-134.7	-125.8	-116.8	-106.1	-93.7	-80.2	-65.9	-55.4
P24b	-134.8	-126.0	-117.0	-106.2	-93.9	-80.3	-66.1	-57.0
P25	-377.8	-334.0	-290.2	-246.4	-202.6	-158.8	-115.0	-24.0

Table B.22 – Shear forces in walls for lateral load applied in negative y-direction with wind as the main action.

Wall	BASEMENT		1ST FLOOR		2ND FLOOR		3RD FLOOR		4TH FLOOR		5TH FLOOR		6TH FLOOR		7TH FLOOR	
	Vx (kN)	Vy (kN)	Vx (kN)	Vy (kN)	Vx (kN)	Vy (kN)	Vx (kN)	Vy (kN)	Vx (kN)	Vy (kN)	Vx (kN)	Vy (kN)	Vx (kN)	Vy (kN)	Vx (kN)	Vy (kN)
P1a	0.0	-0.3	0.0	-0.4	0.0	-0.4	0.0	-0.4	0.0	-0.3	0.0	-0.3	0.0	-0.2	0.0	-0.2
P1b	0.0	-0.3	0.0	-0.4	0.0	-0.4	0.0	-0.4	0.0	-0.3	0.0	-0.3	0.0	-0.2	0.0	-0.2
P3a	0.0	-4.9	0.0	-6.0	0.0	-5.8	-0.1	-5.2	-0.1	-4.3	-0.1	-3.2	-0.1	-2.1	-0.1	-1.5
P3b	0.0	-4.9	0.0	-6.0	0.0	-5.8	0.1	-5.2	0.1	-4.2	0.1	-3.2	0.1	-2.1	0.1	-1.5
P5a	-0.1	-42.0	0.2	-33.3	0.2	-25.5	0.2	-19.3	0.1	-13.6	0.0	-7.8	-0.1	-1.3	-0.2	7.2
P5b	0.1	-42.1	-0.2	-33.0	-0.2	-25.1	-0.2	-18.9	-0.1	-13.3	0.0	-7.6	0.1	-1.3	0.2	7.0
P8a	0.0	-45.4	0.0	-53.4	0.0	-54.9	0.0	-53.6	0.0	-50.3	0.0	-46.1	0.0	-42.5	-0.1	-20.1
P8b	0.0	-46.1	0.0	-52.0	0.0	-53.5	0.0	-52.2	0.0	-49.1	0.0	-45.2	0.0	-42.2	0.1	-20.1
P9	0.0	-11.9	0.0	-1.3	0.0	2.4	0.0	4.0	0.0	4.7	0.0	4.8	0.0	5.2	0.0	6.3
P11a	0.0	-13.9	0.0	-17.6	0.0	-17.6	0.0	-15.9	0.0	-13.2	0.0	-10.0	0.0	-6.5	0.0	-2.3
P11b	0.0	-13.9	0.0	-17.6	0.0	-17.6	0.0	-15.9	0.0	-13.2	0.0	-10.0	0.0	-6.5	0.0	-2.3
P13a	0.0	-21.0	0.0	-19.8	0.0	-18.6	0.0	-16.3	0.0	-13.6	0.0	-10.7	0.0	-7.5	0.0	-3.8
P13b	0.0	-21.0	0.0	-19.8	0.0	-18.5	0.0	-16.3	0.0	-13.6	0.0	-10.6	0.0	-7.5	0.0	-3.8
P16a	0.0	-47.6	-0.1	-44.3	-0.2	-38.8	-0.2	-32.4	-0.2	-25.1	-0.2	-16.9	-0.2	-7.5	-0.3	2.9
P16b	0.0	-47.6	0.1	-44.3	0.2	-38.8	0.2	-32.4	0.2	-25.1	0.2	-16.9	0.2	-7.5	0.3	2.9
P19a	-0.1	-38.0	-0.2	-29.1	-0.2	-21.3	-0.3	-15.4	-0.4	-10.3	-0.4	-5.6	-0.5	-0.2	-0.7	8.6
P19b	0.1	-37.9	0.1	-29.1	0.2	-21.3	0.3	-15.3	0.4	-10.2	0.4	-5.5	0.5	-0.2	0.7	8.6
P22a	0.0	-56.2	0.0	-52.7	0.0	-46.2	0.0	-38.6	0.0	-30.2	0.0	-21.2	-0.1	-12.2	-0.1	4.0
P22b	0.0	-56.0	0.0	-52.2	0.0	-45.4	0.0	-37.6	0.0	-29.0	0.0	-19.9	0.1	-10.6	0.1	5.9
P25	0.0	-12.3	0.0	-2.2	0.0	-1.4	0.0	-0.9	0.0	-0.6	0.0	-0.4	0.0	-0.1	0.0	2.0

Table B.23 – Bending moments in walls for lateral load applied in negative y-direction with wind as the main action.

Wall	BASEMENT		1ST FLOOR		2ND FLOOR		3RD FLOOR		4TH FLOOR		5TH FLOOR		6TH FLOOR		7TH FLOOR	
	Mx (kNcm)	My (kNcm)	Mx (kNcm)	My (kNcm)	Mx (kNcm)	My (kNcm)	Mx (kNcm)	My (kNcm)	Mx (kNcm)	My (kNcm)	Mx (kNcm)	My (kNcm)	Mx (kNcm)	My (kNcm)	Mx (kNcm)	My (kNcm)
P1a	-39.5	-0.7	-56.3	1.1	-57.6	1.3	-52.7	1.5	-44.7	1.8	-35.3	2.2	-25.5	2.6	21.8	-2.7
P1b	-39.4	0.6	-56.3	-1.1	-57.6	-1.3	-52.7	-1.5	-44.7	-1.9	-35.3	-2.3	-25.5	-2.6	21.9	-2.7
P3a	-771.1	3.5	-899.8	5.7	-855.9	6.2	-745.8	6.8	-603.1	7.6	449.4	8.7	306.8	9.9	250.4	-9.5
P3b	-771.1	-3.6	-899.7	-5.9	-855.4	-6.4	-745.1	-6.9	-602.6	-7.7	449.7	-8.7	308.0	-9.8	250.4	9.5
P5a	-13900.0	21.2	-8660.0	-32.6	-5407.0	31.4	-3193.0	26.9	2268.0	18.2	1967.0	7.1	1249.0	8.2	1729.0	25.0
P5b	-13890.0	-21.8	-8625.0	-32.1	-5353.0	-31.1	-3136.0	-26.5	2232.0	-17.8	1955.0	-6.8	1270.0	-8.3	1724.0	-24.0
P8a	-10610.0	-1.0	-9414.0	-0.6	-8521.0	-1.6	-7638.0	1.4	7391.0	0.8	7192.0	1.4	7048.0	-2.1	-3853.0	-7.2
P8b	-10570.0	0.6	-9238.0	0.5	-8310.0	-0.9	-7432.0	-0.9	7236.0	-0.3	7088.0	-2.3	7080.0	-4.1	-4659.0	13.1
P9	-4007.0	2.0	-1093.0	-2.6	-694.4	-1.1	-587.5	-0.9	841.1	1.0	993.1	1.2	1078.0	-1.2	1755.0	3.1
P11a	-2283.0	0.5	-2666.0	-2.6	-2602.0	-3.9	-2304.0	3.9	-1884.0	2.8	-1403.0	0.8	929.7	2.7	-369.6	4.6
P11b	-2283.0	-0.6	-2667.0	2.6	-2604.0	4.0	-2306.0	-4.0	-1885.0	-2.9	-1403.0	-0.9	929.1	-2.6	-368.9	-4.5
P13a	-4757.0	-3.4	-3545.0	-2.5	-2979.0	-4.5	-2400.0	5.0	1981.0	3.9	1690.0	1.3	1321.0	2.4	732.7	6.4
P13b	-4757.0	3.2	-3542.0	2.2	-2975.0	4.5	-2395.0	-5.1	1978.0	-4.0	1686.0	-1.4	1317.0	-2.3	727.0	-6.3
P16a	-14580.0	8.3	-10070.0	16.8	-7339.0	21.9	-5187.0	25.5	3692.0	27.9	3046.0	30.1	1900.0	-30.5	1161.0	44.8
P16b	-14580.0	-8.5	-10070.0	-16.8	-7337.0	-21.8	-5185.0	-25.3	3689.0	-27.7	3042.0	-30.0	1896.0	30.1	1163.0	-44.4
P19a	-11990.0	9.4	-7444.0	22.5	-4555.0	33.6	-2571.0	43.4	1776.0	52.4	1570.0	62.6	962.2	-66.2	1532.0	113.2
P19b	-11990.0	-9.4	-7441.0	-22.1	-4550.0	-32.8	-2563.0	-42.4	1765.0	-51.4	1561.0	-61.7	957.7	65.2	1539.0	-112.2
P22a	-18880.0	-0.4	-12850.0	-2.5	-9165.0	-4.6	-6331.0	4.4	4511.0	2.9	4059.0	2.5	3298.0	7.9	2955.0	-16.1
P22b	-18910.0	-0.5	-12830.0	2.7	-9089.0	5.1	-6213.0	-5.3	4320.0	-3.8	3849.0	-1.4	3059.0	-7.6	3117.0	21.5
P25	-4541.0	-0.1	-1099.0	-0.1	-491.0	-0.1	140.4	-0.1	310.4	-0.1	416.9	0.1	441.6	-0.7	553.2	2.1

Table B.24 – Bending moments and shear forces in beams for lateral load applied in negative y-direction with wind as the main action.

Beam	1ST FLOOR		2ND FLOOR		3RD FLOOR		4TH FLOOR		5TH FLOOR		6TH FLOOR		7TH FLOOR		ROOF	
	M (kNcm)	V (kN)	M (kNcm)	V (kN)	M (kNcm)	V (kN)	M (kNcm)	V (kN)	M (kNcm)	V (kN)	M (kNcm)	V (kN)	M (kNcm)	V (kN)	M (kNcm)	V (kN)
L1a	-613.0	-11.6	-745.0	-13.8	-702.0	-14.3	-600.8	-14.6	615.0	-14.9	843.5	-15.1	1113.0	-14.5	249.8	-5.4
L1b	-573.5	11.5	-702.8	13.7	-662.6	14.2	-564.6	14.5	641.0	14.8	857.5	15.0	1106.0	14.4	249.9	5.4
L2a	564.1	14.0	-695.8	-9.6	-879.6	-10.2	-1067.0	-11.6	-1305.0	-13.8	-1605.0	-17.2	-1958.0	-21.9	334.3	-9.0
L2b	494.9	-13.1	-461.6	-13.4	-415.1	-11.2	-390.4	-7.6	-542.3	9.1	-1014.0	15.3	-1641.0	23.5	440.5	10.0
L3	-307.8	-5.3	-471.9	-11.7	-586.3	-14.7	-667.3	-15.5	-739.2	-15.1	-829.5	-14.0	-973.8	-12.8	-1126.0	-6.3
L4a	-990.5	12.4	-1245.0	14.4	-1243.0	14.3	-1130.0	13.4	-971.2	12.1	-807.1	10.7	-660.9	9.4	-94.1	2.9
L4b	-993.4	12.4	-1249.0	14.4	-1248.0	14.4	-1134.0	13.4	-975.1	12.1	-810.1	10.8	-662.1	9.4	-94.3	2.9
L5a	-459.3	16.8	-524.4	18.6	-488.2	17.5	-405.7	15.2	-301.0	12.4	-188.7	9.3	99.9	6.4	-70.5	-3.6
L5b	-459.4	16.8	-524.6	18.6	-488.3	17.5	-405.7	15.2	-301.2	12.4	-189.3	9.3	99.4	6.4	-70.5	-3.6
L6a	-1905.0	29.3	-2534.0	33.5	-2639.0	32.8	-2472.0	29.8	-2170.0	25.5	-1829.0	20.6	-1555.0	15.8	112.6	4.1
L6b	-1906.0	29.3	-2534.0	33.5	-2638.0	32.8	-2471.0	29.7	-2169.0	25.4	-1827.0	20.6	-1552.0	15.8	112.0	4.1
L7a	-766.0	-15.2	-999.8	-18.8	-1042.0	-19.4	-968.8	-18.3	-827.8	-16.1	-651.5	-13.4	-470.2	-10.7	0.0	-15.2
L7b	-766.1	-15.2	-999.9	-18.8	-1042.0	-19.4	-968.0	-18.3	-826.3	-16.1	-649.9	-13.4	-468.5	-10.6	0.0	-15.2
L8a	-256.9	5.6	722.6	19.9	833.5	22.0	886.7	22.5	904.3	22.2	895.5	21.1	866.5	19.8	731.9	16.1
L8b	-256.7	-5.6	-287.1	6.5	-265.0	6.4	-210.1	5.7	-146.5	4.6	-92.3	-4.1	85.8	-5.1	114.4	-5.4
L9a	1066.0	32.4	1453.0	42.5	1543.0	45.1	-1484.0	43.4	-1319.0	39.1	-1072.0	32.7	-732.8	23.9	-2782.0	19.8
L9b	1060.0	32.1	1435.0	42.0	1518.0	44.4	-1454.0	42.7	-1291.0	38.4	-1047.0	32.0	-709.5	23.3	-2888.0	17.1
L10a	507.1	-15.3	729.6	-20.1	842.4	-22.1	896.3	-22.7	913.8	-22.3	905.0	-21.3	876.1	-20.0	740.2	-16.3
L10b	503.3	15.2	-251.4	-11.9	-286.6	-10.6	-298.2	-8.2	-305.1	-5.2	-378.6	5.2	-488.4	8.3	-363.6	5.4
L11a	-251.7	11.2	-346.8	7.7	-341.3	6.3	-306.1	4.0	-308.1	-5.5	-356.9	-8.9	-384.7	-12.0	-336.8	-9.2
L11b	-252.3	-11.3	-286.8	-6.5	-264.3	-6.4	-209.3	-5.7	-146.0	-4.6	-92.3	4.1	84.8	5.1	113.4	5.4
L12a	-461.2	6.6	-520.3	-10.9	-671.3	-15.0	-755.9	-18.3	981.4	-20.9	1319.0	-23.2	1705.0	-24.9	517.9	-10.1
L12b	-468.1	-6.7	-695.5	9.4	-880.1	10.0	-1068.0	11.4	-1309.0	13.6	-1617.0	17.0	-1983.0	21.8	334.3	9.0
L13a	-463.0	-9.2	-527.6	10.8	-678.8	14.9	-765.7	18.1	953.7	20.8	1291.0	23.1	1679.0	24.8	512.1	10.0
L13b	-462.9	9.1	-514.1	14.4	-465.3	12.1	-408.3	8.5	-530.7	-8.3	-1023.0	-15.0	-1753.0	-24.1	461.5	-10.5
L14	-400.6	-8.7	-511.4	-8.9	-700.3	-9.0	-948.5	-9.1	-1266.0	-9.3	-1693.0	-9.4	-2389.0	-9.5	-4455.0	-9.4

B.3 Load combination III – Seismic force as the main action

Table B.25 – Bending moments and shear forces in beams for lateral load applied in x-direction with seismic force as the main action.

Beam	1ST FLOOR		2ND FLOOR		3RD FLOOR		4TH FLOOR		5TH FLOOR		6TH FLOOR		7TH FLOOR		ROOF	
	M (kNcm)	V (kN)	M (kNcm)	V (kN)	M (kNcm)	V (kN)	M (kNcm)	V (kN)	M (kNcm)	V (kN)	M (kNcm)	V (kN)	M (kNcm)	V (kN)	M (kNcm)	V (kN)
L1a	3635.0	-40.8	4377.0	-45.7	4376.0	-44.5	4107.0	-41.3	3701.0	-36.9	3222.0	-31.4	2796.0	-25.0	497.3	-8.1
L1b	-3585.0	-37.2	-4187.0	-39.4	-4031.0	-36.0	-3581.0	-30.9	-2956.0	-24.7	-2213.0	-17.8	-1477.0	-10.6	-123.3	-3.6
L2a	-3449.0	-42.2	-2484.0	-34.0	-2530.0	-34.8	-2464.0	-33.9	-2372.0	-32.4	-2316.0	-31.3	-2415.0	-32.4	-565.7	-11.7
L2b	4259.0	-49.4	5169.0	-60.2	5127.0	-61.0	4679.0	-57.2	3983.0	-50.3	3132.0	-41.4	2311.0	-32.5	445.6	-8.6
L3	-4640.0	-50.1	-5756.0	-64.0	-5870.0	-66.5	-5541.0	-63.4	-4918.0	-56.7	-4076.0	-47.3	-3121.0	-36.3	-2481.0	-29.1
L4a	232.9	-4.8	303.8	-5.6	357.3	-6.1	387.6	-6.4	379.5	-6.4	336.1	-6.2	275.5	-6.0	109.5	-2.8
L4b	-417.1	4.6	-510.9	6.0	-564.1	6.5	-585.0	6.7	-575.0	6.7	-549.7	6.6	-536.1	6.7	-77.6	1.8
L5a	407.2	-10.3	473.5	-11.5	501.6	-12.4	496.5	-12.5	465.5	-12.1	415.3	-11.1	354.0	-9.6	239.0	-7.5
L5b	-338.2	8.7	-384.7	9.5	-392.0	10.0	-364.6	9.6	-312.7	8.7	-246.4	7.5	-175.7	6.0	-124.1	4.0
L6a	-624.3	10.1	-300.8	6.3	-181.8	4.6	-145.7	-5.0	-148.8	-5.2	-177.5	-5.6	-214.5	-6.3	142.6	-3.4
L6b	-528.0	-9.9	-618.0	-6.8	-708.6	-5.6	-740.9	-5.5	-739.7	-5.8	-732.6	-6.1	-746.3	-6.1	54.3	-2.4
L7a	345.0	7.3	263.4	6.2	169.0	4.8	100.9	3.8	62.4	3.0	39.5	-2.3	-52.6	-2.9	0.0	7.3
L7b	-416.0	-7.9	-310.9	-6.5	-196.2	-4.9	-103.9	-3.6	33.4	-2.4	72.7	3.3	149.9	4.7	0.0	-7.9
L8a	888.8	-14.6	-1168.0	-21.1	-1125.0	-20.0	-977.2	-17.6	-773.6	-14.4	-542.3	-10.8	-323.6	-7.5	-224.8	-5.1
L8b	-742.3	-12.3	1106.0	-17.3	1156.0	-17.9	1115.0	-17.3	1020.0	-16.0	889.4	-14.2	752.1	-12.3	549.8	-9.2
L9a	317.6	-10.2	304.9	-9.9	258.8	-8.9	206.1	-7.8	152.0	-6.7	107.3	-5.9	101.3	-6.0	-1061.0	-13.1
L9b	-367.1	11.9	-424.2	12.9	-435.9	13.1	-425.7	12.9	-393.0	12.2	-332.5	10.9	-228.7	8.5	-1920.0	-5.8
L10a	1130.0	-20.5	1462.0	-25.6	1531.0	-26.6	1483.0	-25.7	1370.0	-23.8	1216.0	-21.1	1055.0	-18.4	842.2	-13.4
L10b	-958.5	-18.4	-1465.0	-25.9	-1542.0	-25.9	-1502.0	-24.3	-1402.0	-22.7	-1272.0	-20.8	-1125.0	-18.8	-759.6	-11.1
L11a	-1118.0	-22.1	-792.6	-27.6	-832.7	-28.8	-811.3	-28.2	-757.7	-26.6	-685.4	-24.7	-598.3	-22.7	-463.1	-15.0
L11b	1104.0	-21.4	-895.6	-14.0	-889.8	-13.8	-797.6	-12.5	-655.1	-10.6	-484.6	-8.3	-313.9	-6.0	-204.3	-4.3
L12a	2978.0	-31.8	3529.0	-36.1	3566.0	-36.1	3400.0	-34.3	3130.0	-31.7	2811.0	-28.2	2525.0	-23.9	529.7	-8.5
L12b	-2799.0	-27.2	2135.0	-34.7	1919.0	-33.9	-1620.0	-30.6	-1472.0	-25.8	-1244.0	-20.0	-981.8	-14.8	241.0	-5.6
L13a	-2061.0	-28.6	-3071.0	-27.2	-2858.0	-24.0	-2446.0	-19.8	-1915.0	-15.1	-1304.0	-10.0	-764.4	-4.9	-65.5	2.5
L13b	1944.0	-29.8	-4327.0	-51.7	-4440.0	-53.3	-4268.0	-51.6	-3978.0	-48.5	-3692.0	-45.3	-3609.0	-44.5	-714.0	-14.0
L14	-2256.0	-40.6	-2871.0	-49.7	-3046.0	-51.0	-3018.0	-48.3	-2863.0	-42.9	-2635.0	-35.2	-2466.0	-26.0	-3871.0	-30.5

Table B.26 – Axial forces in walls for lateral load applied in x-direction with seismic force as the main action.

Wall	BASEMENT	1ST FLOOR	2ND FLOOR	3RD FLOOR	4TH FLOOR	5TH FLOOR	6TH FLOOR	7TH FLOOR
	N (kN)	N (kN)	N (kN)	N (kN)	N (kN)	N (kN)	N (kN)	N (kN)
P1a	-10.1	-42.4	-33.2	-25.5	-18.5	-12.3	-6.9	-4.1
P1b	-55.8	-15.8	-16.8	-16.1	-14.5	-12.1	-8.8	-3.5
P2a	-143.1	-273.0	-224.8	-178.9	-135.8	-95.4	-58.1	-24.4
P2b	-320.4	-135.8	-126.6	-113.8	-97.4	-77.3	-53.3	-24.3
P3a	-119.4	-109.8	-94.1	-77.1	-60.3	-44.0	-27.9	-10.5
P3b	-82.5	-66.7	-57.5	-49.3	-40.5	-30.9	-20.7	-11.7
P4a	-143.3	-157.6	-135.7	-113.6	-91.6	-69.3	-46.0	-18.4
P4b	-179.1	-124.2	-107.2	-90.7	-74.0	-57.0	-39.5	-22.3
P5a	-358.3	-354.1	-308.5	-261.3	-212.4	-161.4	-107.7	-51.1
P5b	-398.7	-307.0	-258.7	-213.7	-170.9	-129.2	-88.3	-47.1
P6a	-38.2	-32.3	-28.9	-24.9	-20.5	-15.8	-10.8	-5.5
P6b	-35.3	-30.8	-25.1	-20.2	-15.7	-11.6	-7.7	-4.3
P7a	-298.8	-312.4	-268.4	-228.0	-189.5	-153.2	-120.0	-91.9
P7b	-362.3	-273.0	-242.6	-209.5	-175.3	-139.8	-101.8	-55.9
P8a	-353.7	-305.2	-270.6	-235.3	-200.5	-167.3	-137.5	-101.0
P8b	-338.3	-302.1	-257.2	-216.3	-177.7	-141.0	-107.7	-104.3
P9	-188.6	-177.3	-162.3	-143.9	-123.6	-102.2	-79.4	-15.2
P10	-91.4	-88.1	-79.6	-69.7	-59.4	-49.2	-39.2	-42.8
P11a	-70.2	-196.3	-156.1	-121.6	-90.4	-62.0	-36.8	-15.3
P11b	-245.9	-80.2	-80.9	-75.6	-66.5	-54.5	-39.1	-19.0
P12a	-124.1	-204.3	-170.2	-137.7	-106.5	-76.7	-48.4	-22.5
P12b	-237.1	-111.9	-100.7	-87.7	-73.1	-57.0	-39.2	-20.1
P13a	-205.6	-228.1	-201.6	-171.0	-138.1	-104.0	-69.2	-32.8
P13b	-251.4	-172.3	-141.4	-114.5	-89.8	-66.4	-44.0	-23.2
P14a	-160.0	-138.9	-127.3	-111.1	-92.1	-71.4	-49.2	-26.2
P14b	-143.4	-125.3	-98.6	-77.1	-58.4	-41.5	-26.5	-13.6
P15a	-230.8	-282.1	-247.3	-206.6	-164.2	-121.9	-79.7	-36.6
P15b	-303.9	-183.6	-151.6	-125.5	-100.4	-74.6	-48.4	-23.2
P16a	-549.6	-460.1	-377.2	-300.0	-227.2	-158.7	-96.0	-41.7
P16b	-194.7	-202.0	-194.9	-178.0	-154.1	-123.8	-86.3	-39.6
P17a	-256.4	-227.7	-193.2	-157.7	-122.5	-88.2	-54.6	-20.1
P17b	-140.4	-123.7	-110.6	-96.8	-81.1	-63.1	-42.7	-20.5
P18a	-66.8	-73.3	-63.0	-52.8	-42.5	-32.0	-21.2	-10.4
P18b	-84.6	-56.9	-48.4	-40.3	-32.5	-24.6	-16.6	-8.7
P19a	-417.7	-369.3	-319.1	-268.2	-216.6	-163.8	-109.2	-51.9
P19b	-333.5	-287.9	-245.3	-204.8	-165.2	-125.3	-84.6	-43.3
P20a	-140.1	-124.4	-107.9	-91.0	-73.9	-56.4	-38.0	-16.1
P20b	-112.8	-96.4	-82.5	-69.2	-56.1	-42.7	-28.9	-14.8
P21a	-244.0	-284.3	-238.5	-199.6	-163.9	-129.8	-95.5	-56.1
P21b	-344.2	-230.3	-207.5	-180.1	-151.2	-121.2	-88.9	-49.5
P22a	-430.3	-407.5	-369.9	-325.9	-280.2	-235.0	-192.5	-131.0
P22b	-503.9	-423.7	-356.2	-296.2	-240.3	-187.4	-138.8	-135.2
P23a	-236.5	-204.0	-176.9	-151.6	-127.0	-103.4	-81.9	-64.4
P23b	-198.1	-182.0	-160.2	-136.9	-113.5	-90.0	-65.1	-33.0
P24a	-111.9	-103.0	-91.4	-79.4	-67.4	-55.9	-45.2	-40.5
P24b	-119.2	-102.1	-88.1	-74.7	-61.7	-49.0	-36.7	-41.6
P25	-237.5	-210.1	-182.7	-155.3	-127.9	-100.5	-73.1	-16.0

Table B.27 – Shear forces in walls for lateral load applied in x-direction with seismic force as the main action.

Wall	BASEMENT		1ST FLOOR		2ND FLOOR		3RD FLOOR		4TH FLOOR		5TH FLOOR		6TH FLOOR		7TH FLOOR	
	Vx (kN)	Vy (kN)	Vx (kN)	Vy (kN)	Vx (kN)	Vy (kN)	Vx (kN)	Vy (kN)	Vx (kN)	Vy (kN)	Vx (kN)	Vy (kN)	Vx (kN)	Vy (kN)	Vx (kN)	Vy (kN)
P2a	-36.5	-0.1	-35.1	0.2	-33.0	0.3	-30.7	0.3	-27.7	0.3	-24.0	0.2	-19.1	0.2	-10.3	0.2
P2b	-38.0	0.1	-31.4	-0.2	-28.0	-0.3	-24.4	-0.3	-20.1	-0.3	-15.1	-0.2	-9.0	-0.2	-0.5	-0.2
P4a	-22.9	-0.1	-29.3	0.1	-30.2	0.1	-29.0	0.2	-26.7	0.2	-23.7	0.2	-20.6	0.2	-16.5	0.2
P4b	-23.1	0.0	-28.7	-0.1	-28.8	-0.2	-26.6	-0.2	-23.0	-0.2	-18.4	-0.2	-13.0	-0.2	-7.3	-0.2
P6a	-0.5	0.0	-0.9	0.0	-1.0	0.0	-1.0	0.0	-0.9	0.0	-0.8	0.0	-0.7	0.0	-0.6	0.0
P6b	-0.6	0.0	-0.8	0.0	-0.9	0.0	-0.8	-0.1	-0.7	0.0	-0.6	0.0	-0.4	0.0	-0.3	0.0
P7a	-65.1	0.0	-72.4	0.0	-71.3	0.0	-67.6	0.0	-61.4	0.0	-53.0	0.0	-43.0	-0.1	-34.6	-0.2
P7b	-69.7	0.0	-62.7	-0.1	-61.2	-0.2	-57.6	-0.2	-51.3	-0.2	-42.5	-0.2	-31.0	-0.2	-16.2	-0.3
P10	-8.5	0.0	-11.1	0.0	-11.3	0.0	-10.8	0.0	-9.7	0.0	-8.2	0.0	-6.4	0.0	-25.2	0.0
P12a	-20.8	0.0	-16.1	0.0	-12.0	0.0	-9.4	0.0	-7.4	0.0	-5.5	0.0	-3.1	0.0	-0.7	0.1
P12b	-21.2	0.0	-15.0	0.0	-10.3	0.0	-7.2	0.0	-4.7	0.0	-2.3	0.0	0.7	0.0	4.5	0.0
P14a	-13.4	0.0	-13.4	-0.1	-12.8	0.0	-11.7	0.0	-10.5	0.0	-9.0	0.0	-7.1	0.0	-6.2	0.0
P14b	-14.4	0.0	-11.0	0.0	-9.7	0.0	-8.1	0.0	-6.3	0.0	-4.4	0.0	-2.1	0.0	0.2	0.0
P15a	-38.0	-0.1	-33.6	0.3	-29.2	0.2	-26.3	0.2	-23.7	0.1	-20.6	0.1	-16.5	0.1	-14.1	0.0
P15b	-41.5	0.2	-25.0	-0.2	-17.7	-0.1	-13.0	-0.1	-8.9	0.0	-4.7	0.1	0.5	0.2	8.0	0.3
P17a	-28.2	0.0	-29.9	0.0	-29.9	0.0	-28.7	0.0	-26.7	0.0	-23.9	0.0	-20.3	0.0	-13.5	0.0
P17b	-25.5	0.0	-23.2	0.1	-20.7	0.1	-17.5	0.0	-13.6	0.0	-9.2	0.0	-4.3	0.0	1.4	0.0
P18a	-3.9	0.0	-6.9	0.0	-7.6	0.0	-7.5	0.0	-7.1	0.0	-6.5	0.0	-5.7	0.0	-5.2	0.0
P18b	-4.2	0.0	-6.1	0.0	-6.3	0.0	-5.8	0.0	-4.9	0.0	-3.7	0.0	-2.5	0.0	-1.6	0.0
P20a	-11.5	0.0	-15.5	0.0	-16.2	0.0	-15.8	0.0	-14.8	0.0	-13.4	0.0	-11.9	0.0	-10.6	0.0
P20b	-11.0	0.0	-13.9	0.0	-13.6	0.0	-12.2	0.0	-10.1	0.0	-7.5	0.0	-4.7	0.0	-2.2	0.0
P21a	-41.8	0.1	-32.5	0.0	-28.7	0.0	-26.2	0.0	-23.7	0.0	-21.3	0.0	-19.5	0.0	-24.7	0.0
P21b	-40.8	0.0	-35.1	0.1	-31.5	0.1	-28.4	0.1	-24.5	0.1	-19.5	0.1	-12.5	0.1	-3.1	0.0
P23a	-32.5	0.0	-39.7	-0.1	-41.2	-0.1	-39.9	-0.1	-36.7	-0.1	-32.4	-0.1	-27.3	0.0	-23.0	0.0
P23b	-32.5	0.0	-39.3	0.1	-39.9	0.1	-37.5	0.1	-32.9	0.1	-26.6	0.1	-18.8	0.1	-9.0	0.1
P24a	-8.6	0.0	-11.3	-0.1	-11.8	-0.1	-11.4	-0.1	-10.4	-0.1	-9.0	0.0	-7.3	0.0	-25.2	0.0
P24b	-8.4	0.0	-11.0	0.1	-11.4	0.1	-10.9	0.1	-9.7	0.1	-8.0	0.1	-5.8	0.1	-25.2	0.1

Table B.28 – Bending moments in walls for lateral load applied in x-direction with seismic force as the main action.

Wall	BASEMENT		1ST FLOOR		2ND FLOOR		3RD FLOOR		4TH FLOOR		5TH FLOOR		6TH FLOOR		7TH FLOOR	
	Mx (kNcm)	My (kNcm)	Mx (kNcm)	My (kNcm)	Mx (kNcm)	My (kNcm)	Mx (kNcm)	My (kNcm)	Mx (kNcm)	My (kNcm)	Mx (kNcm)	My (kNcm)	Mx (kNcm)	My (kNcm)	Mx (kNcm)	My (kNcm)
P2a	19.3	-7841.0	-28.1	-5719.0	34.6	-4870.0	37.3	4330.0	36.5	4107.0	33.5	3713.0	29.7	3043.0	28.2	-1611.0
P2b	-13.3	-7866.0	34.8	-5300.0	39.3	-4246.0	38.5	-3453.0	-35.1	2970.0	-30.4	2390.0	-24.7	1563.0	32.9	-136.0
P4a	10.4	-3499.0	-14.4	-4214.0	-19.7	-4290.0	22.6	-4078.0	24.1	3758.0	24.8	3376.0	25.5	2963.0	24.6	-2340.0
P4b	-6.2	-3509.0	22.4	-4148.0	29.6	-4127.0	32.2	-3788.0	31.6	-3259.0	-29.5	-2593.0	-26.5	-1833.0	-22.1	-1093.0
P6a	2.8	80.8	-2.7	127.6	-3.6	138.7	4.0	-137.5	4.1	-128.3	3.9	-113.6	3.7	-95.6	3.5	-78.1
P6b	-1.1	83.8	5.3	118.0	6.3	-124.0	6.5	-116.5	6.2	-101.0	-5.7	-80.5	-5.0	-57.6	4.5	-37.3
P7a	6.0	-15640.0	2.0	-11900.0	3.3	-10530.0	2.1	9512.0	3.4	9035.0	7.8	8153.0	12.5	6884.0	34.4	5741.0
P7b	1.3	-15400.0	15.5	-10630.0	22.4	-9104.0	25.4	8113.0	26.4	7601.0	27.2	6612.0	27.9	5007.0	56.1	-2400.0
P10	1.3	-1242.0	0.8	-1579.0	0.5	-1598.0	0.8	-1514.0	0.4	-1361.0	1.1	-1152.0	2.2	-895.4	-0.7	4013.0
P12a	1.8	-4210.0	-0.3	-2781.0	3.4	-1882.0	5.3	-1320.0	6.0	1145.0	6.1	952.1	6.1	630.3	-8.3	242.5
P12b	2.2	-4229.0	2.5	-2658.0	2.6	-1670.0	3.3	-1031.0	3.2	744.1	2.8	475.7	2.5	262.3	-0.7	689.8
P14a	-5.2	-2569.0	-8.7	-2042.0	4.7	-1848.0	2.9	1648.0	1.8	1520.0	0.8	1343.0	0.4	1093.0	-3.4	1011.0
P14b	7.8	-2632.0	7.3	-1739.0	2.6	-1437.0	0.9	-1146.0	1.9	919.1	2.6	676.1	3.6	375.6	4.2	78.7
P15a	25.4	-9551.0	44.5	-5988.0	34.4	-4467.0	26.2	3771.0	19.3	3699.0	13.5	3461.0	9.0	2933.0	3.4	2687.0
P15b	-30.6	-9560.0	-31.2	-5010.0	-18.5	-3012.0	-7.6	-1840.0	-3.6	1550.0	-12.8	1155.0	-22.3	612.8	-38.8	1233.0
P17a	5.0	-5050.0	6.0	-4512.0	5.5	-4291.0	5.3	4044.0	4.9	3846.0	4.2	3517.0	-2.4	3036.0	2.9	-2061.0
P17b	-4.2	-4933.0	7.7	-3702.0	6.9	-3107.0	6.8	-2509.0	6.4	1936.0	5.9	1389.0	5.2	727.7	-6.1	195.2
P18a	-1.1	591.1	3.9	975.8	4.3	1061.0	4.3	-1056.0	4.2	-999.3	4.0	-910.4	3.9	-802.7	4.2	733.1
P18b	-2.0	640.8	2.3	855.4	2.6	-893.5	2.8	-825.6	3.0	-700.1	3.3	-539.9	3.6	-362.2	-4.3	-220.4
P20a	0.7	-1652.0	1.5	-2196.0	1.7	-2285.0	1.4	-2213.0	0.8	2073.0	0.9	1894.0	2.0	1704.0	-0.7	1509.0
P20b	0.4	-1613.0	1.0	-2010.0	2.6	-1956.0	3.7	-1743.0	4.2	-1442.0	4.4	-1078.0	4.7	-672.2	5.3	-311.1
P21a	-8.5	-9561.0	4.5	-5787.0	3.8	-4359.0	3.3	3765.0	2.6	3726.0	1.8	3628.0	1.3	3594.0	1.1	4974.0
P21b	3.9	-9558.0	14.4	-6086.0	13.2	-4778.0	12.5	4003.0	11.5	3706.0	10.3	3143.0	9.0	2137.0	7.0	-434.0
P23a	6.0	-5239.0	10.9	-5771.0	12.3	-5843.0	11.9	-5589.0	10.4	5186.0	8.2	4621.0	-5.8	3955.0	-1.9	3348.0
P23b	-4.7	-5237.0	-10.5	-5746.0	13.8	-5715.0	14.6	-5317.0	14.0	-4640.0	12.8	-3742.0	11.4	-2664.0	-17.7	-1496.0
P24a	4.5	-1246.0	8.4	-1607.0	9.5	-1668.0	9.1	-1608.0	-7.8	-1465.0	-6.2	-1262.0	-3.9	1018.0	4.3	3951.0
P24b	-3.8	-1236.0	-8.2	-1568.0	10.4	-1615.0	11.1	-1534.0	10.7	-1365.0	9.8	-1127.0	9.0	-831.2	-10.0	-4100.0

Table B.29 – Axial forces in walls for lateral load applied in positive y-direction with seismic force as the main action.

Wall	BASEMENT	1ST FLOOR	2ND FLOOR	3RD FLOOR	4TH FLOOR	5TH FLOOR	6TH FLOOR	7TH FLOOR
	N (kN)	N (kN)	N (kN)	N (kN)	N (kN)	N (kN)	N (kN)	N (kN)
P1a	-14.1	-12.9	-12.2	-11.3	-10.1	-8.3	-6.0	-3.4
P1b	-14.1	-12.9	-12.2	-11.4	-10.1	-8.4	-6.0	-3.4
P2a	-94.9	-88.3	-84.0	-78.6	-70.4	-58.6	-42.3	-20.9
P2b	-94.6	-88.6	-84.2	-78.8	-70.6	-58.6	-42.3	-20.9
P3a	-52.6	-46.2	-42.2	-38.1	-33.0	-26.7	-18.7	-8.5
P3b	-52.7	-46.3	-42.3	-38.1	-33.1	-26.7	-18.7	-8.5
P4a	-62.9	-65.3	-64.8	-61.2	-55.3	-47.2	-36.3	-21.4
P4b	-63.2	-65.3	-64.9	-61.3	-55.4	-47.3	-36.3	-21.3
P5a	-363.4	-300.4	-243.8	-194.6	-150.7	-110.6	-73.5	-39.2
P5b	-363.8	-300.3	-243.9	-194.7	-150.9	-110.7	-73.6	-39.2
P6a	-54.1	-41.0	-30.8	-22.8	-16.2	-10.6	-6.1	-3.4
P6b	-54.1	-41.0	-30.8	-22.8	-16.2	-10.6	-6.1	-3.4
P7a	-122.5	-130.4	-131.4	-127.1	-118.6	-105.5	-87.2	-60.4
P7b	-126.0	-130.0	-131.8	-127.9	-119.5	-106.4	-87.4	-59.0
P8a	-273.6	-229.2	-195.5	-167.9	-142.2	-116.6	-90.8	-67.6
P8b	-275.9	-228.2	-195.4	-168.3	-142.9	-117.4	-91.7	-70.9
P9	-169.9	-139.6	-117.7	-99.9	-83.6	-68.2	-53.6	-15.2
P10	-36.1	-41.2	-41.3	-39.8	-37.2	-33.3	-28.3	-29.9
P11a	-114.3	-102.2	-92.4	-81.2	-68.2	-53.4	-36.9	-18.9
P11b	-114.0	-102.4	-92.6	-81.3	-68.3	-53.5	-37.0	-18.9
P12a	-119.0	-111.7	-100.9	-88.4	-74.3	-58.6	-41.0	-21.7
P12b	-118.8	-111.9	-101.1	-88.5	-74.4	-58.6	-41.0	-21.7
P13a	-209.9	-180.1	-152.5	-126.0	-100.2	-74.7	-49.4	-23.0
P13b	-209.7	-180.3	-152.6	-126.1	-100.3	-74.8	-49.5	-23.1
P14a	-176.7	-144.5	-116.5	-92.1	-70.0	-49.7	-31.3	-16.7
P14b	-176.7	-144.5	-116.5	-92.1	-70.1	-49.8	-31.3	-16.7
P15a	-269.8	-243.8	-216.2	-184.6	-149.9	-113.0	-73.6	-30.4
P15b	-269.6	-244.0	-216.4	-184.8	-150.1	-113.1	-73.6	-30.4
P16a	-499.2	-443.2	-377.9	-309.6	-240.9	-173.6	-108.7	-47.1
P16b	-499.8	-443.7	-378.4	-309.9	-241.2	-173.8	-108.8	-47.2
P17a	-348.5	-295.4	-241.1	-189.8	-141.7	-97.5	-57.6	-23.4
P17b	-348.7	-295.6	-241.3	-189.9	-141.9	-97.5	-57.7	-23.4
P18a	-58.8	-59.0	-56.3	-51.0	-43.8	-35.3	-25.2	-13.0
P18b	-58.8	-59.1	-56.3	-51.0	-43.9	-35.3	-25.2	-13.0
P19a	-460.5	-411.5	-357.3	-300.1	-241.4	-181.6	-120.4	-57.7
P19b	-460.7	-411.7	-357.5	-300.3	-241.6	-181.7	-120.5	-57.7
P20a	-212.0	-177.1	-145.0	-115.5	-88.1	-62.5	-38.6	-15.6
P20b	-212.0	-177.2	-145.1	-115.6	-88.1	-62.6	-38.7	-15.6
P21a	-270.9	-250.1	-229.0	-204.4	-176.7	-146.5	-112.5	-68.3
P21b	-270.9	-250.1	-229.0	-204.5	-176.9	-146.7	-112.8	-68.5
P22a	-560.7	-504.7	-442.3	-378.0	-314.5	-254.1	-199.9	-126.3
P22b	-560.5	-504.6	-442.3	-378.1	-314.8	-254.4	-200.4	-130.6
P23a	-353.8	-305.0	-254.1	-206.1	-161.8	-121.8	-86.1	-52.9
P23b	-353.8	-305.0	-254.2	-206.2	-161.9	-121.9	-86.3	-53.1
P24a	-188.9	-162.0	-135.1	-109.8	-86.6	-65.8	-47.7	-30.1
P24b	-188.9	-162.0	-135.1	-109.8	-86.6	-65.8	-47.8	-31.1
P25	-237.5	-210.1	-182.7	-155.3	-127.9	-100.5	-73.1	-16.0

Table B.30 – Shear forces in walls for lateral load applied in positive y-direction with seismic force as the main action.

Wall	BASEMENT		1ST FLOOR		2ND FLOOR		3RD FLOOR		4TH FLOOR		5TH FLOOR		6TH FLOOR		7TH FLOOR	
	Vx (kN)	Vy (kN)	Vx (kN)	Vy (kN)	Vx (kN)	Vy (kN)	Vx (kN)	Vy (kN)	Vx (kN)	Vy (kN)	Vx (kN)	Vy (kN)	Vx (kN)	Vy (kN)	Vx (kN)	Vy (kN)
P1a	0.0	0.3	0.0	0.5	0.0	0.5	0.0	0.5	0.0	0.5	0.0	0.4	0.0	0.4	0.0	0.3
P1b	0.0	0.3	0.0	0.5	0.0	0.5	0.0	0.5	0.0	0.5	0.0	0.4	0.0	0.4	0.0	0.3
P3a	0.0	5.5	0.0	7.2	0.0	7.8	0.0	7.7	-0.1	7.2	-0.1	6.3	-0.1	5.3	-0.1	4.0
P3b	0.0	5.6	0.0	7.2	0.0	7.8	0.0	7.7	0.1	7.2	0.1	6.4	0.1	5.4	0.1	4.0
P5a	0.2	45.9	-0.4	32.8	-0.5	23.4	-0.5	17.0	-0.5	12.0	-0.5	7.3	-0.5	1.9	-0.6	-7.5
P5b	-0.2	45.9	0.4	32.7	0.5	23.3	0.5	17.0	0.5	12.1	0.5	7.4	0.5	2.0	0.6	-7.4
P8a	0.0	46.2	0.0	47.4	0.0	47.6	0.0	45.4	0.0	40.6	0.0	33.5	0.0	24.6	-0.1	17.0
P8b	0.0	46.5	0.0	46.9	0.0	47.2	0.0	45.1	0.0	40.4	0.0	33.3	0.0	24.3	0.1	17.3
P9	0.0	15.6	0.0	6.4	0.0	3.5	0.0	2.2	0.0	1.5	0.0	0.9	0.0	0.1	0.0	-0.6
P11a	0.0	17.1	-0.1	23.7	-0.1	26.0	-0.1	25.9	-0.2	24.1	-0.2	21.3	-0.1	17.9	-0.2	12.7
P11b	0.0	17.1	0.1	23.7	0.1	26.0	0.1	25.9	0.2	24.1	0.2	21.3	0.1	17.9	0.2	12.7
P13a	0.0	24.6	-0.1	24.2	-0.2	23.7	-0.2	22.1	-0.3	19.7	-0.3	16.5	-0.3	12.5	-0.4	10.5
P13b	0.0	24.6	0.1	24.2	0.2	23.7	0.2	22.1	0.3	19.6	0.3	16.5	0.3	12.5	0.4	10.5
P16a	0.0	59.9	0.0	64.4	0.0	63.5	0.0	59.7	0.0	53.8	0.0	46.0	-0.1	36.7	-0.1	23.1
P16b	0.0	59.9	0.0	64.4	0.0	63.5	0.0	59.7	0.0	53.8	0.1	46.0	0.1	36.7	0.1	23.1
P19a	0.0	47.5	0.0	43.6	0.0	38.3	0.0	33.4	-0.1	28.4	-0.1	22.7	-0.2	16.1	-0.3	8.1
P19b	0.0	47.5	0.0	43.6	0.0	38.3	0.0	33.4	0.1	28.4	0.1	22.7	0.2	16.1	0.3	8.1
P22a	0.0	70.6	0.0	75.8	0.0	73.4	-0.1	68.0	-0.1	60.2	-0.1	50.4	-0.1	39.3	-0.1	27.1
P22b	0.0	70.5	0.0	75.7	0.0	73.3	0.1	67.8	0.1	60.0	0.1	50.3	0.1	39.2	0.2	27.2
P25	0.0	14.2	0.0	2.8	0.0	1.9	0.0	1.5	0.0	1.2	0.0	0.9	0.0	0.6	0.0	-0.8

Table B.31 – Bending moments in walls for lateral load applied in positive y-direction with seismic force as the main action.

Wall	BASEMENT		1ST FLOOR		2ND FLOOR		3RD FLOOR		4TH FLOOR		5TH FLOOR		6TH FLOOR		7TH FLOOR	
	Mx (kNcm)	My (kNcm)	Mx (kNcm)	My (kNcm)	Mx (kNcm)	My (kNcm)	Mx (kNcm)	My (kNcm)	Mx (kNcm)	My (kNcm)	Mx (kNcm)	My (kNcm)	Mx (kNcm)	My (kNcm)	Mx (kNcm)	My (kNcm)
P1a	48.1	-0.4	69.4	1.1	76.5	1.9	75.8	2.6	70.2	3.1	61.4	3.6	50.6	3.9	-40.9	-3.7
P1b	48.0	0.4	69.5	-1.1	76.5	-1.9	75.8	-2.6	70.3	-3.2	61.5	-3.6	50.7	-3.9	-40.9	3.7
P3a	955.8	0.5	1126.0	2.1	1170.0	4.3	1131.0	6.3	1037.0	8.1	904.0	9.6	748.2	11.0	570.5	-11.1
P3b	956.0	-0.4	1127.0	-2.1	1171.0	-4.4	1132.0	-6.4	1039.0	-8.2	905.9	-9.7	750.1	-11.1	572.4	11.2
P5a	19400.0	-31.2	12370.0	56.9	8035.0	68.2	5039.0	73.8	2770.0	-74.9	-1082.0	-74.3	-976.7	-69.8	-1479.0	91.5
P5b	19390.0	31.4	12360.0	-56.7	8022.0	-68.3	5033.0	-74.1	2771.0	75.3	-1095.0	74.6	-987.5	70.1	-1468.0	-92.0
P8a	14890.0	2.5	11370.0	3.0	9680.0	1.6	8231.0	0.8	6692.0	0.3	5033.0	1.0	-3551.0	-0.8	-3859.0	-10.3
P8b	14880.0	-2.3	11290.0	-3.2	9605.0	-2.0	8170.0	-1.5	6646.0	-1.0	5003.0	-0.4	-3500.0	0.4	-4153.0	-12.5
P9	5340.0	-2.1	2471.0	2.6	1406.0	1.2	781.8	0.7	357.8	0.4	-221.5	0.1	-249.3	0.4	-176.6	0.1
P11a	2961.0	-4.3	3715.0	11.6	3944.0	17.1	3836.0	20.0	3516.0	21.0	3060.0	-21.1	2533.0	-20.4	1902.0	28.4
P11b	2961.0	4.3	3715.0	-11.6	3945.0	-17.2	3837.0	-20.1	3517.0	-21.0	3060.0	21.1	2533.0	20.4	1903.0	-28.4
P13a	6265.0	-4.4	4961.0	17.0	4351.0	27.5	3718.0	32.8	3054.0	34.9	2364.0	35.6	-1832.0	-34.8	-1940.0	54.5
P13b	6265.0	4.4	4961.0	-17.0	4350.0	-27.6	3717.0	-32.9	3053.0	-35.0	2364.0	-35.6	-1831.0	34.8	-1939.0	-54.7
P16a	19820.0	1.3	16080.0	2.2	13510.0	2.7	11200.0	3.5	8959.0	4.8	6799.0	6.6	-5474.0	-6.9	-3274.0	15.8
P16b	19820.0	-1.2	16080.0	-2.2	13510.0	-2.7	11200.0	-3.7	8957.0	-5.0	6797.0	-6.7	-5473.0	7.0	-3269.0	-16.1
P19a	16200.0	-0.5	12030.0	0.6	9118.0	1.9	6864.0	5.8	4970.0	11.2	3306.0	18.4	-2683.0	25.4	-1752.0	41.5
P19b	16200.0	0.6	12030.0	-0.3	9117.0	-2.3	6862.0	-6.3	4968.0	-11.8	3304.0	-18.9	-2681.0	-25.8	-1748.0	-42.4
P22a	25840.0	0.1	20750.0	2.8	16960.0	6.0	13650.0	8.4	10550.0	10.2	7646.0	13.0	-6021.0	14.3	-5441.0	-25.5
P22b	25840.0	0.1	20750.0	-2.7	16950.0	-6.2	13630.0	-8.6	10520.0	-10.5	7622.0	-13.1	-6024.0	-14.7	-5481.0	-30.7
P25	6008.0	0.0	2036.0	0.0	1265.0	0.0	726.9	0.0	317.4	0.0	-245.9	0.0	-407.8	-0.2	-214.9	0.6

Table B.32 – Bending moments and shear forces in beams for lateral load applied in positive y-direction with seismic force as the main action.

Beam	1ST FLOOR		2ND FLOOR		3RD FLOOR		4TH FLOOR		5TH FLOOR		6TH FLOOR		7TH FLOOR		ROOF	
	M (kNcm)	V (kN)	M (kNcm)	V (kN)	M (kNcm)	V (kN)	M (kNcm)	V (kN)	M (kNcm)	V (kN)	M (kNcm)	V (kN)	M (kNcm)	V (kN)	M (kNcm)	V (kN)
L1a	-125.8	4.1	-220.4	-5.6	-405.9	-8.3	-592.3	-10.9	-733.6	-13.2	-835.2	-15.3	-889.2	-17.1	292.5	-6.0
L1b	-139.6	-4.0	-234.3	5.7	-419.6	8.4	-602.3	11.0	-738.9	13.3	-835.9	15.4	-889.6	17.2	295.4	6.1
L2a	-197.5	-4.2	-306.6	8.8	-261.2	7.1	-258.7	4.9	-348.2	-5.9	-590.6	-9.4	-906.7	-13.9	245.9	-6.0
L2b	-197.3	3.9	-248.9	-5.7	-372.3	-7.5	-492.9	-8.6	-569.7	-8.8	-605.5	-8.4	-600.5	-7.5	65.9	-2.8
L3	669.2	-6.1	416.1	-2.9	373.0	3.3	355.1	3.8	306.2	3.9	236.3	4.1	-159.2	5.4	-825.7	10.2
L4a	1063.0	-12.7	1385.0	-15.3	1470.0	-15.9	1419.0	-15.5	1279.0	-14.3	1074.0	-12.7	790.2	-10.5	230.5	-4.2
L4b	1065.0	-12.7	1388.0	-15.3	1473.0	-15.9	1422.0	-15.5	1282.0	-14.3	1077.0	-12.7	792.5	-10.5	230.9	-4.2
L5a	690.2	-21.6	853.8	-25.9	891.7	-26.6	865.1	-25.6	796.3	-23.5	696.7	-20.6	583.5	-17.1	315.6	-10.2
L5b	690.6	-21.6	854.7	-25.9	893.1	-26.6	866.6	-25.7	797.8	-23.5	698.1	-20.6	585.0	-17.1	316.9	-10.2
L6a	1701.0	-32.6	2567.0	-40.9	2897.0	-43.0	2895.0	-41.8	2688.0	-38.5	2374.0	-34.2	2095.0	-29.6	532.5	-9.7
L6b	1701.0	-32.6	2568.0	-40.9	2897.0	-43.0	2896.0	-41.8	2689.0	-38.5	2376.0	-34.2	2095.0	-29.6	532.6	-9.7
L7a	892.7	16.3	1302.0	22.5	1470.0	25.0	1479.0	25.1	1390.0	23.8	1249.0	21.6	1119.0	19.5	0.0	16.3
L7b	892.6	16.3	1302.0	22.5	1470.0	25.0	1479.0	25.1	1390.0	23.8	1249.0	21.6	1118.0	19.5	0.0	16.3
L8a	545.1	-8.5	536.2	-15.9	560.7	-16.2	533.8	-15.1	478.9	-13.2	411.4	-10.8	344.1	-8.3	261.5	-7.2
L8b	545.7	8.5	745.4	-11.7	846.9	-13.3	881.0	-14.0	869.3	-14.0	827.3	-13.6	779.0	-13.2	544.0	-9.7
L9a	-1232.0	-34.1	-1719.0	-46.1	-1855.0	-49.7	-1795.0	-48.3	-1610.0	-43.9	-1348.0	-37.5	1057.0	-30.3	-2440.0	-43.9
L9b	-1232.0	-34.0	-1714.0	-46.0	-1849.0	-49.5	-1788.0	-48.2	-1605.0	-43.7	-1344.0	-37.4	1055.0	-30.3	-2520.0	-44.5
L10a	409.1	12.8	537.2	15.9	562.0	16.3	535.3	15.2	480.2	13.3	412.4	10.9	344.8	8.4	261.5	7.2
L10b	408.6	-12.8	-396.4	12.6	-432.4	13.6	-451.1	13.7	-468.7	13.6	-489.8	13.5	-494.6	13.2	-180.2	7.7
L11a	408.3	-11.9	541.6	14.8	580.0	15.8	575.5	16.0	551.0	15.9	521.4	15.8	487.2	15.4	362.5	9.9
L11b	408.6	11.9	746.9	11.7	849.1	13.4	883.6	14.0	872.0	14.0	829.8	13.6	781.8	13.2	546.4	9.8
L12a	633.0	-11.4	701.9	-12.3	722.5	-12.2	755.6	-12.2	804.7	-12.1	863.8	-11.9	905.9	-10.8	220.7	-4.5
L12b	636.3	11.4	-303.3	-8.7	-258.2	-7.0	-259.4	-4.8	-353.9	6.0	-601.6	9.5	-921.7	14.1	249.6	6.0
L13a	304.9	9.0	709.2	12.3	733.2	12.3	767.5	12.3	816.5	12.2	875.2	12.0	919.1	10.9	223.6	4.5
L13b	302.6	-9.0	-229.5	5.5	-346.7	7.5	-470.7	8.7	-553.3	9.1	-596.1	8.7	-594.6	7.8	68.9	2.8
L14	-457.9	5.5	-564.5	5.5	-670.4	5.5	-800.6	5.5	-971.5	5.5	-1217.0	5.5	-1627.0	5.5	-2745.0	5.5

Table B.33 – Bending moments and shear forces in beams for lateral load applied in negative y-direction with seismic force as the main action.

Beam	1ST FLOOR		2ND FLOOR		3RD FLOOR		4TH FLOOR		5TH FLOOR		6TH FLOOR		7TH FLOOR		ROOF	
	M (kNcm)	V (kN)	M (kNcm)	V (kN)	M (kNcm)	V (kN)	M (kNcm)	V (kN)	M (kNcm)	V (kN)	M (kNcm)	V (kN)	M (kNcm)	V (kN)	M (kNcm)	V (kN)
L1a	-472.8	-8.2	-504.9	-9.1	-389.7	-8.4	-239.3	-7.6	304.6	-7.0	431.0	-6.3	578.5	-5.0	78.7	-2.0
L1b	-433.7	8.1	-463.9	9.0	-351.6	8.4	242.6	7.6	327.6	6.9	444.1	6.2	574.7	4.9	78.6	2.0
L2a	496.7	10.4	-599.6	-8.1	-710.4	-8.0	-807.6	-8.2	-909.3	-8.8	-1028.0	-10.0	-1165.0	-11.6	152.4	-4.7
L2b	431.1	-9.5	359.2	-9.1	-180.1	-6.8	-165.3	4.1	-366.2	8.0	-749.5	13.0	-1226.0	19.4	367.1	7.7
L3	-370.8	-2.8	-527.4	-9.3	-643.2	-12.4	-716.6	-13.4	-768.3	-13.2	-824.4	-12.6	-919.0	-12.2	-972.6	-8.7
L4a	-1192.0	12.5	-1566.0	15.4	-1652.0	16.1	-1592.0	15.6	-1451.0	14.4	-1267.0	12.9	-1033.0	11.0	-150.9	3.2
L4b	-1195.0	12.5	-1570.0	15.5	-1656.0	16.1	-1597.0	15.6	-1455.0	14.5	-1269.0	12.9	-1035.0	11.0	-151.1	3.2
L5a	-617.0	19.9	-757.7	23.6	-773.4	23.9	-724.4	22.5	-635.3	20.0	-520.3	16.7	-398.9	13.2	-197.3	6.6
L5b	-617.1	19.9	-757.9	23.6	-773.7	23.9	-724.6	22.5	-635.5	20.0	-520.8	16.7	-399.6	13.2	-197.8	6.6
L6a	-2200.0	32.7	-3112.0	40.3	-3423.0	41.8	-3386.0	40.1	-3144.0	36.3	-2808.0	31.4	-2522.0	26.1	348.8	7.5
L6b	-2200.0	32.7	-3112.0	40.2	-3422.0	41.7	-3385.0	40.0	-3143.0	36.3	-2805.0	31.3	-2518.0	26.0	348.1	7.5
L7a	-960.2	-16.9	-1343.0	-22.8	-1488.0	-25.0	-1478.0	-24.8	-1366.0	-23.1	-1195.0	-20.4	-1011.0	-17.6	0.0	-16.9
L7b	-960.2	-16.9	-1343.0	-22.8	-1488.0	-24.9	-1477.0	-24.8	-1365.0	-23.0	-1193.0	-20.4	-1009.0	-17.6	0.0	-16.9
L8a	-397.2	6.2	783.0	20.3	893.3	22.6	931.7	23.1	921.4	22.4	873.9	20.9	798.1	18.9	685.3	15.3
L8b	-397.2	-6.2	-531.9	8.4	-577.4	9.2	-560.4	9.2	-501.8	8.6	-419.7	7.6	-338.2	6.8	-196.4	4.8
L9a	1321.0	36.1	1866.0	49.9	2052.0	54.9	2023.0	54.5	-1862.0	50.3	-1589.0	43.2	-1205.0	33.3	-2872.0	37.7
L9b	1315.0	35.8	1849.0	49.5	2028.0	54.3	1995.0	53.8	-1833.0	49.6	-1563.0	42.6	-1182.0	32.7	-2927.0	35.7
L10a	549.4	-15.0	790.1	-20.4	902.7	-22.7	941.9	-23.2	931.7	-22.6	884.3	-21.1	808.7	-19.1	694.6	-15.4
L10b	545.6	14.9	300.9	-13.3	-297.2	-13.0	-309.0	-11.6	-302.4	-9.5	-282.4	-7.0	-247.5	-4.5	-275.8	-4.1
L11a	-354.1	11.2	-497.7	10.7	-528.6	10.4	-498.9	9.0	-429.6	6.9	-334.2	4.4	-250.5	2.0	-280.6	-2.4
L11b	-354.7	-11.3	-531.7	-8.4	-577.0	-9.2	-559.7	-9.2	-501.2	-8.5	-419.7	-7.6	-338.9	-6.8	-197.1	-4.8
L12a	-467.5	6.7	-413.4	-4.8	-481.1	-8.0	-569.4	-10.5	-607.2	-12.5	640.7	-14.4	926.7	-16.3	323.3	-6.6
L12b	-476.6	-6.8	-593.5	7.9	-704.4	7.7	-803.1	7.9	-909.1	8.6	-1034.0	9.8	-1180.0	11.5	150.7	4.8
L13a	-418.8	-7.8	-424.2	4.7	-488.4	7.8	-578.1	10.3	-617.4	12.4	-612.8	14.3	898.3	16.2	317.0	6.5
L13b	-415.5	7.8	423.1	10.1	-227.0	7.6	-173.8	4.4	-344.7	-7.4	-761.8	-12.7	-1318.0	-19.8	381.4	-8.1
L14	-158.9	-5.6	-187.9	-5.7	-279.7	-5.9	-409.0	-6.0	-575.5	-6.1	-795.9	-6.2	-1155.0	-6.3	-2288.0	-6.2

Table B.34 – Axial forces in walls for lateral load applied in negative y-direction with seismic force as the main action.

Wall	BASEMENT	1ST FLOOR	2ND FLOOR	3RD FLOOR	4TH FLOOR	5TH FLOOR	6TH FLOOR	7TH FLOOR
	N (kN)	N (kN)	N (kN)	N (kN)	N (kN)	N (kN)	N (kN)	N (kN)
P1a	-51.7	-45.3	-37.8	-30.2	-22.9	-16.0	-9.7	-4.2
P1b	-51.8	-45.2	-37.7	-30.2	-22.9	-16.0	-9.7	-4.1
P2a	-368.8	-320.5	-267.3	-213.9	-162.4	-113.9	-68.9	-27.7
P2b	-369.1	-320.3	-267.1	-213.7	-162.3	-113.8	-68.9	-27.8
P3a	-149.3	-130.3	-109.3	-88.2	-67.7	-48.1	-29.8	-13.6
P3b	-149.4	-130.4	-109.3	-88.2	-67.6	-48.1	-29.8	-13.6
P4a	-260.3	-215.8	-177.4	-142.6	-110.0	-78.9	-49.1	-19.2
P4b	-258.8	-216.8	-178.0	-142.9	-110.0	-78.7	-48.7	-19.0
P5a	-395.3	-359.9	-322.7	-279.8	-232.0	-179.6	-122.2	-59.0
P5b	-392.7	-362.0	-324.1	-280.7	-232.4	-179.6	-121.9	-58.8
P6a	-19.6	-22.2	-23.1	-22.2	-20.0	-16.8	-12.4	-6.3
P6b	-19.4	-22.3	-23.2	-22.3	-20.1	-16.8	-12.5	-6.3
P7a	-527.8	-447.7	-377.2	-310.4	-247.9	-190.4	-138.3	-89.9
P7b	-517.4	-452.4	-379.6	-311.5	-247.9	-189.3	-135.6	-84.1
P8a	-407.6	-369.4	-328.5	-283.1	-237.4	-194.4	-157.5	-107.4
P8b	-400.3	-374.3	-331.6	-284.8	-238.1	-194.4	-157.1	-112.6
P9	-247.2	-239.0	-218.1	-191.3	-162.1	-132.5	-102.5	-15.2
P10	-162.1	-137.7	-116.6	-96.5	-77.5	-59.8	-43.9	-45.7
P11a	-201.7	-174.4	-144.6	-116.0	-88.8	-63.2	-39.0	-15.4
P11b	-202.2	-173.9	-144.2	-115.7	-88.6	-63.0	-38.9	-15.4
P12a	-242.0	-204.5	-170.0	-137.0	-105.3	-75.0	-46.5	-20.9
P12b	-242.3	-204.2	-169.8	-136.8	-105.1	-74.9	-46.5	-20.9
P13a	-247.3	-220.3	-190.4	-159.4	-127.6	-95.6	-63.8	-32.9
P13b	-247.3	-220.3	-190.4	-159.4	-127.6	-95.6	-63.8	-32.9
P14a	-127.0	-119.7	-109.5	-96.0	-80.4	-63.1	-44.4	-23.0
P14b	-126.8	-119.9	-109.7	-96.1	-80.4	-63.2	-44.4	-23.0
P15a	-264.9	-221.9	-182.8	-147.6	-114.8	-83.6	-54.5	-29.4
P15b	-265.1	-221.6	-182.5	-147.3	-114.6	-83.5	-54.4	-29.4
P16a	-246.0	-219.6	-194.8	-169.0	-140.8	-109.2	-73.8	-34.3
P16b	-244.7	-218.5	-193.8	-168.2	-140.2	-108.8	-73.5	-34.2
P17a	-49.0	-56.6	-63.2	-65.1	-62.1	-53.9	-39.6	-17.3
P17b	-48.6	-56.2	-62.9	-64.8	-61.9	-53.8	-39.6	-17.2
P18a	-92.5	-71.0	-54.9	-42.0	-31.0	-21.2	-12.6	-6.1
P18b	-92.4	-71.1	-54.9	-42.0	-31.0	-21.3	-12.7	-6.1
P19a	-290.4	-245.4	-206.8	-172.6	-140.1	-107.3	-73.2	-37.5
P19b	-290.6	-245.6	-207.0	-172.8	-140.3	-107.5	-73.4	-37.6
P20a	-41.1	-43.8	-45.5	-44.7	-41.8	-36.5	-28.2	-15.3
P20b	-41.2	-43.9	-45.5	-44.8	-41.9	-36.6	-28.3	-15.3
P21a	-316.3	-262.9	-215.6	-174.4	-137.7	-104.0	-71.6	-37.0
P21b	-315.5	-263.6	-216.3	-175.1	-138.3	-104.6	-72.3	-37.7
P22a	-371.5	-324.6	-282.2	-242.8	-204.9	-167.4	-130.2	-76.2
P22b	-373.0	-326.0	-283.5	-244.0	-206.0	-168.5	-131.6	-80.4
P23a	-80.8	-81.0	-82.9	-82.2	-78.4	-71.2	-60.4	-43.7
P23b	-81.0	-81.2	-83.1	-82.4	-78.6	-71.5	-60.8	-44.3
P24a	-42.1	-43.1	-44.4	-44.3	-42.4	-38.9	-33.9	-29.9
P24b	-42.3	-43.2	-44.5	-44.4	-42.5	-39.1	-34.1	-30.9
P25	-237.5	-210.1	-182.7	-155.3	-127.9	-100.5	-73.1	-16.0

Table B.35 – Shear forces in walls for lateral load applied in negative y-direction with seismic force as the main action.

Wall	BASEMENT		1ST FLOOR		2ND FLOOR		3RD FLOOR		4TH FLOOR		5TH FLOOR		6TH FLOOR		7TH FLOOR	
	Vx (kN)	Vy (kN)	Vx (kN)	Vy (kN)	Vx (kN)	Vy (kN)	Vx (kN)	Vy (kN)	Vx (kN)	Vy (kN)	Vx (kN)	Vy (kN)	Vx (kN)	Vy (kN)	Vx (kN)	Vy (kN)
P1a	0.0	-0.3	0.0	-0.5	0.0	-0.5	0.0	-0.5	0.0	-0.5	0.0	-0.4	0.0	-0.4	0.0	-0.3
P1b	0.0	-0.3	0.0	-0.5	0.0	-0.5	0.0	-0.5	0.0	-0.5	0.0	-0.4	0.0	-0.4	0.0	-0.3
P3a	0.0	-5.7	0.0	-7.5	0.0	-7.9	0.0	-7.6	0.0	-6.9	0.0	-5.9	0.0	-4.8	0.0	-3.9
P3b	0.0	-5.7	0.0	-7.5	0.0	-7.9	0.0	-7.6	0.0	-6.9	0.0	-5.9	0.0	-4.8	0.0	-3.9
P5a	-0.2	-47.8	0.3	-37.7	0.4	-29.3	0.4	-23.0	0.4	-17.3	0.3	-11.3	0.2	-4.1	0.2	6.7
P5b	0.2	-47.9	-0.3	-37.4	-0.4	-29.0	-0.4	-22.7	-0.4	-17.0	-0.3	-11.1	-0.2	-4.0	-0.2	6.6
P8a	0.0	-51.5	0.0	-60.7	0.0	-64.2	0.0	-64.2	0.0	-61.2	0.0	-56.2	0.0	-50.4	0.0	-31.2
P8b	0.0	-52.1	0.0	-59.4	0.0	-62.8	0.0	-62.8	0.0	-60.0	0.0	-55.2	0.0	-49.8	0.0	-31.2
P9	0.0	-14.2	0.0	-2.9	0.0	0.9	0.0	2.6	0.0	3.3	0.0	3.7	0.0	4.3	0.0	5.2
P11a	0.0	-16.9	0.1	-23.1	0.1	-24.9	0.1	-24.3	0.1	-22.2	0.1	-19.1	0.1	-15.4	0.1	-9.5
P11b	0.0	-16.9	-0.1	-23.1	-0.1	-24.9	-0.1	-24.3	-0.1	-22.2	-0.1	-19.1	-0.1	-15.3	-0.1	-9.5
P13a	0.0	-24.8	0.0	-24.8	0.1	-24.6	0.1	-23.0	0.1	-20.6	0.1	-17.5	0.1	-13.7	0.1	-10.4
P13b	0.0	-24.8	0.0	-24.8	-0.1	-24.5	-0.1	-23.0	-0.1	-20.6	-0.1	-17.4	-0.1	-13.6	-0.1	-10.3
P16a	0.0	-57.6	-0.1	-59.0	-0.1	-56.7	-0.1	-52.2	-0.2	-45.8	-0.2	-37.4	-0.2	-26.8	-0.2	-12.8
P16b	0.0	-57.6	0.1	-58.9	0.1	-56.7	0.1	-52.2	0.2	-45.8	0.2	-37.4	0.2	-26.8	0.2	-12.8
P19a	0.0	-45.6	-0.1	-38.9	-0.2	-32.4	-0.2	-27.1	-0.3	-22.0	-0.3	-16.6	-0.3	-10.0	-0.5	0.3
P19b	0.0	-45.5	0.1	-38.9	0.2	-32.4	0.2	-27.0	0.3	-22.0	0.3	-16.6	0.3	-9.9	0.5	0.4
P22a	0.0	-68.0	0.0	-70.1	0.1	-67.0	0.1	-61.3	0.1	-53.5	0.0	-43.7	0.0	-32.6	0.0	-17.4
P22b	0.0	-67.8	0.0	-69.6	-0.1	-66.2	-0.1	-60.3	-0.1	-52.3	0.0	-42.5	0.0	-31.2	0.0	-17.4
P25	0.0	-14.2	0.0	-2.7	0.0	-1.9	0.0	-1.4	0.0	-1.1	0.0	-0.8	0.0	-0.5	0.0	1.7

Table B.36 – Bending moments in walls for lateral load applied in negative y-direction with seismic force as the main action.

Wall	BASEMENT		1ST FLOOR		2ND FLOOR		3RD FLOOR		4TH FLOOR		5TH FLOOR		6TH FLOOR		7TH FLOOR	
	Mx (kNcm)	My (kNcm)	Mx (kNcm)	My (kNcm)	Mx (kNcm)	My (kNcm)	Mx (kNcm)	My (kNcm)	Mx (kNcm)	My (kNcm)	Mx (kNcm)	My (kNcm)	Mx (kNcm)	My (kNcm)	Mx (kNcm)	My (kNcm)
P1a	-48.7	-0.3	-72.3	-0.4	-78.6	-0.2	-77.0	0.0	-70.6	0.0	-61.2	0.1	-49.9	0.3	44.6	0.7
P1b	-48.6	0.3	-72.3	0.4	-78.7	0.2	-77.1	0.0	-70.6	0.0	-61.2	-0.2	-49.9	-0.3	44.6	-0.7
P3a	-954.9	2.5	-1158.0	-3.7	-1182.0	-3.2	-1117.0	-2.7	-996.4	2.5	-840.0	2.8	670.9	3.2	568.7	-3.0
P3b	-954.9	-2.6	-1158.0	3.6	-1181.0	3.2	-1116.0	2.8	-996.0	-2.6	-840.1	-2.8	671.8	-3.1	568.6	2.9
P5a	-18520.0	29.0	-12220.0	-49.6	-8236.0	-54.7	-5409.0	54.8	-3179.0	50.8	1851.0	43.1	1463.0	32.7	1654.0	-28.9
P5b	-18510.0	-29.6	-12180.0	48.9	-8185.0	54.1	-5356.0	-54.5	-3131.0	-50.4	1838.0	-42.9	1477.0	-32.6	1652.0	29.6
P8a	-14090.0	-1.5	-12350.0	-1.2	-11340.0	-1.0	-10300.0	-1.1	-9076.0	0.7	8039.0	0.5	7831.0	1.4	-4437.0	2.2
P8b	-14060.0	1.1	-12180.0	1.3	-11130.0	-0.2	-10100.0	-0.4	-8889.0	-0.3	7923.0	-1.4	7806.0	-3.3	-5686.0	6.0
P9	-5146.0	2.3	-1928.0	-3.0	-960.1	-1.4	-745.5	-1.1	-515.7	-1.1	705.4	-1.2	928.2	-1.0	1457.0	2.4
P11a	-2890.0	2.6	-3594.0	-7.6	-3757.0	-11.2	-3596.0	-12.5	-3232.0	12.4	-2735.0	11.2	-2158.0	9.0	-1454.0	-10.8
P11b	-2890.0	-2.7	-3595.0	7.5	-3758.0	11.2	-3597.0	12.5	-3233.0	-12.5	-2735.0	-11.3	-2157.0	-9.1	-1453.0	10.9
P13a	-6094.0	-0.2	-4862.0	-8.3	-4320.0	-16.1	-3719.0	-19.1	-3077.0	19.4	2488.0	18.2	2107.0	15.8	1854.0	-22.3
P13b	-6094.0	-0.1	-4860.0	8.2	-4315.0	16.1	-3714.0	19.1	-3072.0	-19.5	2484.0	-18.3	2102.0	-15.9	1848.0	22.4
P16a	-19250.0	6.3	-14800.0	13.0	-12020.0	17.2	-9654.0	19.8	-7418.0	21.4	-5258.0	22.7	4326.0	-22.9	2346.0	31.4
P16b	-19250.0	-6.5	-14800.0	-13.0	-12020.0	-17.0	-9652.0	-19.6	-7414.0	-21.2	-5254.0	-22.4	4321.0	22.5	2336.0	-30.9
P19a	-15720.0	7.7	-11010.0	18.1	-7878.0	26.2	-5569.0	32.6	-3701.0	37.6	2558.0	42.9	2116.0	-43.6	551.3	73.7
P19b	-15720.0	-7.7	-11010.0	-17.6	-7872.0	-25.4	-5561.0	-31.5	-3691.0	-36.6	2549.0	-41.8	2111.0	42.5	559.1	-72.4
P22a	-25090.0	-0.2	-19110.0	-3.7	-15200.0	-6.9	-11940.0	-7.7	-8932.0	7.3	6144.0	5.7	5682.0	2.5	5477.0	1.4
P22b	-25120.0	-0.2	-19090.0	3.9	-15130.0	7.3	-11830.0	8.4	-8790.0	-8.3	5955.0	-6.7	5474.0	-3.4	5270.0	5.8
P25	-5832.0	-0.1	-1869.0	-0.1	-1115.0	-0.1	-593.9	-0.1	-201.5	-0.1	342.0	0.1	492.5	-0.5	481.0	1.5